STYRELSEN FÖR

VINTERSJÖFARTSFORSKNING

WINTER NAVIGATION RESEARCH BOARD

Research Report No 65

Lennart Fransson

Ice Mechanics and Shipping in Ice-infested Waters, 2008

Finnish Transport Safety Agency
Finnish Transport Agency
Finland

Swedish Maritime Administration
Swedish Transport Agency
Sweden

FOREWORD

In this report no 65, the Winter Navigation Research Board presents the result from a project “Ismekanikk og havnedrift I islagt farvann”.
This report is the main document within this project and all interim reports are also presented in this document.

The Winter Navigation Research Board warmly thanks Mr Lennart Fransson for this report.

Helsinki

June 2014

Jorma Kämäräinen

Finnish Transport Safety Agency

Peter Fyrby

Swedish Maritime Administration

Tiina Tuurnala

Finnish Transport Agency

Stefan Eriksson

Swedish Transport Agency

2008:09

RESEARCH REPORT

Ice Mechanics and Shipping in Ice-infested Waters

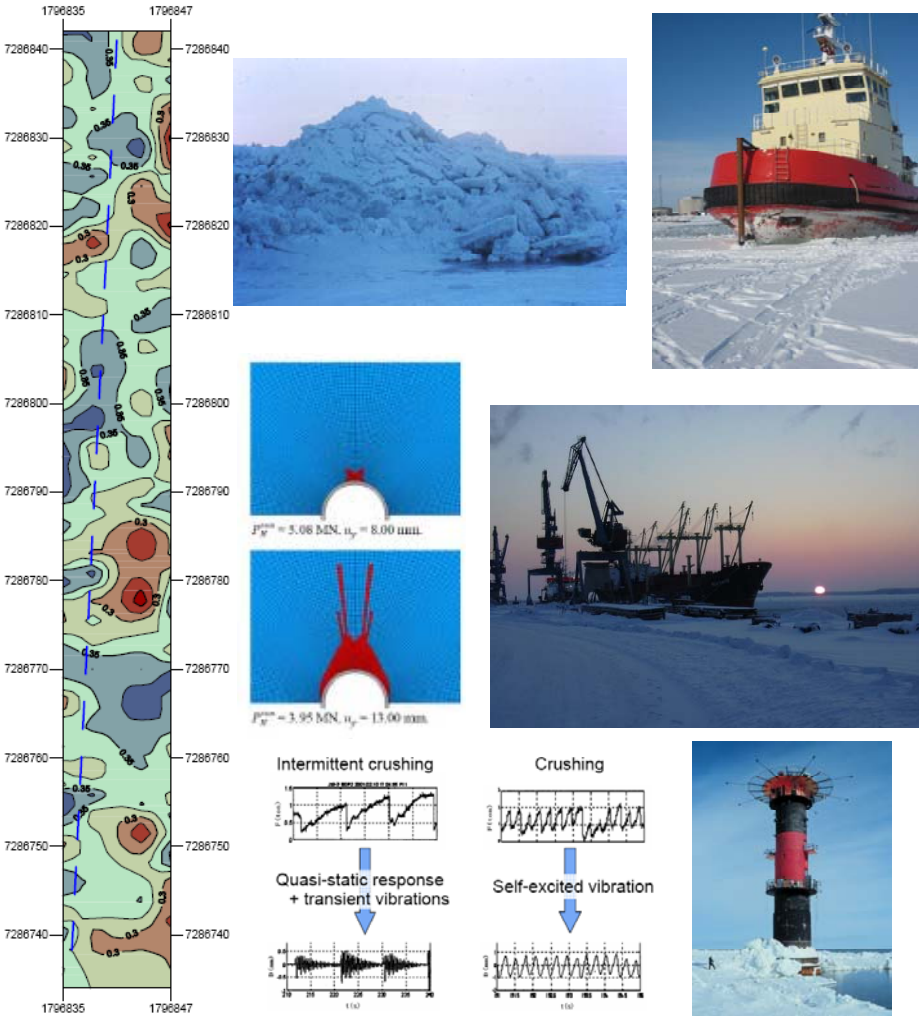

Ed. by Lennart Fransson

Luleå University of Technology
Department for Civil & Environmental Engineering
Division of Structural Engineering

Förord

Följande rapport ingår i projektet ”Ismekanikk og havnedrift i islagte farvann” (delprogrammet Nordkalotten INTERREG III A Nord).

Denna rapport är huvuddokumentet där alla delrapporter inom projektet sammanställts.

Luleå i april 2008

Lennart Fransson

Innehållsförteckning

Nonlinear finite element simulations of ice forces on offshore structures

Björnar Sand

Nonlinear finite element simulations of ice forces on offshore structures

Björnar Sand

Preface

The following report is a part of the project ”Ismekanikk og havnedrift i islagte farvann” (Nordkalotten INTERREG III A Nord).

In this report an extract (section 6.3) from the PhD.-thesis by Björnar Sand is presented.

Luleå, April 2008

Björnar Sand

Contents

1 Summary

The present investigation has been devoted to the development of nonlinear finite element simulations by means of obtaining ice forces on offshore structures. The effects of material nonlinearities and friction between ice and structure are taken into account. The key ingredients of the present approach have been described; a realistic representation of the complex constitutive behaviour of ice, accurate tracking of contact between the ice and the structure including coulomb friction sliding, and an automatic procedure for computation of buoyancy forces on a partially or completely submerged ice features.

A new three-dimensional constitutive model for ice is proposed and the formation of crushing or cracking is treated as a transformation of state, where the ice changes from being a solid to a granular material. The idea is to employ two separate constitutive models to simulate transformation of state due to cracking or crushing of the ice. The first constitutive model describes the material behaviour of unbroken or virgin ice and the second one describes the behaviour of ice after crushing or cracking by using element birth and death capabilities. In this manner, the mechanical behaviour of ice is approximated from the brittle end and it is treated as a rate-independent, elastic-brittle material. In the case of first year-ice, a general anisotropic failure criterion for ice has been applied to predict failure of columnar ice. This criterion accounts for material anisotropy, allows for different strengths in tension and compression, and predicts a nonlinear relation between material strength and hydrostatic stress. The anisotropic failure criterion represents a hyper-elliptic surface in the stress space and nonlinear least square procedures is employed to achieve least square fitting of the associated material parameters to laboratory test data for anisotropic, columnar ice. A similar approach has also been applied to model the behaviour of granular, multi-year ice and an isotropic failure criterion has been employed to predict failure of isotropic ice. This criterion represents an elliptic surface and has been fitted to laboratory test data for isotropic, granular ice. These constitutive models are implemented in the general finite element code ANSYS. To take account for buoyancy and gravity forces acting on floating ice features when the ice is lifted out of or submerged into the water, an iterative procedure for automatic calculation of the buoyancy forces has also been developed and implemented in the general finite element code ANSYS.

In the numerical studies presented herein, the structures are considered fixed and rigid. The contact interaction between the ice and the structure is described by a model based on finite sliding interaction between the ice features and interacting structure. The computation of friction forces acting at the ice-structure interface is based on the Coulomb friction law.

In order to test the constitutive models for ice and the application of the kinematic model including contact and friction, ice sheet interaction with:

- sloping structures
- vertical structures
- upward and downward bending cones

are analyzed by means of nonlinear finite element computations. For sloping and conical structures, a nonlinear, discrete spring model is employed to take account for the effect of buoyancy forces. In these examples, both the forces associated with ice breaking, and ice riding up the face of the sloping and conical structures is considered.

In addition, there have also been carried out nonlinear finite element simulations of:

- upward and downward bending cones
- and cylindrical structures

interacting with a moving multi-year ice ridge embedded into an ice sheet. In these examples, an idealized multi year ridge model with a constant sail to keel ratio and geometry is chosen. The ice within the ice sheet and the ridge is assumed to be isotropic and the strength is constant through the thickness of the ice sheet and ridge. The elliptic failure surface for granular ice was adopted to predict failure of solid isotropic ice. For upward and downward bending cones, the iterative model for automatic calculation of buoyancy and gravity forces has been employed to include the weight and buoyancy forces of the multi-year ice ridge.

The numerical results obtained for the chosen examples are compared with well-established analytical methods, numerical results reported in the literature, and in some examples, experimental field data. Although there is some discrepancy between these methods, the numerical results are in relatively good agreement with both the analytical solutions as well as the experimental field data.

The deviation between the numerical results obtained during finite element computations and the analytical methods might be due to several factors. The analytical solutions are based on simplified approximations of the mechanical behaviour of ice as well as the contact interaction processes. In addition, the failure modes are assumed a priory. The present finite element approach is based on a realistic representation of the complex constitutive behaviour of ice. In addition, the kinematic model includes accurate tracking of contact between the ice and the structure including coulomb friction sliding. The failure patterns and modes obtained during finite element simulations are not assumed a priory, but are a result of the three-dimensional stress state within the ice sheet or the ice ridge.

Extract from PhD.-thesis by Björnar Sand

Section 6.3

6.3 Finite element analysis of ice forces on vertical structures

The interaction of ice sheets with rigid vertical structures is an important problem in the design of arctic offshore structures. These structures often experience an enormous ice load since the ice sheet fails by crushing. In this section the finite element method is adopted to calculate ice forces on vertical structures. The effect of material nonlinearities and friction between the ice and structure is taken into account. The ice is treated as a transversely isotropic, nonlinear material, and the contact interaction between the ice sheet and the structure is simulated with a contact formulation based on finite sliding interaction between a deformable body and a rigid body with Coulomb friction sliding. To verify the applicability of the proposed constitutive models to describe failure of columnar ice, the numerical results obtained during the present study are compared with data from field measurements.

6.3.1 Geometry and ice data for Norströmsgrund lighthouse

In the EU-project LOLEIF (1998-2000) ice pressures were measured on 9 of totally 20 segments around the perimeter of the Swedish lighthouse Norströmsgrund in the Gulf of Bothnia. Much information and important results from these measurements have been published earlier (www.hydromod.de/loleif) and will not be repeated here. Instead one selected events from Jochmann and Schwarz [82] have been chosen to illustrate important characteristics of ice loads. In this study the ice crushing event 0303_022 was chosen to be simulated because the interacting ice thickness was fairly constant with a mean ice thickness of 0.26 m. This event has earlier been described by Fransson et al. [83, 84]. Observed vibrations associated with this event were small and possibly insignificant for the ice load development. The design of the data acquisition system (parallel A/D converters) made it possible to register all loads simultaneously with a high degree of accuracy. In the chosen event, 16 synchronized loads were registered for 20 minutes with a sampling rate of 30 Hz. Important details about the actual loading scenario and geometry of load sensors are shown in Figure 6.10 and the ice data is summarized in Tables 6.4 and 6.5.

Table 6.4 Ice data for event 0303_022, date 2000-03-03, ice type: level ice [83, 84].

Water level[1] [m]	Ice thickness[2] h [m]	Ice speed[3] v [m/s]	Ice movement direction[3] [π/10]	Air temp. [^{o}C]	Salinity [ppt]	compressive strength [4] f_c [MPa]
-0.05	0.26	0.20	4.5	-8	0.6	1.1-1.4

[1] Relative to upper edge of load sensors, [2] Registration (0.14 Hz) with sonar, [3] Estimation from video recordings, [4] Field tests 2000-03-22, compressive load applied on samples cut from the ice sheet.

Table 6.5 Summary of segment loads for event 0303_022 [84].

Segment no.	Reg. Length L (m)	Centre Line X (m)	Reg. Angle φ [π/10]	Mean Pressure p_{mean} ([kN/m]	Max Pressure p_{max} [kN/m]	Stand. dev $p_{\text{st.dev.}}$ [kN/m]	Pressure at max global load $p(P_H^{max})$ [kN/m]	Remarks:
1	1.21	0.605	1	125	372	50	186	
2	1.21	1.865	2	119	361	54	171	
3	1.21	3.125	3	111	414	56	249	
4a	0.50	4.030	4	111	478	58	227	4.1 + 4.3 + 4.5 + 4.7
4b	0.50	4.740	4	114	499	62	302	4.2 + 4.4 + 4.6 + 4.8
4	1.0	4.385	4	112	489	60	265	4a+4b
5	1.21	5.645	5	107	401	59	203	
6	1.21	6.905	6	108	377	59	335	
7	1.21	8.165	7	103	161	27	-	partially out of order
8	1.21	9.425	8	139	410	60	286	
9	1.21	10.685	9	111	297	47	144	
P_y [MN]				0.01	-0.10	0.01	0.14	
P_x MN]				0.921	3.20	0.46	2.01	
P_H [MN]				0.921	3.20	0.46	2.02	
angle φ				89.3	91.8	89.5	86,0	Orientation of P_H

The foundation of the lighthouse is equipped with force measuring panels on 162^o of the perimeter with 9 panels where each panel covers 18^o of the perimeter. Eight of the panels have dimensions 1.20 m × 1.60 m where 1.20 is the width and 1.60 m is the height of the panels. Each of these panels has a load capacity of 3 MN including an overload range of 50%. One panel (Panel no. 4 in Figure 6.10) has the same dimensions as above, but it was assembled from 8 small panels with a load area of 0.50 m × 0.37 m and a normal load capacity of 1 MN. Three basic statistical properties of the measured ice pressure have been studied and summarized in Table 6.5, mean pressure, p_{mean}, maximum pressure p_{max} and standard deviation $p_{\text{st.dev.}}$. In addition to these properties, the pressure distribution $p(P_H)$ at maximum global load during the event 0303_022 is of great interest. According to Fransson [83], the

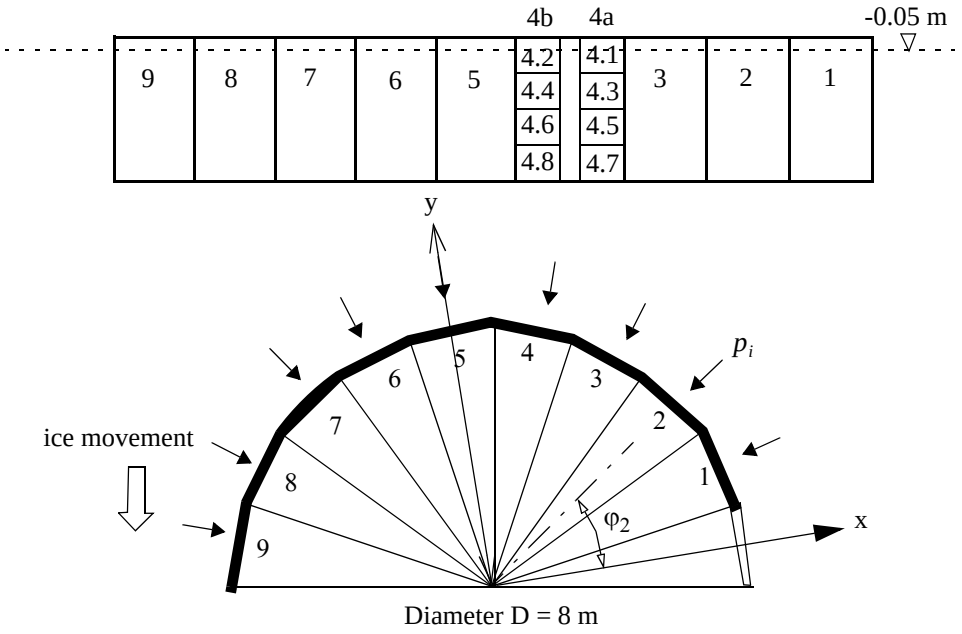

Figure 6.10 Lay-out of pressure sensors and geometry of the segmented lighthouse foundation. Segment 4 was divided into 8 smaller sensors (4.1-4.8).

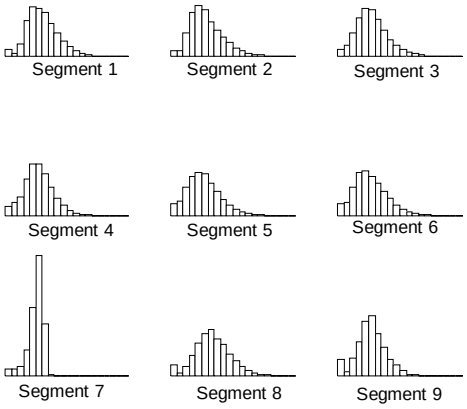

Figure 6.11 Probability density functions for segment pressures (0-414 kN/m), Fransson [84].

ice pressure $p(t)$ as function of time t is defined as

$$p(t) = \frac{F(t)}{L} \tag{6.2}$$

where $F(t)$ is the registered load normal to the segment and L is the corresponding registration length defined in Figure 6.10. When the total load on two or more adjacent segments were considered L was the total registration length. The probability density functions of individual segment pressures, shown in Figure 6.11, were of Weibull type with maximum pressures of about four times the mean level. It

can be seen from the graph that the measurement at segment 7 differs from other segments probably due to a frozen load panel. Segment 7 was therefore omitted in further analysis. Pressure variation on individual segments was in general more dynamic than pressure on the total structure. The maximum pressure decreased substantially with increasing registration length whereas the mean pressure was constant. It can be noticed that the mean pressure level dropped several times over a period of 20 minutes. From video recordings it was observed that the mean pressure drops were caused by large instability failures of the ice sheet in front of the structure. Pressure variations on segment 1 and on the total registration length are shown in Figure 6.12.

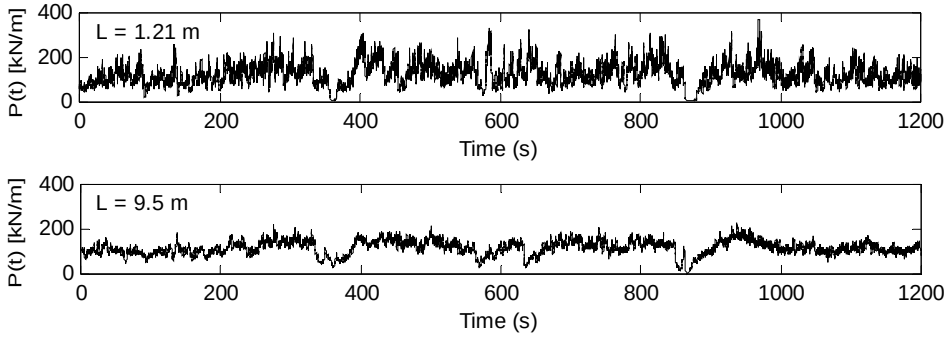

Figure 6.12 Pressure variation on segment 1 (L=1.21 m) and on the total registration length (L=9.5 m), Fransson [83].

Bjerkås et al. [85] discussed a method to calculate the global ice load acting on Norströmsgrund lighthouse. The panels covers each $\varphi = 18°$ of the perimeter and a total perimeter of $n\varphi$ where $n = 9$ is the number of panels as shown in Figure 6.10. A panel is only able to measure normal forces. In theory the ice-structure interaction zone covers a symmetric perimeter of $180°$, while the load panels only covers $162°$. The global ice load P_H, as given in Table 6.5, is calculated from the forces P_x and P_y acting in x-direction and y-direction as shown in Figure 6.10:

$$P_H = \sqrt{P_x^2 + P_y^2} \tag{6.3}$$

where the forces P_x and P_y are expressed by the ice pressures p_i acting on segments i ($i = 1, 2 \ldots 9$):

$$\begin{aligned} -P_x = {} & [(p_9 - p_1)\cos(\varphi) + (p_8 - p_2)\cos 2\varphi \\ & + (p_7 - p_3)\cos(3\varphi) + (p_6 - p_9)\cos(4\varphi)]L_0 \end{aligned} \tag{6.4}$$

$$\begin{aligned} P_y = {} & [p_5 + (p_9 + p_1)\sin(\varphi) + (p_8 + p_2)\sin(2\varphi) \\ & + (p_7 + p_3)\sin(3\varphi) + (p_6 + p_4)\sin(4\varphi)]L_0 \end{aligned} \tag{6.5}$$

Where $L_0 = 1.26$ m is the length of each segment and φ is the inscribed angle as

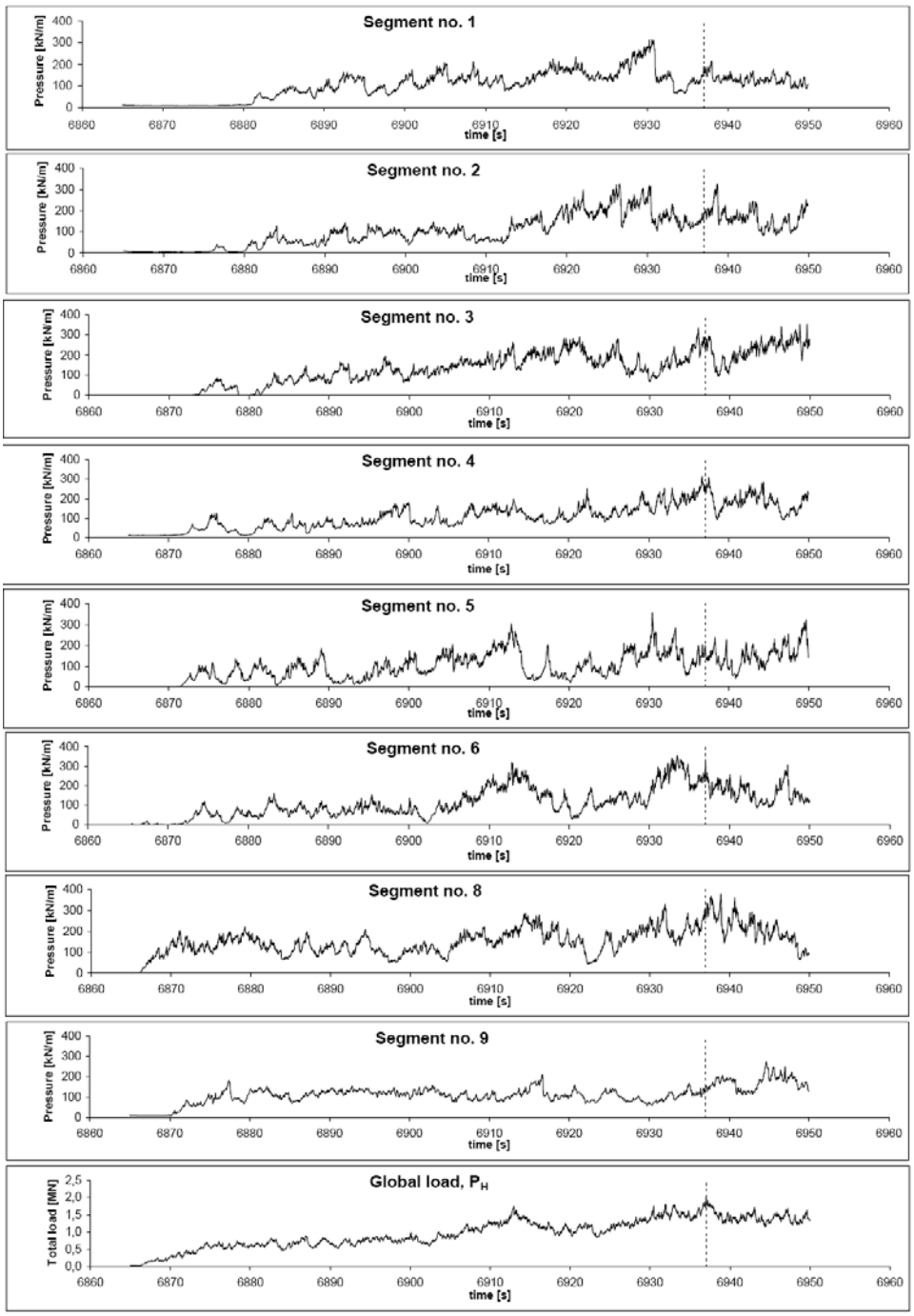

Figure 6.13 Variation of pressure on segments and global load for 85 s duration. Maximum global load P_H occurred at time $t = 6937$ s and is marked as dotted vertical lines.

shown in Figure 6.10. The ice pressure acting on the segments are given in Table 6.5. As described above, the load panel on segment 7 is partially out of order. Therefore, the pressure on segment 7 is substituted by $p_7 = (p_8 + p_6)/2$ when calculating the global load. During the event 0303_022, maximum global force $P_H = 2.02$ MN occurred after $t = 6937$ s. For illustration purposes, a sub-event of 85 s is chosen and Figure 6.13 shows the variation of the ice pressure on the segments and global load P_H. The time for occurrence of maximum global load is marked as dotted vertical lines in these diagrams.

Based on data from full-scale measurements of ice loads on Norströmsgrund lighthouse and a statistical approach to the extreme loads on the lighthouse, Fransson and Lundqvist [84] proposed the following formula for calculating the extreme load on Norströmsgrund lighthouse:

$$P_H = 5.5\left(\frac{D}{h_i}\right)^{-0.54} Dh_i = 5.5\left(\frac{8.0}{0.26}\right)^{-0.54} 8.0 \cdot 0.26 = 1.8 \text{ MN} \tag{6.6}$$

The discrepancy between the horizontal global load predicted by using Eq. (6.6) and the global horizontal force calculated from the measured pressure during event 0303_022 as summarized in Table 6.5 is less than 12%.

6.3.2 Finite element models of lighthouse foundation

The element mesh of the plane ice sheet and segmented lighthouse foundation is shown in Figure 6.10a. The ice thickness $h = 0.26$ m and the diameter D of the segmented lighthouse foundation is equal to 8.0 m. The ice sheet is modelled with length $L = 40D$ and width $B = 80D$, which moves into contact with the segmented lighthouse foundation by applying a uniformly distributed force in the y-direction along the edge ABC of the ice sheet. The boundary conditions of the edge ABC were such as to keep the ice sheet in a horizontal position. The remaining edges of the ice sheet were free. The segmented foundation was modelled with straight lines between the corners as shown in Figure 6.10b. The segmented lighthouse foundation was modeled as a fixed and rigid structure with a total number of 240 hexahedral elements with eighth nodal points and three translational degrees of freedoms associated with each nodal point. To study the effect of stress concentrations at the corners, the segmented foundation was also approximated as a smooth circular structure and the finite element model of the circular foundation is shown in Figure 6.10c.

Contact interaction forces between the ice sheet and the foundation is simulated with a contact formulation based on finite sliding between a deformable body and a rigid body as described in Section 5.2. The primary aim is to distinguish between open (i.e. not in contact) and closed (in contact) situations. This task is accomplished by two different algorithms, the pinball algorithm and pseudo-element algorithm briefly outlined in Section 5.2.2. Contact forces are divided into

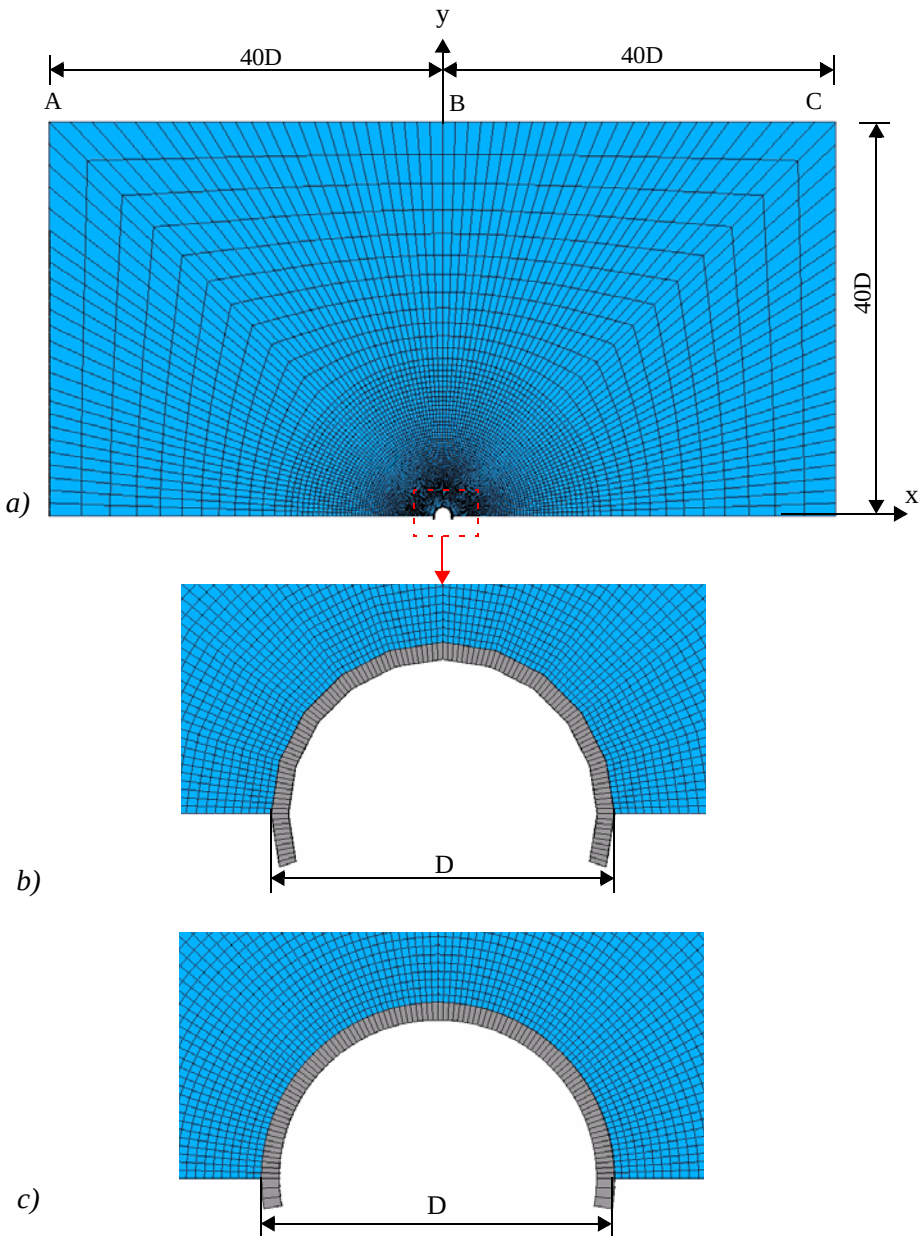

Figure 6.14 a) Finite element mesh of the ice sheet and lighthouse foundation. b) Segmented lighthouse foundation. c) Lighthouse foundation approximated as a smooth circular structure.

normal and tangential components. Forces normal to the structure are calculated with a combined penalty and Lagrange multiplier method as described in Section 5.2.3. In this method, the contact stiffness is variable in order to achieve contact compatibility to a user defined precision. Tangential forces are due to friction that arises as the nodal points on the ice sheet meet the target surface of the structure and

slides along it. In the present study, a Coulomb friction model is employed and the sticking force limit of the Coulomb friction model is function of the friction coefficient μ and the contact forces normal to the target surface on the structure.

The effect of loading rate and strain rate on the deformation characteristics and strength of ice is documented in Ref. 1 and 2. Unconfined tests on granular or columnar grained ice samples have shown that, under high strain rates ($\dot{\varepsilon} > 10^{-3}$ s^{-1}), ice behaves as a elastic brittle material. Michel and Toussaint [65] proposed that the effective strain rate $\dot{\varepsilon}$ is related to the indentation velocity V and the diameter D of the structure as $\dot{\varepsilon} = v/(4D)$, while Ralston [53] defined the strain rate as $\dot{\varepsilon} = v/(2D)$. The last definition has been adopted in API [10, 11]. During the field experiment, the ice speed v = 0.2 m/s is estimated from video recordings. The strain rate $\dot{\varepsilon}$ in the ice sheet is between $6.25 \cdot 10^{-3}$ s^{-1} and $1.25 \cdot 10^{-2}$ s^{-1} for diameter D = 8.0 m. Therefore, the ice can be treated as a elastic, brittle material.

When ice behaves in a brittle manner, cracking or crushing occurs during most interaction with structures. The formation of crushed or cracked ice may be seen as a change of state, where the ice changes from a solid to a cracked or crushed material as described in Section 3.6. To achieve this change of state, the ice sheet was discretized with a dual set of elements using an element mesh of 16400 isoparametric hexahedral elements, with four element through the thickness of the ice sheet, to model the behavior of solid ice as shown in Figure 6.14. The same number of elements was also applied to model the post failure behavior of ice as described in Section 3.6. For the numerical examples presented in this section, it is assumed that the ice sheet is made of columnar ice with constant stiffness and strength through the thickness of the ice sheet.

At the start of the analysis, the virgin, undamaged elements are active ones, while the second set of elements, representing damaged ice, are deactivated. For the first set, consisting of 16400 virgin elements, which represent undamaged ice, the stress rate $\dot{\sigma}_{ij}$ is related to the incremental elastic strain rate $\dot{\varepsilon}^{e}_{ij}$ through Hooke's law given by Eq. (3.36). The following values elastic constants are assumed: elastic moduli; $E_x = E_y$ = 6 GPa, E_z = 8.2 GPa, shear moduli $G_{xy} = G_{zx}$ = 2.26 GPa, and Poisson's ratios $\upsilon_{xy} = \upsilon_{zx}$ = 0.33. The elastic moduli E_x, E_z and Poisson's ratios υ_{xy}, υ_{zx} are based on test data from tensile tests carried out on columnar saline ice at a strain rate of 10^{-3} [13]. When the state of stress at a point reaches the failure surface, i.e. $f = f(\sigma_{ij}) = 0$, failure is said to occur and the virgin elements are deactivated, and the damaged elements are reactivated simultaneously. To predict failure of transversely isotropic ice, Horrigmoe and Zeng's [57] hyper-elliptic failure criterion, given by Eq. (3.31), is applied. The material parameters a_1, a_3, a_5, a_7, a_9 and a_{11} are determined numerically as described in Section 3.4.1 and values for the parameters are summarized in Table 3.4. The failure criterion, given by Eq. (3.31), is evaluated based on the mean values of the stress components in the finite elements, see Eq. (3.30).

After failure, the elasto-plastic approach, as described in Section 3.6.3, is employed to describe the post failure behavior of second set of 16400 damaged elements. To obtain meaningful results, the finite element analysis is based on the updated Lagrange formulation as described in Section 5.1. The geometries of the newly reactivated damaged elements are then evaluated in the current geometric configuration of the deactivated virgin elements. In this manner the current strains in the virgin elements are transferred to the damaged elements. In the cracked or crushed state, it is assumed that the elastic behavior is the same in tension and compression and the total strain rate $\dot{\varepsilon}_{ij}$ is the sum of elastic strain rate $\dot{\varepsilon}^{e}_{ij}$ and plastic strain rate $\dot{\varepsilon}^{cr}_{ij}$ as given by Eq. (3.42). The elastic strains is given by Eq. (3.41) and the post failure modulus E^c MPa and Poisson's ratio υ^c are assumed to be equal to equal to E_x and υ_{xy}, respectively. To account for different plastic yielding and hardening in tension and compression, a composite yield surface is introduced to describe the post failure behavior of ice. Rankine's maximum stress criterion, given by Eq. (3.42), is adopted to describe the tension behavior in the damaged state with tensile yield strength f_t, while von Mises yield criterion, Eq. (3.43), is employed to describe the compressive behavior with compressive yield strength f_c. To achieve an reduced residual strength of the cracked or crushed ice, the tensile yield strength f_t and compressive yield strength f_c in the post failure state are taken as 30% of the uniaxial tensile and compressive strength of the columnar, virgin ice, i.e. $f_t = 0.3T_x$ and $f_c = 0.3C_x$, where the uniaxial tensile strength $T_x = 0.35$ MPa and compressive strength $C_x = 3.65$ MPa, see Table 3.5. Linear isotropic hardening is specified by the elasto-plastic tangent modulus $E^{pl} = E^c/500$.

6.3.3 Global ice forces and ice failure

The ice sheet was considered as made of columnar ice and Horrigmoe and Zeng's criterion was employed to predict failure of the ice. To examine the effect of magnitude of friction coefficient on the global ice forces and distribution of ice pressure acting on the structure, six different values was selected between $\mu = 0.0$ and $\mu = 0.5$. Figure 6.15 shows plots of global ice force versus the displacement u_y as obtained during finite element analysis of the segmented and circular foundations, respectively. The displacement u_y of the ice sheet is takene at point B in Figure 6.14. These diagrams also demonstrate the effect of magnitude of the ice-structure friction coefficient. In general, the global ice forces increases almost linearly as the foundation penetrates the ice sheet until approximately 85% - 90% of the maximum load. As foundation penetrates deeper into the ice sheet, the stiffness of the ice decreases gradually due to initiation of fracture of ice and maximum ice load on the foundation occurs. Thereafter, the ice force decreases gradually as ice fracture propagates further into the ice sheet and the ice force reaches a stable load level as shown in Figure 6.15. The maximum global ice force P_H^{num}, corresponding effective pressure, $p_e = P_H^{num}/(hD)$, and normalized effective pressure contact factor, p_e/C_x, are summarized in Table 6.6. When calculating the contact factor k_b, the horizontal, uniaxial compressive strength of columnar ice $C_x = 3.62$ MPa is used, see Table 3.5.

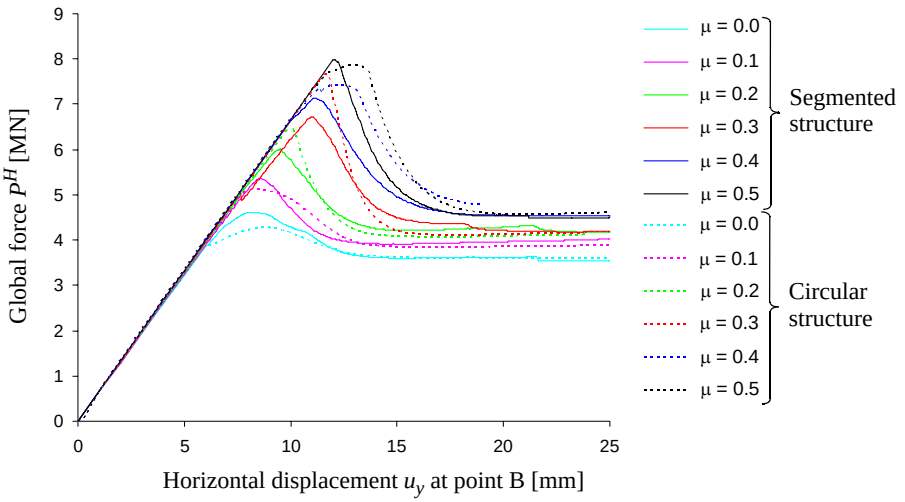

Figure 6.15 Global ice force vs. displacement obtained during finite element simulations of an ice sheet interacting with a segmented or circular foundation.

Table 6.6 Maximum global ice forces, indentation pressure and contact factor obtained during nonlinear finite element analysis of ice sheet interacting with segmented or circular structure.

Coefficient of friction μ [-]	Maximum global force P_H^{num} [MN]	Displacement at point B (u_y) [mm]	Effective pressure p_e [MPa]	Normalized effective pressure p_e / C_x [-]
Segmented foundation.				
0.0	4.61	8.1	2.22	0.61
0.1	5.37	8.7	2.58	0.71
0.2	6.00	9.5	2.89	0.80
0.3	6.71	11.0	3.23	0.89
0.4	7.14	11.1	3.43	0.95
0.5	7.97	12.00	3.83	1.06
Circular foundation				
0.0	4.26	8.9	2.05	0.57
0.1	5.12	8.4	2.46	0.68
0.2	6.47	10.0	3.11	0.86
0.3	7.68	11.7	3.69	1.02
0.4	7.43	11.9	3.57	0.99
0.5	7.87	13.0	3.78	1.04

6.3.4 Failure pattern and ice pressure for segmented structure

The development of the failure pattern of the ice is studied by gradually increasing the magnitude of ice-structure friction μ from 0.0 to 0.5, and the numerical results are portrayed in Figures 6.16 to 6.21 where the failure patterns of the ice sheet are shown at different load levels. These figures also demonstrates the variation of contact pressure acting in the direction normal to the load panels of the segmented structure.

The ice pressure obtained by finite element simulations is plotted as function of the registration angle φ in the range of $0°$ and $180°$ for different load levels. The Registration angle φ is defined in Figure 6.10. By post-processing of the numerical results, only the normal contact pressure acting at the centre plane of the ice sheet is considered. The tangential contact stress due to friction is neglected, i.e. in the same manner as for the measured ice pressure. Comparisons of the measured ice pressure, given in Table 6.5, and the ice pressure obtained by finite element computations are compared and discussed later in this chapter.

Two kinds of primary failure modes were obtained for the segmented structure, i.e. radial cracking and shear failure as described below.

For lower magnitudes of friction, i.e. $\mu \leq 0.3$, as shown in Figures 6.16 to 6.19, the ice slides along the surfaces of the segmented structure, which leads to relatively low confinement of the ice in front of the structure. When the ice is in the elastic state, i.e. the lowest load levels in Figures 6.16 to 6.19, maximum ice pressure acting on each segment occurs at the corners of the structure. At approximately 85% - 90% of the maximum global, radial cracks starts to form due to stress concentrations in the ice near the corners of the segmented structure. Formation of radial cracks leads to small regions of low-pressure zones near the corners of the structure. High-pressure zones will tend to form at the edges of low-pressure zones, responding to the occurrence of ice failure. Formation of radial cracking reduces the stiffness of the ice sheet as shown in global force- displacement curves as shown in Figure 6.15. As the load increases further and reaches maximum load, the radial cracks coalesce due to crushing of the ice in the front of the structure, which has a great influence on the ice pressure distribution. The location of the high-pressure zones moves as the size of the region of ice failure expands, which in turn increases the magnitude of maximum ice pressure. As the structure penetrates deeper into the ice sheet, the stiffness of the ice is partially lost as a large crack in front of the structure start to form and propagates along the centre line if the ice sheet, i.e. a splitting type of failure. This is characterizes the softening behavior of the ice sheet and the global ice force reaches a stable load level as shown in Figure 6.15. At this stage, the ice pressure is almost uniform along the entire ice-structure contact surface, except for small regions of high-pressure zones near the corners of the structure for $\varphi = 0°$ and $\varphi = 180°$.

Higher magnitudes of friction, $\mu > 0.3$, prevents the ice from sliding along the surfaces of the segmented structure, which increases the confinement pressure in the ice. When the ice is in the elastic state, i.e. the lowest load levels in Figures 6.20 to 6.21, maximum ice pressure on each segment occurs near the corners of the structure at the end farthest off the centre of the structure and decreases towards the end of the segments nearest the centre of the structure, i.e. similar pressure distribution as obtained for lower magnitudes of friction, but the level of the ice pressure level is somewhat higher. At approximately 90% of the failure load, shear failure start to form in the ice at each side of the structure as shown in Figures 6.20 and 6.21. Ice failure tends to decreases the ice pressure at previous high-pressure zones. At the same time, ice pressure increases elsewhere. However, initiation of shear failure does not influence on the overall behavior of the ice sheet. In same manner as for lower magnitudes of friction, radial cracks still forms near the corners of the segmented structure as the ice load increases towards maximum. As the structure penetrates deeper into the ice sheet, the radial cracks coalesce due to crushing of the ice in the front of the structure, which has a great influence on the ice pressure distribution. The location of the high-pressure zones moves as the size of the region of ice failure expands, which in turn increases the magnitude of maximum ice pressure. Final failure occurs as the structure penetrates even deeper the ice and the stiffness of the ice sheet is partially lost due to formation of a large crack in front of the structure along the centre line i.e. a splitting type of failure in same manner as obtained for lower magnitudes of friction. This characterizes by softening behavior of the ice sheet and the global ice force reaches a stable load level as shown in Figure 6.15. At this stage, the ice pressure is almost uniform, except for small regions of high-pressure zones near the corners of the structure.

Due to low spatial resolution of the measured ice pressure, it is difficult to make any well-built conclusions by directly comparing the distribution of the measured and simulated ice pressure. However, the simulated and measured ice pressure shows similar trends. The distribution of the ice pressure are considerable more dynamic than the global ice forces acting on the structure. It is commonly assumed that the ice pressure acting on circular or near circular structure follows a cosine distribution, with a maximum ice pressure in the direction of the moving ice sheet [83, 85]. This summation may be valid in a global sense, but the simulated shows strong variation along the length of each individual segment. The simulated ice pressure, fluctuate considerable both in space and time (or global load level), with most of the force concentrated intensely in regions. This is similar to what Jordaan et al. [86] called high-pressure and low pressure zones. High-pressure zones will tend to locate in the most confined regions or due to stress concentrations near corners. As the global load increases, the pressure within the high-pressure zones increases accordingly and moves about, responding to the occurrence of fracture, sometimes moving away from the "most likely" locations. Fracture will tend to occur where there are location of the stress concentration associated with the high-pressure zones themselves.

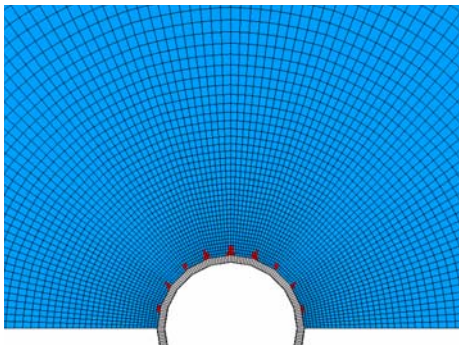

P_H^{num} = 3.86 MN, u_y = 6.00 mm.

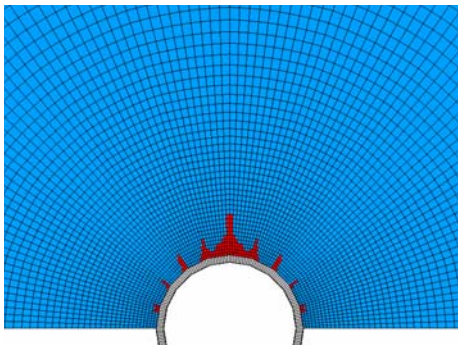

P_H^{num} = 4.34 MN, u_y = 7.00 mm.

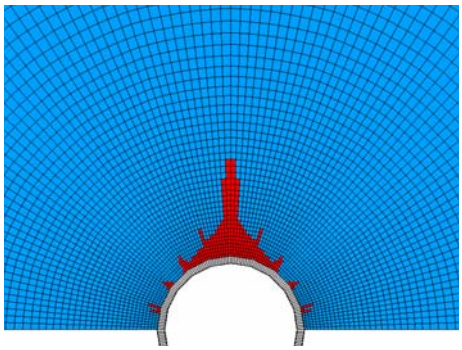

P_H^{num} = 4.61 MN, u_y = 8.13 mm.

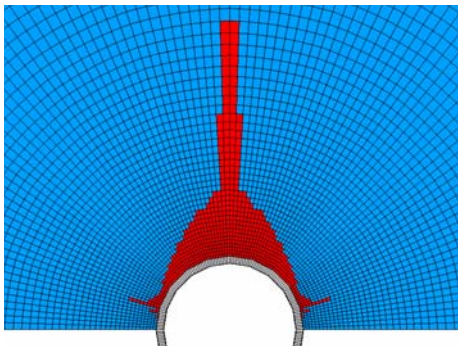

P_H^{num} = 4.09 MN, u_y = 11.00 mm.

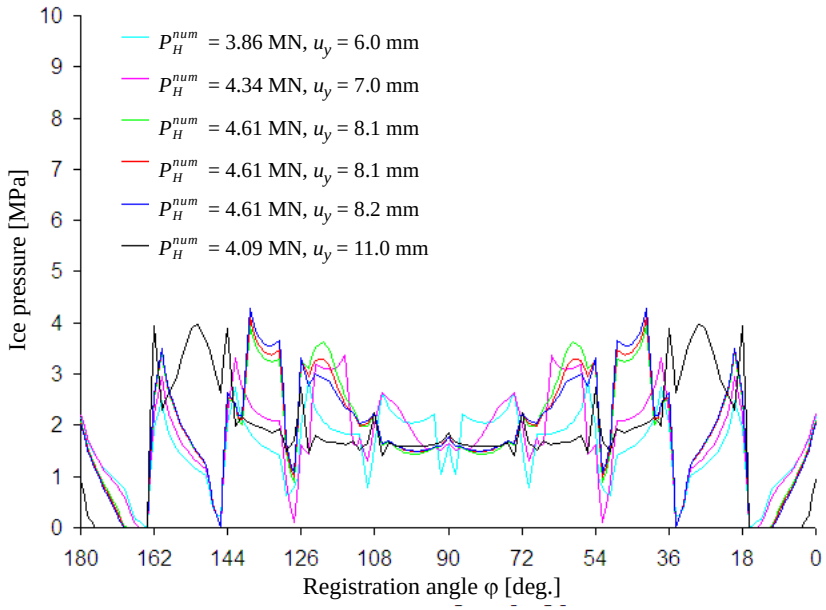

Figure 6.16 Calculated failure pattern and distribution of ice pressure obtained for the segmented structure with μ = 0.0.

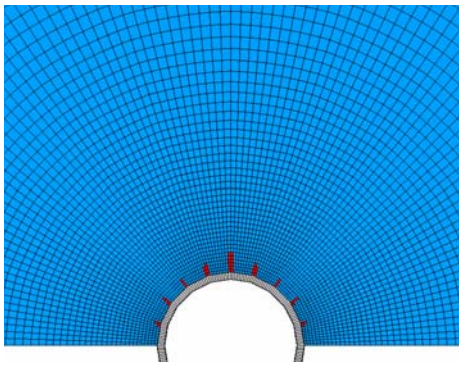

P_H^{num} = 4.51 MN, u_y = 7.00 mm.

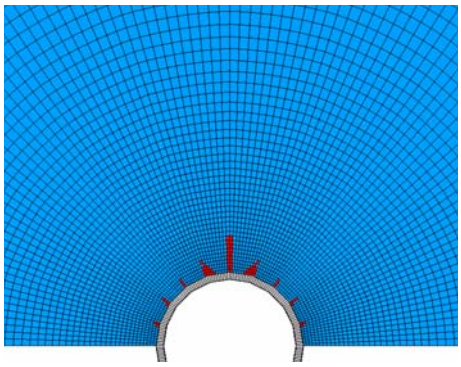

P_H^{num} = 5.13 MN, u_y = 8.00 mm.

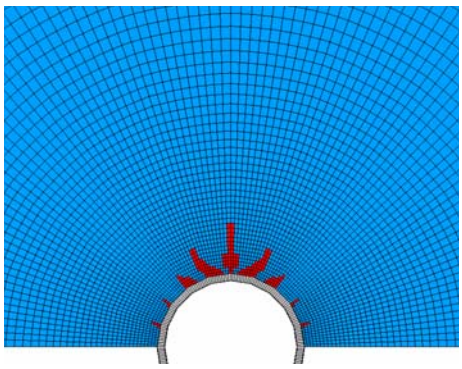

P_H^{num} = 5.36 MN, u_y = 8.56 mm.

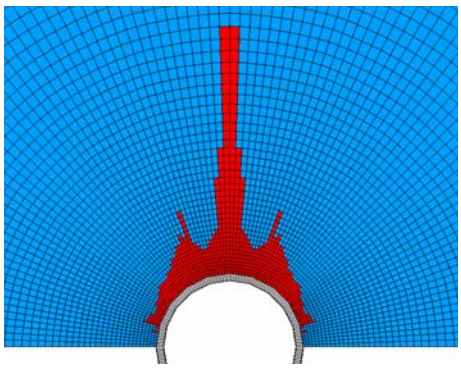

P_H^{num} = 3.95 MN, u_y = 13.00 mm.

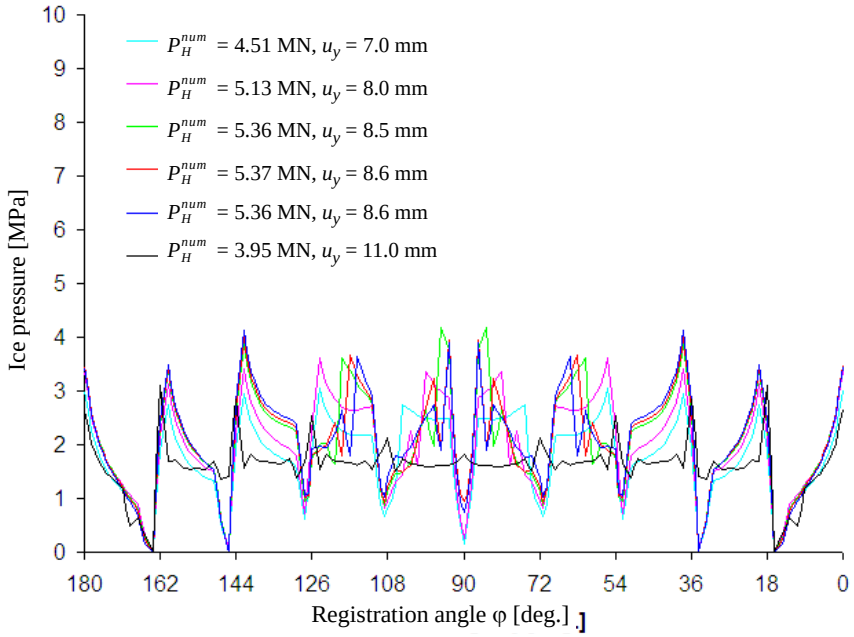

Figure 6.17 Calculated failure pattern and distribution of ice pressure obtained for the segmented structure with μ = 0.1.

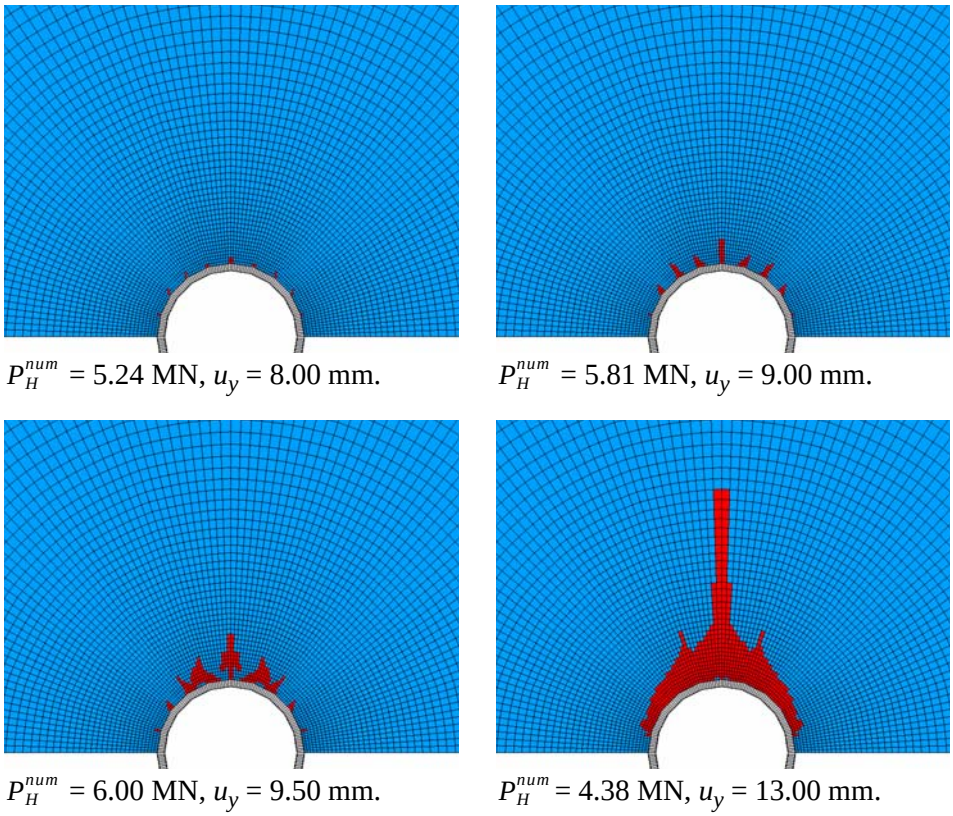

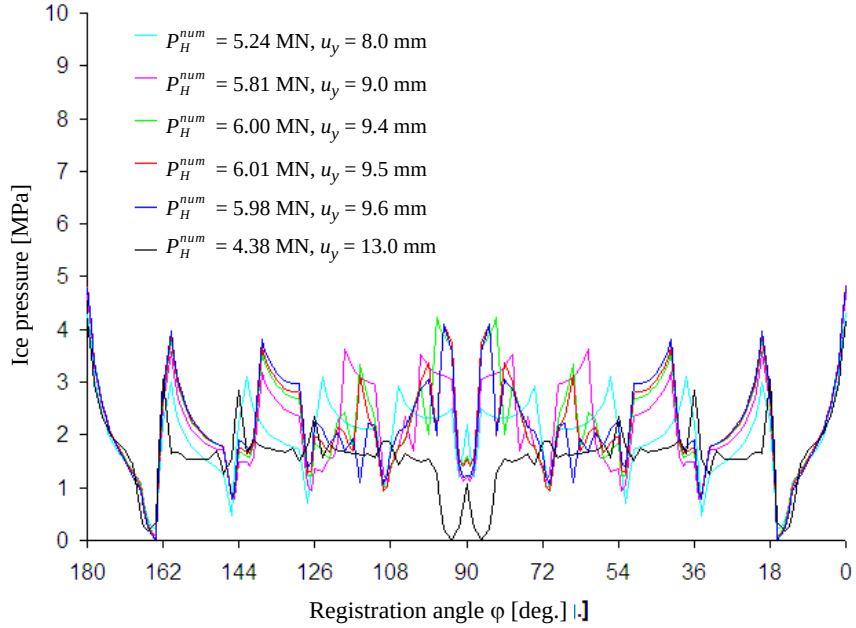

Figure 6.18 Calculated failure pattern and distribution of ice pressure obtained for the segmented structure with μ = 0.2.

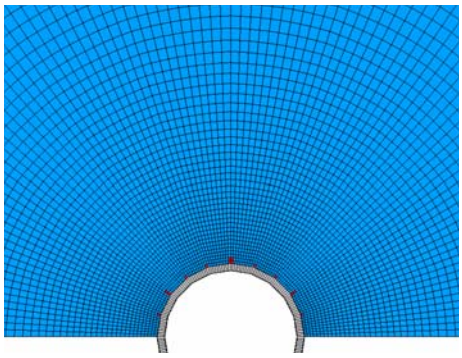

P_H^{num} = 5.64 MN, u_y = 9.00 mm.

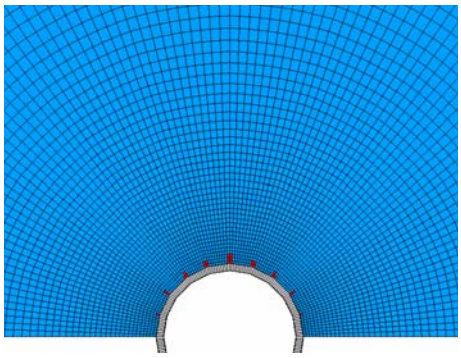

P_H^{num} = 6.24 MN, u_y = 10.00 mm.

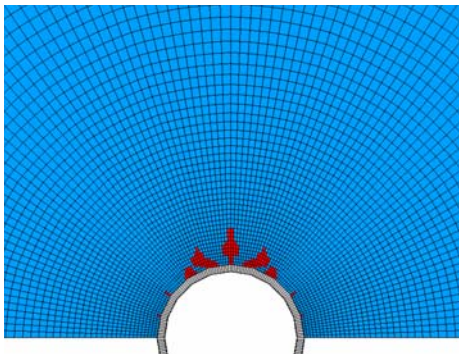

P_H^{num} = 6.71 MN, u_y = 11.00 mm.

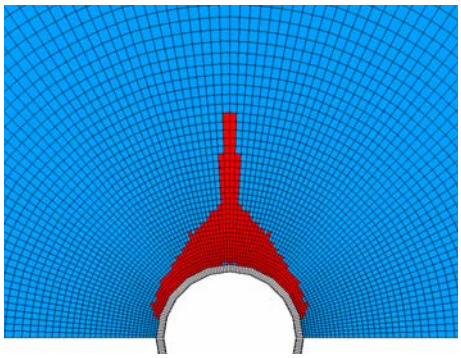

P_H^{num} = 6.26 MN, u_y = 13.00 mm.

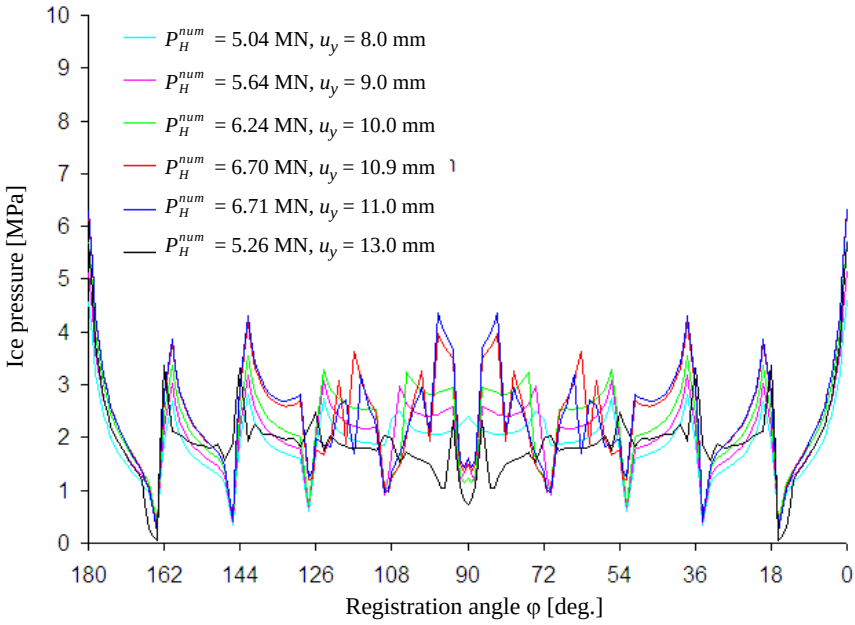

Figure 6.19 Calculated failure pattern and distribution of ice pressure obtained for the segmented structure with μ = 0.3.

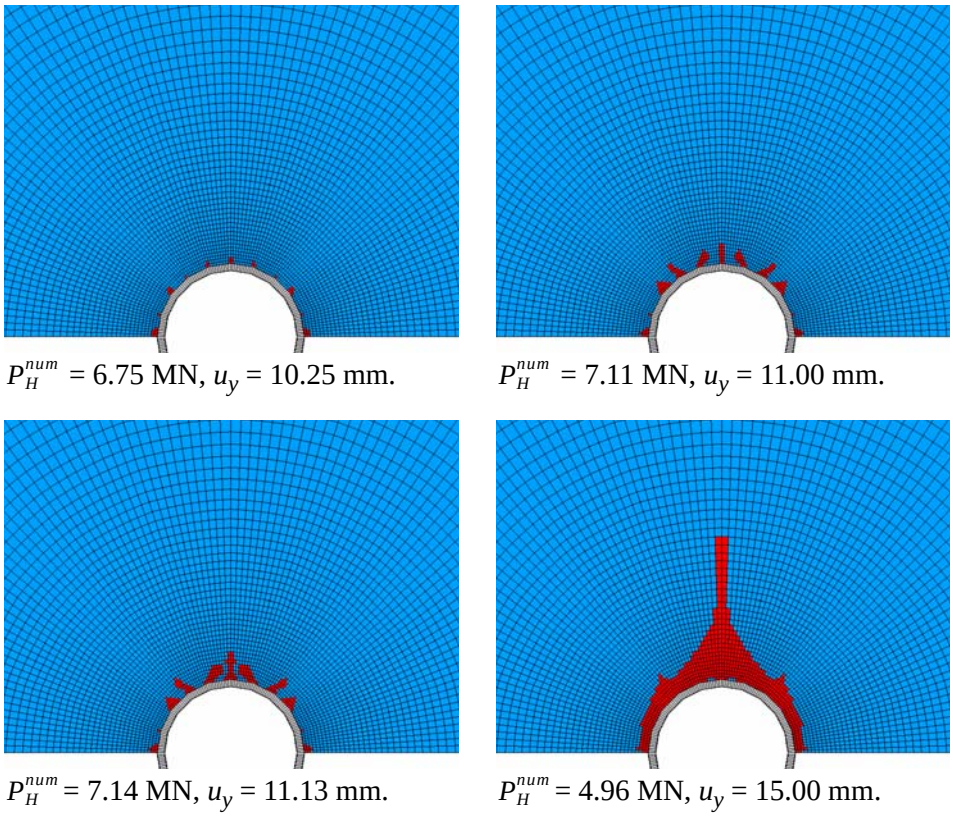

Figure 6.20 Calculated failure pattern and distribution of ice pressure obtained for the segmented structure with μ = 0.4.

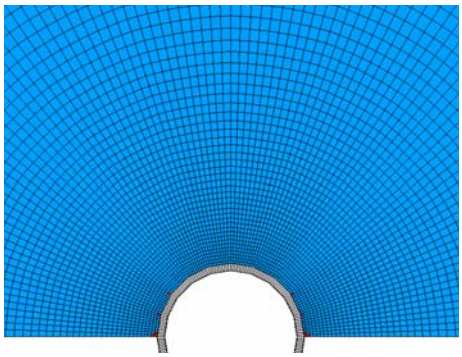

P_H^{num} = 7.32 MN, u_y = 11.00 mm.

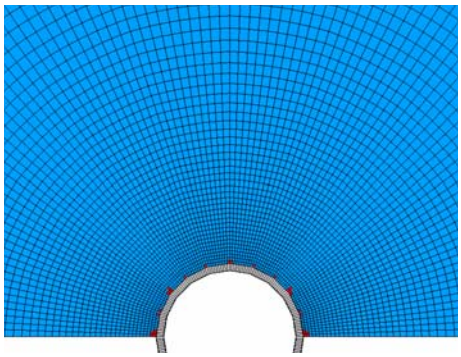

P_H^{num} = 7.97 MN, u_y = 12.00 mm.

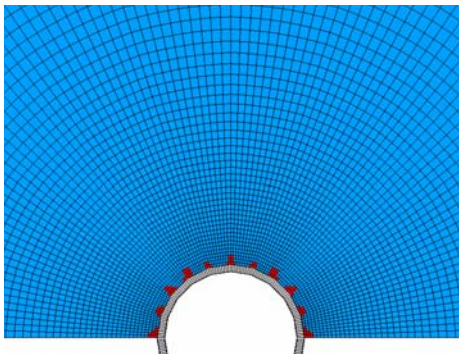

P_H^{num} = 7.95 MN, u_y = 12.13 mm.

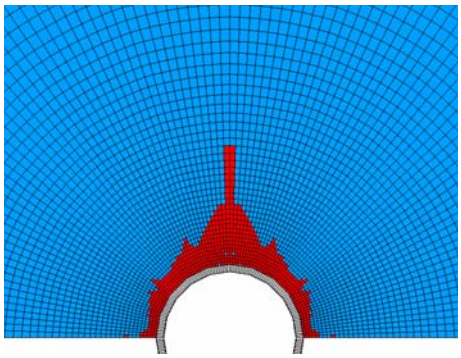

P_H^{num} = 5.16 MN, u_y = 15.00 mm.

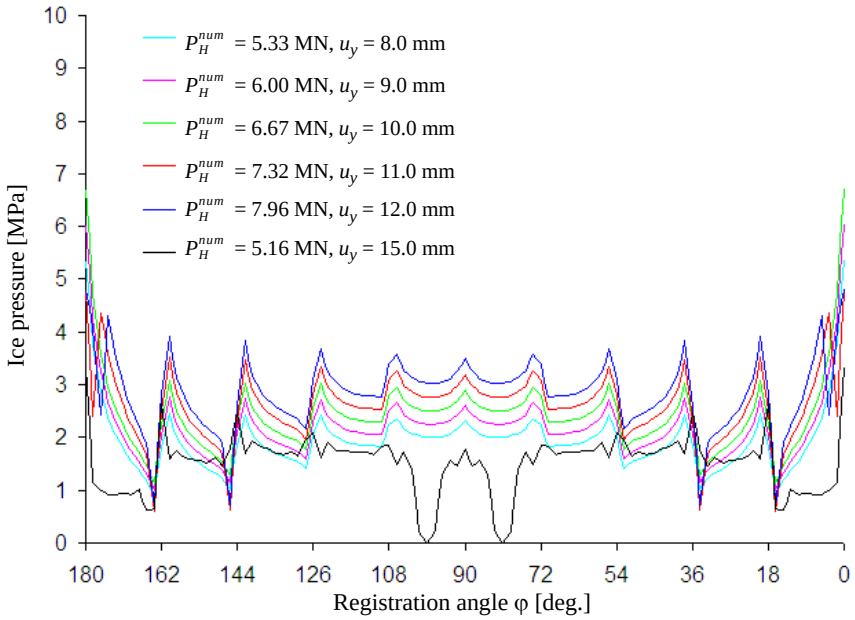

Figure 6.21 *Calculated failure pattern and distribution of ice pressure obtained for the segmented structure with μ = 0.5.*

6.3.5 Failure pattern and ice pressure for circular structure

In same manner as for the segmented structure, the development of ice failure process and distribution of ice pressure obtained for the circular structure for magnitudes of friction μ between 0.0 and 0.5 are illustrated in Figures 6.22 to 6.27. Three different kinds of primary failure modes where identified for the circular structure: crushing, radial cracking, and shear failure as described below.

For the lowest magnitudes of friction, i.e. $\mu = 0.0$ and $\mu = 0.1$, as shown in Figures 6.22 to 6.23, the ice slides along the surface of the circular structure, which lead to relative low confinement pressure in front of the structure. When the ice is in the elastic state, the ice pressure shows a concave pressure distribution on the circular surface and maximum ice pressure occurs in front of the structure as shown for the lowest load levels in Figures 6.22 to 6.23. Formation of ice crushing in front of the structure dominates primary failure of the ice sheet at approximately 85% - 95% of the maximum global load. Ice crushing leads to low-pressure zones in front of the structure. At the same moment high-pressure zones forms at the edges of the ice crushing zone. As the load increases to maximum, the size of ice crushing areas and corresponding low-pressure zones increases accordingly, which is followed by either initiation of, a single centre crack as shown in Figure 6.22 ($\mu = 0.0$), or initiation of multiple, radial cracks as shown in Figure 6.23 ($\mu = 0.1$). This in turn moves the locations of the high-pressure zones and increases magnitudes of ice pressure within these regions. As the structure penetrates deeper into the ice, the cracks propagates and forms either a final splitting type of failure shown in Figure 6.22, or a wedge-shaped type of failure as shown in Figure 6.23. Due to formation of splitting or wedge-shaped failure, the ice sheet looses some of its stiffness, which characterizes the softening behavior of the global force-displacement curves shown in Figure 6.15. At this stage, the low-pressure zone covers almost the entire ice-structure contact surface, except for small regions of high-pressure zones at each side of the structure.

For intermediate magnitudes of friction, $\mu = 0.2$ and $\mu = 0.3$, as shown in Figures 6.24 and 6.25, the relative sliding between the ice sheet and structure reduces and the confinement pressure in the ice in front of the structure increases. In the elastic state, the ice pressure distribution shows a local maximum in front of the structure, and the ice pressure decreases towards each side of the structure and shows a local minimum at registration angles $\varphi \approx 10°$ and $\varphi \approx 170°$ and increases rapidly towards maximum values at each side of the structure. Primary failure starts at approximately 90% of the maximum global load as radial cracks forms in the ice. Radial cracking leads to small regions of low-pressure zones shown as drops in the ice pressure distribution. As the load increases, the radial cracks propagates for $\mu = 0.2$, while for $\mu = 0.3$, the ice starts to crush in front of the structure and the low-pressure zones increases in size accordingly. The development of high-pressure zones is not as pronounced as for the lowest magnitudes of friction ($\mu = 0.0$ and $\mu = 0.1$), but small spots of high-pressure occurs at the edge of the low-pressure zones. As the penetration continuous, final failure occurs due to a combination of

crushing and radial cracking for $\mu = 0.2$, which form a wedge-shaped failure mode as shown in Figure 6.24. For $\mu = 0.3$, final failure is dominated by crushing and the stiffness of the ice sheet is partially lost due to formation of a splitting type of failure as shown in Figure 6.25. At this stage, the low-pressure zones expand and cover almost the entire ice-structure contact surface, except for small regions of high-pressure zones at each side of the structure.

For the highest magnitudes of friction, ($\mu = 0.4$ and $\mu = 0.5$), the ice is prevented from sliding along the surface of the circular structure, and the confinement pressure in the ice increases even further in front of the structure, which in turn increases the ice strength. In the elastic state, the ice pressure distribution shows a local maximum in front of the structure, and the ice pressure decreases towards each side of the structure and shows a local minimum at registration angles $\varphi \approx 18°$ and $\varphi \approx 162°$ and increases rapidly towards maximum values at each side of the structure. The increased confinement pressure in the ice in front of the structure prevents radial cracking, which leads to formation of primary shear failure at each side of the structure as shown in Figures 6.26 and 6.27 for $\mu = 0.4$ and $\mu = 0.5$, respectively. At approximately 90% of the maximum global ice load. The formation of shear failure in the ice at each side of the structure leads to reduced magnitudes of ice pressure in the previous high-pressure zones, which in turn increases the overall ice pressure acting elsewhere on the ice-structure contact surface. As the load increases, the size of the ice failure zone due to combined shear and crushing increases accordingly. This in turn moves the locations of the high-pressure zones and increases magnitudes of ice pressure within these regions. At the same time, low-pressure zones develop at previous high-pressure zones due to ice failure. As structure penetrates deeper into the ice, final failure occurs due to a combination of shear failure at each side of the structure and crushing in front of the structure as shown in Figures 6.26 and 6.27. At this stage, the low-pressure zones expand and cover almost the entire ice-structure contact surface, except for small regions of high-pressure zones at each side of the structure.

Even if the global behavior of the segmented and circular structure does not differ significant as illustrated by the global ice force - displacement curves given in Figure 6.15, there are several differences in the predicted failure patterns and distribution of the ice pressure. In the elastic state, the simulated ice pressure distribution for the circular structure is smooth and show a cosine distribution, at least for friction coefficient $\mu = 0.0$ and crushing occurred due to high compressive stresses in front of the structure. For higher coefficient of friction, maximum ice pressure occurs at registration angles equal to $0°$ and $180°$, which in turn lead to a shear type failure at each side of the structure. The ice pressure obtained for the segmented structure is considerable more dynamic both in space and load level. Due to stress concentrations at the corner of the segmented structure, high-pressure zones occurs in the ice, which in turn lead to radial cracking for lower values of friction, this is combined with a shear failure for higher values of friction.

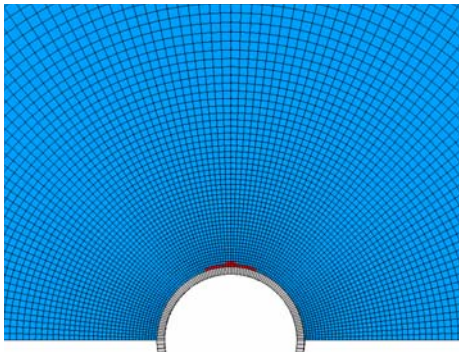

P_H^{num} = 3.85 MN, u_y = 6.00 mm.

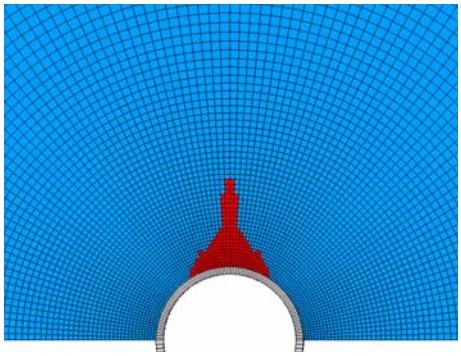

P_H^{num} = 4.04 MN, u_y = 7.00 mm.

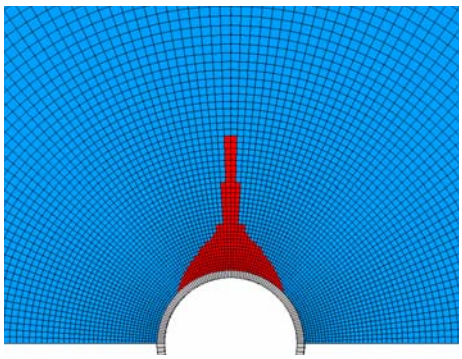

P_H^{num} = 4.26 MN, u_y = 8.88 mm.

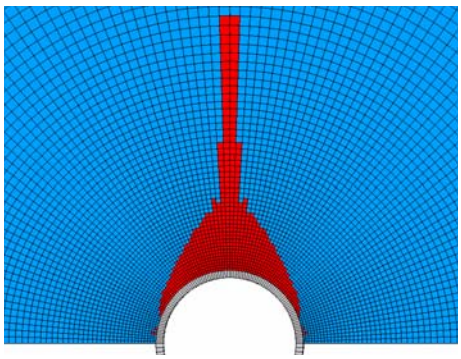

P_H^{num} = 3.96 MN, u_y = 11.00 mm.

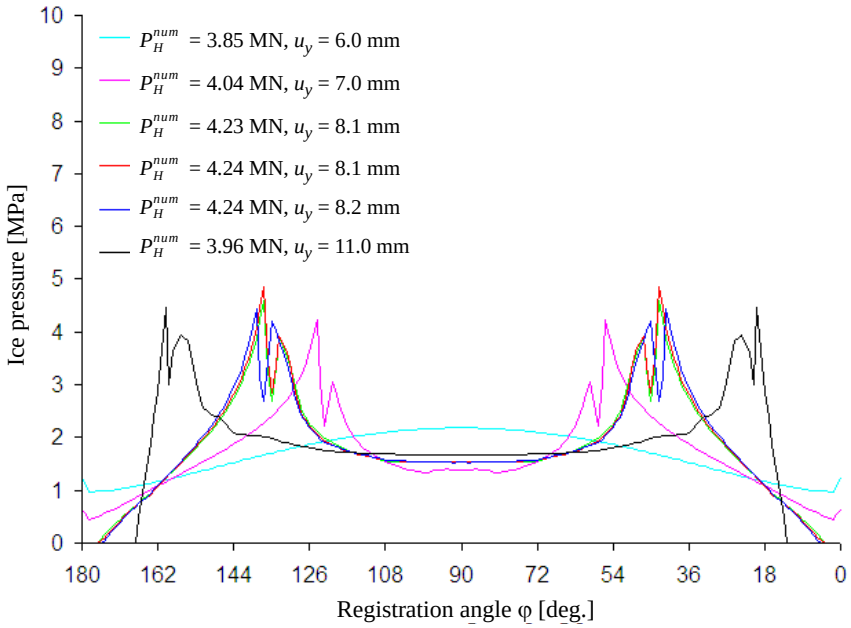

Figure 6.22 Calculated failure pattern and distribution of ice pressure obtained for the circular structure with μ = 0.0.

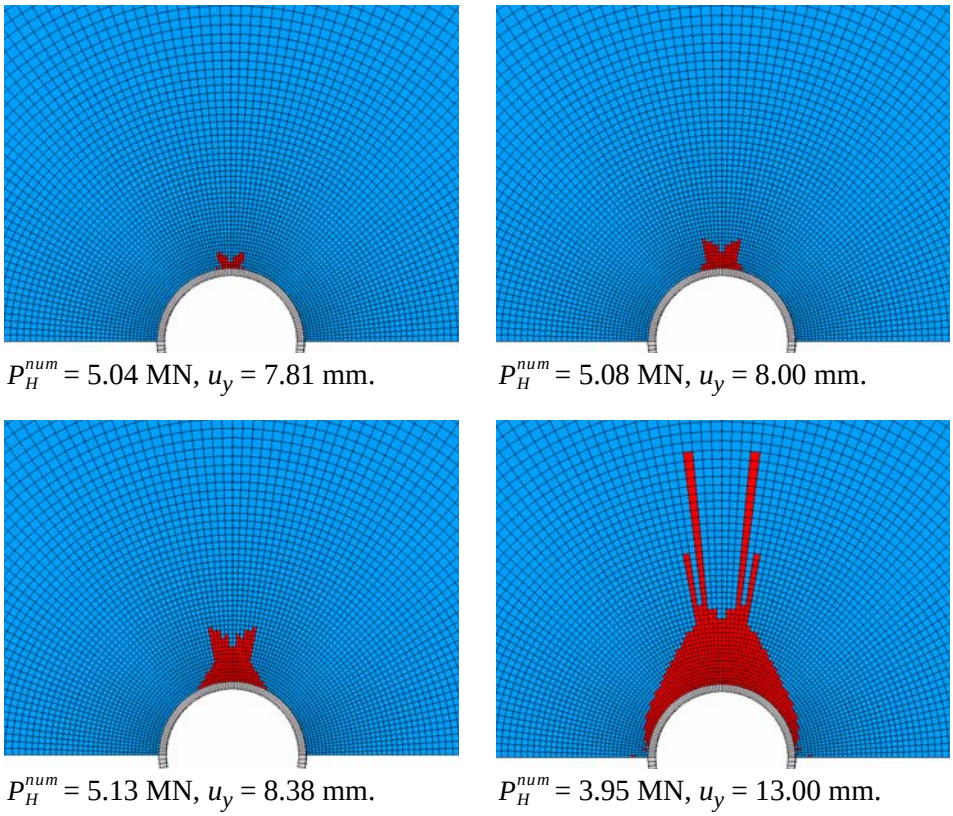

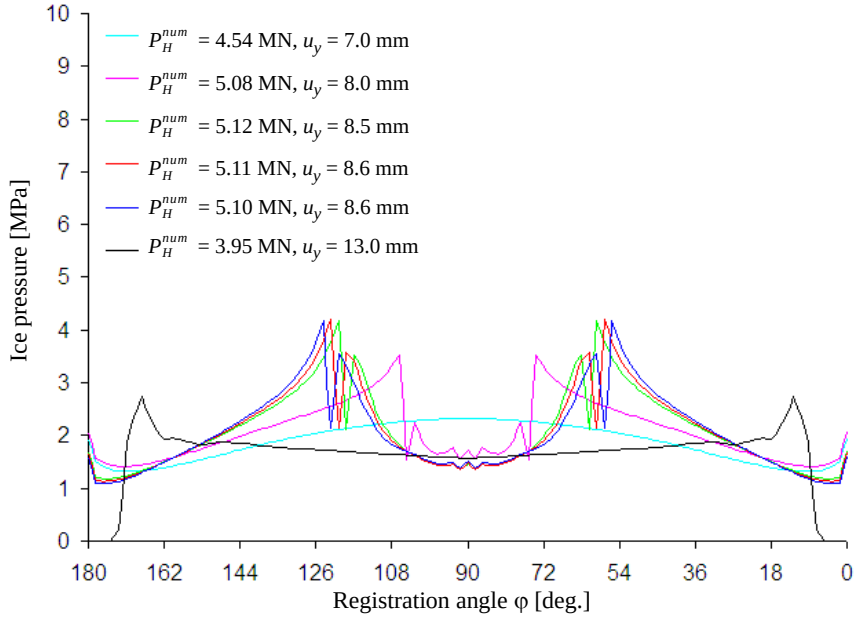

Figure 6.23 Calculated failure pattern and distribution of ice pressure obtained for the circular structure with μ = 0.1.

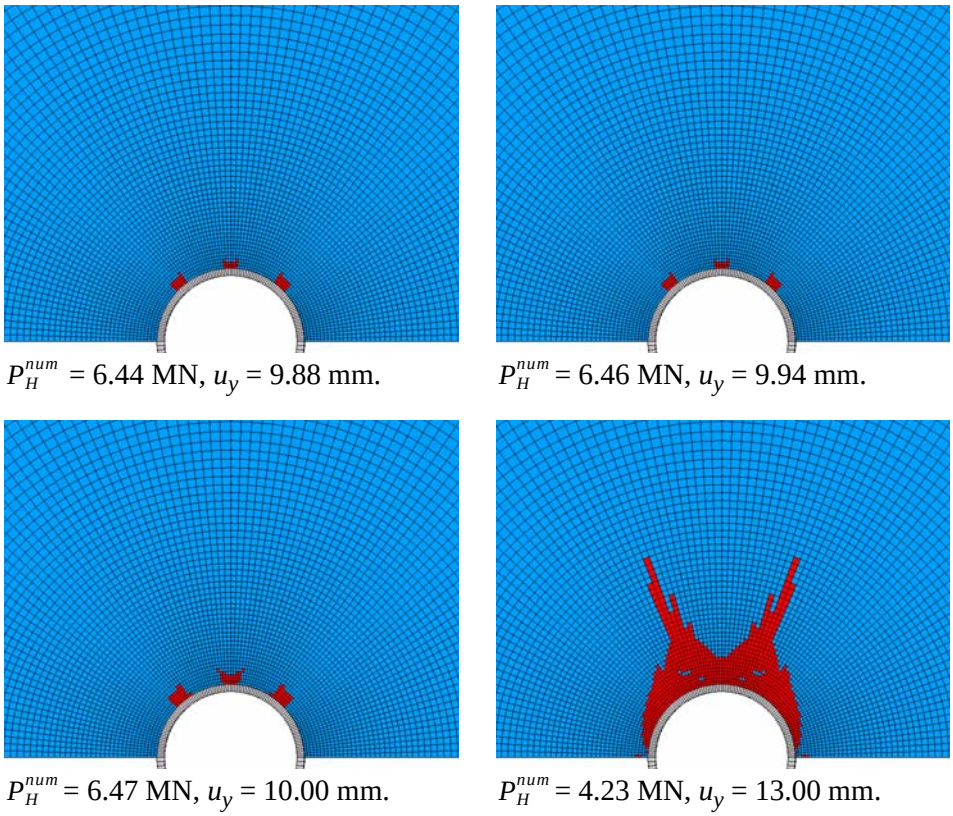

Figure 6.24 Calculated failure pattern and distribution of ice pressure obtained for the circular structure with μ = 0.2.

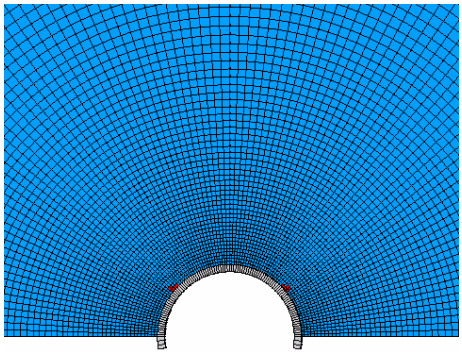

P_H^{num} = 7.66 MN, u_y = 11.63 mm.

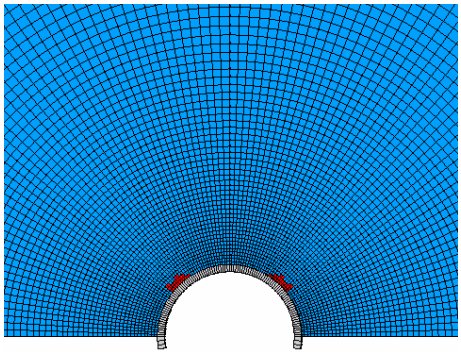

P_H^{num} = 7.68 MN, u_y = 11.68 mm.

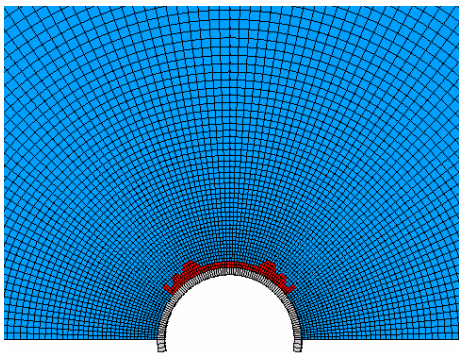

P_H^{num} = 7.67 MN, u_y = 11.75 mm.

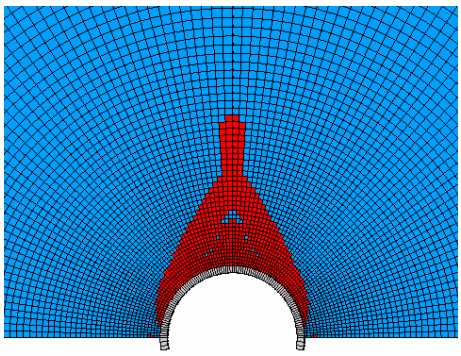

P_H^{num} = 5.26 MN, u_y = 13.00 mm.

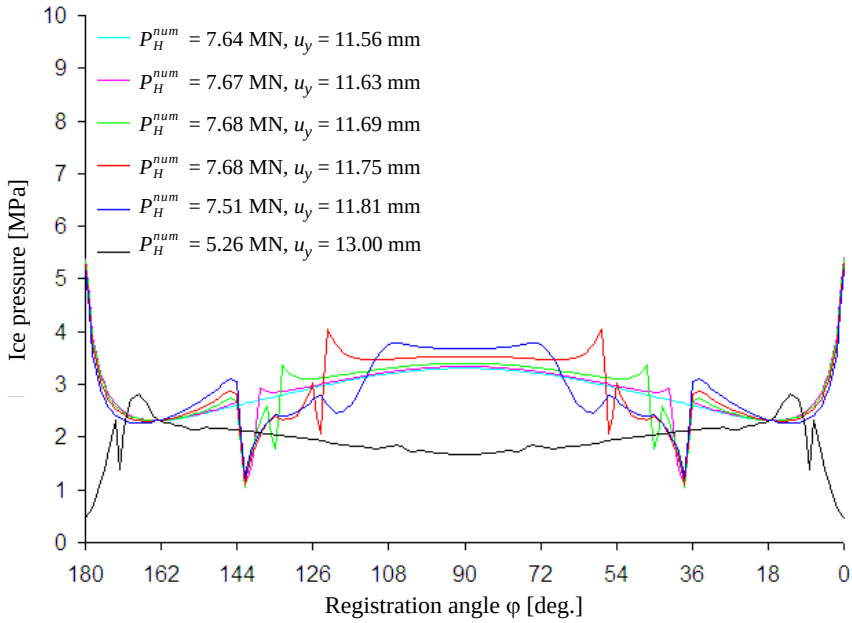

Figure 6.25 Calculated failure pattern and distribution of ice pressure obtained for the circular structure with μ = 0.3.

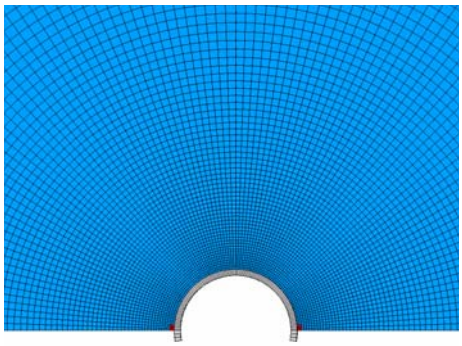

P_H^{num} = 6.81 MN, u_y = 10.25 mm.

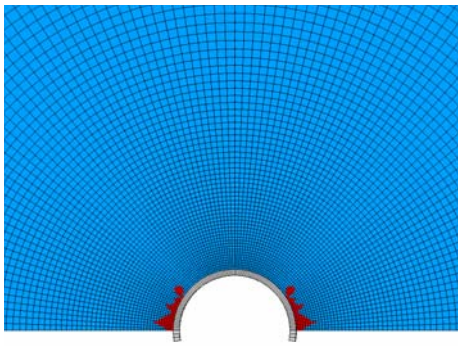

P_H^{num} = 7.31 MN, u_y = 11.50 mm.

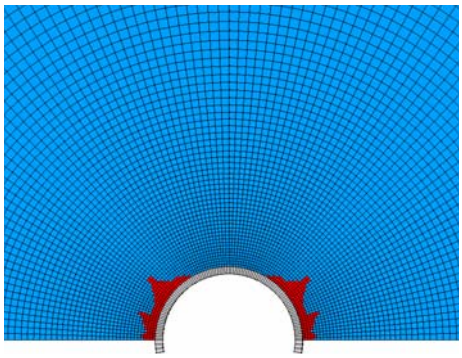

P_H^{num} = 7.43 MN, u_y = 11.94mm.

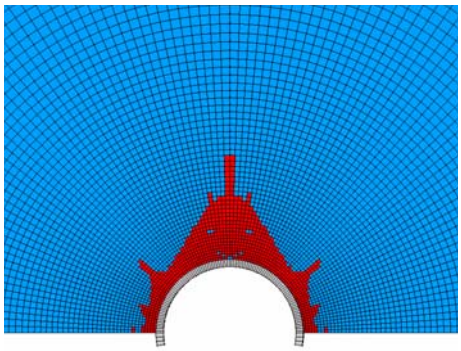

P_H^{num} = 5.65 MN, u_y = 15.00 mm.

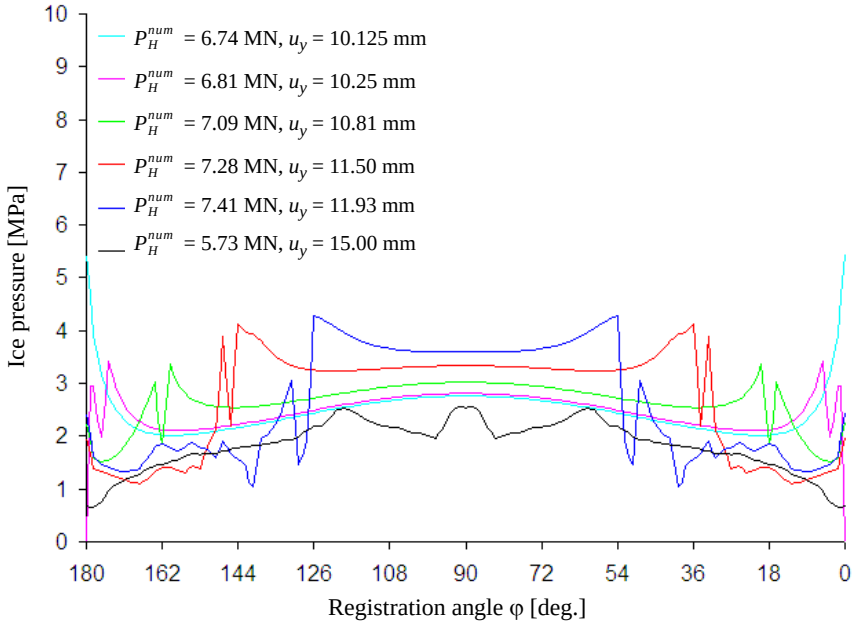

Figure 6.26 Calculated failure pattern and distribution of ice pressure obtained for the circular structure with μ = 0.4.

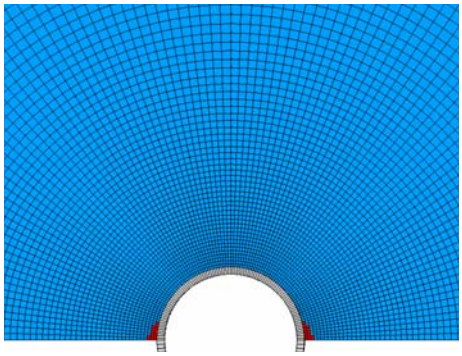

P_H^{num} = 6.68 MN, u_y = 10.00 mm.

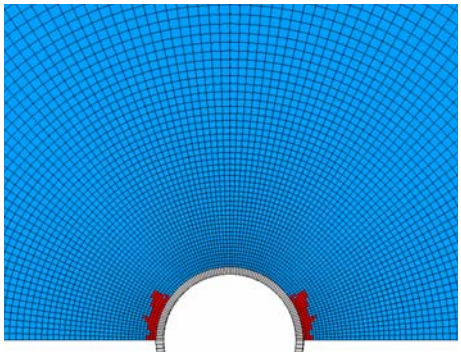

P_H^{num} = 7.34 MN, u_y = 11.00 mm.

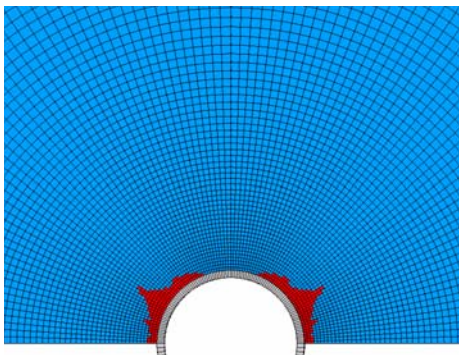

P_H^{num} = 7.87 MN, u_y = 13.00 mm.

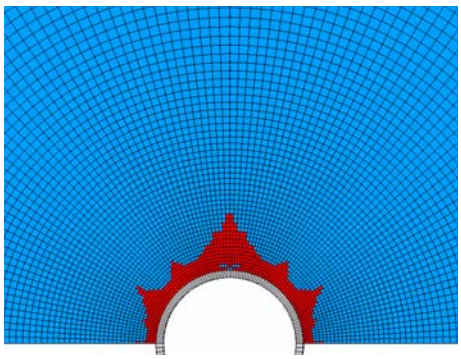

P_H^{num} = 5.90 MN, u_y = 15.00 mm.

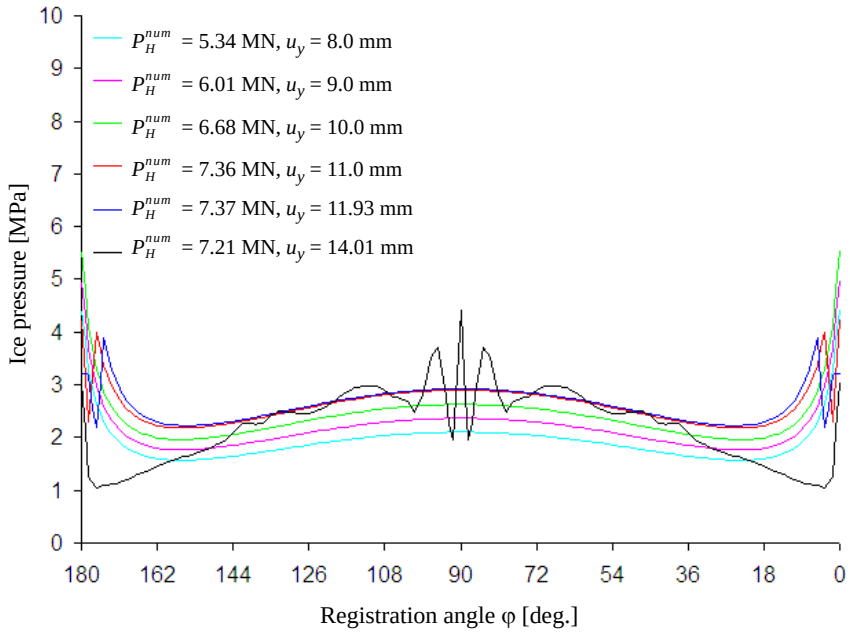

Figure 6.27 Calculated failure pattern and distribution of ice pressure obtained for the circular structure with μ = 0.5.

6.3.6 Comparison of simulated and measured ice pressure

Without further post-processing of the numerical results, it is difficult to make any well-built conclusions by comparing the ice pressure distribution obtained by simulations and the ice pressure measured on the lighthouse during the event 0303_022. One reason is the material parameters involved in Horrigmoe and Zeng's failure criterion, which are determined based on mechanical properties of laboratory grown ice as described in Section 3.4.1. The horizontal uniaxial compressive strength of the laboratory ice is equal to 3.6 MPa, while the lighthouse interacts with brackish sea ice in the northwestern Gulf of Bothnia with horizontal uniaxial compressive strength 1.2 MPa as average, see Table 6.4. Another reason is due to the low resolution of the measured ice pressure, i.e. each individual segment were covered by only one single load panel, except segment no. 4, which is divided into 8 load panels as shown in Figure 6.10.

For making meaningful comparisons some kind of normalization of the numerical and experimental results is introduced. The average ice pressure p_k^{num} acting on segment no. k ($k = 1, 2 \ldots 9$) obtained by finite element computations is calculated as

$$p_k^{num} = \frac{h_{ice}}{L_k} \sum_{i=1}^{n} p_i \left[\frac{(x_{i+1} - x_i)}{2} + \frac{(x_i - x_{i-1})}{2} \right] \tag{6.7}$$

where h_{ice} is the ice thickness, L_k is the length of the panel, x_{i-1}, x_i and x_{i+1} are the coordinates of the nodal points along the contact interface on each segment, and n is the total number of nodal points along the segment. Normalized value for the average ice pressure p_k^{norm} acting on segment no. k, is calculated as

$$p_k^{norm} = \frac{p_k^{num}}{h_{ice} C_x} \tag{6.8}$$

where ice thickness $h_{ice} = 260$ mm and horizontal uniaxial compressive strength ice $C_x = 3.62$ MPa. The calculated values for the averaged and normalized segment loads p_k^{norm} at maximum global load P_H^{num} are summarized in Table 6.7 for both the segmented and circular foundation and for magnitudes of friction between 0.0 and 0.5.

Figure 6.28 compares normalized ice pressure vs. position on the fundament for event 0303_020 and average ice pressure p_k^{norm} at maximum global load obtained by finite element computations for the segmented and circular structure. The load panels mounted on the foundation are made of coated steel. As described in section Section 2.3.8, static friction between ice and coated steel is between 0.07 and 0.18, while the dynamic friction is between 0.04 and 0.08. In this comparison, the magnitude of friction $\mu = 0.1$ is therefore chosen. The statistical properties, p_{mean}, p_{max}, $p_{\text{st.dev.}}$ and the pressure distribution $p(P_H^{max})$ at maximum global given in Table 6.5 is treated in similar manner, i.e, normalized by dividing the ice pressure by the average uniaxial compressive strength (equal to 1.2 MPa, see Table 6.4) and ice thickness 260 mm.

Table 6.7 Summary of average and normalized segment loads p_k^{norm} obtained by finite element computations at maximum global load P_H^{num}.

Segment no.	$\frac{p_k^{num}}{h_i C_x}$ μ = 0.0 [-]	$\frac{p_k^{num}}{h_i C_x}$ μ = 0.1 [-]	$\frac{p_k^{num}}{h_i C_x}$ μ = 0.2 [-]	$\frac{p_k^{num}}{h_i C_x}$ μ = 0.3 [-]	$\frac{p_k^{num}}{h_i C_x}$ μ = 0.4 [-]	$\frac{p_k^{num}}{h_i C_x}$ μ = 0.5 [-]
Segmented structure						
1	0.23	0.45	0.57	0.73	0.68	0.88
2	0.55	0.58	0.67	0.68	0.81	0.74
3	0.86	0.78	0.75	0.85	0.62	0.84
4	0.82	0.70	0.59	0.64	0.85	0.92
5	0.50	0.63	0.76	0.79	0.76	0.98
6	0.50	0.63	0.76	0.79	0.76	0.98
7	0.82	0.70	0.59	0.64	0.85	0.92
8	0.86	0.78	0.75	0.85	0.62	0.84
9	0.55	0.58	0.67	0.68	0.81	0.74
Circular structure						
1	0.13	0.38	0.67	0.83	0.48	0.86
2	0.58	0.57	0.68	0.82	0.54	0.69
3	1.00	0.87	0.61	0.70	0.64	0.75
4	0.55	0.86	0.95	0.90	1.20	0.83
5	0.47	0.48	0.92	1.13	1.10	0.88
6	0.47	0.48	0.92	1.13	1.10	0.88
7	0.55	0.86	0.95	0.90	1.20	0.83
8	1.00	0.87	0.61	0.70	0.64	0.75
9	0.58	0.57	0.68	0.82	0.54	0.69

The distribution of mean pressure p_{mean} was almost constant at all segments with some minor peaks at segments 1 and 8, and lower ice pressure occurs at segment 5 and 6. The pressure distribution at maximum global load $p(P_H^{max})$ for event 0303_022 and distribution of maximum pressure p_{max} are more dynamic compared to the distribution of mean pressure p_{mean}. The distributaion of maximum pressure p_{max} shows pressure peaks at segments 4 and 8, and lower pressure at segments 2 and 6. The pressure distributions at maximum global load $p(P_H^{max})$ shows higher pressure at segment 6 and 5 and lower pressure at centre for segment 5 and at each end, i.e. segments 1, 2 and 9. For all the pressure distributions compared in Figure 6.28, the lowest pressure occurred at segment 9; therefore segment 9 appeared to be at the end of the crushing zone.

Comparisons of the distribution averaged and normalized segment loads p_k^{norm} at maximum global load obtained by finite element computations for the segmented and circular foundations shows similar trends as the pressure distribution at

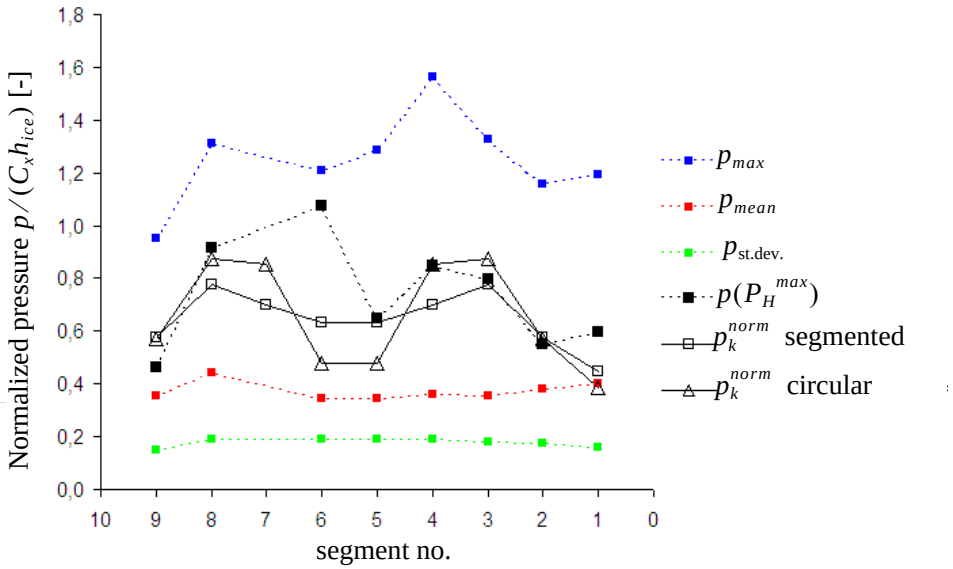

Figure 6.28 Spatial distribution of normalized pressure on segments.

maximum global load $p(P_H{}^{max})$. Pressure peaks for p_k^{norm} occurred at segments 3 and 7, while lower pressure occurred at the centre for segments 5 and 6, and at each end for segments 1 and 9. However, the finite element models do not capture the maximum pressure peak, which occurred for segment 6 as shown for the pressure distribution at maximum global load $p(P_H{}^{max})$.

The pressure distribution of averaged and normalized segment loads p_k^{norm} obtained for the circular structure is more dynamic compared to the pressure distribution on the segmented structure. The pressure peaks are higher at segments 3 and 7, while the pressure is lower at the centre for segments 5 and 6, and at the ends for segments 1 and 9.

6.3.7 Flat and wedge shaped structures

It is interesting to compare global ice forces acting on different structural shapes. Therefore a Quadratic structure is chosen and two different scenarios are considered as shown in Figure 6.29. In the first scenario, the ice sheet is pushed into contact with the flat side of the quadratic structure of width D equal to 8.0 m. In the second scenario, the quadratic structure is rotated 45 degrees and the ice movement is directly onto the corner of the structure. This scenario is therefore referred to as a wedge shaped structure. In this case, the effective contact width $D = 8\sqrt{2}$ m.

Finite element modelling of the flat and wedge shaped structures are carried out in the same manner as described in Section 6.3.2 for the segmented and circular structure. The finite element meshes of the flat and wedge shaped structure are shown in Figure 6.30. The ice sheet was considered as made of columnar ice and Horrigmoe and Zeng's criterion was employed to predict failure of the ice. The thickness of the plane ice sheet h = 0.26 m, with length $L = 40D$ and width $B = 80D$.

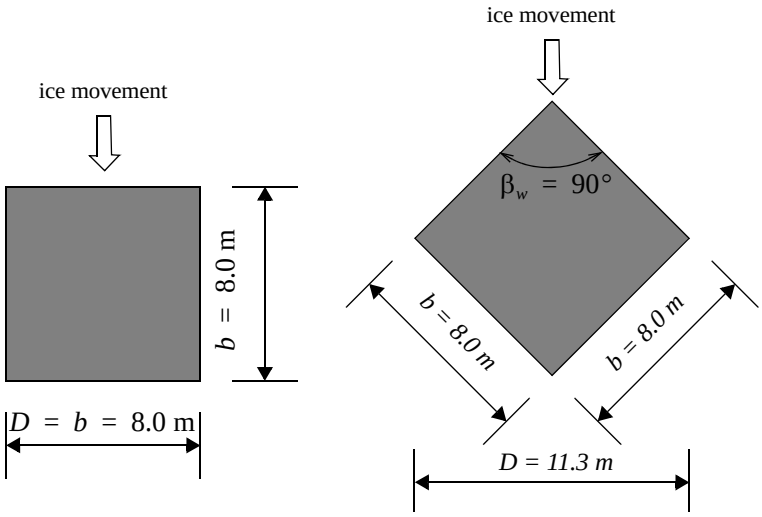

Figure 6.29 Geometry of quadratic structure. a) Quadratic (flat) structure. b) Wedge shaped structure.

The ice sheet was moved into contact with the structures by applying a uniformly distributed force in the y-direction along the edge ABC of the ice sheet. The remaining edges of the ice sheet were free. To avoid buckling of the ice sheet, the nodal degrees of freedom normal to the plane of the ice sheet (u_z) were fixed. The structures was modelled as fixed and rigid and the contact interaction forces is modelled with a contact formulation based and a Coulomb friction model and finite sliding as described in Section 5.2.

To examine the effect of magnitude of friction coefficient on the global ice forces and distribution of ice pressure acting on the structures, six different values was selected between $\mu = 0.0$ and $\mu = 0.5$. Figure 6.31 shows plots of global ice force versus the displacement u_y by finite element analysis of the flat and wedge shaped structures. The displacement u_y of the ice sheet is takene at point B in Figure 6.30. These diagrams also demonstrate the effect of magnitude of the ice-structure friction coefficient. The maximum global ice force P_H^{num}, corresponding effective pressure, $p_e = P_H^{num}/(hD)$, and normalized effective pressure p_e/C_x are summarized in Table 6.8. When calculating the contact factor k_b, the horizontal, uniaxial compressive strength of columnar ice $C_x = 3.62$ MPa is used, see Table 3.5.

For the flat structure, the global ice force increases in an almost linear manner until approximately 90% of the failure load is reached. As the structure is pushed further against the ice, the overall stiffness decreases due to failure of the ice and the maximum ice load is reached. As the flat structure is pushed even further against the ice, the global ice force decreases gradually due to ice failure and reaches a stable load level. In contradiction to the trend observed for the segmented and circular structure, the maximum global load for the flat structure decreases as the magnitude of friction increases. For $\mu = 0.5$, the global ice force decreases by 10% compared

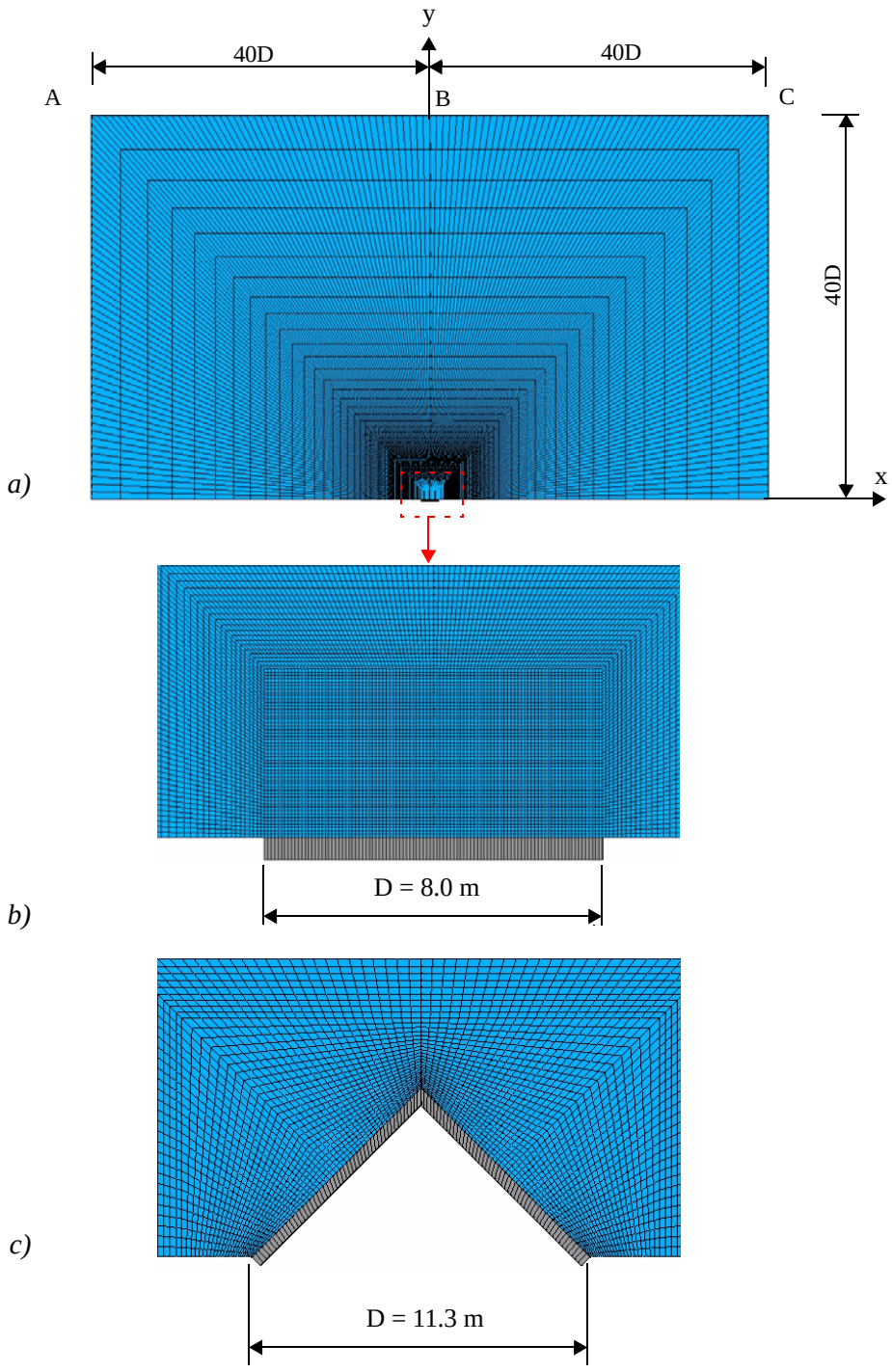

Figure 6.30 a) Finite element mesh of the ice sheet and structure. b) Flat structure. c) Wedge shaped structure.

to my $\mu = 0.0$. The indentation pressure is between 4.10 MPa for $\mu = 0.1$ and decreases to and 3.72 for $\mu = 0.5$, i.e., from 13% to 2% larger than the uniaxial compressive strength of the columnar ice ($C_x = 3.62$ MPa)

.

Table 6.8 Maximum global ice forces, indentation pressure and normalized effective pressure obtained by finite element analysis of ice sheet interacting with a flat or wedge shaped structure.

Coefficient of friction μ [-]	Maximum global force P_H^{num} [MN]	Displacement at point B (u_y) [mm]	Effective pressure p_e [MPa]	Normalized effective pressure p_e / C_x [-]
flat structure				
0.0	8.52	16.3	4.10	1.13
0.1	8.17	15.1	3.93	1.08
0.2	8.04	16.8	3.86	1.07
0.3	7.83	14.5	3.76	1.04
0.4	7.70	15.1	3.70	1.02
0.5	7.72	14.6	3.71	1.02
Wedge shaped structure				
0.0	5.36	11.0	1.82	0.50
0.1	6.34	13.3	2.16	0.60
0.2	6.80	13.0	2.31	0.64
0.3	7.24	13.8	2.46	0.68
0.4	7.26	13.5	2.47	0.68
0.5	7.32	13.5	2.49	0.69

The wedge shaped structure shows similar trends in the global load-displacement behavior as obtained for the segmented and circular structure, but first failure occurs at the tip of the wedge at approximately 10% of the failure load, which is quite low compared to what is obtained for the other studied structures. This effect is due to a singularity in the stress field in the ice near the tip of the wedge shaped structure. For lower magnitudes of friction, the global load-displacement shows a softening behavior until maximum load is reached. As the magnitude of friction increases, the global load - deflection behavior becomes more linear until maximum failure load. Thereafter, the load decreases gradually due to ice failure and reaches a stable load level. For the wedge shaped structure, both the maximum global load and indentation pressure increases to approach a constant value when the friction is higher than 0.3. The indentation pressure is always lower than the uniaxial compressive strength of the columnar ice and increases from 2.6 MPa ($\mu = 0.0$) to 3.5 MPa ($\mu \geq 0.3$).

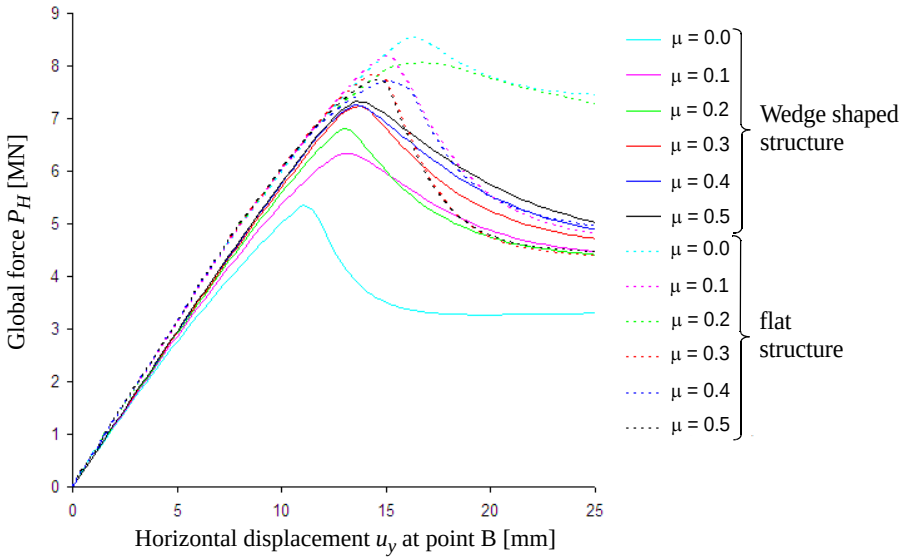

Figure 6.31 Global ice force vs. displacement obtained by finite element simulations of an ice sheet interacting with a flat and wedge shaped structure.

6.3.8 Failure pattern and ice pressure for flat and wedge shaped structures

Development of ice failure pattern and ice pressure is demonstrated in Figure 6.32 for the flat structure. In this case the friction coefficient $\mu = 0.1$ and similar failure pattern and distribution of ice pressure is obtained for the other magnitudes of friction. In the elastic state, (lowest load level in Figure x), maximum ice pressure occurs at each end of the structure for $x = 0$ and $x = 8.0$ m, and shows a convex ice pressure distribution between the pressure peaks. At approximately 60% of the maximum load, shear failure starts to form near the corners of the structure due to large shear stresses in these regions. Formation of shear failure leads to reduced ice pressure and at the same time, the ice pressure increases in front of the structure. As the load increases, the shear failure developed towards the centre of the structure and forms arc shaped failure zones at each side of the structure and high pressure zones forms at the edge of the failure zone. As the flat structure is pushed even further against the ice, ice crushing starts to form in front of the structure and the localization of the high-pressure zones moves as the region of ice failure expands from each side towards the centre of the structure. At maximum load, crushing has occurred along the entire ice-structure contact interface, except for small regions near the corners of the structure. As structure penetrates into the ice sheet, the stiffness is partially lost as ice crushing occurs along the entire ice-structure interface, which is characterized by the softening branch as shown in the global force-displacement curves show in Figure 6.31.

Figure 6.33 demonstrates the development of failure pattern and ice pressure distribution for the wedge shaped structure. In the elastic state, maximum pressure occurs at the tip of the wedge shaped structure ($x = 4.0$ m) and decreases rapidly

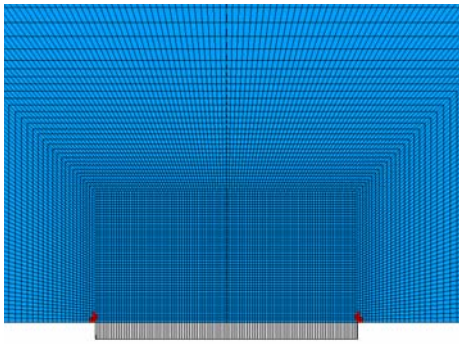

P_H^{num} = 4.96 MN, u_y = 8.00 mm.

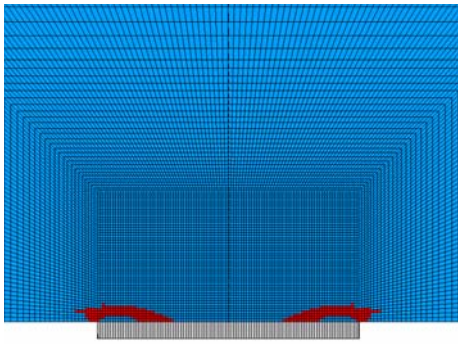

P_H^{num} = 5.87 MN, u_y = 9.75 mm.

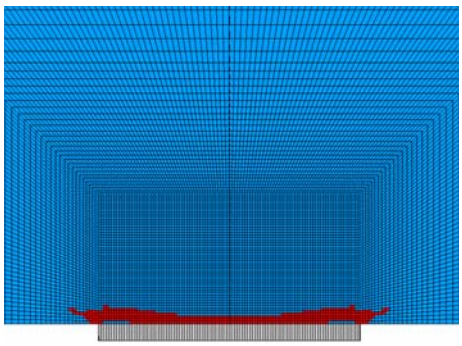

P_H^{num} = 8.17 MN, u_y = 15.10 mm.

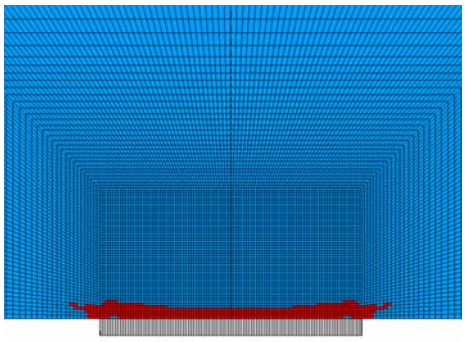

P_H^{num} = 5.87 MN, u_y = 19.00 mm.

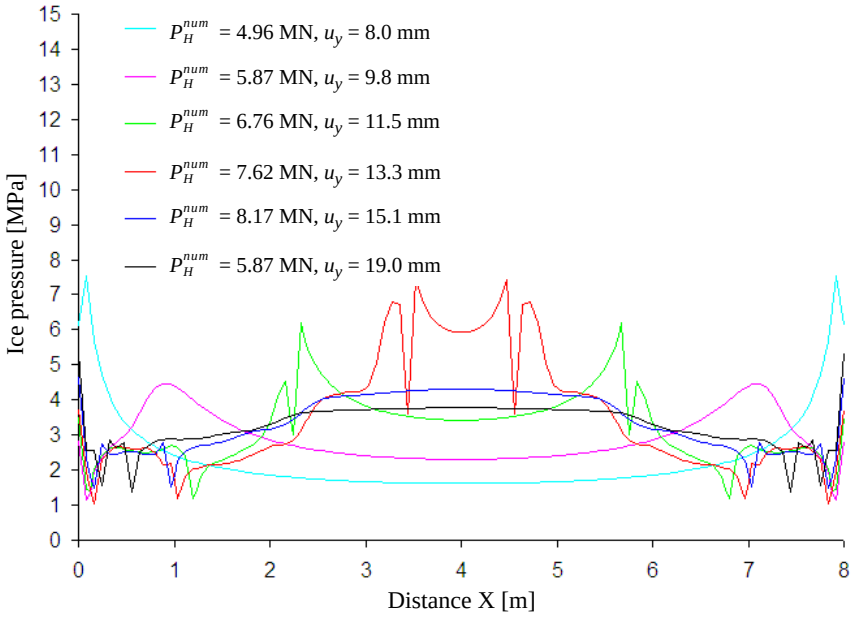

Figure 6.32 Calculated failure pattern and distribution of ice pressure obtained for the flat structure with μ = 0.1.

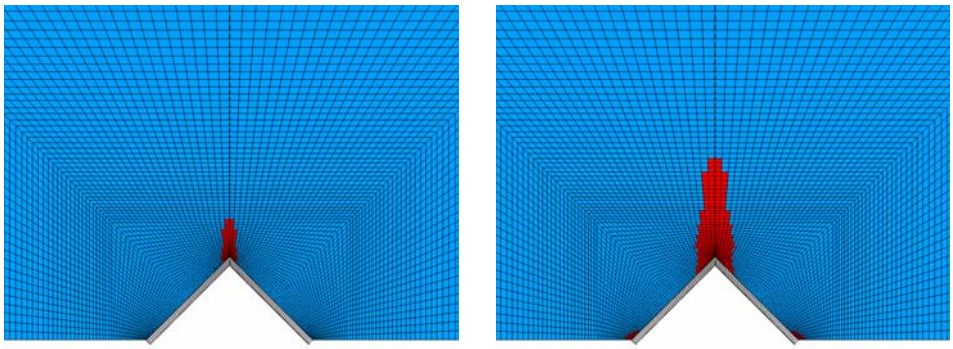

P_H^{num} = 2.73 MN, u_y = 4.8 mm. P_H^{num} = 4.92 MN, u_y = 9.0 mm.

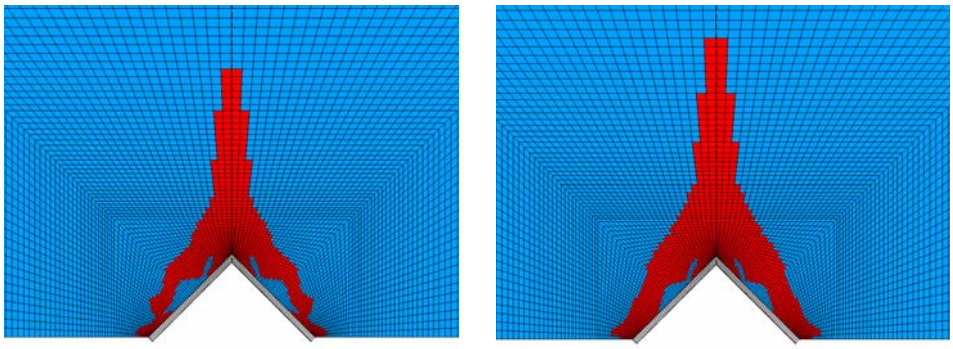

P_H^{num} = 6.34 MN, u_y = 13.3 mm P_H^{num} = 5.97 MN, u_y = 15.0 mm

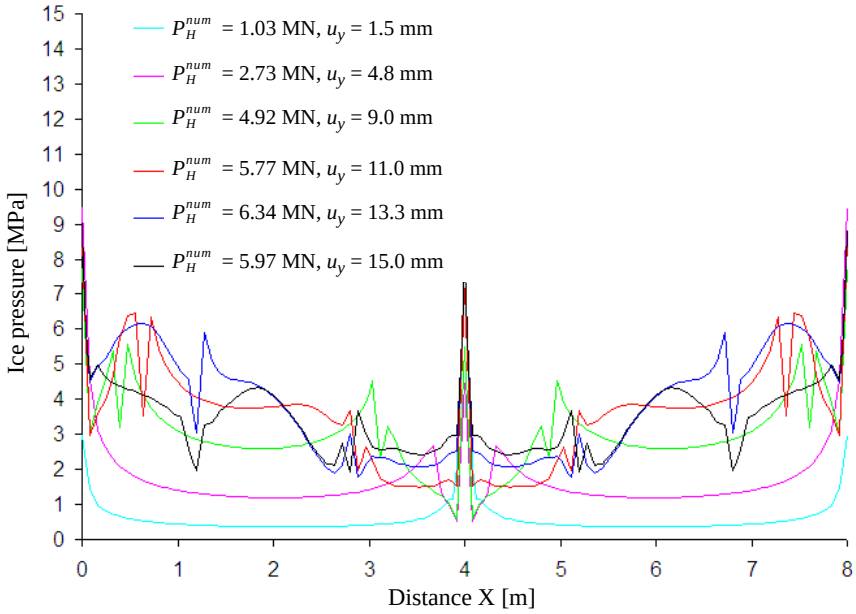

Figure 6.33 Calculated failure pattern and distribution of ice pressure obtained for the wedge shaped structure with μ = 0.1.

and reaches a local minimum pressure at each side of the tip of wedge at $x = 3.9$ m and $x = 4.1$ m. Due to stress concentration at the tip of the wedge, initiation of failure occurs at a very low load level, i.e. 10% of the maximum global load. As the load increases, the ice pressure increases all over the contact surface and maximum ice pressure at this load level occurs at $x = 0.0$ m and $x = 8.0$ m, which in turn leads to ice failure at the corners of the structure. As the global ice force increases to maximum, ice failure developed further and forms an arc-shaped failure zone at each side of the structure. At the same time, the localization of high-pressure zones moves with the edge of ice failure zone. Final failure occurs as the structure penetrates deeper into the ice and the stiffness of the ice sheet is partially lost due to propagation of a centre crack in front of the wedge, which is characterized by the softening behavior and the global force reaches a stable load level as shown in Figure 6.31.

6.3.9 Comparison of effective pressure on structures of different shapes

As described earlier, the material parameters involved in Horrigmoe and Zeng's failure criterion are determined based on mechanical properties of laboratory ice with horizontal uniaxial compressive strength $C_x = 3.62$ MPa, while the lighthouse interacts with brackish sea ice in the northwestern Gulf of Bothnia with horizontal uniaxial compressive strength 1.2 MPa as average, see Table 6.4.

The normalized effective pressure $p_e/C_x = P_H^{num}/(hDC_x)$ obtained by finite element simulations for different structural shapes are plotted vs. the ice-structure friction μ in Figure 6.34. In general, the normalized ice pressure increases as the magnitude of friction increases, except for the flat structure, where the maximum force decreases by 10% as the magnitude of friction μ increases from 0.0 to 0.5. For the highest magnitude of friction, the normalized effective pressure converge towards the same value for the flat, segmented and circular structures (within 3% difference), while for the wedge shaped structure, the effective pressure is 33% less than predicted for the other structural shapes.

For the segmented structure, the normalized effective pressure increases approximately linearly as the magnitude of friction increases, and the maximum load increases by 73% as the magnitude of friction μ increases from 0.0 to 0.5.

As described in section Section 6.3.5, three different kinds of primary failure modes where identified for the circular structure: crushing ($\mu \leq 0.1$), radial cracking ($0.2 \leq \mu \leq 0.3$), and shear failure $\mu \geq 0.4$. The transition between radial cracking and shear failure has considerable influence on the normalized effective pressure predicted for the cylindrical structure. The normalized effective pressure increases approximately linearly as the magnitude of friction increases from 0.0 to 0.3 (increases by 80%). But, the predicted global load is almost constant as the magnitude of friction is higher than 0.3 (increases by 4% as magnitude of friction increases from 0.3 to 0.5), i.e. transition between radial cracking and shear failure.

A similar trend in the normalized pressure is obtained for the wedge shaped

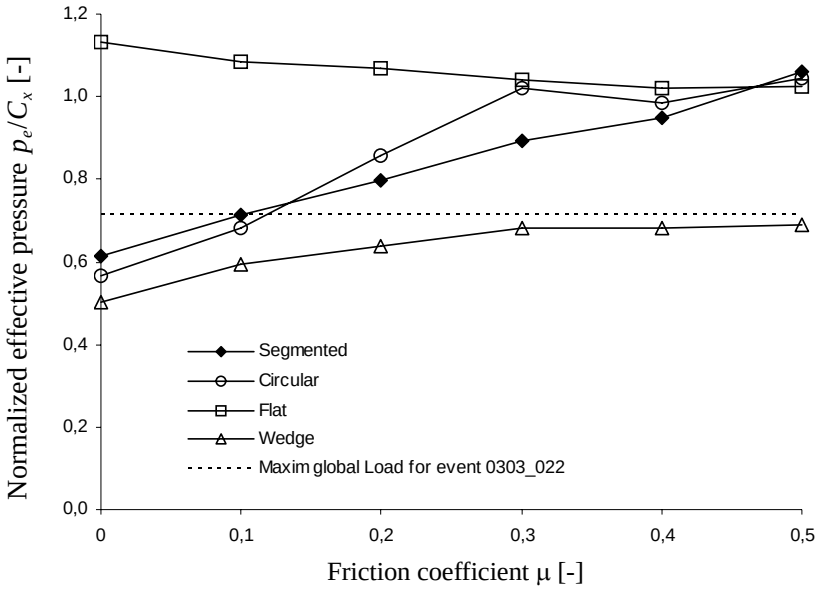

Figure 6.34 Normalized effective pressure vs. ice - structure friction coefficient.

structure. The normalized effective pressure increases by 35% as the magnitude of friction increases from 0.0 to 0.3. As the friction increases above 0.3, the effective pressure is almost constant, increases by 2% as the magnitude of friction increases from 0.3 to 0.5.

The normalized effective pressure calculated for event 0303_020, given in Table 6.5, is plotted as a horizontal dotted line in Figure 6.34. The load panels on the lighthouse is made of coated steel, therefore, the magnitude of friction $\mu = 0.1$ is chosen in this comparison. For friction coefficient $\mu = 0.1$ the discrepancy between the normalized effective pressure for event 0303_020 and value predicted for the segmented structure is less than 0.04%, while the difference in normalized effective pressure for the circular structure is 4%.

In Figure 6.35, the shape factor m for different structural shapes are plotted vs. the ice-structure friction coefficient. The shape factor m is the ratio between the global force on a structure with arbitrary shape and a flat structure. It is seen from Figure 6.35 that the coefficient of friction has a great influence on the shape factor and in general, the shape factor m increases as the magnitude of friction increases.

As described in section Section 2.3.8, static friction between ice and coated steel is between 0.07 and 0.18, while the dynamic friction is between 0.04 and 0.08. The load panels on the lighthouse is made of coated steel, therefore, the magnitude of friction $\mu = 0.1$ is chosen in this comparison. For $\mu = 0.1$, the numerical simulations resulted in the following shape factors: $m = 0.63$ for the segmented structure, $m = 0.60$ for circular and $m = 0.52$ for the wedge shaped structure. The

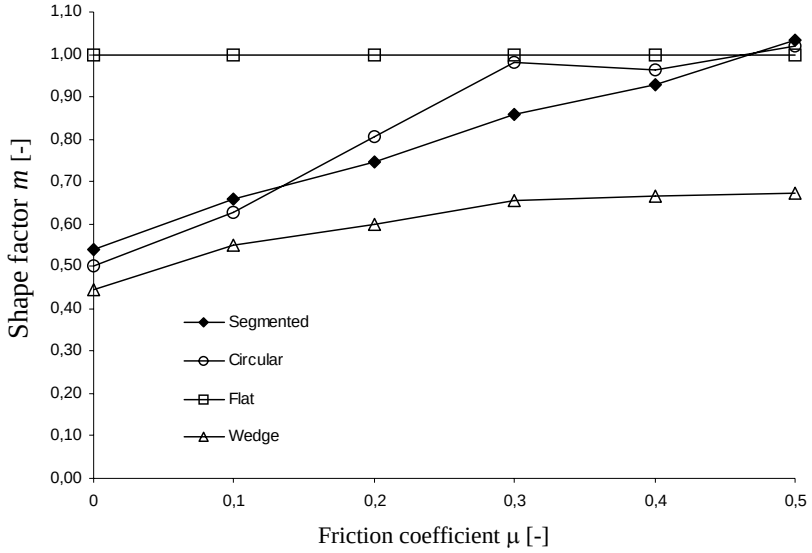

Figure 6.35 Shape factor m vs. ice - structure friction coefficient for different structural shapes.

shape factor obtained for the circular structure can be compared with several experimental results that have been obtained on narrow structures in the past. Hirayama et al. [87] obtained a shape factor of $m = 0.77$ for narrow models in laboratory conditions. Saeki et al. [88, 89] made tests using freshwater ice of the Saroma Lagoon in Hokkaido. They obtained a shape factor of $m = 0.74$, whereas Afanasiev [90] has obtained a value of $m = 0.9$ for a circular structure, while for the segmented structure the shape factor is dependent on the wedge opening angle angle β_w as shown in Figure 6.29. For wedge angle $\beta_w = 90°$, Afanasiev [90] proposed a shape factor $m = 0.69$.

It is interesting to compare the effective ice pressure obtained by finite element analysis of ice forces acting on structures of different shapes with corresponding values of effective pressure calculated based on empirical formulas. The following assumptions are made: ice velocity is 0.2 m/s, continuos crushing, plane strain and the uniaxial compressive strength $f_c = 1.0$ MPa. Values for the indention coefficient I, contact factor k and shape factor m are taken as given in Table 4.1. Values for the normalized effective pressure p_e/C_x are summarized in Table 6.9.It is observed from Table 6.9 that Korzhavin's formula [64] results in the highest values for the normalized effective pressure p_e/C_x, which are 3.3 times higher than the lowest values predicted by using Eq. (4.3) and with Ralston's [53] parameters for granular ice.

Michel and Toussaint's formula [65], given by Eq. (4.4), resulted in 26% higher values compared to Eq. (4.3) with Ralston's [53] parameters for granular ice, while the Ralston's [53] parameters for columnar ice is 2.15 times higher values for the normalized effective pressure.

Table 6.9 Normalized effective pressure calculated for empirical formulas.

Author	Indent. cough. I	Cont. fact. k	Normalized effective pressure p_e/C_x [-]		
			Flat $m = 1.0$	Circular $m = 0.9$	Wedge $m = 0.69$
Korzhavin [64], Eq. (4.2)	2.5	0.4	1.71	1.54	1.18
Michel and Toussaint [65], Eq. (4.4)	3.0	0.3	0.65	0.59	0.45
Ralston [53] Granular ice, Eq. (4.3)	1.15	0.45	0.52	0.47	0.36
Ralston [53], Columnar ice, Eq. (4.3)	3.13	0.45	1.41	1.27	0.97

By comparing the normalized effective pressure given in Table 6.9 and corresponding values obtained by finite element simulations for different structural shapes, as shown in Figure 6.34, it is observed that the normalized effective pressure obtained by finite element for the flat structure is 1.13 for $\mu = 0.0$ and decreases to 1.02 for $\mu = 0.5$, which is lower than predicted using Eq. (4.3) with Ralton's parameters for columnar ice, but higher than Michel and Toussaint's formula, given by Eq. (4.4).

For the wedge shaped structure, the finite element analysis resulted in normalized effective pressure in the range of 0.50 ($\mu = 0.0$) to 0.69 $\mu = 0.5$, which for the lowest magnitude of friction is closer to Michel and Toussaint's formula, given by Eq. (4.4). For the highest magnitude of friction, the numerical result is approximately in the middle of the values predicted by Michel and Toussaint's formula and Eq. (4.3) with Ralston's [53] parameters for columnar ice.

For the segmented and circular structure, the normalized effective pressure obtained by finite element analysis is in the lower range for $\mu = 0.0$. For the circular structure the normalized pressure $p_e/C_x = 0.57$, while for the segmented structure $p_e/C_x = 0.61$ and are very close to $p_e/C_x = 0.59$, which is predicted by using Michel and Toussaint's formula. The normalized effective pressure increases as the magnitude of friction increases. For $\mu = 0.5$, $p_e/C_x = 1.06$ and $p_e/C_x = 1.04$ for the segmented and circular structure, respectively, which still are lower than $p_e/C_x = 1.27$ predicted by using Eq. (4.3) with Ralton's parameters for columnar ice.

Mätning av islaster med isbrytare

Lennart Fransson, Lars Åström,

Mats Petersson, Håkan Thun

Forskningsrapport

Mätning av islaster med isbrytare

Lennart Fransson, Håkan Thun, Lars Åström, Mats Petersson

Luleå University of Technology
Department for Civil & Environmental Engineering
Division of Structural Engineering

Förord

Följande rapport ingår i projektet ”Ismekanikk og havnedrift i islagte farvann” (delprogrammet Nordkalotten INTERREG III A Nord).

I denna rapport beskrivs hur provningsutrustning som används för att mäta isens krafter på en konstruktion tillverkades och monterades på en isgående bogserbåt. Rapporten innehåller också resultat och diskussion av de mätningar som utfördes på Bottenvikens islagda vatten under vintern 2007/08.

Luleå i juni 2008

Lennart Fransson och Håkan Thun

Innehållsförteckning

1 Introduktion

I denna rapport beskrivs bakgrunden till hur provningsutrustning (provrigg) för att mäta iskrafter tillverkades och senare monterades på Luleå Bogserbåts AB:s bogserbåt Viscaria.

Provningarna har utförts under mars och april 2008 och själva provriggen tillverkades av Verkstads AB Eric Erlandsson i Luleå.

Den personal från Luleå tekniska universitet (LTU) som deltagit i projektet är Henrik Andrén, Claes Fahleson, Lennart Fransson, Mats Petersson, Håkan Thun och Lars Åström. Fartygschefer på bogserbåten Viscaria under provningstillfällena har varit Mikael Rönnbäck, Robert Karlsson och Staffan Bramberg, alla vid Luleå Bogserbåts AB.

I bilaga A finns tillverkningsritningarna till provriggen.

2 Utformning av provningsutrustning

När ett stort isflak passerar och pressar mot t.ex. en fyr uppstår stora krafter. För att enklare kunna simulera detta fall med islast mot en konstruktion med cirkulärt tvärsnitt, användes idén med att göra ”tvärtom”. Istället för att isflaket skulle driva omkring mha av vindriktning och så småningom nå fyren och dess lastceller, så kunde man istället ”flytta på fyren”. Detta skulle vara möjligt om man skalade ner fyren med avseende på dimensionen genom att montera en rörkonstruktion i fören på en lämplig båt och sedan köra genom isen.

I de konstruktioner som diskuterades i början av projektet, var en önskad funktion att provningsriggen skulle kunna fällas upp så att den inte var i kontakt med isen under färden ut till testplatsen. Denna idé resulterade dock i en mycket komplicerad och otymplig konstruktion. För att undvika detta togs beslutet att provningsutrustningen skulle vara fast monterad under hela provningstillfället, dvs. från kaj till testplats (men möjligheten att enkelt kunna bygga om de så att den skulle kunna fällas upp skulle behållas).

Principen för hela provningsarrangemanget byggde på att ett mothåll (här kallad ”kölpuck”) skulle svetsas fast på bogserbåtens köl, mot vilken sedan en 50 tons lastcell skulle trycka. Denna tryckraft skulle överföras via ett horisontell rör från det vertikala rör med ytterdiametern 300mm (längd 6,5 m) som trycktes mot isen när isbrytaren körde framåt.

Efter diskussioner och beräkningar bestämdes det att konstruktion som visas i Figur 1 skulle vara en lämplig kompromiss mellan styrka och hanterlighet. De röda ytorna i Figur 1 representerar isbrytarens skrov. Det horisontella röda strecket till vänster i Figur 1 symboliserar ungerfärlig isnivå.

Vid dimensionering av provriggen var utgångspunkten lastcellens kapacitet på 50 ton. I ekvationen ingick även tanken att om lasterna skulle bli för stora, skulle provriggen – dvs. bultinfästningen – gå sönder före isbrytarens reling.

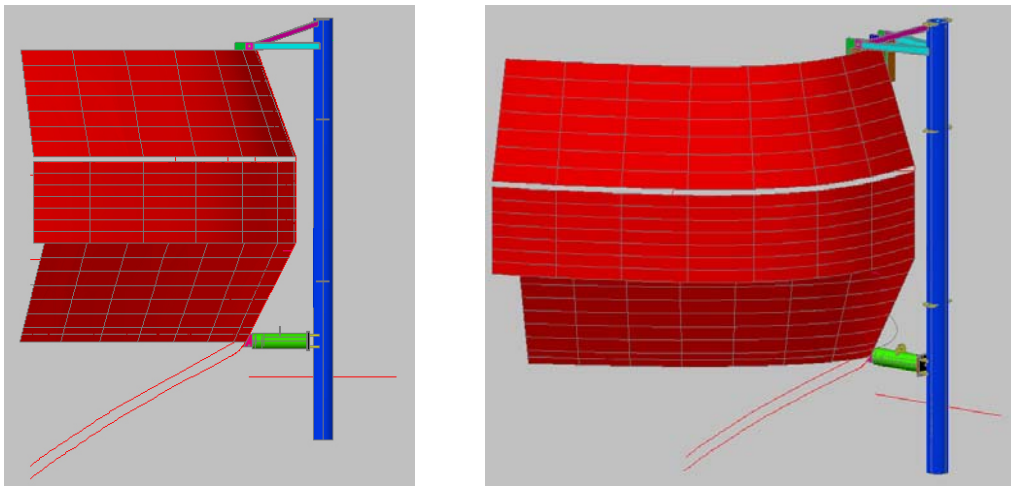

Figur 1 3D-ritning av provningsrigg.

Huvudprincipen för montaget av provriggen var att den skulle lyftas på plats innan varje försökstillfälle och sedan lyftas av när man mätt klart. Själva tillvägagångssättet var att man först skulle hänga den på relingen, sedan montera bultar för att avsluta med att ”vika in den” mot kölpucken så att kontakt uppstod.

Överdelen utformades på så sätt att provriggen skulle fästas i isbrytaren mha två ”öron” av plattstål som skulle svetsas fast i relingens spant. Själva provriggen skulle i sin tur fästas i dessa två öron mha av M30-bultar som skulle göra det möjligt att enkelt montera provriggen genom att ta bort/sätta dit dessa (möjligheten att ”hissa” upp röret behölls också i och med att dessa ”gångjärn” skapades). I Figur 2 visas överdelen av provriggen. De gröna delarna är ”öronen” som svetsades fast och dessa två plattstål satt därmed kvar på isbrytaren även när inte försök gjordes.

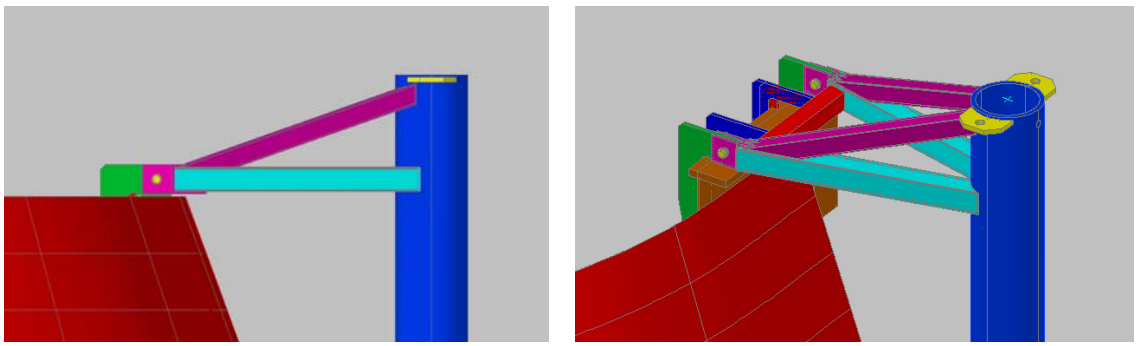

Figur 2 3D-ritningar som visar provriggens överdel.

I Figur 3b visas lastcellen – orange del närmast kölpucken – och övriga delar som möjliggör att tryckkraften överförs från det vertikala röret (kölpucken är den rosa delen till vänster i Figur 3).

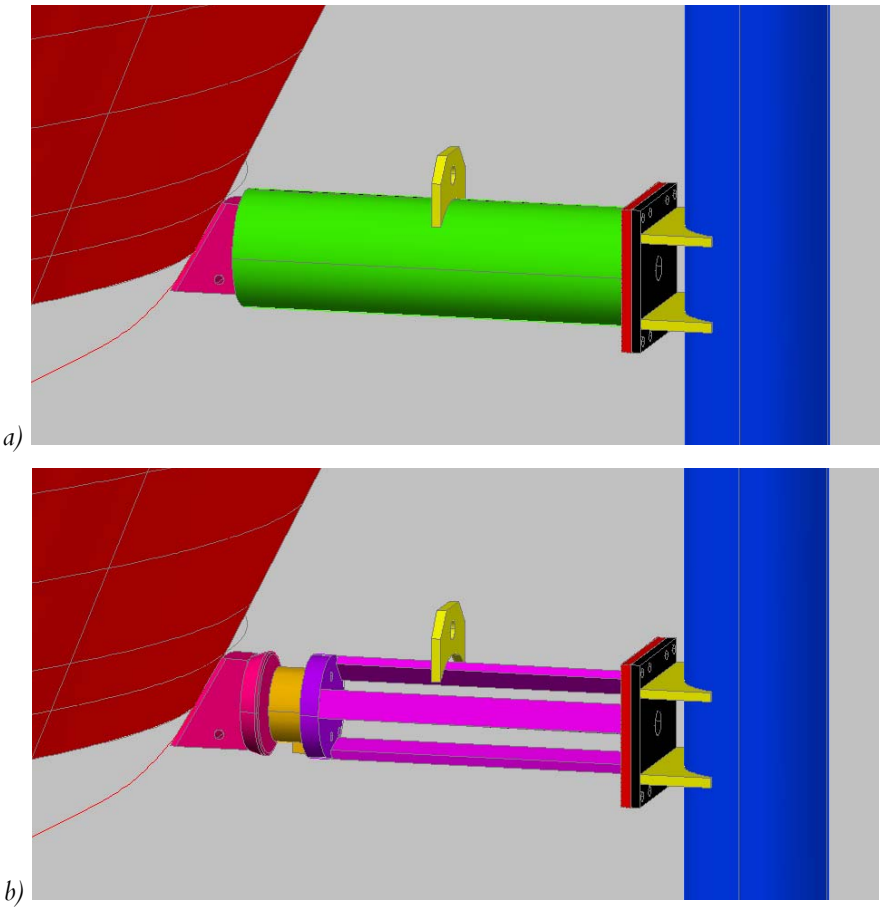

Figur 3 3D-ritningar som visar provriggens underdel.

Eftersom provriggens underdel endast vilade mot kölpucken spändes den mha vantskruvar och kättingar (vars ena ände var fastsatt i isbrytarens ankare och den andra i det vertikala röret) mot kölpucken så att kontakt mellan kölpuck och lastcell uppstod.

Trådtöjningsgivare monterades i höjd med det horisontella röret för att mäta töjningarna i det vertikala stålröret.

Datainsamlingen under försöken har skett med en Spider8 och Catman datorprogram tillverkade av HBM.

3 Montering

Nedan följer ett antal fotografier som visar monteringen av provriggen på bogserbåten och hur det såg ut när försök utfördes.

Figur 4 Fotografi som visar mothållet (”kölpuck”) för lastcellen som svetsats fast på bogserbåtens köl.

Figur 5 Fotografi som visar montage av provrigg. Första gången användes en lastbil för att montera provriggen pga. dess bättre manöverbarhet jämfört med traktor. Vid senare tillfällen användes en traktor. Bogserbåt: Viscaria.

Figur 6 Fotografi som visar när provningsriggen “hänger på relingen” och M30-bultarna monteras.

Figur 7 Fotografi som visar när provningsriggen "hänger på relingen" och montaget av den undre, horisontella, delen skall påbörjas.

Figur 8 Fotografi som visar när montaget/svetsningen av den undre delen är färdigställd.

Figur 9 Fotografi som visar när kättingarna spänns mha vantskruvar för att skapa anliggning mellan "kölpuck" och lastcell. Personer på bild: Mats Petersson till vänster och Lennart Fransson till höger.

Figur 10 Fotografi som visar när kättingarna har spänts. En kätting på vardera sida om röret. Dessa kättingar är fästa i bogserbåtens ankare i ena änden och i röret i den andra.

Figur 11 Fotografi som visar när ett försök skall påbörjas

Figur 12 Fotografi som visar en närbild på hur isen krossas mot det vertikala röret när bogserbåten kör genom isen.

Figur 13 Fotografi som visar en översiktsbild på hur provningsriggen är monterad på bogserbåten.

4 Resultat och diskussion

4.1 Uppmätta islaster

4.1.1 Försöksprogram

Försöksutrustningen var klar att tas i bruk i mitten av mars och försöken pågick tillslutet av april då isen börjat smälta. Totalt genomfördes 28 kontrollerade tester med registrering av islaster. Testerna kan delas upp i tre kategorier:

- kollisioner med uppbruten is
- kontinuerlig krossning i fast is
- oscillerande last för tjock is

Kollisionerna med uppbruten is skedde i rännan där isblocken var av varierande storlek och tidigare hade brutits upp med isbrytare och andra fartyg. Kollisionshastighet varierade mellan 1 och 8 knop.

Krossningen i den fasta isen utfördes i ett stort isområde utanför Klubbviken där istjockleken var 20-30 cm. Isens egenskaper undersöktes stickprovsmässigt genom analyser i LTU:s laboratorium. Isens termomekaniska egenskaper och fysikaliska egenskaper redovisas i en separat del, kapitel 5.

Vid krossning av tjock is förekom hastigt oscillerande islast vilket orsakade överlast av försöksutrustningen. Extremt höga lasttryck uppkom också vid igångsättning av iskrossningen men lastnivån var då något lägre. Dessa lastfall anser vi vara mycket viktiga och resultatet av dessa tester diskuteras i slutet av detta kapitel.

Islastens beroende av istjocklek h, iskvalitet σ och framdrivnings-hastighet v, studerades primärt. Röret som kan ses som en nedskalad modell av ett cirkulärt fundament hade en konstant geometri, styvhet och dämpning i samtliga test. Istjockleken mättes i borrade hål längs penetreringsvägen och med hjälp av en markradarutrustning som anpassats med en GHz antenn för att få bra upplösning på tunn is, se kapitel 6. Iskvaliteten antas vara bestämd av den horisontella tryckhållfastheten (bestämd vid hastig belastning) vilket i sin tur är en funktion av den relativa saltlake-volymen och defekter orsakade av smältningen. Framdrivningshastigheten mättes endast med gps, men kan vid behov bestämmas mer noggrant med hjälp av videoinspelningar

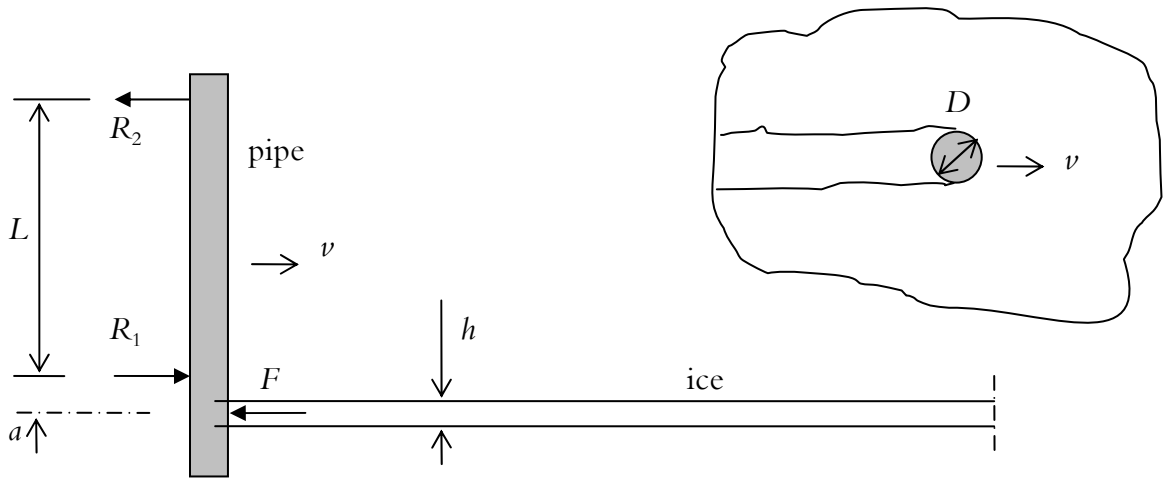

Figur 14 Principle of the ice load measurement. The reaction force R_1 was registered with a load cell and the ice load F was calculated from $F = R_1L/(L+a)$.

4.1.2 Kalibrering

Islasten F mättes indirekt via reaktionskraften R_1 från sambandet

$$F = R_1 \frac{L}{L+a}, \qquad (1)$$

där L = 4.54 m och a är definierade i figur 14. Avståndet a påverkar alltså förhållandet mellan verklig islast och uppmätt reaktionskraft och eftersom a kunde variera under försökets gång mättes även momentet i röret vid stödet 1. Töjningsgivare placerades utanpå röret på den dragna sidan för att även kunna övervaka påkänningarna i stålröret. Avståndet a som funktion av tiden t ges av

$$a(t) = M(t)/F(t) \qquad (2)$$

där vi antar att momentet vid stödet M är proportionellt mot den uppmätta töjningen och att kraften R_1 registreras vid samma tidpunkt. Under antagande om linjärt elastisk deformation och enkel balkteori fås sambandet mellan töjning och moment ur $\sigma = E\varepsilon$ och $\sigma = \frac{M}{W}$, där tvärsnittskonstanten W är böjmotståndet för ett cirkulärt rör. Om spänningen sätts lika får vi ett teoretiskt värde på momentet

$$M(t) = WE \cdot \varepsilon(t) \qquad (3)$$

där ε(t) är den registrerade töjningen. Ekvationerna (1) och (3) insatta i (2) ger det tillämpade uttrycket för att bestämma variationen hos avståndet a enligt

$$a(t) = \frac{WE\varepsilon(t)}{R_1(t) - WE\varepsilon(t)} L \qquad (4)$$

Utrustningen kalibrerades under antagandet att istryckets resultant angriper h/2 från isytan varför konstanterna *WE* kunde ersättas med ett kalibrerat värde. Avståndet mellan stöden uppmättes till 4.54 m. En sådan kalibrering gjordes vid Test 5 då istjockleken varierade mellan 0.2 och 0.4 meter och även fartygets hastighet varierade. För att vara säker på att töjning och reaktionslast har uppkommit vid samma tidpunkt gjordes en resampling av rådata från 400 till 1 Hz. Den kalibrerade islasten jämfört med uppmätt reaktionslast visas i Figur 15, där även lastens beräknade avstånd från stödet *a*(t) har plottats.

Vid mycket dynamiska lastförhållanden varierade *a* med ± 0.2 m vilket motsvarade istjockleken. Det fanns också en långvågig variation som förmodligen berodde på isbrytarens vertikala rörelse då isen bröts. Men i stort påverkas inte lastförhållandena mellan reaktionskraft och islast i någon högre grad eftersom *a* är litet i förhållande till *L*. Med medelvärdet a = 0.5 m blir F = 0.9 R_1. Töjningsgivarna skadades vid flera tillfällen under försöksseriens gång och vi har därför genomgående valt att redovisa reaktionskraften. Man ska dock vara uppmärksam på att vissa egenfrekvenser som möjligen indikeras vid senare analyser kan bero på isbrytarens eller angreppspunktens vertikala rörelse.

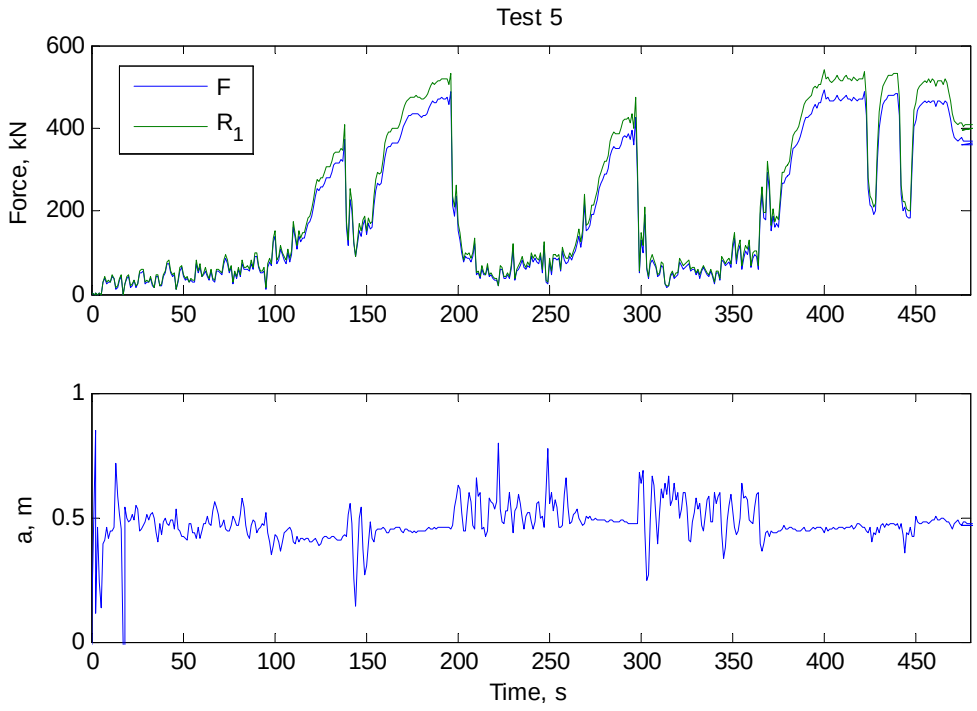

Figur 15 Ice load compared with the registered reaction force (a). Variation of the centre of ice force (b).

4.1.3 Sammanställning

I tabellen nedan finns en summering av alla test med röret i Bottenviken under vintern 2008. I de flesta fall har lasten registrerats med en samplingshastighet på 400 Hz. Reaktionskraften R_1 som funktion av tiden och ett histogram som visar fördelningskurvan finns som diagram i Bilaga C.

Table 4.1 Summary of test with the 300 mm pipe in front of Viscaria, 2008

No.	Date	Time	Max Load	Speed	Ice thickness	Comments
	yymmdd	hh:mm:ss	kN	knt.	cm	
1	080319	15:28:05	67	5		broken ice
2	080319	15:55:58	276	<1	18-25	
3	080319	17:52:31	61			broken ice
4	080319	18:08:23	218			broken ice
5	080325	13:02:27	649	<1	25-38	
6	080325	13:02:37				
7	080325	14:02:22	463	8		broken ice
8	080325	14:43:30	523	1	25	
9	080329	09:00:38	384			broken ice
10	080329	09:41:33	323			broken ice
11	080329	10:10:36	322	0.5-1.5	25	
12	080329	15:08:43	166	0.5-0.8	25	
13	080329	15:27:15	209	1.2-1.4	25	
14	080329	15:41:01	266	2.2-2.5	25	
15	080329	15:55:17	459			
16	080329	15:58:18	537	0-4	25-35	
17	080329	16:30:53	541			
18	080410	09:34:12	336			broken ice
19	080410	11:12:35	283	0.5-1	25	
20	080410	11:26:06	277	1-1.5	25	
21	080410	11:38:25	269	1.8-2	25	
22	080410	13:20:50	845	<1	40-45	overloading
23	080425	09:47:59	77	0.7	20	melting
24	080425	10:02:53	140	1.2	20	melting
25	080425	10:16:56	347	2	20	melting
26	080425	10:30:05	191	8	20	melting
27	080425	09:28:44	135			broken ice
28	080425	11:41:59	768	<1	40-45	melting

4.1.4 Kollision med uppbruten is

Resultaten har delats in i tre likartade grupper (bruten is, fast is, oscillerande last) där främst isens egenskaper över tid varierar. Lasten från flytande isblock antas variera med isens massa, form och kollisionshastighet. Här är det naturligtvis helt avgörande om rännan har brutits omedelbart före försöket eller om det översta skiktet täcks av fast is. Fördelningen av de höga kollisionslasterna har typiskt en jämnt nedåtgående del som verkar vara exponentiell, se fig 16.

Figur 17 visar detaljerna på maxlasten i en annan tidsskala. Överensstämmelsen med splines är utmärkt utom vid maxpunkten där mätningen trots den relativt höga samplingshastigheten förmodligen underskattar den verkliga maxlasten. Varaktigheten av en kollision är här ca en tiondels sekund. Frekvensen av den oscillerande lasten under själva krossningen är sannolikt kopplat till rörets egensvängning.

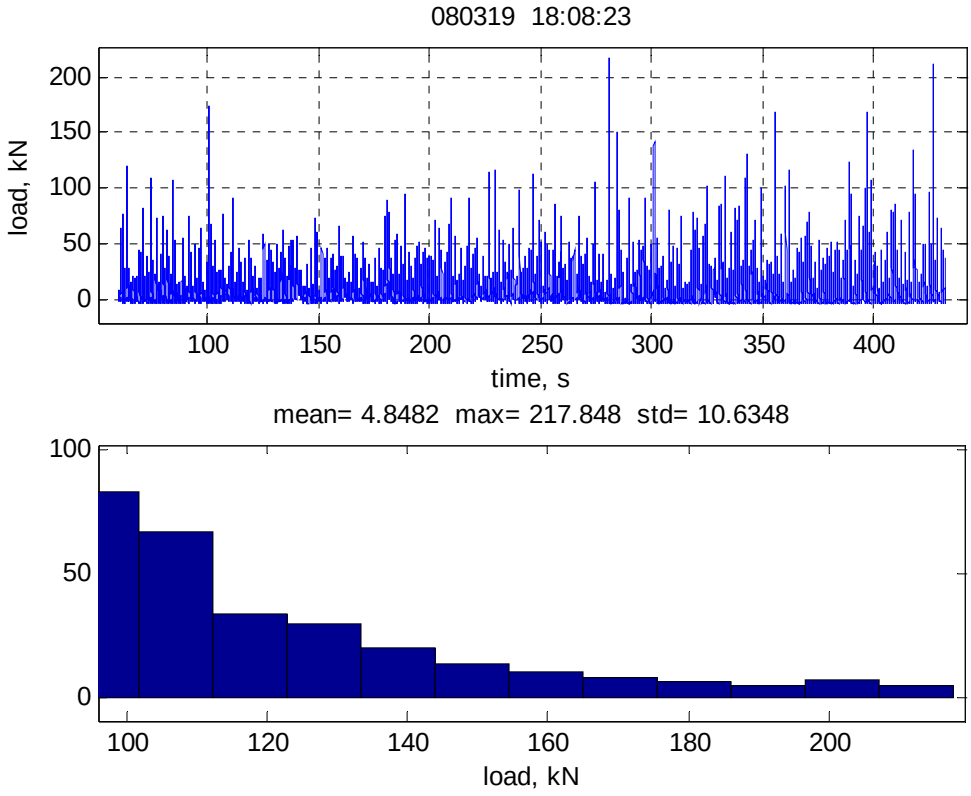

Figur 16 Typical load and probability at collisions with broken ice in the track during 7 minutes. Only loads above 100 kN are shown in the histogram.

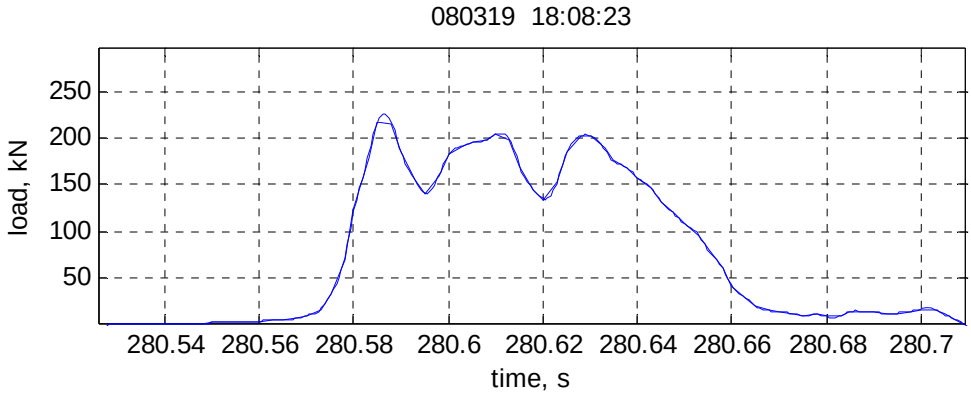

Figur 17 Max load at time t = 280.6 s when the pipe collides with an ice block. The figure includes two lines, measured values and fitted spline functions.

4.1.5 Kontinuerlig krossning i fast is

Islastens beroende av istjocklek

Att mäta istjocklek med precision över en stor yta är en svår uppgift. I strömmande vatten bildas en vågformig underyta på isen och isflak som tillsammans bildar en fast is påverkar istjockleken i högsta grad. Därtill kommer variationer i snödjup vilket påverkar istillväxten/smältningen och istemperaturen. Vanligen förekommer det ett system med råkar och breda igenfrusna sprickor som också antas påverka islastens storlek vid kontinuerlig krossning. I våra tester mättes istjockleken stickprovsmässigt längs en linje med ca 10 metes mellanrum och med markradar. I test 5 mättes isen i flera parallella linjer som indata till en tre-dimensionell numerisk modell (surfer) av isen, se fig 18.

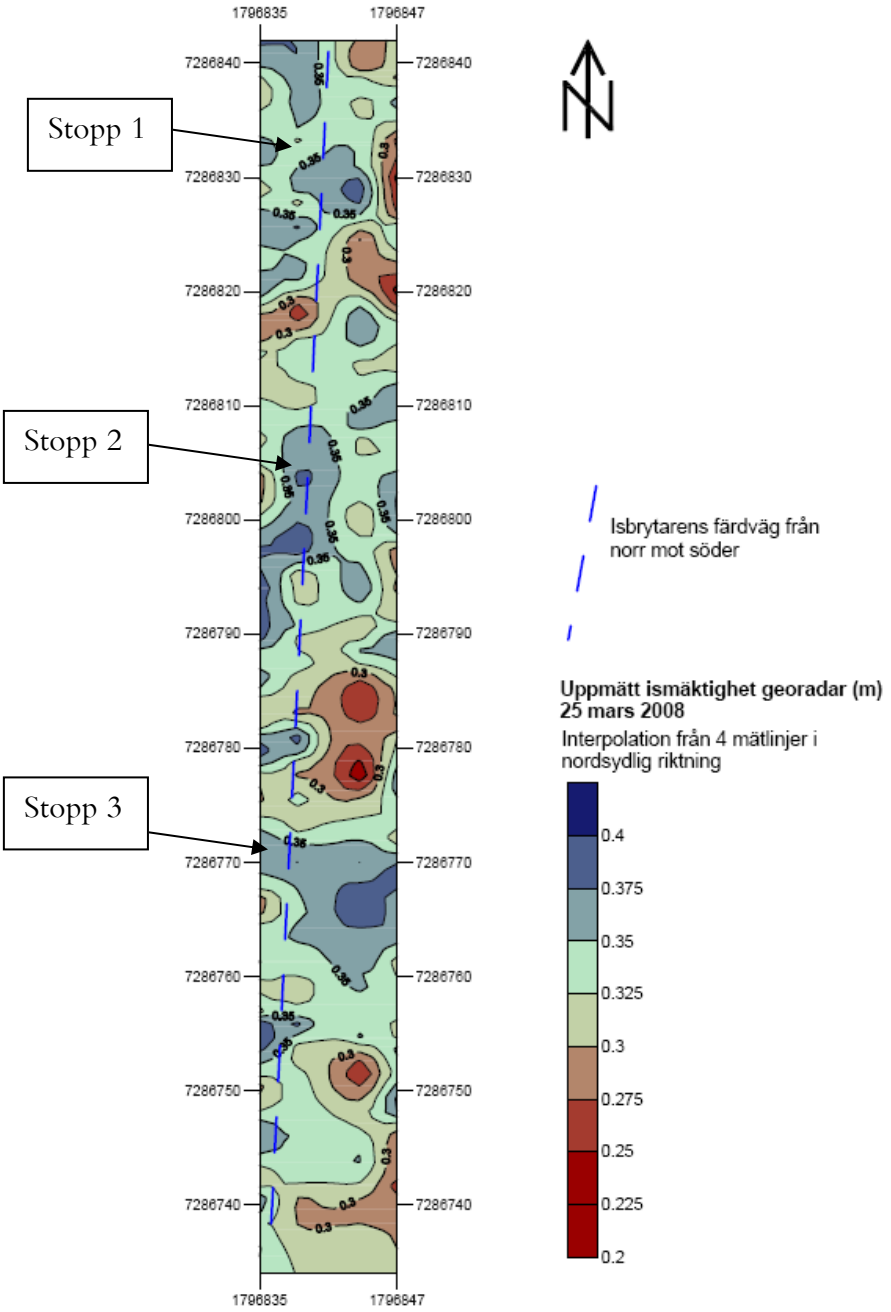

Figur 18 Istjocklekens variation i Test 5.

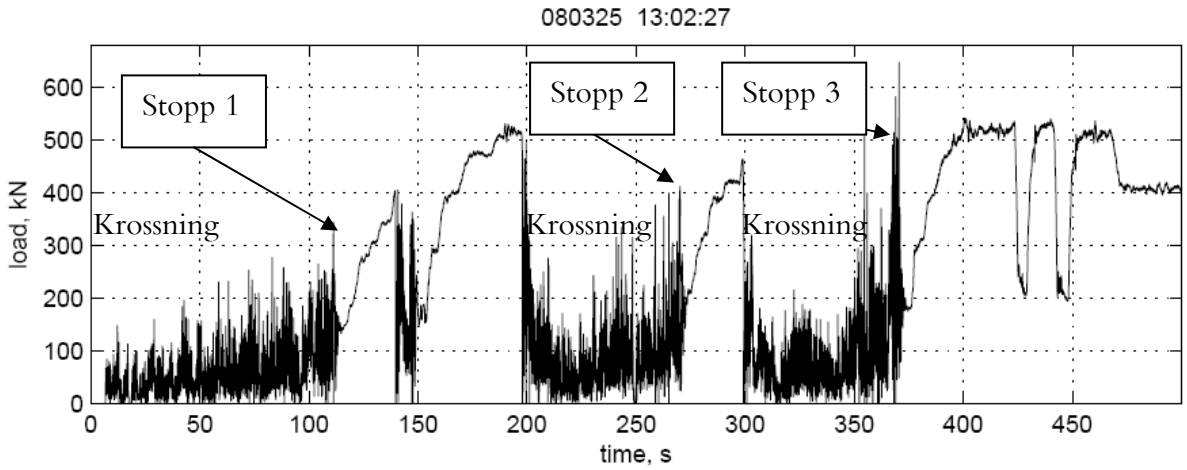

Figur 19 Load variation in Test 5. The icebraker stopped at three occations due to insufficient driving force.

I detta försök, fig 19, var det svårt att korrelera islasten F med istjockleken h eftersom isbrytaren inte kunde hålla en jämn hastighet. Resultatet antyder ändå att stoppen inträffade där isen var som tjockast. Det effektiva p_e istrycket brukar definieras ur

$$p_e = F / Dh \qquad (5)$$

I detta fallet var trycket som högst 4-8 MPa beroende på vilken istjocklek man väljer. Det lägre värdet fås om man antar att maxlasten uppkom där istjockleken var störst. Men vi ser också att islasten varierar inom vida gränser och att den statiska lasten efter varje stopp är betydligt högre än den dynamiska lasten vid krossning.

Åtta tester utfördes med isradarn fastsatt ca 5 m framför det isbrytande röret (Test 12-16 och Test 19-21). Istjockleken och islasten har normerats så att ett värde mellan noll och ett visas i figurerna 7 och 8. Isdjupet som funktion av tillryggalagd sträcka har också plottats i figurerna 20 och 21. Hastigheten varierade mellan 0.5 och 1 knop och den plottade sträckan är något godtyckligt vald att representera en medelhastighet på 0.68 knop eller 0.35 m/s. Figurerna visar att stora istjockleksminskningar (förmodligen igenfrusna sprickor) ger en tydlig minskning av islasten, i övrigt är korrelationen svag. För att minska dynamiken i de uppmätta lasterna visas medelvärdet under varje 0.5 sekunders mätning.

Sammanfattningsvis tyder resultaten på att det krävs relativt stora ytor med jämn istjocklek för att man ska kunna spåra förändringar i islasten. Variationerna mätt längs en linje är inte kritisk för islasten eftersom hållfasthet, inhomogenitet och inspänningsförhållanden och diverse andra faktorer maskerar eventuell korrelation.

För att få en uppfattning om hur maxlasten varierade med istjockleken har samtliga försök med iskrossning i fast is plottats i figur 22. Genomgående antas maxlasten vara korrelerad till den största istjockleken (Tabell 1) i de fall den inte har mätts med georadar. Två värden för 8-10 cm is i Test 19 har också plottats.

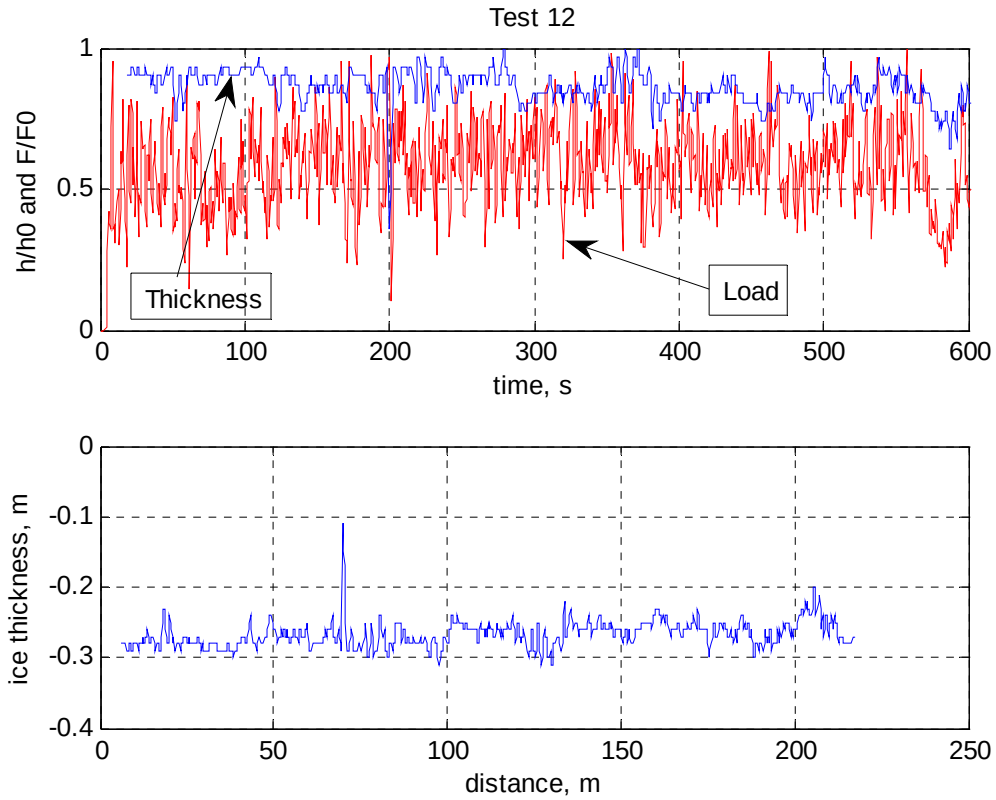

Figur 20 Comparison of load (average on 0.5 sec) and ice thickness in Test 12.

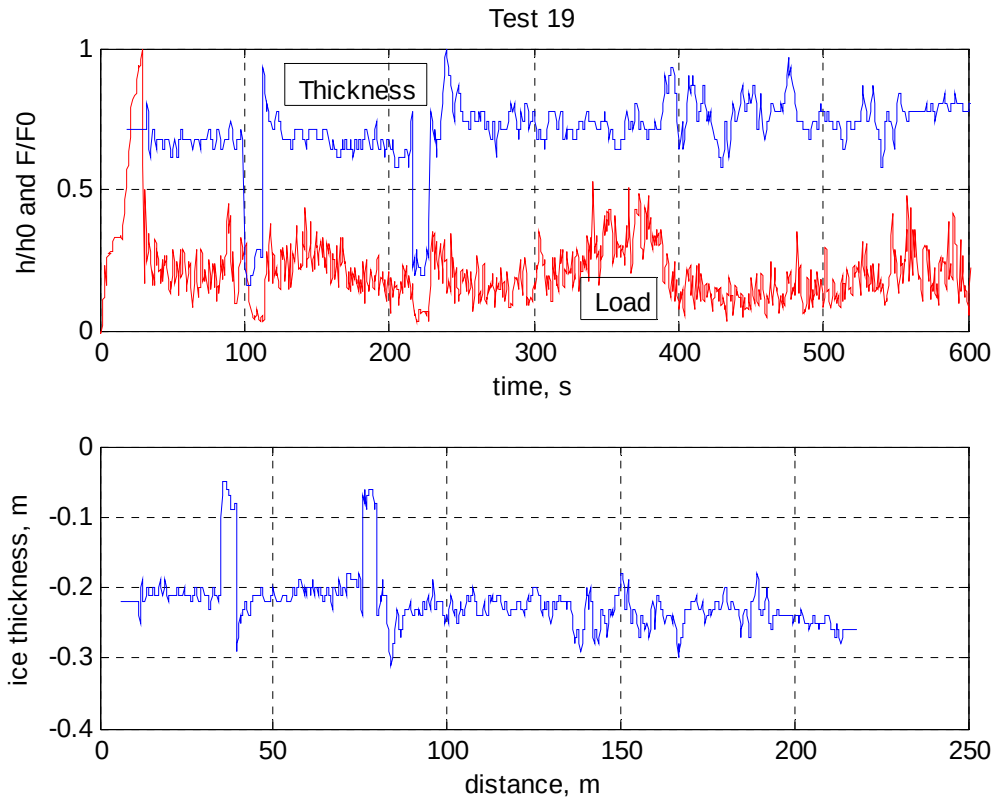

Figur 21 Comparison of load (average on 0.5 sec) and ice thickness in Test 19.

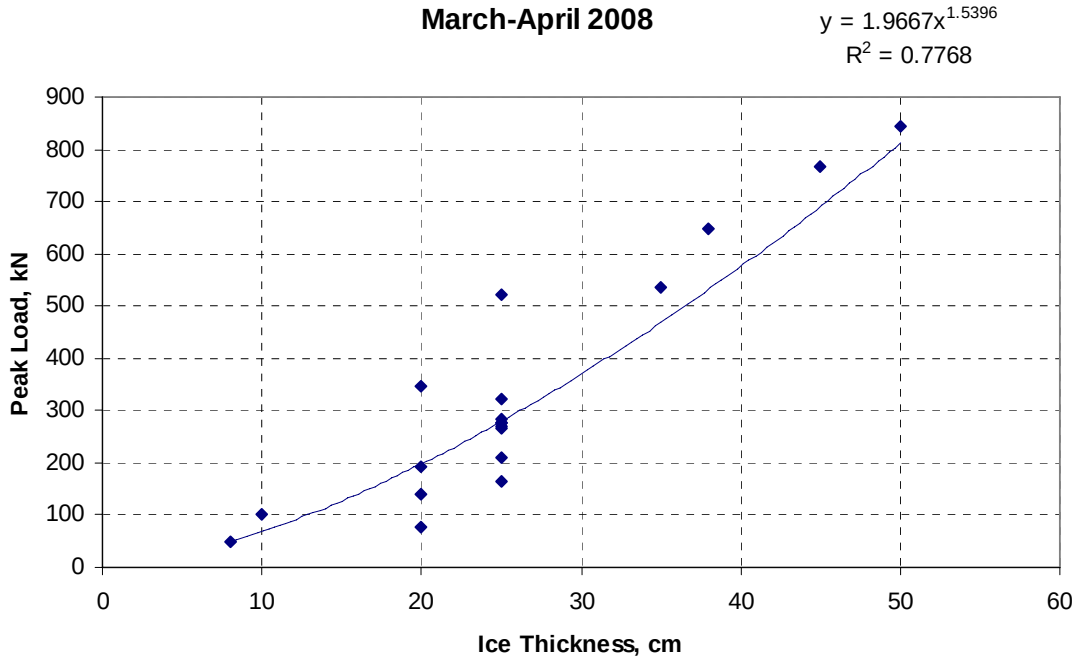

Figur 22 Peak Load vs. Ice Thickness plotted for all tests on level ice in the Gulf of Bothnia,

Islastens beroende av iskvalitet

Enbart genom att se på hur islasterna förändrades under issäsongen 2008 upptäcker man att såväl maxlast som medelvärde sjunker efter mitten av april, fig 23 och 24. Med hänsyn till hur istjockleken varierade ser man däremot att det maximala istrycket verkar sjunka under hela testperioden, se figur 25. Spridningen är ganska stor beroende på att maximal last tycks vara så starkt beroende av penetreringshastighet. Det är intressant att höga istryck kan uppstå så sent som den 29 april då det 20 cm tjocka istäcket rent subjektivt kunde klassificeras som ruttet.

Figur 23 Ice cover appearance 2008-03-29.

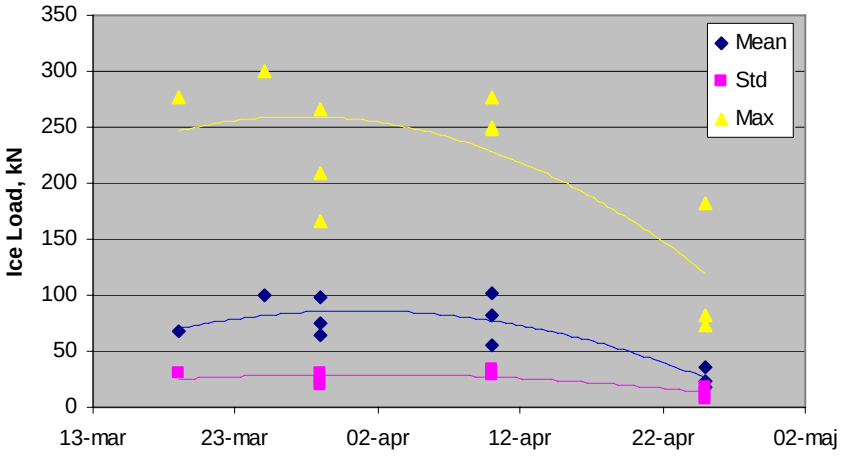

Figur 24 Development of ice load during the winter 2008.

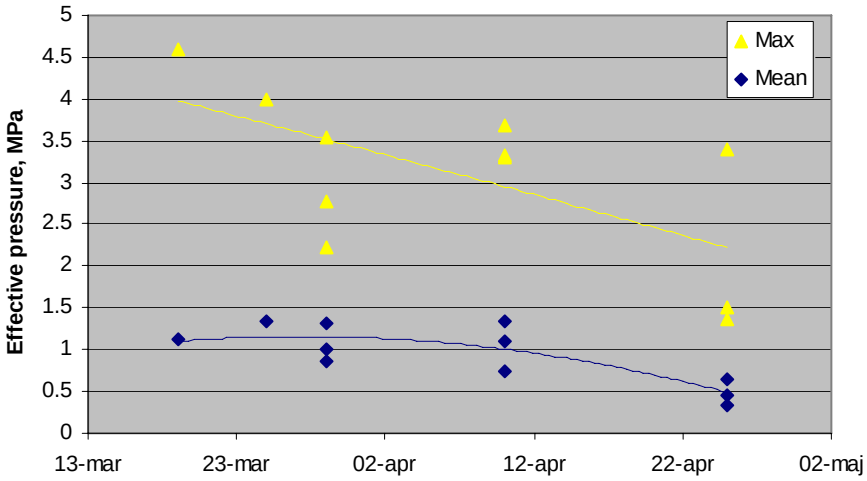

Figur 25 Development of effective ice pressure during the winter 2008.

Islastens beroende av penetreringshastighet

Det är svårt att uttala sig generellt om hur islasten på en konstruktion varierar med den annalkande isens hastighet. Om konstruktionen är flexibel kommer penetreringshastigheten att variera över tiden även om isfältet rör sig med konstant hastighet. Detta gäller i viss mån även för denna försöksuppställning med den skillnaden att vibrationerna i röret har en hög frekvens (ca 70 Hz) och att det är konstruktionen som rör sig inte isen. Vi kom att driva fram röret med olika medelhastigheter (0.7 - 4 knop) men den verkliga hastigheten varierade något beroende på brytningsmotståndet. Trögheten i systemet var stort vilket medförde att hastigheten endast förändrades långsamt. De 10 hastighetskontrollerade försök som gjordes på 25 cm tjock is (Test 2, 8, 11, 12, 13, 14, 16, 19, 20, 21) visas i figur 26. Medellasten och maxlasten ökade med hastigheten. Resultatet tyder också på att maxlasten skiljer sig alltmer från medellasten vid höga hastigheter. Lastkurvorna vid tre försök med olika hastighet (12, 13, 14) jämförs i figur 27.

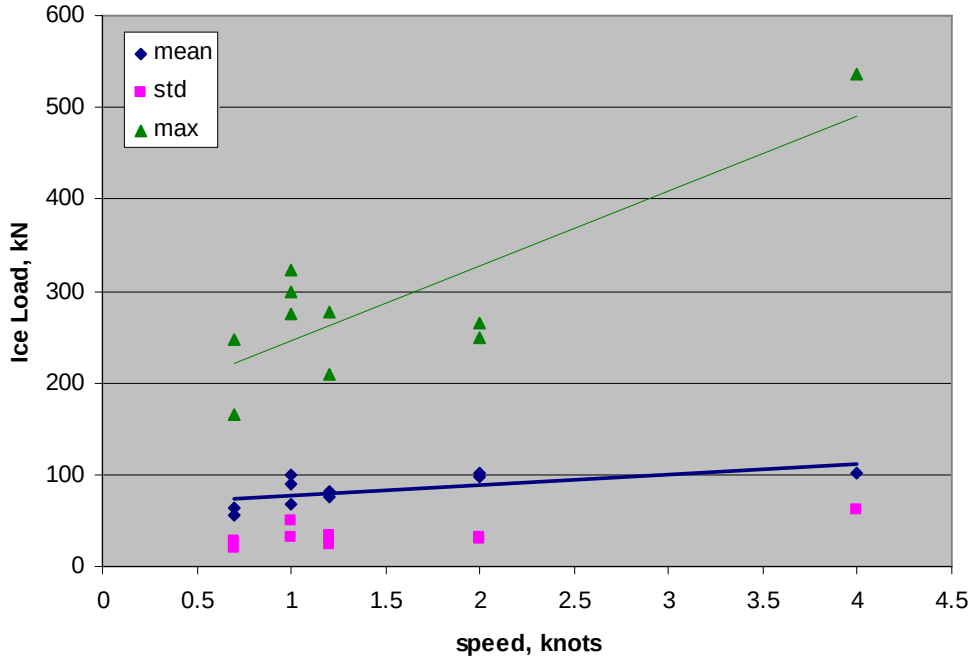

Figur 26 Ice load as function of penetration speed (h = 25 cm).

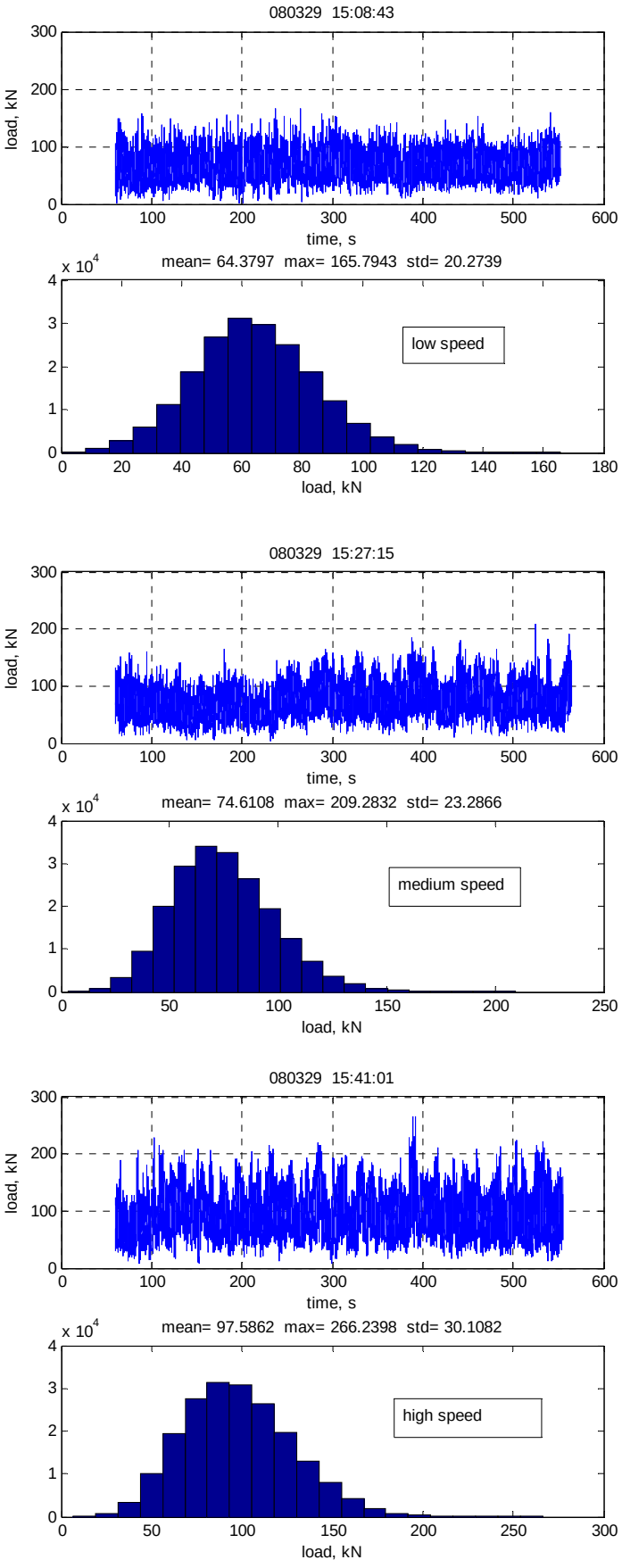

Figur 27 Influence of penetration speed on ice load, at Port of Luleå 2008-03-29.

4.1.6 Oscillerande last vid höga lastnivåer

Vid Test 22 I 40-45 cm tjock is blev lasten till slut så hög att röret böjdes permanent. Överlastningen föregicks av en period med oscillerande last. Vid normal iskrossning var dynamiken en annan, se figur 28. Svängningsmoden och dess frekvens bestämdes troligtvis helt av rörets lägsta grundfrekvens (ca 40 Hz). I den valda samplingshastigheten ser man att svängningen är sinusformad. Vid höga lastnivåer övergår kurvan till av vara sågtandad och lasten sjunker snabbt till noll efter varje maxnivå. Amplituden är därmed hela lasten 845 kN och frekvensen är ca 5 Hz, se figur 29.

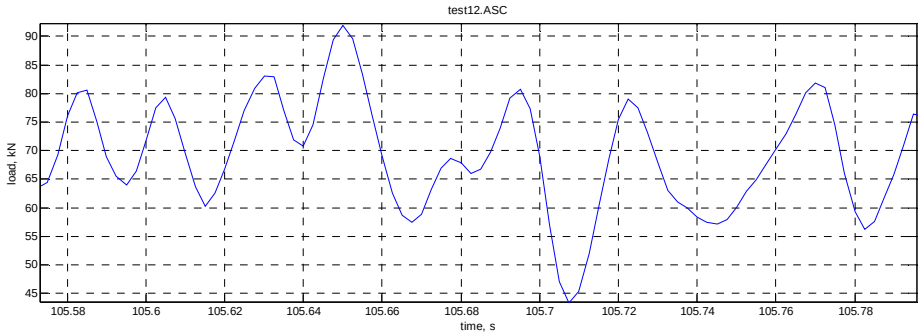

Figur 28 Ice crushing of 25 cm ice resulting in a harmonic load curve with the frequency of abt. 40 Hz.

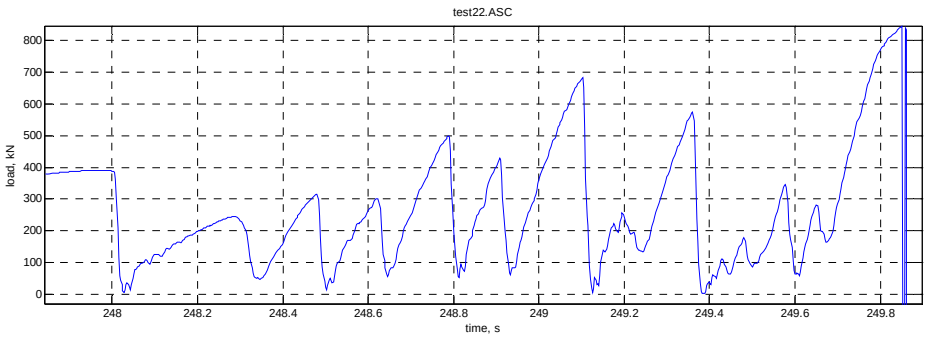

Figur 29 Ice crushing of 45 cm ice resulting in saw-tooth shaped load curve with the frequency of abt.5 Hz.

4.2 Isens Egenskaper

4.2.1 Metodik

Isprover samlades in stickprovsmässigt i samband med varje fältförsök där islasterna mot röret mättes. Isproven bestod av 200 mm borrkärnor där överytan markerades och proven förpackades i 100 liters sopsäckar av plast. Proven förvarades endast en kort tid på isbrytardäcket i snö varefter de lagrades i frysrum i -10°C tills hållfasthetsprovning och övriga analyser utfördes. Densitet och porositet bestämdes på olika djup genom att mäta och väga provkropparna som bestod av 70 mm cylindrar med plansågade ändytor. Provkropparna tryckbelastades i ett frysskåp med en servohydraulisk lastmaskin (Dartec). För att mildra problem med spänningskoncentrationer bestod kontaktytan med isprovet av polyuretan som var inspänd i en aluminiumhylsa (komplians-platttor) enligt IAHR:s standard för isprovning. Provningsmetodiken förklaras i figurerna 30-32.

Kvarvarande rester av borrkärnorna användes för kristallanalys. Skivor med tjocklek på ca 2 mm sågades ut horisontellt och vertikalt med hjälp av en bandsåg. Iskristallernas storlek och utseende bestämdes från fotografier i korspolariserat ljus. Istyperna delades in i tre klasser: Granulär (G), Kolumnär (K) och en mix mellan dessa två (M). Ett exempel på klassad is visas i figur 33. G2 i figurtexten betyder granulär is med 2 mm medeldiameter och K 14-160 betyder kolumnär is med medeldiametern 14 mm och längden 160 mm. Ett vertikalt snitt på samma istyp visas i figur 34. Man kan också säja att isen bestod av 16 cm kärnis överlagrad med 6 cm fast stöpis.

4.2.2 Översikt av utförda analyser

Totalt utfördes enaxlig tryckprovning på 91 is-cylindrar från sex olika istäcken varav 87 prov med kompliansplattor och 4 prov med tryckplattor av stål. I kontakten med stela stålytor uppstod förtida sprickbildning i isens ändytor vilket satte ned tryckhållfastheten. Dessa prov har inte tagit med i fortsatt analys. Tryckhållfastheten, som visas i figur 35, beräknades som maximal last dividerat med provets tvärsnittsarea (A=35.4 cm^2). Hållfastheten varierade starkt med isens temperatur, utom i ett fall (Kallax 2008-01-08) där isen var helt fri från salt. Intressant är att isen som var inhämtad under slutet av issäsongen hade det största hållfasthetstappet vid noll grader trots att all is hade förvarats i -10°C under en tid före provningen och vid själva provprepareringen.

Alla resultat finns i tabeller och diagram med last plottat mot tid i bilaga D.

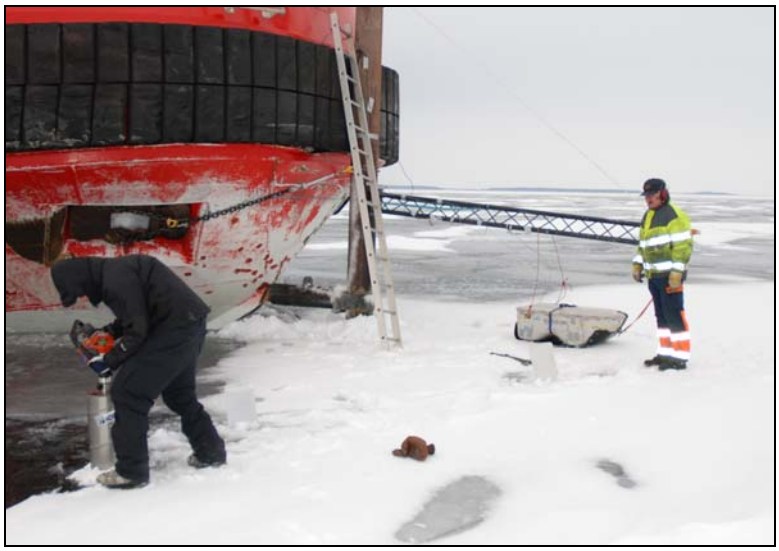

Figur 30 Taking ice cores from the ice cover in front of the icebreaker, 2008-04-10.

Figur 31 Drilling of 70 mm test samples from a vertical core at different depths in the ice cover.

Figur 32 The loading machine and the cold cabinet used for ice strength tests.

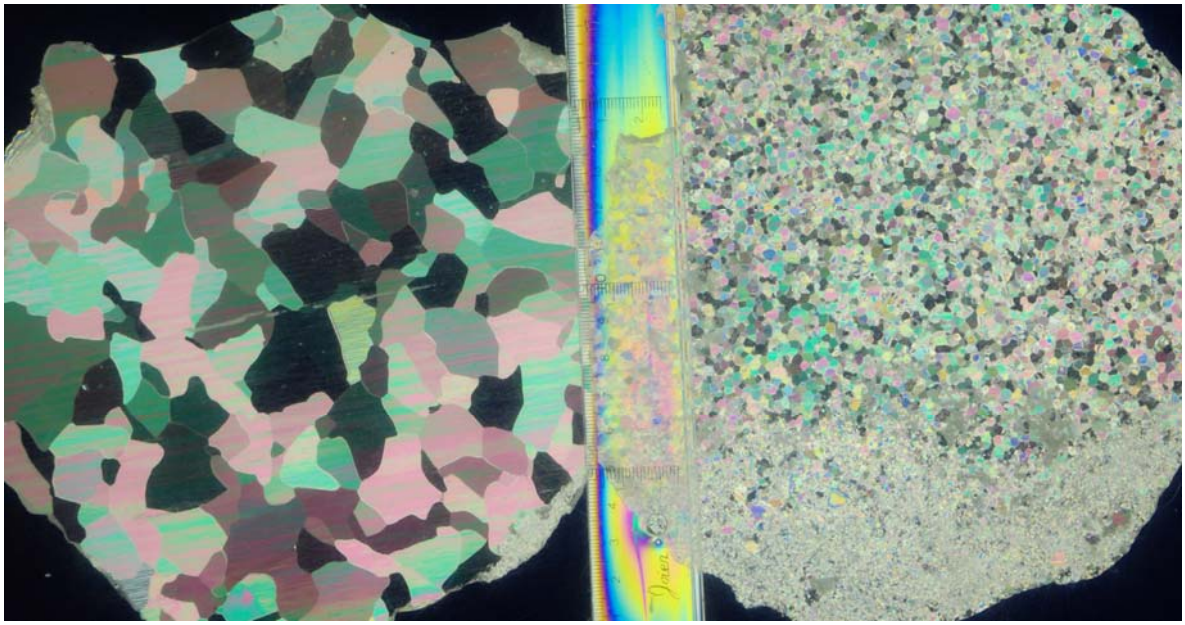

Figur 33 Horizontal sections from ice core showing the crystals at the bottom (left) and at the top (right). The ice was classified as K14-160, G2, G1, Klubbviken 2008-04-10.

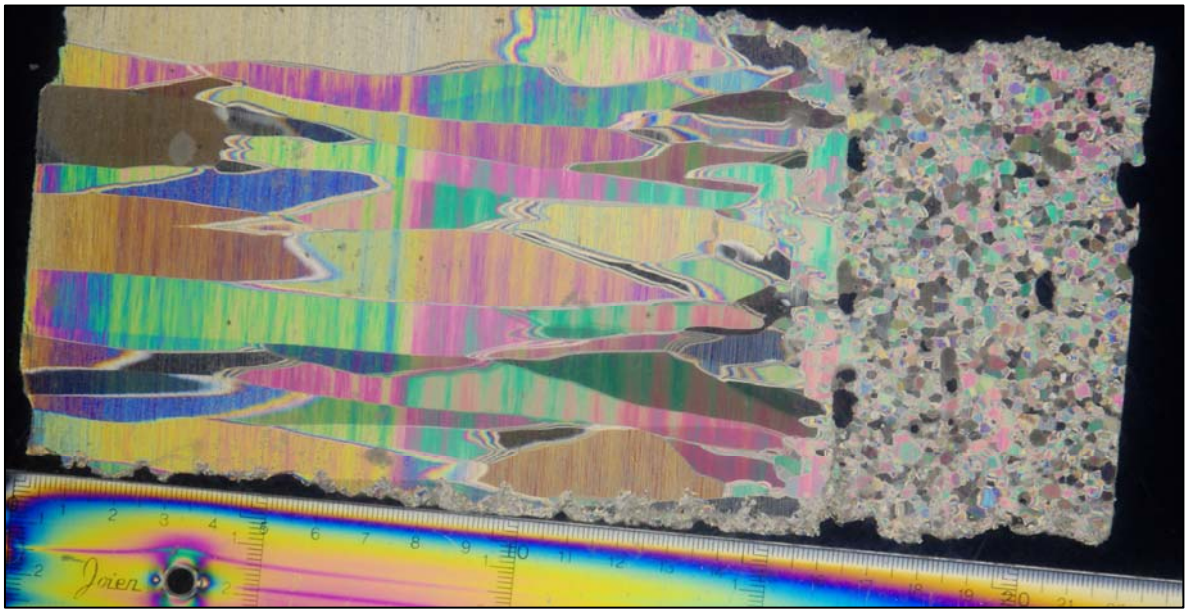

Figur 34 Vertical section from ice core showing the crystals from bottom (left) to the top (right). Total length of this core was 22 cm, Klubbviken 2008-04-10.

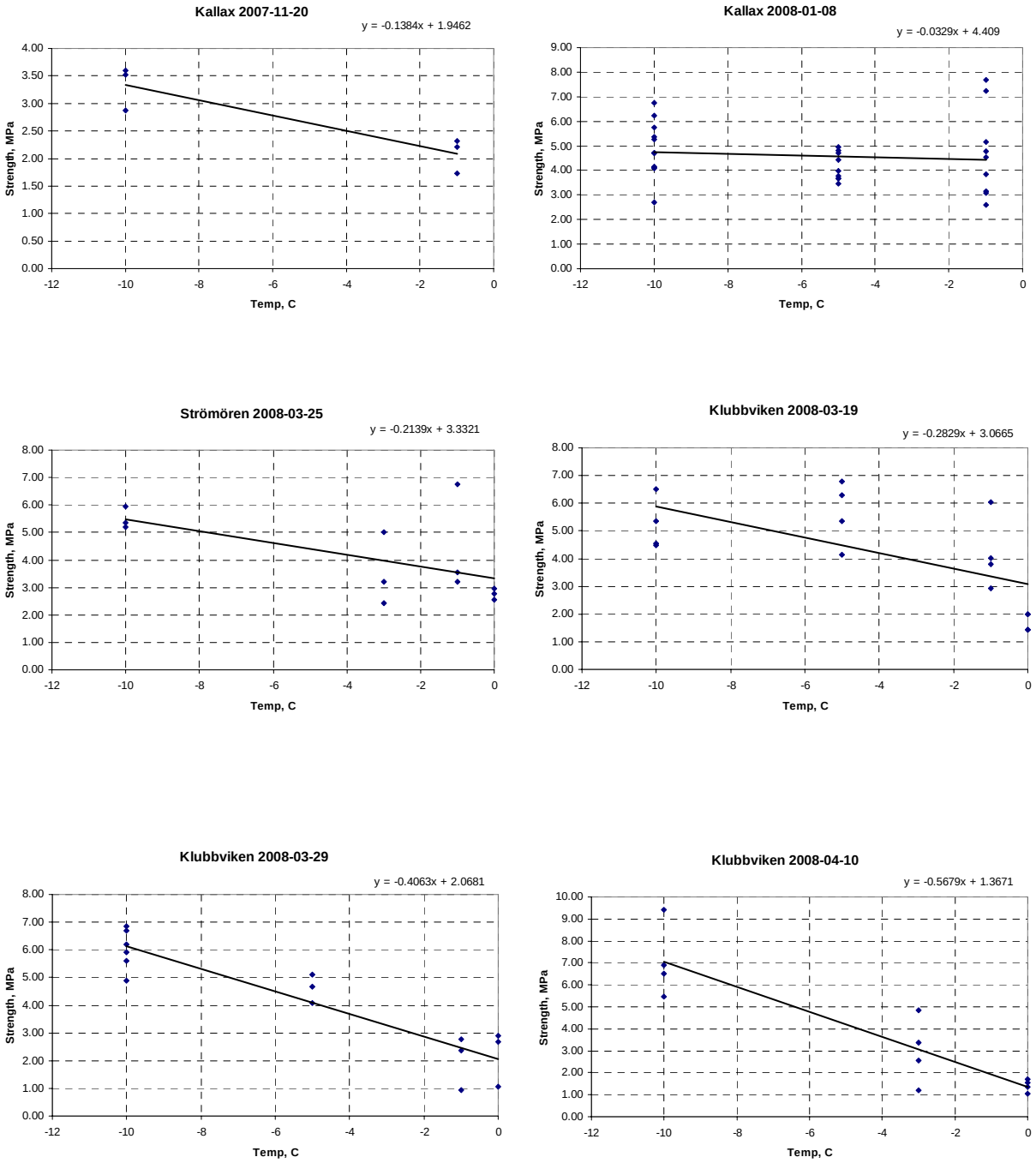

Figur 35 Ice Strength vs. Temperature on 87 compressive tests, Gulf of Bothnia 2007/08.

Bilaga A Tillverkningsritningar

Version 080228

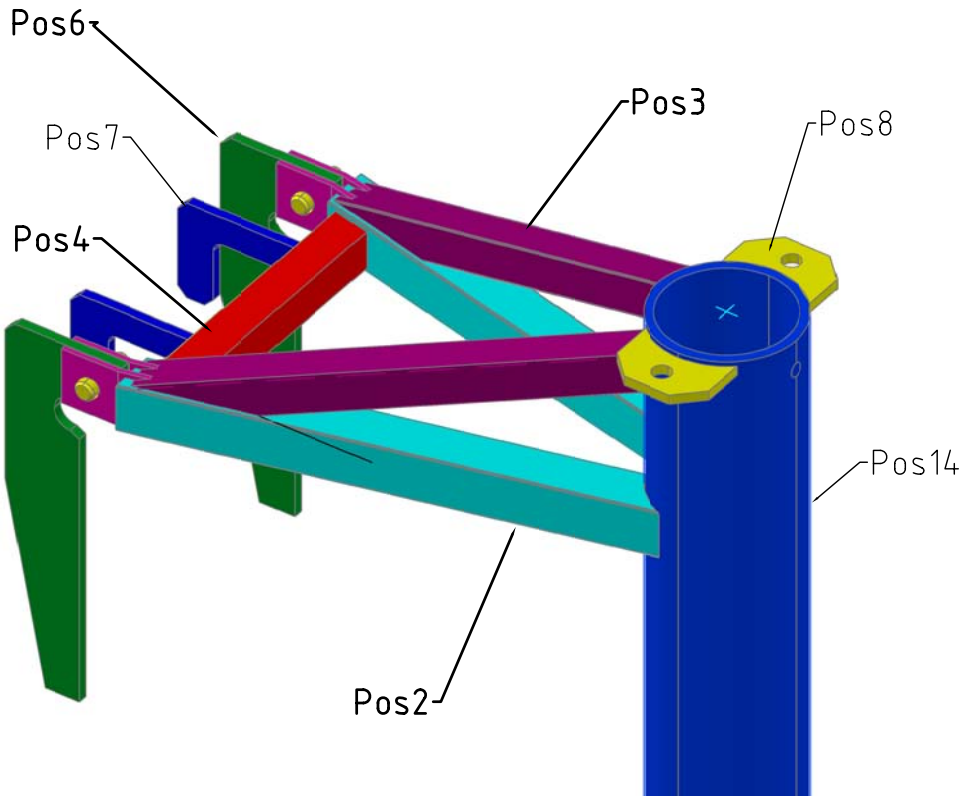

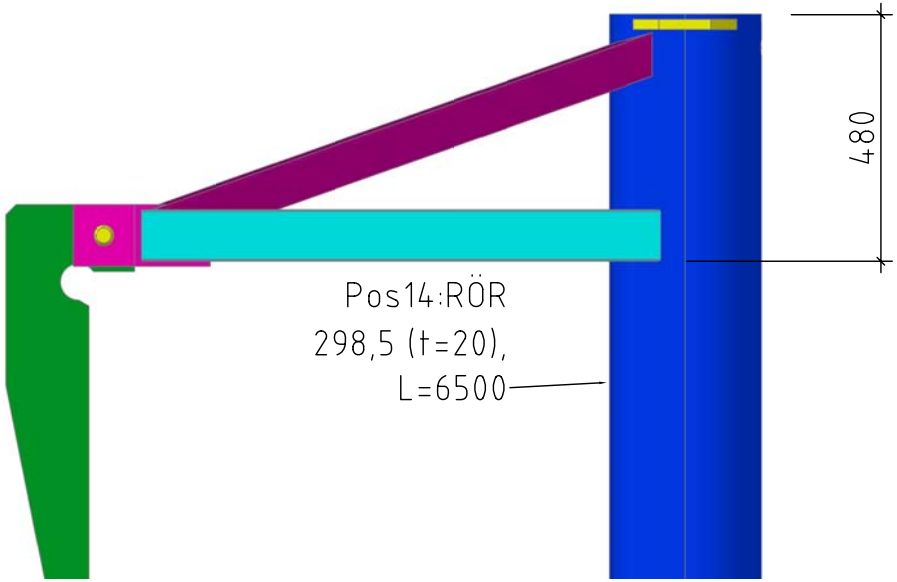

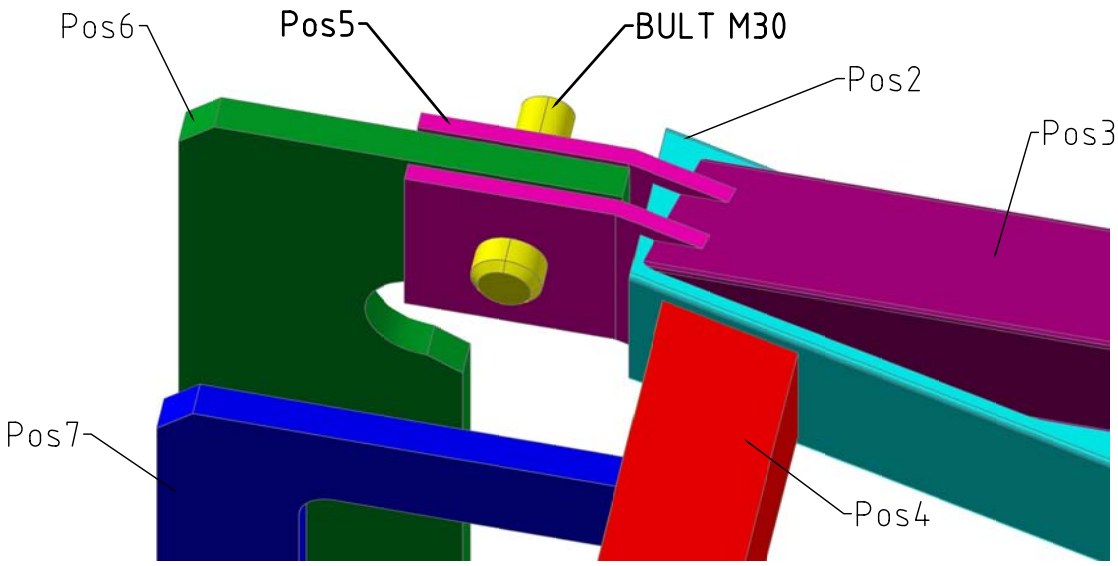

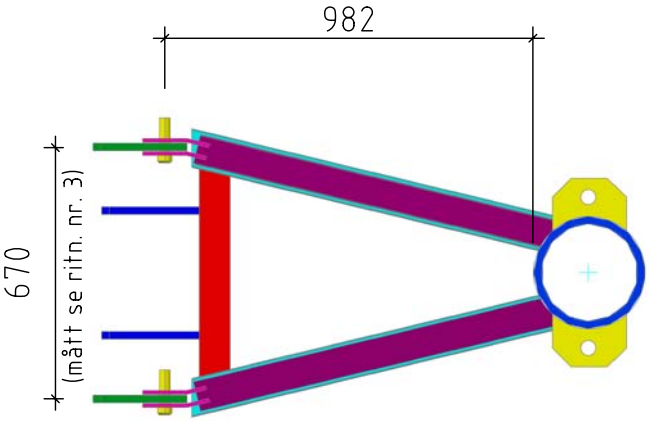

FÖRKLARINGAR
STÅL: S235J0
SVETS: a5 kälsvets om inget annat anges
Pos 14 levereras av LTU

OBJEKT			
Planer och vyer (IS-INTERREG)			
SKALA	RITAD AV LTU	RITN NR 1	DATUM

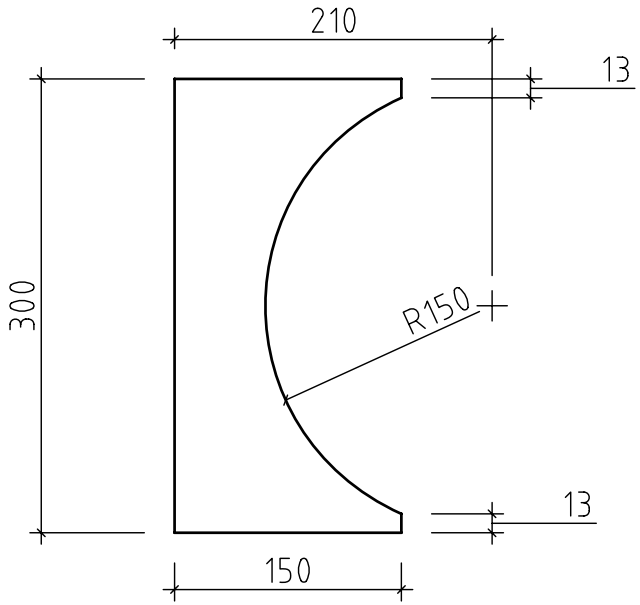

Pos 12 - 2st, Tjocklek 20 mm
---1:5----

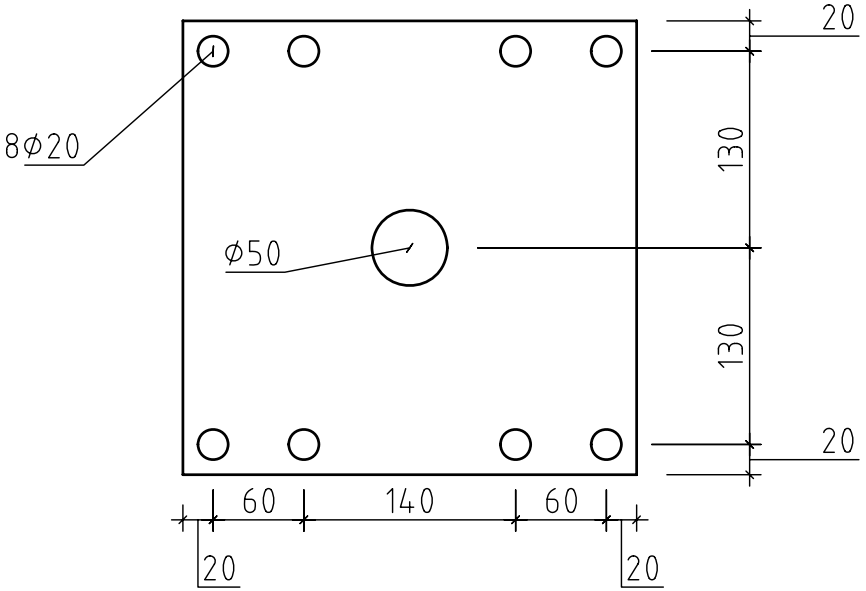

Pos 11 - PL300×300×20, 2st
---1:5----

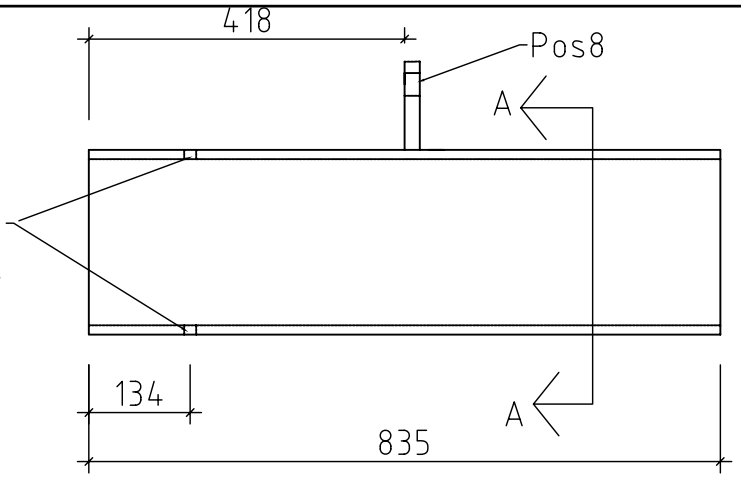

Pos 13 - VKR 244,5 t=12,5
---1:5----

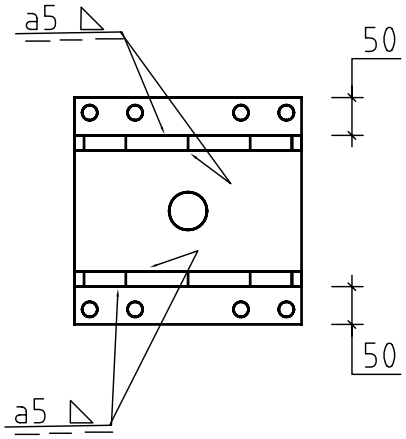

Pos12 svetsas på pos11, se vy
ritn 8

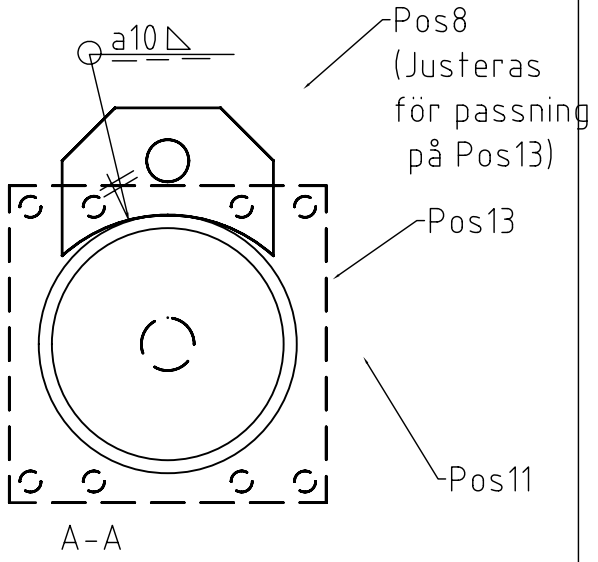

FÖRKLARINGAR
STÅL: S235JO
SVETS: a5 kälsvets om inget annat anges
Pos 14 levereras av LTU

88

OBJEKT			
Pos11, 12 och Pos13 (IS-INTERREG)			
SKALA	RITAD AV LTU	RITN NR 10	DATUM

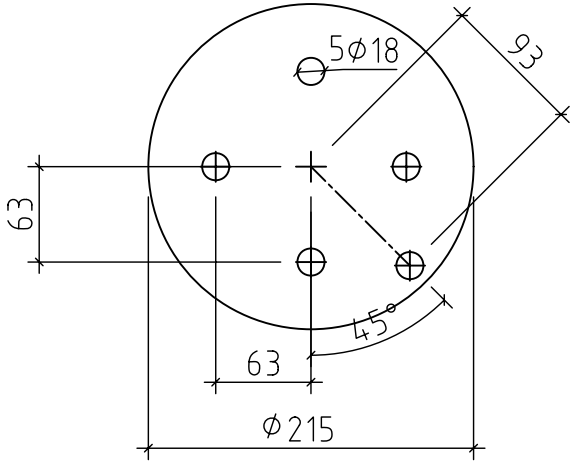

Pos 9 - Tjocklek 40 mm
---1:5----

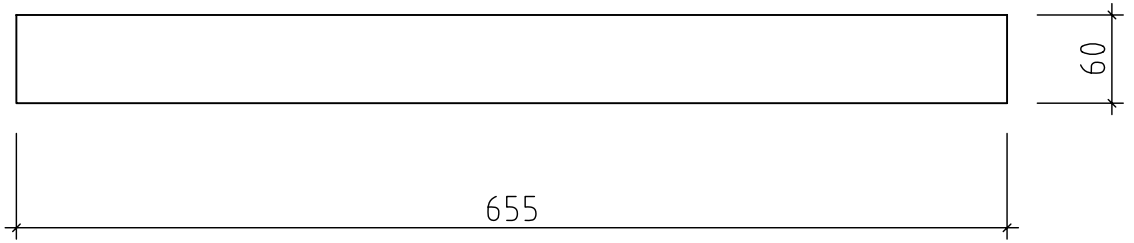

Pos 10 - PL655×60×20, 3st
---1:5----

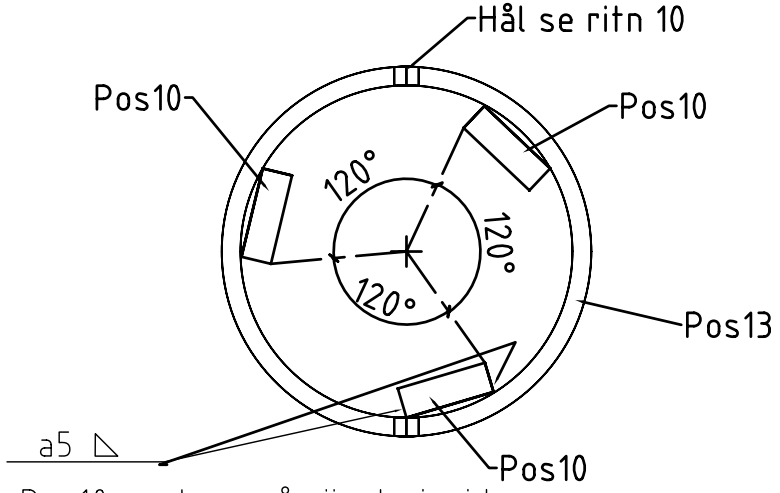

Pos10 svetsas på rörets insida så lång sträcka som möjligt i var ände (gäller alla tre)

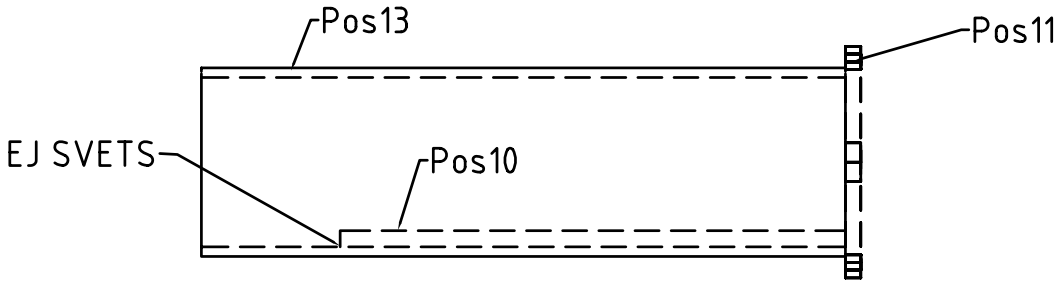

Principskiss montering av
Pos10, Pos11 och Pos13

FÖRKLARINGAR
STÅL: S235J0
SVETS: a5 kälsvets om inget annat anges
Pos 14 levereras av LTU

OBJEKT			
Pos9 och Pos10 (IS-INTERREG)			
SKALA	RITAD AV	RITN NR	DATUM
	LTU	9	

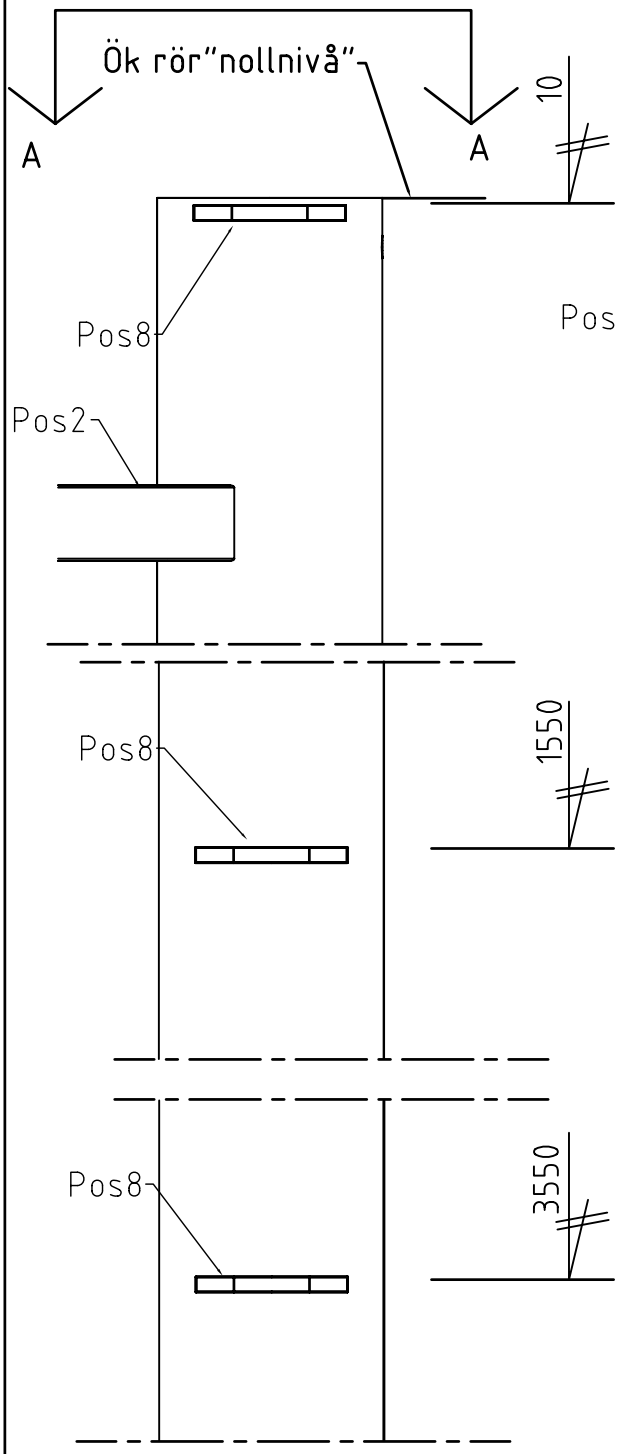

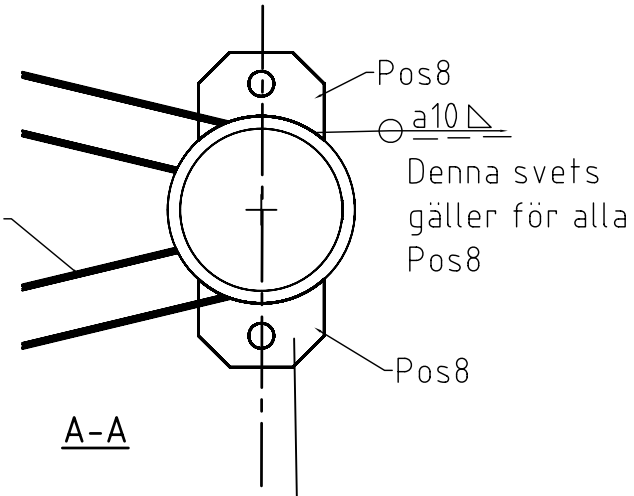

OBJEKT	DATUM
Pos8 (IS-INTERREG)	
SKALA	RITN NR 2
	RITAD AV LTU

FÖRKLARINGAR
STÅL: S235J0
SVETS: a5 kälsvets om inget annat an
Pos 14 levereras av LTU

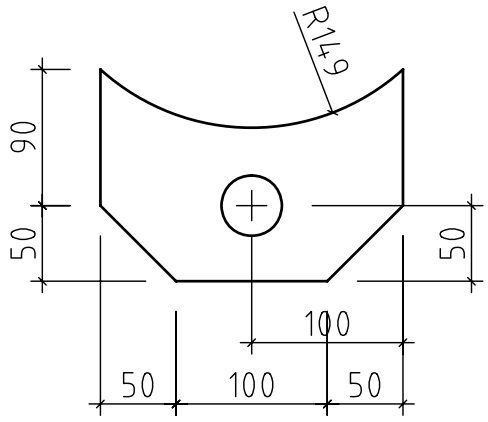

Montering av Pos8 på Pos14 (Ø298,5 (t= 20 mm) med längden 6500 mm)

Pos 8 - PL200×140×20, 7st

---1:5----

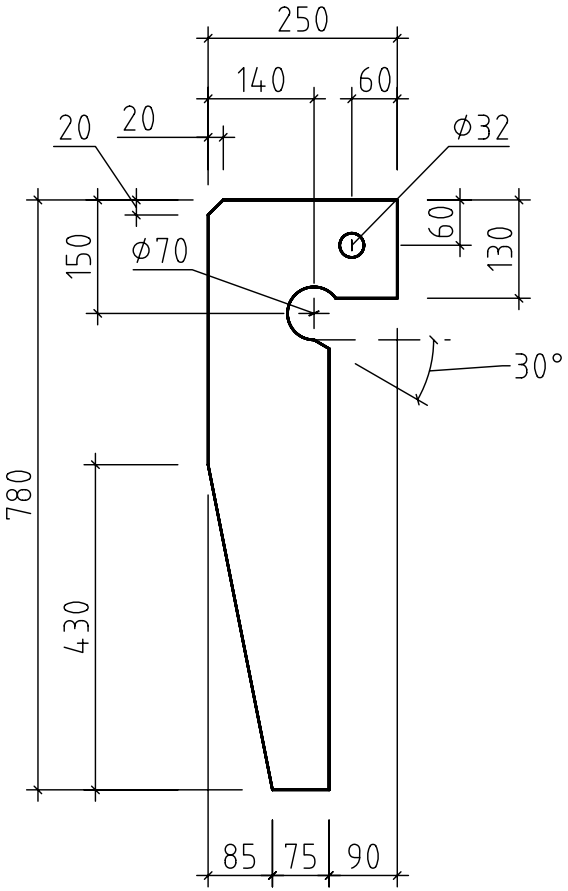

Pos6 - PL 780×250×20, 2st

--- 1:10 ----

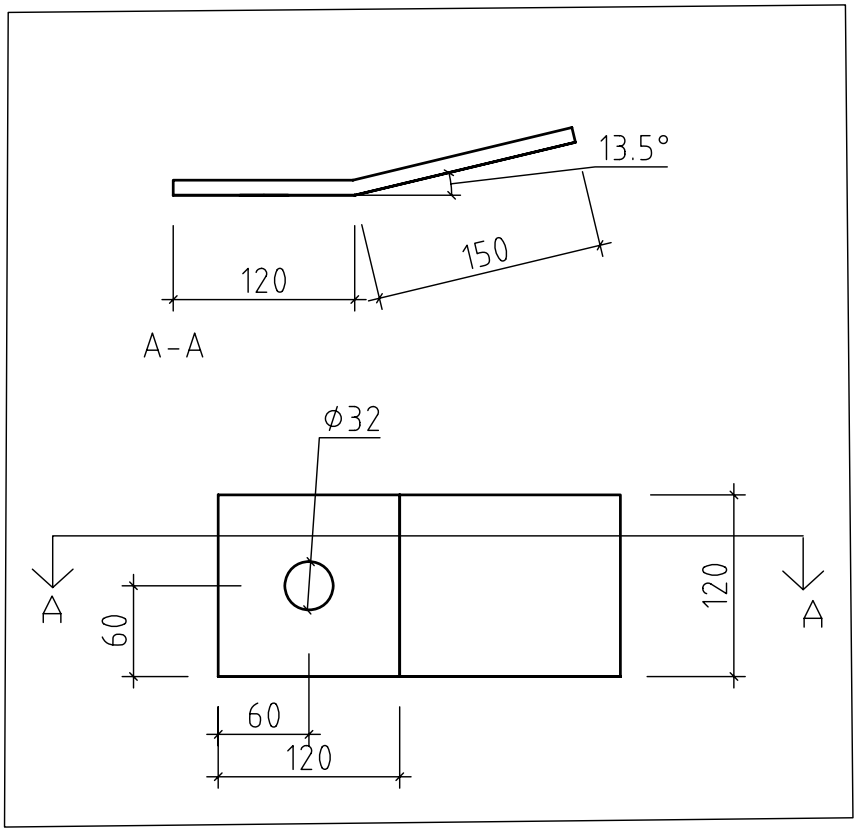

Pos 5 - PL 270×120×10, 2+2st

(2st är spegelvända)

---1:5----

FÖRKLARINGAR

STÅL: S235J0

SVETS: a5 kälsvets om inget annat anges

Pos 14 levereras av LTU

OBJEKT			
Pos5 och Pos6 (IS-INTERREG)			
SKALA	RITAD AV	RITN NR	DATUM
1:5, 1:10	LTU	6	080221

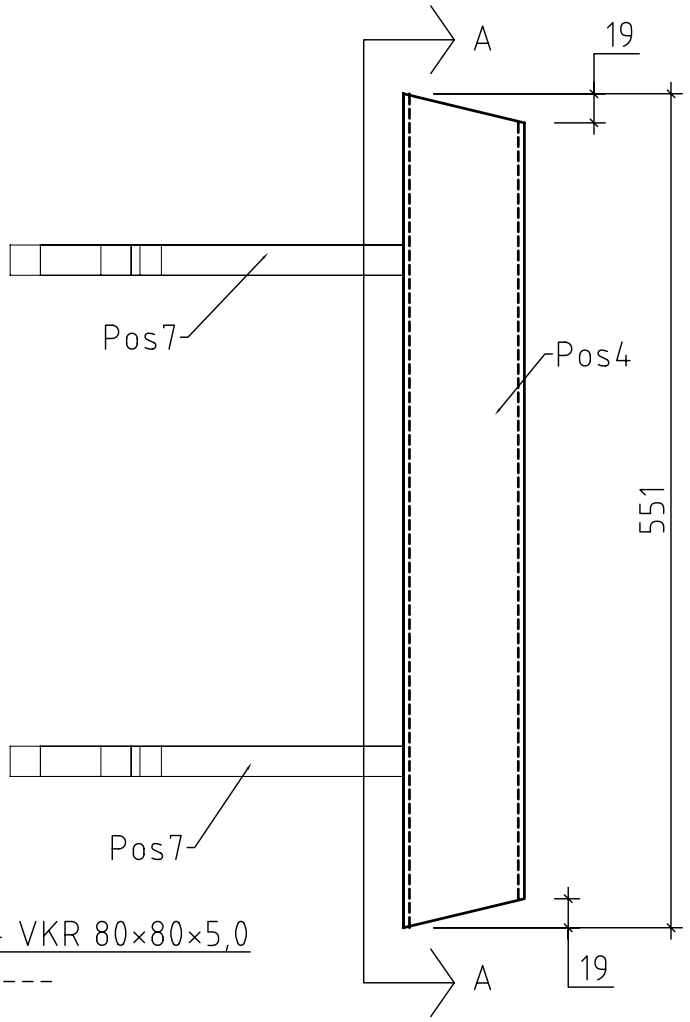

Pos 4 - VKR 80×80×5,0

---1:5----

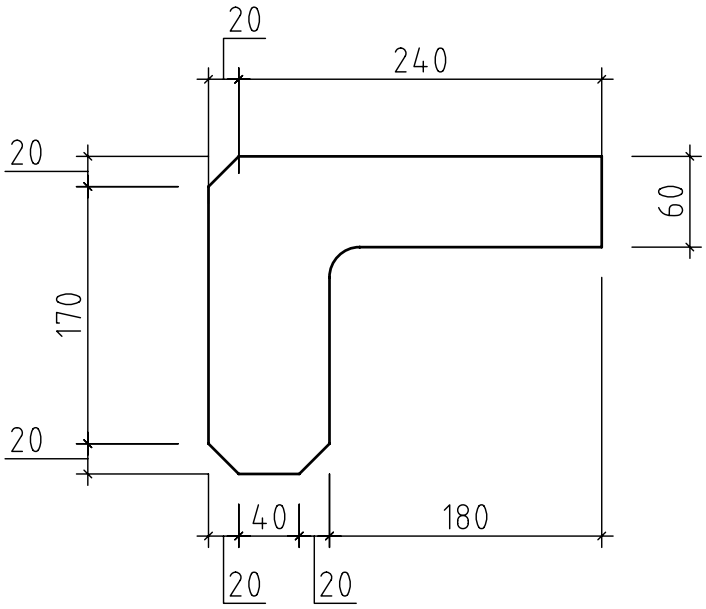

Pos 7 - PL260×210×20, 2st

---1:5----

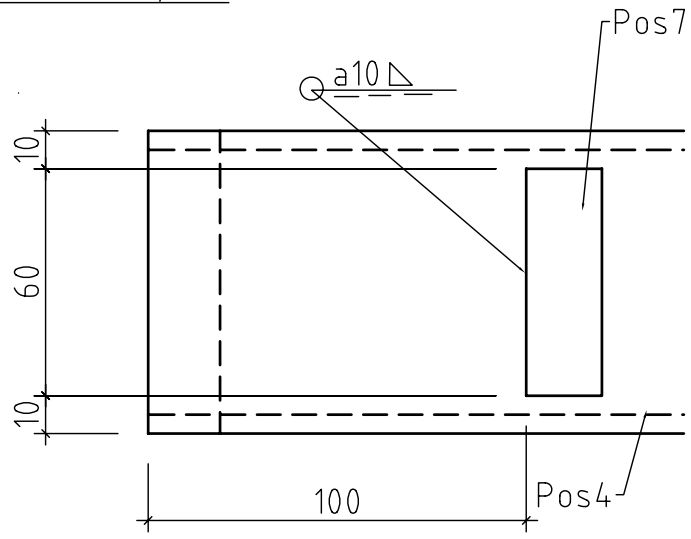

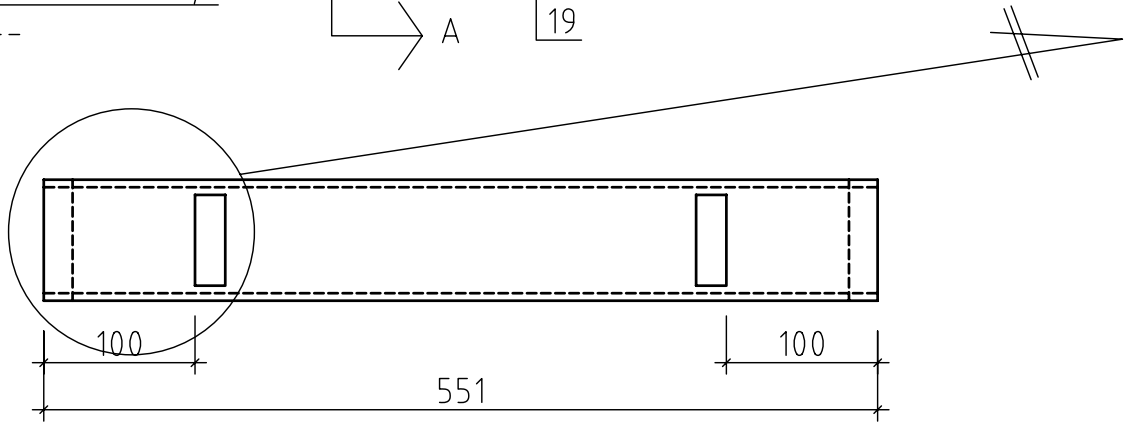

A-A

FÖRKLARINGAR: SE ÖVRIGA RITNINGAR

92

OBJEKT			
Pos4 och Pos7 (IS-INTERREG)			
SKALA	RITAD AV	RITN NR	DATUM
	LTU	4	

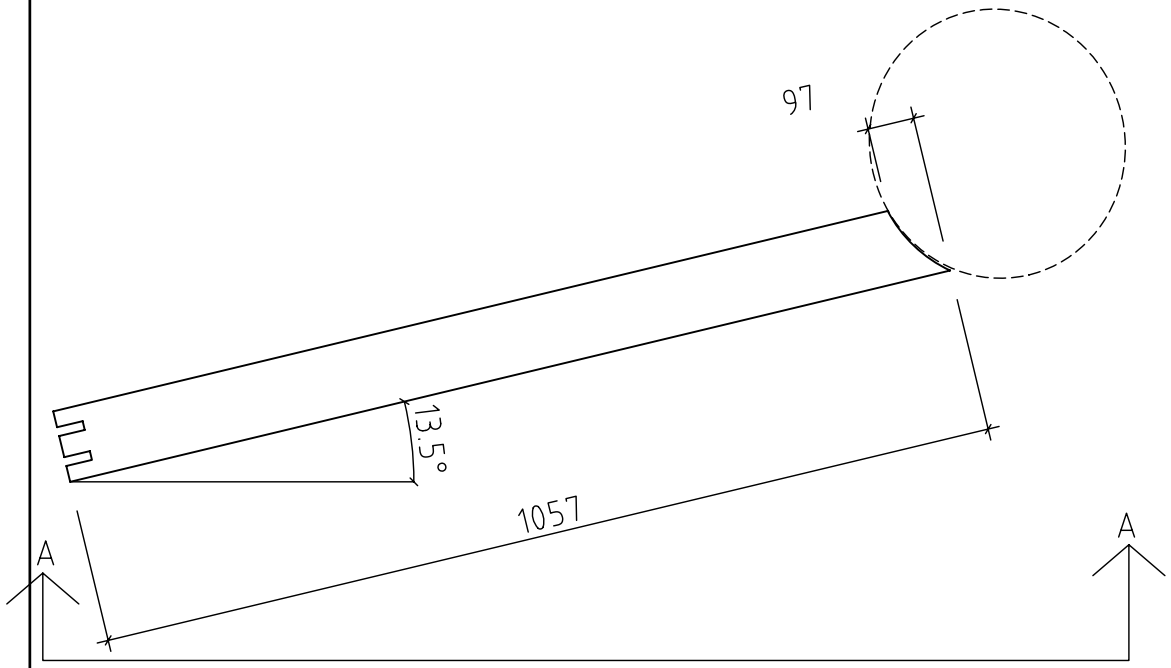

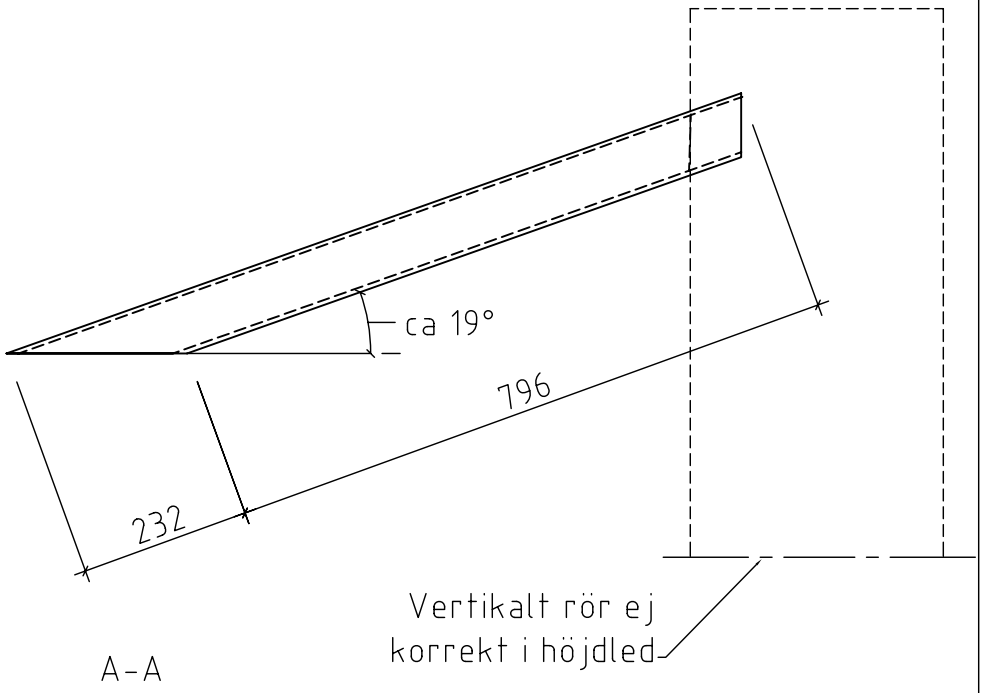

Pos3 bör justeras in på plats,
ovanpå Pos2

Pos 3 - VKR180×80×5,0, 2st (spegelvända)

---1:5----

FÖRKLARINGAR
STÅL: S235J0
SVETS: a5 kälsvets om inget annat anges
Pos 14 levereras av LTU

OBJEKT			
Pos3 (IS-INTERREG)			
SKALA	RITAD AV	RITN NR	DATUM
1:5, 1:10	LTU	7	080227

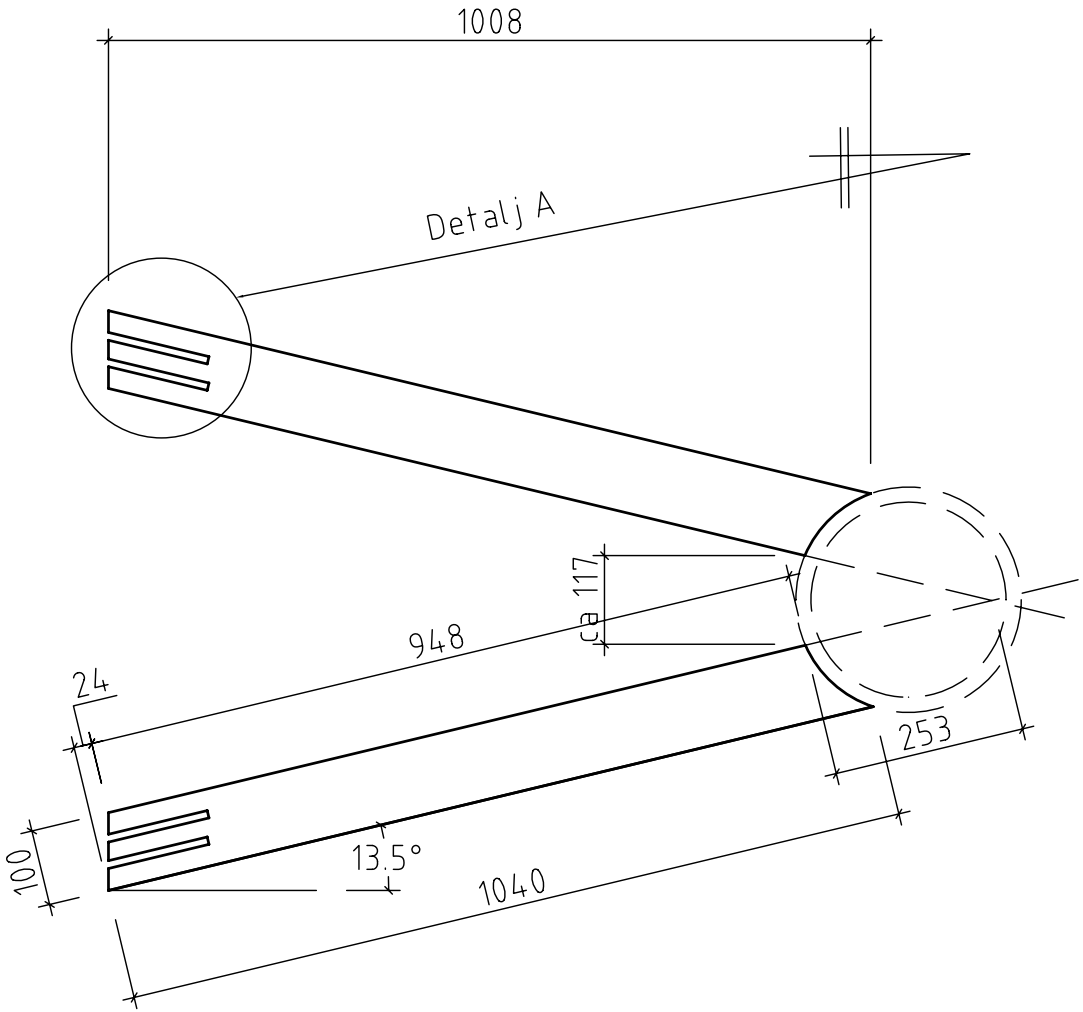

Pos 2 - VKR 100×100×6,3

---1:10----

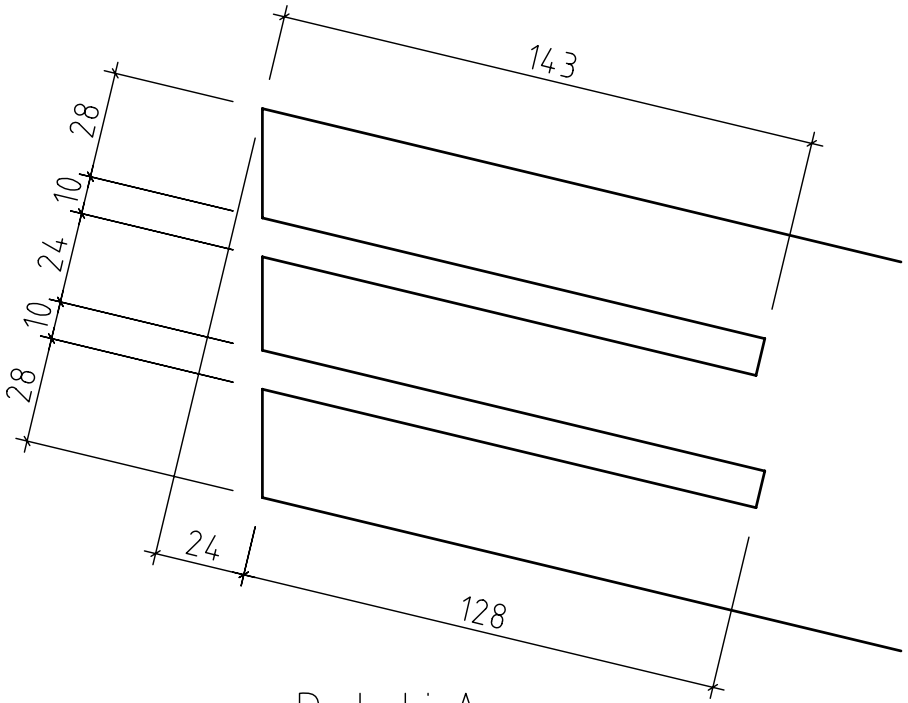

Detalj A

---1:2----

FÖRKLARINGAR

STÅL: S235JO

SVETS: a5 kälsvets om inget annat anges

Pos 14 levereras av LTU

94

OBJEKT			
Pos2 (IS-INTERREG)			
SKALA	RITAD AV LTU	RITN NR 5	DATUM

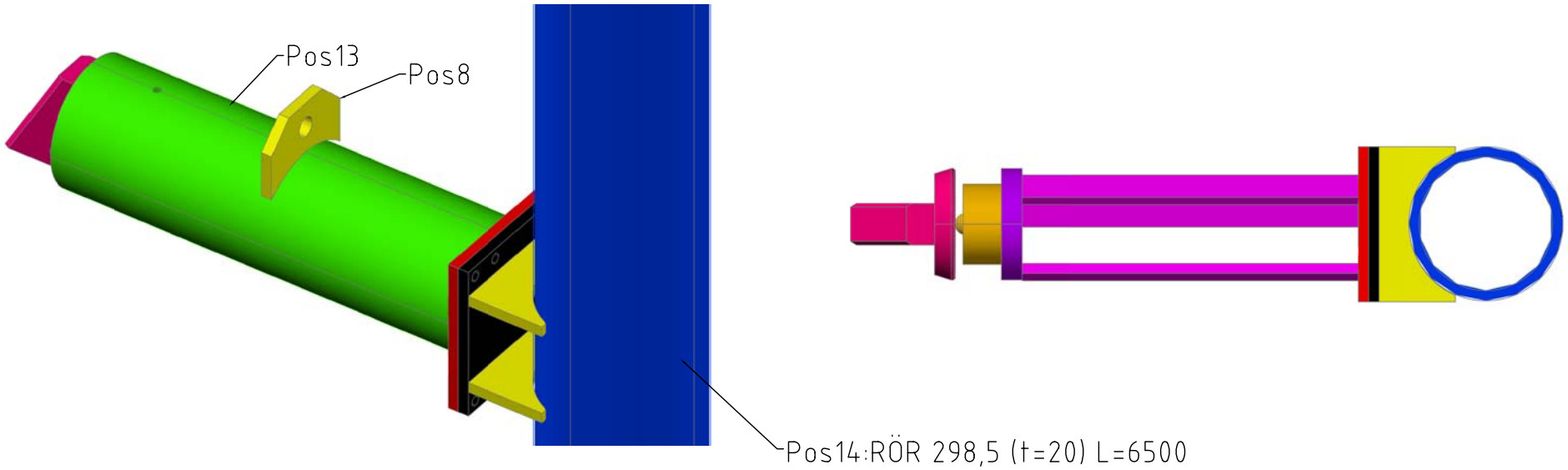

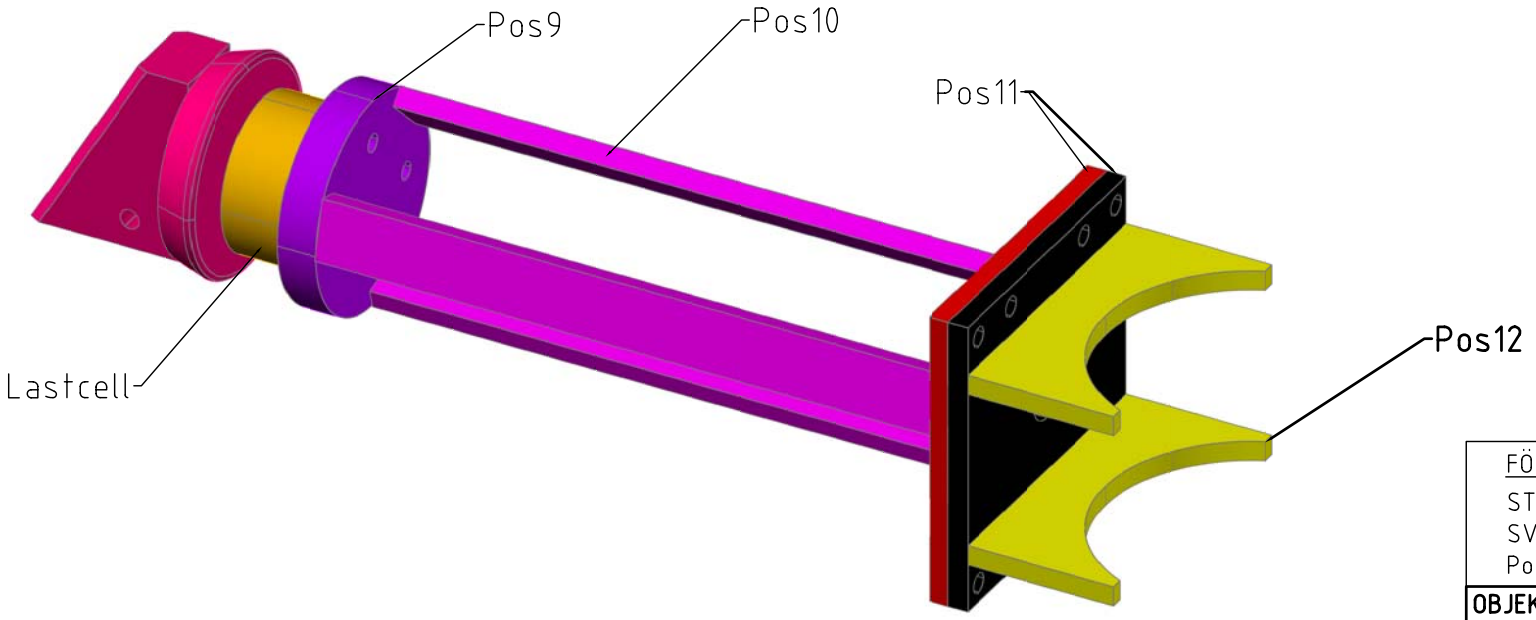

FÖRKLARINGAR

STÅL: S235J0

SVETS: a5 kälsvets om inget annat anges

Pos 14 levereras av LTU

OBJEKT			
Planer och vyer (IS-INTERREG)			
SKALA	RITAD AV LTU	RITN NR 8	DATUM

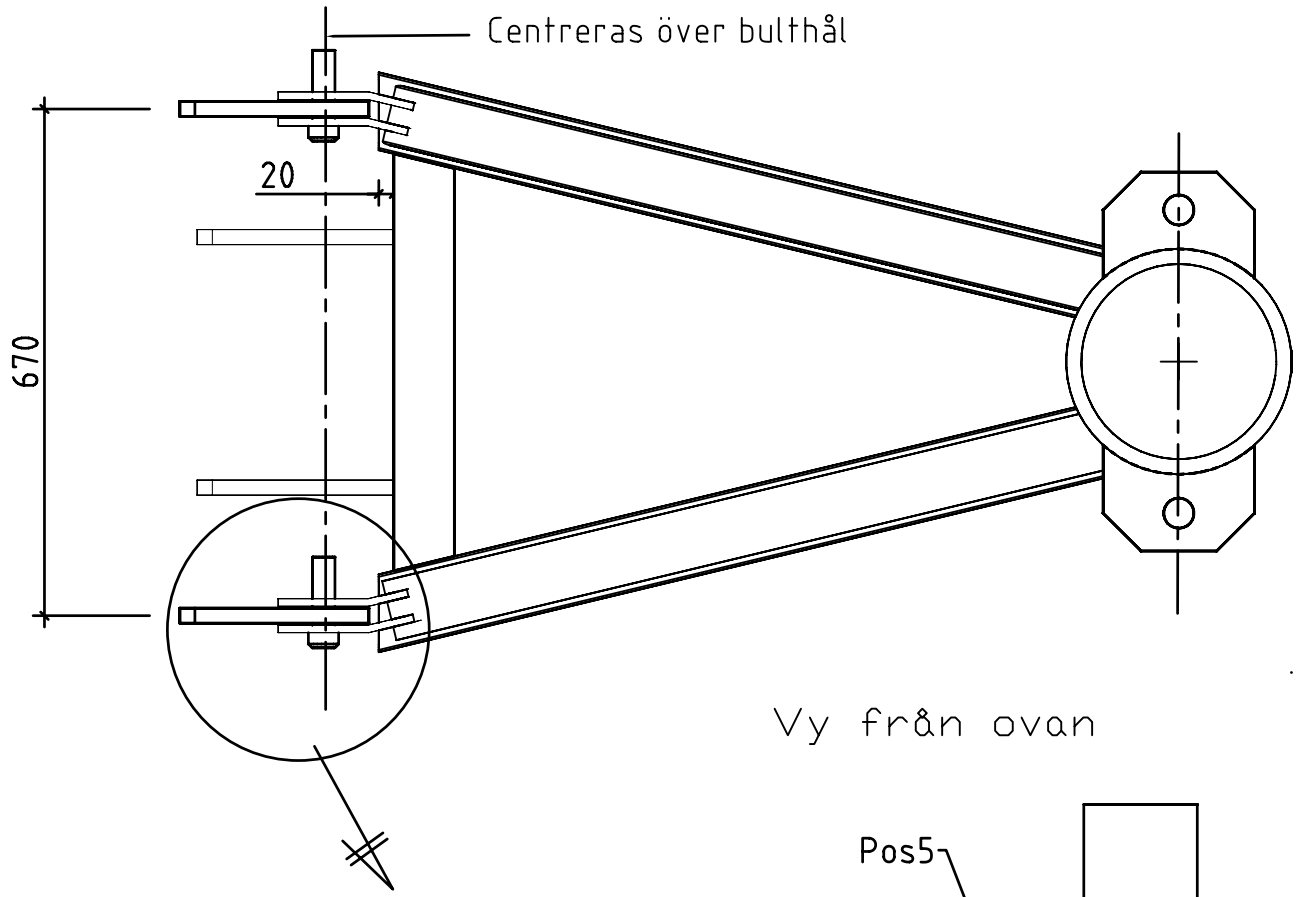

Vy från ovan

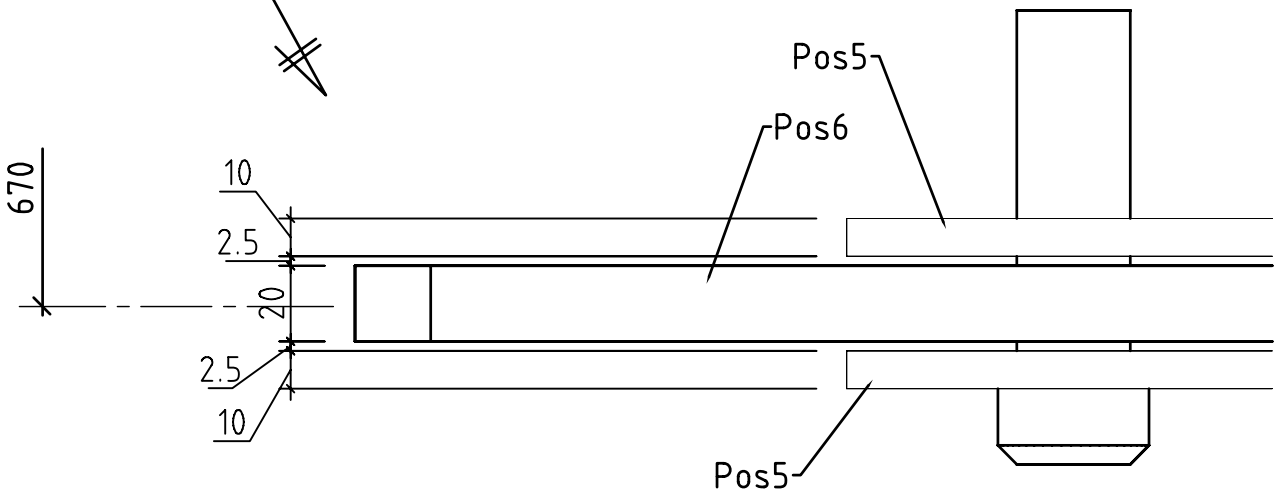

Montering

FÖRKLARINGAR
STÅL: S235J0
SVETS: a5 kälsvets om inget annat anges
Pos 14 levereras av LTU

96

OBJEKT			
Montering Pos2 och 8 (IS-INTERREG)			
SKALA	RITAD AV LTU	RITN NR 3	DATUM

Bilaga B Mätning av istjocklek med georadar

Mätning av istjocklek med georadar i Luleå Hamn, perioden 25 mars – 10 april 2008

Inledning

MRM Konsult AB har på uppdrag av Luleå Tekniska Universitet utfört mätning med georadar i Luleå Hamn under vårvintern 2008. Mätningen ingår som en del i ett forskningsprojekt där man mäter isens tryck mot ett vertikalt stående rör som pressas genom isen. Praktiskt har försöket gått till så att ett vertikalt järnrör försett med tryckgivare monterats i stäven på hamnisbrytaren Viscaria.

Georadarmätningen har syftat till att jämföra istjocklekens variation med övriga mätdata från rörkonstruktionen.

Fältmätningar och mätutrustning

Mätningar har utförts vid 3 tillfällen: den 25 mars, den 29 mars och den 10 april 2008 enligt nedan. Vid samtliga mättillfällen har georadarsystem RAMAC och 1000 MHz antenn använts.

25 mars

- Mätning längs en 12 m bred och 100 m lång korridor som i efterhand bröts med isbrytaren. Mätningen, som gjordes manuellt, omfattar 4 parallella linjer med inbördes avstånd ca 4 m.
- Manuell mätning framför isbrytaren (mätperiod ca 5 minuter).

29 mars

- Mätning med antennen fast monterad ca 4 m framför röret på isbrytaren. Mätning gjordes i sammanlagt 5 st omgångar, de flesta ca 10 minuter långa.

10 april

- Mätning med antennen fast monterad ca 3 m framför röret på isbrytaren. Mätningen gjordes i sammanlagt 3 omgångar, var och en ca 10 minuters lång.

Vid samtliga mättillfällen jämfördes georadardata mot istjocklek i ett fåtal borrhål. Jämförelse mellan radarvågens gångtid i is och isens tjocklek ger ett genomsnittligt värde på isens dielektricitetstal på 3,6 motsvarande en utbredningshastighet på ca 160 m/µs. Detta är något lägre än vad man normalt finner i torr sötvattenis (ca 165 m/ µs).

Resultat

25 mars

Resultaten från mätningen i den 12 m breda korridoren redovisas som kurvdragen karta i bilaga 1. Som framgår av kartan varierar isens tjocklek i korridoren mellan drygt 20 och 40 cm. På ritningen är isbrytarens (senare) färdväg genom korridoren införd med streckad linje.

Registreringen från den manuella mätningen framför isbrytaren redovisas i bilaga 2. Registreringen visar isens tjocklek mot mättid i sekunder.

MRM Konsult AB
Box 63
971 03 LULEÅ

Telefon 0920-60460
Laboratoriet 0920-60487 / -89
Telefax 0920-60474

E-post mrm@mrm.se
Internet www.mrm.se

Organisationsnummer
556263-5077

Besöksadress
Gammelstadsvägen 5
972 41 LULEÅ

29 mars
Registreringarna från de 5 olika mätomgångarna (betecknade test 12 – test 16) redovisas i bilagorna 3–7. I överkant på registreringarna är starttid (satellittid) införd.

I bilaga 11 (Excel-fil) redovisas beräknad istjocklek utifrån mätningen med ett värde per 0,5 sek.

Generellt för detta mättillfälle är att mätdata ofta är störda, dels av förhållandena på isen (drevsnö och ibland vatten på isytan) och av att antennen var monterad så att den ibland lyftes upp från isytan på grund av isbrytarens gungning. De mätdata som av dessa anledningar bedöms som osäkra har i bilagorna markerats med rött. I vissa fall har också mätdata utelämnats längs kortare partier.

10 april
Registreringarna från de 3 mätomgångarna (betecknade försök 1 – försök 3) redovisas i bilagorna 8-10. I överkant på registreringarna är starttid (satellittid) införd.

I bilaga 12 (Excel-fil) redovisas beräknad istjocklek utifrån mätningen med ett värde per 0,5 sek.

Vid denna mätomgång monterades antennpulkan på ett sätt så att den aldrig kom att lyftas upp från isen. Förhållandena på isytan var även torrare än tidigare, vilket sammantaget ledde till stabilare registreringar än vid den tidigare mätningen. På ställen med drevsnö på isen kan dock radarmätningen indikera en något för hög istjocklek. Dessa partier är markerade med rött.

MRM Konsult AB 2008-04-15

Bo Löfroth

Bilagor

Bilaga 1 - 12

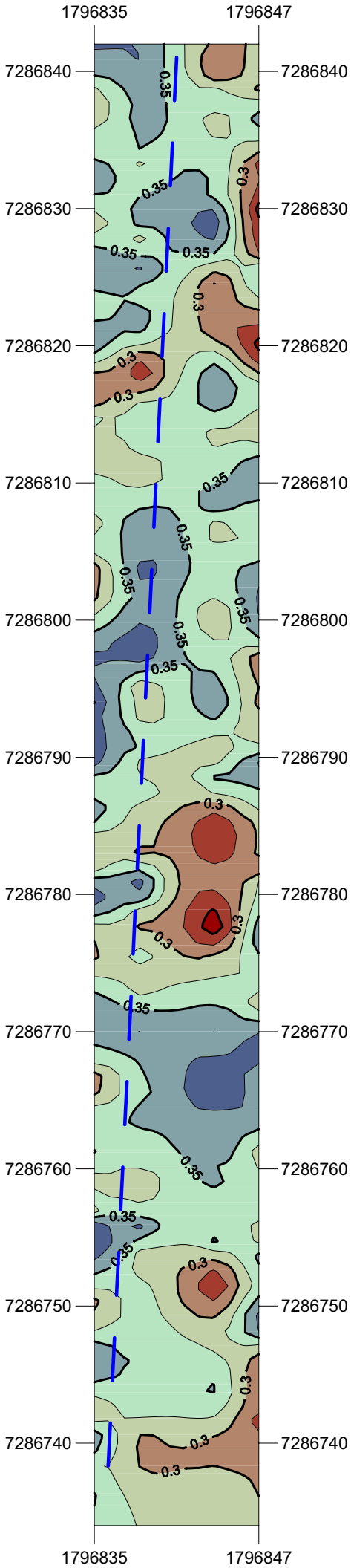

Isbrytarens färdväg från norr mot söder

Uppmätt ismäktighet georadar (m) 25 mars 2008

Interpolation från 4 mätlinjer i nordsydlig riktning

0.4
0.375
0.35
0.325
0.3
0.275
0.25
0.225
0.2

Manuell mätning framför isbrytare 2008-03-25

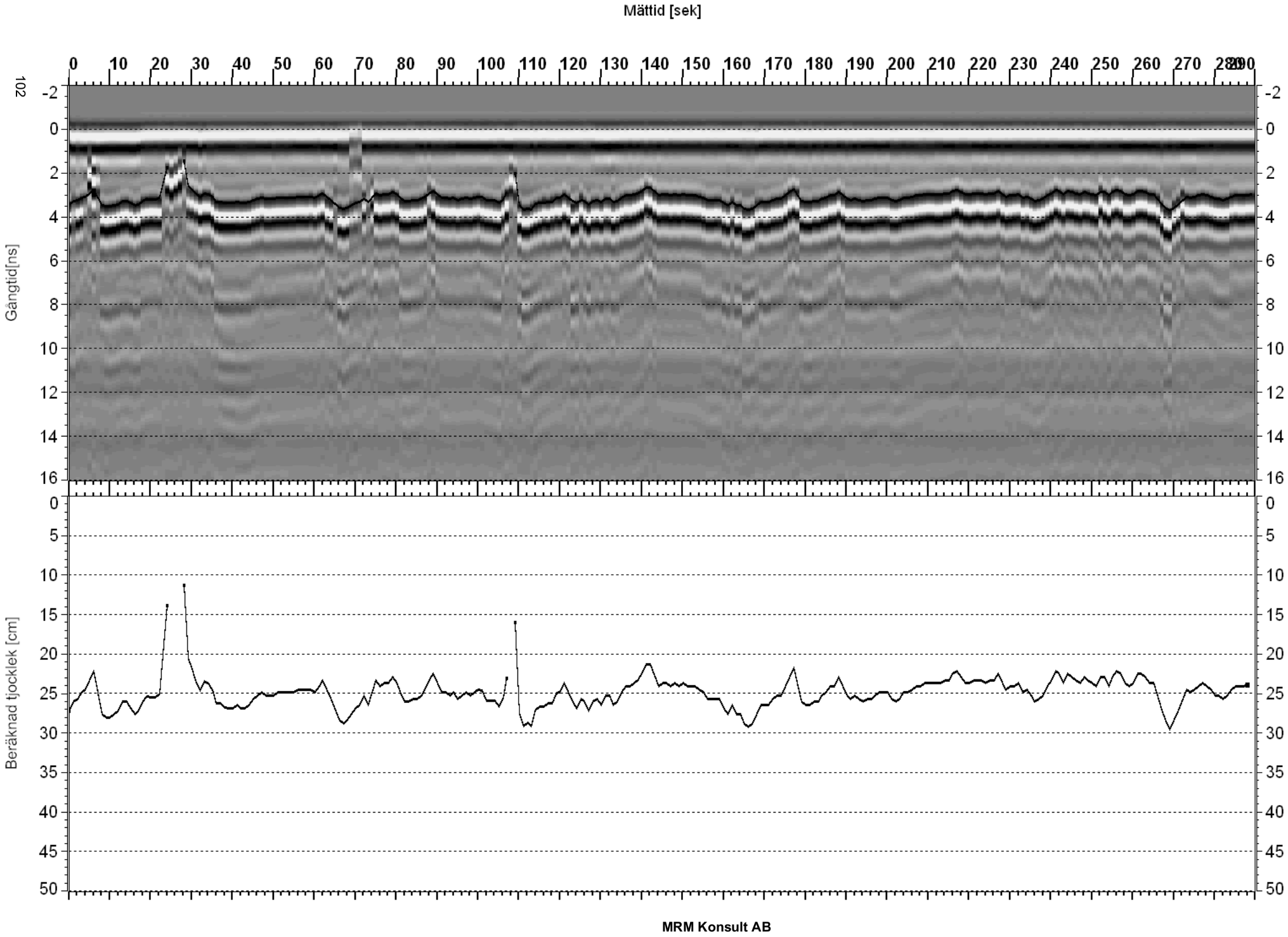

Test 12 29 mars 2008

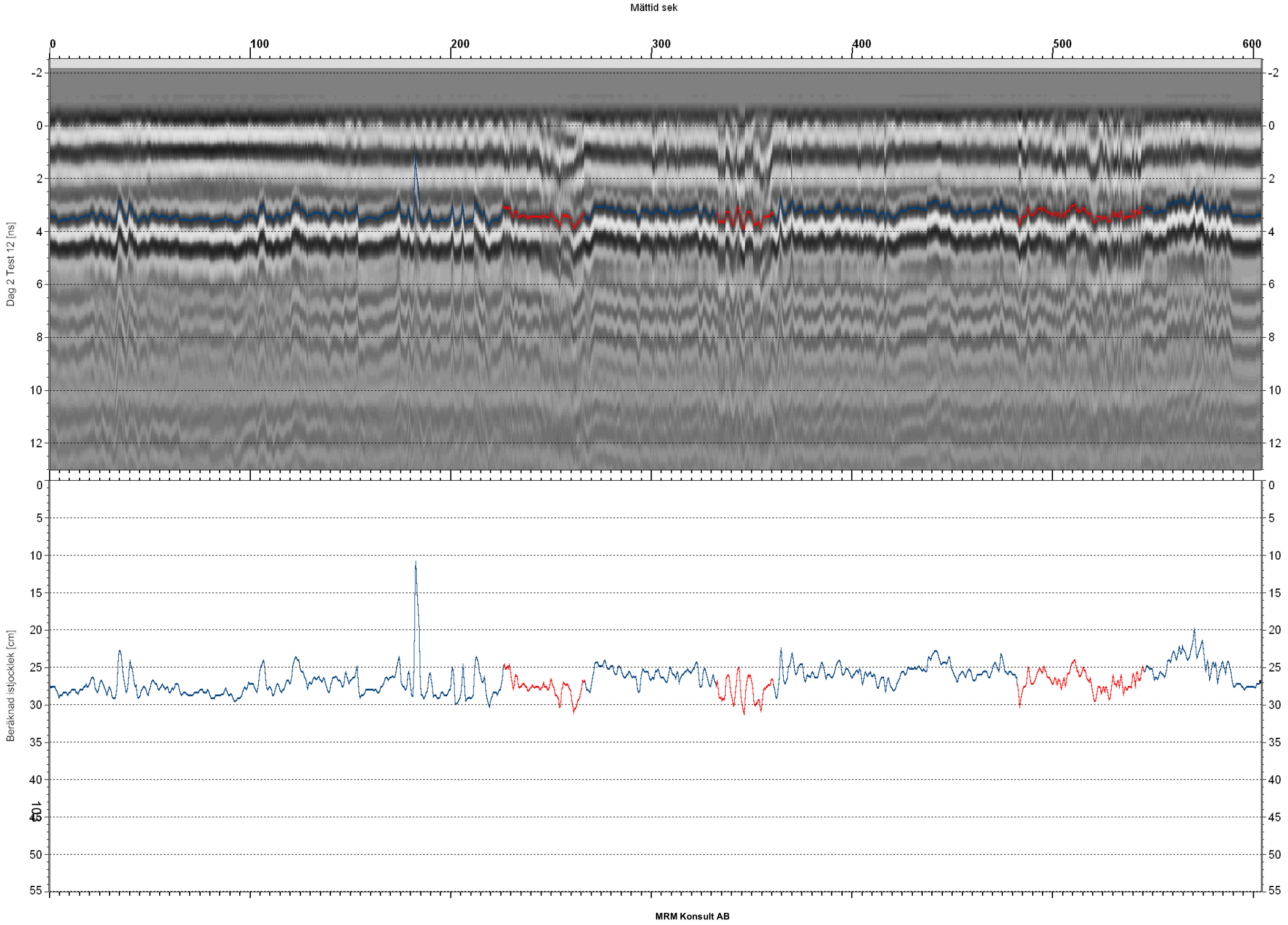

Test 13 29 mars 2008

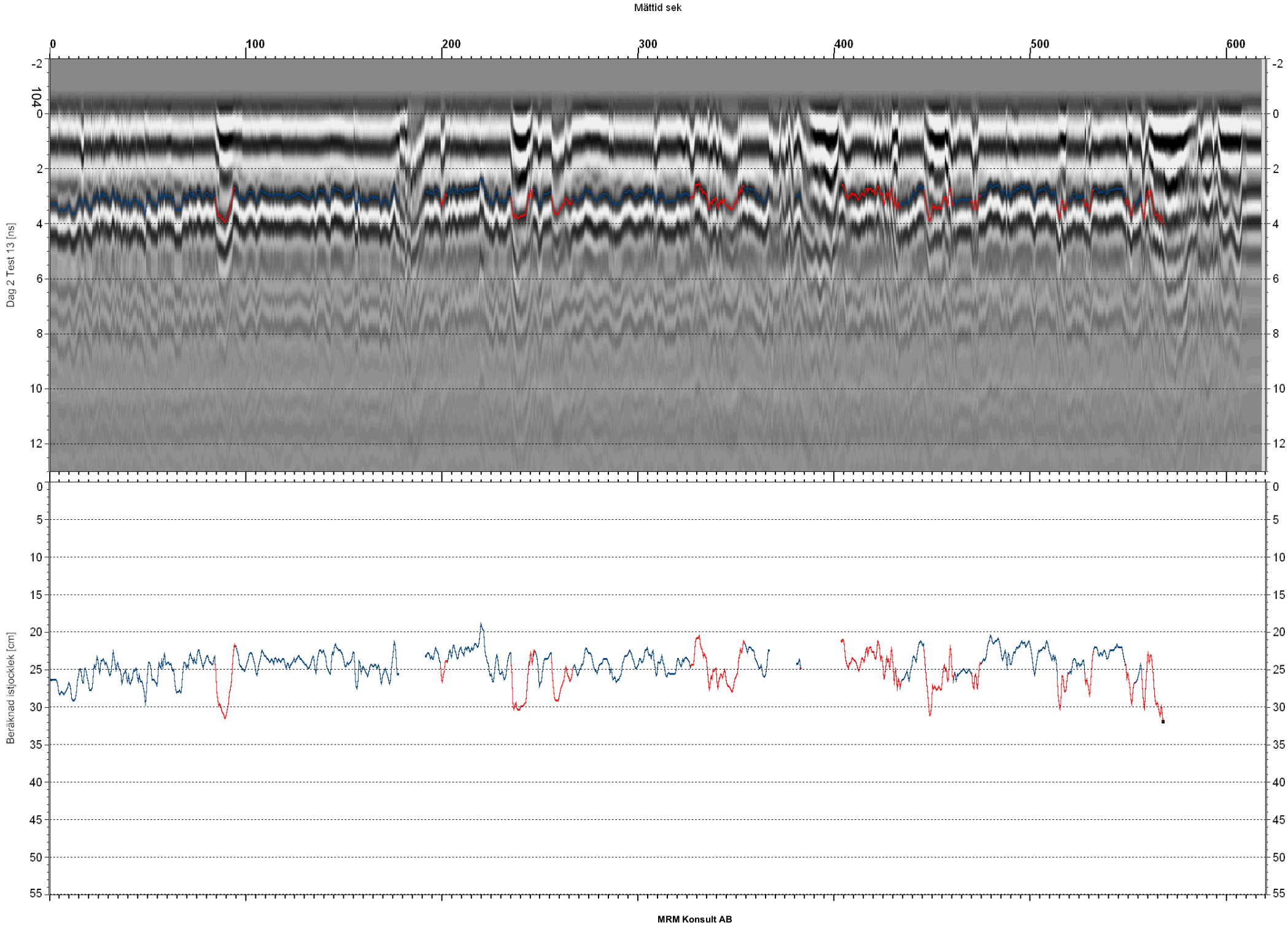

Test 14 29 mars 2008

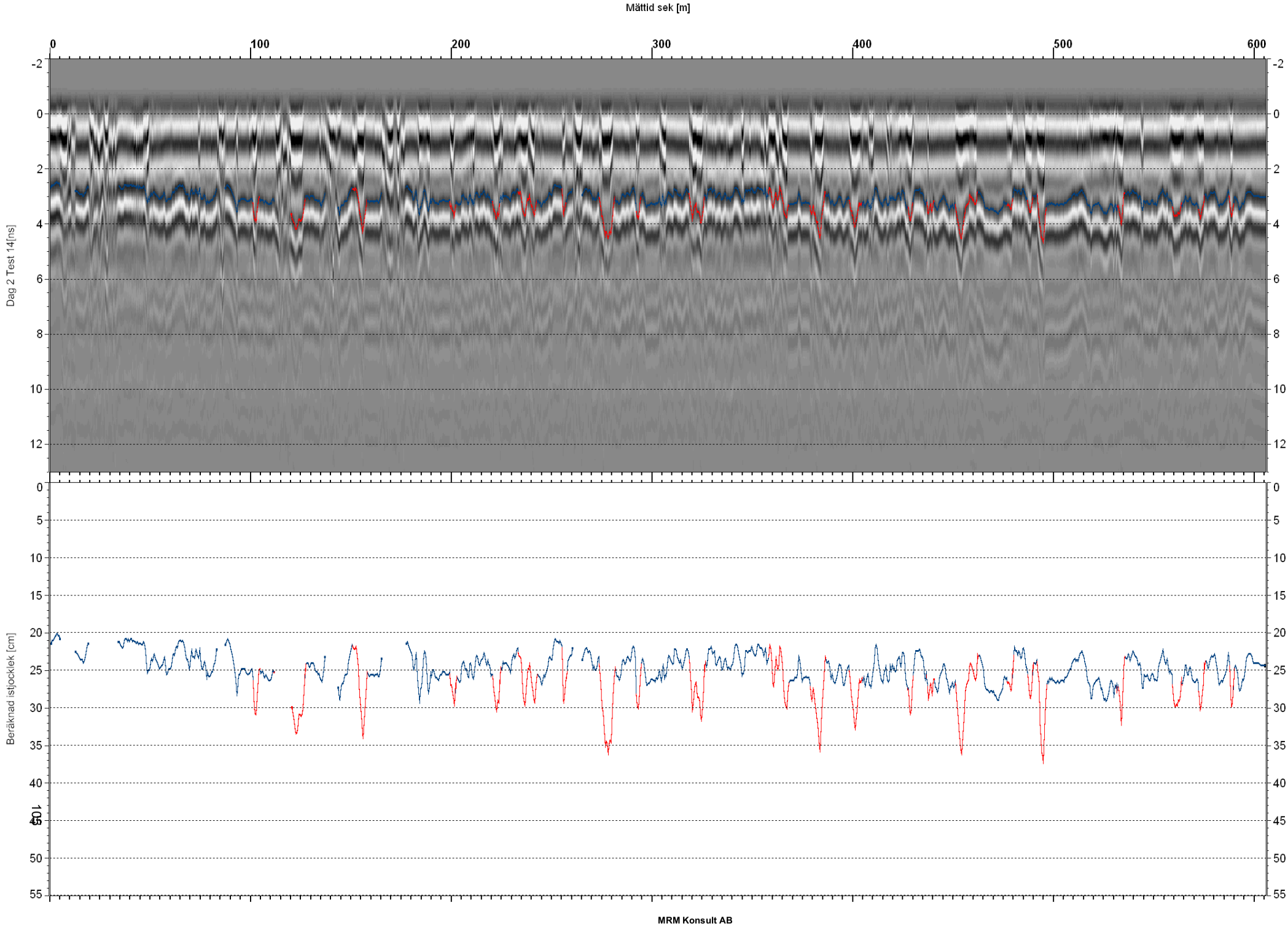

Test 15 29 mars 2008

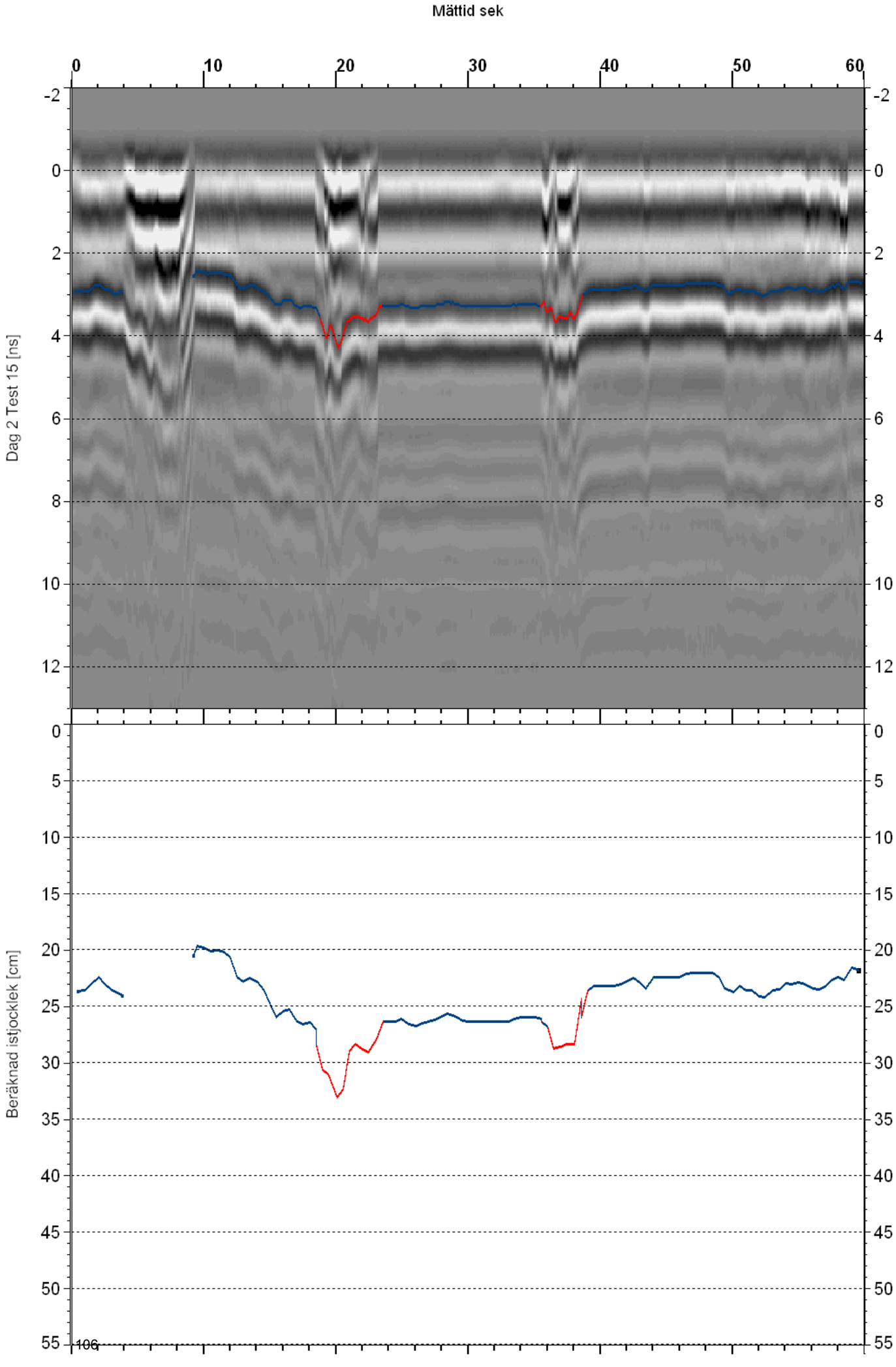

Test 16 29 mars 2008

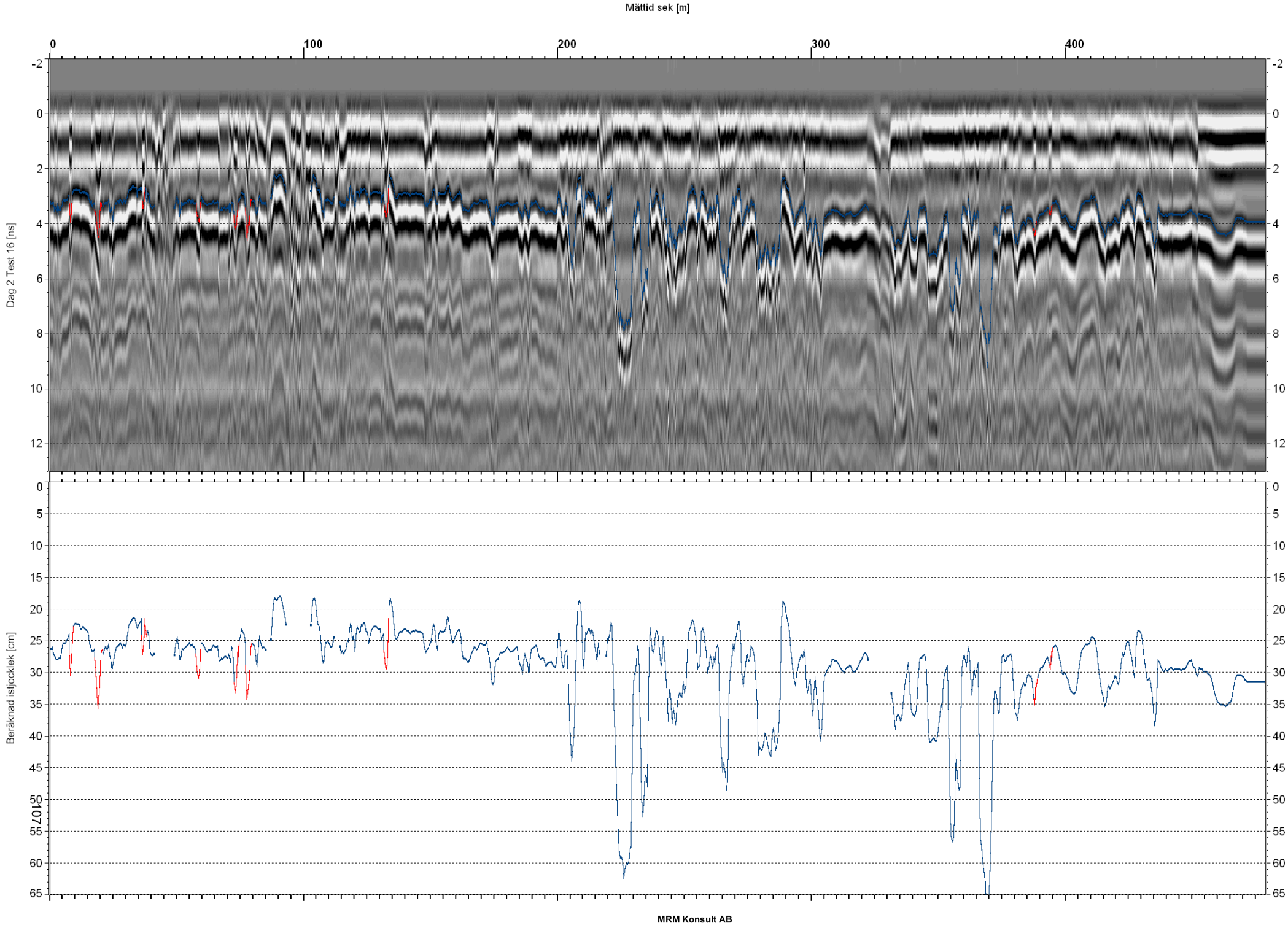

MRM Konsult AB

Försök 1 10 april 2008

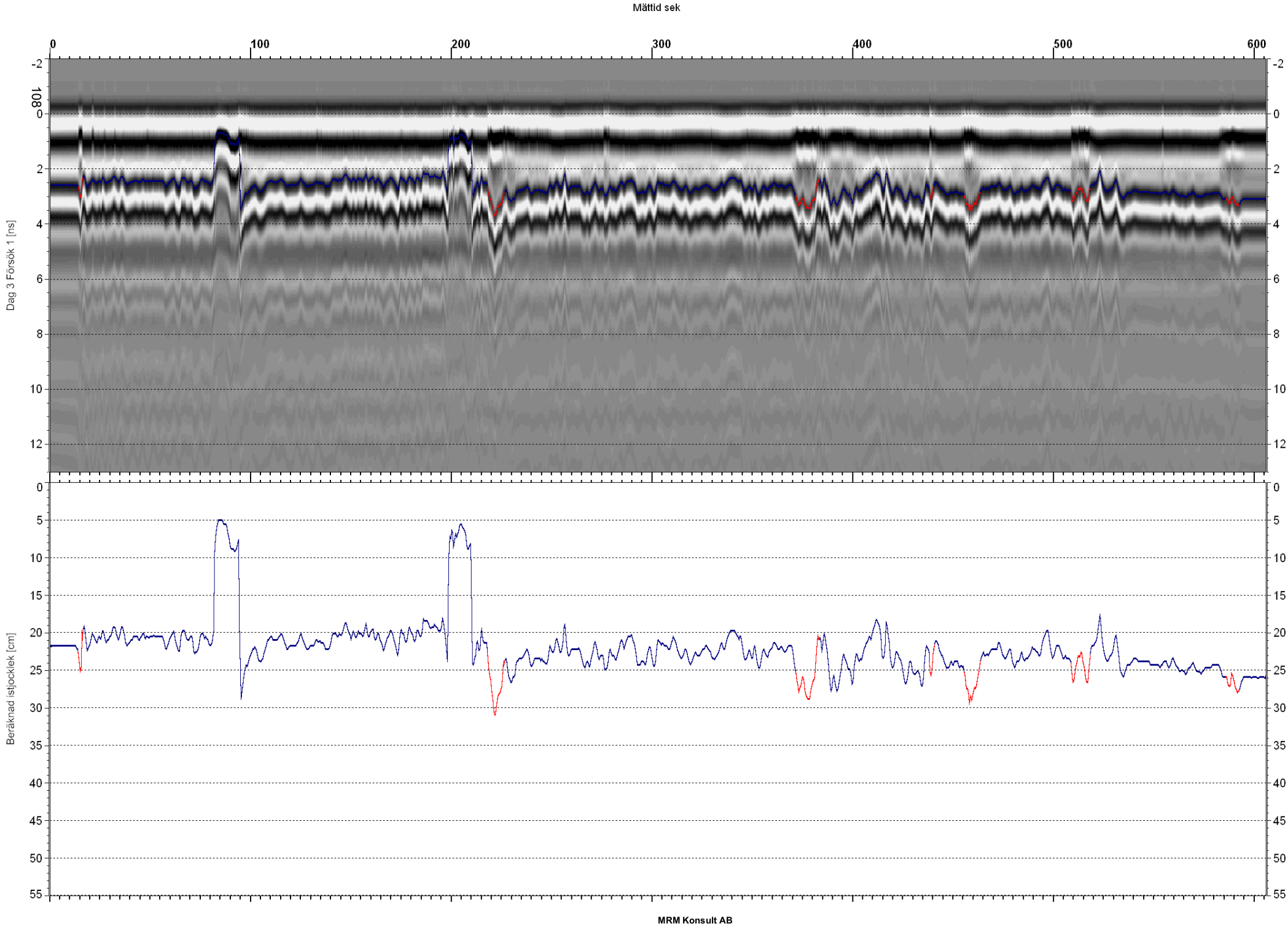

Försök 2 10 april 2008

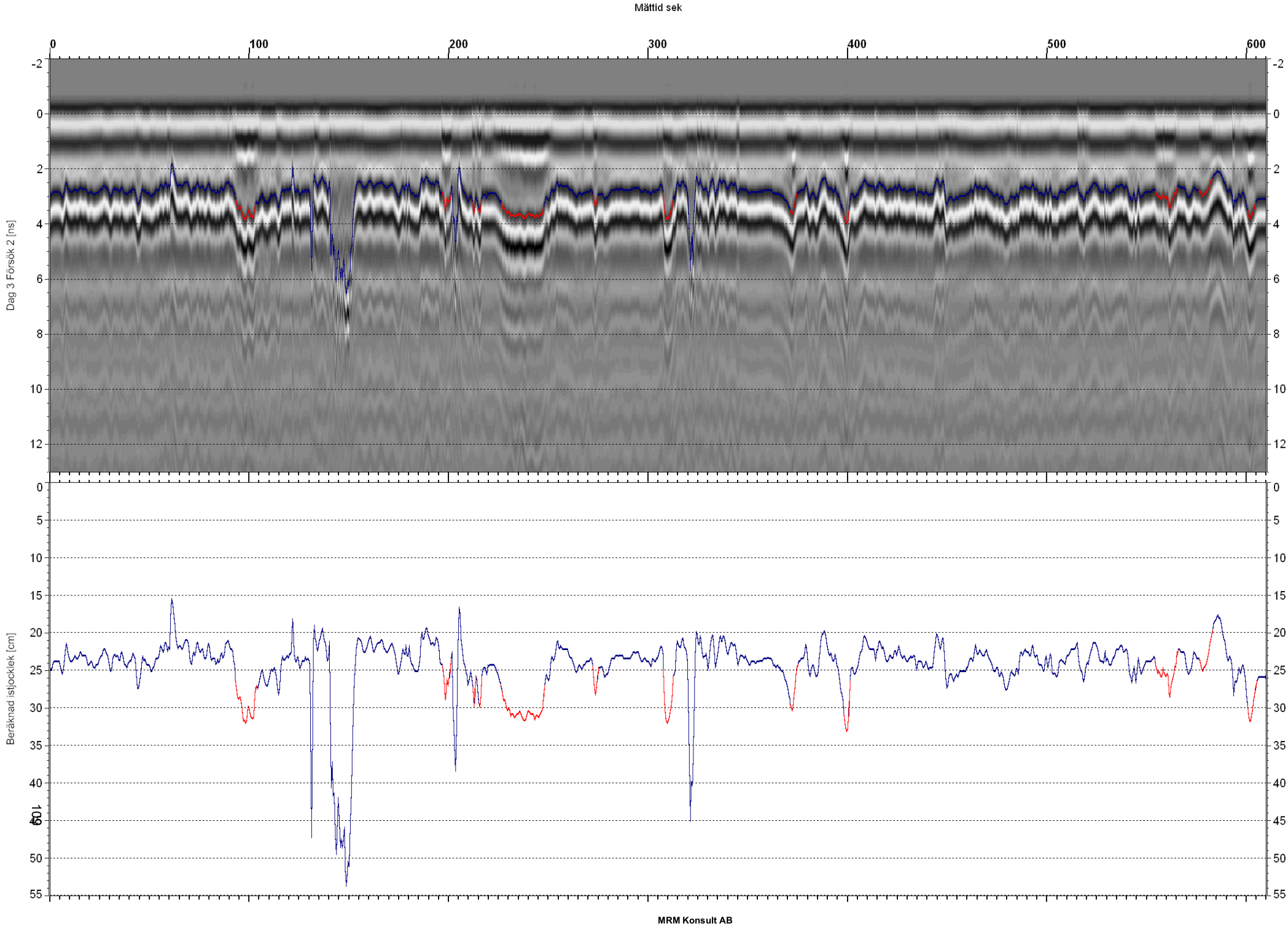

Försök 3 10 april 2008

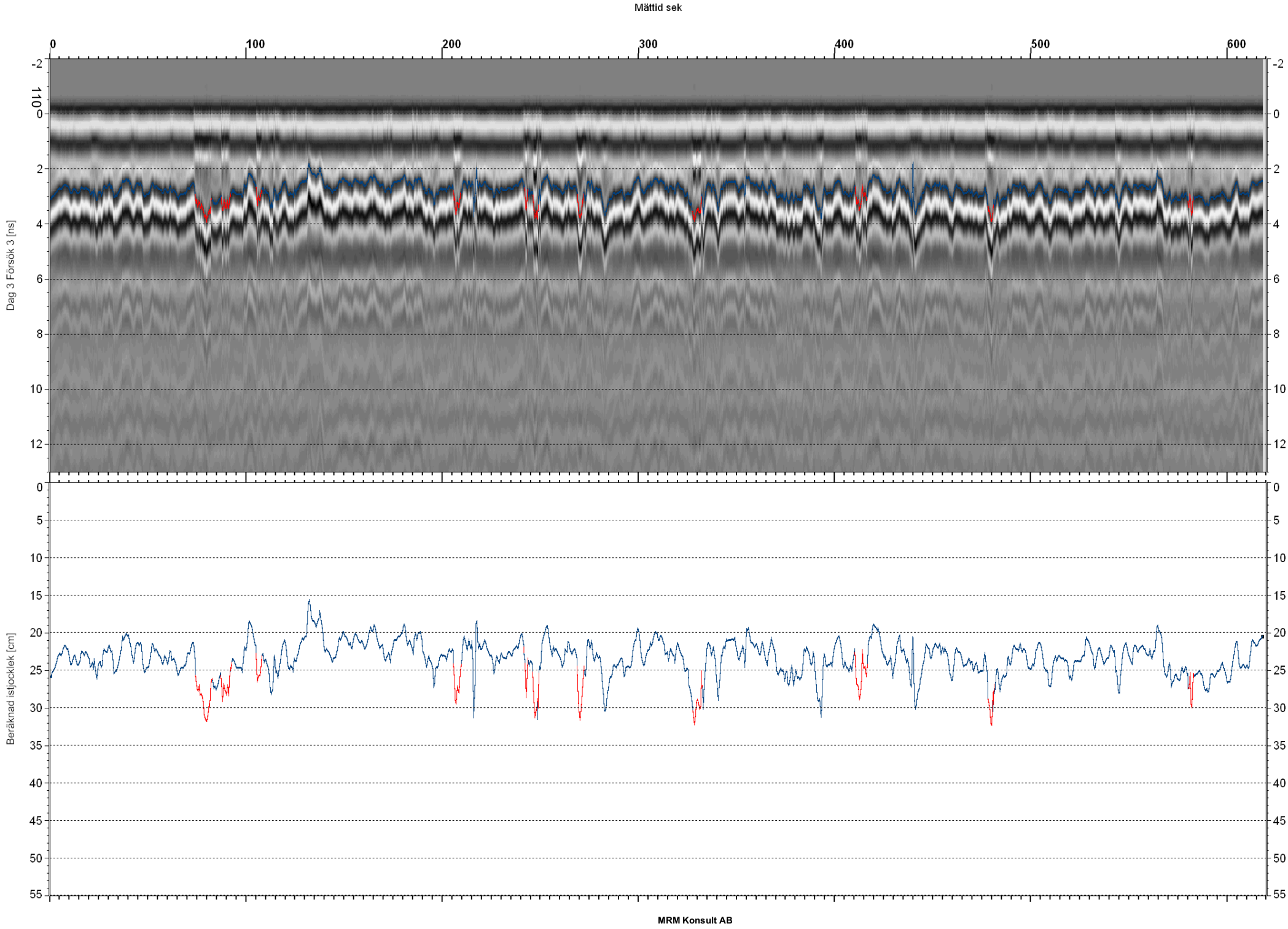

Bilaga C Islaster mot stålrör, diagram

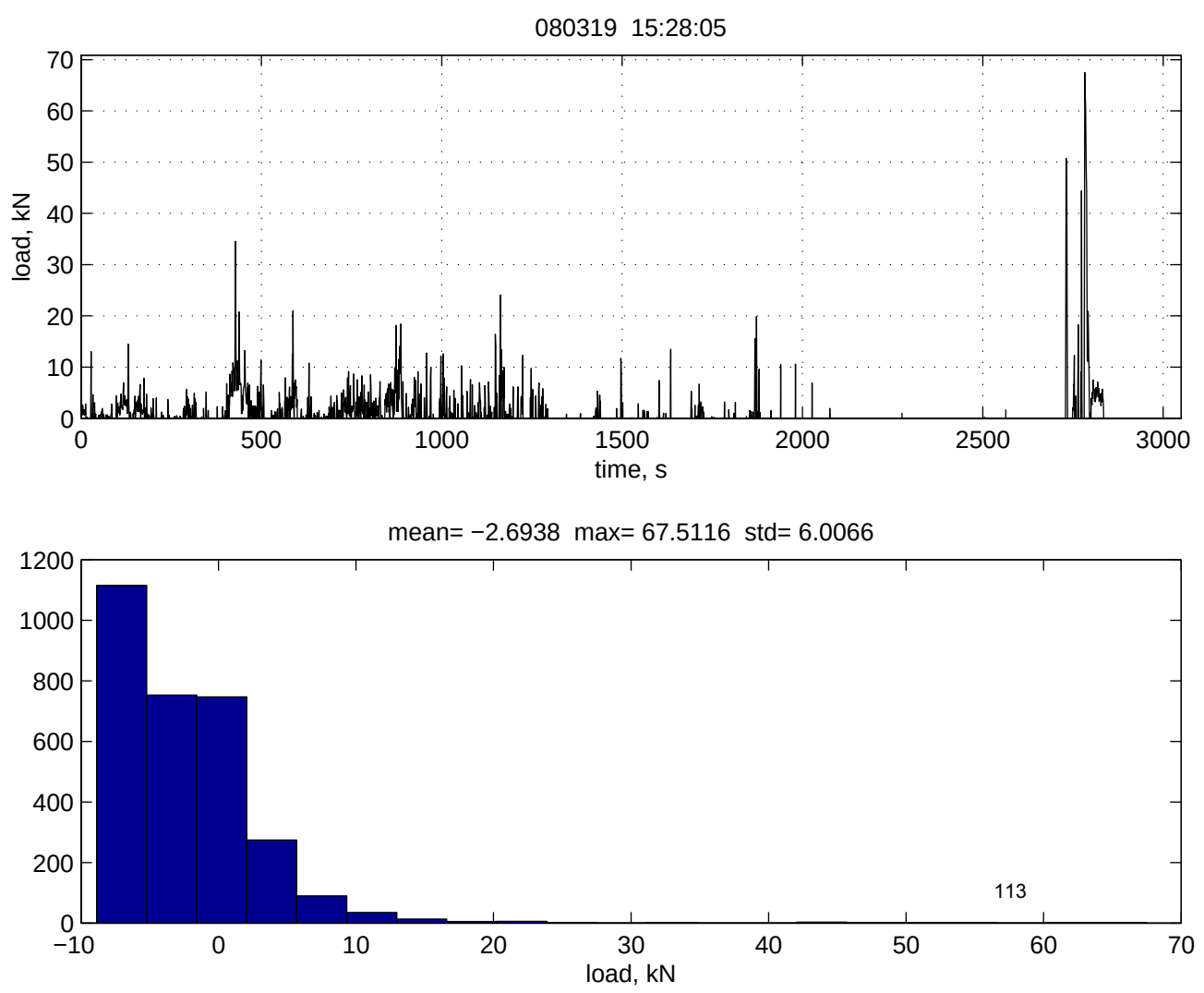
080319 15:28:05
load, kN
time, s
mean= −2.6938 max= 67.5116 std= 6.0066
113
load, kN

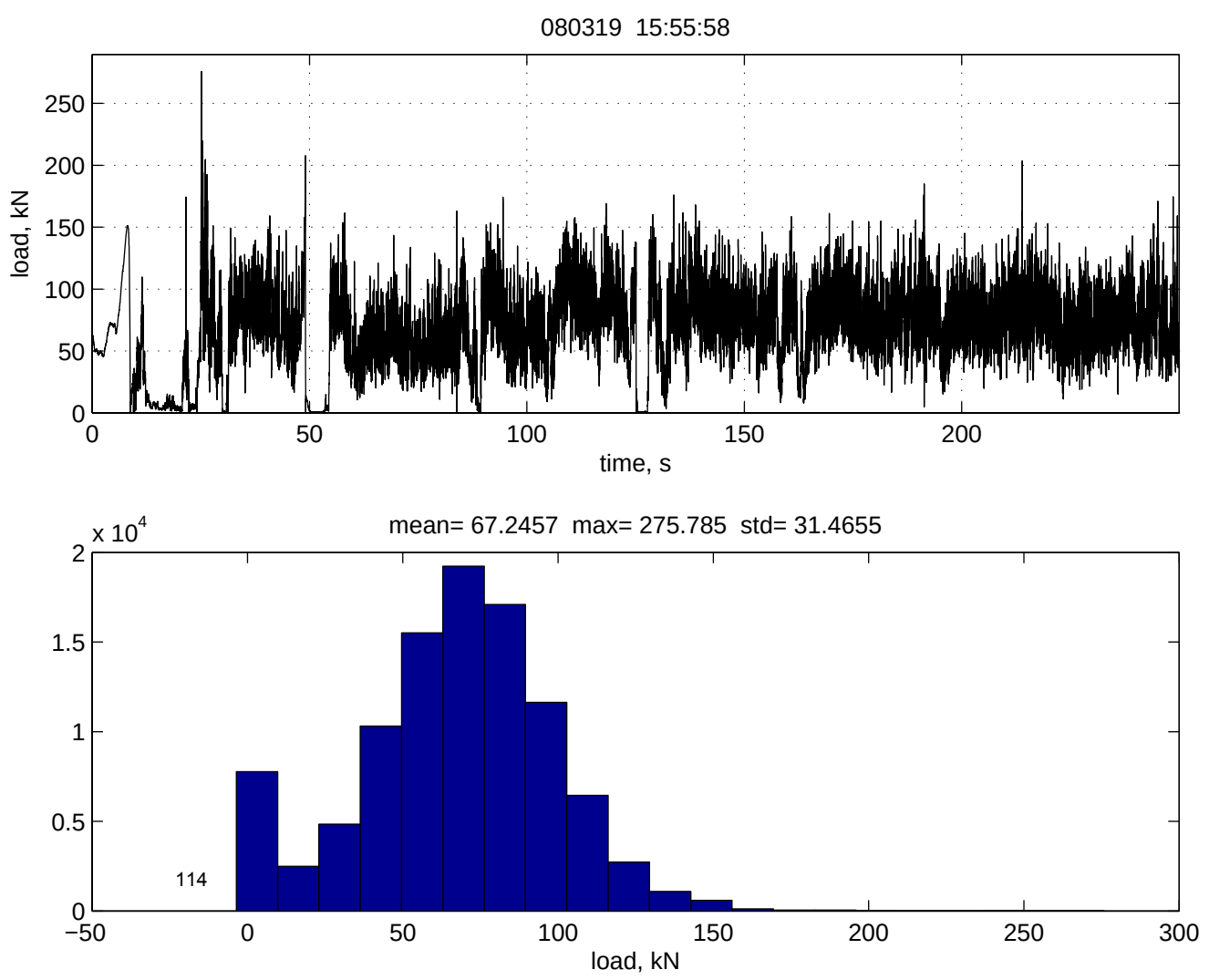
080319 15:55:58
load, kN
time, s
0
50
100
150
200
250
mean= 67.2457 max= 275.785 std= 31.4655
x 10^4
2
1.5
1
0.5
0
114
−50
0
50
100
150
200
250
300
load, kN

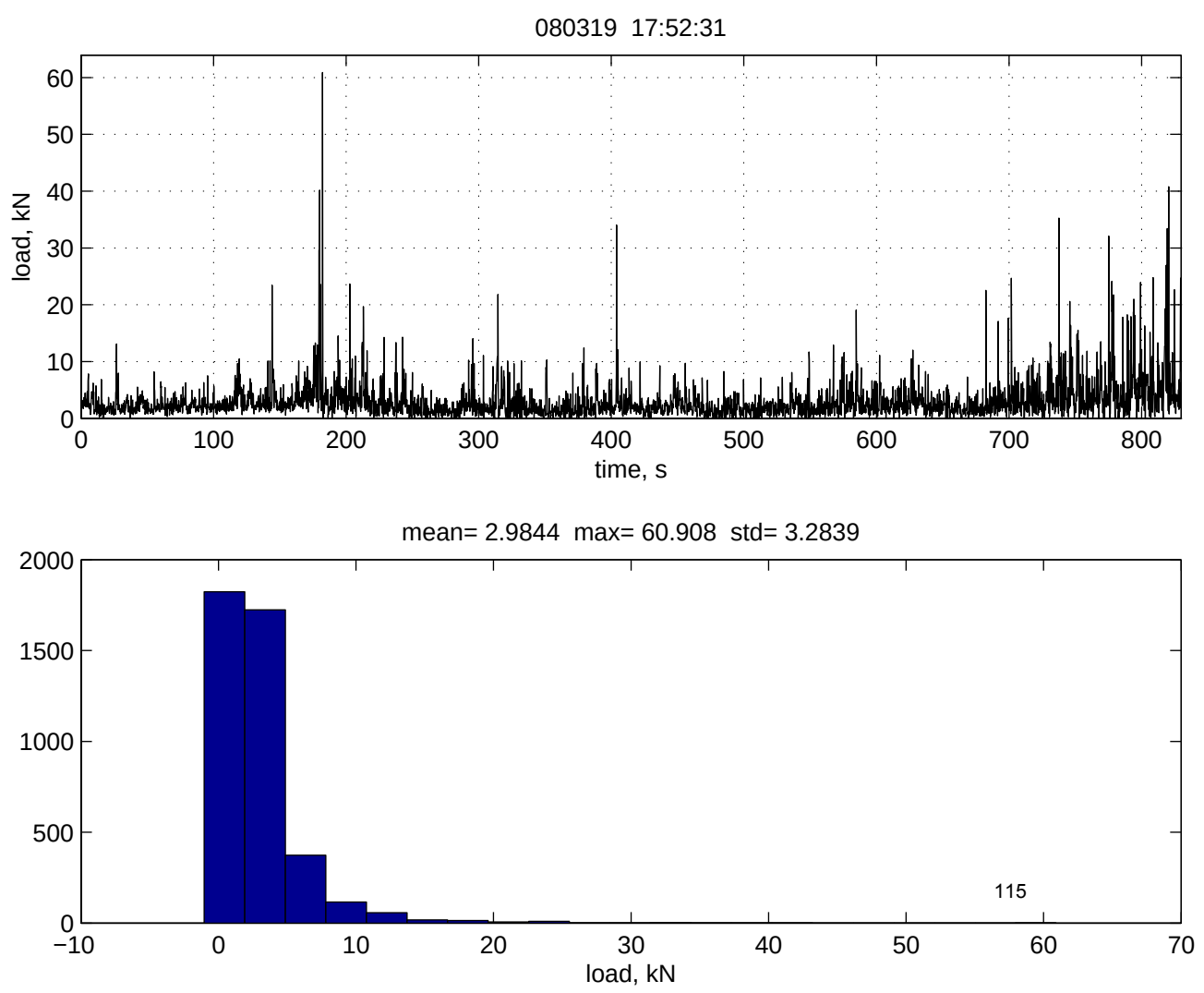
080319 17:52:31
load, kN
time, s
mean= 2.9844 max= 60.908 std= 3.2839
load, kN
115

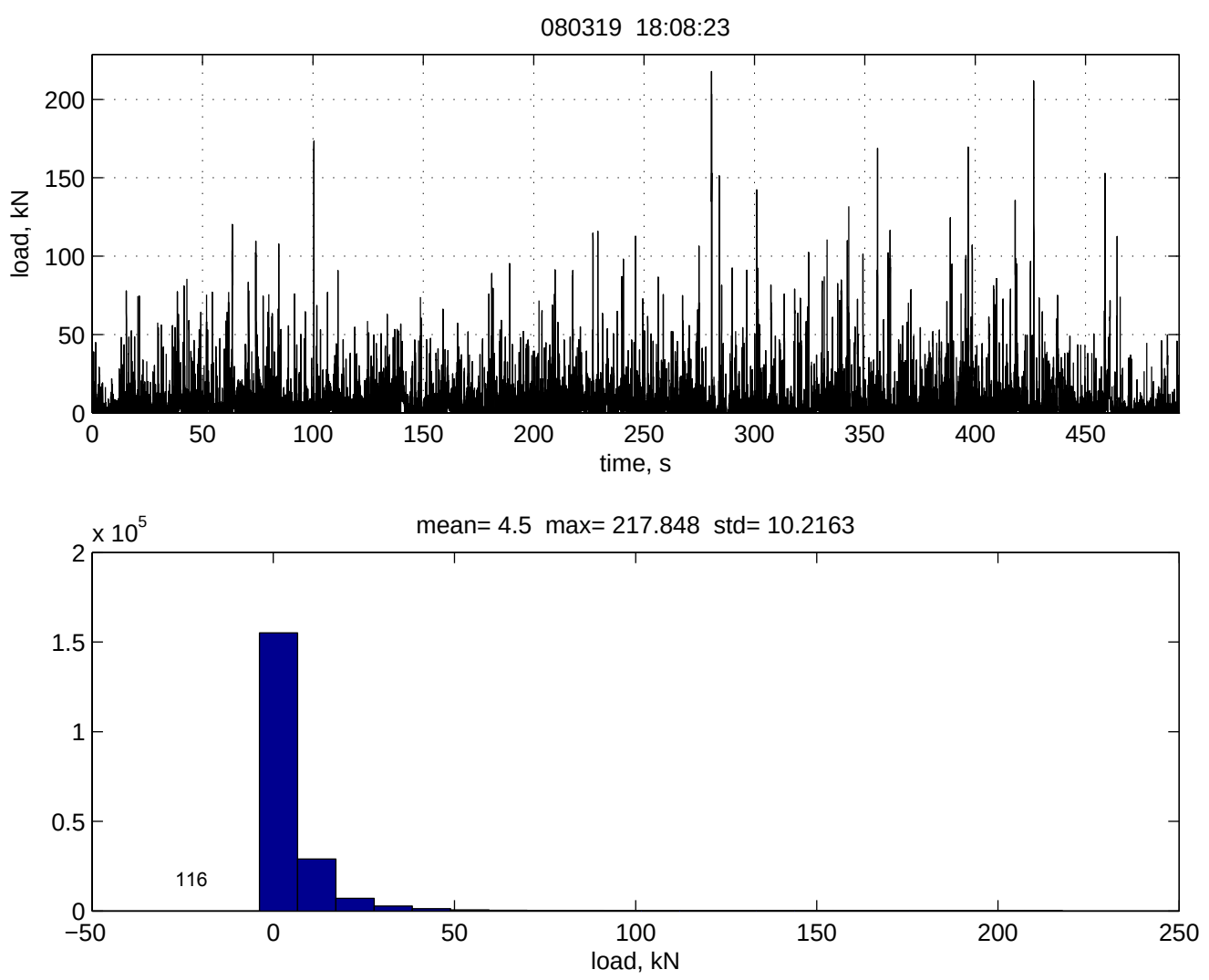
080319 18:08:23
load, kN
time, s
0
50
100
150
200
250
300
350
400
450
mean= 4.5 max= 217.848 std= 10.2163
x 10^5
2
1.5
1
0.5
116
−50
load, kN

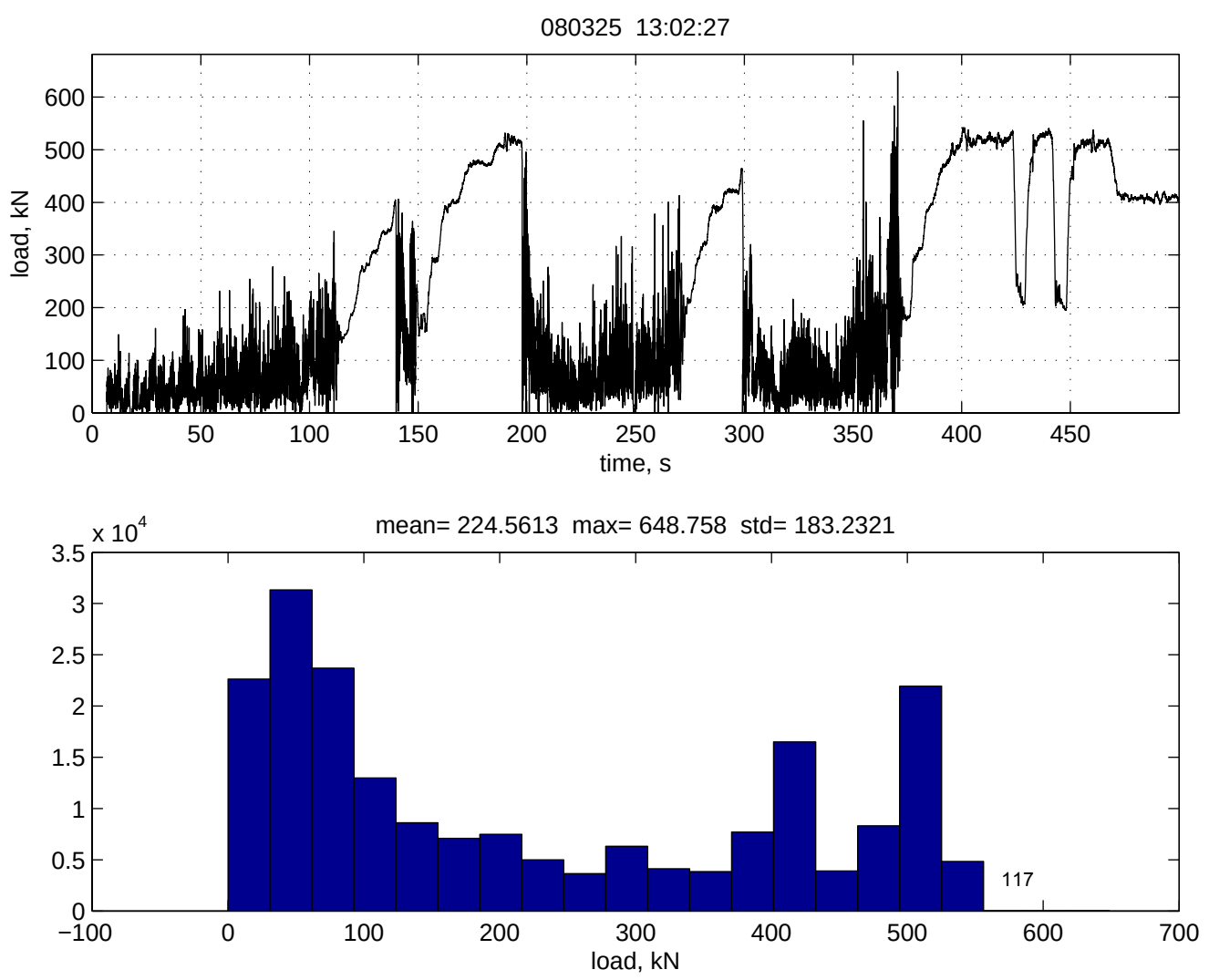
080325 13:02:27
load, kN
time, s
0
50
100
150
200
250
300
350
400
450
100
200
300
400
500
600
x 10^4
mean= 224.5613 max= 648.758 std= 183.2321
3.5
3
2.5
2
1.5
1
0.5
117
−100
700
load, kN

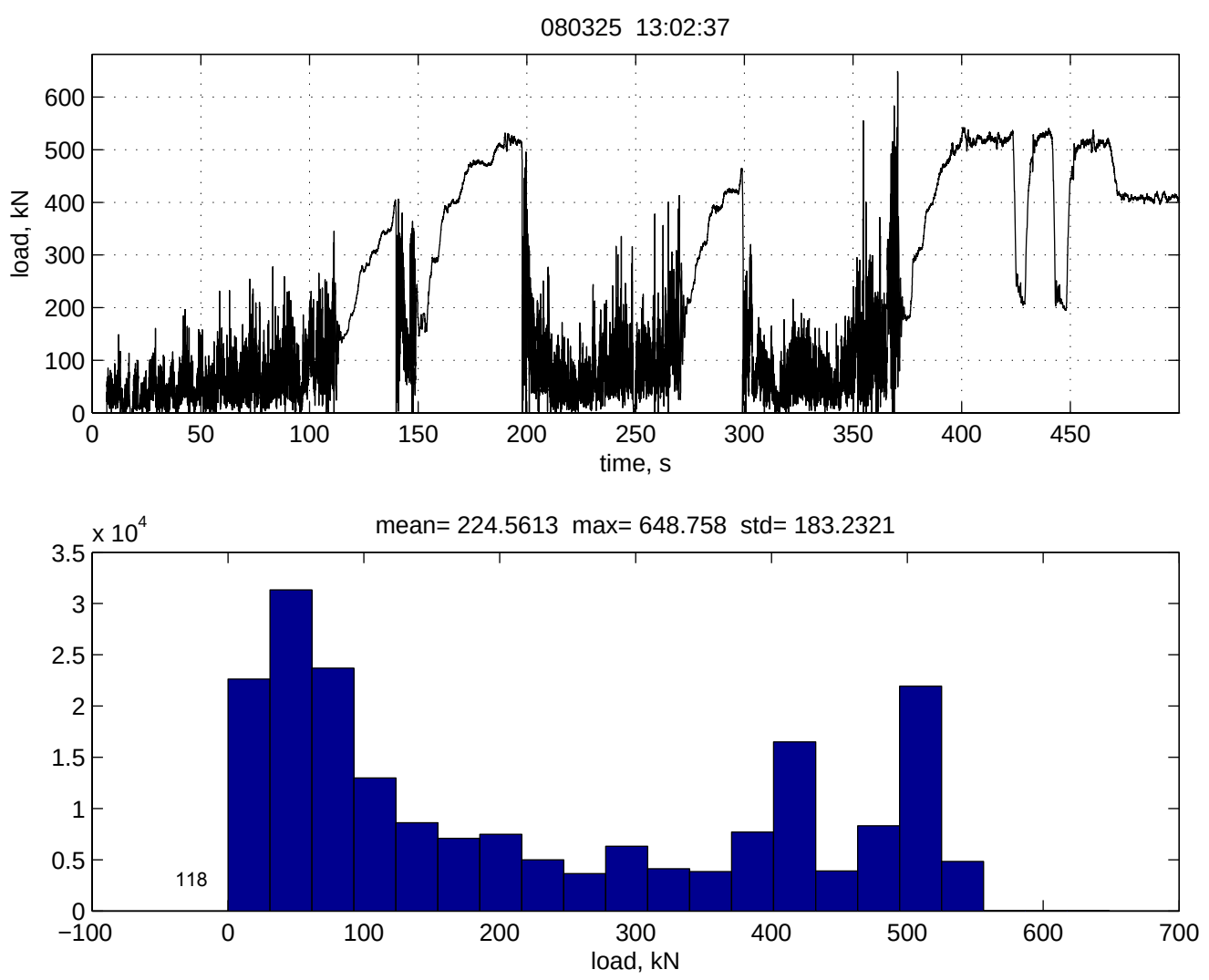
080325 13:02:37
load, kN
time, s
0
50
100
150
200
250
300
350
400
450
100
200
300
400
500
600
x 10^4
mean= 224.5613 max= 648.758 std= 183.2321
118
load, kN
−100
0
100
200
300
400
500
600
700
0.5
1
1.5
2
2.5
3
3.5

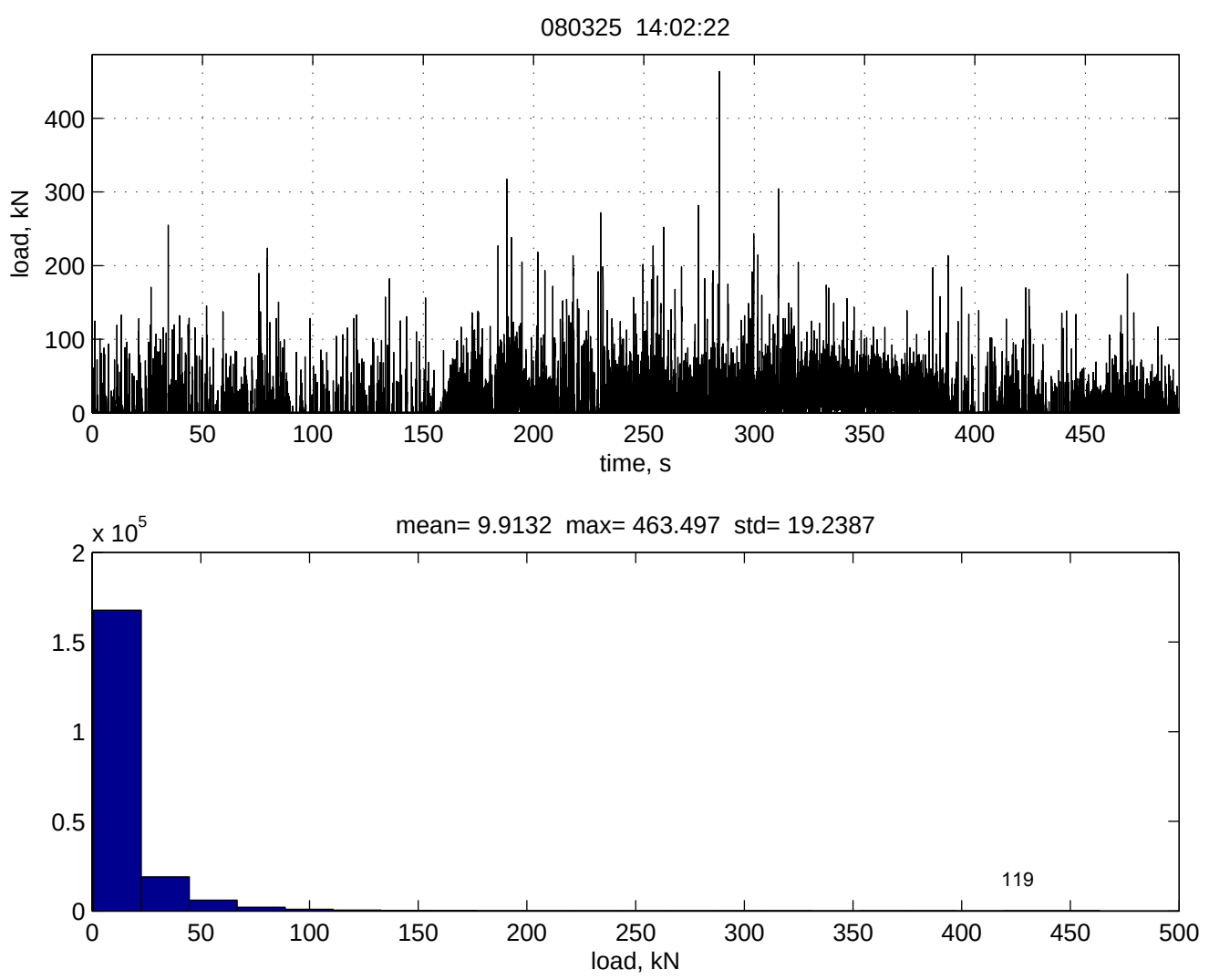
080325 14:02:22
load, kN
time, s
mean= 9.9132 max= 463.497 std= 19.2387
x 10^5
load, kN
119

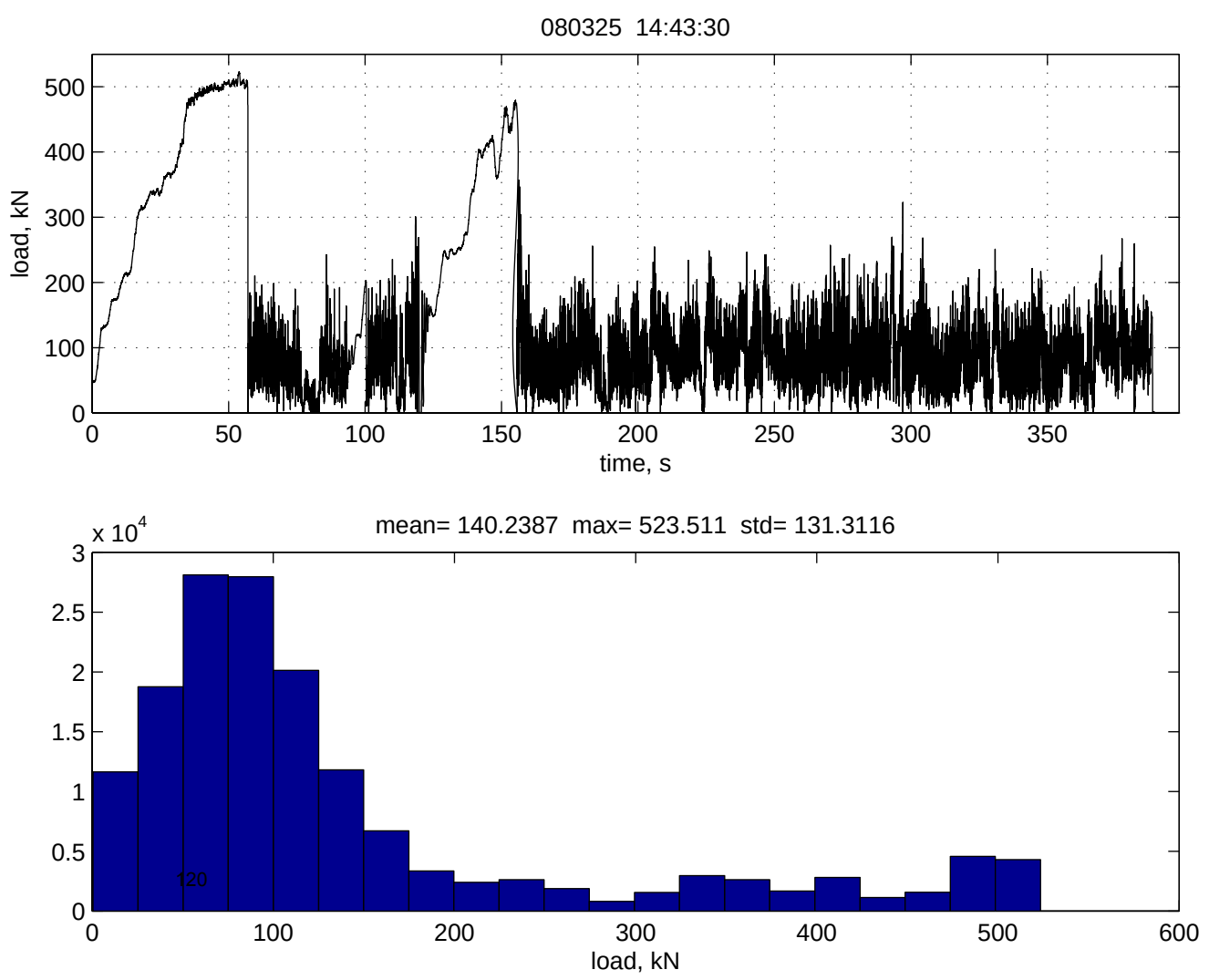
080325 14:43:30
load, kN
time, s
x 10^4
mean= 140.2387 max= 523.511 std= 131.3116
120
load, kN

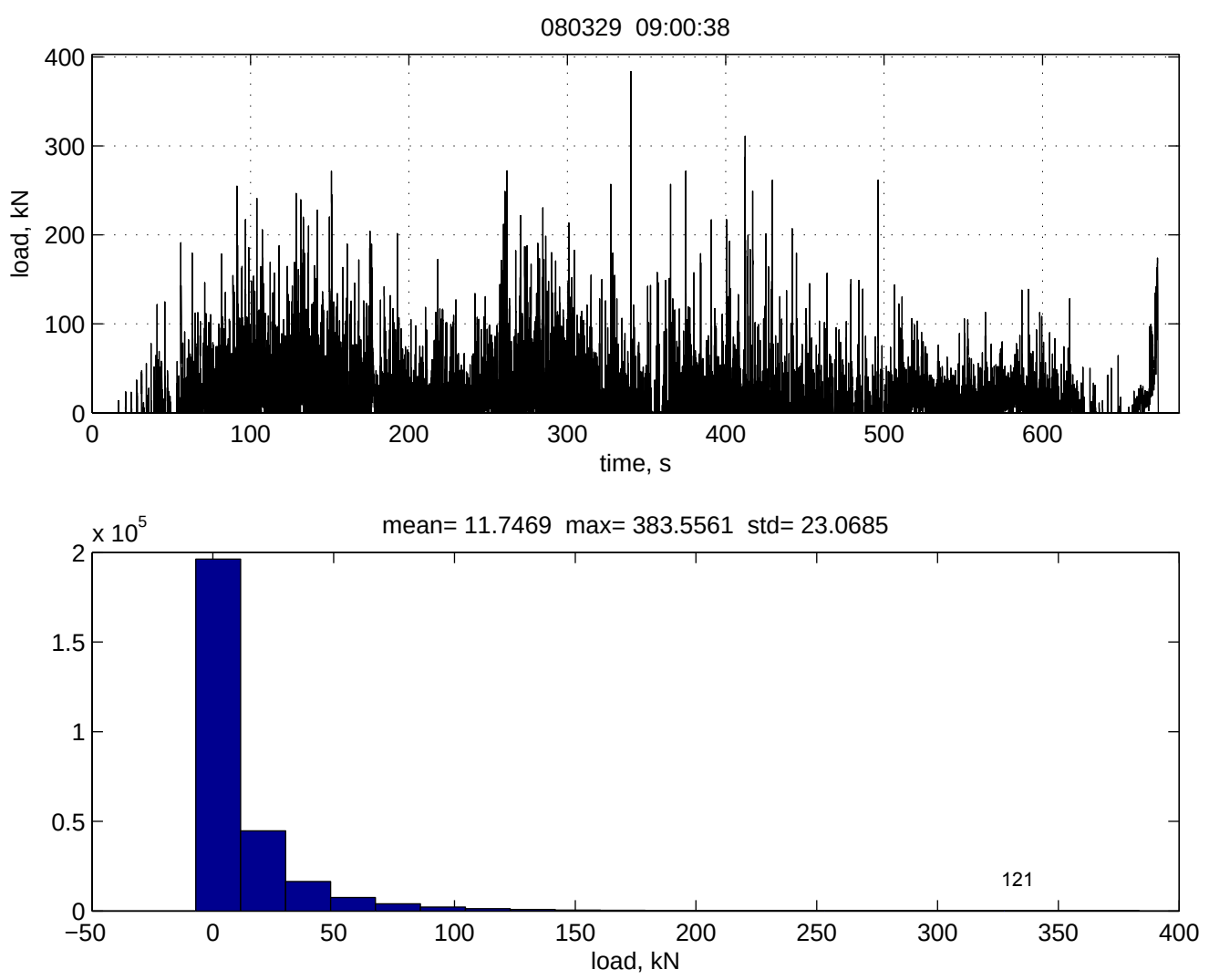
080329 09:00:38
load, kN
time, s
0
100
200
300
400
500
600
mean= 11.7469 max= 383.5561 std= 23.0685
x 10^5
2
1.5
1
0.5
0
−50
0
50
100
150
200
250
300
350
400
load, kN
121

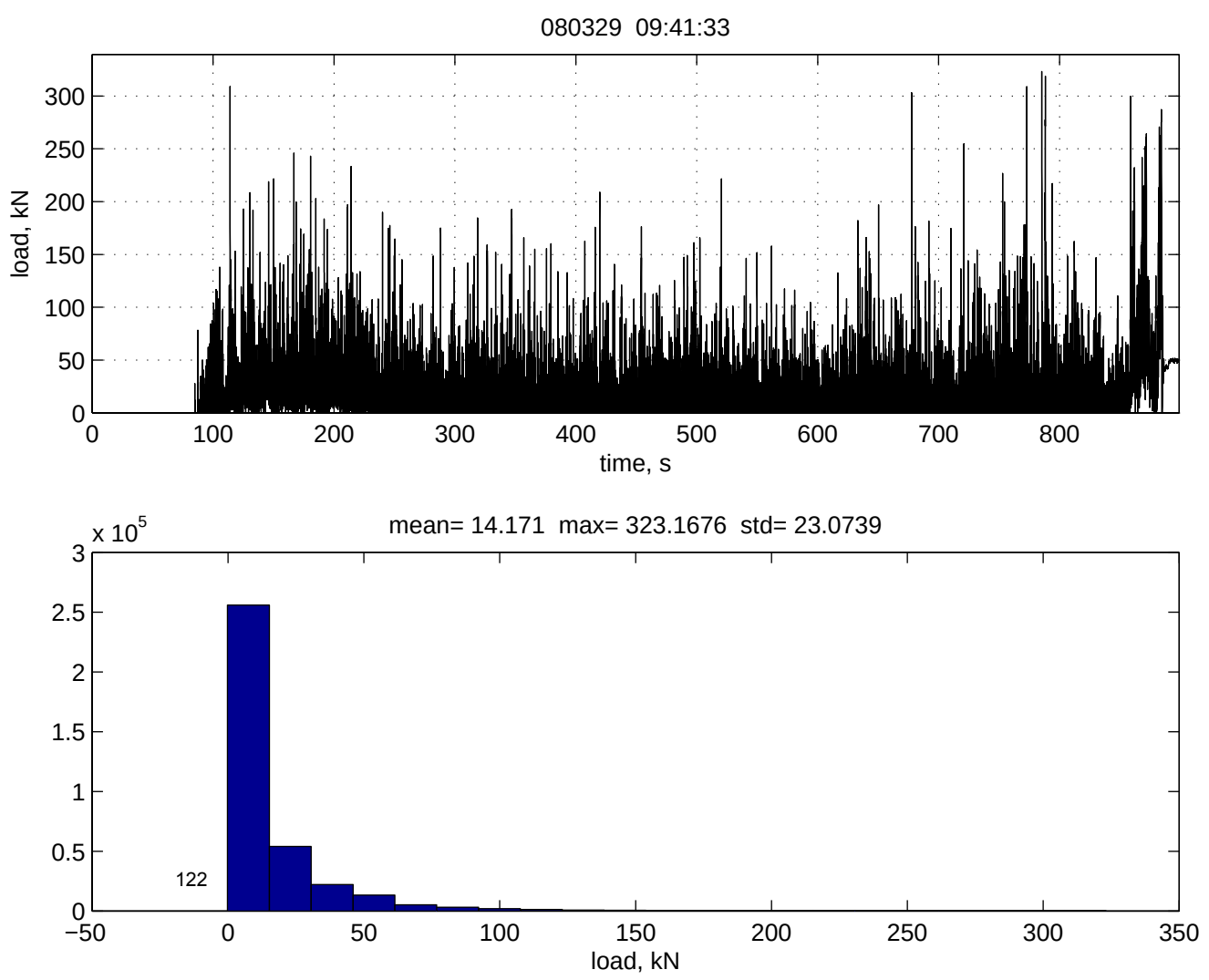
080329 09:41:33
load, kN
time, s
0
50
100
150
200
250
300
0
100
200
300
400
500
600
700
800
x 10^5
mean= 14.171 max= 323.1676 std= 23.0739
122
load, kN
−50
0
50
100
150
200
250
300
350
0
0.5
1
1.5
2
2.5
3

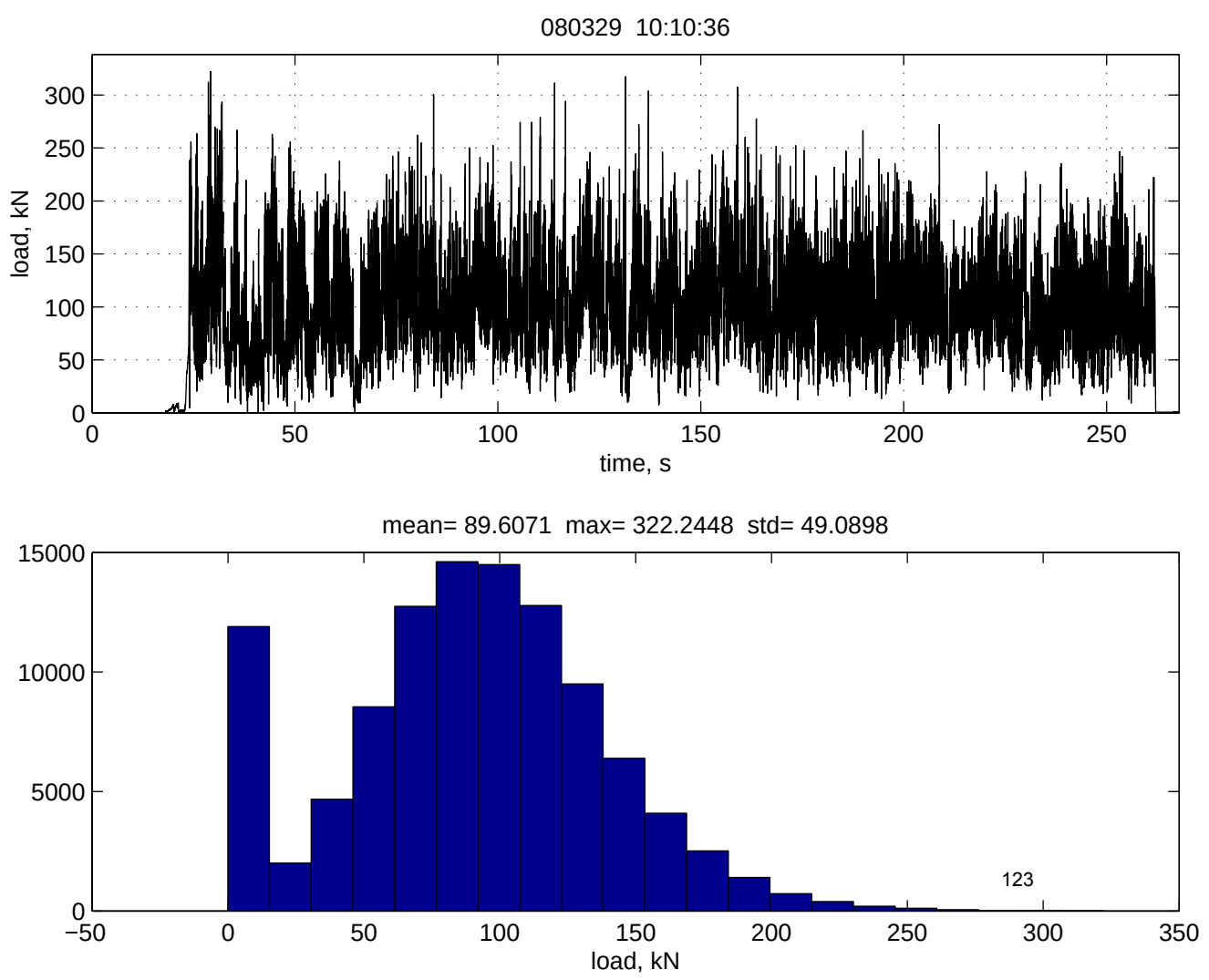
080329 10:10:36
load, kN
time, s
0
50
100
150
200
250
300
mean= 89.6071 max= 322.2448 std= 49.0898
15000
10000
5000
0
−50
0
50
100
150
200
250
300
350
load, kN
123

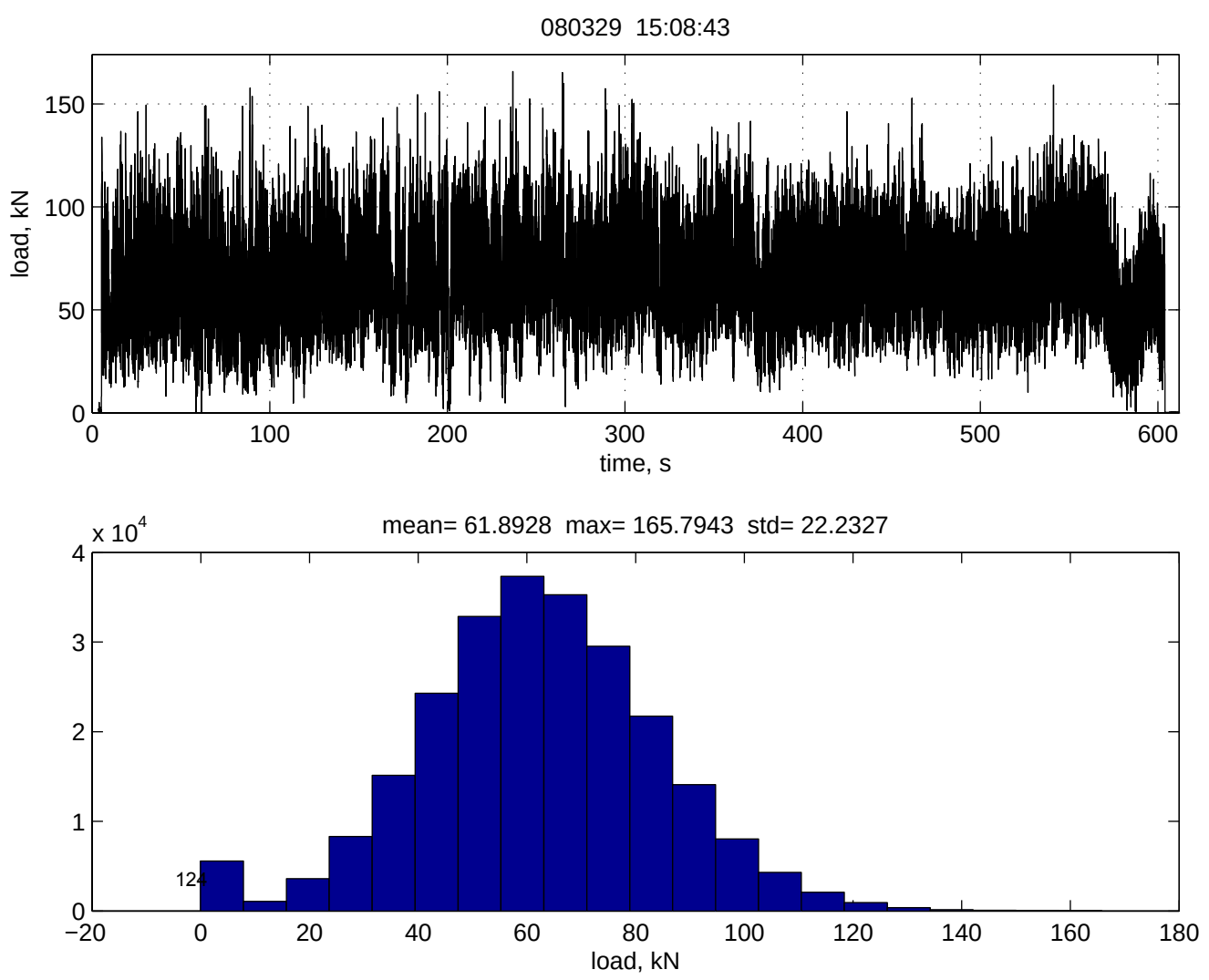
080329 15:08:43
load, kN
time, s
mean= 61.8928 max= 165.7943 std= 22.2327
x 10^4
load, kN

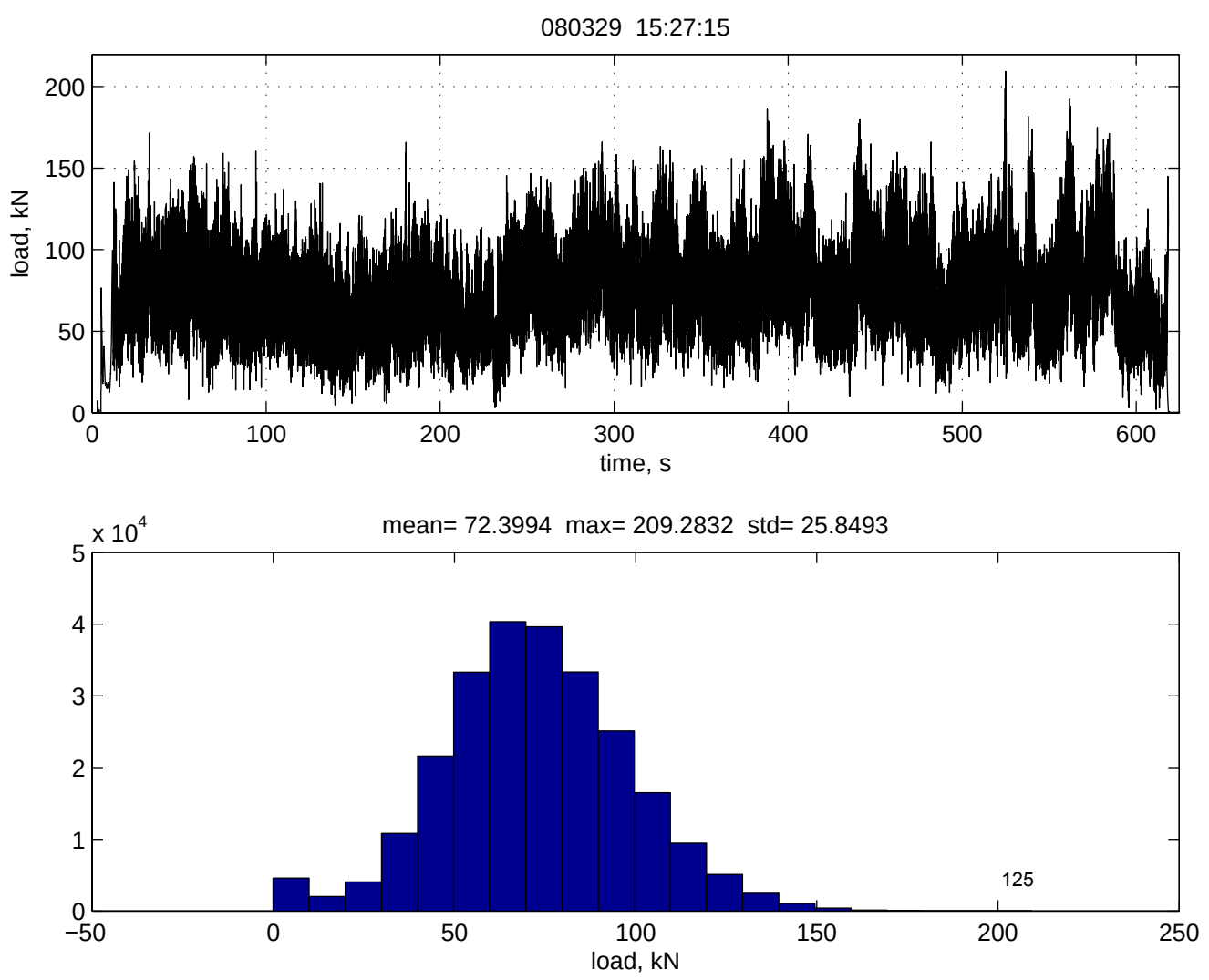
080329 15:27:15
load, kN
time, s
0
50
100
150
200
0
100
200
300
400
500
600
x 10^4
mean= 72.3994 max= 209.2832 std= 25.8493
125
load, kN
−50
0
50
100
150
200
250
1
2
3
4
5

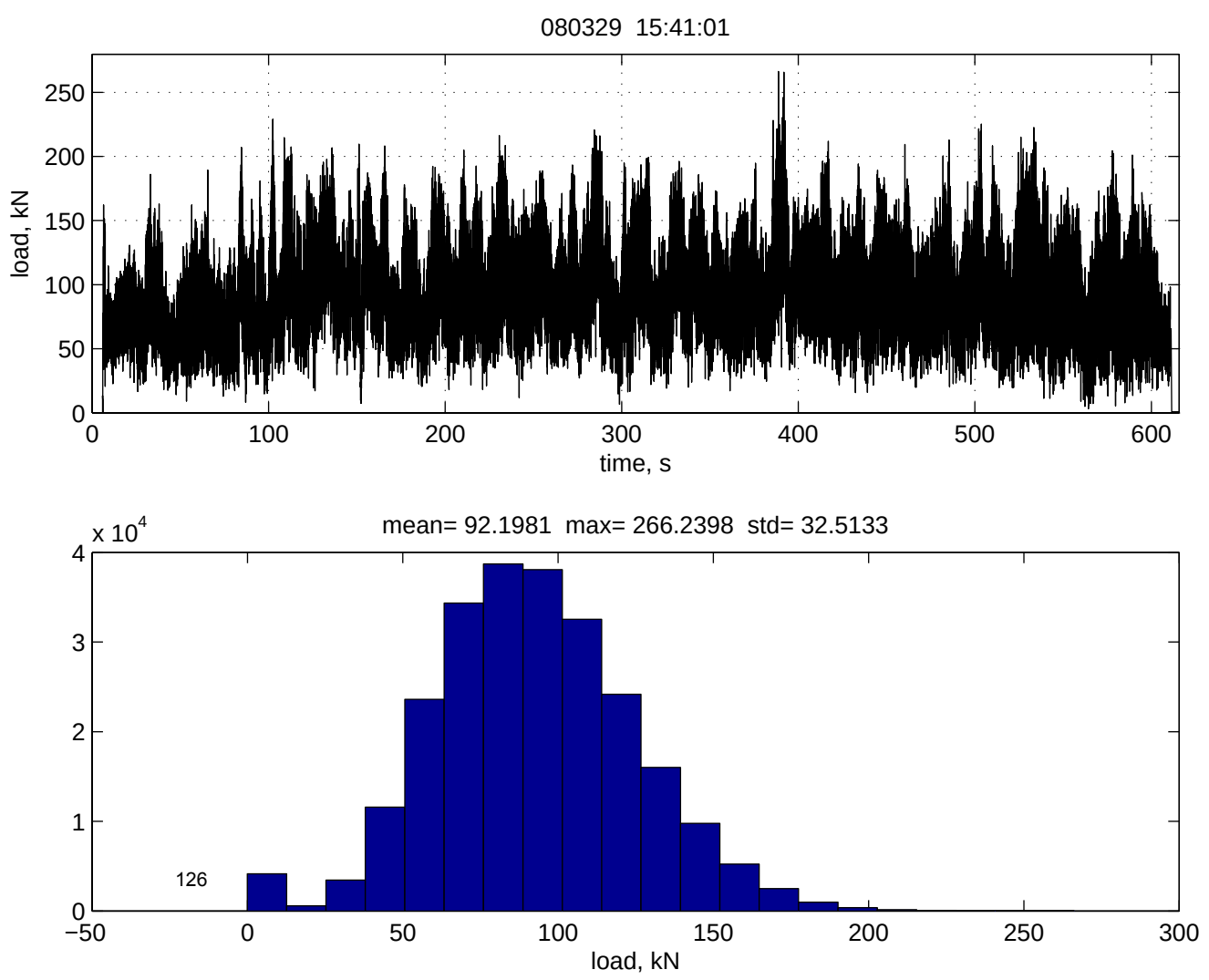
080329 15:41:01
load, kN
time, s
mean= 92.1981 max= 266.2398 std= 32.5133
x 10^4
126
load, kN

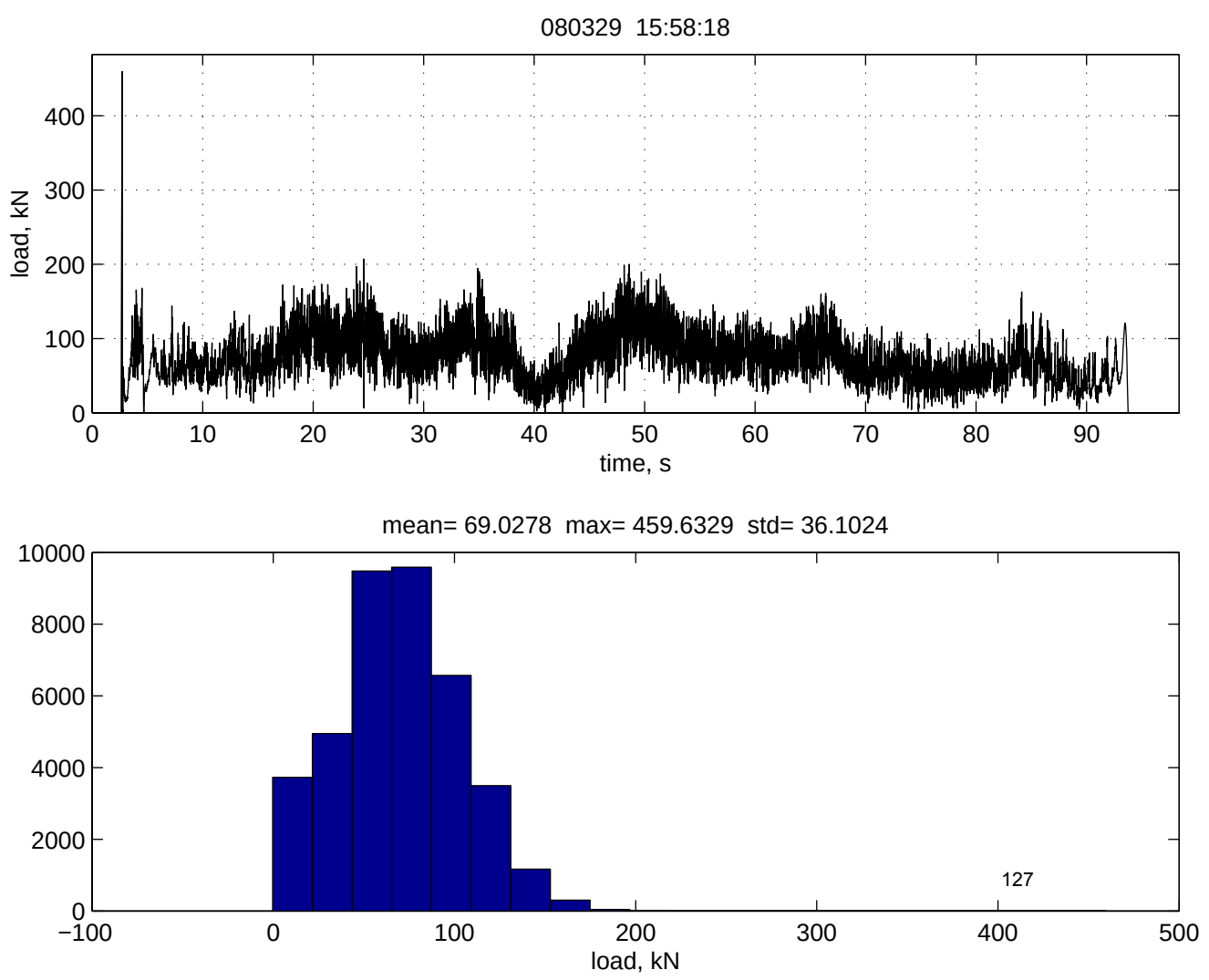
080329 15:58:18
load, kN
time, s
mean= 69.0278 max= 459.6329 std= 36.1024
127
load, kN

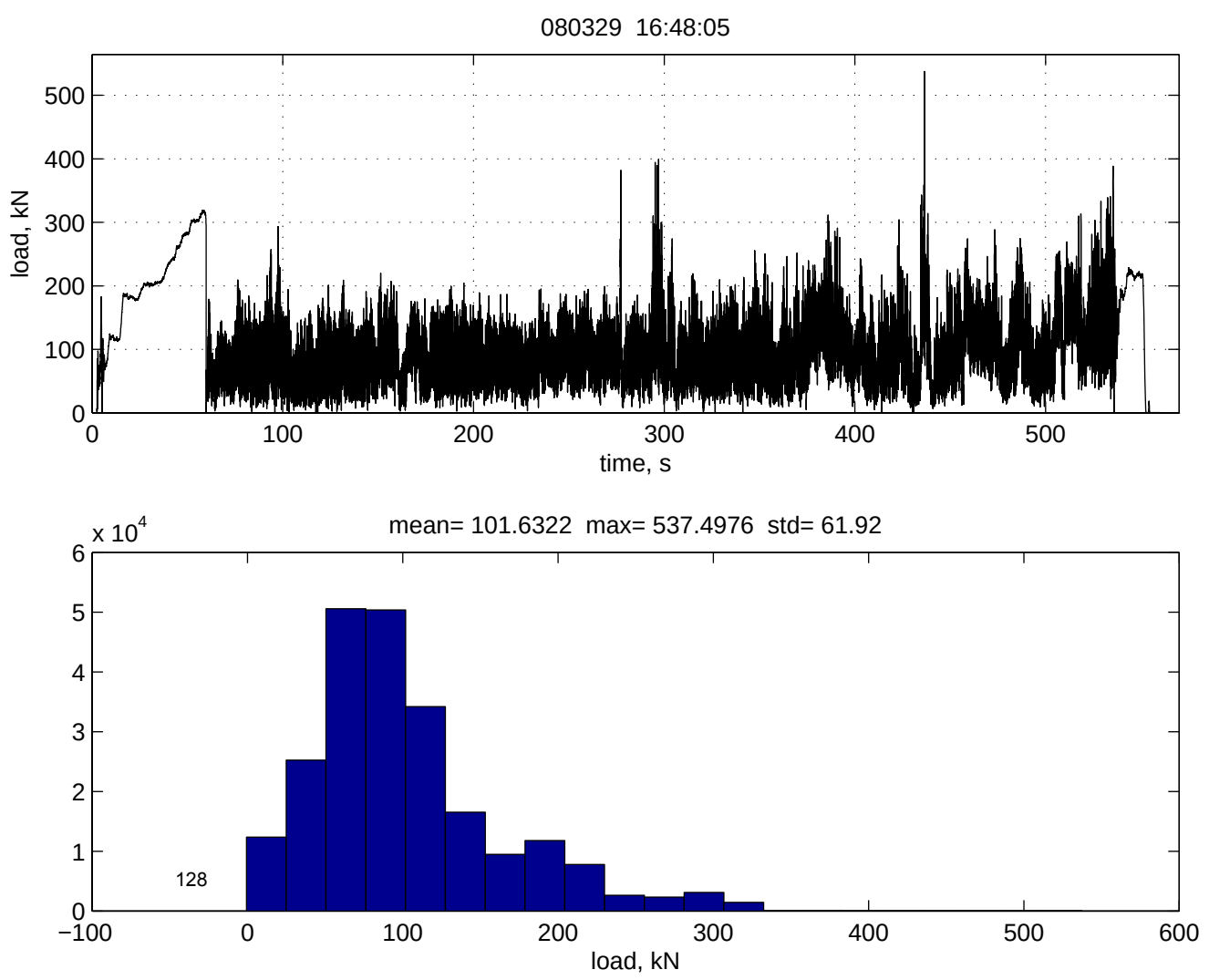
080329 16:48:05
load, kN
time, s
0
100
200
300
400
500
x 10^4
mean= 101.6322 max= 537.4976 std= 61.92
128
load, kN
−100
600

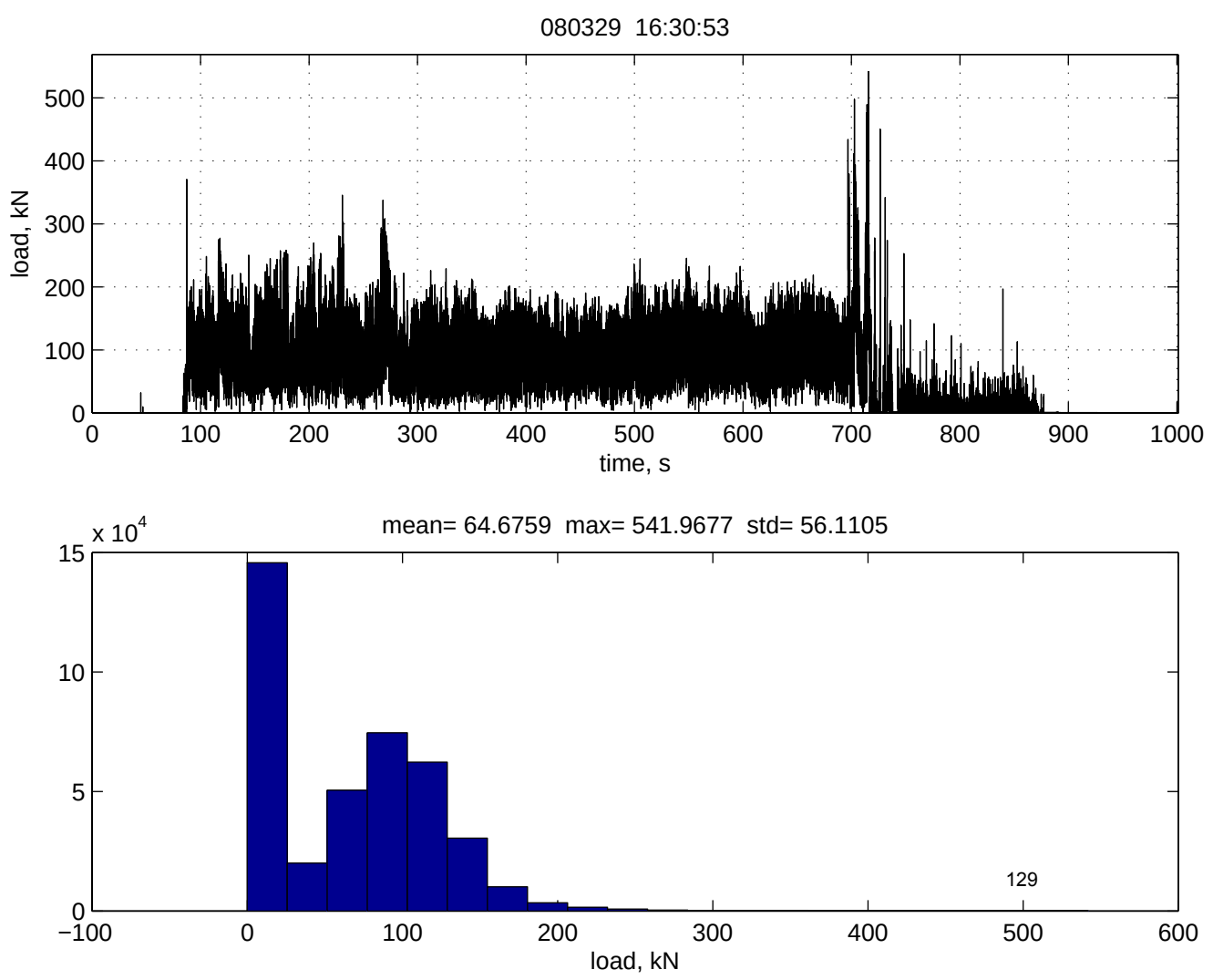
080329 16:30:53
load, kN
time, s
mean= 64.6759 max= 541.9677 std= 56.1105
x 10^4
load, kN
129

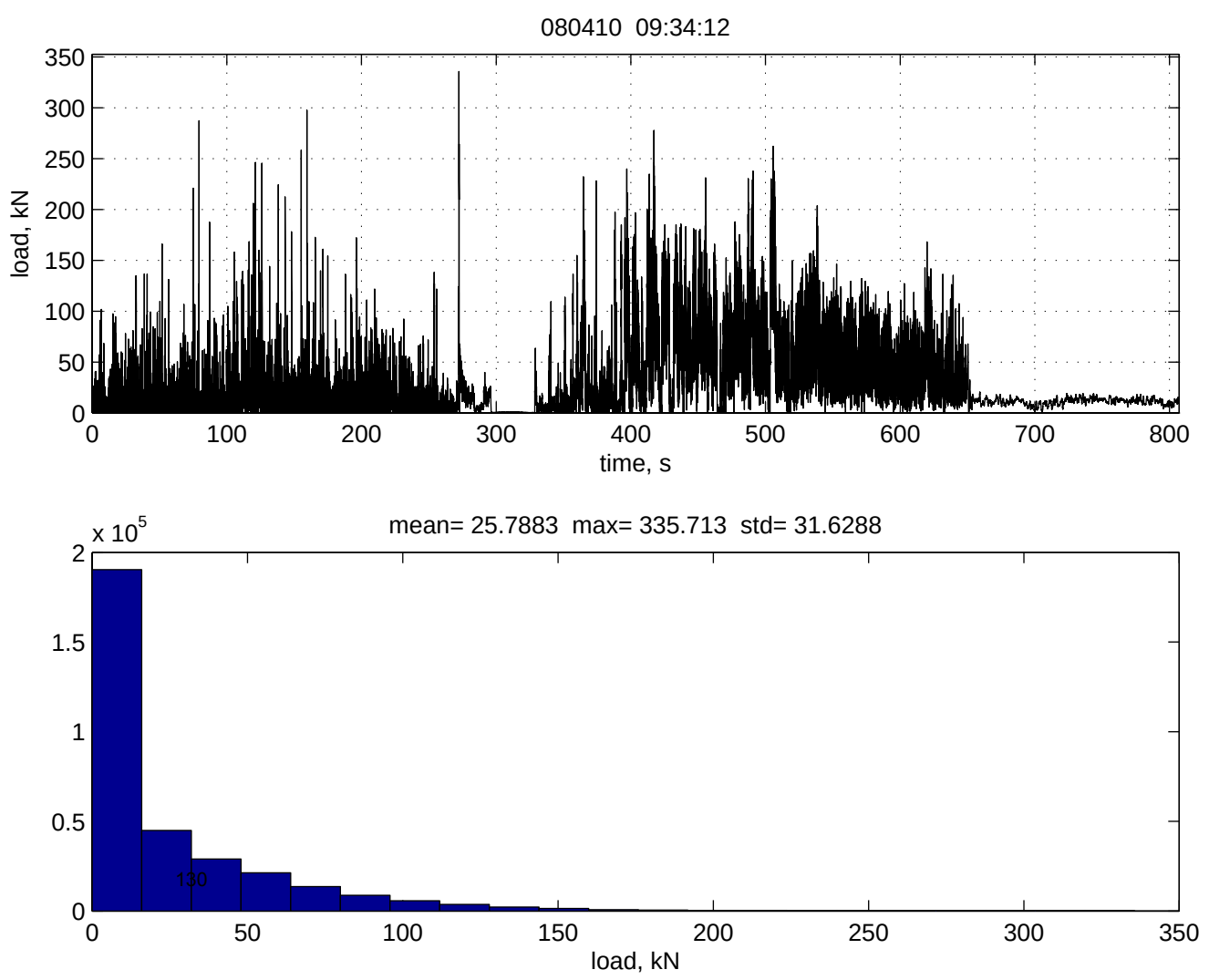
080410 09:34:12
load, kN
time, s
mean= 25.7883 max= 335.713 std= 31.6288
x 10^5
load, kN
130

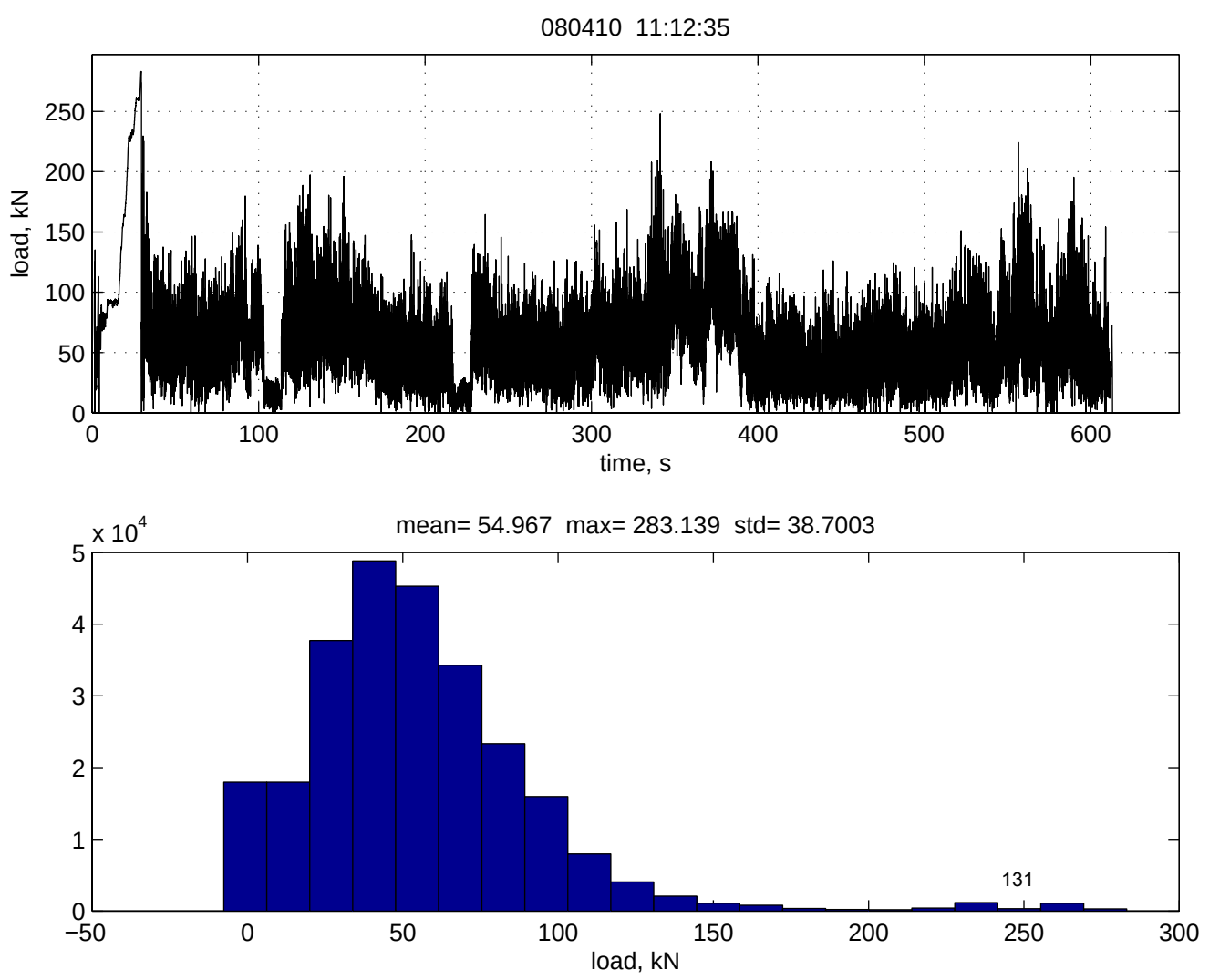
080410 11:12:35
load, kN
time, s
0
50
100
150
200
250
0
100
200
300
400
500
600
x 10^4
mean= 54.967 max= 283.139 std= 38.7003
131
load, kN
−50
0
50
100
150
200
250
300
1
2
3
4
5

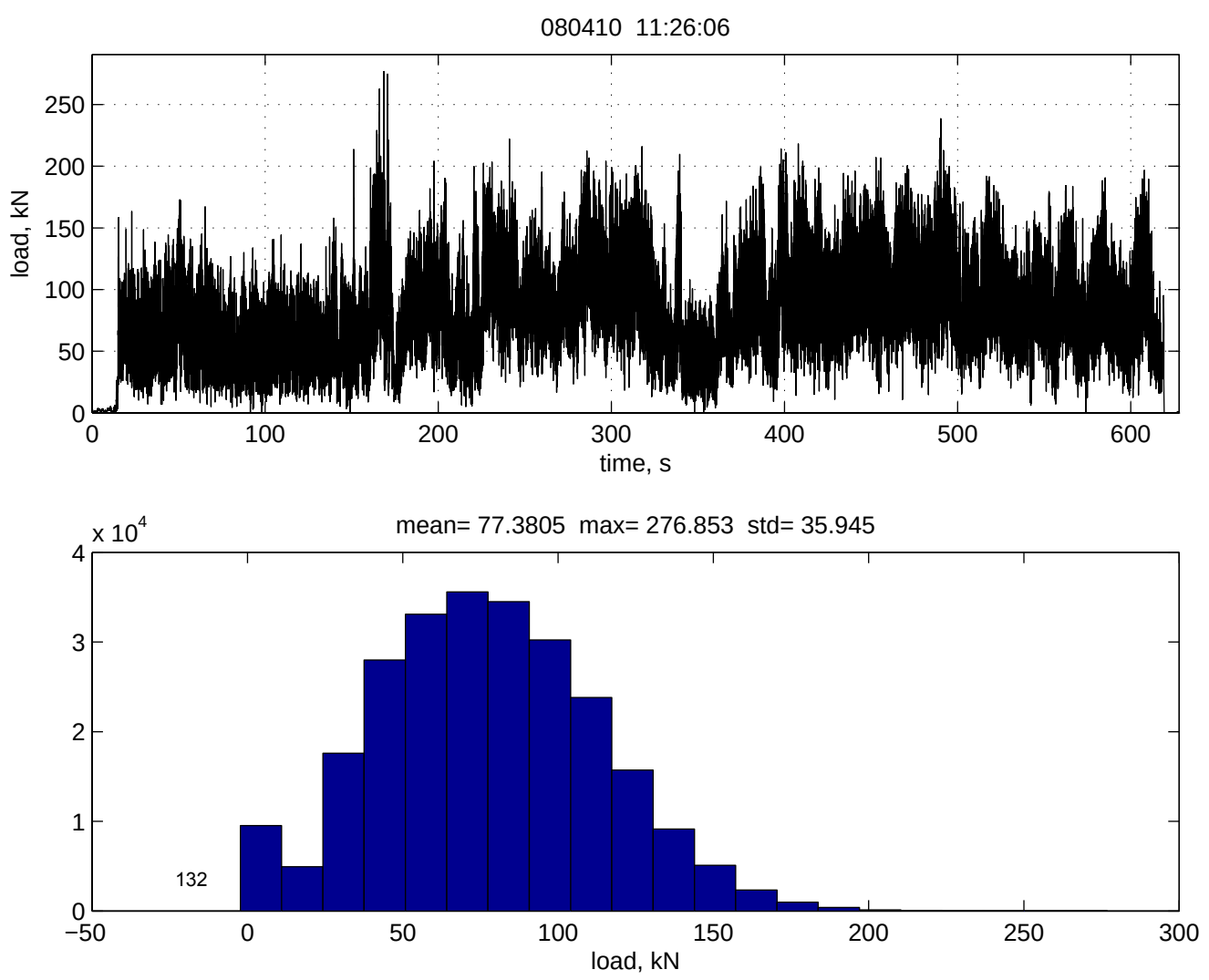
080410 11:26:06
load, kN
time, s
0
50
100
150
200
250
0
100
200
300
400
500
600
x 10^4
mean= 77.3805 max= 276.853 std= 35.945
132
load, kN
−50
0
50
100
150
200
250
300
1
2
3
4

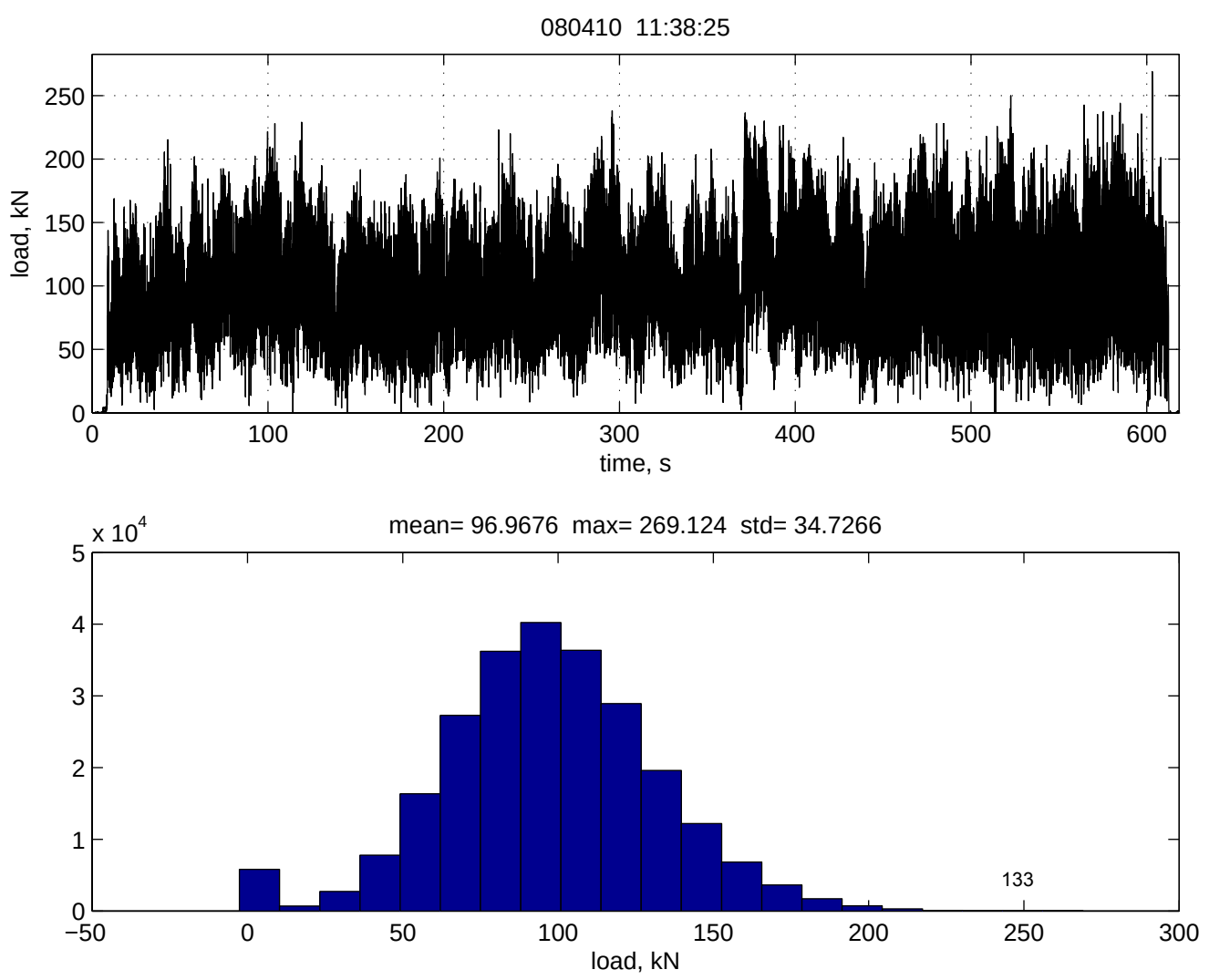
080410 11:38:25
load, kN
time, s
0
50
100
150
200
250
0
100
200
300
400
500
600
x 10^4
mean= 96.9676 max= 269.124 std= 34.7266
load, kN
133
−50
0
50
100
150
200
250
300
1
2
3
4
5

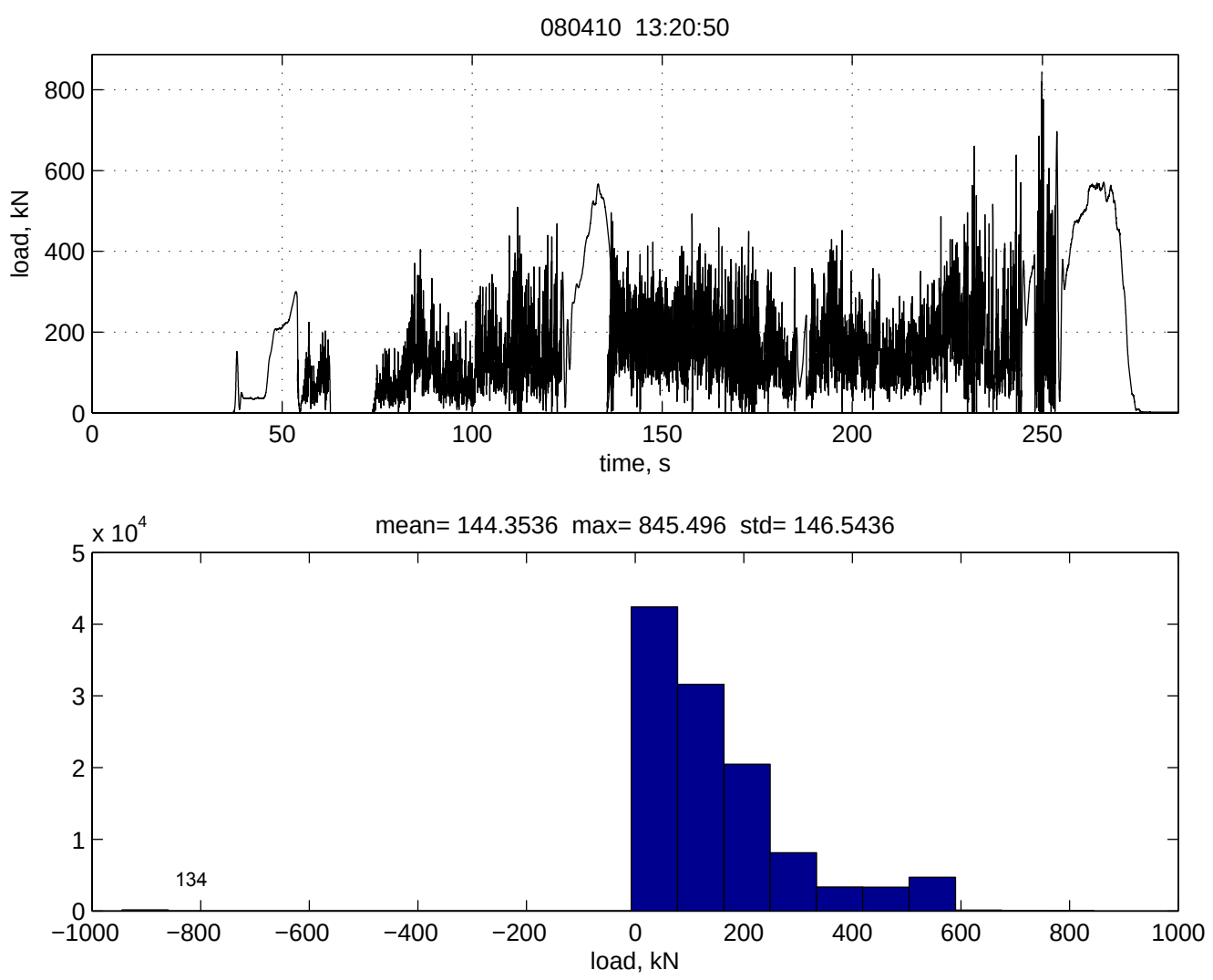
080410 13:20:50
load, kN
time, s
mean= 144.3536 max= 845.496 std= 146.5436
x 10^4
134
load, kN

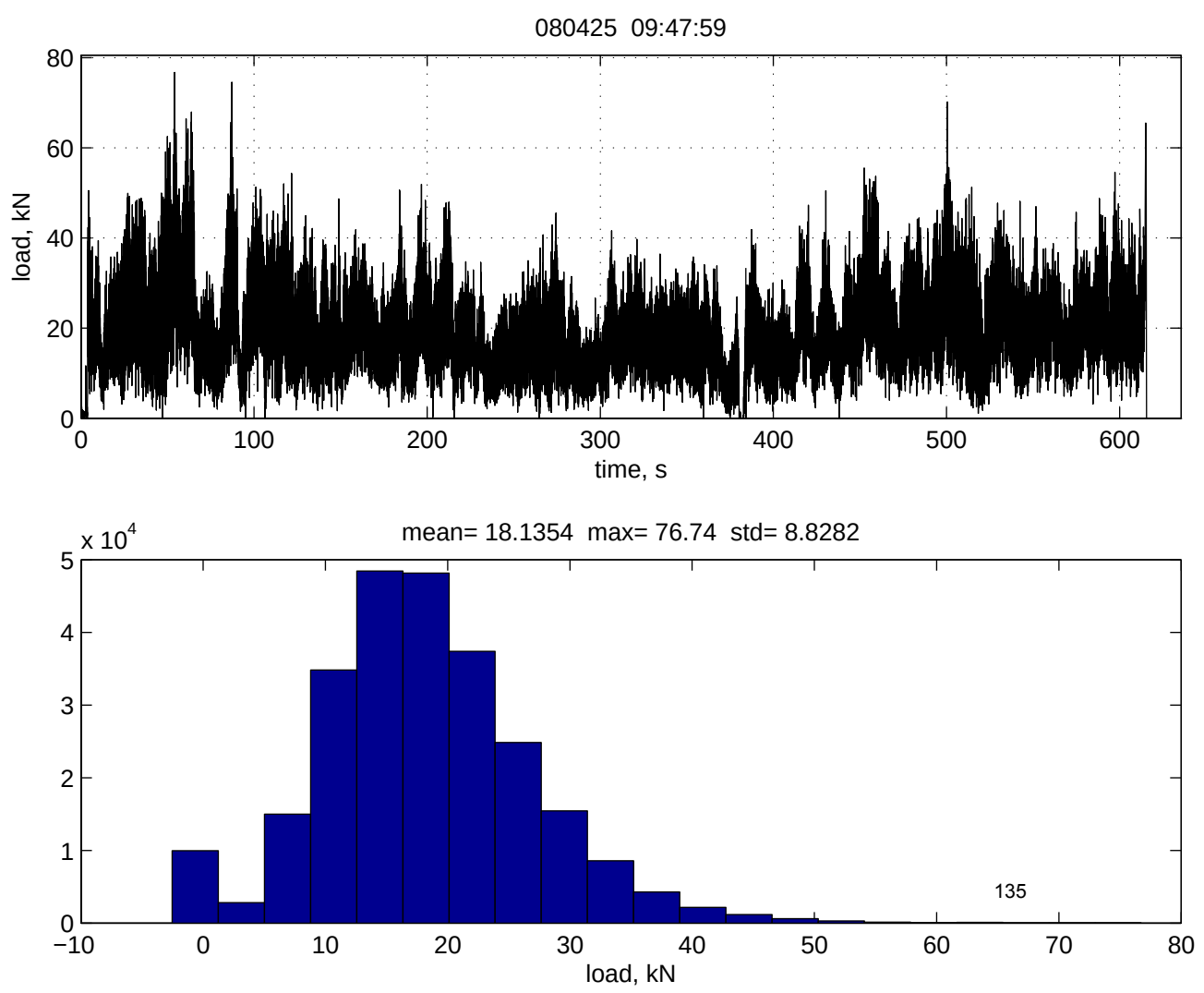
080425 09:47:59
load, kN
time, s
mean= 18.1354 max= 76.74 std= 8.8282
x 10^4
load, kN
135

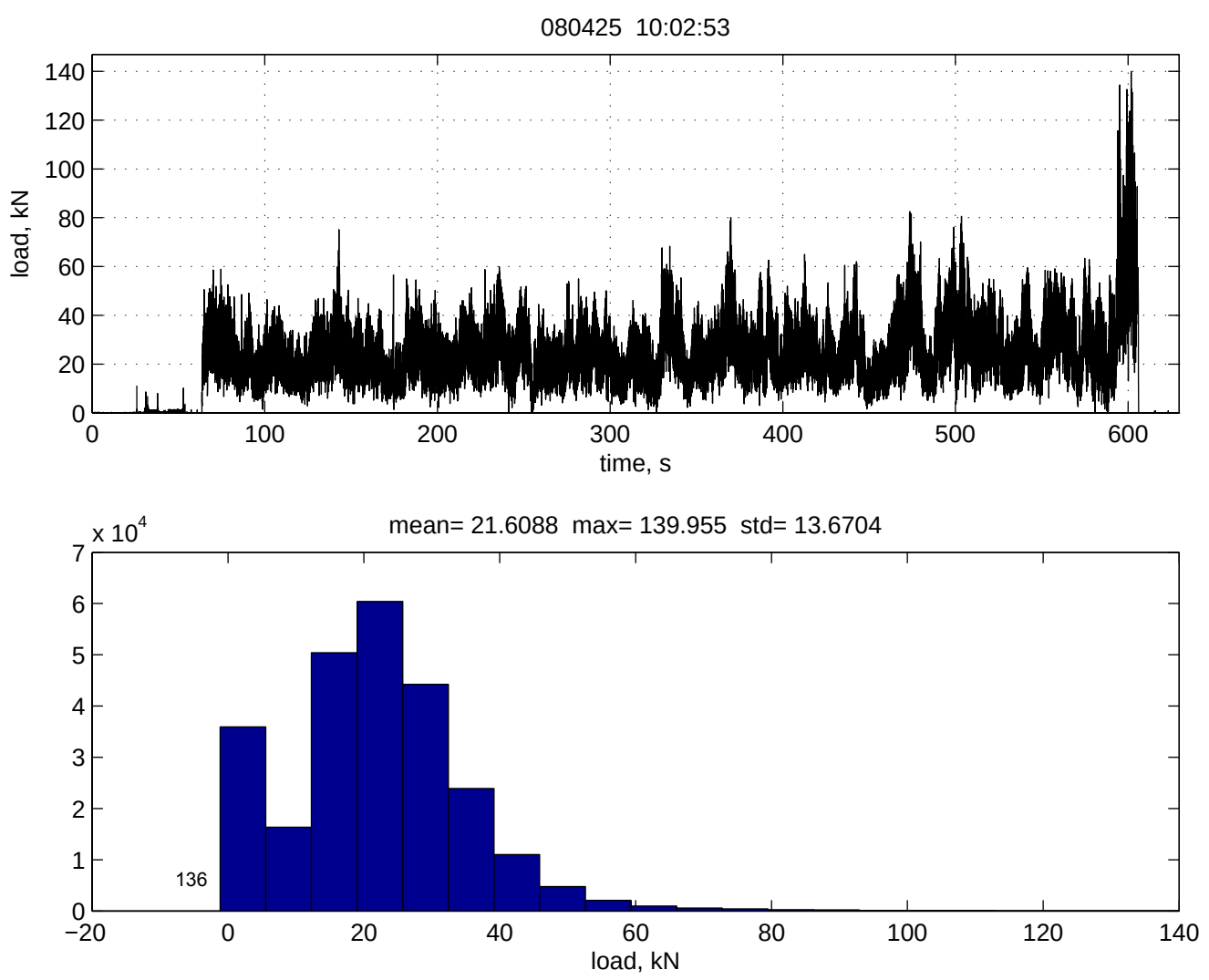
080425 10:02:53
load, kN
time, s
x 10^4
mean= 21.6088 max= 139.955 std= 13.6704
136
load, kN

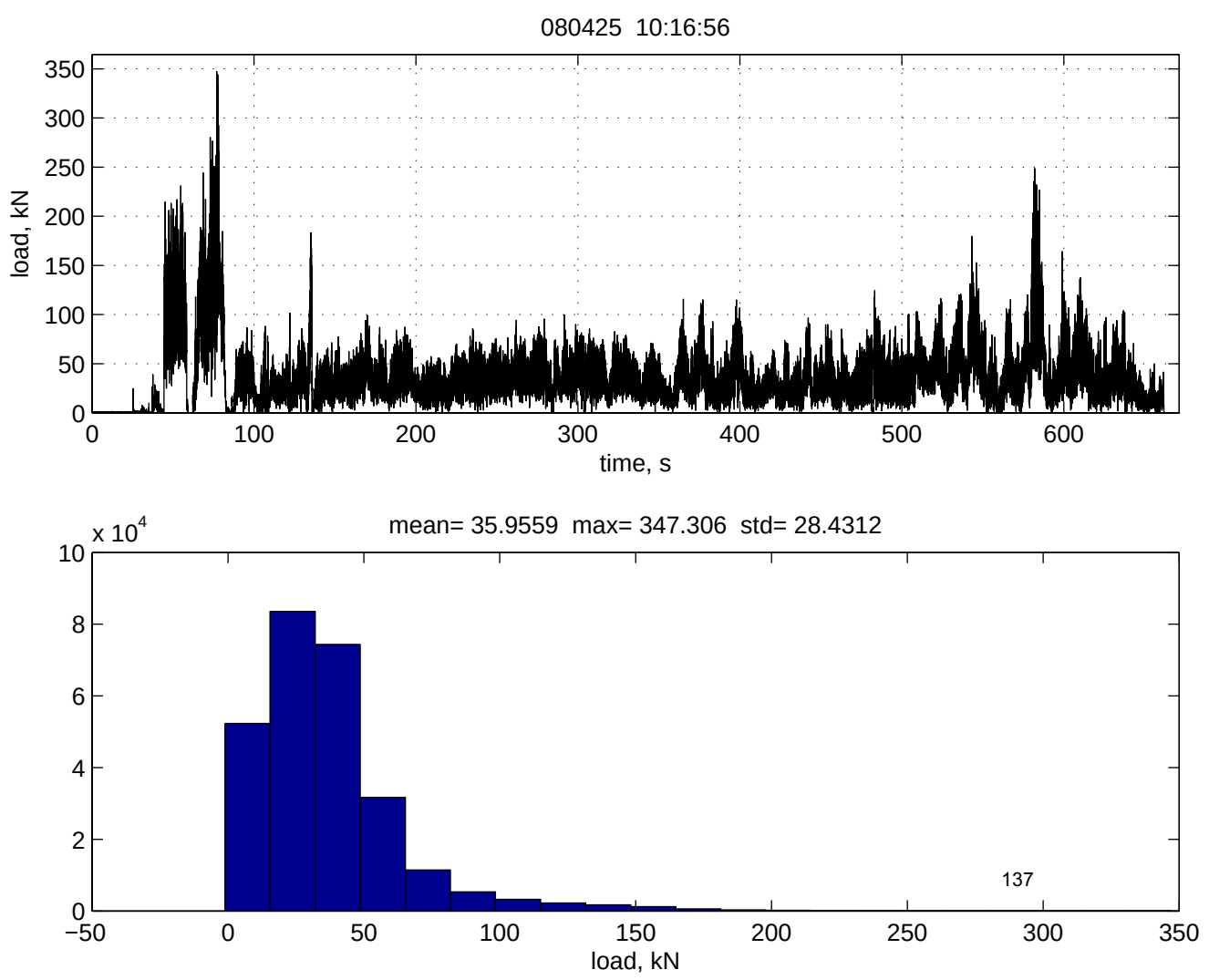
080425 10:16:56
load, kN
time, s
mean= 35.9559 max= 347.306 std= 28.4312
x 10^4
137
load, kN

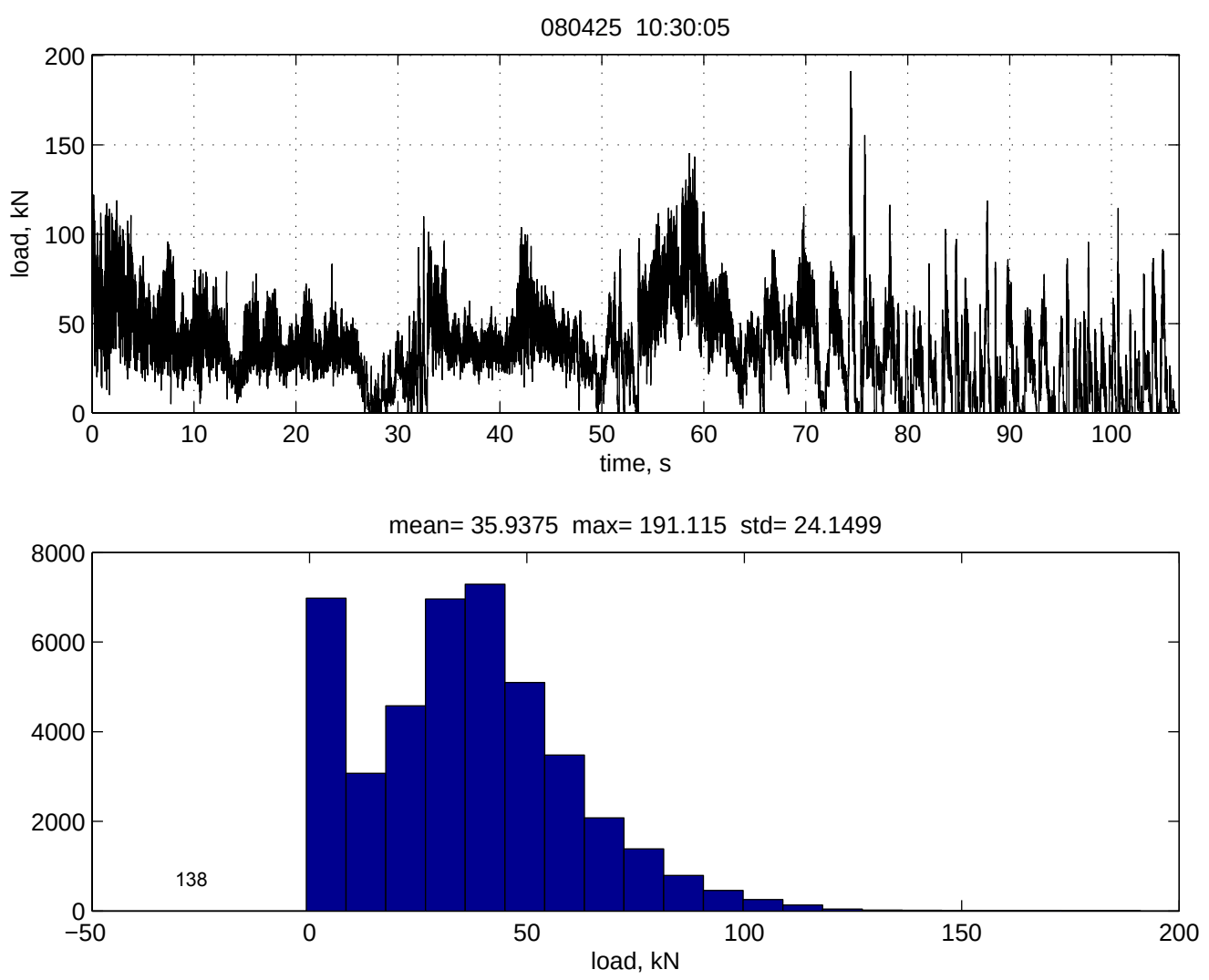
080425 10:30:05
load, kN
time, s
mean= 35.9375 max= 191.115 std= 24.1499
138
load, kN

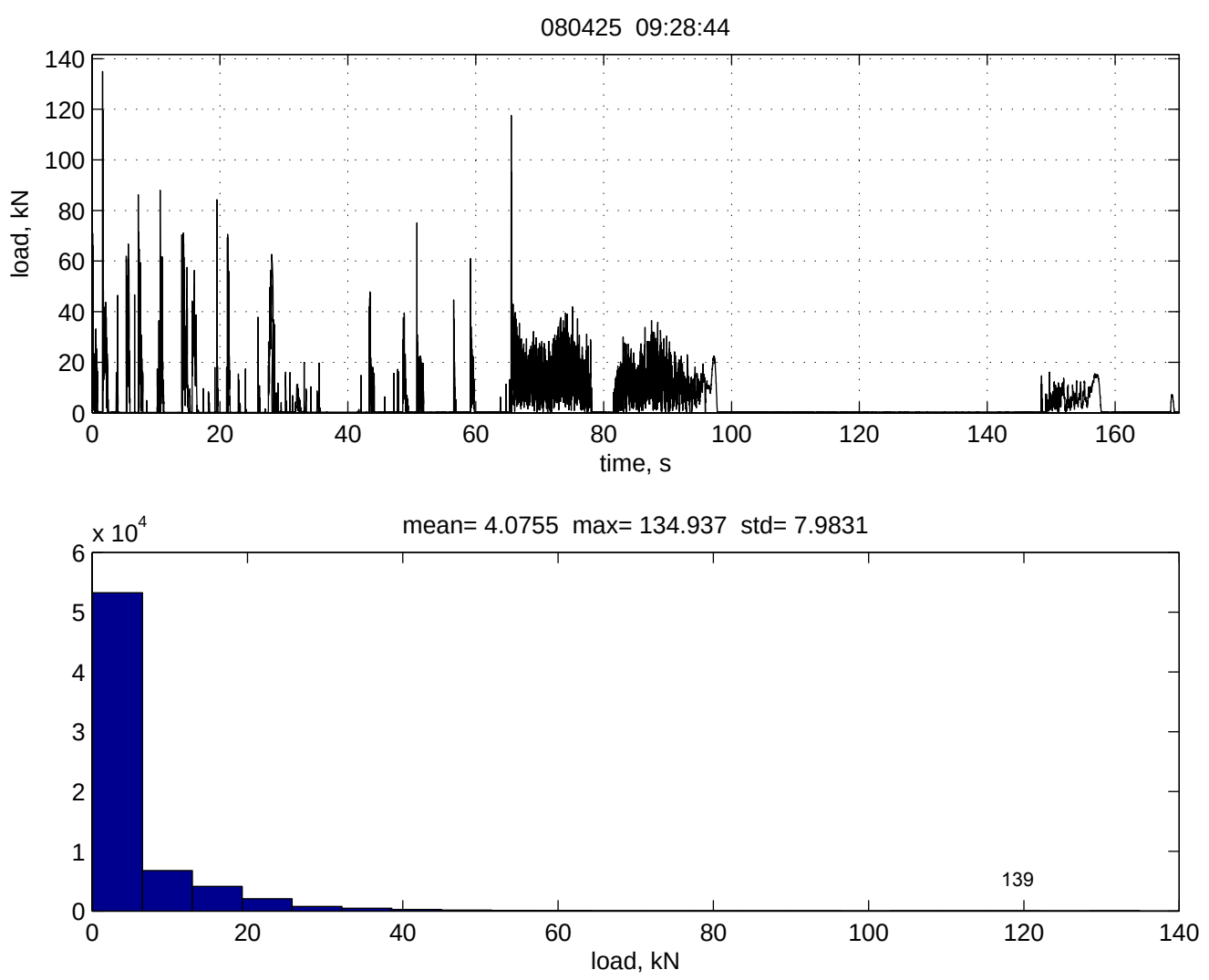
080425 09:28:44
load, kN
time, s
mean= 4.0755 max= 134.937 std= 7.9831
x 10^4
load, kN
139

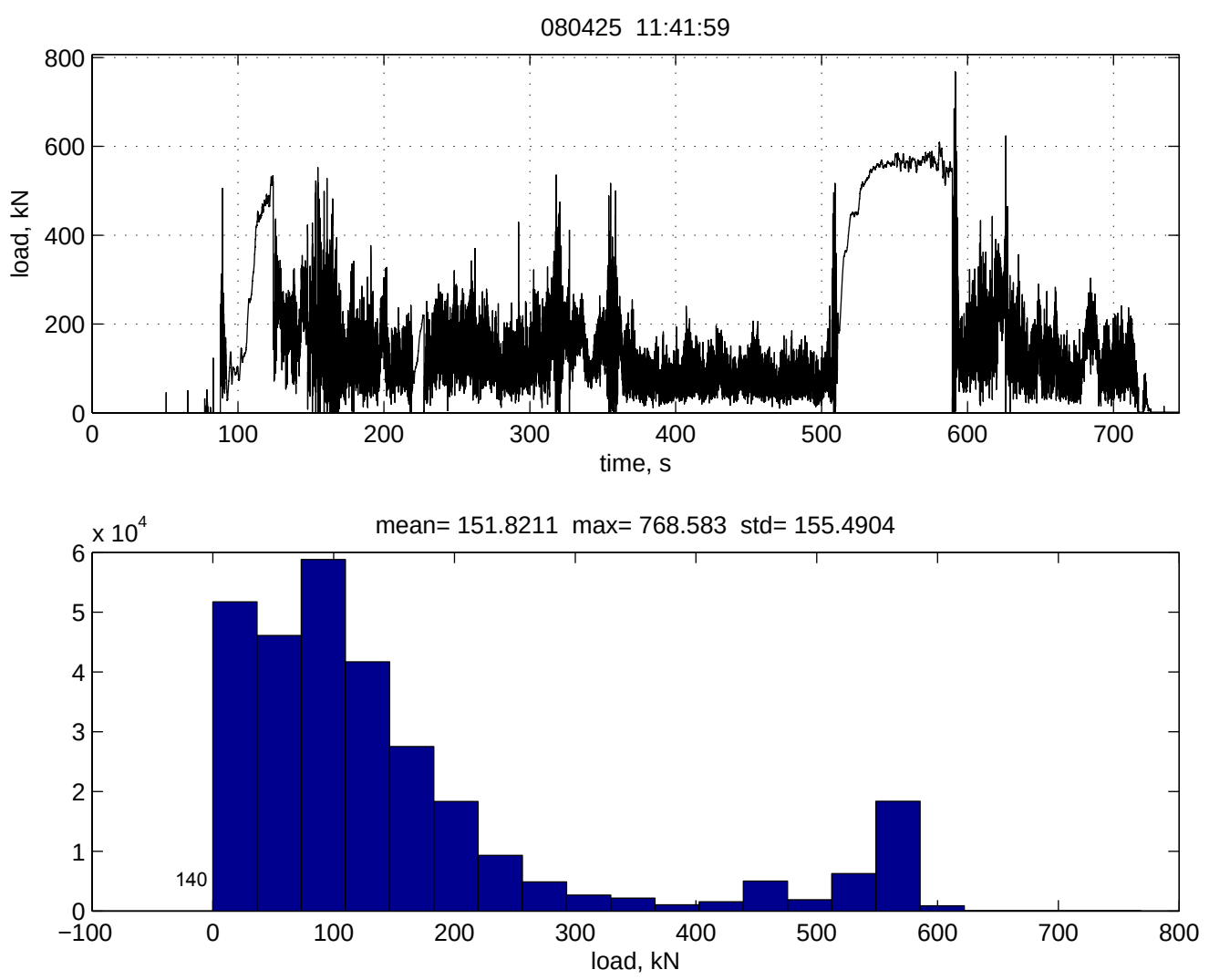
080425 11:41:59
load, kN
time, s
mean= 151.8211 max= 768.583 std= 155.4904
x 10^4
140
load, kN

Bilaga D Tryckprovning av is

Kallax 1

Sample	Temp	Diam D	Length L	Mass	Load	Depth z	Speed	Density	Strength	Salinity	GrainSize
20-nov	T (C)	(mm)	(mm)	M (g)	P (kN)	(cm)	mm/s	(kg/m3)	(MPa)	(μS)	(mm)
111	-10	67.1	157.0	505.9	12.446	5	0.080	911.2	3.52	202	17.5
112	-10	67.1	156.9	505.4	10.135	5	0.157	910.9	2.87	145	17.5
113	-10	67.1	139.7	449.3	12.747	5	0.279	909.5	3.60	158	17.5
114	-1	67.0	151.4	486.1	8.161	5	0.074	910.7	2.31	174	17.5
115	-1	67.0	145.7	469.3	7.764	5	0.147	913.6	2.20	161	17.5
116	-1	67.1	152.9	491.7	6.142	5	0.305	909.4	1.74	132	17.5

Kallax 2

Sample	Temp	Diam D	Length L	Mass	Load P	Depth z	Speed	StrRate	Density	Strength	Salinity	GrainSize
08-jan	T (C)	(mm)	(mm)	M (g)	(kN)	(cm)	mm/s	(e-4/s)	(kg/m3)	(MPa)	(μS)	(mm)
211	-10	67.2	173.7	547.3	22.04	5	0.086	5.0	888.4	6.22	33	M*
212	-10	67.2	173.6	558.1	14.67	15	0.086	5.0	906.4	4.13	6	33.3
213	-10	67.2	173.5	553.4	19.01	25	0.086	5.0	899.3	5.36	8	37.0
214	-10	66.9	173.6	554.8	16.54	5	0.173	9.9	909.2	4.71	19	M
215	-10	66.9	173.7	557.9	18.54	15	0.173	9.9	913.7	5.27	7	33.3
216	-10	66.9	173.6	544.9	23.69	25	0.173	9.9	892.9	6.74	6	37.0
217	-10	67.2	173.9	553.3	14.46	5	0.173	9.9	897.1	4.08	17	M
218	-10	67.2	173.8	557.3	16.66	15	0.173	9.9	904.1	4.70	5	33.3
219	-10	67.2	173.7	553.9	16.75	25	0.173	9.9	899.1	4.72	5	37.0
221	-5	67.1	173.9	554.2	13.02	5	0.086	5.0	901.2	3.68	28	M
222	-5	67.1	173.8	558.7	12.20	15	0.086	5.0	909.1	3.45	20	33.3
223	-5	67.1	168.9	540.8	13.34	25	0.086	5.1	905.5	3.77	8	37.0
224	-5	67.1	173.6	551.7	14.05	5	0.173	9.9	898.7	3.97	52	M
225	-5	67.1	173.7	557.9	17.56	15	0.173	9.9	908.3	4.97	18	33.3
226	-5	67.1	173.6	555.1	16.66	25	0.173	9.9	904.2	4.71	15	37.0
227	-5	67.1	173.6	553.7	15.68	5	0.345	19.9	902.0	4.43	26	M
228	-5	67.1	173.5	557.5	16.99	15	0.345	19.9	908.7	4.81	7	33.3
229	-5	67.1	170.9	545.4	12.98	25	0.345	20.2	902.5	3.67	5	37.0
231	-1	66.7	173.8	555.9	13.41	5	0.086	5.0	915.4	3.84	18	M
232	-1	66.7	173.6	557.6	25.30	15	0.086	5.0	919.2	7.24	12	33.3
233	-1	66.7	173.7	555.1	26.86	25	0.086	5.0	914.6	7.69	5	37.0
234	-1	66.7	173.6	555.4	18.04	25	0.171	9.8	915.6	5.16	8	37.0
235	-1	66.7	173.7	558.1	15.89	15	0.173	9.9	919.5	4.55	13	33.3
236	-1	66.7	173.7	551.6	9.03	5	0.345	19.9	908.8	2.58	35	M
237	-1	66.7	173.8	550.6	10.98	5	0.345	19.9	906.7	3.14	60	M
238	-1	66.7	173.6	557.6	10.72	15	0.345	19.9	919.2	3.07	10	33.3
239	-1	66.7	173.9	555.2	16.63	25	0.345	19.9	913.7	4.76	12	37.0
241	-10	67.1	168.5	535.9	9.54	5	0.345	20.5	899.4	2.70	97	M
242	-10	67.1	169.9	545.2	14.65	15	0.347	20.4	907.5	4.14	11	33.3
243	-10	67.1	169.6	542.0	20.27	25	0.345	20.4	903.7	5.73	9	37.0

M=Mixade istyper

Klubbviken 1

Sample	Temp	Diam D	Length L	Mass	Load	Depth z	Speed	StrRate	Density	Strength	Salinity	GrainSize
19-mar	T (C)	(mm)	(mm)	M (g)	P (kN)	(cm)	mm/s	(e-4/s)	(kg/m3)	(MPa)	(μS)	(mm)
11	-10	67.0	160.6	518.7	15.835	5	0.08	5.0	916.1	4.49	6	M
12	-10	67.1	160.5	519.1	16.079	15	0.08	5.0	914.6	4.55	6	6.2
41	-10	67.2	161.1	517.8	19.024	5	0.08	5.0	906.2	5.36	8	M
42	-10	67.2	161.2	519.4	23.05	15	0.08	5.0	908.5	6.50	4	6.2
71	-5	67.2	160.7	497.9	24.110	5	0.08	5.0	873.6	6.80	17	M
72	-5	67.2	160.5	519.2	14.721	15	0.08	5.0	912.1	4.15	11	6.2
81	-5	67.2	160.7	498.5	22.340	5	0.08	5.0	874.6	6.30	11	M
82	-5	67.1	160.6	519.0	18.963	15	0.08	5.0	913.9	5.36	8	6.2
51	-1	67.1	161.0	514.0	21.380	5	0.08	5.0	902.8	6.05	41	M
52	-1	67.1	161.1	519.4	13.462	15	0.08	5.0	911.7	3.81	12	6.2
61	-1	67.2	160.6	492.8	14.202	5	0.08	5.0	865.2	4.00	45	M
62	-1	67.2	160.4	518.8	10.368	15	0.08	5.0	911.9	2.92	5	6.2
21	0	67.0	160.8	513.1	13.394	5	0.08	5.0	905.0	2.01	15	M
22	0	67.3	160.8	518.9	5.032	15	0.08	5.0	910.4	1.43	64	6.2
31	0	67.1	160.8	514.6	7.092	5	0.08	5.0	905.0	2.01	45	M
32	0	67.2	160.8	519.2	5.085	15	0.08	5.0	910.4	1.43	13	6.2

M=Mixade istyper

Klubbviken 2

Sample	Temp	Diam D	Length L	Mass	Load	Depth z	Speed	StrRate	Density	Strength	Salinity	GrainSize
29-mar	T (C)	(mm)	(mm)	M (g)	P (kN)	(cm)	mm/s	(e-4/s)	(kg/m3)	(MPa)	(μS)	(mm)
51	-10	67.2	165.2	511.7	17.338	5	0.08	4.8	873.3	4.89	36	M
52	-10	67.1	165.2	521.3	21.94	15	0.08	4.8	892.4	6.20	12	7.9
53	-10	67.2	165.2	532.7	20.95	25	0.08	4.8	909.2	5.91	5	16.6
11	-10	67.2	165.3	511.6	24.28	5	0.08	4.8	872.6	6.85	46	M
12	-10	67.2	165.5	517.6	23.79	15	0.08	4.8	881.8	6.71	18	7.9
13	-10	67.2	165.3	534.2	19.825	25	0.08	4.8	911.2	5.59	4	16.6
31	-5	67.2	165.3	494.2	18.093	5	0.08	4.8	842.9	5.10	32	M
32	-5	67.1	165.4	521.3	16.510	15	0.08	4.8	891.3	4.67	14	7.9
33	-5	67.1	165.3	533.5	14.446	25	0.08	4.8	912.7	4.09	3	16.6
21	-1	67.1	165.6	491.7	9.758	5	0.08	4.8	839.7	2.76	26	M
22	-1	67.2	165.3	525.8	8.408	15	0.08	4.8	896.8	2.37	19	7.9
23	-1	67.1	165.4	534.0	3.346	25	0.08	4.8	913.0	0.95	6	16.6
41	0	67.2	165.4	500.5	9.510	5	0.08	4.8	853.2	2.68	39	M
42	0	67.2	165.2	523.6	10.281	15	0.08	4.8	893.6	2.90	11	7.9
43	0	67.1	165.2	533.1	3.742	25	0.08	4.8	912.6	1.06	7	16.6

M=Mixade istyper

Klubbviken 3

Sample **10-apr**	Temp T (C)	Diam D (mm)	Length L (mm)	Mass M (g)	Load P (kN)	Depth z (cm)	Speed mm/s	Density (kg/m3)	Strength (MPa)	Salinity (μS)	Grain Size (mm)	Comments
11	-10	67.1	162.0	523.7	19.348	5	0.08	914.2	5.47	22	M	
12	-10	67.4	162.0	523.5	23.190	15	0.08	905.7	6.50	10	7.9	
21	-10	67.2	162.1	523.2	24.420	5	0.08	910.0	6.89	21	M	
22	-10	67.2	162.0	523.1	33.420	15	0.08	910.4	9.42	12	7.9	
31	-10	67.1	162.2	523.5	12.295	5	0.08	912.7	3.48	9	M	utan poluretan
32	-10	67.1	162.1	522.8	8.072	15	0.08	912.0	2.28	12	7.9	utan poluretan
41	-10	67.1	162.0	522.4	9.598	5	0.08	911.9	2.71	16	M	utan poluretan
42	-10	67.2	162.0	523.4	19.207	15	0.08	910.9	5.42	12	7.9	utan poluretan
51	-3	67.2	165.1	523.3	11.948	5	0.08	893.7	3.37	17	M	
52	-3	67.1	161.8	522.9	17.098	15	0.08	913.9	4.84	10	7.9	
61	-3	67.2	161.9	522.3	4.257	5	0.08	909.6	1.20	15	M	
62	-3	67.1	161.9	522.6	9.056	15	0.08	912.8	2.56	14	7.9	
71	0	67.1	161.9	523.0	4.814	5	0.08	913.5	1.36	9	M	
72	0	67.2	161.9	523.3	5.470	15	0.08	911.3	1.54	10	7.9	
81	0	67.1	162.0	522.6	6.088	5	0.08	912.3	1.72	21	M	
82	0	67.1	162.0	521.9	3.769	15	0.08	911.0	1.07	9	7.9	

M=Mixade istyper

Strömören

Sample **25-mar**	Temp T (C)	Diam D (mm)	Length L (mm)	Mass M (g)	Load P (kN)	Depth z (cm)	Speed mm/s	StrRate (e-4/s)	Density (kg/m3)	Strength (MPa)	Salinity (μS)	GrainSize (mm)
11	-10	67.3	162.3	524.6	21.190	5	0.08	4.9	908.6	5.96	24.60	2.8
12	-10	67.1	162.4	523.5	18.353	15	0.08	4.9	911.6	5.19	5.20	8.3
13	-10	67.1	162.3	522.7	18.925	25	0.08	4.9	910.7	5.35	3.70	13.8
31	-3	67.4	162.4	526.4	8.717	5	0.08	4.9	908.5	2.44	7.30	2.8
32	-3	67.3	162.3	526.9	11.452	15	0.08	4.9	912.6	3.22	3.10	8.3
33	-3	67.4	162.2	527.2	17.903	25	0.08	4.9	911.0	5.02	2.80	13.8
21	-1	67.2	162.4	521.5	11.425	5	0.08	4.9	905.4	3.22	5.70	2.8
22	-1	67.1	162.4	523.8	12.559	15	0.08	4.9	912.1	3.55	4.00	8.3
23	-1	67.2	157.7	509.1	23.930	25	0.08	5.1	910.2	6.75	4.80	13.8
41	0	67.3	162.4	526.2	9.079	5	0.08	4.9	910.8	2.55	25.70	2.8
42	0	67.4	162.3	526.9	9.895	15	0.08	4.9	909.9	2.77	4.90	8.3
43	0	67.3	162.2	526.7	10.479	25	0.08	4.9	912.8	2.95	4.00	13.8

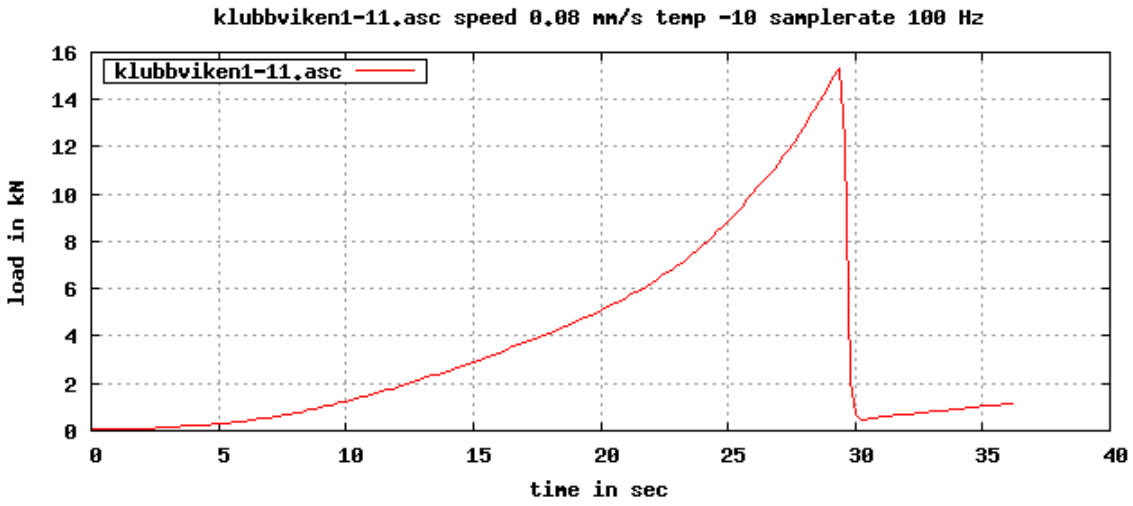
klubbviken1-11.asc speed 0.08 mm/s temp -10 samplerate 100 Hz
klubbviken1-11.asc
load in kN
time in sec
0
2
4
6
8
10
12
14
16
0
5
10
15
20
25
30
35
40

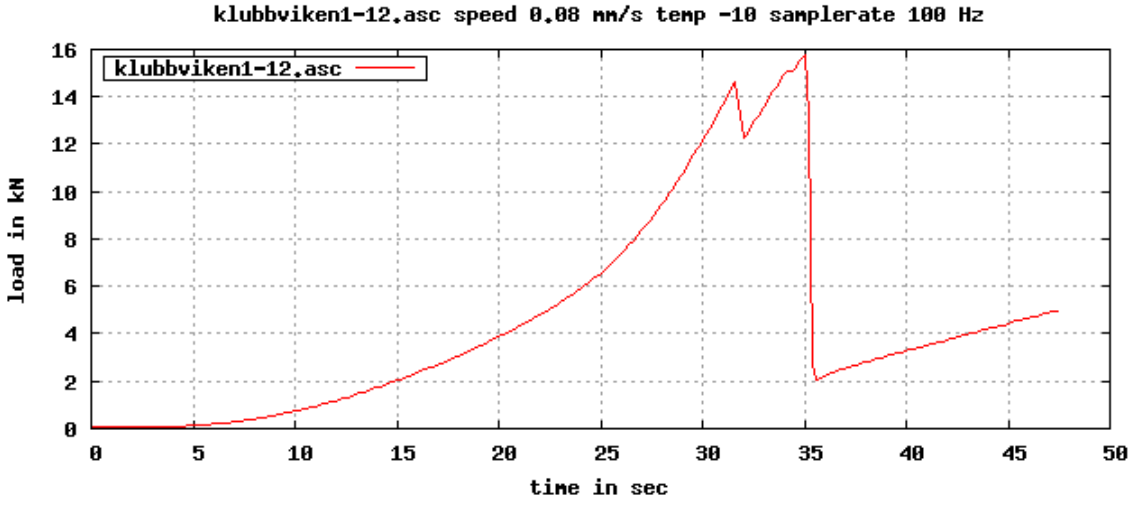
klubbviken1-12.asc speed 0.08 mm/s temp -10 samplerate 100 Hz
klubbviken1-12.asc
load in kN
time in sec
0
2
4
6
8
10
12
14
16
0
5
10
15
20
25
30
35
40
45
50

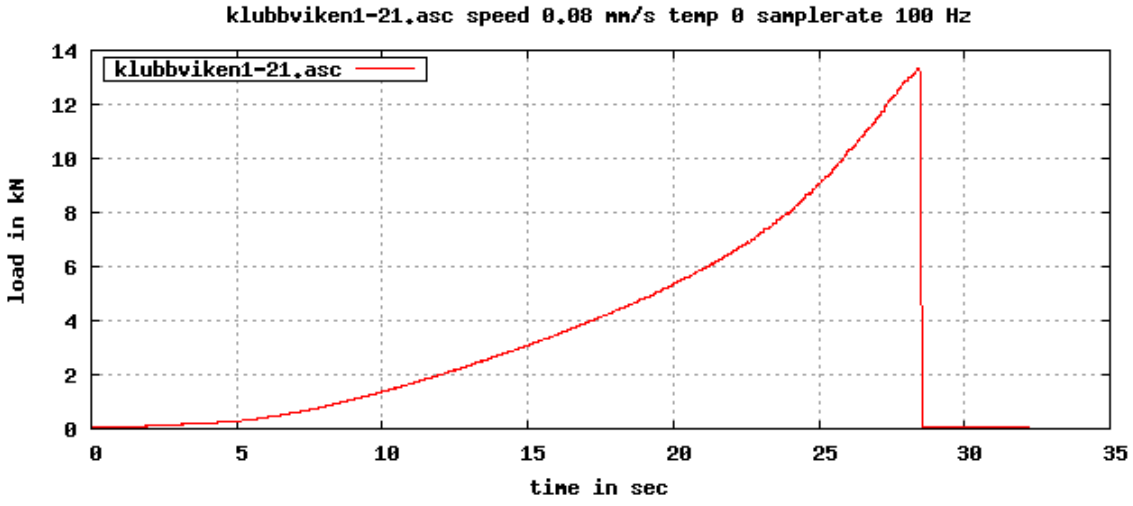
klubbviken1-21.asc speed 0.08 mm/s temp 0 samplerate 100 Hz
klubbviken1-21.asc
load in kN
time in sec
0
2
4
6
8
10
12
14
0
5
10
15
20
25
30
35

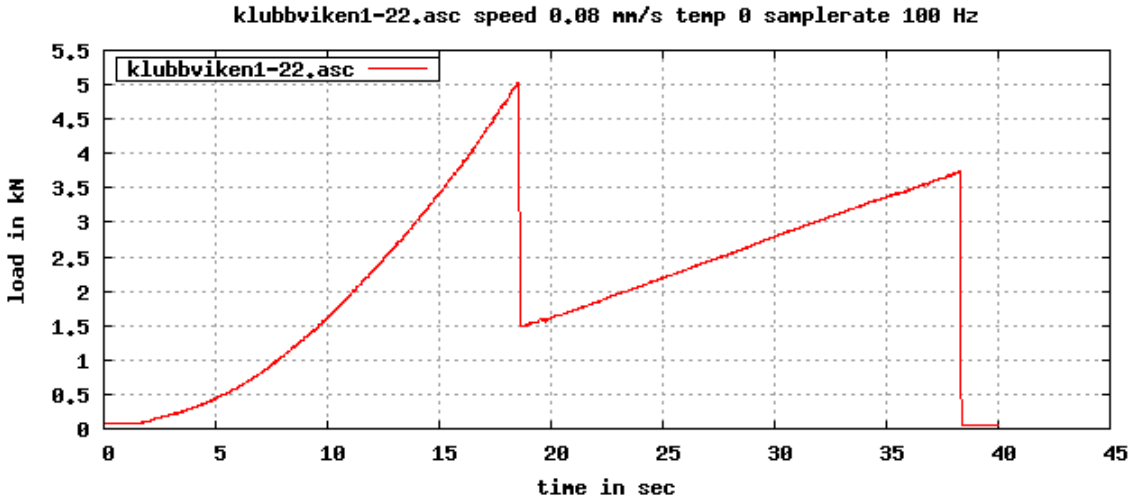
klubbviken1-22.asc speed 0.08 mm/s temp 0 samplerate 100 Hz
klubbviken1-22.asc
load in kN
time in sec
0
0.5
1
1.5
2
2.5
3
3.5
4
4.5
5
5.5
0
5
10
15
20
25
30
35
40
45

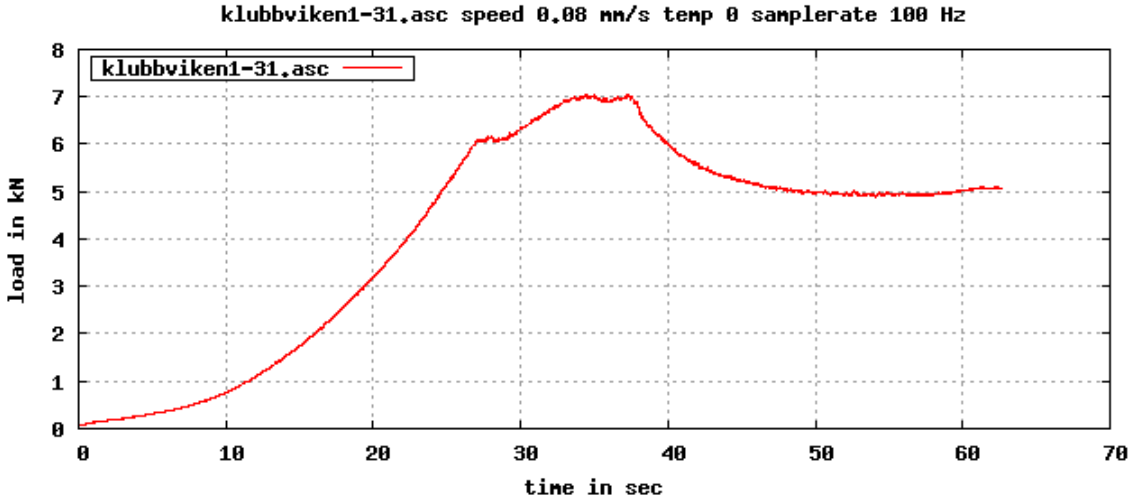
klubbviken1-31.asc speed 0.08 mm/s temp 0 samplerate 100 Hz
klubbviken1-31.asc
load in kN
time in sec
0
1
2
3
4
5
6
7
8
0
10
20
30
40
50
60
70

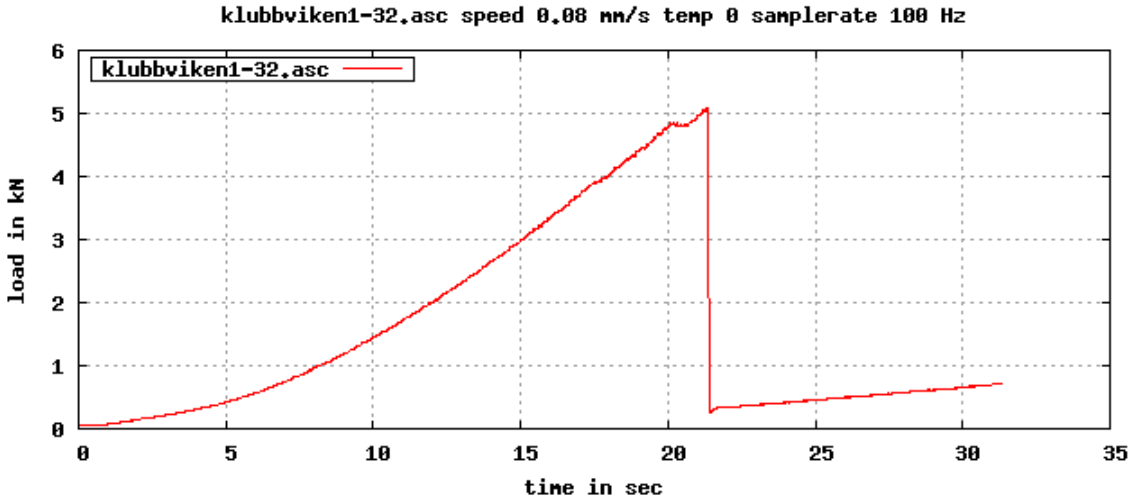
klubbviken1-32.asc speed 0.08 mm/s temp 0 samplerate 100 Hz
klubbviken1-32.asc
load in kN
time in sec
0
1
2
3
4
5
6
0
5
10
15
20
25
30
35

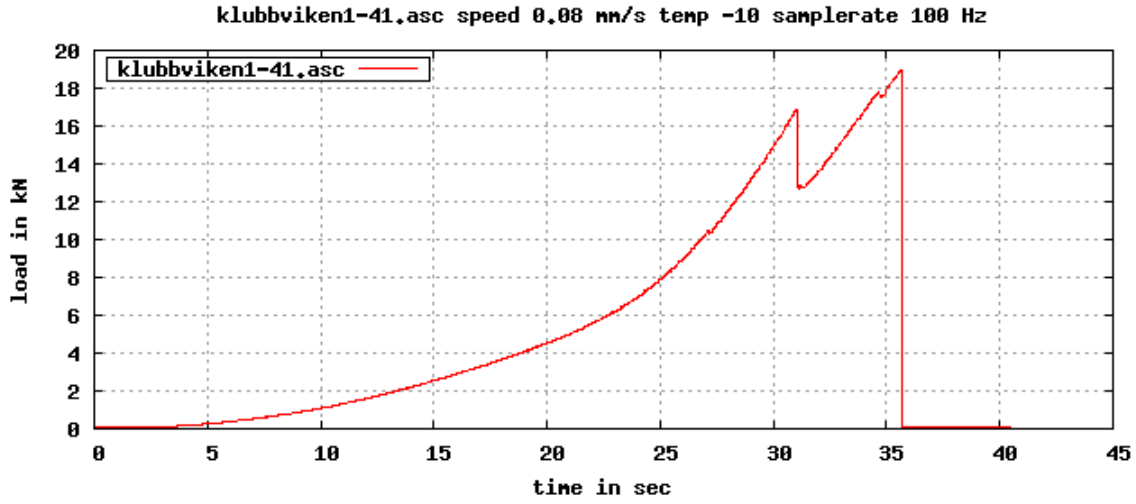
klubbviken1-41.asc speed 0.08 mm/s temp -10 samplerate 100 Hz
klubbviken1-41.asc
load in kN
time in sec
0
2
4
6
8
10
12
14
16
18
20
0
5
10
15
20
25
30
35
40
45

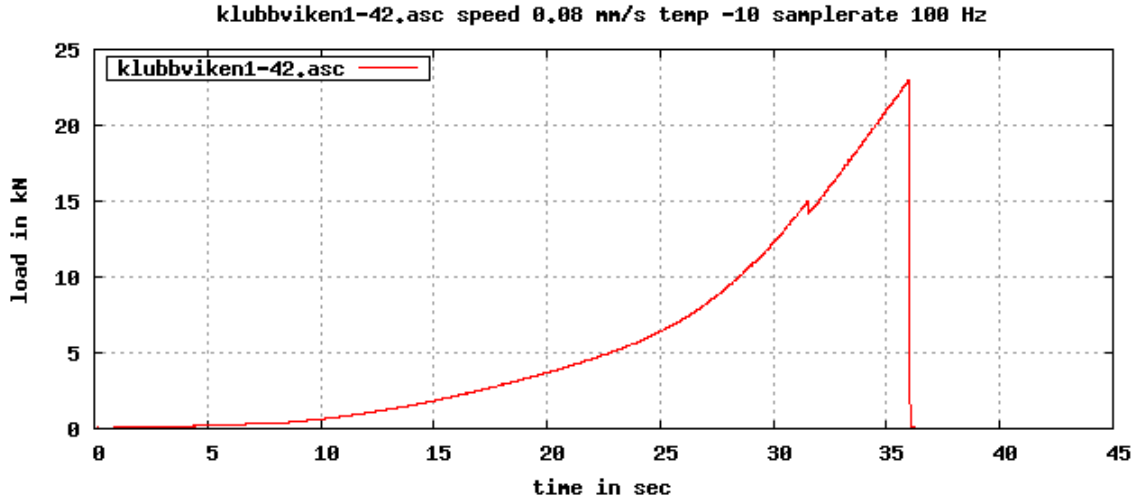
klubbviken1-42.asc speed 0.08 mm/s temp -10 samplerate 100 Hz
klubbviken1-42.asc
load in kN
time in sec
0
5
10
15
20
25
0
5
10
15
20
25
30
35
40
45

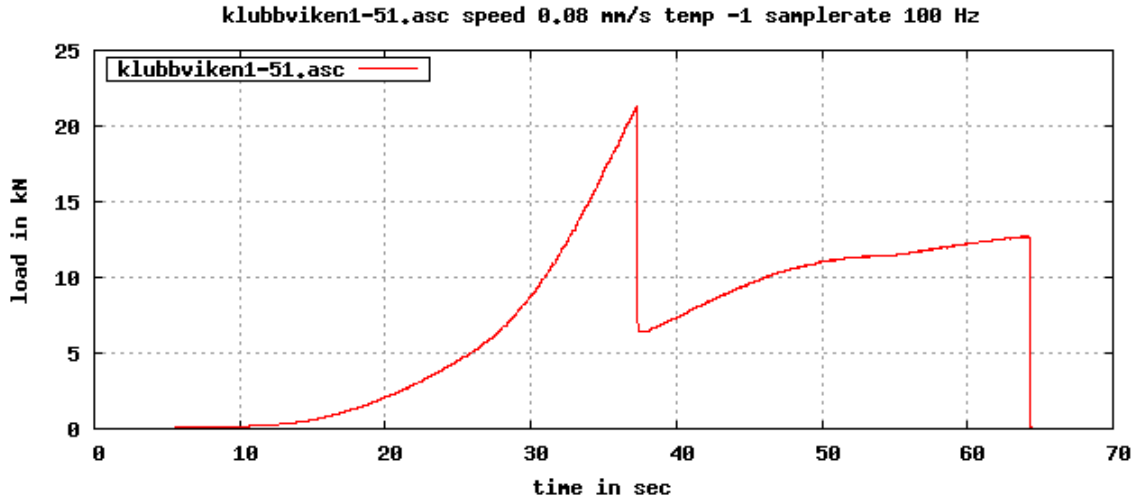
klubbviken1-51.asc speed 0.08 mm/s temp -1 samplerate 100 Hz
klubbviken1-51.asc
load in kN
time in sec
0
5
10
15
20
25
0
10
20
30
40
50
60
70

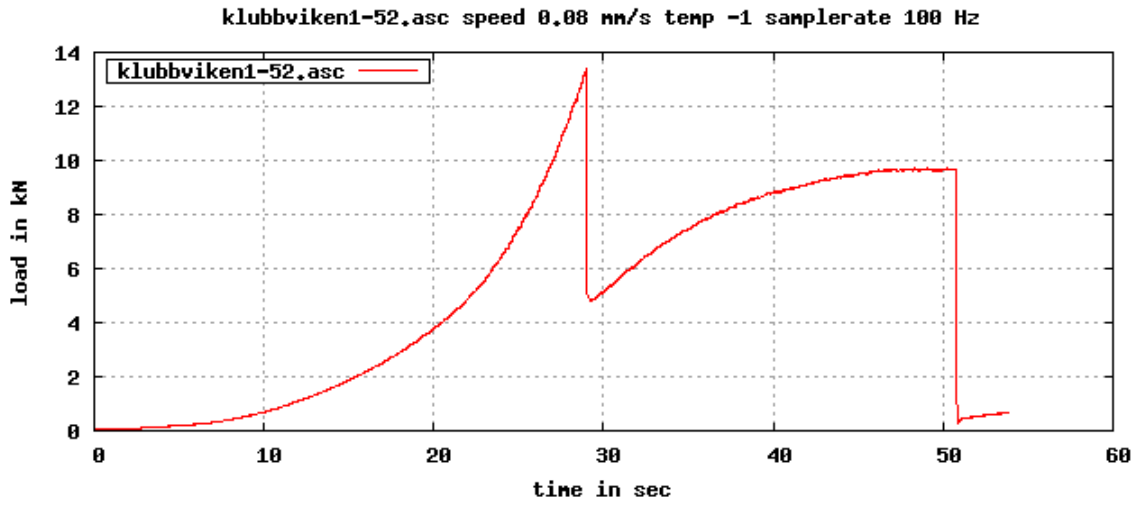
klubbviken1-52.asc speed 0.08 mm/s temp -1 samplerate 100 Hz
klubbviken1-52.asc
load in kN
time in sec
0
2
4
6
8
10
12
14
0
10
20
30
40
50
60

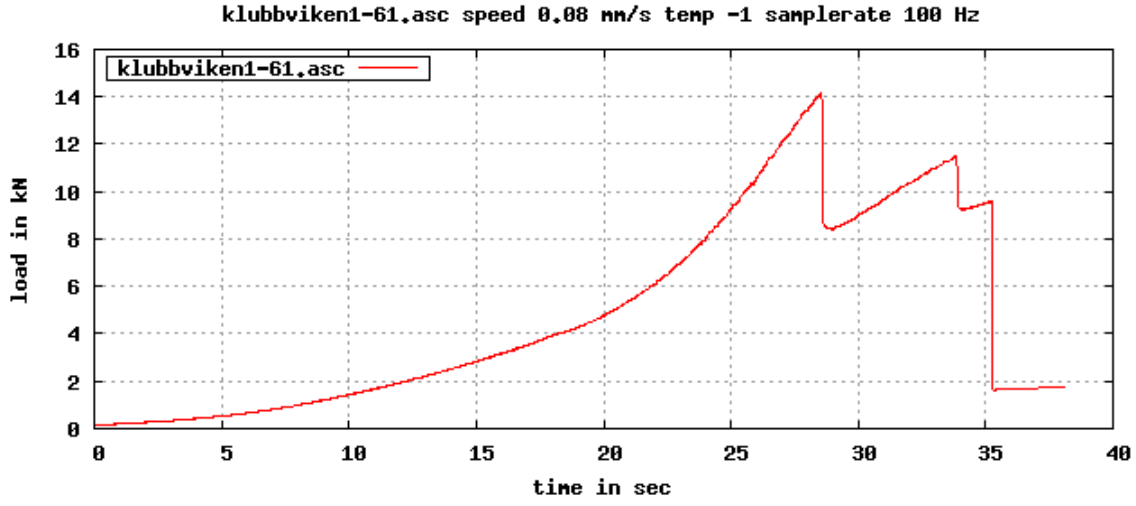
klubbviken1-61.asc speed 0.08 mm/s temp -1 samplerate 100 Hz
klubbviken1-61.asc
load in kN
time in sec
0
2
4
6
8
10
12
14
16
0
5
10
15
20
25
30
35
40

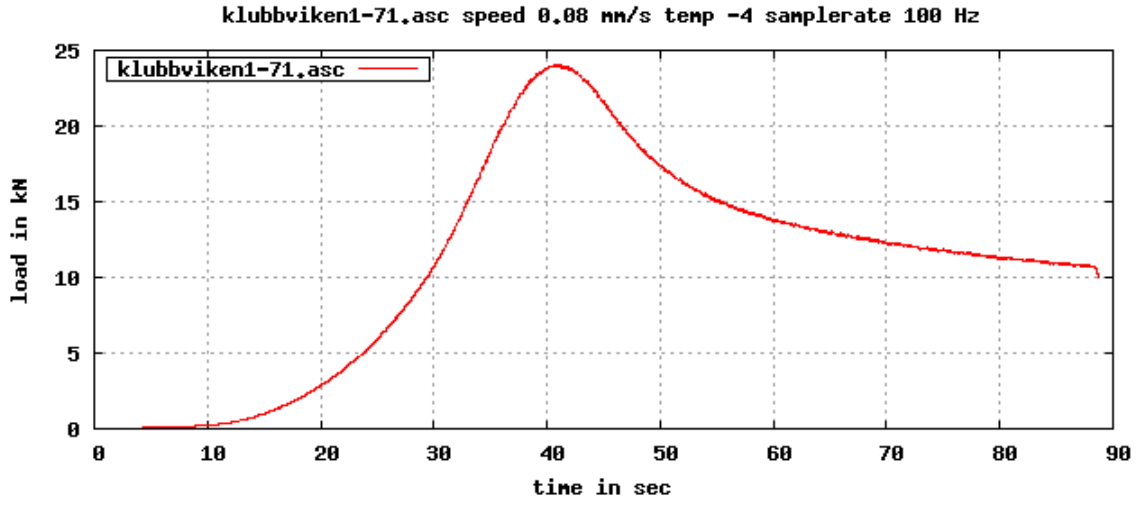
klubbviken1-71.asc speed 0.08 mm/s temp -4 samplerate 100 Hz
klubbviken1-71.asc
load in kN
time in sec
0
5
10
15
20
25
0
10
20
30
40
50
60
70
80
90

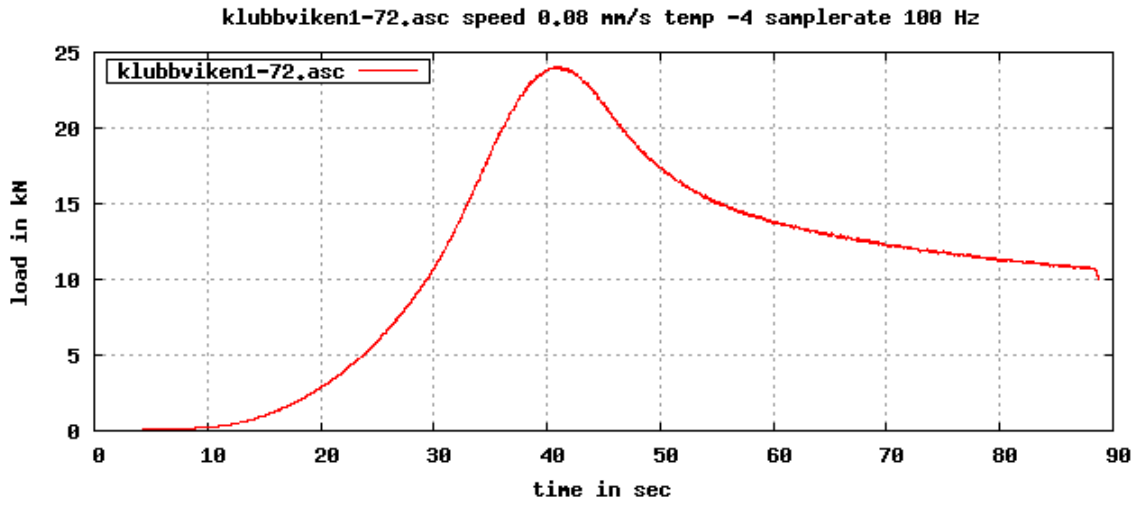
klubbviken1-72.asc speed 0.08 mm/s temp -4 samplerate 100 Hz
klubbviken1-72.asc
load in kN
time in sec
0
5
10
15
20
25
0
10
20
30
40
50
60
70
80
90

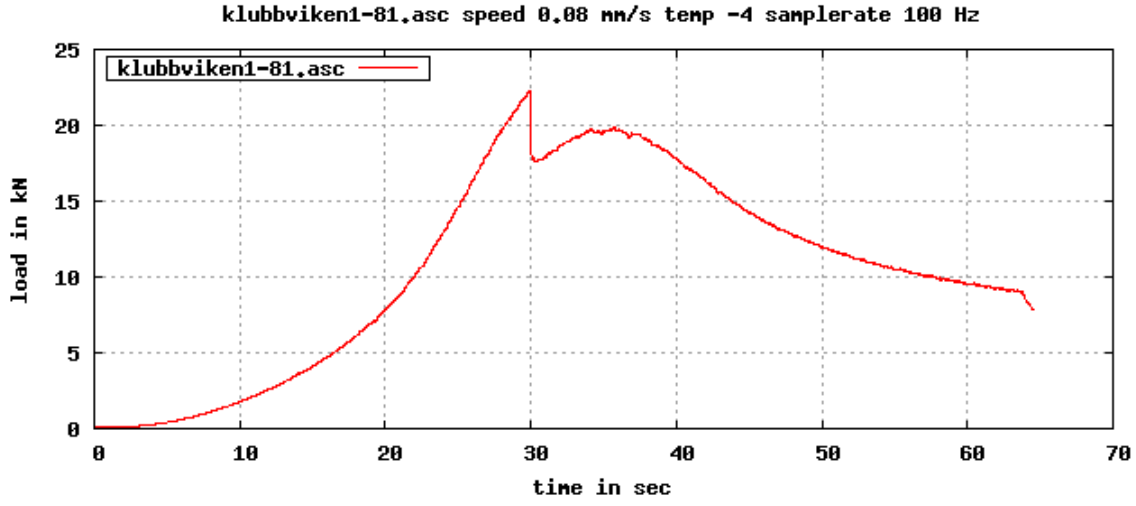
klubbviken1-81.asc speed 0.08 mm/s temp -4 samplerate 100 Hz
klubbviken1-81.asc
load in kN
time in sec
0
5
10
15
20
25
0
10
20
30
40
50
60
70

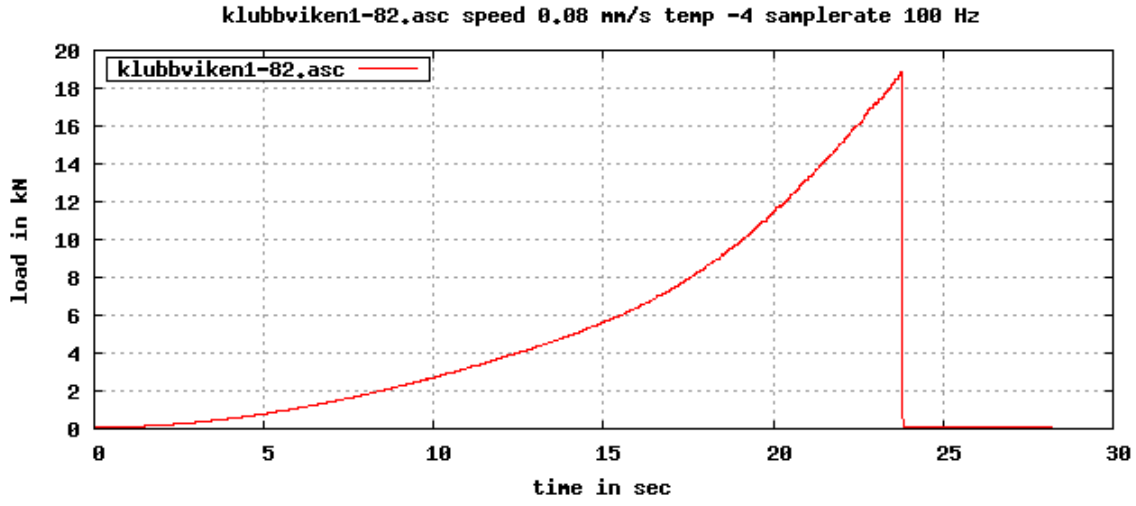
klubbviken1-82.asc speed 0.08 mm/s temp -4 samplerate 100 Hz
klubbviken1-82.asc
load in kN
time in sec
0
2
4
6
8
10
12
14
16
18
20
0
5
10
15
20
25
30

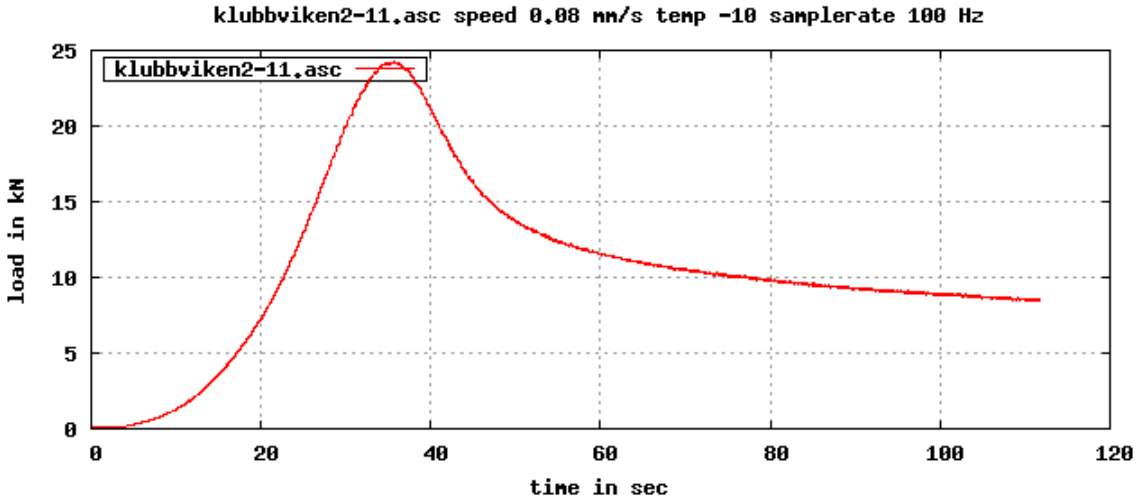
klubbviken2-11.asc speed 0.08 mm/s temp -10 samplerate 100 Hz
klubbviken2-11.asc
load in kN
time in sec
0
5
10
15
20
25
0
20
40
60
80
100
120

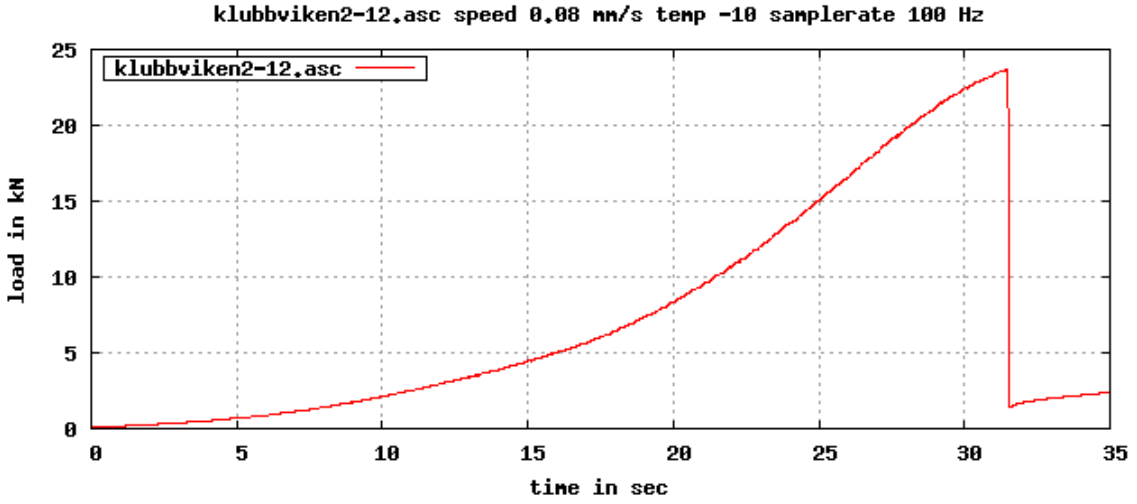
klubbviken2-12.asc speed 0.08 mm/s temp -10 samplerate 100 Hz
klubbviken2-12.asc
load in kN
time in sec
0
5
10
15
20
25
0
5
10
15
20
25
30
35

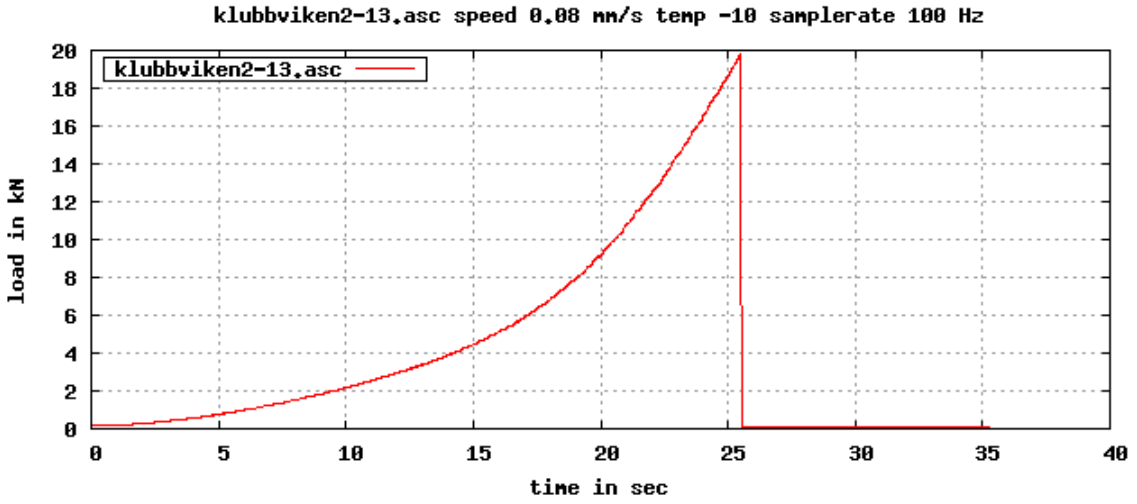
klubbviken2-13.asc speed 0.08 mm/s temp -10 samplerate 100 Hz
klubbviken2-13.asc
load in kN
time in sec
0
2
4
6
8
10
12
14
16
18
20
0
5
10
15
20
25
30
35
40

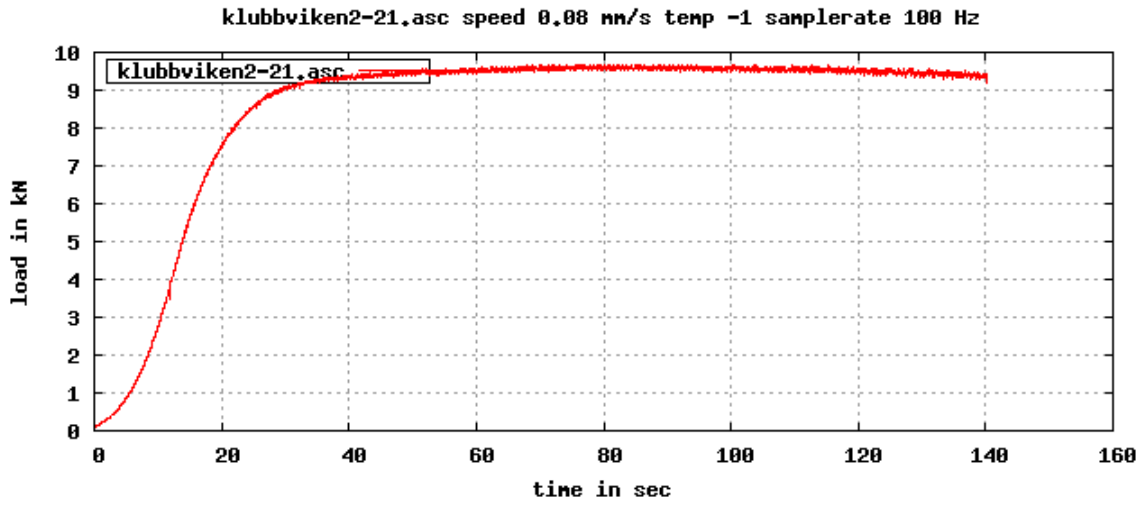
klubbviken2-21.asc speed 0.08 mm/s temp -1 samplerate 100 Hz
klubbviken2-21.asc
load in kN
time in sec
0
1
2
3
4
5
6
7
8
9
10
0
20
40
60
80
100
120
140
160

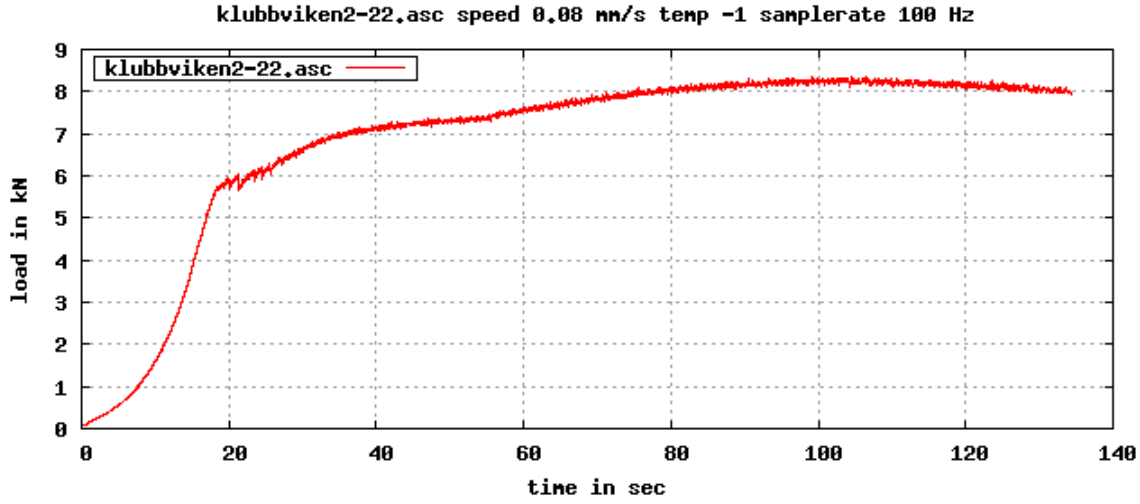
klubbviken2-22.asc speed 0.08 mm/s temp -1 samplerate 100 Hz
klubbviken2-22.asc
load in kN
time in sec
0
1
2
3
4
5
6
7
8
9
0
20
40
60
80
100
120
140

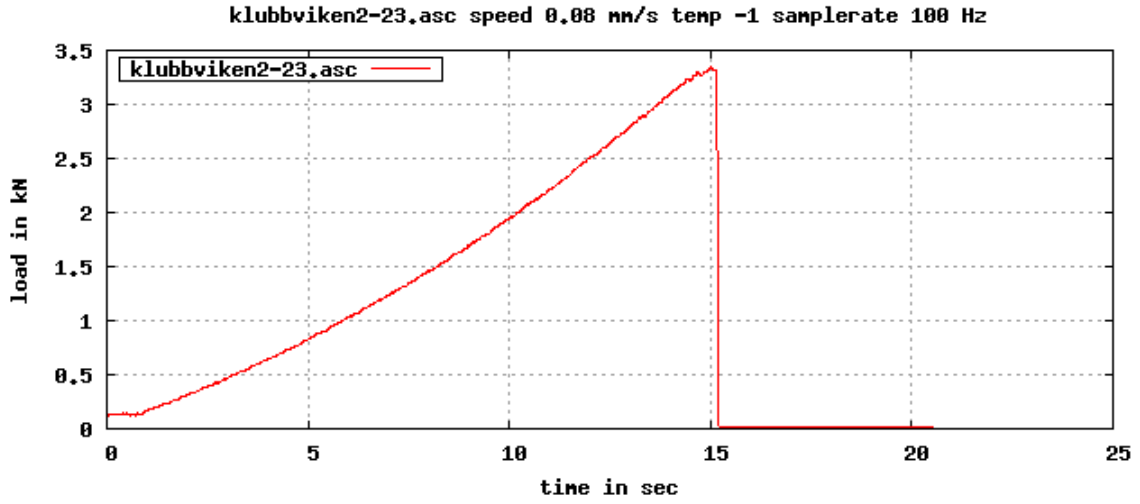
klubbviken2-23.asc speed 0.08 mm/s temp -1 samplerate 100 Hz
klubbviken2-23.asc
load in kN
time in sec
0
0.5
1
1.5
2
2.5
3
3.5
0
5
10
15
20
25

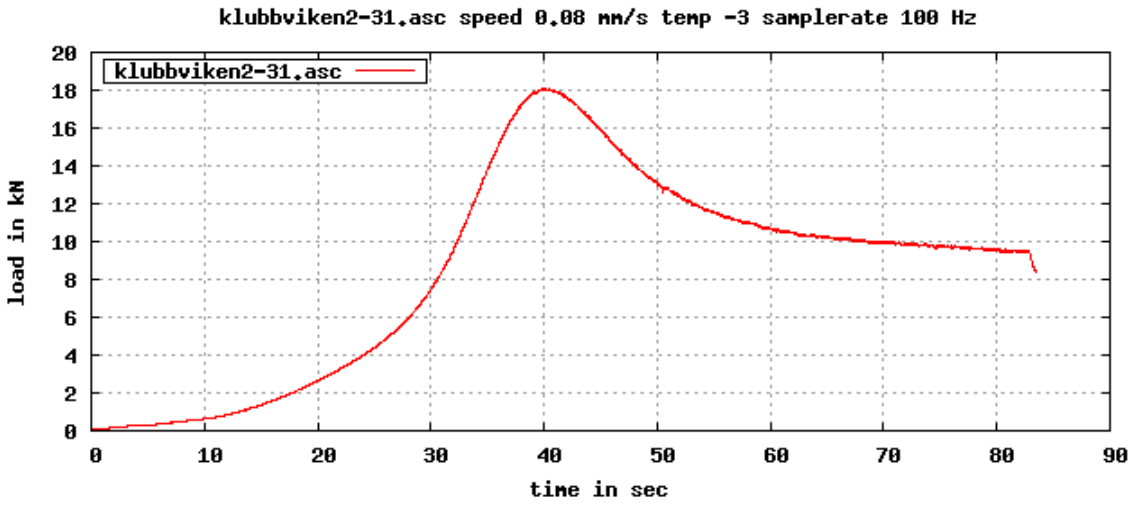
klubbviken2-31.asc speed 0.08 mm/s temp -3 samplerate 100 Hz
klubbviken2-31.asc
load in kN
time in sec
0
2
4
6
8
10
12
14
16
18
20
0
10
20
30
40
50
60
70
80
90

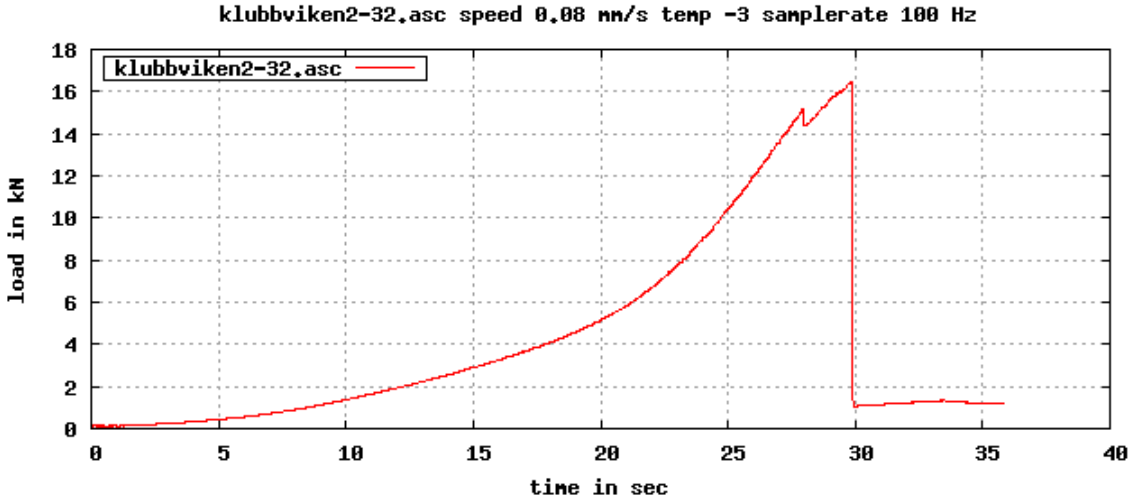
klubbviken2-32.asc speed 0.08 mm/s temp -3 samplerate 100 Hz
klubbviken2-32.asc
load in kN
time in sec
0
2
4
6
8
10
12
14
16
18
0
5
10
15
20
25
30
35
40

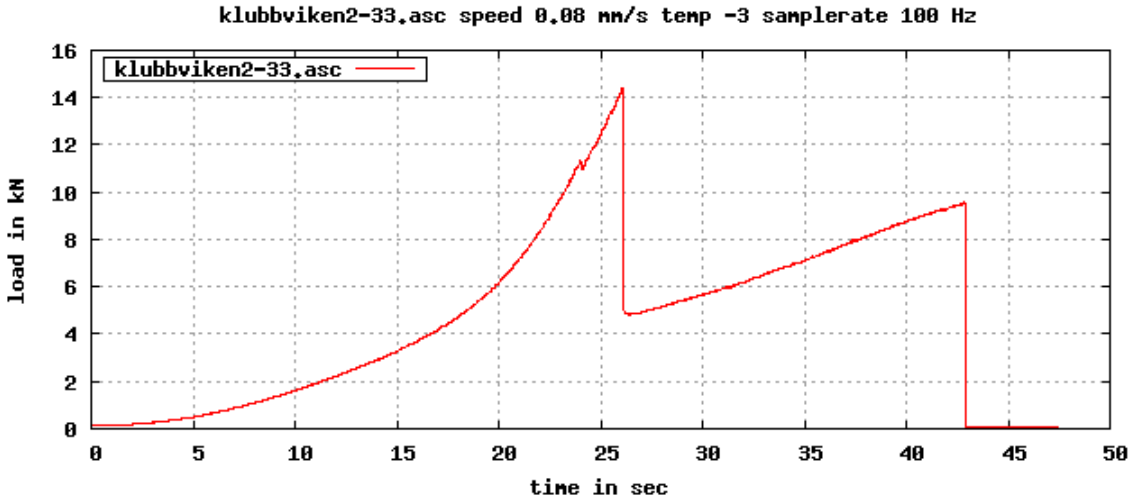
klubbviken2-33.asc speed 0.08 mm/s temp -3 samplerate 100 Hz
klubbviken2-33.asc
load in kN
time in sec
0
2
4
6
8
10
12
14
16
0
5
10
15
20
25
30
35
40
45
50

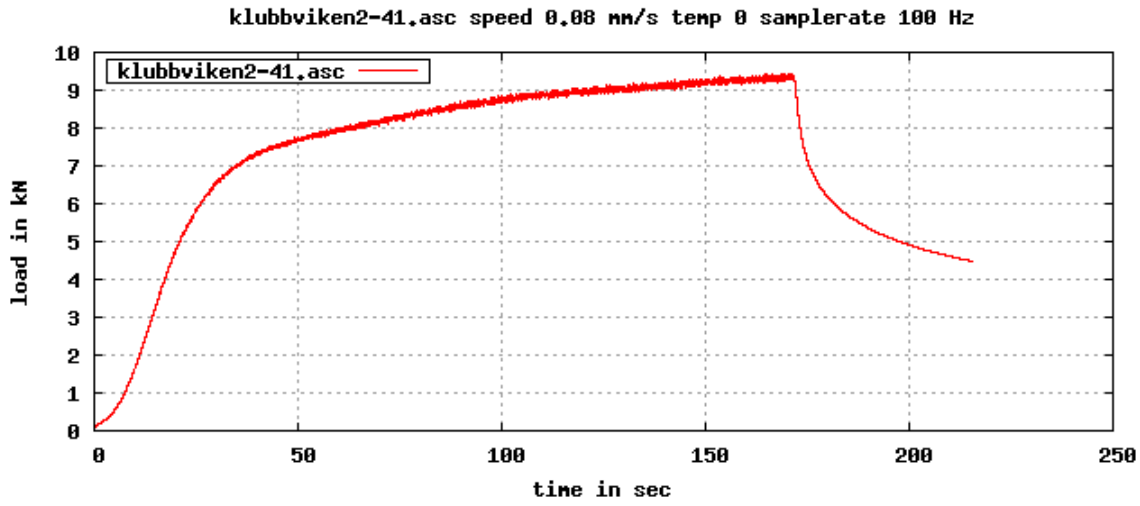
klubbviken2-41.asc speed 0.08 mm/s temp 0 samplerate 100 Hz
klubbviken2-41.asc
load in kN
time in sec
0
1
2
3
4
5
6
7
8
9
10
0
50
100
150
200
250

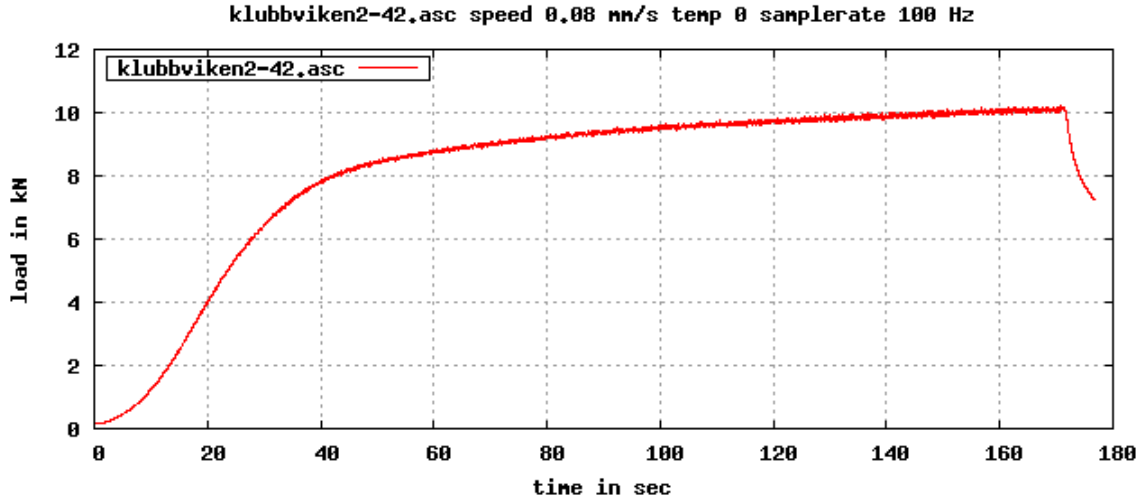
klubbviken2-42.asc speed 0.08 mm/s temp 0 samplerate 100 Hz
klubbviken2-42.asc
load in kN
time in sec
0
2
4
6
8
10
12
0
20
40
60
80
100
120
140
160
180

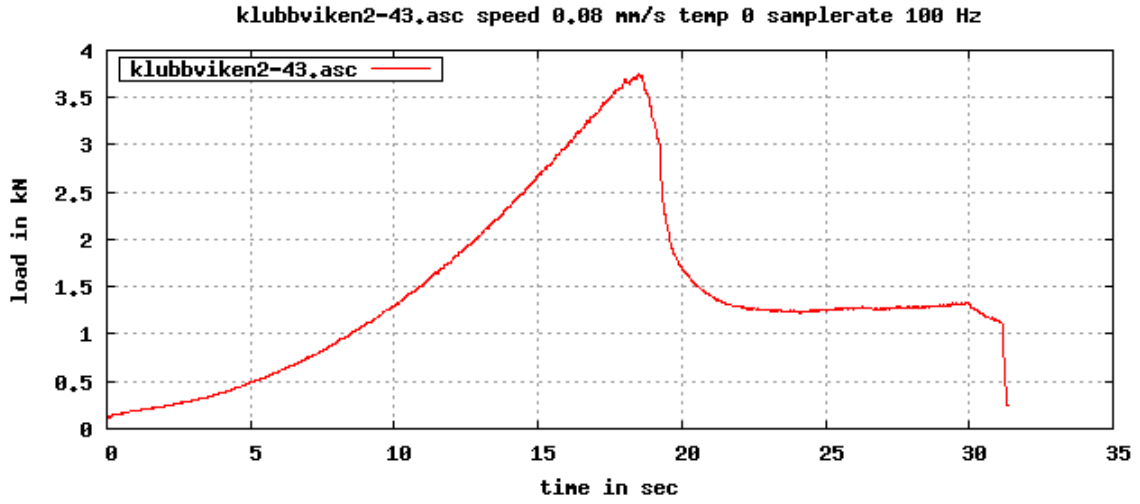
klubbviken2-43.asc speed 0.08 mm/s temp 0 samplerate 100 Hz
klubbviken2-43.asc
load in kN
time in sec
0
0.5
1
1.5
2
2.5
3
3.5
4
0
5
10
15
20
25
30
35

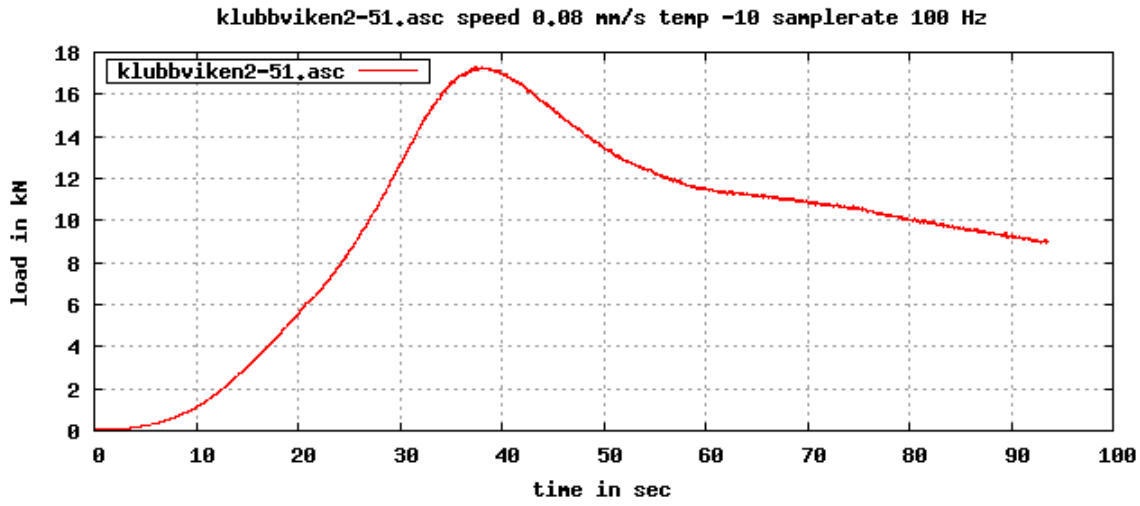
klubbviken2-51.asc speed 0.08 mm/s temp -10 samplerate 100 Hz
klubbviken2-51.asc
load in kN
time in sec
0
2
4
6
8
10
12
14
16
18
0
10
20
30
40
50
60
70
80
90
100

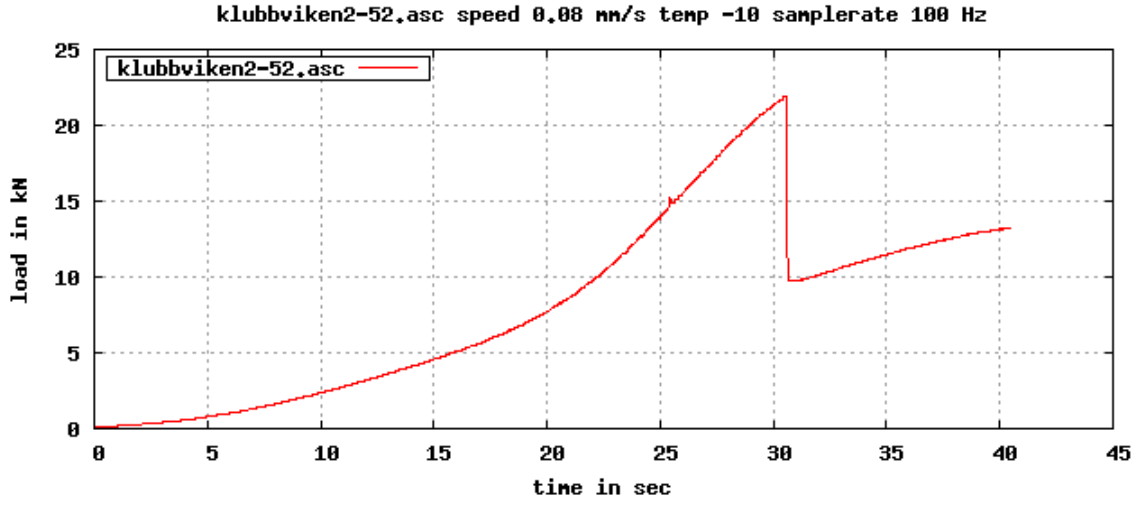
klubbviken2-52.asc speed 0.08 mm/s temp -10 samplerate 100 Hz
klubbviken2-52.asc
load in kN
time in sec
0
5
10
15
20
25
0
5
10
15
20
25
30
35
40
45

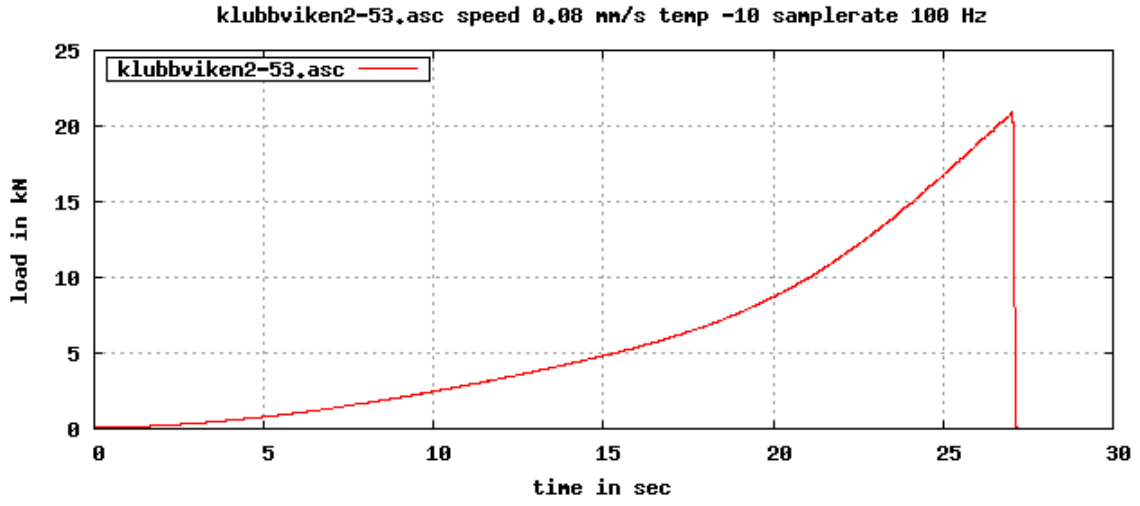
klubbviken2-53.asc speed 0.08 mm/s temp -10 samplerate 100 Hz
klubbviken2-53.asc
load in kN
time in sec
0
5
10
15
20
25
0
5
10
15
20
25
30

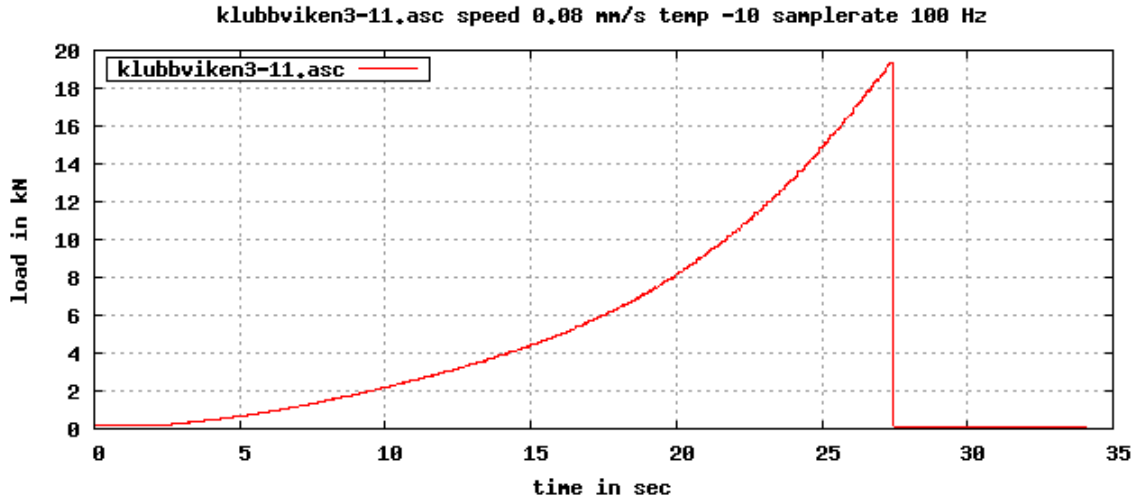
klubbviken3-11.asc speed 0.08 mm/s temp -10 samplerate 100 Hz
klubbviken3-11.asc
load in kN
time in sec
0
2
4
6
8
10
12
14
16
18
20
0
5
10
15
20
25
30
35

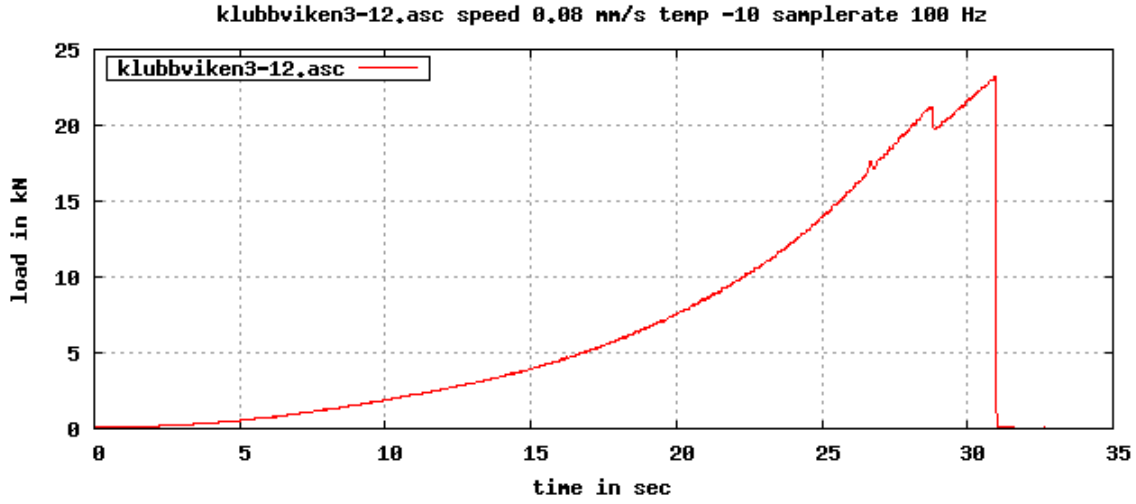
klubbviken3-12.asc speed 0.08 mm/s temp -10 samplerate 100 Hz
klubbviken3-12.asc
load in kN
time in sec
0
5
10
15
20
25
0
5
10
15
20
25
30
35

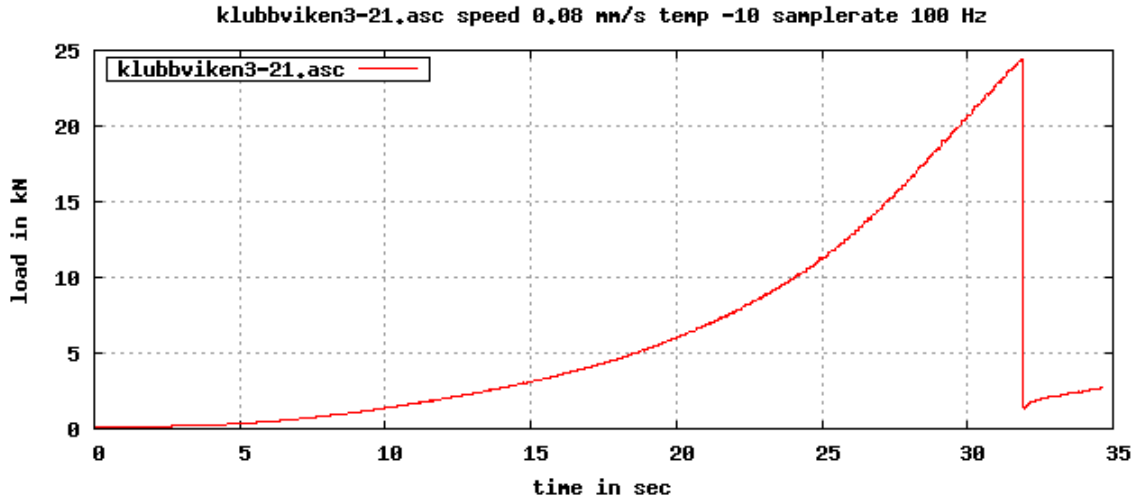
klubbviken3-21.asc speed 0.08 mm/s temp -10 samplerate 100 Hz
klubbviken3-21.asc
load in kN
time in sec
0
5
10
15
20
25
0
5
10
15
20
25
30
35

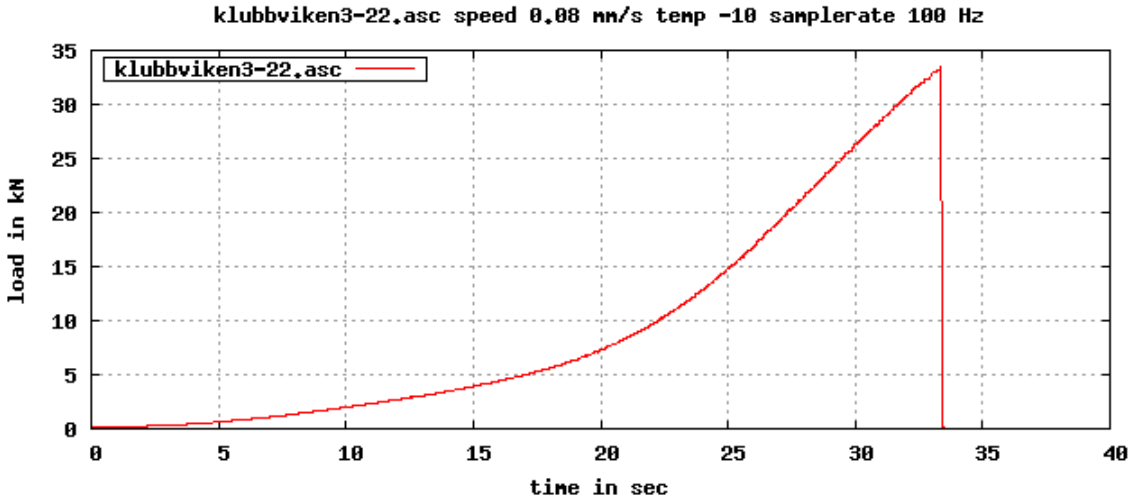
klubbviken3-22.asc speed 0.08 mm/s temp -10 samplerate 100 Hz
klubbviken3-22.asc
load in kN
time in sec
0
5
10
15
20
25
30
35
40

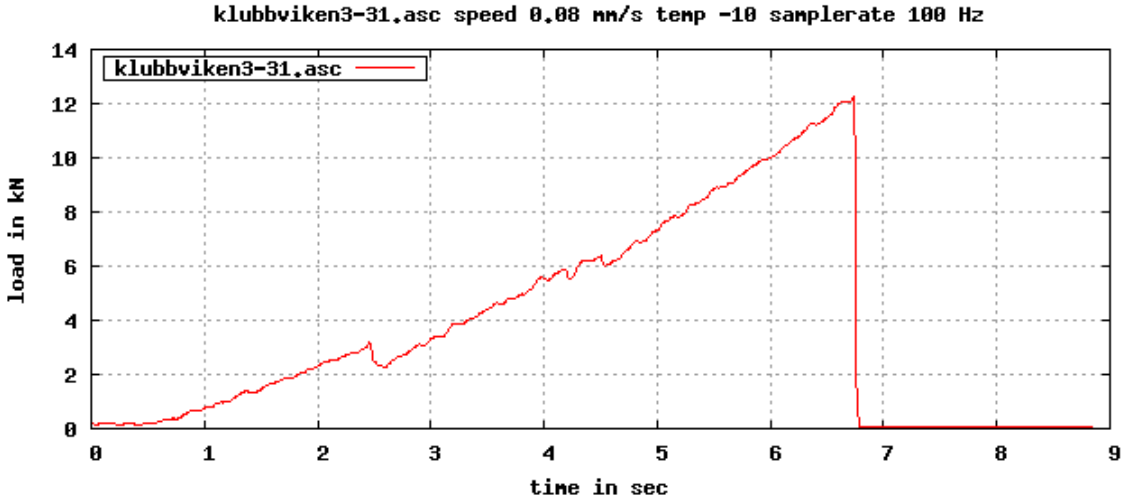
klubbviken3-31.asc speed 0.08 mm/s temp -10 samplerate 100 Hz
klubbviken3-31.asc
load in kN
time in sec
0
1
2
3
4
5
6
7
8
9

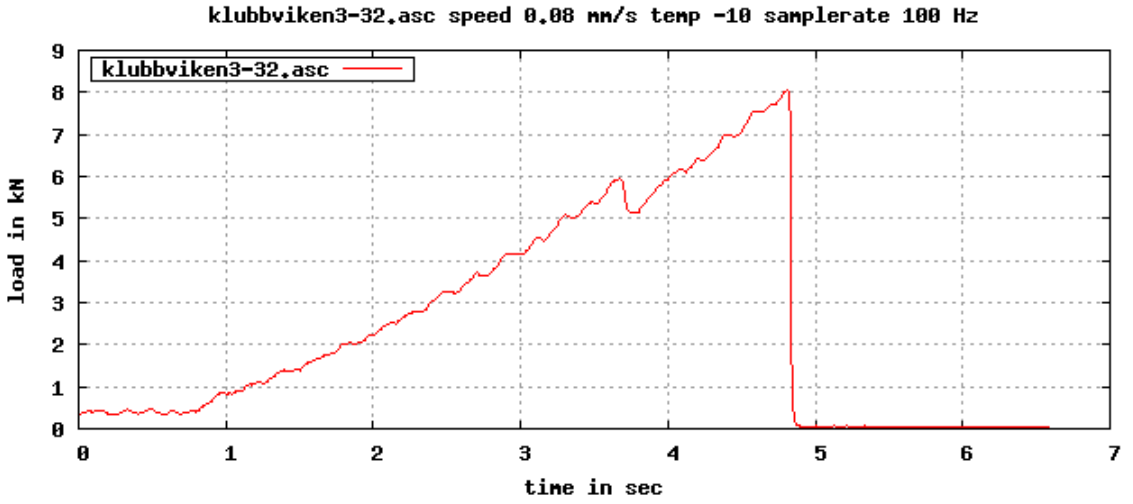
klubbviken3-32.asc speed 0.08 mm/s temp -10 samplerate 100 Hz
klubbviken3-32.asc
load in kN
time in sec
0
1
2
3
4
5
6
7

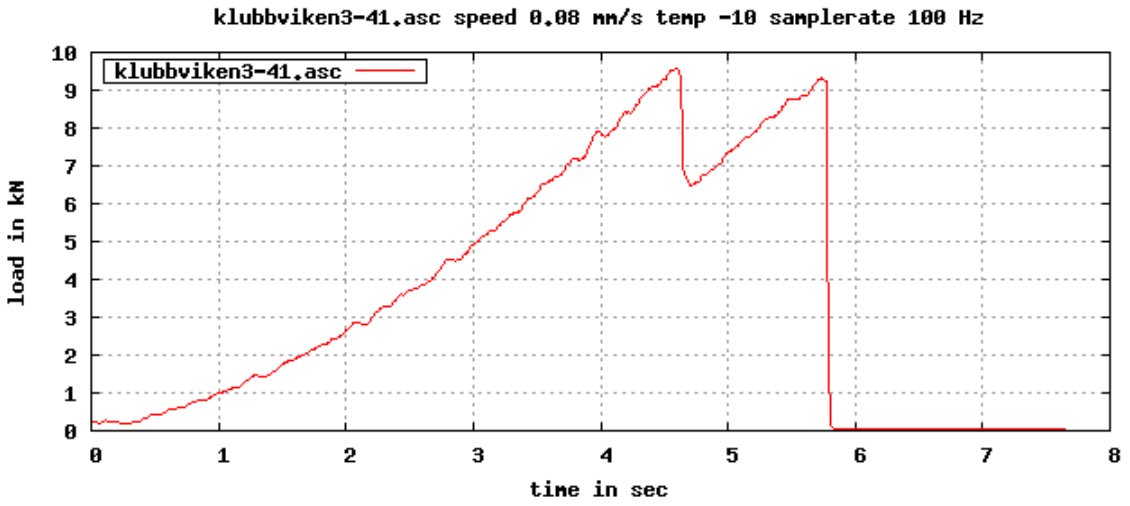
klubbviken3-41.asc speed 0.08 mm/s temp -10 samplerate 100 Hz
klubbviken3-41.asc
load in kN
time in sec
0
1
2
3
4
5
6
7
8
9
10

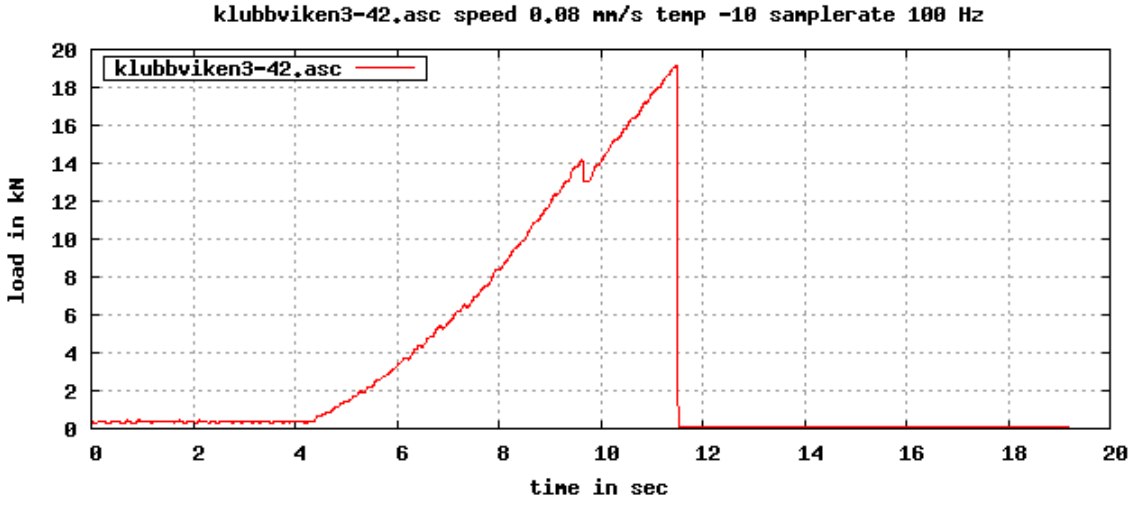
klubbviken3-42.asc speed 0.08 mm/s temp -10 samplerate 100 Hz
klubbviken3-42.asc
load in kN
time in sec
0
2
4
6
8
10
12
14
16
18
20

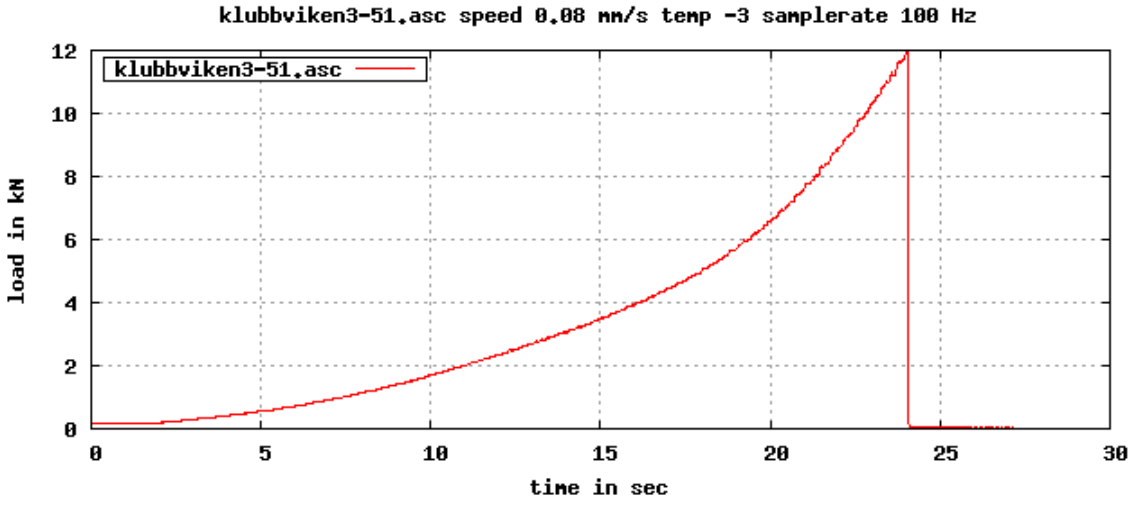
klubbviken3-51.asc speed 0.08 mm/s temp -3 samplerate 100 Hz
klubbviken3-51.asc
load in kN
time in sec
0
5
10
15
20
25
30
2
4
6
8
10
12

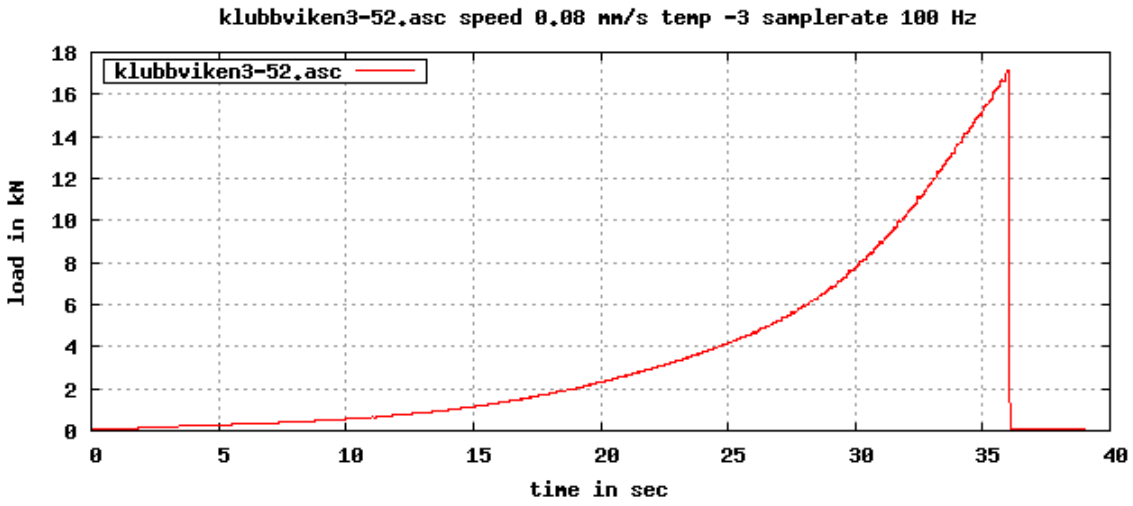
klubbviken3-52.asc speed 0.08 mm/s temp -3 samplerate 100 Hz
klubbviken3-52.asc
load in kN
time in sec
0
2
4
6
8
10
12
14
16
18
0
5
10
15
20
25
30
35
40

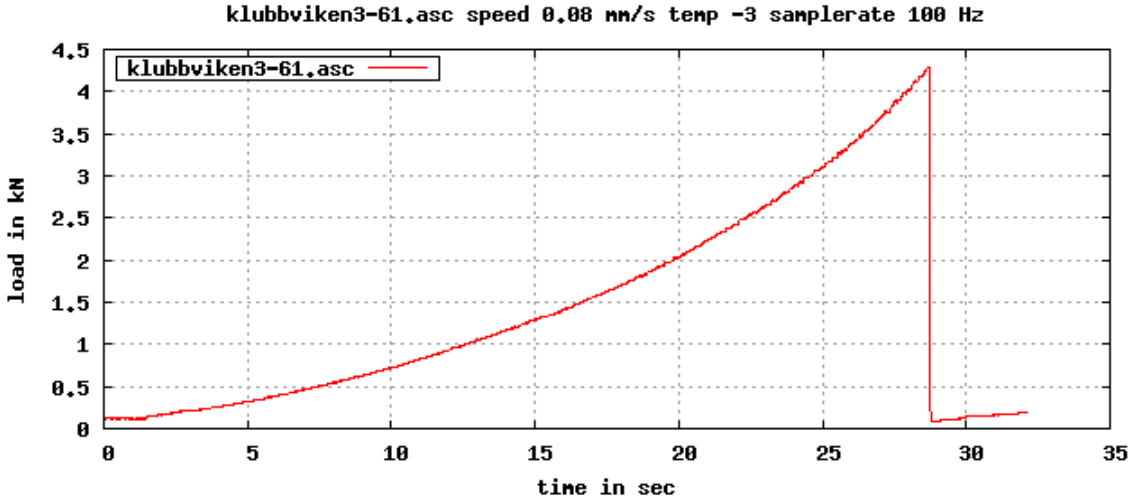
klubbviken3-61.asc speed 0.08 mm/s temp -3 samplerate 100 Hz
klubbviken3-61.asc
load in kN
time in sec
0
0.5
1
1.5
2
2.5
3
3.5
4
4.5
0
5
10
15
20
25
30
35

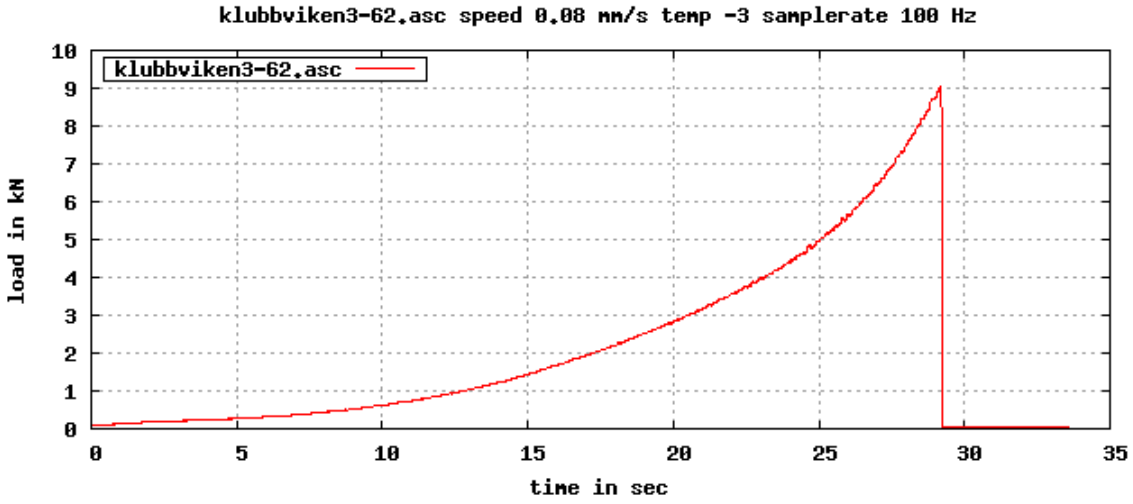
klubbviken3-62.asc speed 0.08 mm/s temp -3 samplerate 100 Hz
klubbviken3-62.asc
load in kN
time in sec
0
1
2
3
4
5
6
7
8
9
10
0
5
10
15
20
25
30
35

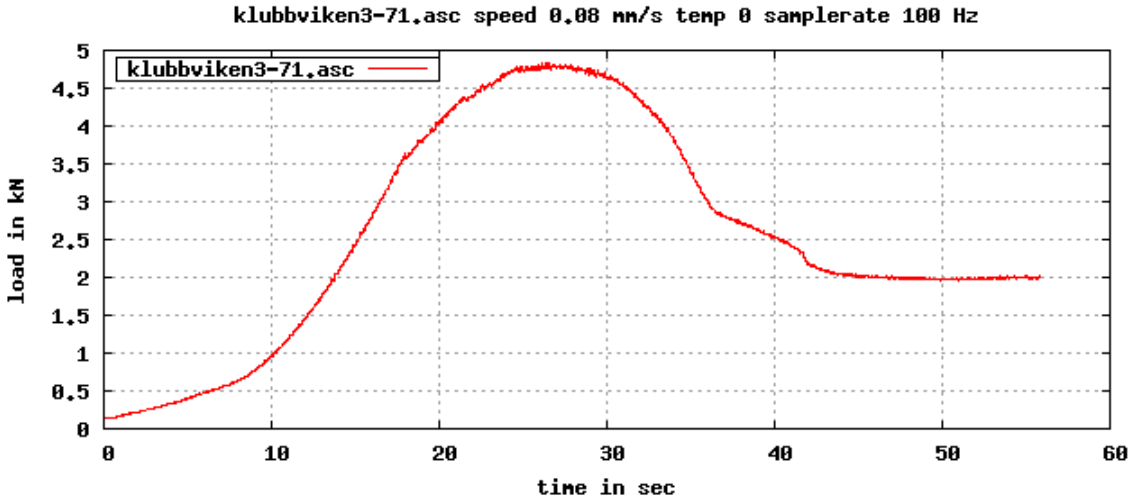
klubbviken3-71.asc speed 0.08 mm/s temp 0 samplerate 100 Hz
klubbviken3-71.asc
load in kN
time in sec
0
0.5
1
1.5
2
2.5
3
3.5
4
4.5
5
0
10
20
30
40
50
60

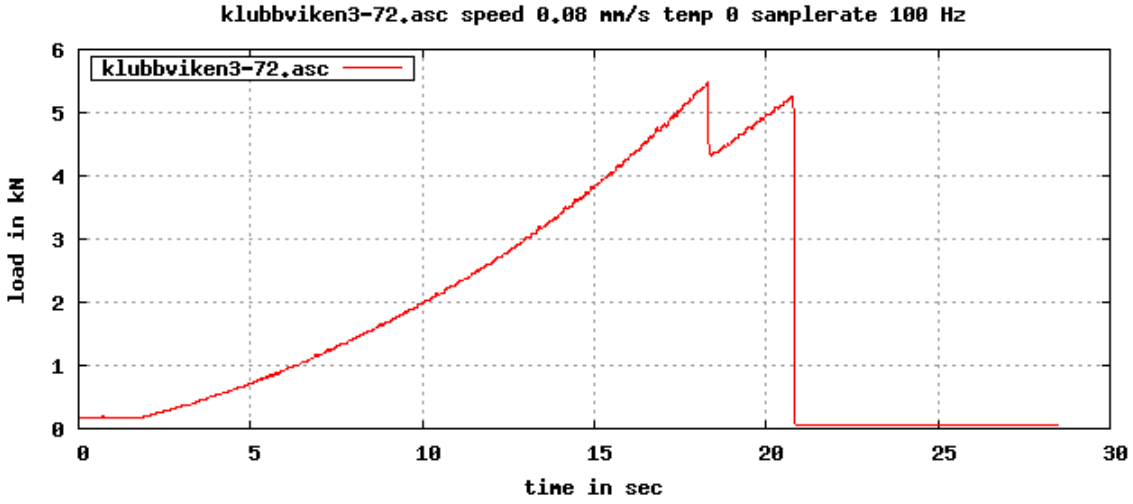
klubbviken3-72.asc speed 0.08 mm/s temp 0 samplerate 100 Hz
klubbviken3-72.asc
load in kN
time in sec
0
1
2
3
4
5
6
0
5
10
15
20
25
30

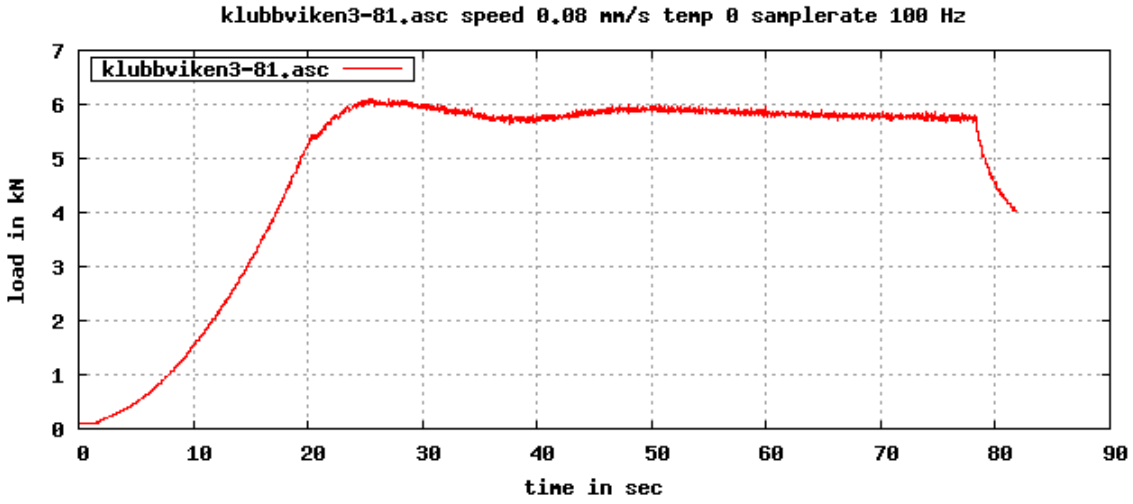
klubbviken3-81.asc speed 0.08 mm/s temp 0 samplerate 100 Hz
klubbviken3-81.asc
load in kN
time in sec
0
1
2
3
4
5
6
7
0
10
20
30
40
50
60
70
80
90

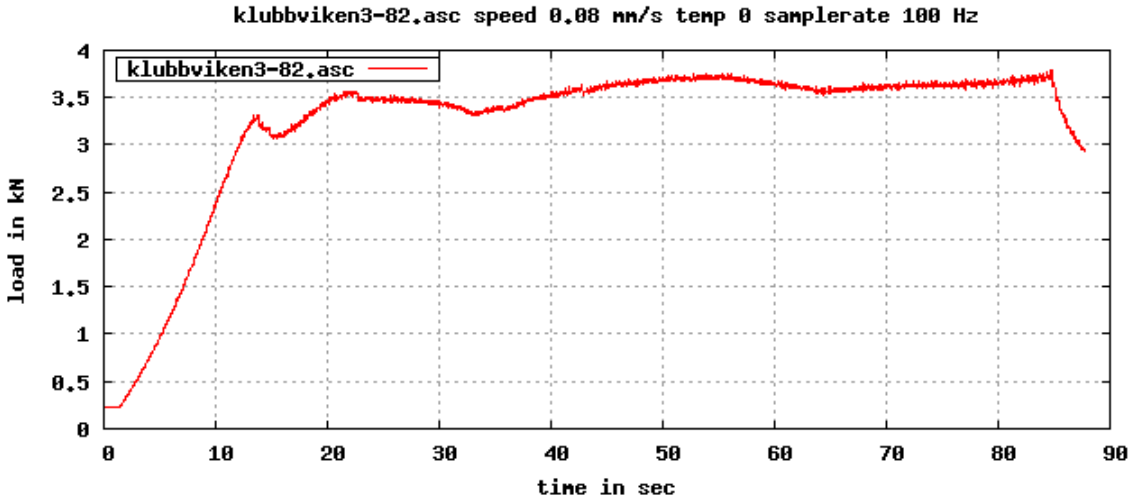
klubbviken3-82.asc speed 0.08 mm/s temp 0 samplerate 100 Hz
klubbviken3-82.asc
load in kN
time in sec
0
0.5
1
1.5
2
2.5
3
3.5
4
0
10
20
30
40
50
60
70
80
90

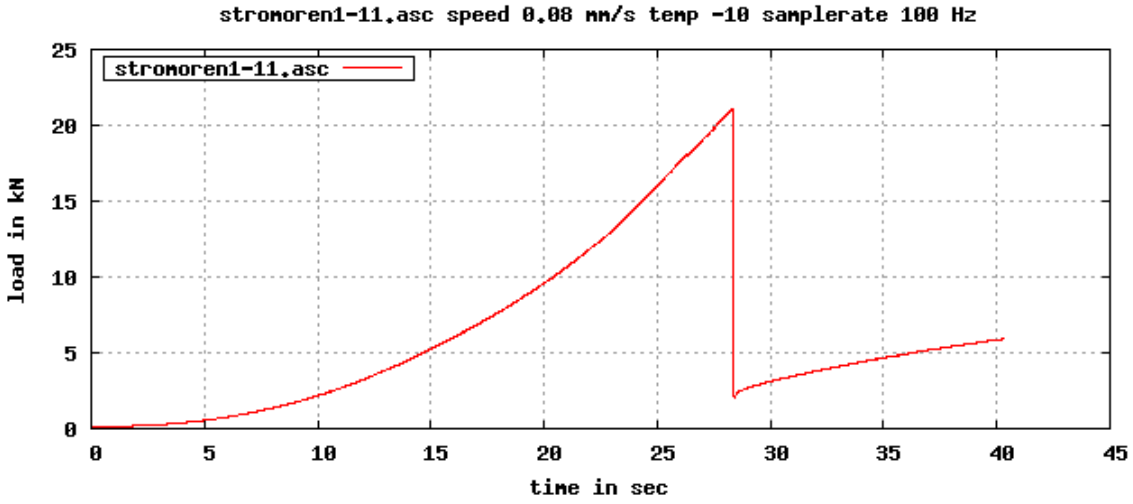
stromoren1-11.asc speed 0.08 mm/s temp -10 samplerate 100 Hz
stromoren1-11.asc
load in kN
time in sec
0
5
10
15
20
25
0
5
10
15
20
25
30
35
40
45

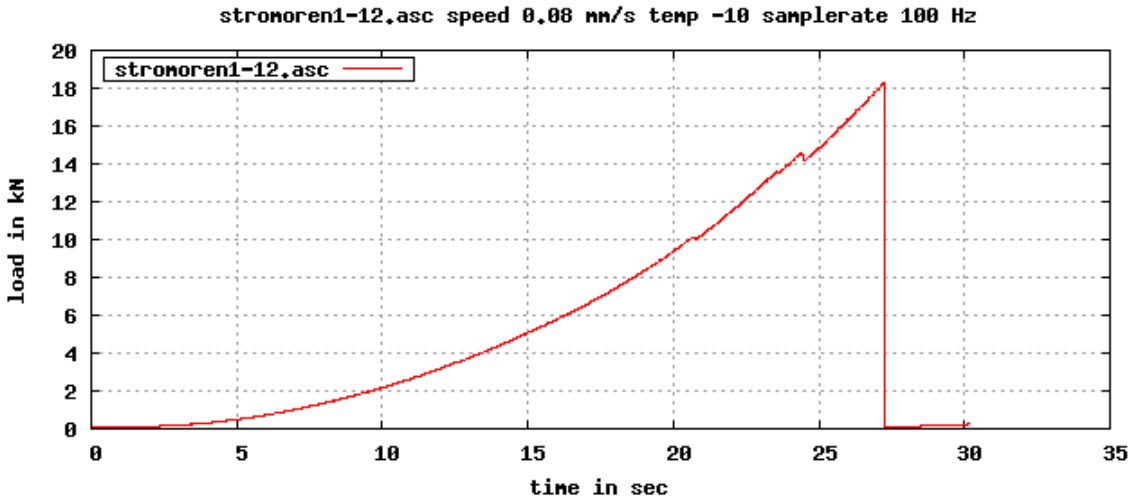
stromoren1-12.asc speed 0.08 mm/s temp -10 samplerate 100 Hz
stromoren1-12.asc
load in kN
time in sec
0
2
4
6
8
10
12
14
16
18
20
0
5
10
15
20
25
30
35

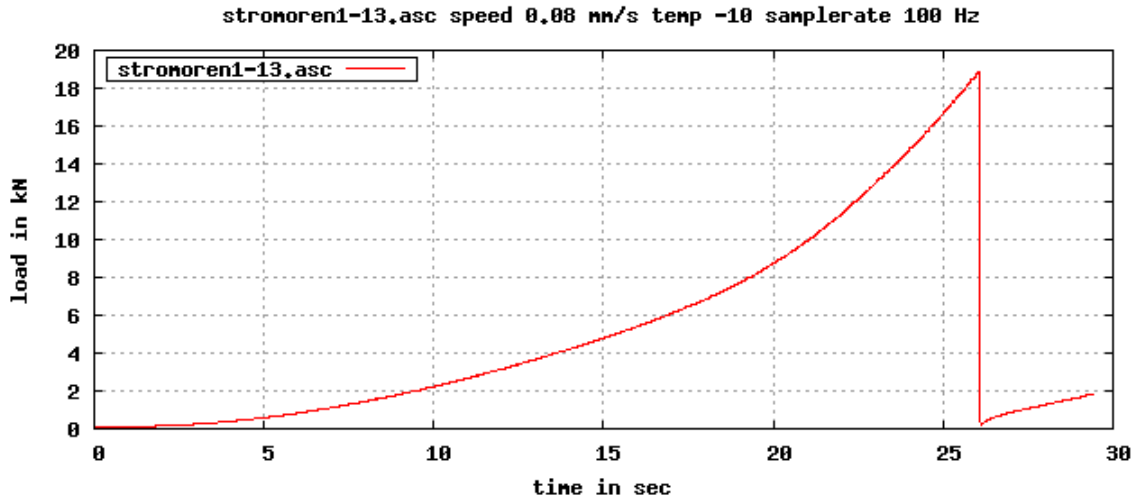
stromoren1-13.asc speed 0.08 mm/s temp -10 samplerate 100 Hz
stromoren1-13.asc
load in kN
time in sec
0
2
4
6
8
10
12
14
16
18
20
0
5
10
15
20
25
30

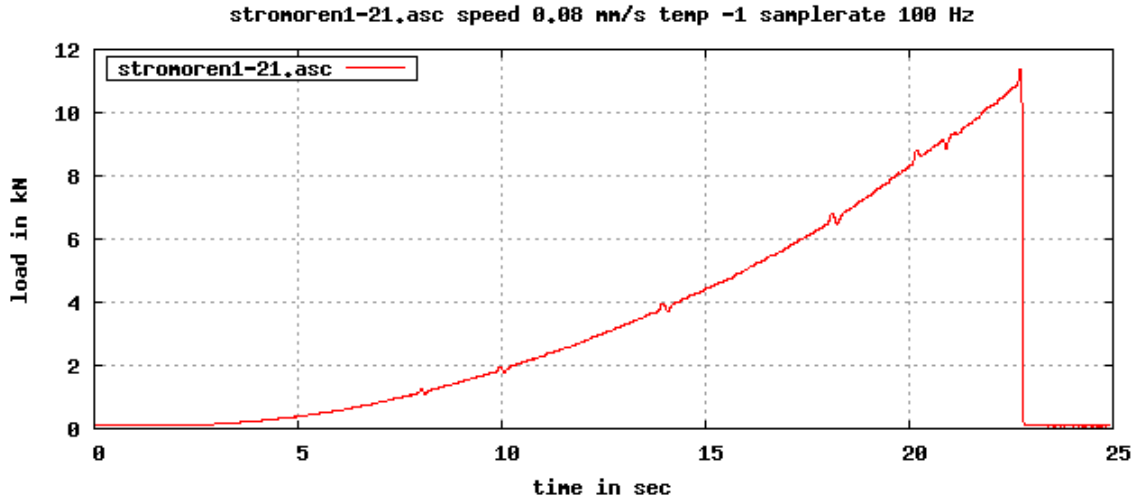
stromoren1-21.asc speed 0.08 mm/s temp -1 samplerate 100 Hz
stromoren1-21.asc
load in kN
time in sec
0
2
4
6
8
10
12
0
5
10
15
20
25

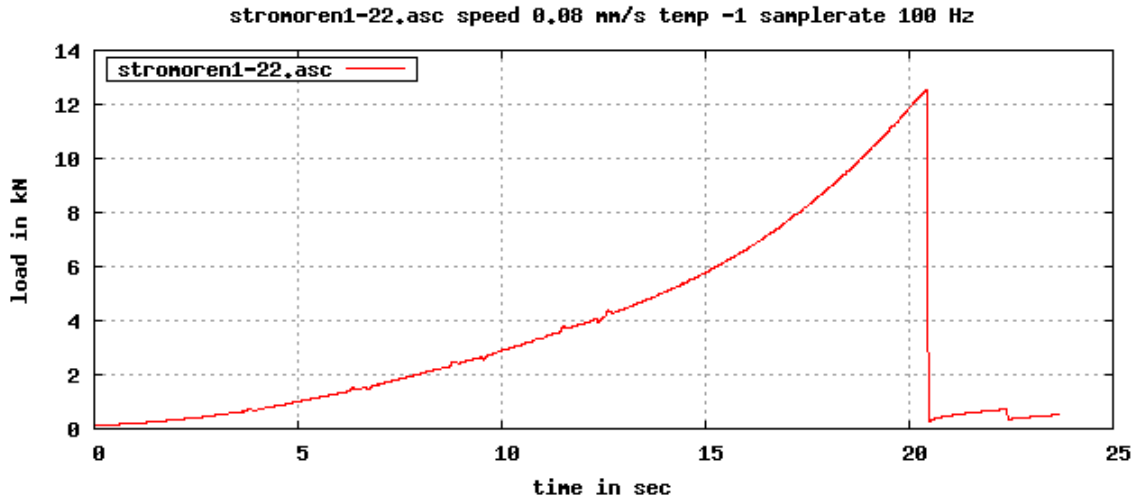
stromoren1-22.asc speed 0.08 mm/s temp -1 samplerate 100 Hz
stromoren1-22.asc
load in kN
time in sec
0
2
4
6
8
10
12
14
0
5
10
15
20
25

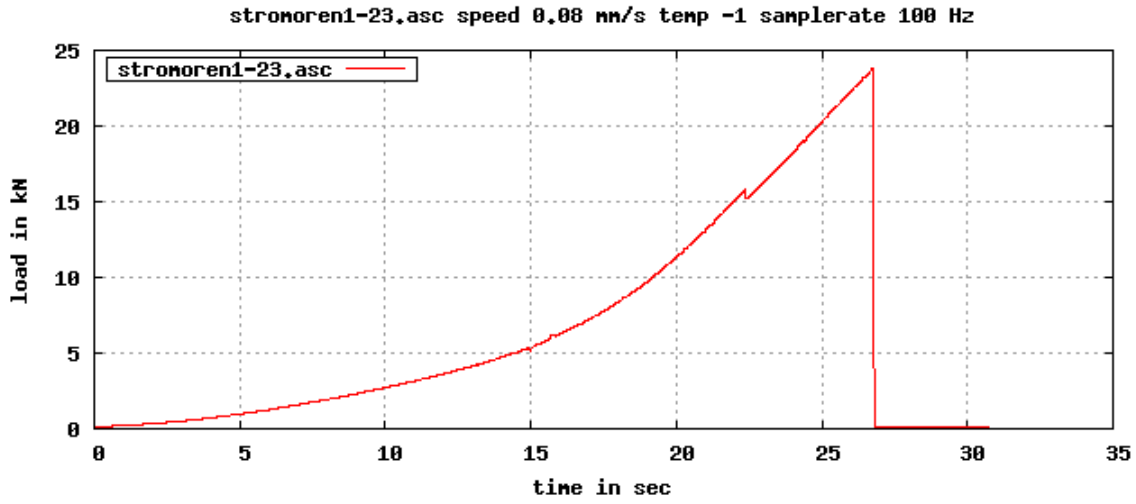
stromoren1-23.asc speed 0.08 mm/s temp -1 samplerate 100 Hz
stromoren1-23.asc
load in kN
time in sec
0
5
10
15
20
25
30
35

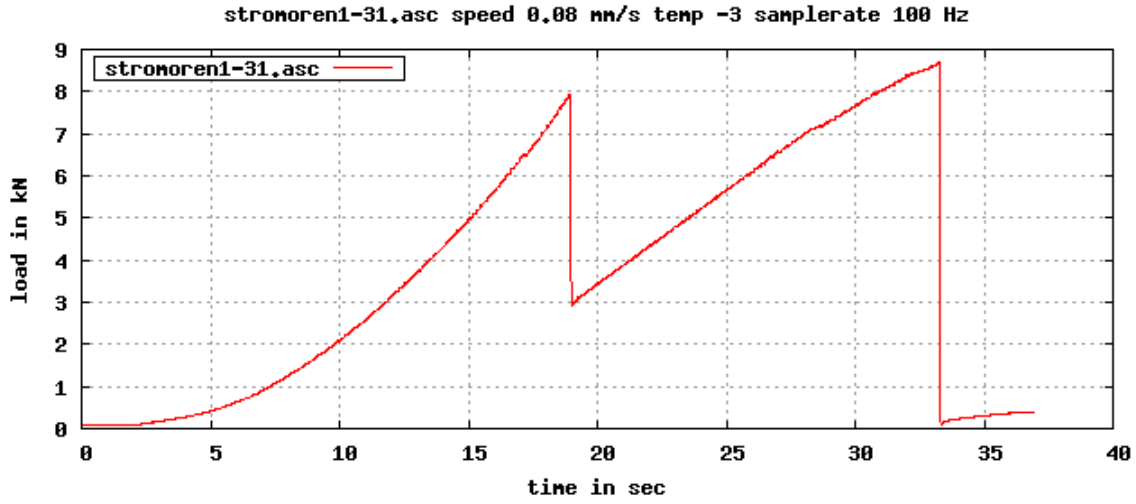
stromoren1-31.asc speed 0.08 mm/s temp -3 samplerate 100 Hz
stromoren1-31.asc
load in kN
time in sec
0
5
10
15
20
25
30
35
40

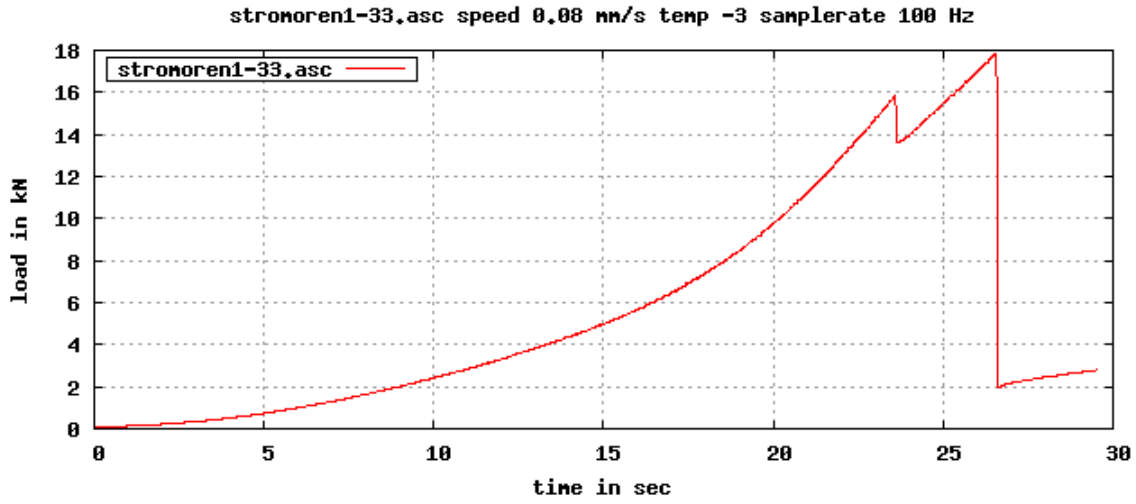
stromoren1-33.asc speed 0.08 mm/s temp -3 samplerate 100 Hz
stromoren1-33.asc
load in kN
time in sec
0
5
10
15
20
25
30

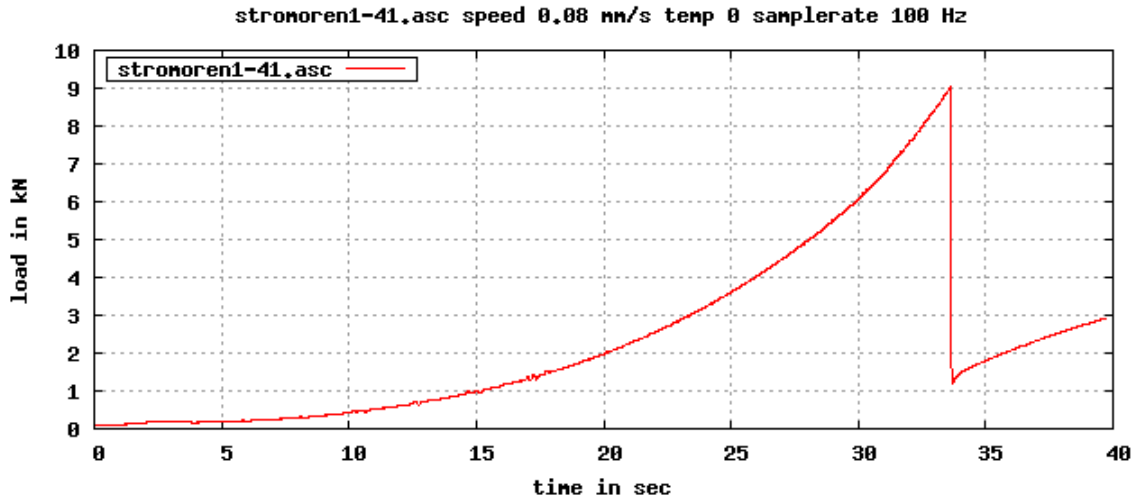
stromoren1-41.asc speed 0.08 mm/s temp 0 samplerate 100 Hz
stromoren1-41.asc
load in kN
time in sec
0
1
2
3
4
5
6
7
8
9
10
0
5
10
15
20
25
30
35
40

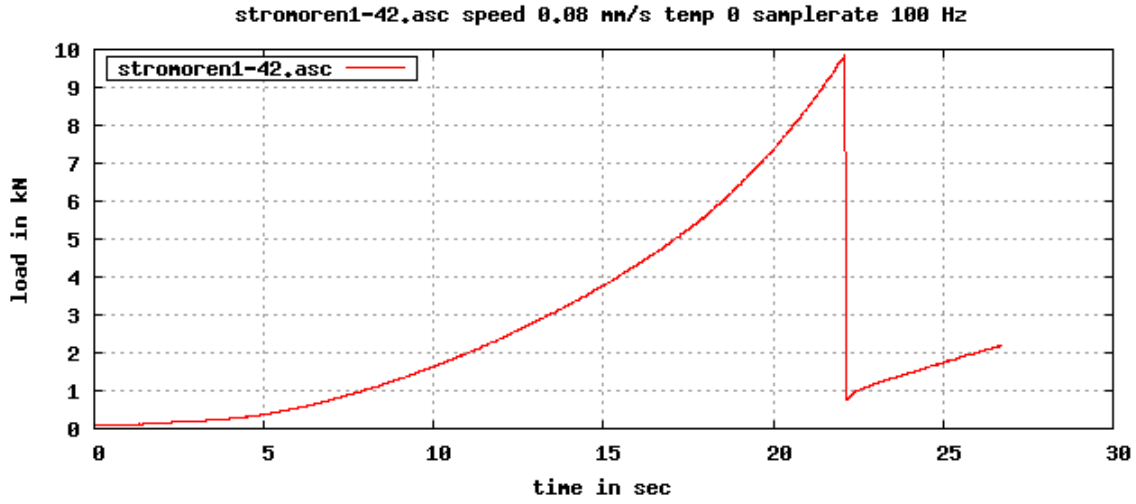
stromoren1-42.asc speed 0.08 mm/s temp 0 samplerate 100 Hz
stromoren1-42.asc
load in kN
time in sec
0
1
2
3
4
5
6
7
8
9
10
0
5
10
15
20
25
30

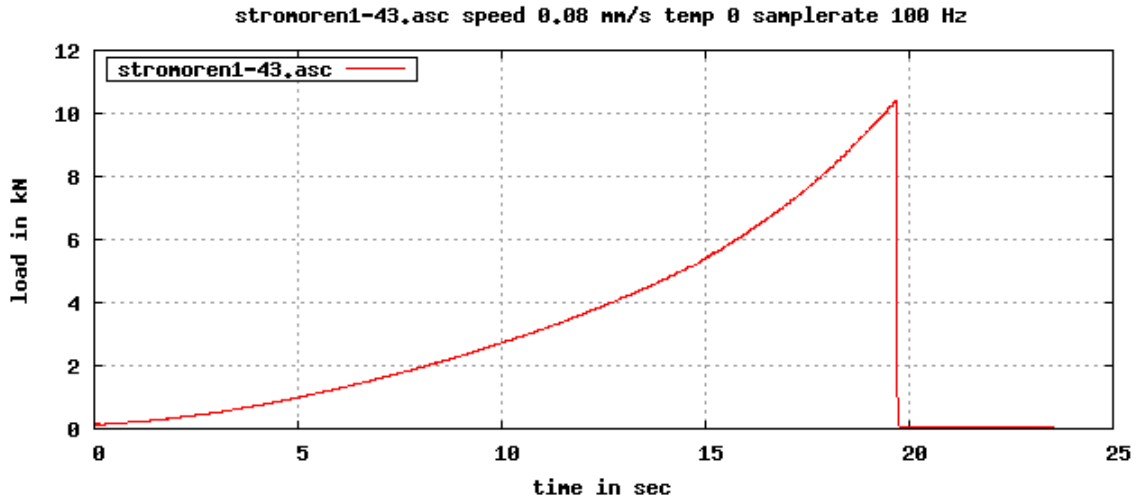
stromoren1-43.asc speed 0.08 mm/s temp 0 samplerate 100 Hz
stromoren1-43.asc
load in kN
time in sec
0
2
4
6
8
10
12
0
5
10
15
20
25

Ice Induced Vibrations of Slender Structures

Tuomo Kärnä

Modelling Ice-induced Vibrations of Vertical Structures

Karna Research and Consulting
Lauttasaarentie 31
00200 Helsinki
tuomo.karna@gmail.com
Puhelin: 044-033 6642

CONTENTS

1. Introduction

Dynamic ice loads are generated when a drifting ice floe or an iceberg impacts against an offshore structure. Generally, slender structures exhibit a dynamic behaviour that must be considered in the design. A soft foundation and moderate velocities of the ice floes lead to a similar situation. A commonly observed form of interaction between an ice floe and structure can be characterized as quasi-static. In this case the ice crushes intermittently and causes transient vibrations which decay before the next event of ice crushing. Occasionally, steady state vibrations may arise. An amplification of the dynamic response is generated in these cases.

Simple design rules do not always provide reliable predictions of the ice effects in dynamic interaction conditions. Therefore, Määttänen (1977, 1978, 1982) made theoretical and experimental studies and presented a numerical interaction model for narrow structures and subsequently (1998) expanded the model. Based on further measurements (Nordlund et al., 1988) of steady state vibrations, Kärnä & Turunen (1989) developed another model for narrow structures. Further developments made by Eranti (1992a, 1992b) and Kärnä et al. (1990, 1994a, 1999) led to a nonlinear numerical interaction model “PSSII” for compliant wide structures. This model will be described in this report.

Ice forces on offshore structures are limited by the failure of the drifting ice features. The dynamic interaction between the structure and the failing ice sheet is a complicated process. Therefore, the present numerical model exploits experimental data on this process. A short overview of the experimental background is presented.

1.1 Ice failure – experimental background

We are concerned with ice-structure interaction phenomena occurring at the transient and brittle ranges of ice failure. For vertical structures the highest global loads are created at confined conditions where the ice fails by crushing and horizontal splitting, which is associated with flaking (spalling). Due to this failure mode the ice edge has a wedge shape. Horizontal splits emanating from the ice edge have an essential effect on the ice failure process (Fig. 1). Hirayama et al. (1975) (see also Schwarz 1993) used data from both field tests and laboratory experiments to show that this failure mode is driven by the vertical tensile stresses in front of the horizontal cracks.

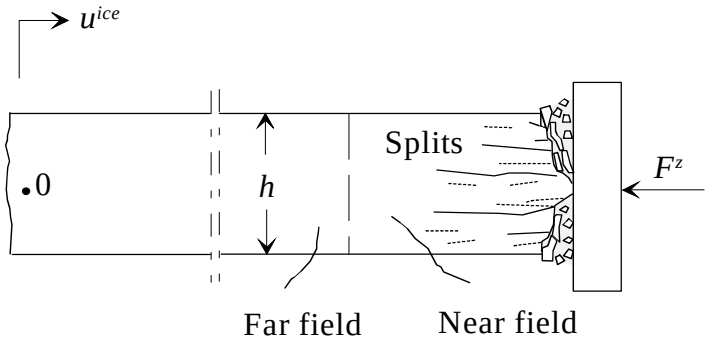

Figure 1. Ice sheet with a stepwise wedge-shaped edge and horizontal splits.

Figure 2 illustrates different kinds of experiences on the ice crushing process. Assur (1971) assumed that the failure of the ice edge is caused by shear stresses. This view was supported by Croasdale et al. (1977) who proposed a shear failure mode across the ice sheet as depicted in Fig. 2A - B. The symmetric failure mode (Fig. 2A) was considered relevant for the first impact between flat surfaces of the ice edge and the structure. The asymmetric failure (Fig. 2B) was assumed to take place while the structure continues penetrating into the ice sheet. Pure crushing (Tsuprik 1992, Kamesaki et al 1997) and pressure melting (Gagnon 2007) have also been proposed to contribute to the ice failure process (Fig. 2B). After a failure due to crushing with horizontal splitting, the ice edge has often a stepwise wedge shape. To study the failure process on this kind of ice edge, Joensuu & Riska (1989) and Fransson et al. (1991) conducted laboratory tests on wedge shaped ice samples. They found that the ice pressure concentrated in a narrow line-like area. Based on these experiments, Daley (1991) modelled the failure process as sequential asymmetric flaking due to shear failure.

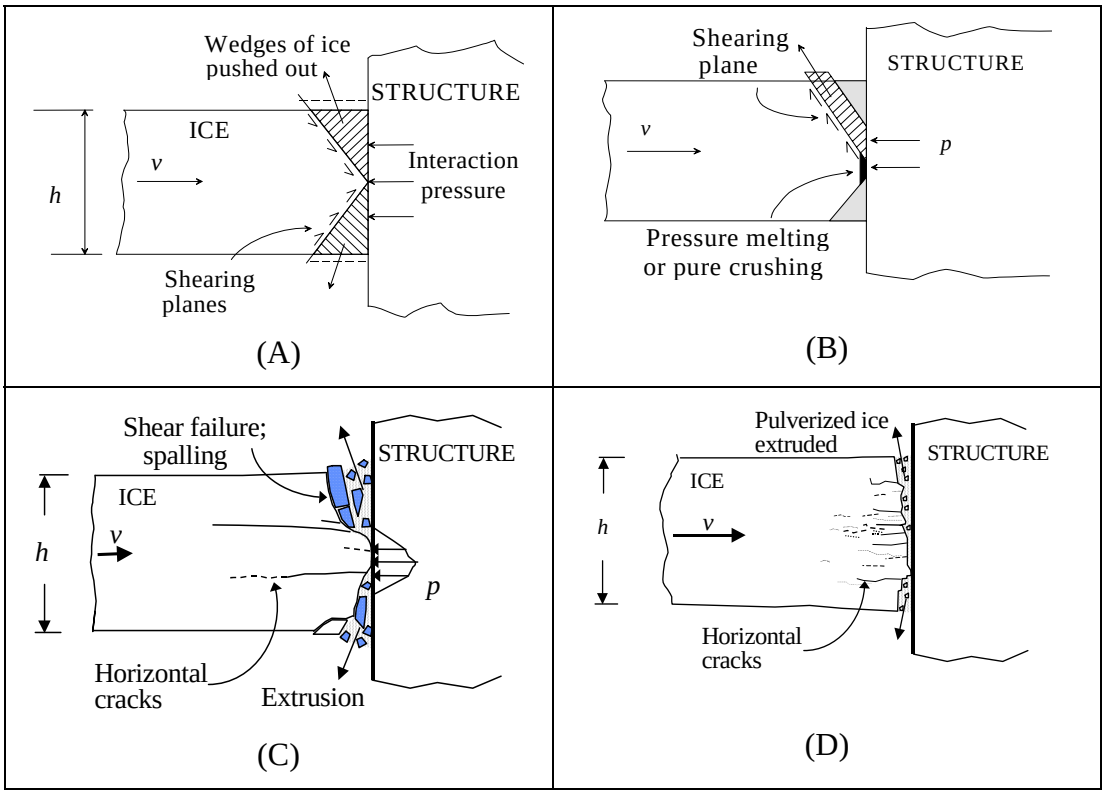

Figure 2. Observed/assumed variants of the ice failure mode titled here as crushing with horizontal splitting (known also as crushing with spalling or crushing with flaking). (A) Symmetric shear failure; (B) Asymmetric shear failure, (C) Fracture with a combination of horizontal and shear cracks; compliant structure, v = 30 mm/s, (D) Fracture with horizontal cracks; compliant structure, v = 80 mm/s.

Hirayama et al. (1975) used strain gauges to measure the strains in the ice sheet in front of a pile that was penetrating into the ice sheet. They concluded that the maximum ice force occurs concurrently with the development of horizontal cleavage cracks that emanate from the ice edge due to the vertical strains in the ice sheet. Similar horizontal cracks have been reported from indentation tests made both in-situ (Zabilansky et al. 1975, Tsuprik 1992, Fransson 1995, Kawamura et al. 1996, Takeuchi et al. 1999) and in laboratory (Fransson et

al. 1991, Muhonen et al. 1992/Fig. 52; Kärnä 1994b/Fig. 6, Tuhkuri 1996). Taylor (1981) reported about indentation tests, where the crushing failure mode incorporated a combination of horizontal tensile cracks and inclined shear cracks. Fig. 2C depicts this phenomenon as observed in thin sections taken after the indentation test No 54 reported by Muhonen et al (1992). A high speed video record taken in similar tests showed that after each major failure event, fractured ice was extruded simultaneously up and down form the ice-structure interface. Figure 1D depicts how the ice failure mode was changed when the nominal indentation velocity was increased from 30 mm/s (in Fig. 2C) to 80 mm/s. It is evident that the indentation velocity influences the length of the horizontal cracks as well as the wedge shaped form of the ice edge.

1.2 Response of the structure

When a drifting ice flow acts on a structure, a continuous ice failure process may produce different kinds of dynamic response modes in the structure. The main categories of structural response are: a quasi static response followed by transient vibration, steady state vibration and the random response to wide-band stochastic excitation. A dynamic model of ice-structure interaction should account for all these modes of response.

Quasi-static response with transient vibration

Figure 3 shows the set-up of an indentation test where a compliant structure was pushed into an ice sheet with a nominally constant rate $u_2 = v$. The resultant ice force as well as the velocity response vs. time and displacement u_1 are shown in Fig. 4. This test result shows that the acceleration and the associated mass forces are very small when the global ice force approaches its peak value during a major loading phase. A nearly static equilibrium exists between the internal and external forces acting on the structures at the events of maximum ice force. Therefore, we characterize the response as quasi-static.

At the events of major peak ice force (Fig. 4) the ice fails almost simultaneously in front of the structure and the structure starts moving forward against the ice edge. This occurs as a transient vibration termed also as “spring-back”. The first part of this period with a monotonously decreasing ice force is termed the unloading phase.

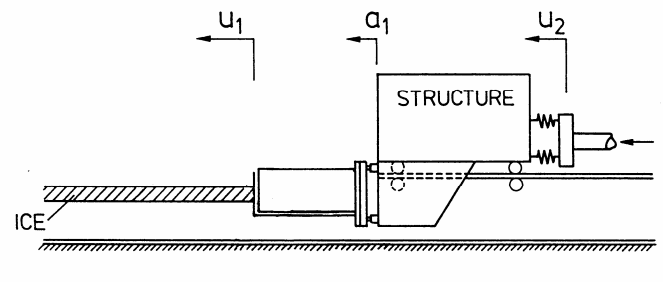

Figure 3. Single-degree-of-freedom structure used in a series of indentation tests (Muhonen et al. (1992)).

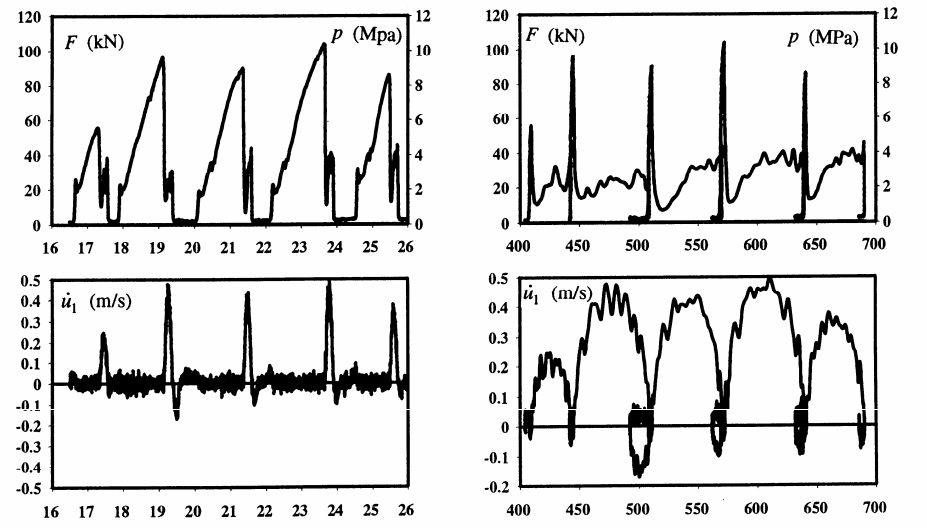

Figure 4. Quasi-static response with transient vibration for the structure shown in Figure 2 (Kärnä & Järvinen 1994a). (Structural mass M = 15 000 kg; rate of indentation v = 30 mm/s; natural frequency f = 2.0 Hz; ice thickness h = 100 mm; indentor width D = 100 mm.)

If the structure is stiff the spring-back phase is often practically the same as the unloading phase. However, a compliant structure may continue its transient motion after a minimum load has been reached. In this case the global ice force fluctuates at a low level. This force fluctuation is associated with non-simultaneous ice failure. An important feature of the transient is that it stops abruptly after one or two cycles if the structural damping is high as in the test system depicted in Fig. 3. This basic feature can be seen also in other reported measurements on compliant structures (Jefferies et al. 1988, 2008; Sodhi 1992; Kamesaki et al. 1995, 1997).

The dynamic interaction process described above includes a lot of phenomena that influence the global load on a wide offshore structure. Therefore, the experiment represented by Figs. 3 - 4 is used below as a benchmark test for the numerical model.

Ice-induced vibration

The drifting ice field may occasionally induce steady state vibration in the structure. This kind of response was measured frequently on two channel markers in the Baltic Sea (Määttänen (1977) Nordlund et al. (1988). The measured acceleration data shows that the time signal is smooth and almost sinusoidal. The effects of the ice force are magnified by the dynamics of the structure. Kärnä & Turunen (1990) proved that if a steady state vibration arises, the velocity amplitude of the structure at the waterline is approximately the same as the ice velocity. Experimental verification of this results has been provided by Toyama et al. 1983; Izumiyama et al. 1996, 1997 and Engelbrektson 1977, 1983, 1985, 1987). New data on steady-state vibrations is provided by Yue and Bi (1998, 2000).

Random response

Kärnä et al. (1993b) analyzed a test condition where a very stiff concrete cylinder was pushed against sea ice at high velocity. The measured time signal of the global force had a

random character. The amplitudes of the force fluctuation were small compared to the mean level of the force. Similar results obtained by Sodhi (1991a, 1991b) suggest that this kind of force pattern is typical in conditions where the relative velocity between the structure and the ice edge is higher than about 0.1 m/s. Tests with segmented indentors show that random global forces occur in conditions where the local forces fluctuate non-simultaneously in front of the structure (Fransson 1995, Kawamura et al. 1996, Sodhi 1992).

2. A numerical model for vertical structures

Määttänen (1978) presented a model for the ice-induced vibrations of narrow structures. The model was subsequently expanded for wide structures (Määttänen, 1998). A different model known as PSSII was derived by Kärnä et al. (1989, 1992, 1994, 1997, 1999) in co-operation with Eranti (1991, 1992). This model is described below and applied for the ice conditions met in winter 2000 at the Norströmsgrund lighthouse. Dynamic ice actions on a compliant wind turbine structure are also simulated.

2.1 Substructure technique

The model PSSII (Procedure for dynamic Soil-Structure-Ice Interaction, Kärnä et al. 1989, 1992, 1994, 1997, 1999; Eranti 1991, 1992) is a substructure technique for the dynamic analysis of compliant structures subjected to the action of ice sheets. Impact of an iceberg can also be analysed by this model.

Consider the dynamic interactions illustrated in Fig. 5. While building up the numerical model, the soil, structure and ice are considered as separate substructures. Separate equations are written for each of them. The motion of the structure is described with the general equation of equilibrium as

$$\mathbf{M}\ddot{\mathbf{U}}(t) + (\mathbf{C} + \mathbf{C}^n)\dot{\mathbf{U}}(t) + \mathbf{K}\mathbf{U}(t) = \mathbf{F}\left[\mathbf{w}^{dz}(t), \dot{\mathbf{w}}^{dz}(t)\right] \qquad (1)$$

where **M**, **C** and **K** are respectively the mass, damping and stiffness matrices of the structure; $\ddot{\mathbf{U}}$, $\dot{\mathbf{U}}$ and **U** are the displacement, velocity and acceleration vectors of the discretized system. $\mathbf{C}^n$ is a separate matrix for non-proportional damping effects. Standard FE techniques are used in modelling the structure. The vector **F** of Eq. 1 represents the ice loading. The ice force exciting the structure is not known a-priori as a function of time. Therefore, **F** is assumed to be a nonlinear function of a relative displacement $\mathbf{w}^{dz}(t)$ and its time derivative between the structure and the ice edge.

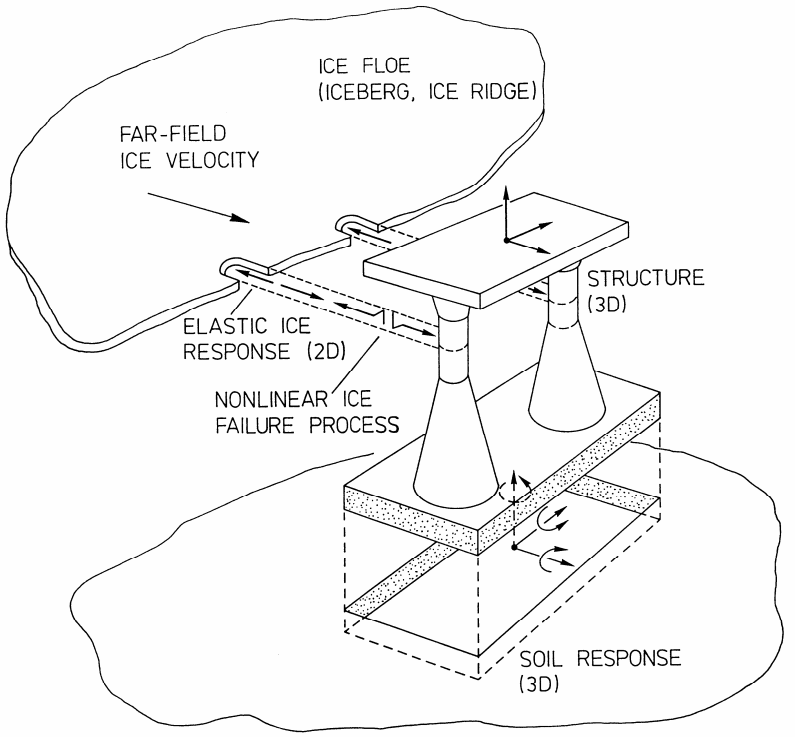

Figure 5. Subsystems in the dynamic analysis of the soil-structure interaction.

2.2 Soil-structure interaction

An impedance function technique is applied in describing the soil behaviour. Consider an embedded foundation as depicted in Fig. 6. A linear relationship between the displacement vector $\mathbf{u}^S = [u_1, u_2, u_3, u_4, u_5, u_6]$ and the corresponding force vector $\mathbf{R}^S$ is needed. Such a relationship can be found by assuming that the foundation is rigid and that it is resting on a homogeneous half-space. The relation between the applied force $\mathbf{R}^S$ and the displacement $\mathbf{u}^S$ is obtained as

$$\mathbf{R}^s(\omega) = \left[\mathbf{K}^s(\omega) + i\,\omega\,\mathbf{C}^s(\omega)\right]\mathbf{u}^s(\omega) \qquad (2)$$

where i is the imaginary unit and $\mathbf{K}^S(\omega)$ and $\mathbf{C}^S(\omega)$ are stiffness and damping matrices for the soil. Analytical expressions are available for the coefficients k^S_{ij} and c^S_{ij} of these matrices. The embedment of the foundation can be considered as well as the radiation and material damping of the soil.

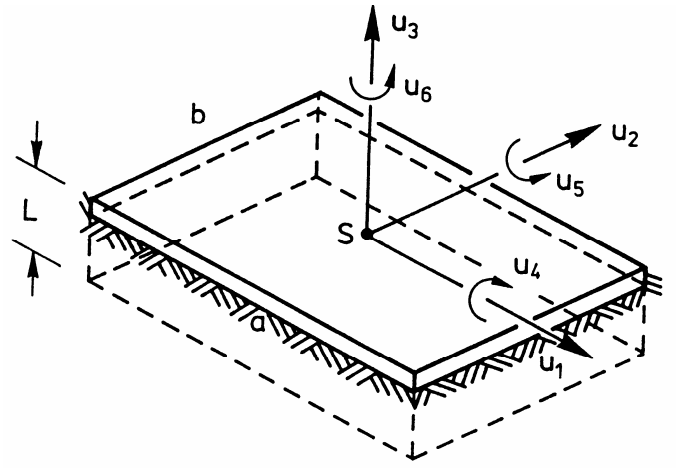

Figure 6. Embedded foundation resting on the seabed.

This impedance function technique describes the soil behaviour as a function of the frequency ω of excitation. On the other hand, the global solution of the present problem entails a time-domain solution where frequency dependent parameters can not be used. However, the soil-structure-ice interaction is in most significant cases a narrow band random process with a dominant frequency. The matrices $\mathbf{K}^S(\omega)$ and $\mathbf{C}^S(\omega)$ are evaluated at this frequency. The soil stiffness $\mathbf{K}^S$ is included directly in the FE model of the structure. The soil effects are introduced in one nodal point of the structural model if a simple gravity base structure is considered. For piled base structures, Eq. 2 can be extended to incorporate a set of lateral springs and dashpot elements that are fixed at the nodal points of the piles. The damping effects due to the soil often exceed the structural damping by an order of magnitude. This difference causes non-proportional damping effects which should preferably be considered in the solution of the equations. Therefore, the soil damping $\mathbf{C}^S$ is incorporated in the separate damping matrix $\mathbf{C}^n$ of Eq. 1.

2.3 Far-field ice sheet

The next subsystem to be incorporated in the model is the ice floe that exerts a nonlinear interaction with the structure. Experimental data shows that most of the nonlinear phenomena occur quite close to the ice-structure interface. Therefore, the ice volume is separated into a near-field and a far-field area as shown in Figs. 7 and 8. All the nonlinearities due to ice crushing and relative displacements are described within the near-field layer. Both the near-field and the far-field area are divided further into zones where the interactive forces as well as relative displacements between the ice and structure are defined at specific contact points. This approach allows the non-simultaneous features of the ice crushing to be considered.

Two equations are needed to describe the far-field response of the ice feature. First, the equation of the rigid body motion of the ice mass is written as

$$M_{ice}(1 + C_a)\ddot{u}_{ice} + C_{dr}\dot{u}_{ice} = F_{dr} - F_{ice} \qquad (3)$$

where M_{ice} is the mass of the ice field, C_a takes account of the hydrodynamic added mass and u_{ice} describes displacement of the ice field at a master point *O*. Eq. 3 allows treatment of situations where the interaction resembles a transient impact. The total ice force F_{ice} retards the motion of the ice feature. On the other hand, a constant driving force F_{dr} due to wind and currents acts on the ice mass.

The ice feature is assumed to drift at a constant velocity *v* at the beginning of interaction. Therefore, a damping effect is included in Eq. 3 to balance the driving force in the initial condition. The damping factor C_{dr} is given by $C_{dr} = F_{dr}/v$.

The second equation pertaining to far field behaviour is written as

$$\mathbf{C}^e\dot{\mathbf{w}}^e + \mathbf{K}^e\mathbf{w}^e = \mathbf{F}^z \qquad (4)$$

where $\mathbf{w}^e$ is a vector that incorporates the nodal elastic displacements of the ice edge relative to the master point O_{ice}. It is defined at the boundary between the far- and near-field areas. $\mathbf{F}^z$ is the corresponding vector of compressive contact forces at the contact points and $\mathbf{K}^e$ stands for the elastic stiffness of the ice floe.

Two options are available for determining the stiffness matrix $\mathbf{K}^e$. First, the far-field area can be modelled using a standard FE technique. An application of unit forces at the boundary yields a flexibility matrix $\mathbf{F}^e$ and further the stiffness matrix $\mathbf{K}^e = (\mathbf{F}^e)^{-1}$. The second option is to use an approximate technique as described by Kärnä and Turunen (1989).

In many cases the ice floe can be assumed to be semi-infinite. In such cases proper account should be taken of the radiation damping effects. The diagonal damping matrix $\mathbf{C}^e$ is used for this purpose. The coefficients of this matrix are approximated as described by Kärnä and Turunen (1989).

2.4 Near-field area

2.4.1 Relative displacements

The ice force interacting between the structure and the ice edge depends on the relative displacements and velocity. The basic approach used in the PSSII model (version 2.1, Kärnä 1991) can be illustrated by considering the uniaxial condition shown in Fig. 7. The layered structure of the ice edge (compare Fig. 8) is omitted here for a while.

The displacement of the structure's surface is denoted by u^z ($u^z \equiv u^c$, Figs. 7-8) and is defined positive in the direction of the compressive ice force acting on the structure. The displacement of a reference point O of the ice floe, in the normal direction to the structure's surface, is denoted u^{ice}. The third displacement parameter used is w^e, which is the displacement of the boundary B_{nf} between the far field and near field. This

displacement is defined positive in the direction of the compressive force acting on the far field.

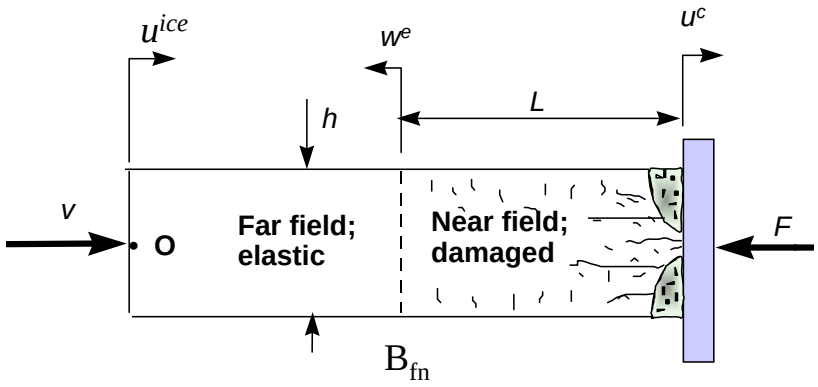

Figure 7. Uniaxial presentation of the displacement parameters.

An implicit time integration technique is used to simulate the time-varying interaction process to calculate the ice force F as a function of the relative displacements between the structure's surface and the boundary B_{fn}. This displacement is defined by the incremental equations

$$ {}^{t+\Delta t}w^z = {}^{t}w^z + \Delta w^z \tag{5}$$

where

$$ \Delta w^z = \Delta u^{ice} - \Delta u^c - \Delta w^e \tag{6}$$

The initial condition at the beginning of the simulation is given by

$$ {}^{0}w^z = - g^{ap} \tag{7}$$

where g^{ap} is the gap between the structure and the near field element. Eq (5) shows that positive values of w^z indicate a compressive strain (w^z /L) in the near field element. Also, positive values of w^z mean that there is a contact between the ice edge and the structure. Negative values mean a loss of a direct contact. However, crushed ice between the structure and the ice edge may transmit loads even for $w^z < 0$.

The contact force F depicted in Fig. 7 is calculated as a function of the near field displacement w^z and its time derivative (relative velocity) as

$$ F = F\left[w^z(t), \dot{w}^z(t)\right] \tag{8}$$

During the loading phase $F(w^z)$ will grow in accordance with a non-linear force-displacement relationship. At a time t_F of ice failure, w^z will experience a sudden change:

$$ w^z(t_F^+) = w^z(t_F^-) - d^f \tag{9}$$

where

$$ d^f = \beta^f \; w^z(t_F^-) \tag{10}$$

To consider the non-simultaneous ice failure process, the near field area is divided into a set of elements E_i, i = 1, ..., NS with a width *B*, length *L* and thickness *h* (Fig. 8). The displacement vector of the structure's boundary is defined as

$$\mathbf{u}^z = (u_i^z), \quad i = 1, \ldots, NS \tag{11}$$

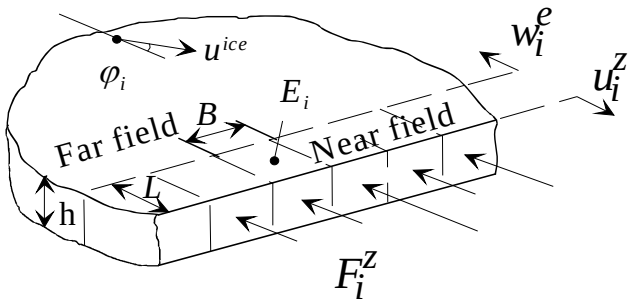

Figure 8. Near field and far field areas of the ice floe acting on structure.

The preceding review of experimental data showed that brittle failure of the ice edge occurs frequently by crushing with horizontal splits in the ice. Therefore, the version 2.4 of the PSSII model (Kärnä et al. 1997, 1999) adopted a more detailed near field model described in Fig. 9. The near field elements E_i depicted in Fig. 9 are here divided further into horizontal layers L_{ik} (i = 1, ..., NS; k = 1, ..., NDZ), which are bounded by the horizontal splits.

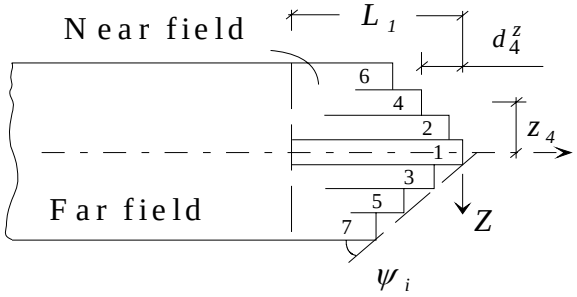

Figure 9. Model of the layered structure of the near field.

The geometry of the wedge shaped ice edge is defined in PSSII-2.4 by the wedge angel ψ_i and the cavities d^z between the structure and the layer. The wedge angle depends on the rate of interaction. Experimental records show that the longest horizontal splits appear close to the central plane of the ice sheet. Therefore, we assume that the length of the near field element E_i is the same as the length of the central layer L_{ik} and is given by

$$L_1 = h \cot \psi_i \tag{12}$$

The other layers are assumed to be shorter as illustrated in Fig. 9. Details of the determination of the parameters ψ_i and d^z are given by Kärnä et al. (1997).

2.4.2 Major and secondary failure events

Ice failure can be either symmetric or asymmetric (Kärnä and Järvinen, 1999). These two failure modes are termed here also as major and secondary crushing with splitting (Fig. 10). High-speed photography of laboratory tests (Muhonen et al., 1992) shows that a major failure event appears as a rapid expansion in the middle level of the ice sheet. The failure occurs symmetrically up and down (Fig. 9A).

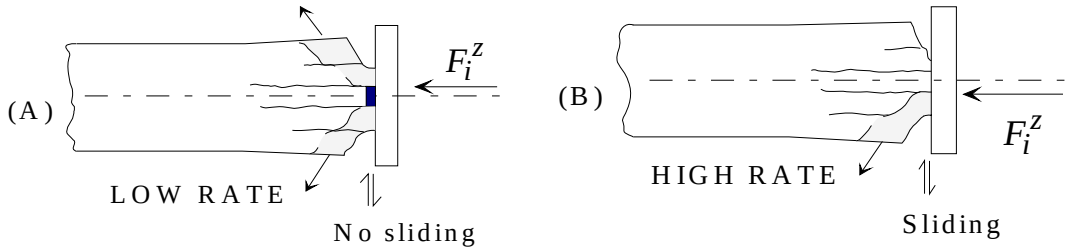

Figure 10. (A) Major flaking at low rate of interaction; (B) Secondary flaking at high rate.

Figure 10B depicts an event of asymmetric secondary ice failure that occurs sequentially on the upper and lower layers of the ice sheet. Experimental data shows that asymmetric crushing with splitting takes place at high rate (Daley 1991) of indentation whereas symmetric, major failure is typical for low stress rates (Muhonen et al. 1992). The physical reasoning and detailed description of these two failure modes are found in Kärnä et al. (1997).

Further details of the symmetric ice failure mode are shown in Fig. 11. This illustration is based on high-speed photography and direct measurements of the displacement u_1 of the structure depicted in Fig. 3..

A typical loading cycle starts with a loading phase where the ice force increases as the indentor penetrates to the ice edge. This is indicated by the point A in the force signal of Fig. 11. Some fractured ice exists between the indentor's surface and the upper and lower parts of the ice edge. One or several cleavage cracks exist in the ice edge. Observations with the transparent window of the indentor showed that this crushed ice did not flow at the contact surface during the loading phase in tests where the mean rate of indentation was in the range of 10 mm/s to 80 mm/s.

The ice extrusion begins at an instant when the ice force passes its peak value. The structure starts moving forward at an increasing velocity. The source of ice extrusion is indicated by the black area ***S*** in Fig. 11. High-speed photography revealed that this are is almost always close to the middle level of the ice sheet, where the highest pressures are encountered.

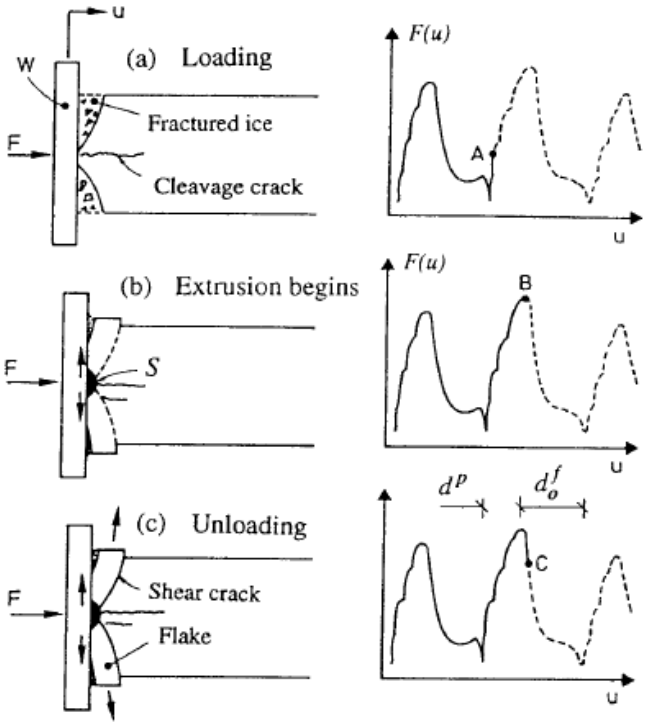

Figure 11. Mechanics of ice crushing and flaking as seen in a laboratory test. Pile-up crushed is not shown. Extract from Kärnä and Järvinen 1994.

During the unloading, the ice force drops as depicted by the point C in Fig. 11. At the same time, the indentor pushes the ice flakes up and down. An important observation is that the flakes are pushed simultaneously up and down. Hence, the distance d_0^f indicated in Fig. 11 can be related to the amount of ice that is crushed and extruded during unloading. This leads to a concept of finite ice failure depth that is applied in the PSSII model.

2.4.3 Ice failure depth

The lateral depth of ice that is failed in one failure event is one of the important parameters of the present model. This parameter, termed as ice failure depth is discussed by studying data shown in Fig. 11. This result was obtained with the test set-up that is shown in Fig. 3 by using a very compliant model structure.

A traditional approach to the problem of ice induced vibrations assumes that the dominant frequency of ice force variations can be expressed as a ratio of the ice velocity (v) to the "damage" (or crushed) length (d_s or δ_c) shown in Fig. 12. This approach suggests that ice sheets have a characteristic crushing frequency that is given as $f = v/d_s$.

However, the results depicted in Fig 12 (and in Fig. 11) show that the distances d_s and δ_c are not ice properties. Instead, they depend both on the ice and the compliance of the structure. It can be shown that that the extent δ_c of the transient spring-back phase can be approximates as

$$\delta_c = \lambda \frac{F^p}{K} + \frac{v}{2f} \tag{13}$$

where F^p is the peak ice force acting on the whole structure, K is the stiffness and f is the fundamental natural frequency.

Therefore, the parameters d_s or δ_c are not used in the PSSII model as parameters to describe ice behaviour. Instead, the ice failure parameter d^f (Eq. 9, Fig. 12) that pertains only to the unloading phase, not for the whole spring-back phase that may continue after the unloading.

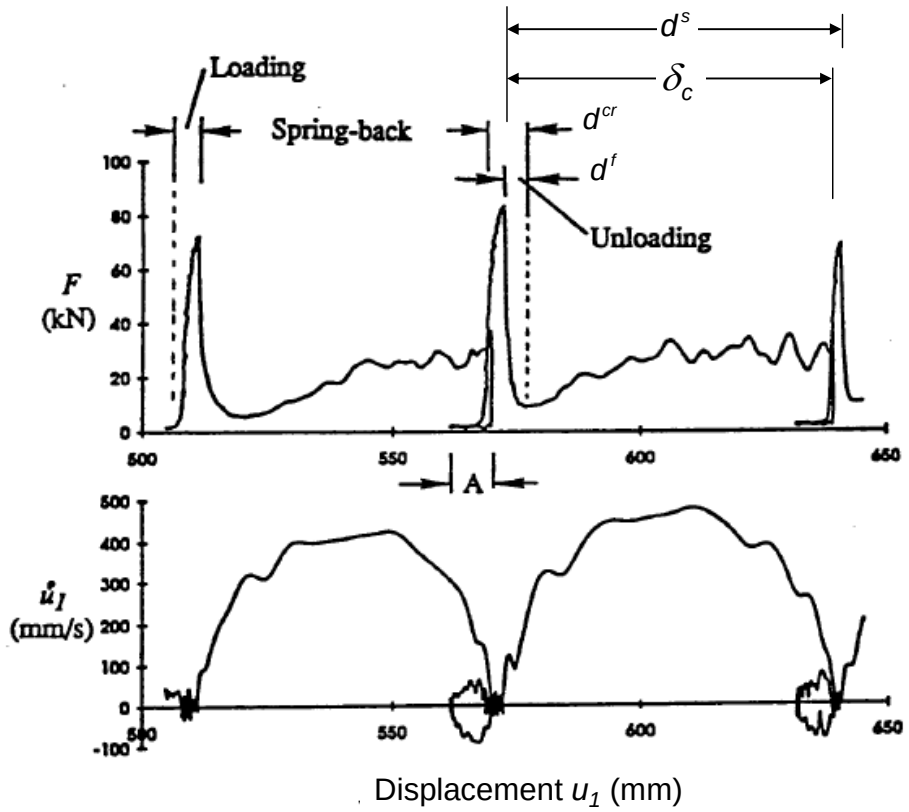

Figure 12. Details of the force and velocity records in dynamic ice actions on a very compliant model structure. Extract from Kärnä et al. 1993c.

2.4.4 Strength distribution

The real failure phenomena are simplified in PSSII_2.4 by assuming that each layer fails due to the compressive force applied on it. The failure force of the layer L_{ik} is determined as

$$F_{ik}^p = c(z_k)\,\varsigma_i\,\frac{h\,B}{NDZ}\,p_i^{cr} \tag{14}$$

where p_i^{cr} is a characteristic ice failure pressure at the near field element E_i. This parameter is obtained by adopting first a constant base value p^{cro}, which depends on the ice thickness h and the width B of the local contact area (Kärnä et al. 2006). A random number generator is then used to obtain log-normal distributed values for the failure pressure p_i^{cr}. In numerical simulations, the width B of the near field elements is usually selected as 0.5 to 1.0 times the ice thickness.

The parameters ζ_i and $c(z_k)$ are used in Eq. 13 to consider two kind of strength distributions. First, ζ_i takes account for the differences between the local ice failure forces. Experiments show (Muhonen et al. 1992, Fransson 1995) that the failure strength assumes its lowest value in the middle of the structure. Second, the parameter $c(z_k)$ is used to consider the vertical strength distribution within the near field element. The central layers can sustain higher pressures than the outer layers. A simple cosine strength distribution is assumed (Kärnä et al. 1997).

It should be appreciated that p_i^{cr} characterises the effective strength of a zone at the ice edge. Due to lateral confinement, p_i^{cr} is usually higher than the uniaxial strength of ice.

In the original model PSSII-2.1, the peak values of the local forces F_i^z (Fig. 8) are determined as

$$F_i^p = \varsigma_i \; h \, B \, p_i^{cr} \tag{15}$$

where p_i^{cr} is a local full-thickness pressure, which depends on the ice thickness h and the width B (Kärnä et al. 2006).

2.4.5 Influence of ice speed and structural compliance

Figure 13 shows results from a series of laboratory tests where vertical model structures were pushed against model ice. The compliance of the structures were varied. The results show that the peak values of the ice load were did not vary much if the indentation speed was in the range of $v > 0.1$ m/s. However the load was significantly magnified when the indentation speed was in the range of $v < 0.1$ m/s.

This feature was first discovered by Peyton (1966 and Blenkarn (1970) and confirmed in subsequent laboratory studies conducted by Sodhi et al. (1991a, 1991b, 1992, 1998, 2001) and others. The same phenomenon was also observed by Jefferies et al (1988, 2008) in full-scale measurements of the Molikpaq structure while it was deployed in the Beaufort Sea in 1980's.

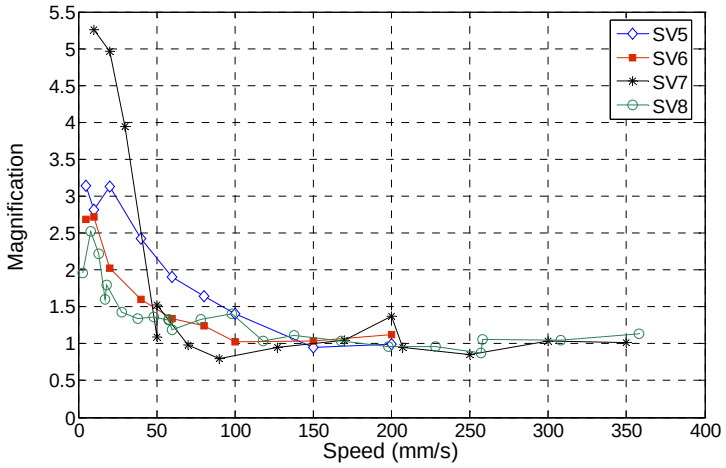

Figure 13. Magnification of ice load on narrow, compliant model structures (Kärnä et al. 2008).

The rate dependence of the ice crushing pressure is p^{cr} is considered in the model version PSSII-2.1 by simulating the ice pressure as shown in Fig. 14. This figure shows the mean value of the ice crushing pressure as a function of the relative speed. The relative speed is defined as the difference between the ice drifting velocity u^{ice} and the velocity u^{c} of the structure (Fig. 6).

The abrupt drop of the crushing pressure (Fig. 14) is caused be a transition form simultaneous to non-simultaneous failure. Both laboratory tests and field experience show that this transition occurs while the ice velocity approximately 0.1 m/s.

The crushing pressure p^{cr} is used in the PSSII model as a log-normally distributed random parameter. The coefficient of variation is taken typically as 0.20. The randomness of the ice strength is indicated by the hatched are in Fig. 14.

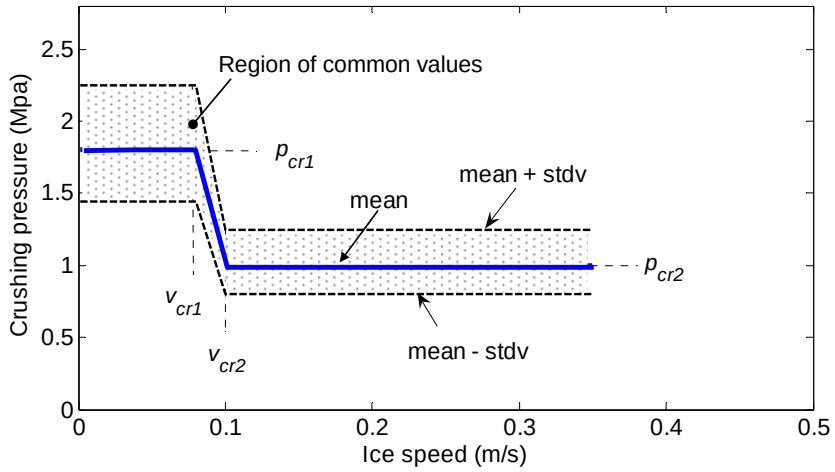

Figure 14. Mean value of the full-thickness ice pressure as a function of relative ice speed.

In the model version PSSII-2.4, the rate dependence is of the ice load is modelled by assuming that the wedge angle ψ (Fig. 9) depends on the relative velocity. This assumption is based on laboratory tests as described by Kärnä et al. (1994b, 1996, 1997, 1999)

2.5 Ice force

2.5.1 The interaction process

A central variable in the simulation of the dynamic ice-structure interaction is the compressive displacement vector. In the model version PSSII-.4 this defined by (see Figs. 8 and 9)

$$\mathbf{w}^{dz} = (w_{ik}^{dz}), \qquad \begin{cases} i = 1,\ldots, NS \\ k = 1,\ldots, NDZ \end{cases} \tag{16}$$

which incorporates the relative near field displacements of the layers. The incremental updating equation for these displacement is

$$^{t+\Delta t}w_{ik}^{dz} = {}^{t}w_{ik}^{dz} + \Delta w_{ik}^{dz} \tag{17}$$

$$\Delta w_{ik}^{dz} = \Delta u^{ice}\cos\varphi_i - \Delta u_i^z - \Delta w_i^e \tag{18}$$

The initial condition is given by

$$^{0}w_{ik}^{dz} = -g_i^{ap} \tag{19}$$

where g_i^{ap}, i = 1, ..., NS is an initial gap between the ice edge and the structure. The local forces acting on the layers are determined as a function of the relative displacements,

$$F_{ik}^{dz} = F_{ik}^{dz}(w_{ik}^{dz}) \tag{20}$$

The compressive local forces acting on the near field elements E_i are calculated as

$$F_i^z = \sum_{k=1}^{NDZ} F_{ik}^{dz} \tag{21}$$

and the global force is obtained as

$$F = \sum_{i=1}^{NS} F_i^z\Big|_n \tag{22}$$

where $F_i^z\Big|_n$ is the component of the local ice force in the direction of the ice motion.

Corresponding expressions are used in PSSII_2.1, where the near-field area is not divided into separate layers (Sect. 2.4.1).

2.5.2 Loading phases

An implicit time integration technique is used to evaluate the ice force as a function time and the relative displacement. Corresponding to the experimental findings, the interaction process is simulated considering four different loading phases termed as loading, unloading, pure crushing with extrusion and the hysteretic unloading.

Loading

A loading phase is defined as a period of ice-structure interaction where the ice force increases. This condition prevails if the structure and the ice edge are in contact with each other and are moving against each other. In the versionPSSII-2.1 (Kärnä 1992) the ice force is assumed to increase as a linear function of the compressive strain at the near field element. A nonlinear relationship derived by Kärnä and Sippola (1996) is used in PSSII_2.4 (Kärnä et al. 1997, 1999). The anisotropy of the ice sheet can be considered in PSSII_2.4 by assigning an appropriate modulus for each layer of the sheet.

Unloading

The ordinary loading phase in a layer is followed by an unloading phase when a major or secondary failure event occurs at the ice edge. During unloading fractured ice is extruded from the ice-structure interface. Kärnä & Järvinen (1994a) considered this ice extrusion as a dynamic process that is driven by the lateral force interacting between the ice sheet and the structure. On the other hand the extrusion is retarded by the mass forces as well as frictional forces on the crushed ice. This dynamic model of ice extrusion is very sensitive to the parameters involved. Furthermore, considering the difficulties posed by the edge geometry, a simplified version of the extrusion process is used here.

Laboratory data shows that the drop from a peak load to the next minimum occurs within a time T_i^u that is typically 10% to 20% of the preceding loading time. A further natural feature of the ice extrusion is that the extrusion velocity is zero at the event of ice failure. Then, assuming that the acceleration of the extruded ice material decreases as a linear function of time, Kärnä et al. (1997) showed that the unloading after a major event of crushing with splitting can be simulated by the incremental force function

$$\Delta F_i^z(t) = 6\left(F_i^{cr} - F_i^{ex}\right)\left\{\left(\frac{t}{T_i^u}\right)^2 - \left(\frac{t}{T_i^u}\right)\right\}\frac{\Delta t}{T_i^u} \tag{23}$$

where F_i^{cr} is the peak load at the preceding event of ice failure and F_i^{ex} is the minimum force level at the end of the unloading. A similar force vs. time function is used to describe the unloading in the case of secondary crushing.

Pure crushing with extrusion

At the event of major crushing with splitting, the near field element E_i looses ice material from the whole contact area. Therefore, all the relative displacements $w_{ik}^{dz}, k = 1, \ldots, NDZ$ become negative. This condition prevails during the unloading phase. Our simplified equation (23) for the unloading phase is a function of time and not of the relative displacement. Accordingly, the relative displacements w_{ik}^{dz} may remain negative after the minimum level F_i^{ex} has been reached. Therefore, we define an intermittent phase of pure crushing with extrusion, where the ice force remains at a constant level until the next loading phase.

Hysteretic unloading

A new loading phase at a layer begins when w_{ik}^{dz} becomes positive. The loading phase will continue as long as the incremental relative displacement Δw_{ik}^{dz} remains positive but can be interrupted before an ice failure. This happens if the relative displacement increment Δw_{ik}^{dz} becomes negative. An intermittent drop in the contact force will occur in this situation. A plausible physical explanations for this hysteretic damping effect can be given by considering the frictional forces associated with the layered near field model. Due to the compressive force, the central layer expands in vertical direction causing compressive vertical stresses on the adjacent layers. At a load reversal the structure departures from the ice edge. Therefore, the compressive force at the central layer is released. The friction acting on the layer surfaces may prevent the sliding at the surfaces for a while. When the force is sufficiently low, sliding occurs at the boundaries and the central layer rebounds towards the structure. After a while the structure moves again against the ice edge due to its transient vibration. The frictional forces on the boundaries of the central layer are also now opposing the sliding at the horizontal boundaries of the layer.

Accordingly, we propose that the ice edge provides Coulomb damping which is sufficient to cause a rapid stop of the transient vibration of the structure. In the numerical model we simulate the Coulomb damping by a viscose model (Kärnä et al. 1997) that is activated for an intermittent time interval in the beginning of the loading phase.

2.6 Solution of the equations

While solving the equations of equilibrium, a few separate steps are taken. First, a general purpose finite element program is used to model the structure, Eq. 1. The same program is used to find a solution to the eigenproblem

$$\mathbf{K}\Phi = \mathbf{M}\mathbf{F}\Omega^2 \tag{24}$$

where $\Phi = \left[\phi_1, \ldots, \phi_n\right]$ is a matrix whose columns are the eigenvectors and the diagonal Ω stores the eigenvalues ω_i on its diagonal. The mode shape matrix Φ is used to define a vector **R** of modal generalized displacements as

$$\mathbf{U} = \Phi\mathbf{R} \tag{25}$$

Using mode-shape orthogonality properties (Clough & Penzien, 1975) and introducing Eq. 25 as well its second time derivative into Eq. 1 leads to the following set of equations for the unknown displacement and contact forces:

$$\mathbf{M}^*\ddot{\mathbf{R}}+\mathbf{C}^*\dot{\mathbf{R}}+\mathbf{K}^*\mathbf{R}=\mathbf{Q}-\mathbf{DR} \tag{26a}$$

$$M_{ice}(1+C_a)\ddot{u}_{ice}+C_{dr}\dot{u}_{ice}=F_{dr}-F_{ice} \tag{26b}$$

$$\mathbf{C}^e\dot{\mathbf{w}}^e+\mathbf{K}^e\mathbf{w}^e=\mathbf{F}^z \tag{26c}$$

$$\mathbf{F}^{dz}=\mathbf{F}^{dz}\left[\mathbf{w}^{dz}(t),\dot{\mathbf{w}}^{dz}(t)\right] \tag{26d}$$

The new symbols are defined as

$\mathbf{M}^*$ = diag(M_n) where $M_n=\phi_n^T\mathbf{M}\phi_n$

$\mathbf{C}^*$ = diag(2 ξ_n ω_n M_n)

$\mathbf{K}^*$ = diag(ω_n^2 M_n)

$\mathbf{Q}=\Phi^T\mathbf{F}\left[\mathbf{w}^{dz},\dot{\mathbf{w}}^{dz}\right]$

$\mathbf{D}=\Phi^T\mathbf{C}^n\Phi$

The final step is to perform a dynamic interaction analysis by solving the Eqs. 26 simultaneously. These equations are nonlinear. Furthermore, the ice crushing constitutes a random process. The equations are therefore solved by an implicit step-by-step algorithm. While solving the equations, the generalized displacements **R** are transformed to global displacements **U** and further to local displacements $\mathbf{u}^z$ at the boundary. The relative displacement $\mathbf{w}^{dz}$ can then be calculated as described above. A computer subroutine is used to calculate the contact force $\mathbf{F}^{dz}\left[\mathbf{w}^{dz}(t),\dot{\mathbf{w}}^{dz}(t)\right]$. Transformations are used between the local contact force $\mathbf{F}^{dz}$, the global force **F** and the generalized force **Q**.

3. Numerical simulations

3.1 A benchmark test

To verify the present formulation, the test described in Figs. 3 - 4 was simulated using the new model described above (PSSII-2.4). The result of this simulation is shown in Fig. 15. The comparison to Fig. 4 shows a good agreement between the experiment and the simulation. Two details of the simulation are of special interest, First, the transient vibration after a major peak force decays to a low level after each cycle. The hysteretic unloading phase of the present model accounts for this effect. The second interesting feature of this simulation is that the force signal *F(u)*, as a function of the displacement

shows a growing trend during the transient spring-back phase. The secondary failure process on the wedge-shaped ice edge accounts for this effect.

Figure 6 shows that the global ice force fluctuates at a relatively low level during the "spring-back" periods where the relative velocity is high. Nonsimultaneus secondary crushing process occurs at the near field elements during these periods. The events of large peak forces occur in quasi-static conditions as simultaneous events of major crushing with splitting.

Further comparison between numerical simulations and test results are shown in Kärnä et al. (1999).

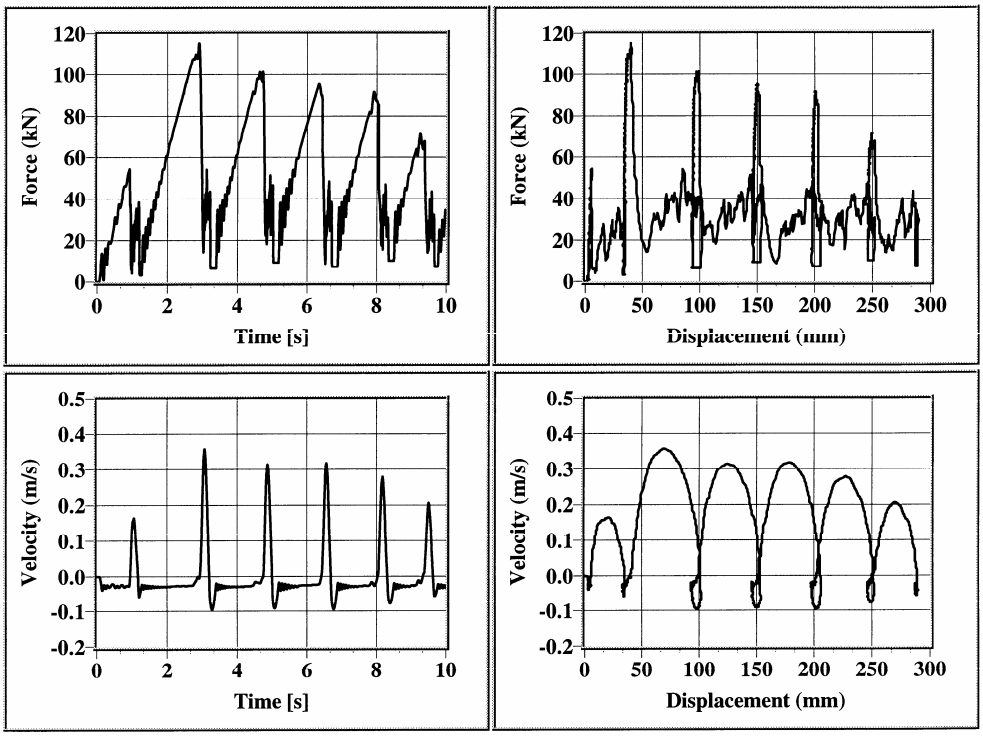

Figure 15. Simulated ice force and structural response in test condition explained in Figs. 3 - 4. Number of near field elements and layers, NS = 3 NZD = 7.

3.2 Simulations - Lighthouse Norströmsgrund

Ice force measurements were carried out at the Norströmsgund lighthouse (Fig. 7) in 1970's and 1980's as described by Engelbrektson (1977, 1983, 1985, 1987) and Björk (1981). This effort was continued by an other research team in 1999-2003 (Swarz and Jochmann 2001, Jochmann and Scwarz 2000, 2001, 2005, Kärnä et al. 2005, 2006). We will simulate numerically selected test conditions. In addition, some parametric studies will be carried out.

3.2.1 Natural modes and frequencies

Based on a FEM analysis and experiments Engelbrektson (1987) reports that the first and second natural frequencies of this lighthouse are f_1 = 2.32 - 2.35 Hz and f_2 = 11.7 Hz. The first natural mode was found to exhibit an amplitude ratio

$$x_T/x_L = 4 \qquad (27)$$

where x_T is the mode amplitude at the top (elevation +39.5 m) and x_L is the mode amplitude at a low level (the force level at the elevation +14.2 m). The damping factor as a fraction of critical was assumed by Engelbrektson as 0.04.

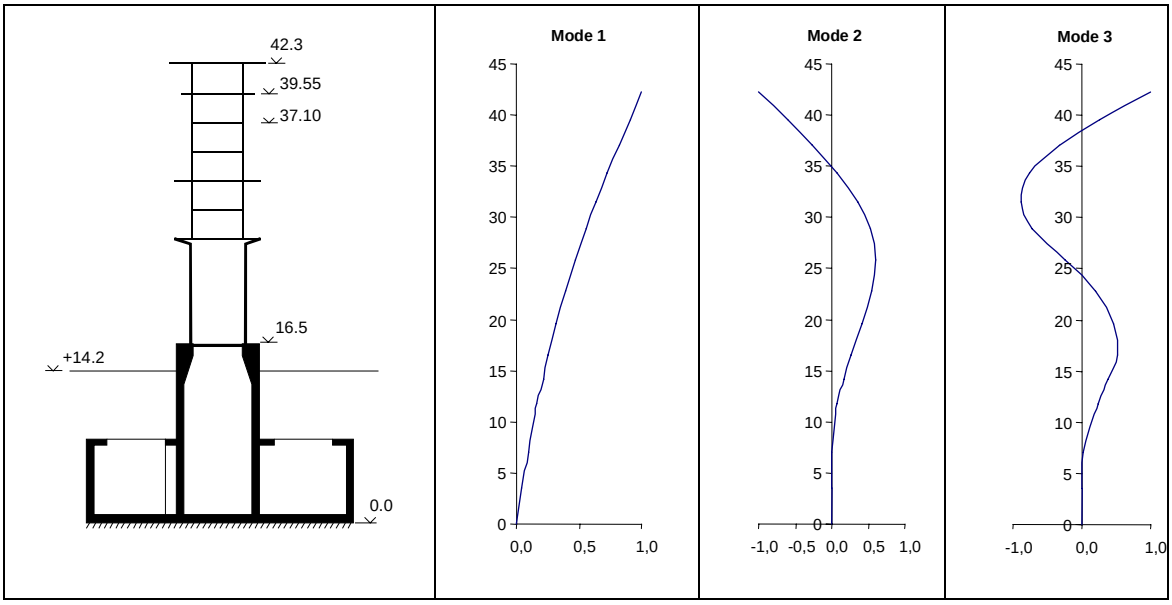

Figure 16. Norströmsgrund lighthouse and lowest natural modes.

During the ice force measurements in winter 2000 some ambient tests were done to evaluate the dynamic characteristics of the lighthouse. The tests were done by using abrupt dynamic forces arising from the ice-structure interaction. On (15.4.2000) several isolated floes with very low large-scale confinement impacted the structure. Due to the low confinement, the floes failed several times due to a large split that divided the floe in two parts. At the event of splitting, the ice force dropped suddenly from a peak value to zero. Transient vibrations arising from these unloading events were measured and analysed. The results are shown in Table 1.

Table 1. Natural frequencies f_n *and damping factors* ξ_n.

	Natural mode		
	1	2	3
f_n [Hz]	3.0	11.7	28.8(*)
ξ_n	0.01	0.01	0.01(**)

(*) Based on FEM analysis only
(**) Assumed value

The natural modes were also evaluated by a FEM analysis. As the foundation conditions were not known accurately, the computed fundamental mode was corrected considering the recorded mode amplitude ratio, which in these measurements was evaluated as

$$x_T/x_L = 3.2 \quad (28)$$

where now x_T = 37.10 m and x_L = 16.50 m. The three lowest natural modes are given in Table 2 and depicted in Fig. 16.

Table 2. Natural modes and nodal masses used in the analysis. Node No 5 is at the water level.

Node	z	Mass	Natural modes		
	[m]	[kg]	Mode 1	Mode 2	Mode 3
1	0	2051853	0.00E+00	0.00E+00	0.00E+00
2	3.5	1555677	4.88E-02	1.24E-03	5.83E-03
3	7	688260	9.78E-02	4.58E-03	2.06E-02
4	11.75	309250	1.70E-01	8.28E-02	2.44E-01
5	14.18	0	2.15E-01	1.76E-01	3.78E-01
6	16.5	212100	2.57E-01	2.70E-01	5.10E-01
7	19.65	100566	3.22E-01	4.14E-01	4.66E-01
8	22.8	59521	3.93E-01	5.42E-01	2.06E-01
9	25.85	55417	4.70E-01	5.99E-01	-2.44E-01
10	28.95	52146	5.59E-01	5.24E-01	-7.16E-01
11	31.5	26405	6.38E-01	3.55E-01	-8.88E-01
12	34.3	21217	7.29E-01	7.70E-02	-7.56E-01
13	37.1	22788	8.23E-01	-2.70E-01	-3.11E-01
14	39.55	22321	9.07E-01	-6.07E-01	2.62E-01
15	42.3	22321	1.00E+00	-1.00E+00	1.00E+00

3.2.3 Simulations using the model version PSSII-2.4

Numerical simulations on ice actions on the lighthouse were conducted in the LOLEIF project in 2000, before details of the force measurements were available (Karna et al. 2001). Results of this simulation are shown below.

Modelling parameters

In the numerical analysis the ice-structure was assumed to consist of nine flat panels as in the field tests. Each panel was divided further into four contact zones as illustrated in Fig. 17.
Numerical analysis was performed using the following assumptions:

- Ice thickness h = 0.3 m
- Number of contact zones: 36
- Width of each zone B = 0.3 m
- Number of layers: 7

- Effective modulus of the near field zone E^z = 400 MPa
- Basic crushing pressure at each zone; p^{cr} = 3 MPa; Specified at low rate for a contact area of $A = B\,h$; p^{cr} is log-normally distributed (coeff. of var. = 0.20)

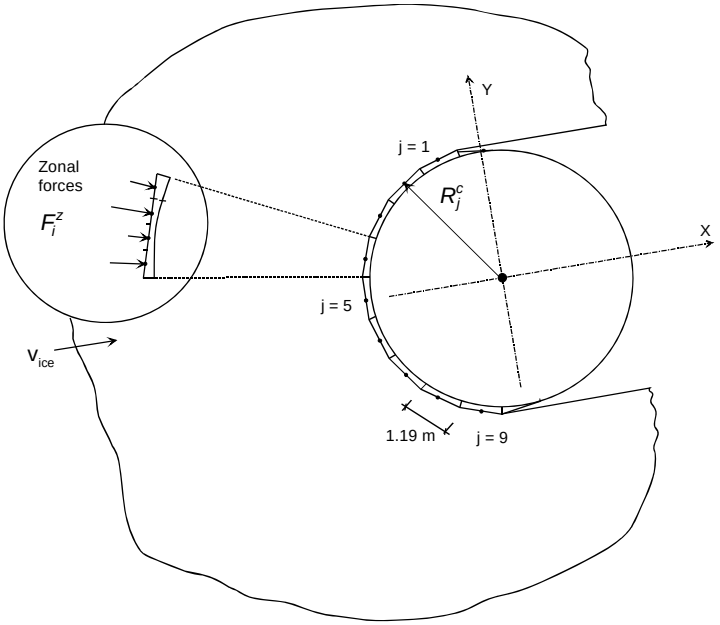

Figure 17. Contact geometry. Radius R^c *=3.6 m. Panels No 1 to 9 with panel No 5 at the centre.*

Numerical simulations

The dynamic ice-structure at the lighthouse was simulated by describing the dynamic behaviour of the structure with the three lowest modes for both X and Y direction. The far field ice velocity v_{ice} was varied. Figure 18 shows the simulated time function of the ice force when v_{ice} = 200 mm/s. The corresponding structural response is shown in Fig. 19. A selected time window for the same parameters is shown in Fig. 20.

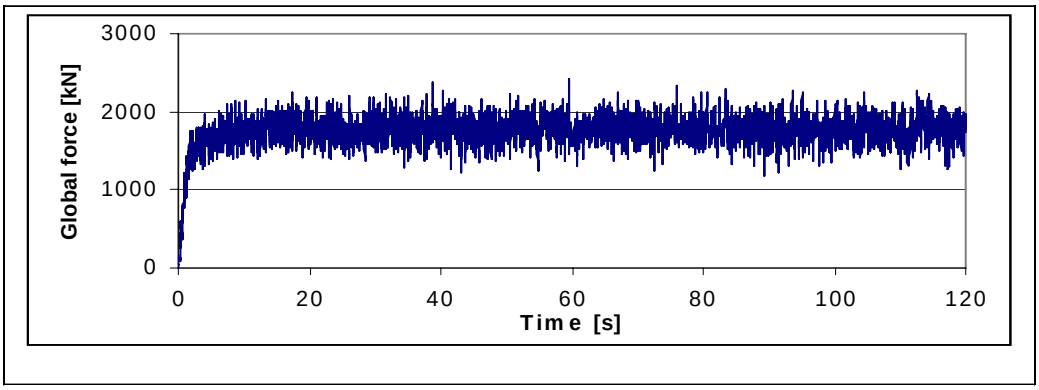

Figure 18. Simulated total ice force for v_{ice} = 200 mm/s.

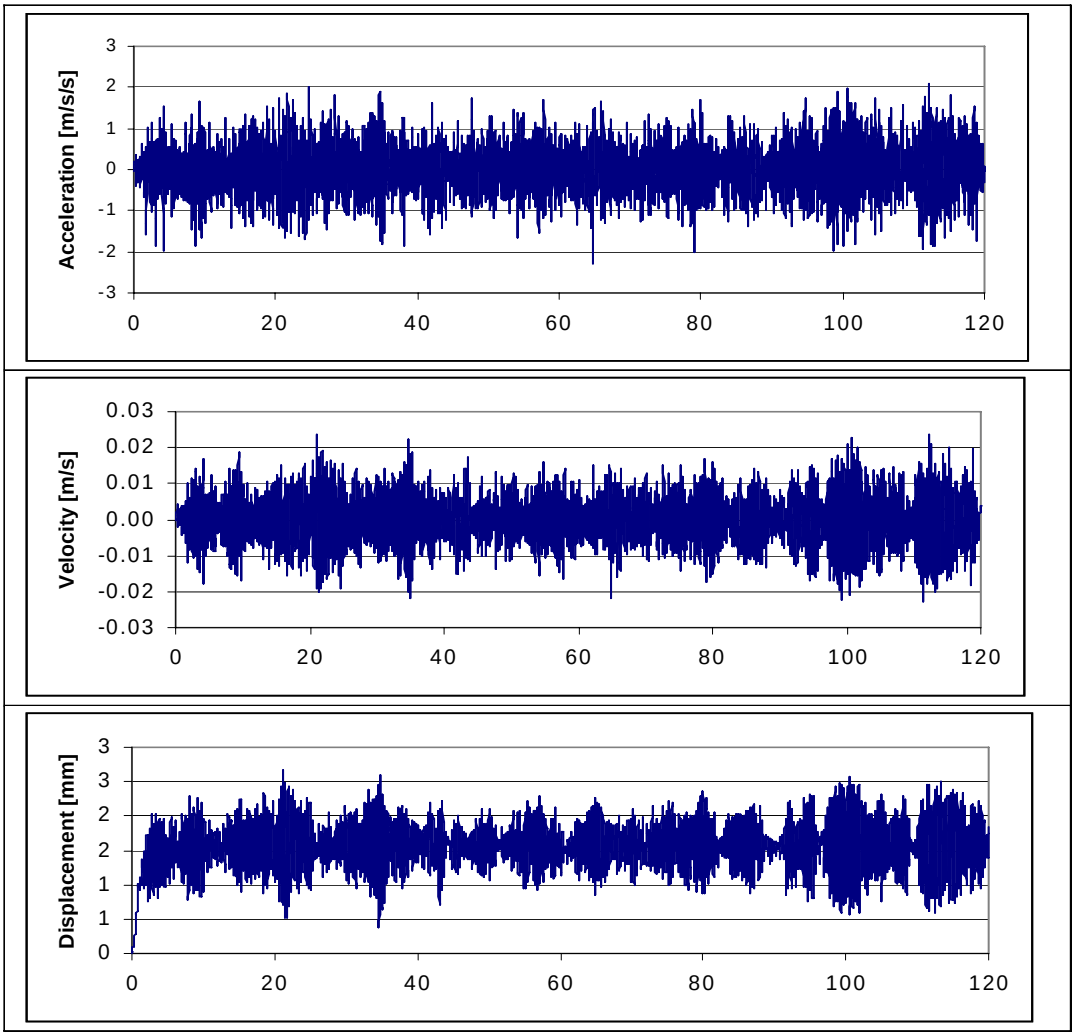

Figure 19. Simulated response for v_{ice} *= 40 mm/s. Acceleration at the level +37.10, Velocity and displacement at the water level.*

Figure 18 suggest that under the conditions considered (v_{ice} = 200 mm/s) the ice failure occurs almost nonsimultaneously on different panels. This is shown in more detail in Fig. 21, which gives the simulated force signals of the panels No 1 to 5. On the other hand, the signals in Fig. 20 show that the response has a narrow band character, the first natural frequency dominates.

The dynamic interaction was simulated further by assuming a low ice velocity, v_{ice} = 40 mm/s. The panel forces for this situation are shown in Fig. 22. A comparison with Fig. 21 shows that the panel forces are higher than in the case of v_{ice} = 200 mm/s. This occurs because the model predicts a tendency for simultaneous ice failure at this range of ice velocities.

Further results for the case of a low velocity are shown in Fig. 23. The velocity amplitudes shown in this figure refer to the structural velocity response at the water level. It can be seen that the amplitude of the structural velocity is almost the same as the far field ice velocity. This is a typical characteristics of steady state vibration (self-induced vibration) caused by ice action. This feature was reported earlier by Toyama et al. (1983) and Kärnä

and Turunen (1989, 1990). In earlier measurements on the Norströmsgrund lighthouse Engelbrektson (1977, 1983, 1985, 1987) found steady state vibrations at the velocity range of v_{ice} < 50 mm/s. He also reports that in this condition the structural velocity amplitude at the ice level is close to the ice velocity.

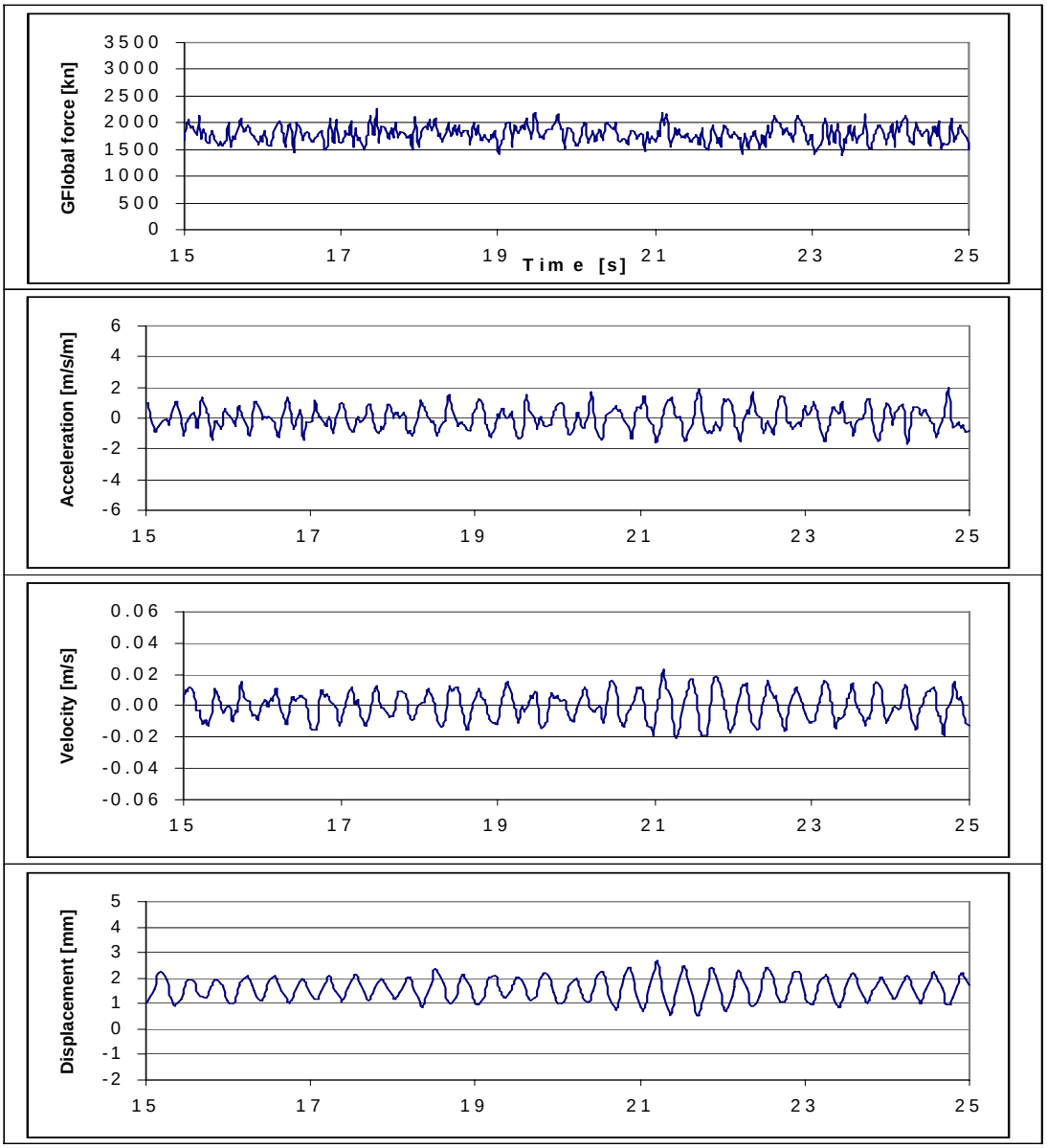

Figure 20. Details of the simulated total ice force and structural response for v_{ice} *= 200 mm/s.*

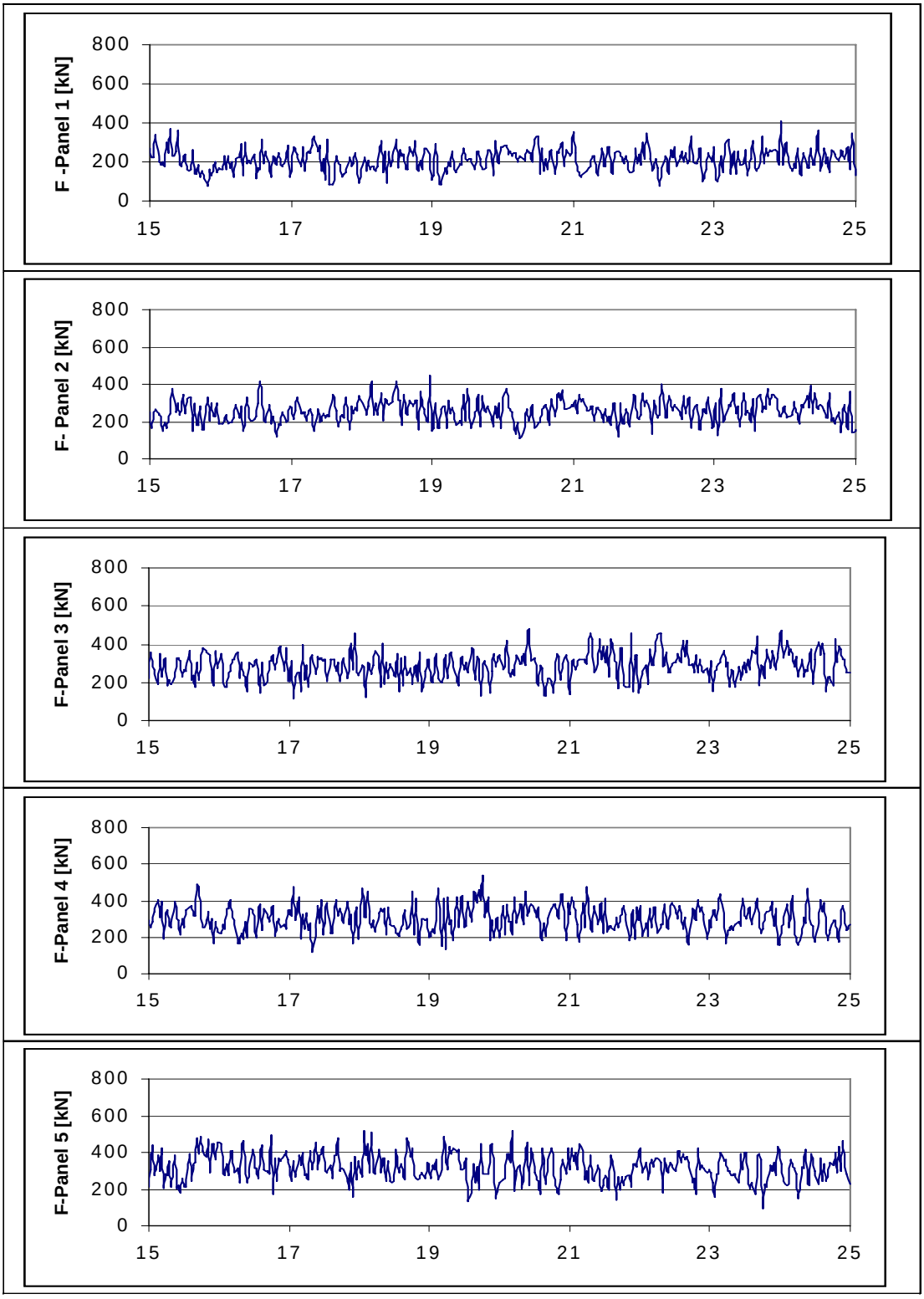

Figure 21. Simulated panel forces for v_{ice} *= 200 mm/s.*

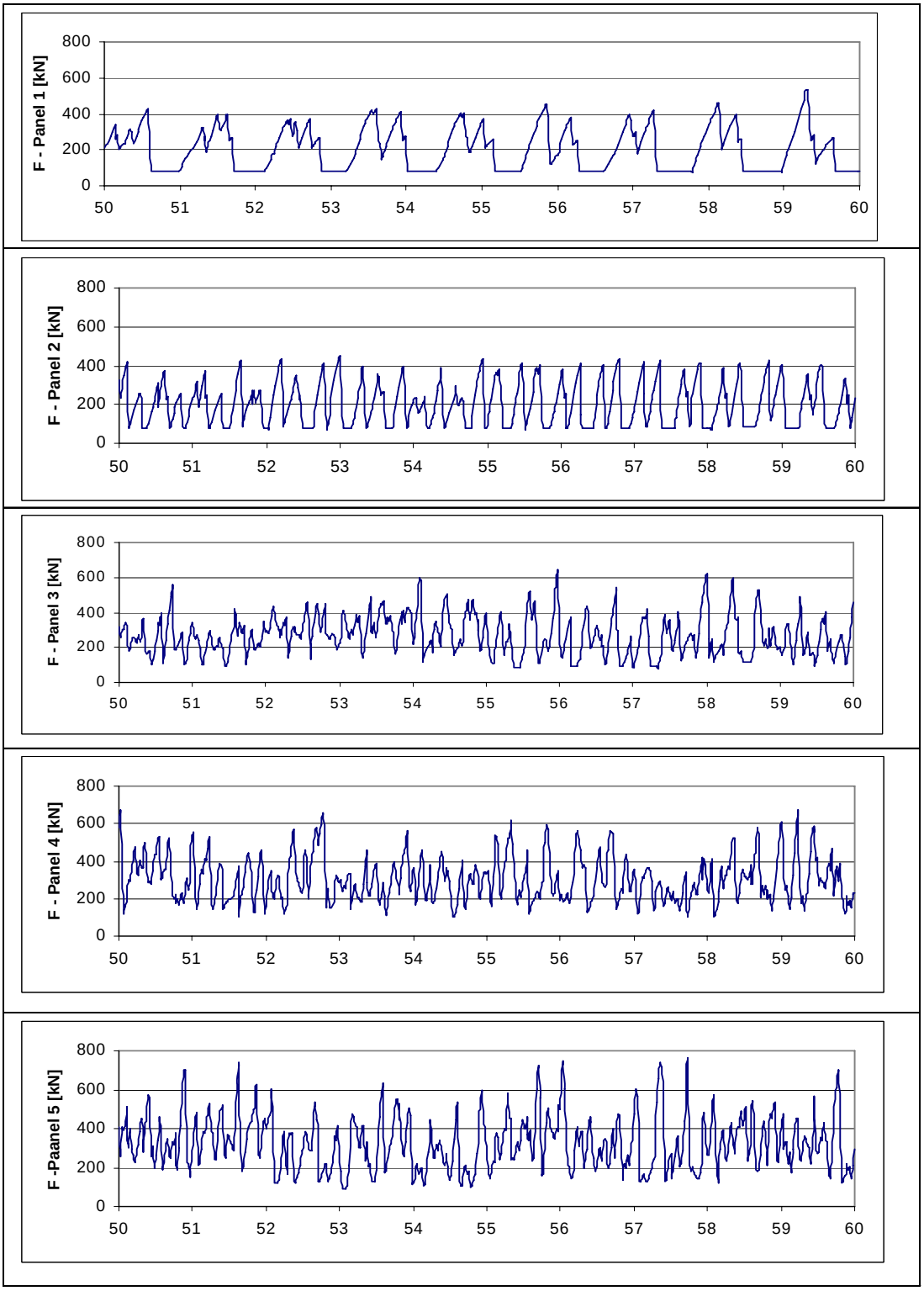

Figure 22. Simulated panel forces for v_{ice} *= 40 mm/s.*

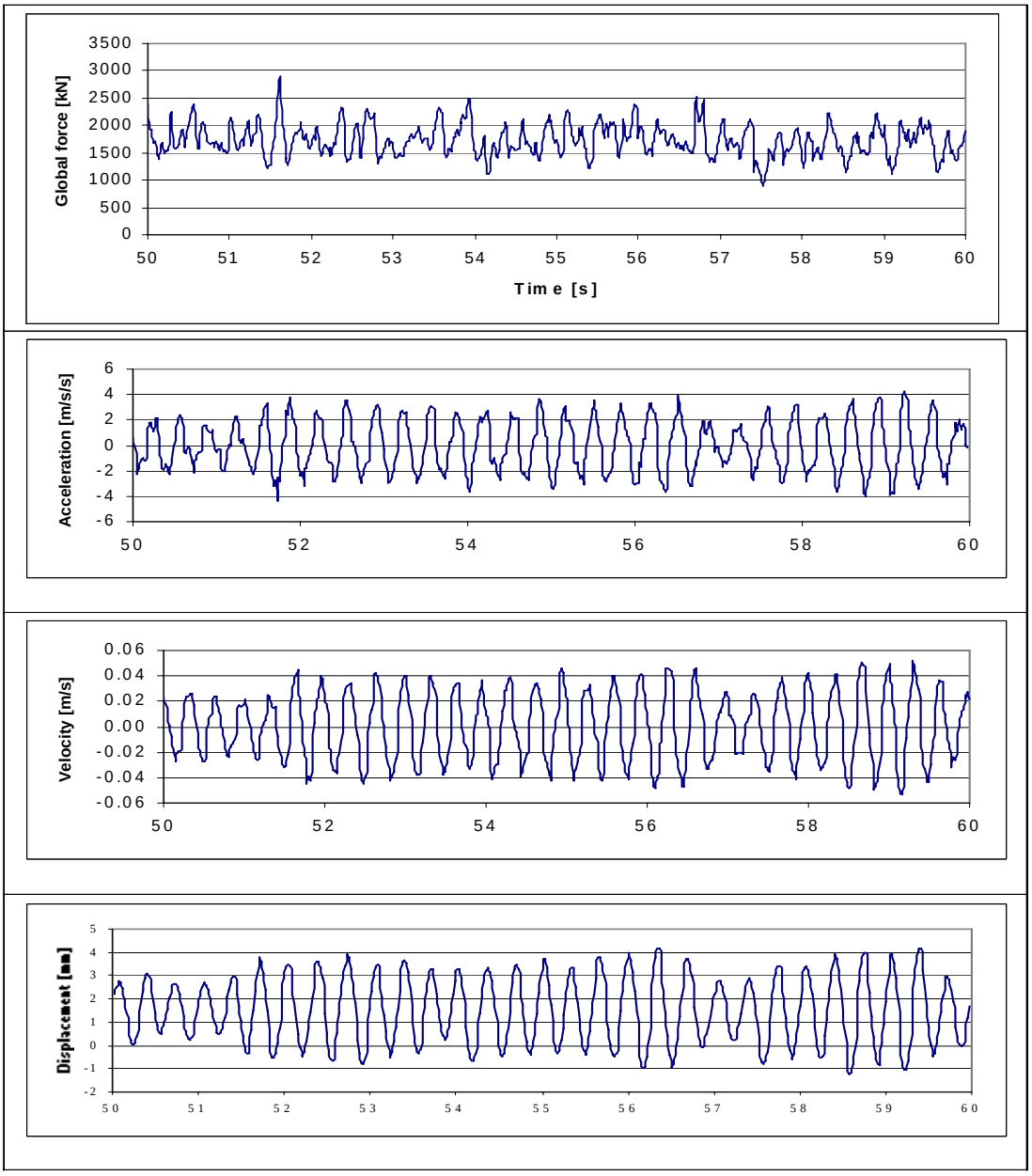

Figure 23. Details of the simulated total ice force and structural response for v_{ice} *= 40 mm/s.*

Further simulations were carried out by varying the ice velocity in the range of 5 mm/s to 400 mm/s. Figure 24 shows how the far field ice velocity influences the calculated maximum values of global ice load, the force at the central panel and the velocity amplitude at the water line. The maximum ice force is predicted for v_{ice} = 50 mm/s. In this case the ice tends to fail simultaneously on different panel forces. When the ice velocity increased the ice failure process becomes more random and the ice force decreases.

At ice velocities v_{ice} < 50 mm/s ice induced vibration is predicted. At some range of ice velocities the response amplitude is directly proportional to the ice velocity. The influence of ice creep is not included in this dynamic model. Hence, the accuracy of the results can not be evaluated at low ice velocities of less than about 5 mm/s.

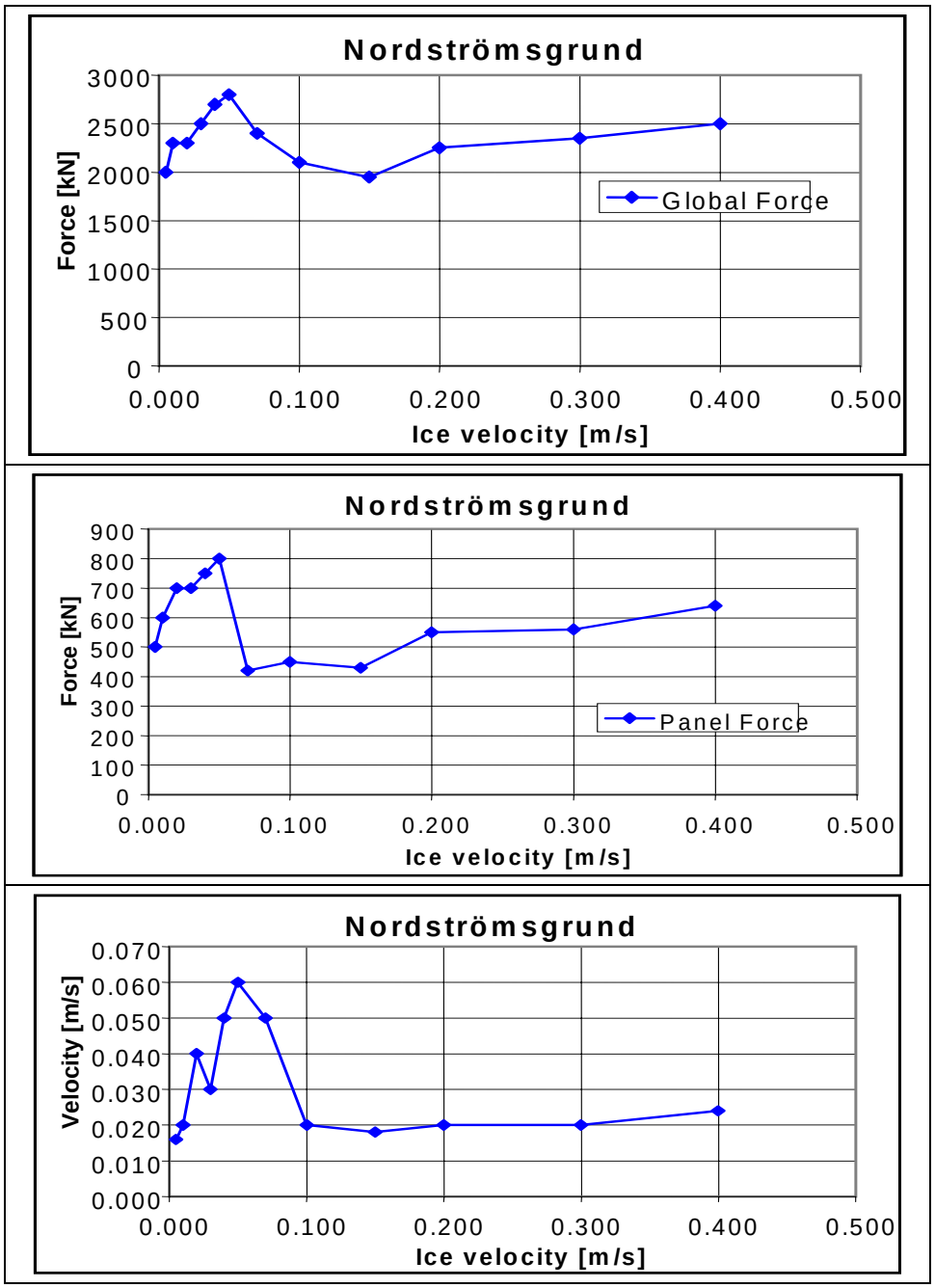

Figure 24. Maximum ice forces and velocity response at the water level as a function of ice velocity.

3.3 Simulations – An offshore wind turbine structure

Structural parameters

In the previous two case studies the dynamic ice-structure interaction and the structural vibrations were dominated by the lowest eigenmode. Määttänen (1975) provides full-scale data a very slender lighthouse that was subjected to dynamic ice actions in the Gulf of Bothnia. Self-excited vibrations occurred at the first and second natural frequencies, 0.85 Hz and 3.85 Hz. Due to this experience, the influence of higher natural modes is studied here by making simulations on a gravity based wind turbine that is illustrated in Fig. 25. This is a fictive structure, which is not directly connected to any particular real design. However, the structure is very slender like any offshore wind turbine that may be designed for the ice-infested waters of the Baltic Sea.

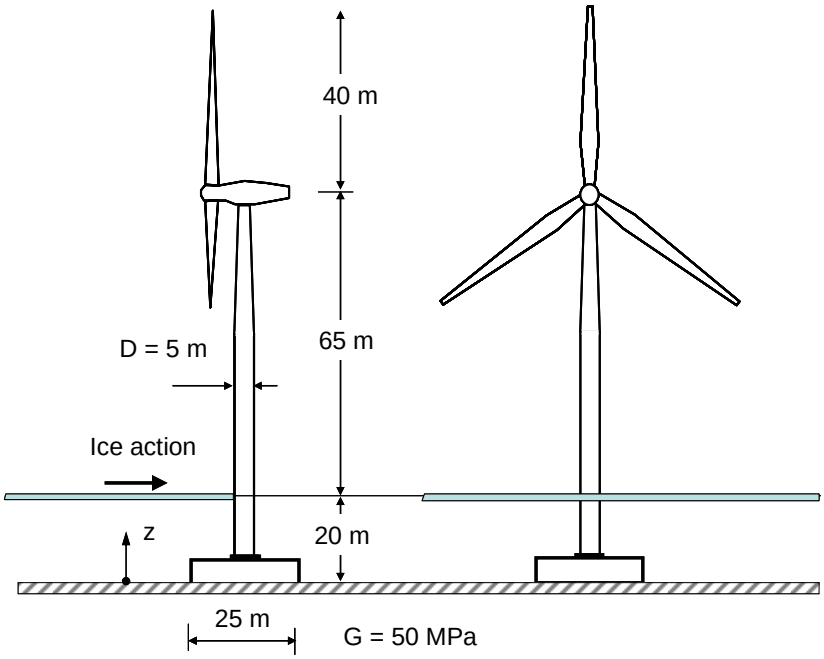

Figure 25. A fictive offshore wind turbine structure subjected to ice actions.

The main structural characteristics of this structure were selected as follows:

- dimensions of the GBS foundation: 5x25x25 m^3, mass 4 500 t,
- diameter of the tower: 5,0 m from z = 15 m to 40 m and 3.0 at the tower tip,
- wall thickness of the tower variable from 50 mm to 15 mm,
- total mass of the hub and nacelle 120 000 kg
- stiffness of a blade is variable

Dynamic soil-structure interaction was considered by applying horizontal and rotational springs as the level z = 0. The soil underneath the foundation was assumed as semi-infinite medium with a shear modulus of G = 50 MPa. The springs coefficients were then obtained from Wolf (1997) as K_x = 2 GN/m and K_θ = 100 GNm.

A FEM model was used to obtain eigenmodes and eigenfrequencies for this structure. Figure 26 shows eight of the lowest mode shapes and Table 3 shows natural frequencies. Table 3 also shows generalized masses M_n, waterline amplitudes ϕ_{nc} and the aerodynamic damping for ten modes. The aerodynamic damping was obtained from the expression

$$\xi_n^d = \frac{\rho_a}{4\pi \cdot f_n} \cdot \frac{\int_S D(z) \cdot C_D(z) \cdot v_m(z) \cdot [\phi_n(z)]^2 \quad dz}{M_m} \tag{29}$$

where ρ_a = 1.25 kg/m^3 is air density, $D(z)$ is the width of a cross-section as seen by the wind, $C_D(z)$ is the drag coefficient and $v_m(z)$ is the mean wind velocity. The drag coefficient was taken as C_D = 0.7 for the tower and C_D= 2.0 for the rotor blade (flapwise). The wind profile $v_m(z)$ was determined in accordance with the Eurocode EN 1991-1-4 assuming that the wind velocity is 10 m/ s at the hub height.

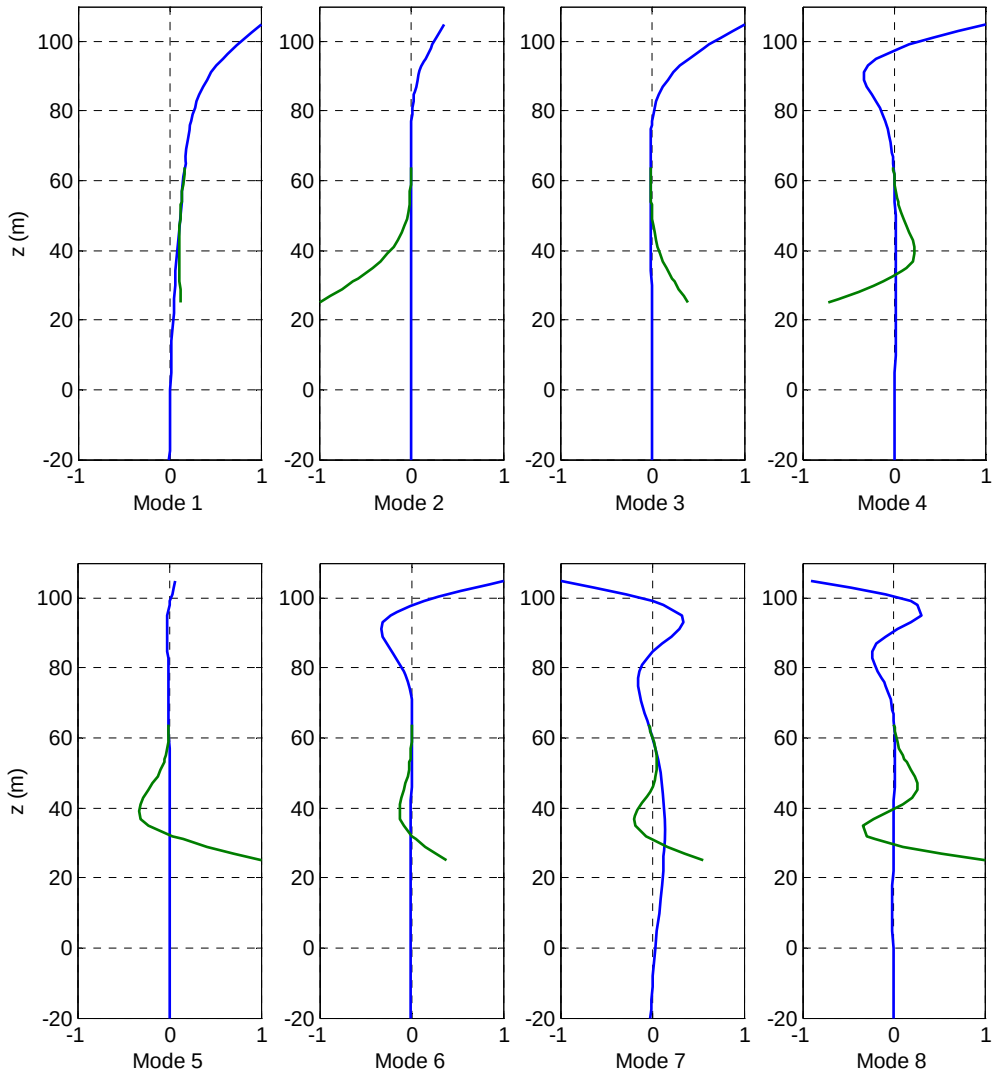

Figure 26. A fictive offshore wind turbine structure subjected to ice actions.

Table 3. Eigenfrequencies and related parameters.

	Modes									
	1	2	3	4	5	6	7	8	9	10
f_n (Hz)	0.56	0.77	0.80	2.30	2.44	2.48	3.40	5.40	5.60	6.89
M_n (kg)	6070	410	430	680	330	395	4200	430	390	2900
$\phi_{nc} \cdot 10^3$	10.1	-0.39	-1.11	11.5	5.47	-5.66	33.6	-6.49	1.47	-53.1
ξ_n^{da} (%)	1.0	4.7	4.7	0.9	1.0	1.0	0.1	0.6	0.6	0.05
ξ_n^{crit} (%)	4.8	0.1	0.6	13.3	5.9	5.2	12.5	2.9	0.2	22.1

Preliminary assessment of susceptibility to frequency lock-in

Lighthouses and very slender channel markers that have been used in the Baltic Sea as aids to navigation provide a long-term experience on ice-induced vibrations. Based on this experience (Määttänen 1978, ISO/CD 19906), the susceptibility of a narrow structure can be estimated in a straightforward way. To ensure dynamic stability of a natural mode *n*, the damping coefficient ξ_n of the structure should be larger than the opposite contribution of ice action to dynamic instability. In the case of a single point action, this criterion can be expressed for a mode of vibration as

$$\xi_n \geq \frac{\phi_{nc}^2}{4\pi\ f_n\ M_n} \cdot h \cdot \theta \qquad (30)$$

where f_n and M_n are described above and,

ξ_n is the total damping of the eigenmode as a fraction of critical,
ϕ_{nc} the modal amplitude at the ice action point,
θ coefficient, suggested value $\theta = 40 \cdot 10^6$ kg/(m·s).

The expression shown in Eq, (30) is denoted as ξ_n^{crit} and is shown in Table 3 for the modes 1 to 10. It is of interest to note that the mode 4 at the frequency or 2.30 Hz appears to be dynamically more sensitive than the modes 1 to 3. The modes 7 and 10 with the natural frequencies of 3.40 Hz and 6.89 Hz also appear to be sensitive. Table 3 reveals that this situation arises partly due to the relatively high values of the waterline amplitudes of these three eigenmodes.

Numerical simulations

Numerical ice-structure interactions were simulated by using the model version PSSII_2.1. The ice-structure interface was divided into $n = 18$ local contact zones as illustrated in Fig. 27. Ten eigenmodes were used while solving the equations (26). Following the instructions of the guideline document GL Wind 2005 (see list of references), the total damping was first assumed as 7% for all eigenmodes.

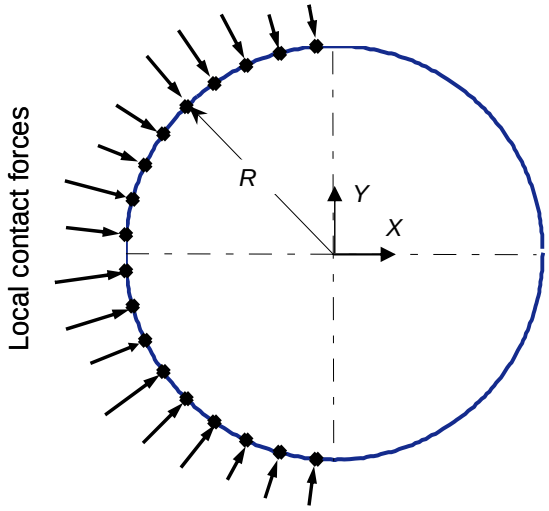

Figure 27. Contact geometry.

The ice parameters were assumes as follows:

- Ice thickness h = 0.5 m
- Waterline diameter w = 5.0 m
- Number of contact zones: 18
- Width of each zone B = 0.44 m
- The mean values of the ice crushing pressures (Fig. 14) were assumed as p_{cr1} = 1.8 MPa and p_{cr2} = 1.0 MPa with the coefficient of variation as 0.20. The corresponding critical ice speeds were v_{cr1} = 0.07 m/s and v_{cr1} = 0.10 m/s,
- Ice speed was varied from 0.03 m/s to 0.300 m/s.

A parametric study was made by varying the ice speed from 0.03 m/ s to 0.30 m/s. The duration of the each simulated event was 30 s. Figure 28 shows how the maximum peak values occurring in each simulation varied with the ice speed. Appendix 1 shows simulated time signals for the global load and for the structural response at selected positions.

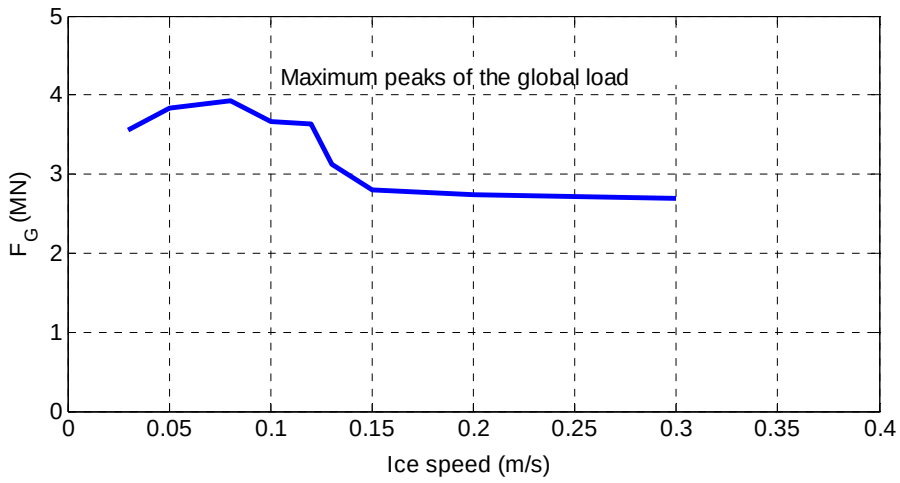

Figure 28. Maximum force values as a function of ice speed.

The role of higher modes in dynamic ice-structure interaction

Further simulations were made to study the possibility that different eigenmodes may dominate the response at different ice speed. This is a problem that may be relevant for other structures besides offshore wind turbine structures. To study this, simulations were repeated assuming that the total damping factor is 0.01 for all then modes involved in the analysis. Results are shown in Figs. 29a, 29b, 30a and 30b for two ice speeds.

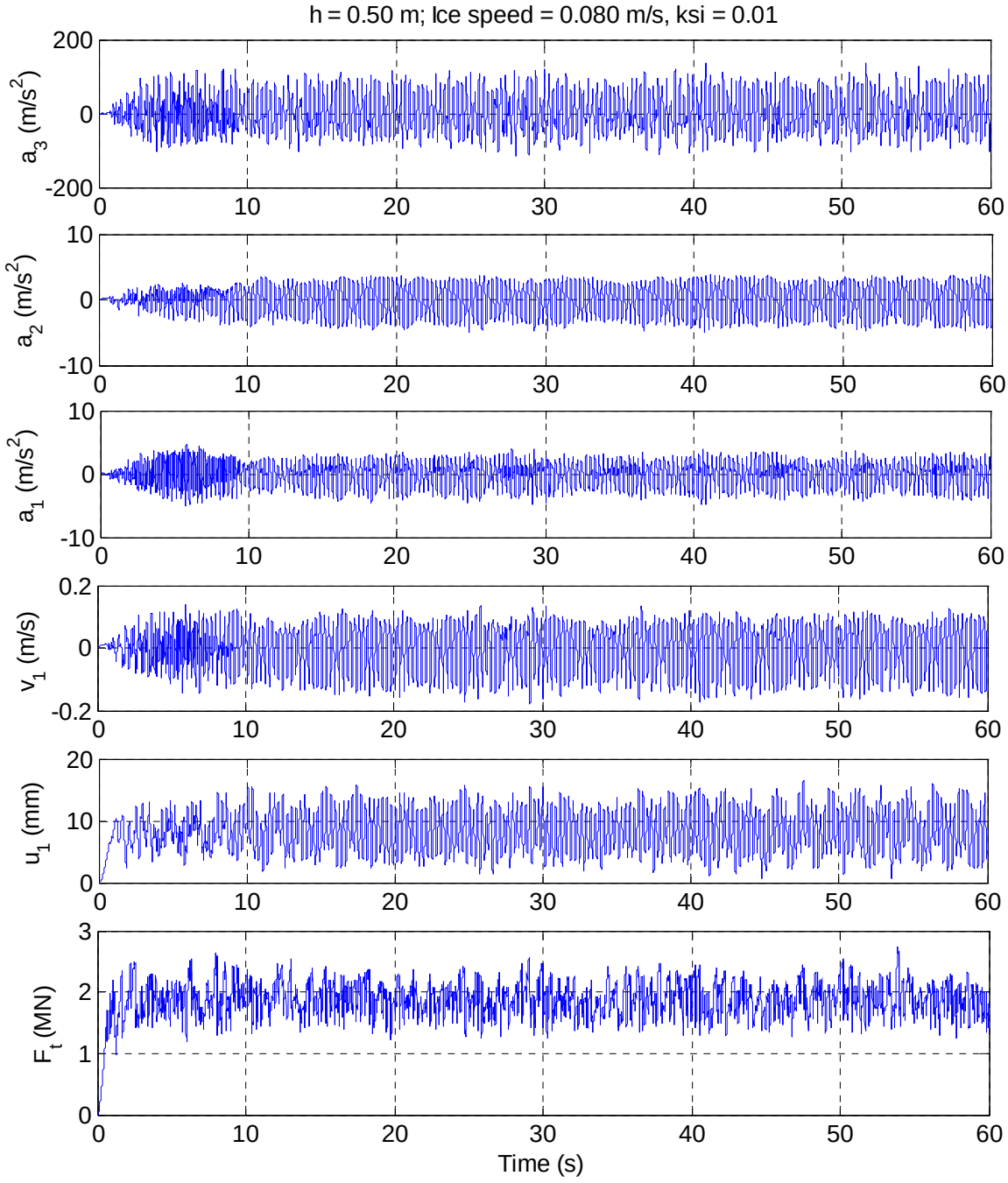

Figure 29a. Simulated time signals assuming a low ice speed (0.08 m/s) and small damping in all modes.

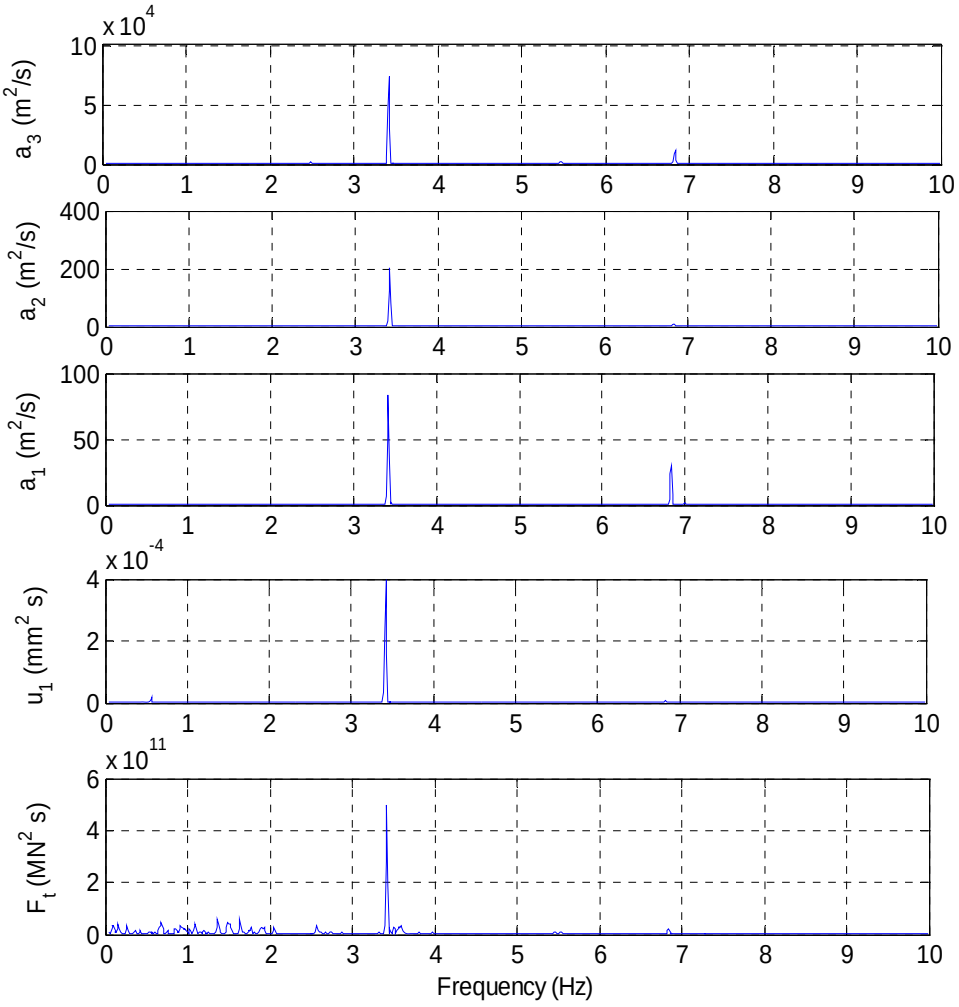

Figure 29b. Power spectral density functions (PSD) for signals shown in Fig. 29a.

The results shown in Figs. 29a and 29b relate to a condition where the ice speed is 0.08 m/s. Experiences from both laboratory tests and from the field indicate that this is a typical condition where ice-induced vibrations may occur at the lowest natural frequency. In this case, however, self-excited vibrations (lock-in) arises at the frequency of 3.4. This is the frequency of the seventh mode. The sensitivity study shown in Table 3 indicates that this one of the modes that can be considered as very sensitive for vibrations.

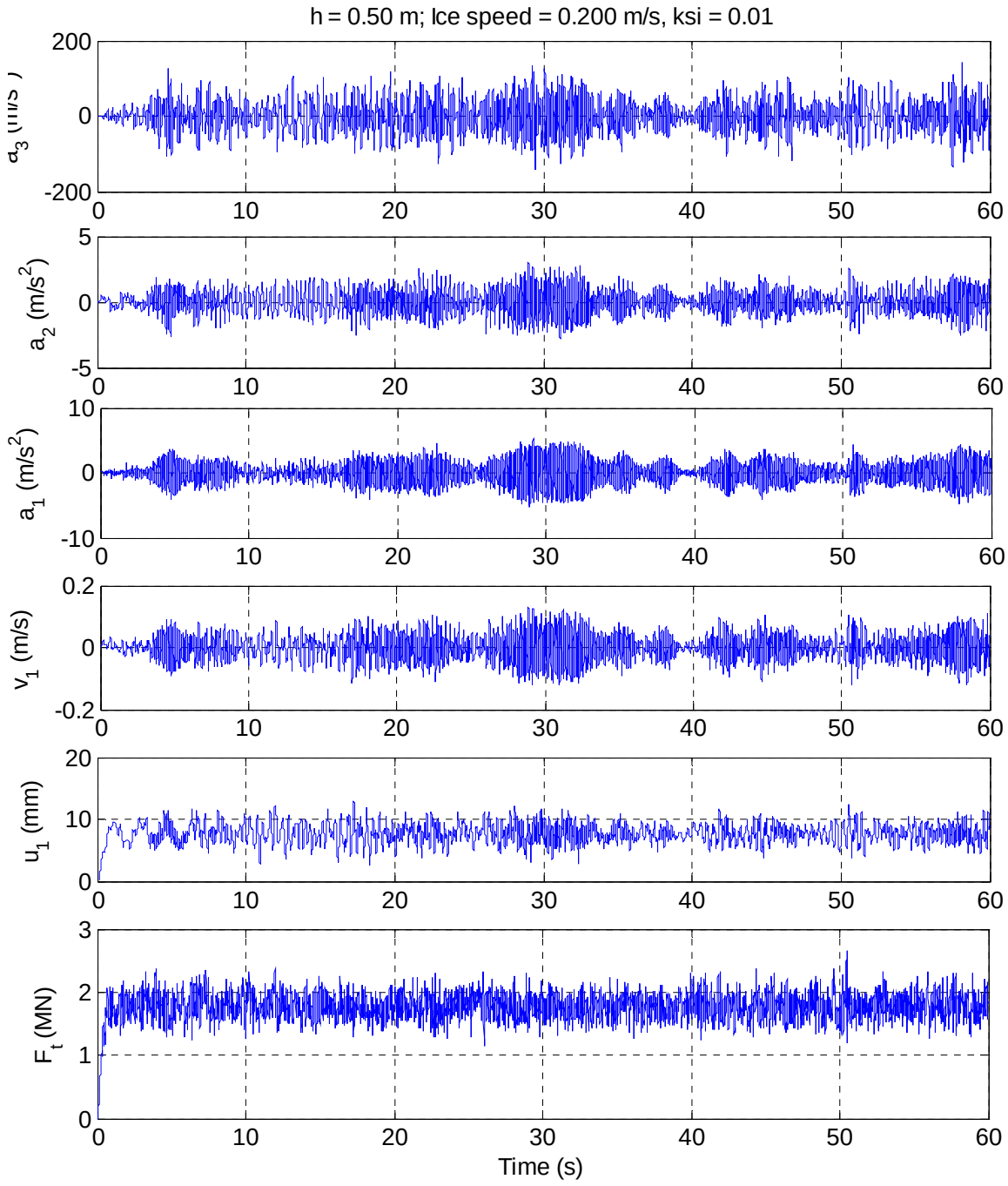

Figure 30a. Simulated time signals assuming a higher ice speed (0.2 m/s) and small damping in all modes.

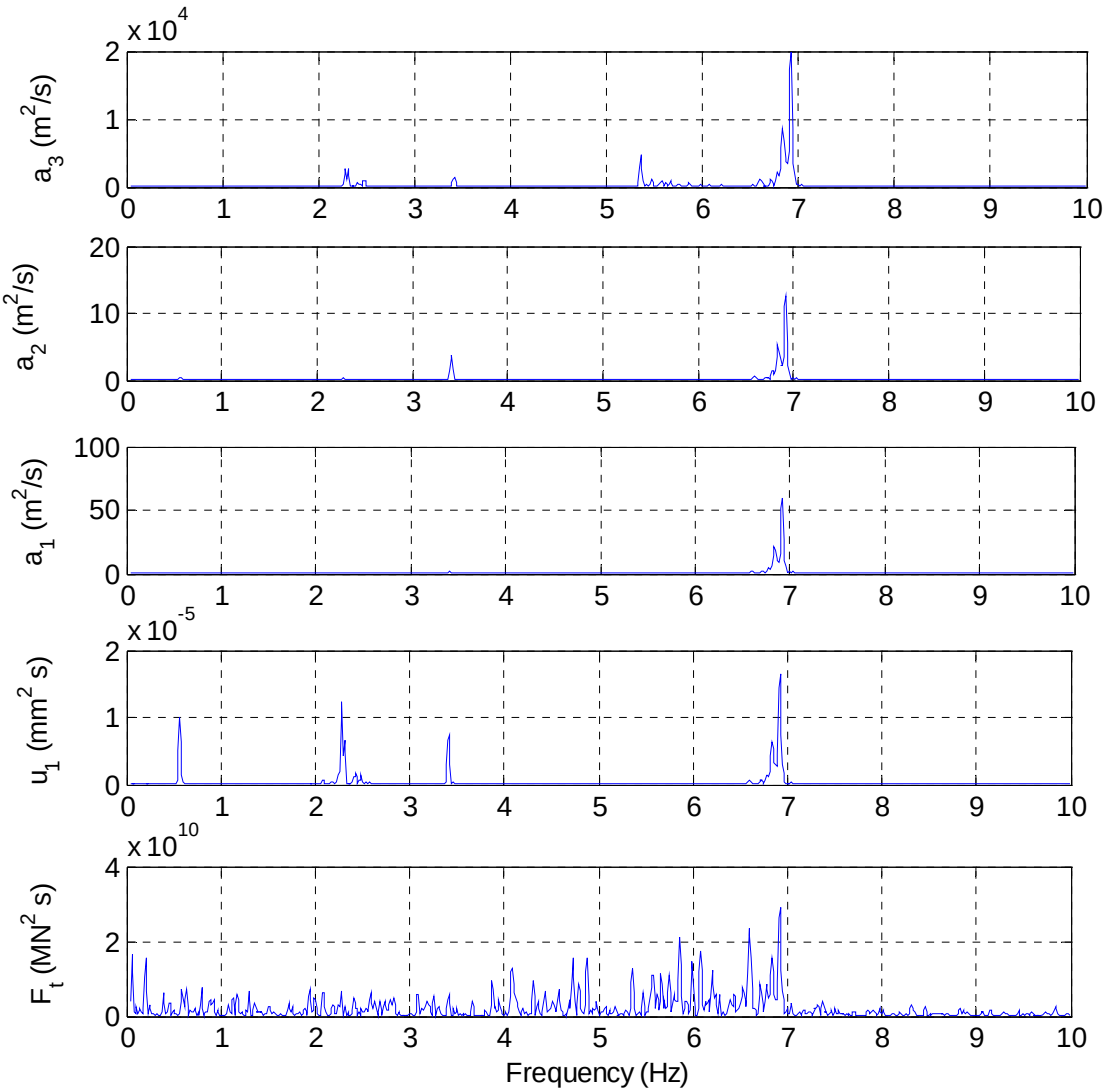

Figure 30b. Power spectral density functions (PSD) for signals shown in Fig. 30a.

The figures 30a and 30b predictions for the condition where the ice speed is 0.20 m/s. The PSD function for the ice force shows that the excitation is now a wide-band process. The modes No 1 (0.56 Hz), 4 (2.30 Hz), 7 (3.4 Hz) and 10 (6.89 Hz) are involved in the response signals. However, the mode 10 clearly dominates the response.

The time signals reveal further that the frequency content of the response may vary during the ice-structure interaction process.

4. Conclusions

This report provides a description of the numerical model PSSII, which can be used to simulate dynamic ice actions on vertical structures. The model takes account of dynamic soil-structure interaction as well as the dynamic ice-structure interaction while a sheet of level ice or rafted ice is acting on the structure. The ice-structure interactions are modelled using experimental information on the physical processes involved. These processes are briefly described.

Different features of this mode were illustrated by making case studies for three different structures. The numerical studies show that three different modes of dynamic ice-structure interaction may occur:

- Intermittent crushing,, which is associated with quasi-static response and transient vibrations
- self-excited vibrations, known also as lock-in
- wide-band random excitation.

These three modes or excitation/response have been seen and reported in several test conditions. The self-excited vibration is the most severe mode of dynamic ice-structure interaction. Some interesting results were obtained in the numerical studies.

- First, a simple formula proposed by Määttänen (1978) was used to obtain a first estimate of the eigenmodes that are likely to dominate the structural response. The subsequent numerical studies show a good agreement with the preliminary predictions.
- Second, the case studies suggest that the lowest eigenmode is not always the most critical mode for ice-induced vibrations. In the case of a fictive wind turbine structure the lowest natural frequency was estimated as 0.56 Hz. However, self-excited vibrations were predicted at the mode no 7, at the frequency or 3.4 Hz.
- The numerical study shows that the wide-band random exitation tends to occur at ice speeds higher than about 0.2 m/s. In spite of this, the response can show characteristics of a narrow-band random process it the structural damping of a mode is very low.

The features listed above were observed in a recent series of laboratory tests (Kärnä et al. 2003a, 2003b).

5. Acknowledgements

This work was supported by the EU funded project INTERREG-ICE, which was coordinated by Dr. Lennart Fransson at Luleå University of Technology. Fruitful discussions with Dr. Fransson and with a member of the project board, Mr. Göran Dalén are acknowledged. Mr. Guo Fengwei of the Dalian University of Technology provided valuable help by calculating PSD functions for this report.

6. References

Björk, B. (1981). Ice-induced vibration of fixed offshore structures. Part 2: Experience with Baltic lighthouses. Marine Structures and ships in ice, A Joint Norwegian Research Project. Report No: 81-06/2.

Blenkarn, K. (1970). Measurements and analysis of ice forces on Cook Inlet structures. Offshore Technology Conference. Houston, TX, USA, April 22-24. OTC 1261.

Clough, R. & Penzien, J. (1975). *Dynamics of Structures*. McGraw-Hill. New York 1975. pp. 191 - 201.

Daley, C. (1991). Ice edge contact – a brittle failure process model. Acta Polytechnica Scandinavica, Mechanical Engineering series No. 100. Finnish Academy of Technology. Helsinki, 92 p.

Daley, C., Tuhkuri, J. & Riska, K. (1998). The role of discrete failures in local ice loads. *Cold Regions Science and Technology* 27 (1998) pp. 197-211.

Engelbrektson, A. (1977). Dynamic ice loads on a lighthouse structure. Proc. Int. Conf. Port & Ocean Eng. under Arctic Cond., St.John´s, Canada, pp. 654 - 663.

Engelbrektson, A. (1983). Observations of a resonance vibrating lighthouse structure in moving ice. Proc. Int. Conf. Port & Ocean Eng. under Arctic Cond., Espoo, Finland. Vol. 2, pp. 855 - 864.

Engelbrektson, A. & Janson, E. (1985). Field observations on concrete structures in the Baltic Sea. *Concrete International*, August 1985. Pp. 48 - 52.

Engelbrektson, (1987). A. Study project ice forces against offshore structures. VBB Project M7334. Reports, No 2, 3 and 5.

Eranti, E. (1992a). Dynamic ice structure interaction – Theory and applications. *VTT Publications No 90.* 81 p.

Eranti, E. (1992b). Ice forces in dynamic ice/structure interaction. *Int. J. of Offshore and Polar Engineering*, vol2, N3, pp. 204 - 211.

Fransson, L., Olofsson,T., Sandkvist, J. (1991). Observation of the failure process in ice blocks crushed by a flat indentor. Proc. 11th Conf. Port and Ocean Engineering under Arctic Conditions (POAC´91), Vol. 1.Memorial University of Newfoundland, St.John´s, pp. 501 - 514.

Fransson, L. (1995). Ice load on Structures. Ice testing in Luleå Harbour 1993. *Cold Tech Report 1995:06*, 21 p + Apps.

GL Wind 2005. Guideline for the Certification of Offshore Wind Turbines. Edition 2005. Germanischer Lloyd, Wind Energie, Hamburg, Germany, 480 p.

Hirayama, K., Schwarz, J. & Wu, H.C. (1975). Ice forces on vertical piles: Indentation and penetration. Proc. 3th IAHR Ice Symp. Hanover, New Hampshire. pp. 429 - 445.

ISO/CD 19906. Arctic Offshore Structures.

Izumiyama, K., Irani, M.B. & Timco, G.W. (1996). Influence of compliance of structure on ice load. Proc. 12th IAHR Ice Symp., Vol. 1, pp.229 - 238.

Izumiyama, K. & Uto, S. (1997). Ice loading on a compliant indentor. Proc 14th Int. Conf. Port Ocean Eng. Arctic Conditions. Yokohama, Vol IV. pp. 431 - 436.

Jefferies, M.G. & Wright, W.H. (1988). Dynamic response of "Molikpaq" to ice-structure interaction. Proc. 7th Int. Conf. Offshore Mech. and Arctic Eng., Houston. Vol. IV, pp. 201 - 220.

Jefferies, M., Kärnä, T. and Løset, S. (2008). Field data on the magnification of ice loads on vertical structures. Proc. 19th IAHR Symposium on Ice. Vancouver, Canada, 6-11 July. (accepted).

Jochmann, P. and Schwarz, J. (2000). Ice Force Measurements at Lighthouse Norströmsgrund. Winter 1999. LOLEIF Report No 5. EU Contract MAS-CT-97-0098. 48 p + Appendix. Hamburg, Germany, December 2000.

Jochmann, P. and Schwarz, J. (2001). Ice Force Measurements at Lighthouse Norströmsgrund. Winter 2000. LOLEIF Report No 9. EU Contract MAS-CT-97-0098. 170 p + Appendix. Hamburg, Germany December 2001.

Jochmann, P. and Schwarz, J. (2005). The influence of individual parameters on the effective pressure on level ice against lighthouse "Norströmsgund". Proc. 18th International Conference on Port and Ocean Engineering under Arctic Conditions. Clarkson University, Potsdam, NY, USA. June 26-30, 2005. Vol. 3.

Joensuu, A. & Riska, K. (1989). Contact Between Ice and a Structure. ESPOO, Helsinki University of Technology, Ship Laboratory, Report M-88, 57 p. (In Finnish).

Kamesaki, K., Yamauchi, Y., Horikawa, T, Kawasaki, T., Ishikawa, S. & Tozawa, S. (1995). Experimental Study on independent failure zone of ice crushing. Proc. 10th Int. Symp. Okhotsk Sea Ice & Peoples, pp. 146 - 151.

Kamesaki, K., Yamauchi, Y & Kärnä, T. (1996). Ice force as a function of structural compliance. Proc. 13th IAHR Ice Symp., Beijing. Vol. I, pp. 395 - 402.

Kamesaki, K., Tsukuda, H. & Yamauchi, Y., (1997). Indentation tests with vertically placed ice sheet. Proc. 13th Int. Conf. Port & Ocean Eng. under Arctic Cond., Yokohama, Japan.

Kawamura, M., Takeuchi, T., Akagawa, S., Terashima, T., Nakazawa, N., Matsushita, H., Aoshima, M, Katsui, H. & Sakai, M. (1996). Ice-structure Interacions in medium scale field indentation tests. Proc. 13th IAHR Ice Symp., Beijing. Vol. 1, pp. 228 - 236.

Kärnä, T. & Turunen, R., (1989). Dynamic response of narrow structues to ice crushing. Cold Regions Science and Technology. 17(1989) 173 - 187.

Kärnä, T. & Turunen, R., (1990). A straightforward technique for analysing structural response to dynamic ice action. Proc. 9th Int. Conf. Offshore Mech. and Arctic Eng., Houston. Vol. IV, pp. 135 - 142.

Kärnä, T. (1992). A procedure for dynamic soil-structure-ice interaction. Proc. 2nd Int. Offshore and Polar Eng. Conf., San Francisco, Vol II, pp. 764 - 770

Kärnä, T., Nyman, T., Vuorio, J. & Järvinen, E. (1993b). Results from indentation tests in sea ice. Proc. 12th Int. Conf. Offshore Mech. and Arctic Eng., Glasgow. Vol. IV, pp. 177 - 185.

Kärnä, T., Muhonen, A., & Sippola, M. (1993c). Rate effects in brittle ice crushing. Proc. 11th Int. Conf. Port & Ocean Eng. under Arctic Cond., Hamburg, vol 1, pp 50 - 72.

Kärnä, T. & Järvinen, E. (1994a). Dynamic unloading accross the face of a wide structure. Proc. 12th IAHR Ice Symp., Trondheim, Vol. 3, pp. 1018 - 1039.

Kärnä, T. (1994b). Finite ice failure depth in penetration of a vertical indentor into an ice edge. *Annals of Glaciology*, 19 (1994), pp. 114 - 120.

208

Kärnä, T. & Sippola, M. (1996). Nonlinear loading phase in ice indentation. Proc. 6th Int. Offshore and Polar Eng. Conf., Los Angeles. Vol. II, pp. 349 - 353.

Kärnä, T., Kamesaki, K. & Tsukuda, H., (1997). A flaking model of dynamic ice-structure interaction. VTT Building Technology. *Internal Report* RTE38-IR-7/1997, 51 p.

Kärnä, T. & Järvinen, E. (1999). Symmetric and asymmetric flaking process. Proc. 15th Int. Conf. Port & Ocean Eng. under Arctic Cond., Espoo, Finland, pp. 988 - 1000.

Kärnä, T., Kamesaki, K. & Tsukuda, H. (1999). A numerical model for dynamic ice-structure interaction. *Computers and Structures* 72(1999) 645 - 658.

Kärnä, T., Shkhinek, K., Kapustiansky, S., Jilenkov, A. Määttänen, M. And Kolari, K. (2001). Ice-Structure Dynamics. Validation of Low Level Ice Forces on Coastal Structures (LOLEIF). Report No 8. EU MAST III Project CT97-0098. 135 p.

Kärnä, T. Kolari, K., Jochmann, P. Evers, K-U., Bi X., Määttänen, M. & Martonen, P. (2003a). Tests on dynamic ice-structure interaction. Proc. 22nd Int. Conf. Offshore Mechanics and Arctic Engineering. Cancun. Mexico, 8-13 June 2003.

Kärnä, T. Kolari, K., Jochmann, P. Evers, K-U., Bi X., Määttänen, M. & Martonen, P. (2003b). Ice action on compliant structures, Laboratory indentation tests. VTT Research Notes 2223, 43 p. + Apps.

Kärnä, T. and Qu Y. (2005). Analysis of the size effect in ice crushing – edition 2. VTT Technical Report RTEU50-IR-6/2005. 203 p. (enters public domain in January 2009).

Kärnä, T., Qu, Y. and Yue, Q.J. (2006). Baltic model of global ice forces on vertical structures. Proc. 18th International Symposium on Ice. Int. Ass. Hydr. Eng. Res. Sapporo, Japan, 28-31 Aug. 2006. Vol 1, pp. 253-260.

Kärnä, T., Guo, F., Løset, S. and Määttänen, M. (2008). Small-scale data on magnification of ice loads on vertical structures. Proc. 19th IAHR Symposium on Ice. Vancouver, Canada, 6-11 July. (accepted).

Muhonen, A., Kärnä, T., Eranti, E., Riska, K. & Järvinen, E (1992). Laboratory indentation tests with thick freshwater ice. Vol I. *VTT Research Notes 1370.* Espoo, 92 p.

Määttänen, M. (1975). Experiences of ice forces against a steel lighthouse mounted on the seabed, and proposed constructional refinements. Proc. 3rd Int. Conf. Port Ocean Eng. under Arctic Cond., Fairbanks, Alaska, 11-15 August,, Vol. II, pp. 875-869.

Määttänen, M. (1977). Ice force measurements at the Gulf of Bothnia by instrumented Kemi I lighthouse. Proc. 4th Int. Conf. Port and Ocean Eng. under Arctic Cond., St. John´s, Canada.

Määttänen, M. (1978). On conditions for the rise of self-excited ice-induced autonomous oscillations in slender marine pile structures. *Winter Nav. Board, Finland, Res. Rep., 25.*

Määttänen, M. (1982). Laboratory tests for dynamic ice-structure interaction. *Eng. Struct., 3(1982),* pp. 111 - 116.

Määttänen, M. (1998). Numerical model for ice-induced vibration load lock-in and synchronization. Proc. 14th IAHR Ice Symp., Potsdam NH, USA. Vol 2. pp. 923 - 930.

Nordlund, O.P., Kärnä. T. & Järvinen E. (1988). Measurements of ice-induced vibrations of channel markers. Proc. 9th IAHR Ice Symp., Sapporo. Vol. 2, pp. 537 - 548.

Olofsson, T., Fransson, L. & Sandkvist, J. (1991). Ice Crushing. Failure Mechanisms. Report of Luleå Technical University, 33 p.

Peyton. H. (1966), Sea Ice Strength. University of Alaska, Geophysical Institute, Report No UAG R-182, December 1966, 285 p.

Schwarz, J. (1993). Ice forces on offshore structures. Proc. 1st Int. Conf. on Development of the Russian Arctic Offshore. St.Petersburg, Russia. pp. 154 - 160.

Schwarz, J. and Jochmann, P. (2001). Ice force measurement within the LOLEIF-project. Proc. 16th Int. Conf. on Port and Ocean Engineering under Arctic Conditions. Ottawa, Canada, August 12-17, 2001. pp. 669 - 680.

Sodhi, D. (1991a). Effective pressures measured during indentation tests in freshwater ice. Proc. 6th Int. Cold Regins Eng. Specialty Conf. Hanover, NH. February 1991. pp. 619 - 627.

Sodhi, D.S. (1991b). Ice-structure interaction during indentation tests. Proc. IUTAM-IAHR Ice Symposium, St.Johns pp 619 - 637.

Sodhi, D., (1992). Ice-structure interaction with segmented indentors. Proc. 11th IAHR Ice Symp., Banff, Alberta. Vol 2, pp. 909 - 929.

Sodhi, D.S., Takeuchi, T., Nakazawa, N., Akagawa, S. & Saeki, H. (1998). Medium-Scale Indentation tests on Sea Ice at Various Speeds. *Journal of Cold Regions Science and Technology*, 28, pp. 161 - 181.

Sodhi, D. (1998). Nonsimultaneous crushing during edge indentation of freshwater ice sheets. *Cold Regions Science and Technology* 27 (1998) 179-195.

Sodhi, D. (2001). Crushing failure during ice-structure interaction. *Engineering Fracture Mechanics* 68 (2001) 1889-1921.

Takeuchi, T., Sasaki, M., Akayawa, S., Kawamura, M., Sakai, M., Haman, Y., Kurokawa, A. & Saeki, H. (1999). Contact Ratio in Ice/Structure Interaction Based on Statistical Generation of Ice Failure Surface. Proc. 9th ISOPE Conference, Vol. II, pp. 505 - 511.

Toyama, Y., Sensu, T., Minamami, M. & Yashima, N. (1983). Model tests on ice-induced self-excited vibration of cylindrical structures. Proc. 7th Int. Conf. Port Ocean Eng. Arctic Conditions, Helsinki, Vol. II, pp. 834 - 844.

Tuhkuri, J. (1996). Computational fracture mechanics analysis of flake formation in brittle ice. Proc. 13th IAHR Ice Symp., Beijing, China. Vol. 1, pp. 54 - 61.

Wolf, J. (1997). Spring-dashpot-mass models for foundation vibrations. *Earthquake Engineering and Structural Dynamics*, Vol. 26, 931-949.

Yue, Q.J. & Bi, X.J. (1998). Full-scale tests and analysis of dynamic interaction between ice sheet and conical structures. Proc. 14th IAHR Ice Symposium. Potsdam, USA. Vol 2.

Yue, Q.J. & Bi, X. (2000). Ice-induced jacket structure vibrations in Bohai Bay Sea. *Journal of Cold Regions Engineering*. Vol. 14, No 2, June 2000, Paper No 21698, pp. 81 - 92.

APPENDIX 1

Plots of the simulation results for a wind turbine

This appendix summarises the results obtained while simulating the dynamic ice-structure interaction of a fictive offshore wind-turbine structure (Sect. 3.3).The simulations were conducted with the model version PSSII_2.1 as described in Set. 3.3. The waterline diameter was assumed as 6.0 m in these simulations. The damping factor was assumed as 7 % for all ten modes that were considered.

Notation for the plots that are shown in the next pages

a_3 is the acceleration response at z = 105 m (blade tip),

a_2 the acceleration response at z = 65 m (hub height),

a_1 the acceleration response at z = 20 m (water level),

v_1 the velocity response at z = 20 m (water level),

u_1 the displacement response at z = 20 m (water level),

F_t the total ice force acting at z = 20 m (water level),

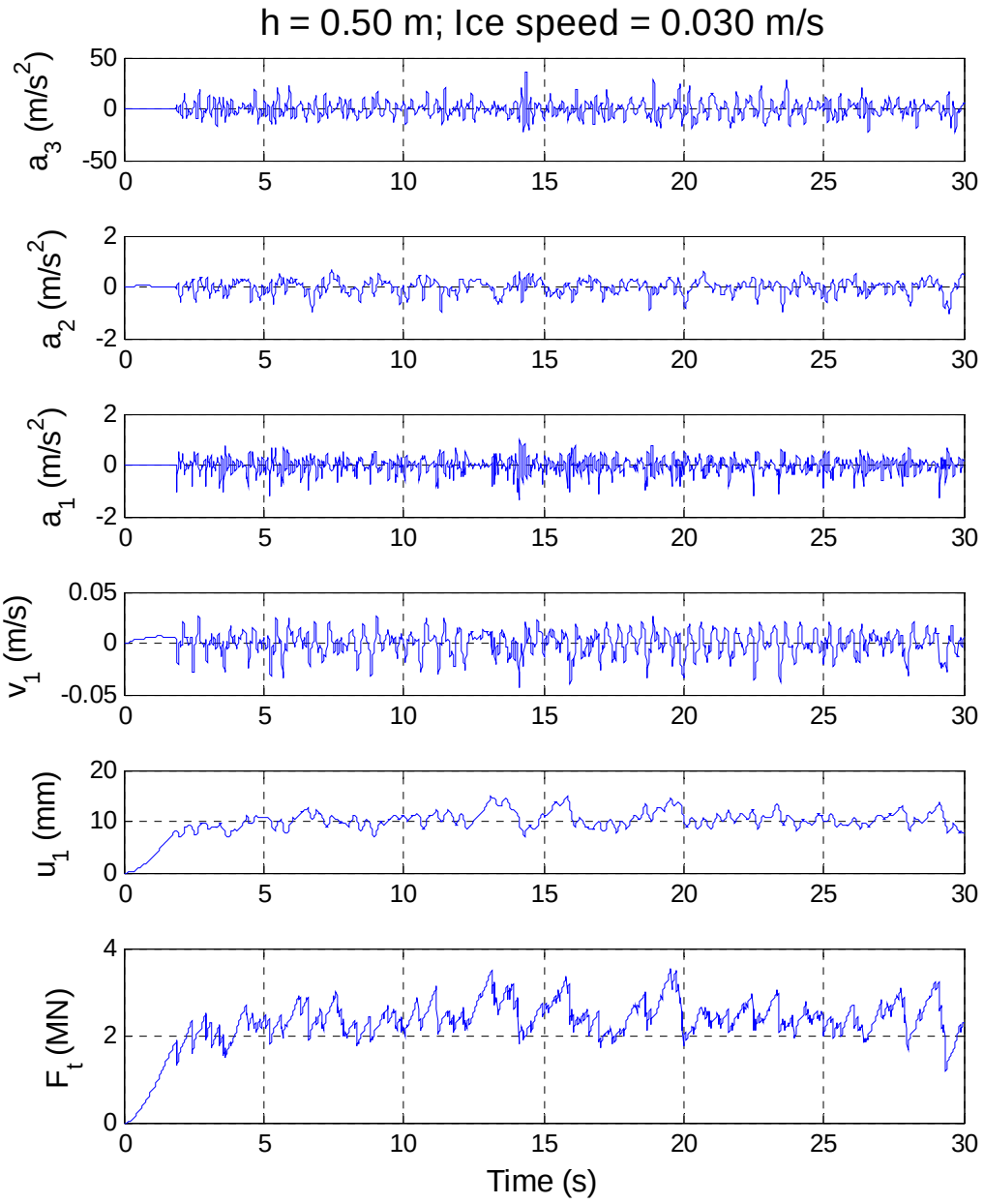
h = 0.50 m; Ice speed = 0.030 m/s
a3 (m/s2)
a2 (m/s2)
a1 (m/s2)
v1 (m/s)
u1 (mm)
Ft (MN)
Time (s)

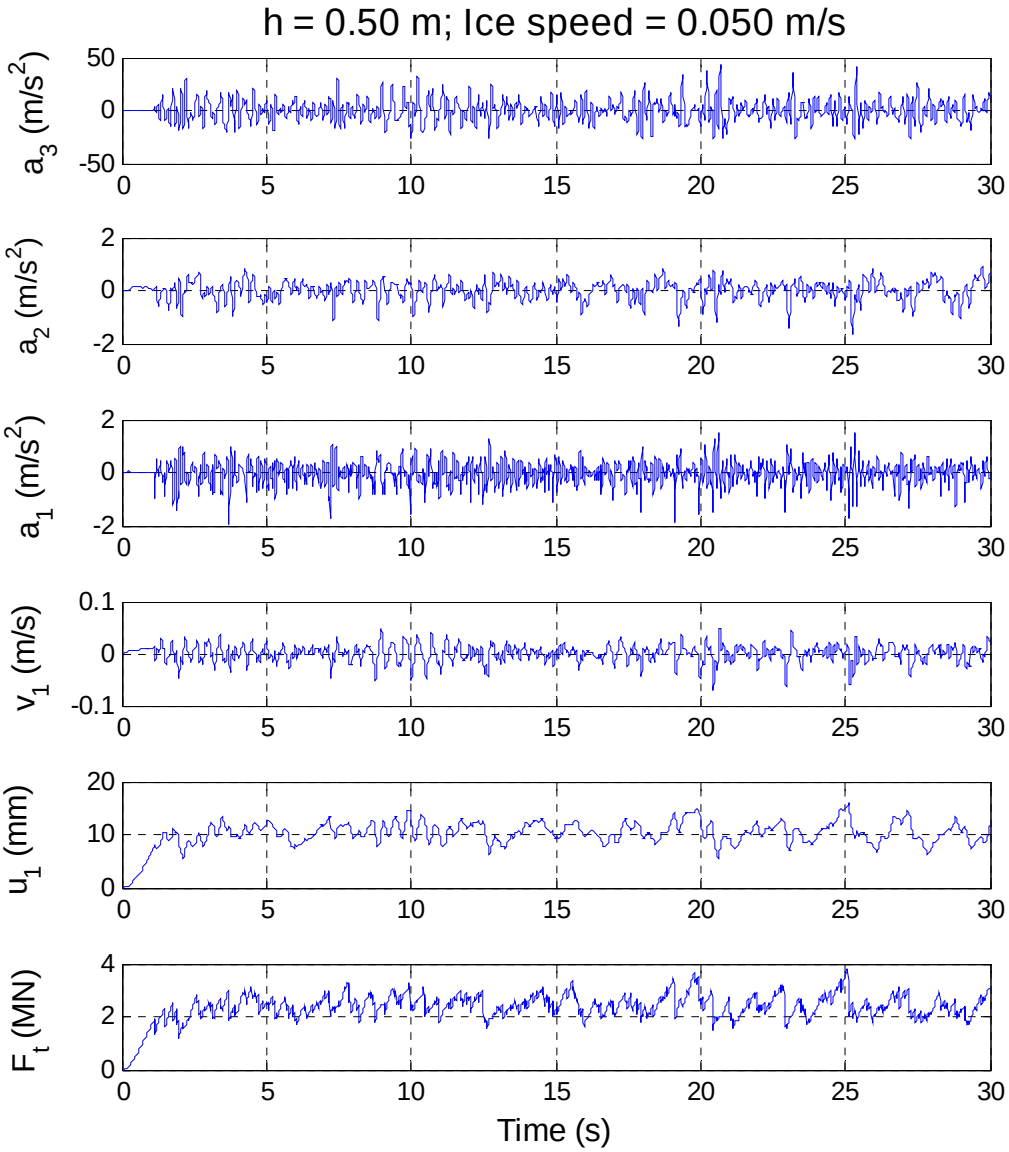
h = 0.50 m; Ice speed = 0.050 m/s
a3 (m/s2)
a2 (m/s2)
a1 (m/s2)
v1 (m/s)
u1 (mm)
Ft (MN)
Time (s)

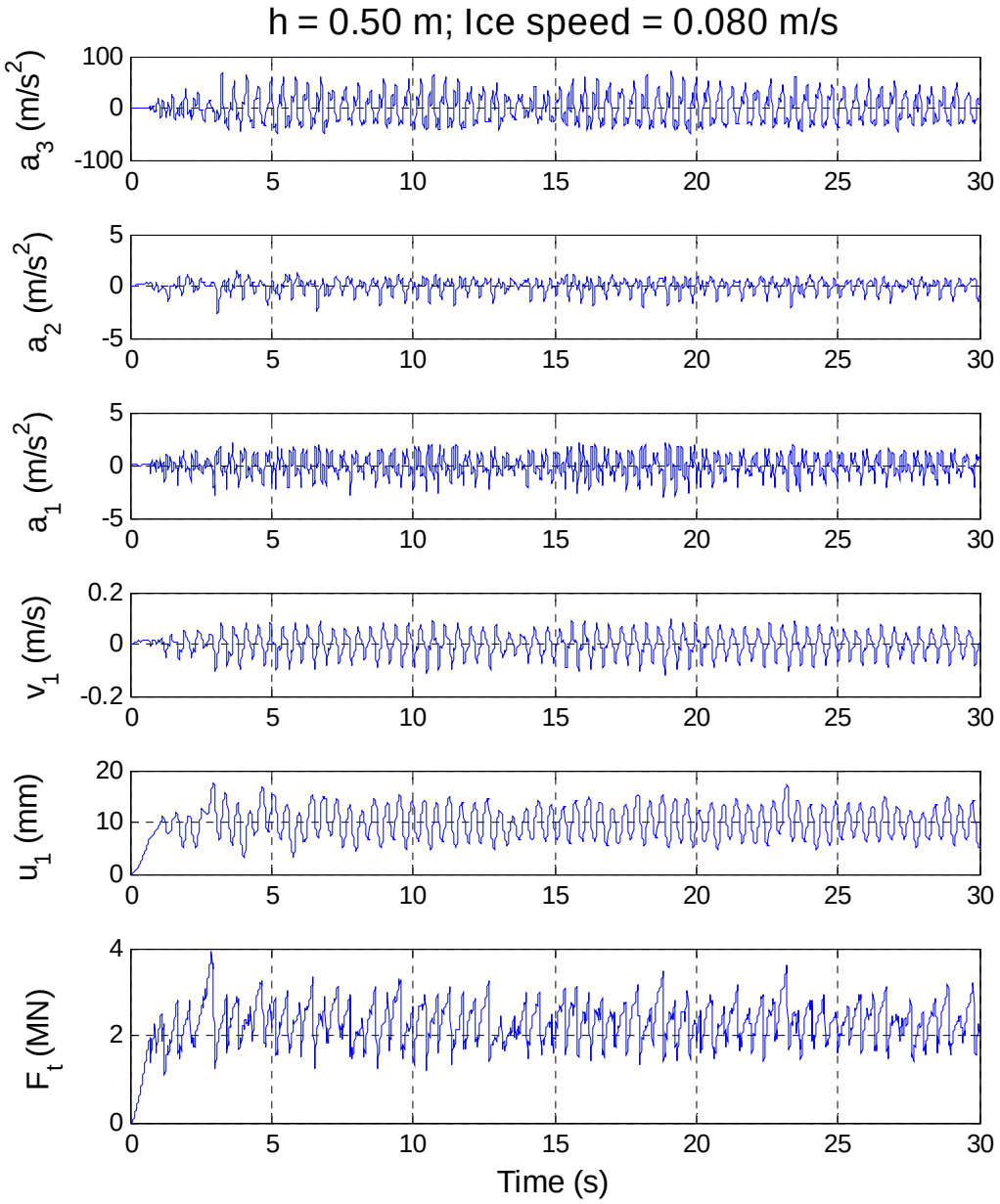
h = 0.50 m; Ice speed = 0.080 m/s
a3 (m/s2)
a2 (m/s2)
a1 (m/s2)
v1 (m/s)
u1 (mm)
Ft (MN)
Time (s)

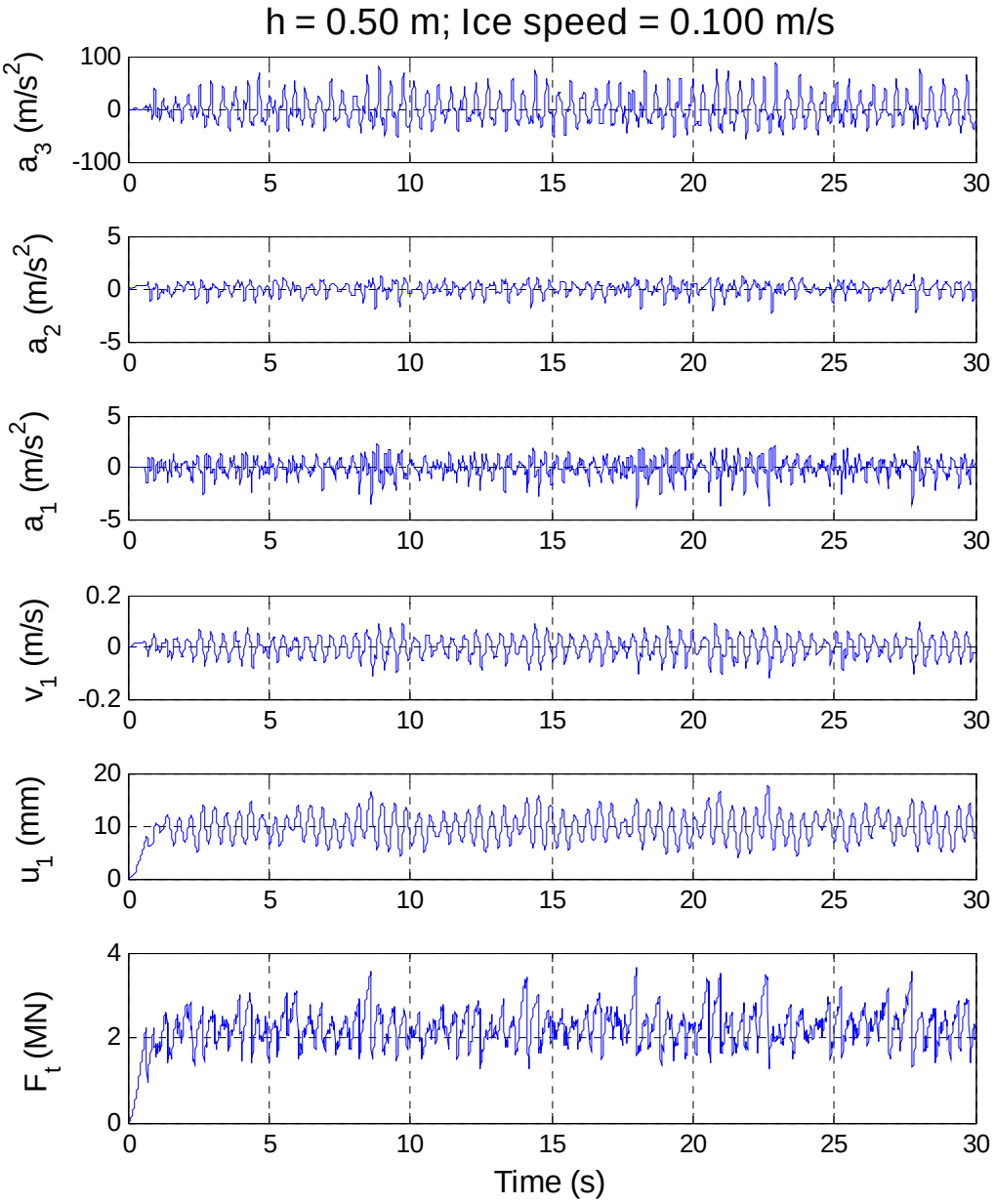
h = 0.50 m; Ice speed = 0.100 m/s
a3 (m/s2)
a2 (m/s2)
a1 (m/s2)
v1 (m/s)
u1 (mm)
Ft (MN)
Time (s)

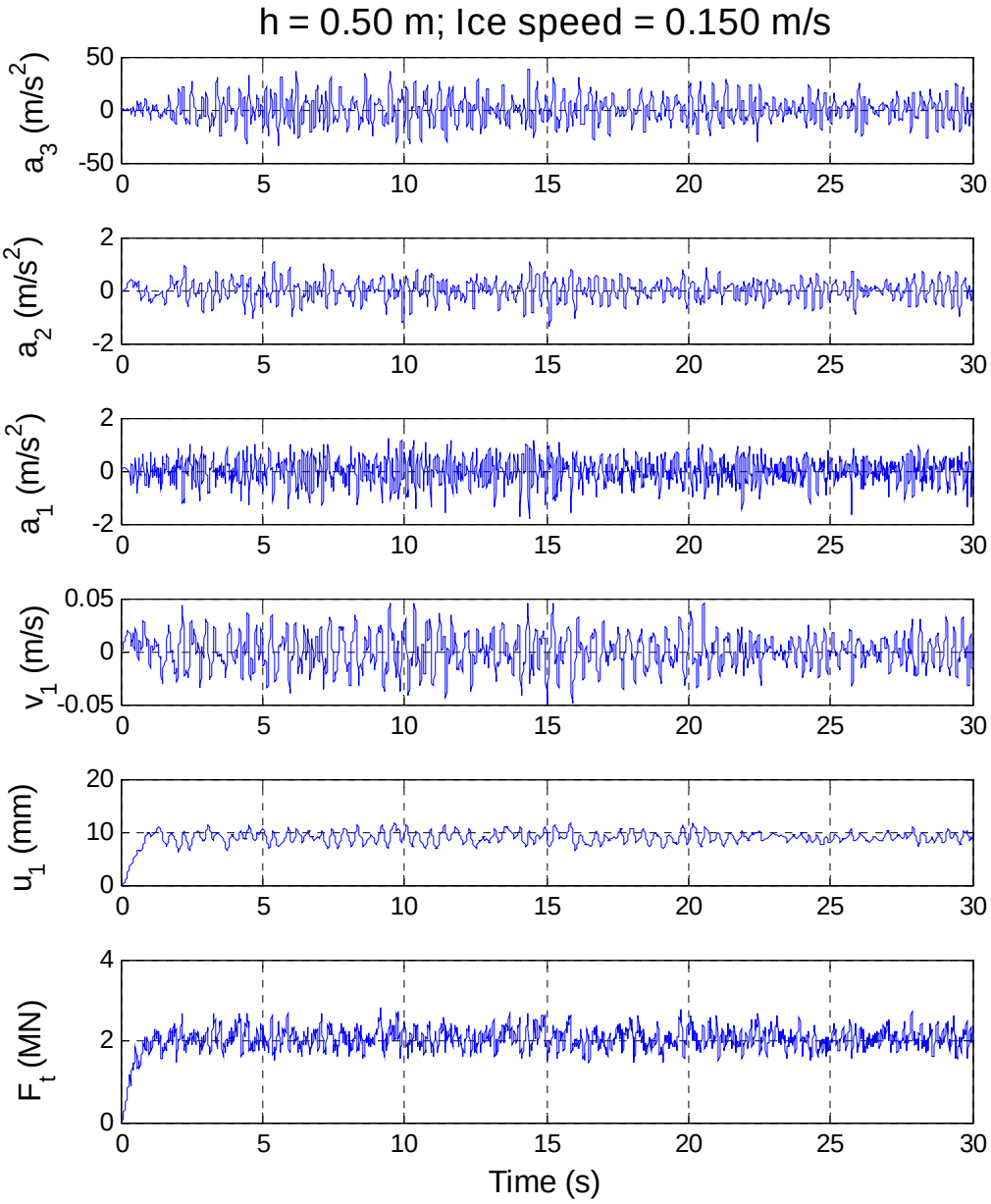
h = 0.50 m; Ice speed = 0.150 m/s
a3 (m/s2)
a2 (m/s2)
a1 (m/s2)
v1 (m/s)
u1 (mm)
Ft (MN)
Time (s)

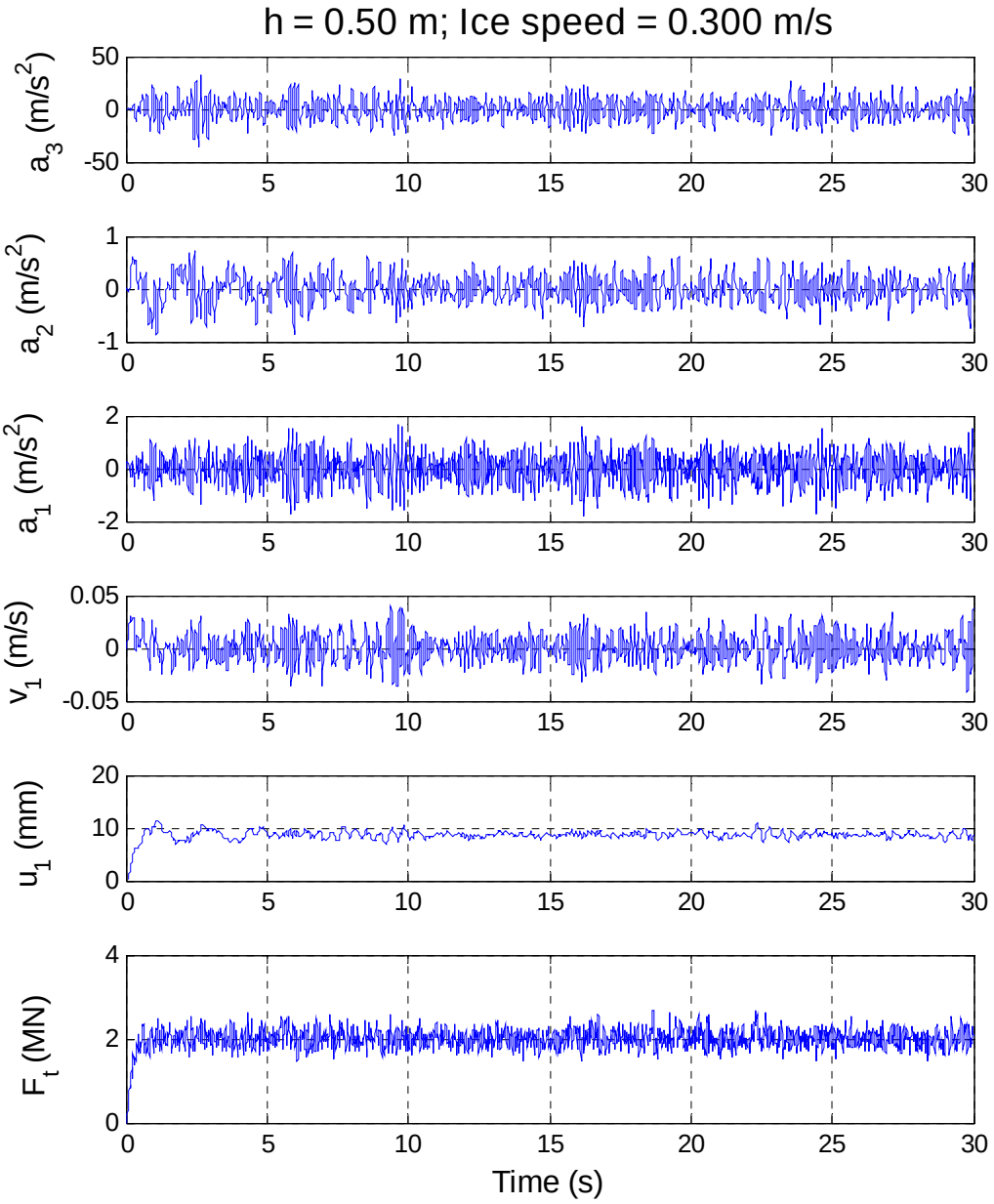
h = 0.50 m; Ice speed = 0.300 m/s
a3 (m/s2)
a2 (m/s2)
a1 (m/s2)
v1 (m/s)
u1 (mm)
Ft (MN)
Time (s)

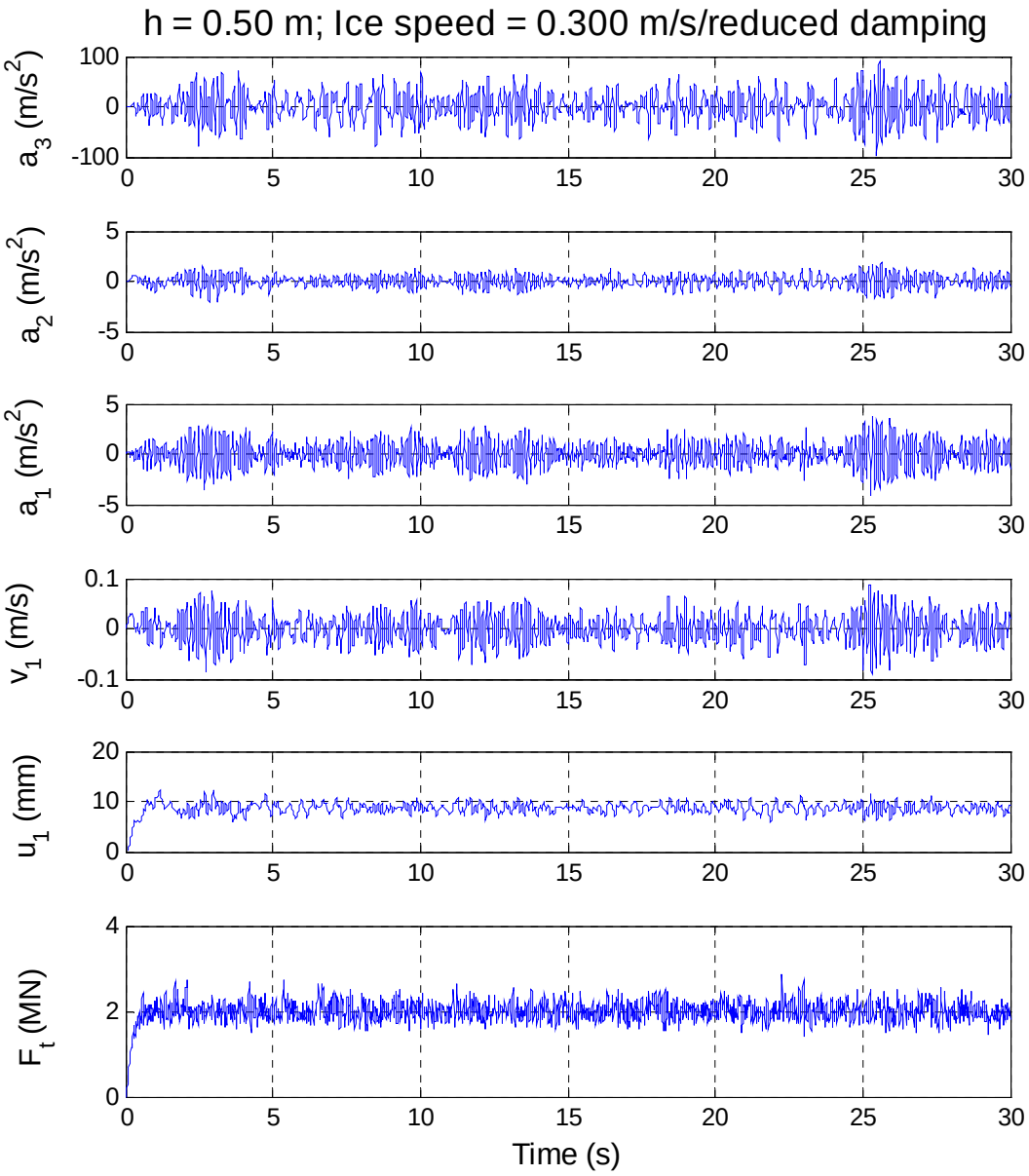
h = 0.50 m; Ice speed = 0.300 m/s/reduced damping
a3 (m/s2)
100
0
-100
a2 (m/s2)
5
0
-5
a1 (m/s2)
5
0
-5
v1 (m/s)
0.1
0
-0.1
u1 (mm)
20
10
0
Ft (MN)
4
2
0
0
5
10
15
20
25
30
Time (s)

Isförhållanden längs svenska kusten, Bottenviken, Bottenhavet och Barents hav

Jan-Eric Lundqvist

Isförhållanden längs svenska kusten, Bottenviken, Bottenhavet och Barents hav

Jan-Eric Lundqvist

Förord

Följande rapport ingår i projektet ” Ismekanikk og havnedrift i islagde farvann” Del programmet Nordkalotten INTERREG III A Nord).

I rapporten beskrivs isutvecklingen och isutbredningen under en lindrig, normal och sträng isvinter i främst Bottenviken och Bottenhavet. Nutida metoder för iskartläggning presenteras. Olika former av is beskrivs och isens topografi i form av vallar, hopskjutningar och sammanpackning. Rapporten tar också upp väderförhållandenas inverkan på isdrift och skapande av extrema issituationer. Vissa kustområden som är särskilt utsatta för svår ispress poängteras. Dessutom presenteras en sammanfattande statistik över istjockleken till sjöss och i skärgårdar.

Rapporten avslutas med en kort rapport över isförhållandena i Barents hav med avseende på kustområdet utanför Nordkalotten.

Norrköping i april 2008

Jan-Eric Lundqvist
meteorolog med marin inriktning

Innehållsförteckning

1 Isförhållanden längs svenska kusten

Sen början av 1960-talet har intresset för en ökad kartläggning och forskning kring isförhållandena i Bottenviken ägt rum. Genom ett riksdagsbeslut 1972 genomdrev man tillsammans med Finland ett beslut att verkställa året runt sjöfart till Bottenvikens hamnar. Ett särskilt vintersjöfartsprogram togs fram, som därmed ökade kunskapen och erfarenheten om isförhållandena i hela Östersjön.

Isförhållandena har under de senaste 50 åren varierat en hel del. Kalla vintrar har avlöst milda och ett statistiskt värde för en normal isutveckling har beräknats. Isvintrarna har skiftat beroende på väderförhållandena framför allt under högvintern januari, februari, mars. Årets (2007/2008) mycket lindriga issituation i Bottenviken blev en av de lindrigaste under perioden 1900 – 2008, jämförbar med isvintern 1992.

1.1 Lindrig isvinter

Under en lindrig isvinter, se exempel i Figur 1.1, har Bottenviken och Norra Kvarken någon period under vintern varit helt istäckt om än kortvarigt. Milda vindar mestadels från en sydlig eller västlig riktning dominerar. Kortvariga kalla perioder medför tillfällig isläggning både vid svenska kusten och den finska men även till sjöss i de centrala delarna. Den nybildade isen bryts dock upp av milda och friska västliga vindar. Isen packas samman oftast utanför finska kusten, där svårforcerade vallar bildas med en stampisvall vid iskanten. Isvintrar klassas även som lindriga då is tillfälligt förekommer utanför svenska och finska kusterna i Bottenhavet. Denna is brukar bli relativt tunn och orsakar inte till några större problem för vintersjöfarten. Bälten med sammanpackad is kan tillfälligt bildas närmast kusterna och i inloppen till hamnarna.

1.2 Normal isvinter

Under en isvinter där maximala isutbredningen täcker hela Bottniska viken, Ålands hav och nordligaste Östersjön till i höjd med Stockholm betecknas som normal, se exempel i Figur 1.2. Kalla nordliga eller nordostliga vindar dominerar tillsammans med högtryckssituationer med klart och kallt väder. I Bottenviken växer isen till alltmer under vintern och driver sydvart. Mycket grov is med vallar spärrar ofta genomfarten i Norra kvarken. I ett tidigt skede av isutvecklingen kan is driva genom Norra Kvarken sydvart längs svenska kusten och skapa ett bälte av grövre is. Det mest anmärkningsvärda under en isläggningsperiod är att is packas samman hårt mot svenska kusten i Gävlebukten, likaså i Ålands hav. Isen i de centrala delarna av t.ex. Bottenhavet brukar mestadels vara relativt jämn med infrusna bälten av grövre is.

I samband med milda och hårda syd- eller sydvästliga vindar i mars bryter isen upp och driver nordvart. Isen i Norra Östersjön packas samman mot Ålands och Åbo skärgård.

Senare släpper isen från kusten och driver sydvart och skingras. I Bottenhavet packas isen samman mot norra delen och mot Norra Kvarken. Ett kompakt och mycket svårforcerat isfält bildas och tidvis förekommer svår ispress. Efterhand släpper ispressen och isfältet bryter upp och driver sydvart. Under den fortsatta islossningen brukar bälten av sammanfrusen grov is med vallar förekomma ute till sjöss långt frampå våren. I Bottenviken öppnas till en början mindre råkar under april månad den men först i maj sker islossningen och isavsmältningen snabbare.

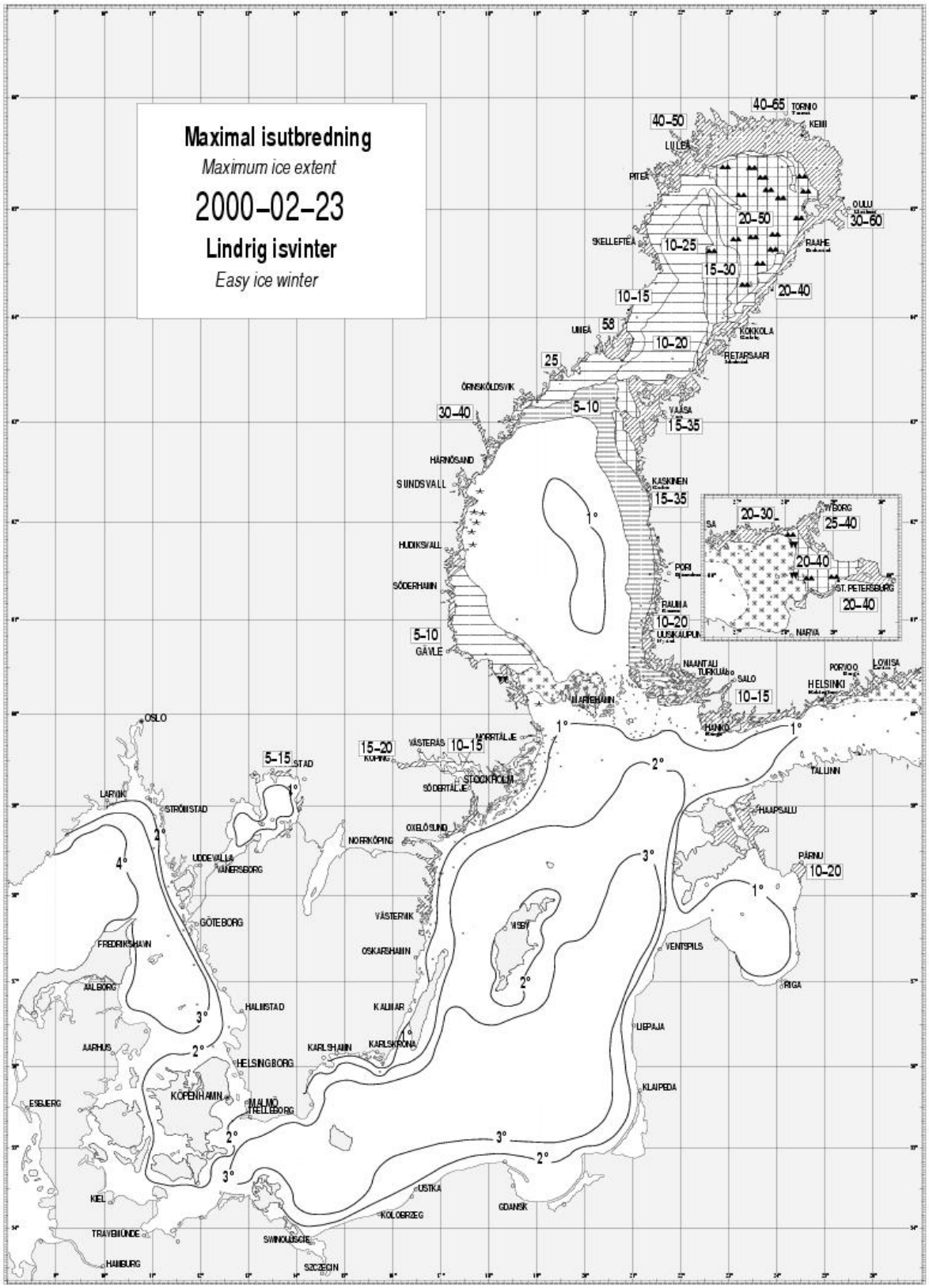

Figur 1.1 Exempel på isutbredning för en lindrig isvinter (2000).

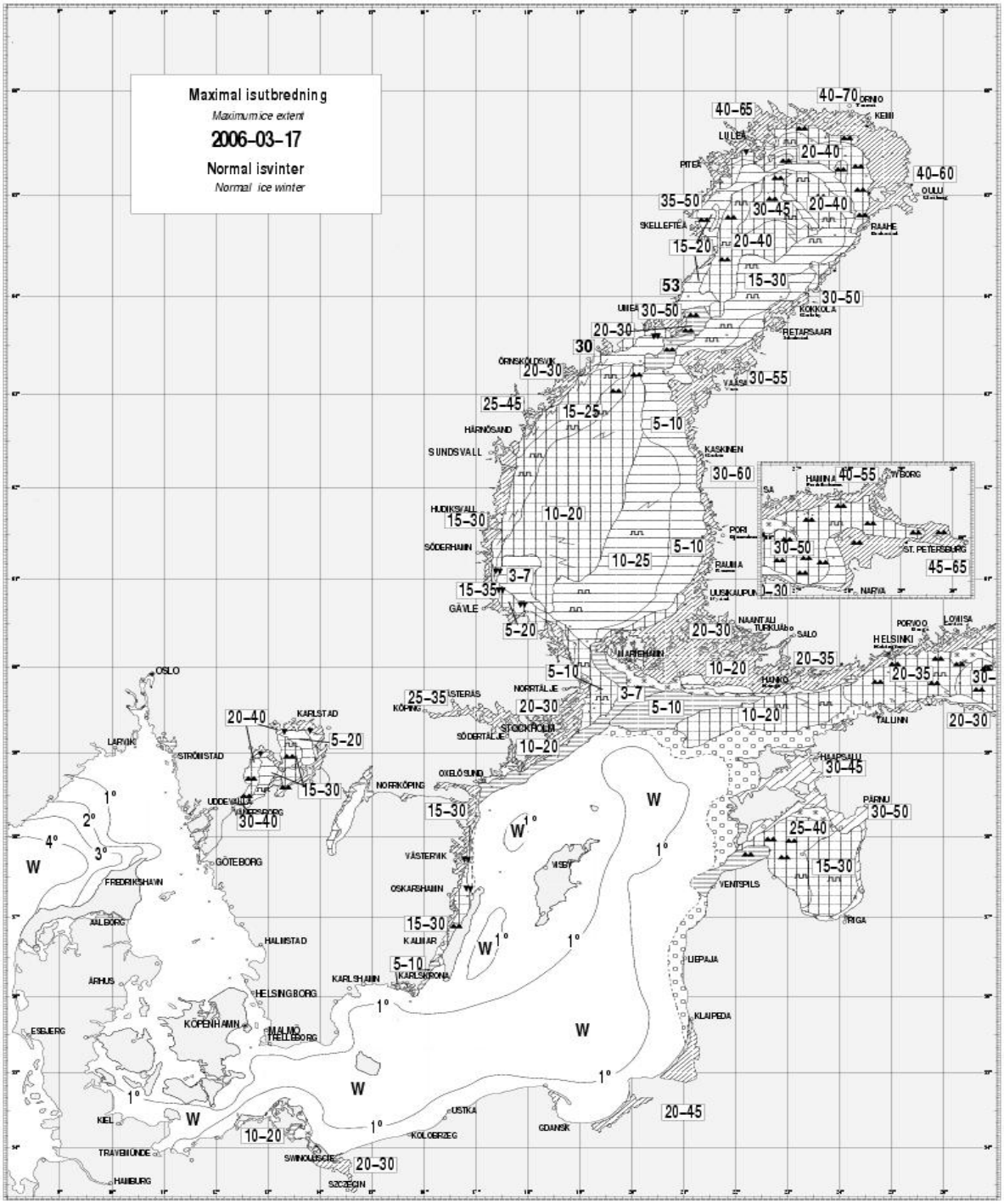

Figur 1.2 Exempel på isutbredning för en normal isvinter (2006).

1.3 Sträng isvinter

Under en sträng isvinter, se exempel i Figur 1.3, sker isutvecklingen i stort sett som under en normal isvinter. Perioder med sträng kyla förekommer oftare och berör även stora delar av Östersjön, Syd- och Västkusten. Kalla nordostliga och ostliga vindar dominerar. I Bottniska viken och söderut till Ålands hav är isförhållandena svåra eller mycket svåra under perioden januari till slutet av mars. I norra Östersjön påverkas isläget från Finska viken. Is som bildas i västra delen av Finska viken driver över mot svenska kusten samtidigt som isen växer till i tjocklek. Efterhand fylls området mellan Gotland och svenska fastlandet med sammanfrusen

grov is med vallar. Isläget brukar vara lindrigare vid baltiska kusten. Isen som bildas där utanför kusten driver västvart och fyller på isfältet på svenska sidan.

Islossningen brukar vara dramatisk med tidvis mycket svår ispress. I samband med hårda sydost- eller sydvästliga vindar i regel i slutet av mars driver isen norrut och packas samman i nordligaste Östersjön. Ett mycket svårforcerat isfält bildas i nordligaste Östersjön och i inloppen till Finska viken och Ålands hav. Efterhand släpper ispressen, isen driver sydvart, sprider ut sig och upplöses långsamt i det varmare vattnet i norra Östersjön. I Bottenhavet öppnas smala råkar i sydligaste delen medan svår ispress sker i norra Bottenhavet. Isfältet brukar vara mycket svårframkomligt med talrika vallar. Efterhand bryter isfältet upp i vidsträckta flak blandat med små flak och krossis. Isen sprider ut sig delvis sydvart och skingras. Först mot slutet av april är det i stort sett isfritt i Bottenhavet. I Bottenviken går islossningen något långsammare och först i slutet av maj är det öppet vatten, även om enstaka isbumlingar förekommer på grynnor och skär in bit in i juni.

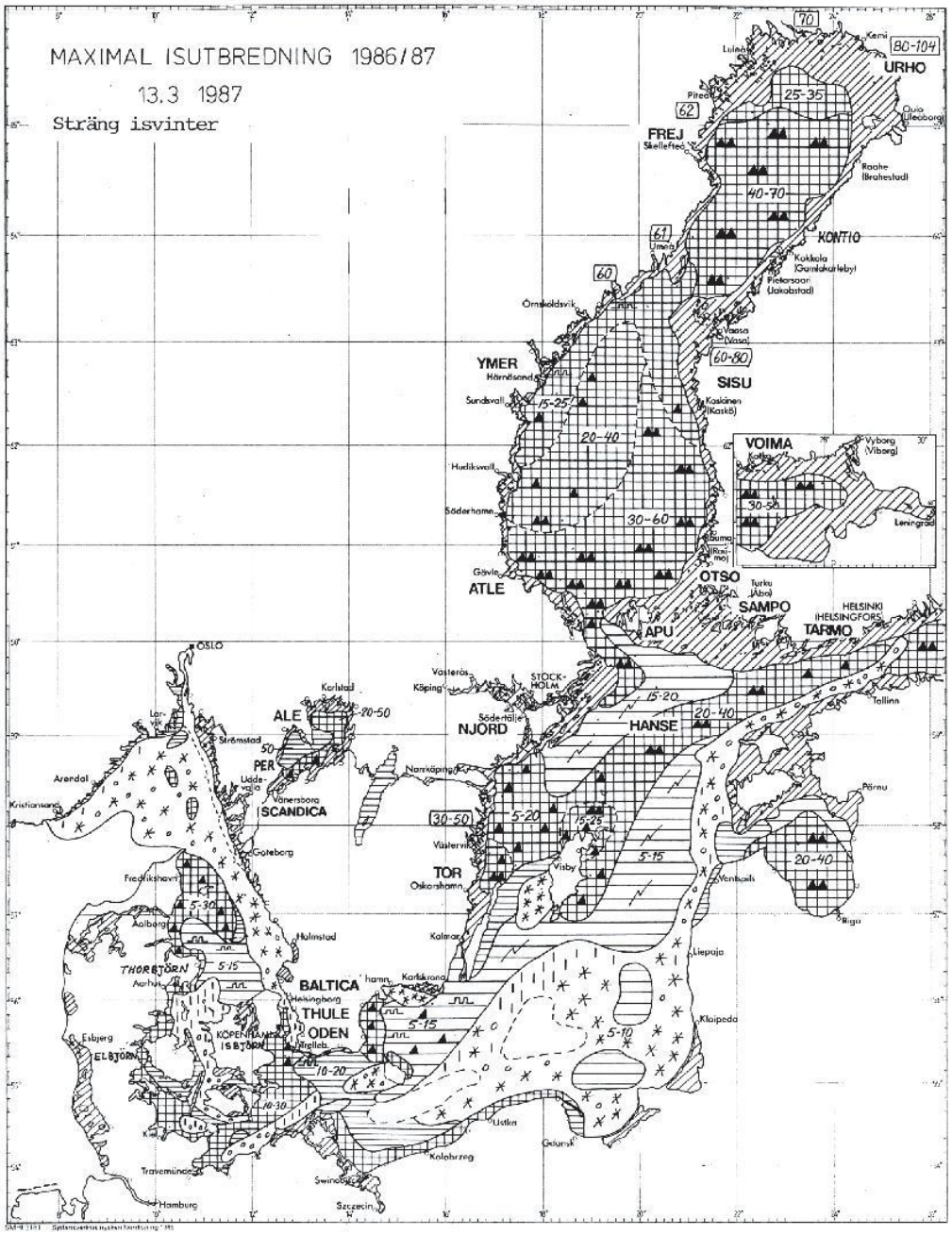

Figur 1.3 Exempel på isutbredning för en sträng isvinter (1987).

1.4 Iskartläggning med satellit

Isutbredningen kartläggs bl.a. av SMHI (Sveriges Meteorologiska och Hydrologiska Institut) samt av FHI (Finska Havsforskningsinstitutet). I modern tid används satellitbilder, dels NOAA (infraröda och visuella spektrat) och dels den kanadensiska kommersiella RADARSAT (radarreflektion från satellit), se exempel i Figur 1.4 - Figur 1.5. Dessa satellitbilder länkas över till isbrytarna som även plottar fartygsrörelser i isfarvatten. Istjockleksmätningar förekommer regelbundet från vissa kuststationer. Till sjöss uppskattas istjockleken från isbrytarna och i vissa fall uppmätta från vistelse på isen.

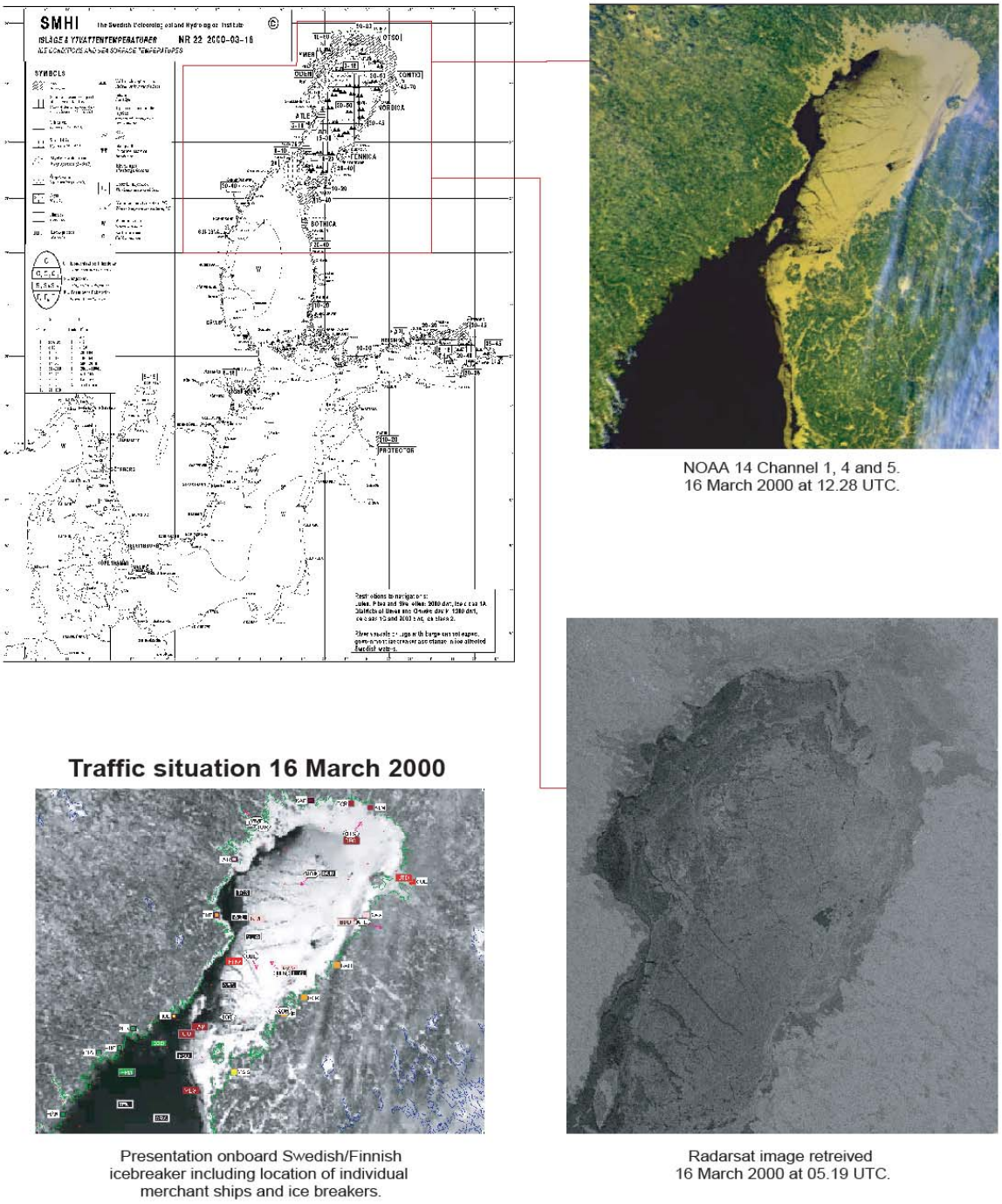

Figur 1.4 Figuren visar isutbredningen från år 2000 och skillnaden mellan de båda satellitbilderna. Bild från aktuell satellitbild med plott över trafikflödet i Bottenviken

Figur 1.5 Figur visar detalj från radarsat - bild över Gävlebukten. Bilden visar grov sammanpackad is med vallar mot svenska kusten i södra Gävlebukten. Isen ger stor reflektion av radarekot och ger vitaktig bild, öppet vatten eller tunn nyis dålig reflektion och mörk bild.

2 Bottenviken

Sedan hundratals år tillbaka har Bottenviken alltid varit helt istäckt under någon del av issäsongen, framför allt under februari – mars. Stora områden med öppet vatten till sjöss förekommer tidvis i de centrala delarna även en normal isvinter, främst under januari.

Den första isen lägger sig i norra Bottenvikens inre skyddade vikar och hamnbassänger normalt under andra halvan av november. Isläggningen fortsätter därefter ut över skärgården i norr och närmast därutanför samt kustnära längre söderut. Isläggningen går långsamt och etappvis under december. Vanligast breder isen ut sig längst utanför finska kusten i nordöstra delen. Friska eller hårda vindar och tillfälligt mildare väder bryter dock upp isen, skingrar den eller packar den nybildade isen in mot de inre skärgårdsöarna. Den sammanpackade drivisen fryser ofta samman och bildar ett bälte med tjockare fastistäcke än den släta och ofta snötäckta skärgårdsisen innanför.

I slutet av december har Bottenviken under kalla vintrar i stort sett varit helt istäckt. Ofta bryter den än så länge relativt tunna isen upp och packas samman främst vid kusterna och den

fasta iskanten med vallbildning som följd. Isutvecklingen fortskrider och under februari förekommer allt mindre områden med öppet vatten. Dessa täcks dock snabbt med nyis.

Under mars månad når isen maximal utbredning och hela området förblir helt istäckt. Istillväxten avstannar men fortfarande under april månad förekommer isbildning i nyöppnade råkar och områden med smält snö. Så kallad stöpis (frusen blöt snö) bildas och ökar isens tjocklek, men den är inte lika bärkraftig som kärnis.

Under andra hälften av april eller början av maj bryter isen till sjöss upp i stora vidsträckta flak blandat med små flak eller krossis. Därmed tilltar islossningen och isavsmältningen. I de inre skärgårdarna börjar islossningen söderifrån i mitten av april men först mot slutet av maj är det isfritt i skärgården längst i norr. Islossningen går långsammare i den yttre skärgården. Ett mindre isfält med gamla packisvallar kan beroende på vindförhållandena bli liggande nära kusten några dagar in i juni månad.

3 Bottenhavet

Statistiskt sett har det förekommit öppet vatten i de centrala och södra delarna av Bottenhavet i 25-30 procent de senaste 50 åren. I de sydligaste inre skärgårdarna har det förekommit isvintrar med endast kortvarig tunn is men norr om Sundsvall är förekomsten av is mer än 90 procent. Även vid den finska kusten söderut till Åland är förekomsten av is under vintrarna 90-100 procent.

Isläggningen börjar i skyddade vikar i norr i mitten av december och i de sydligaste delarna normalt vid årsskiftet. I början av januari bildas den första isen i Norra Kvarken och söderut längs främst finska kusten. Isutbredningen sker sedan en normal isvinter etappvis norrifrån. Is från Norra Kvarken driver sydvart längs svenska kusten med kalla nordostliga vindar och skyndar på isläggningen. Även is utanför finska kusten driver ut till sjöss och växer till i tjocklek medan nyis snabbt bildas i nyöppnade råkar närmast kusten. Vid fortsatt kallt väder och nordostlig vind isläggs Gävlebukten i slutet av januari eller början av februari. Milda vintrar med skiftande vind- och temperaturförhållanden bildad tillfälligt is till sjöss. Isen bryts upp och packas kraftigt samman mot svenska och finska kusten i norr och bildar tillfälligt mycket svårforcerad stampis vid kusten. Den maximala isutbredningen inträffar i regel i mitten av mars.

Islossning börjar i regel söderifrån i samband med kraftiga sydvindar. Isen packas hårt samman i norr med kraftiga vallar och ispress. Men under april brukar istäcket till sjöss släppa från kusten och driva sydvart. Ganska ofta driver grov is med isbumlingar sydvart längs svenska kusten ner till i höjd med Sundsvall, där det blir liggande och sakta upplöses. I Gävlebukten är det i regel isfritt i skärgården första veckan i april och i vikar från Härnösand och norrut i mitten av april.

4 Extrema isförhållanden

Extrema eller mycket svåra isförhållanden har sedan 1950-talet inträffat 6 isvintrar, varav den svåraste över Bottniska viken 1966. De andra isvintrarna, som bedömts som mycket svåra, var 1956, 1969, 1978, 1985 och 1987. Som exempel kan nämnas de väl utforskade och kartlagda förhållandena isvintern 1986/87. I norra Bottenvikens skärgård var fastisen 80-105 cm (rekord från tidigare 122 cm), i södra Bottenviken 60-70 cm och i Bottenhavets skärgårdar allmänt 50-60 cm. Till sjöss i Bottenviken var istjockleken på den relativt jämna isen 40-75 cm (1963 lär isen varit upp till 100 cm), i Bottenhavet 30-60 cm. Nordliga och nordostliga vindar dominerade och vallförekomsten var stor i de södra delarna av Bottenviken och Bottenhavet, exempel på isvallar se Figur 4.1.

Figur 4.1 Bild som visar exempel på ett område med flera svårforcerade vallar.

De lindrigaste isvintrarna, också 6 till antalet, var 1973, 1975, 1989, 1992, 1993 och 1995. Issäsongen 1992 var den lindrigaste, jämförbar med 2008. Då var det isfritt till sjöss i Bottenhavet hela vintern, bortsett från Norra Kvarken. Där var istjockleken till sjöss max 15 cm medan det var upp till 30cm tjock is i skärgårdarna. I Bottenviken förekom under lång till ett bälte med upp till 35 cm tjock sammanpackad is vid den finska kusten norr om Brahestad, i övigt till sjöss 5-15 cm relativt jämn is. Milda sydvästvindar dominerade. Öppna råkar bildades ofta vid svenska kusten och nyis och issörja som dessemellan bildades drev över till finska kusten och fyllde på isbältet där.

5 Isdrift

Isdriften orsakas huvudsakligen av vindförhållandena och i viss mån även av ström, som främst orsakas av vattenståndsändringar, exempel kan ses i Figur 5.1. Vattenståndsändringar i Bottenviken påverkar främst strömmen i Norra Kvarken. I allmänhet är isdriften relativt svag upp 0.2- 0.5 knop vid sammanhängande eller mycket tät drivis. I samband med hård vind kan isdriften vara ca 1.0 knop eller i extremfall upp mot 1.5 knop i samband med lös sönderbruten is. I Norra Kvarken i passagen vid Nordvalen kan isdriften vara upp mot 2 knop. Strömmarna är huvudsakligen sydgående vid den svenska kusten och nordgående vid den finska. Stora variationer förekommer dock p.g.a. väderförhållandena. Kusterna och därutanför liggande isfält med grov is dämpar isdriften. Den fortsatta isdriften mot kusten medför att isen skjuts ihop och bildar vallar eller upptornad is. Ispressen kan vara kraftig.

Figur 5.1 Bild som visar hur ”spåret” från en fyr ändras pga isdriften.

6 Isvallar

Man skiljer på olika typer av vallar beroende på isens utveckling och topografi, se exempel i Figur 6.1- Figur 6.2. Inom isnomenklaturen skiljer man på hopskjuten is (engelska rafted ice), stampisvall (jammed brash barrier), packisvall (ridge) och upptorning (hummock).

Figur 6.1 Exempel på en mindre isvall. Lägg märke till sick-sackformen

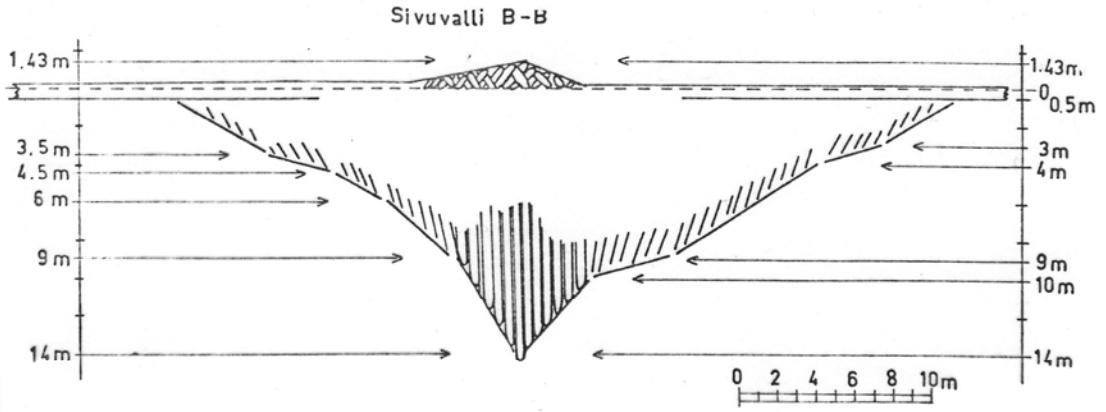

Fig. 26 . Transverse cross-section of the ridge seen in Fig. 21 The vertical position of the floes in the middle of yhe keel are caused by shearing of ice.

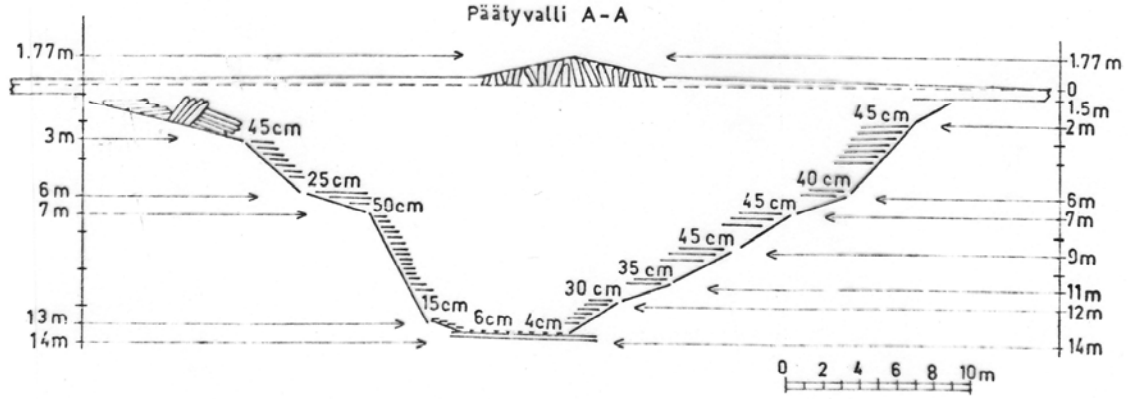

Fig. 25. Transverse cross-section of the ridges seen in fig. 21 .

Figur 6.2 Schematisk skiss på vallar och fördelningen av isflakens tjocklek, från Palosuo (1975).

Det första stadiet för bildandet av en vall är att isen glider upp över varandra. Isdriften är ganska svag och s.k. **finger hopskjutning** (finger rafting) förekommer. Istjockleken är i allmänhet mindre än 10 cm. Vågrörelsen är svag och en svag dyning kan ha startat processen. Vid ökad vind skjuter isen ihop alltmer, isen bryts upp i flak och packas hasardartat samman ett eller flera flak över ett annat i form av en mindre vall. Till sjöss brukar en mindre vall ligga i sicksack form, se Figur 6.1. Ett hinder, som t.ex en kust eller fastiskant blir vallen mer långsträckt.

Vid kraftig vind och isdrift riktad mot kusten bildas en s.k. **stampisvall**, ofta en bit in i skärgården vid fastiskanten. Ofta är det öppet vatten utanför med vågor, som pressar på mot kusten. Stampisvallen består av en ansamling vattenbemängd issörja, snösörja, krossis och små grova flak högst 1-2 m i diameter. Topografin är låg och ibland syns ett vågmönster, då vågor utifrån dämpats längre in i vallen. Stampisvallen blir oftast 500 -1000 m bred. Extremfall, där stampisen når 2-3 nm ut från kusten, förekommer främst vid den grundare finska kusten. Stampisvallen går i allmänhet 2-4m djupt men kan i yttre kustbandet vid mycket hård ispress gå ner mer än 6 m djupt. Då vinden mojnar eller ändrar riktning flyter isen isär och breder ut sig. I vissa fall ligger isen kvar och bildar snabbt ett grövre isbälte jämfört med det omgivande isfältet. Stampisvallar är ett stort hinder för sjöfarten i inloppet till en hamn. Isbrytarassistans är oftast nödvändig. I samband med islossningen och isvallen släpper från t.ex. skärgården och driver ut till sjöss kan stora metertjocka flak/isbumlingar förekomma.

Då isutvecklingen fortskrider och istjockleken överstiger 10-15 cm skjuter isen i samband med frisk eller hård vind ihop och bildar **vallar** (även kallade ”packisvallar”). Isen trycks kaotiskt ihop flera flak över var andra och kan liknas vid en ”timmerbråte”. Topografin blir mycket ojämn. Den övre delen ovan vattenytan med ibland upprättstående flak kallas ”seglet”, den undre, där isflaken staplas på varandra kallas ”kölen”. Isflaken behöver där inte vara hopfrusna med varandra utan vatten förekommer mellan delar av flaken. Det kan vara ett isfält med tunnare is med något snabbare isdrift, som trycks upp mot ett grovt isfält. Ofta varierar tjockleken i den sammanhängande eller mycket täta drivisen från 10 cm till upp mot 40-50 cm. Om vinden är hård och istrycket pågår flera timmar går vallen djupt ner, 6-10m djupt är inte ovanligt, (rekordet i Bottenviken uppmätt till 28 m). Pågår istrycket åtskilliga timmar bildas alltfler vallar längre in i isfältet eller närmast kusten. När vinden mojnar eller vrider till annan riktning avtar istrycket i den undre delen och flak försöker flyta upp mot ytan. Därmed breddas vallen i horisontellt. Vid islossningen eller då isfältet bryter upp från vidsträckta till små flak förekommer under lång tid för issmältningen stora grova flak av gamla vallar, s.k. ”**isbumlingar**”. Storleken på isbumlingar är i regel mindre än 10 m i diameter men upp mot 1m grova.

En annan typ av vallbildning, som är mycket svårartad är **isskjuvning**. I gränsen mellan isfält med olika hastighet på isdriften men också tjocklek skapas en skjuvning eller ett vridmoment på fasta konstruktioner. Isskjuvning uppstår oftast vid kusten eller vid fastiskanten med drivisen därutanför.

Vallbildning över grynnor och grund bildar **upptorningar**, se exempel i Figur 6.3**.** Vallen går helt enkelt på grund. Isflaken tornar upp sig i stora högar och liknar nästan isberg. I ett grundområde typ Norströmsgrund med 3-8 m grundklackar bildas flera upptorningar eller ishögar med ett kraterliknande område i mitten. Upptorningen ligger kvar under isvintern och utgör främst ett problem i samband med islossningen, då grova isbumlingar lossnar från grunden och flyter ut.

Figur 6.3 Bild som visar exempel på upptorning.

7 Kustområden som är utsatta för ispress

Svenska kusten i Bottenviken är främst utsatt för ispress och isskruvning vid nordostlig vind, se exempel i Figur 7.1.

Då isen driver sydvästvart hakar isflaken fast vid de yttre öarna och över grundområden strax utanför fastiskanten. Skillnader i isdriftens hastighet medför vallbildning. Typiska områden är grunden kring *Marakallen* och *Norströmsgrund* utanför Luleå samt *Klockgrund* och *Nygrån* utanför Piteå

Figur 7.1 Exempel på resultatet av ispress.

Skelleftebukten är speciellt utsatt vid långvarig nordostlig vind. Flertal kraftiga vallar bildas långt in i bukten. Högar med upptornad is har förekommit vid buktens södra stränder. Längre sydvart utanför Holmöarna är den nordöstra stranden (*Stora Fjäderägg*) mycket utsatt. Ett bälte 500 – 1000 meter brett med täta vallar bildas ofta och därutanför samt vidare längs östra sidan av ön bildas ofta en glidkant p.g.a. stark ström. Istillväxt och snöfall är en vanlig kombination.

Vid kraftig sydlig eller sydvästlig vind pressas isen norrut och vallbildning sker i området kring *Malören, Björnklack/Farstugrunden* samt *Norströmsgrund/Marakallen*. På *Simpgrund* långt utanför Piteå bildas ofta en upptorning/ishög. Däremot släpper isen från kusten en bit ut i Skelleftebukten. Det bildas en råk, som sedan vidgas om sydvinden består. Temperaturen i samband med sydvinden är åtminstone under mars – april förhållandevis mild med ibland plusgrader. Isflakens kanter blir relativt ”våta” och därmed förbättras möjligheten för isflaken att klättrar på varandra. (Interna friktionen minskar). Senare under islossningperioden krossas isflakens kanter mot varandra och issörja bildas mellan flaken.

Även vid finska kusten utanför Kemi och Uleåborg bildas kraftiga vallar som staplas till varandra och ett mycket brett område med talrika vallar bildas. Upptornad is bildas på grunden *Artunmatala* och *Merikallat*. Vid *Nahkiainen, Ulkokalla* och *Tankar* längre söderut förekommer kraftig vallbildning främst vid västlig och nordvästlig vind.

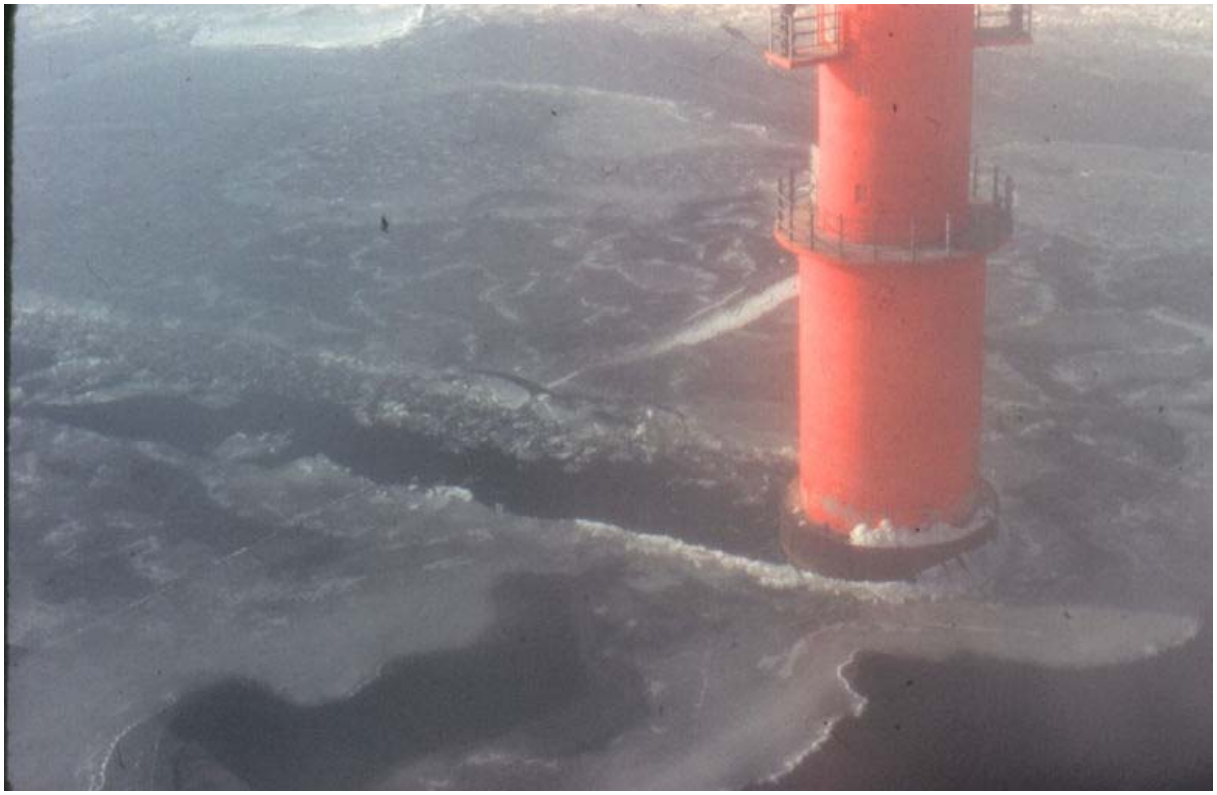

Figur 7.2 Fyr som utsätts förisdrift och lätt ispress.

I norra Bottenhavet är den svenska kusten utsatt för ispress och isskjuvning under isläggningsperioden. Grov is från södra Bottenviken och Norra Kvarken driver sydvästvart längs kusten samtidigt som ny is bildas p.g.a. kyla. Sammanfrusen drivis hakar i utskjutande uddar typ Husumbukten och i ett senare skede även i Sundsvallsbukten. Under en svår isvinter förekommer ofta en besvärande glidkant med isskruvning vid fastiskanten. Den svåraste ispressen och vallbildningen förekommer i samband med sydliga eller sydostliga vindar under februari och mars. Om större delen av Bottenhavet varit istäckt och sydliga vindar tränger in bryter isen upp, driver norrut och packas samman den vid norra kusten. Inloppen till Umeå och Örnsköldsvik drabbas främst. Norra Kvarken utgör en spärr. Ispressen brukar bestå även om vinden vrider mot sydväst och den kraftiga ispressen riktas mot den finska kusten utanför Vasa. Först vid nordlig eller nordvästlig vind släpper ispressen och isen driver ut till sjöss och glesnar.

I södra Bottenhavet är det oftast stampisvallar närmast kusten som dominerar. Kalla ostliga eller nordostliga vindar med snöfall skapar dessa till en början smala bälten med ispress. Med fortsatt kyla och isläggning ute till sjöss fryser även stampisvallarna ihop och blir grova och svårforcerade. En svår isvinter med återkommande kalla nordliga eller nordostliga vindar skapar hopskjuten is och vallar, som fastnar på grundklackarna över Västra Banken och Finngrunden. Gävlebuktens södra kust ut till Öregrundsgrepen och Grundkallen drabbas också. Ispressen kan vara mycket kraftig i samband med kuling och storm, då vind och vågor har en lång fetch/stryklängd över hela Bottenhavet.

Då milda sydliga vindar tränger in öppnas mindre råkar en bit ut från kusten. Grundstötta vallar och upptorningar bromsar till en början uppbrytningen av isen men efterhand öppnas en mer sammanhängande råk. Grundstötta vallar blir ofta kvar och efterhand lossnar enstaka flak/isbumlingar i samband med att vattenståndet stiger och driver sedan ut och smälter.

Finska kusten i södra och mellersta Bottenhavet är inte lika hårt drabbat av kraftig ispress. Under milda vintrar med ofta förekommande milda sydväst- eller västliga vindar bildas ett

bälte med sammanpackad drivis utanför kusten. Vallarna är ofta frekventa men inte särskilt kraftiga. Det förekommer dock isvintrar då en kraftig nordvästlig vind packat samman is i den sydöstra delen mellan Åland och finska fastlandet. Vallar bildas då utanför fastiskanten vid Skärgårdshavet. Under islossningsperioden öppnas ofta först en råk längs kusten i södra delen och i ett senare läge kan ett isbälte med sönderbruten drivis bli liggande en tid utmed kusten innan isen upplöses.

8 Istjockleksstatistik jämn is

Vallar ökar medelistjockleken i norra Bottenhavet med 20-40 cm främst under mars månad. I södra Bottenhavet är det främst i Gävlebukten och nordost om Åland som det statistiskt sett sker en ökning av istjockleken med 10-20 cm. I Tabell 8.1 presenteras istjockleksstatistik för jämn is.

Tabell 8.1 Istjockleksstatistik för jämn is.

	Normal (cm)	Max (cm)
Norra Bottenviken skärgård	50-80	100
till sjöss	40-60	70-80
Södra Bottenviken skärgård	50-70	60-80
till sjöss	30-50	40-60
Norra Bottenhavet skärgård	40-50	50-70
till sjöss	30-50	40-60
Södra Bottenhavet skärgård	30-40	40-60
till sjöss	20-30	30-50

9 Barents hav

I Barents hav är det normalt öppet vatten till havs söder om latituden 75 grader N och österut till ungefär 40 grader E. Längst in i skyddade delar av de norska fjordarna kan det tillfälligt förekomma tunn is (10-15 cm), som dock inte ställer till problem för sjöfarten. I Varangerfjorden förekommer längst in i fjorden tunn is kalla vintrar. I inloppet till Kirkenes hamn kan det vid i samband med islossningen i älven driva ut en del isflak under april. I området kring Murmansk kan det vissa vintrar driva till en del spridd drivis österifrån men Golfströmmen hindrar fortsatt isdrift västerut.

Det är tack vare den varma Golfströmmen som löper österut via Nordkap som håller Norska kusten isfri. Ytvattentemperaturen utanför Varangerfjorden håller i regel under vintermånaderna 2-4 plusgrader, i de inre fjordarna ner mot noll.

Vita havet är däremot drabbat av is varje år och under vissa år mycket besvärliga isförhållanden med grov is och ispress med vallbildning. I Figur 9.1 visar kartan maximala isutbredningen normalt under februari-mars.

Figur 9.1 Kartan nedan visar maximala isutbredningen normalt under februari-mars. Från Meteorological Office Bracknell.

10 Referenser

Palosuo, E. (1975). Formation and structure of ice ridges in the Baltic, Winter Navigation Research Board, Rep. No. 12, Board of Navigation, Helsinki.

Sammanfattning av Isvintern och Isbrytarnas Verksamhet. Årliga publikationer från 1972 till 2007. SMHI i samarbete med Sjöfartsverket.

Climatological Ice Atlas for the Baltic Sea, Kattegat, Skagerrak and Lake Vänern (1963-1979). SMHI och Havsforskningsinstitutet i Helsinki Finland. ISBN 91-86502-00-X.

Meteorological Office Bracknell, Berkshire. Monthly Ice Charts, Sea Ice Normals.Not published after 1984.

Bilder ur SMHI diabild arkiv. (Istjänsten)

Ice Control Measures in Swedish Harbours

Johannes Hüffmeier

Ice Control Measures in Swedish Harbours

SSPA Sweden AB
30 April 2008

REPORT

Subject	Report
Ice situation and ice control measures in the Gulf of Bothnia and the Bothnia Bay	2007 4693-1
	Project manager Johannes Hüffmeier
Customer/Contact Lennart Fransson Luleå Technical University	Author Johannes Hüffmeier Jim Sandkvist
Order By mail	Date 2008-04-30

The purpose of the work was to get an overview of the present ice situation in the northern Swedish harbours and to get to know the thermal and mechanical ice control measures in the harbours. Interviews with mainly harbour masters and managers have been made; personally, by phone and by email. Often even the local ice experts had been asked about the situation.

Jim Sandkvist
Vice President

Johannes Hüffmeier
Project Manager

SSPA Sweden AB

POSTADRESS *POSTAL ADDRESS*	BESÖKSADRESS *STREET ADDRESS*	TELEFON *TELEPHONE*	TELEFAX *TELEFAX*	E-MAIL *E-MAIL*	ORG NR *REG NO.*	BANKKONTO *BANK ACCOUNT*	BANKGIRO *BANK GIRO*
BOX 24001 SE-400 22 GÖTEBORG SWEDEN	CHALMERS TVÄRGATA 10 GÖTEBORG SWEDEN	NAT 031 - 7729000 INT +46 - 31 7729000	NAT 031 - 7729124 INT +46 - 31 7729124	postmaster@sspa.se	556224-1918	SE-BANKEN 5027-1002190	152-4875

TABLE OF CONTENTS

SUMMARY

Scandinavian ports, especially the ports in the northern Baltic Sea, face a regular challenge every year – ice. In an INTERREG-project led by the Luleå University of Technology, SSPA Sweden AB conducted a study to gain insight in the problems related to winter traffic in Swedish ports. This research is intended to lead to an identification of technical solutions that could ease winter navigation in the ports.

The state icebreakers made navigation possible all around the year since the seventies by assisting ships sailing in ice-covered sea. In Sweden, the local port owner is responsible to break channels and assist arriving and departing vessels.

All port owners along the east coast of Sweden have been interviewed to get an overview of the local ice conditions and their impact on the traffic. Specific emphasis was put on the collection and analysis of different ice-reducing measures currently used in the ports. These include mechanical (e.g., ice breaking) and thermal (e.g., waste water discharge) measures. The distribution and range of applications and most important the experiences with the different measures have been described and summarised.

The efficiency of the different measures has been investigated and compared to predictions of theoretical calculations. In the analyses of the ice-reducing measures, the effects of different measures have been studied, a cost-benefit assessment for different ice-reducing measures has been included and the environmental impact studied. Most of the ports base their ice management only on an icebreaking tug boat even though other measures could play a decisive roll in the ice handling.

High pressure on quay structures occurs because of the berthing of ships in ice-covered ports. This pressure represents a regular source of damages. Manoeuvring and backing in ice can further lead to damages of the propeller and rudder of the ice-going vessels. Even other problems like icing on ships and equipment was looked at.

The costs for repairing and other extra costs due to winter navigation for the port and – indirectly – the ship owners can be seen as a commercial disadvantage. Therefore, an identification of costs caused by the winter conditions was an important part of our analysis.

The results of the research have been compared with a similar study performed in Finland and a further literature study was conducted to recommend efficient improvements for the port owners.

1 INTRODUCTION

Many ports on the east cost of Sweden, especially in the north, experience ice on a yearly basis. To avoid a drawback for industries, to keep the European transport system functioning and to avoid geographical disadvantages, year-around navigation has to be possible in all harbours. Since 1970 all Swedish harbours are open through the winter, which has been guaranteed by the Swedish government and its state-owned icebreakers. Even in the harbours efficient ice control measures have had to be implemented in order to enable year-round maritime traffic. This paper presents a compilation of the normal ice conditions and the typical ice control measures. Also problems that occur are mentioned, together with the solutions used to overcome them.

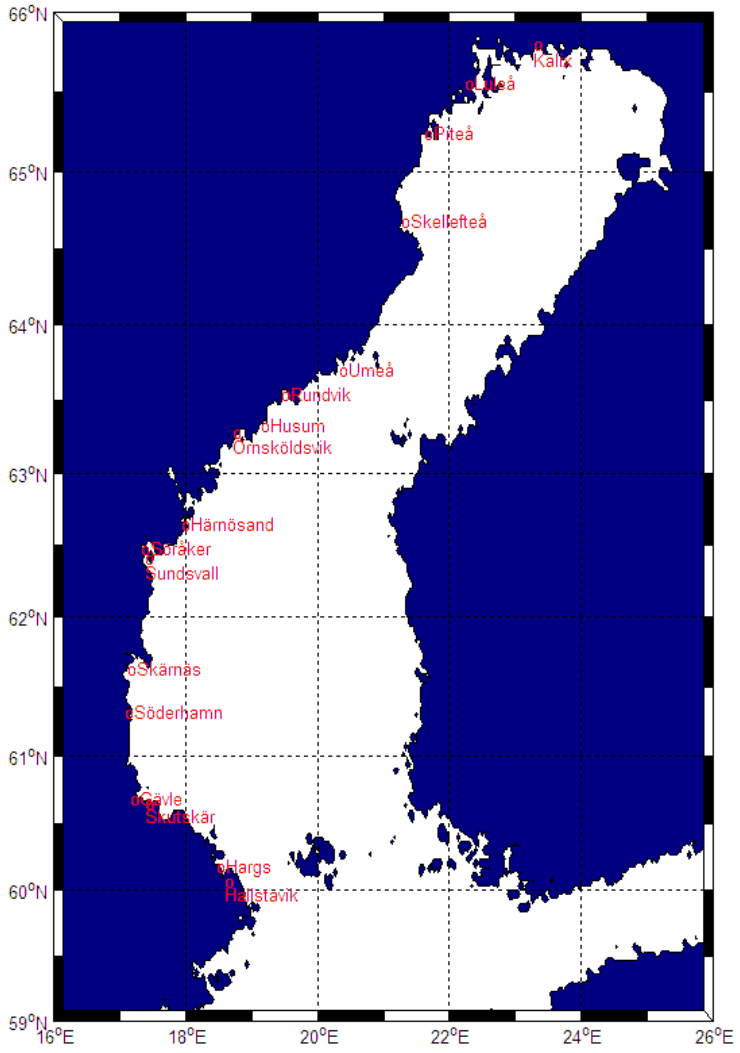

Almost all Swedish ports north of Stockholm have been interviewed to get an overview of the state-of-the-art in ice management in the harbours. The different ice-handling methods have been collected, analysed and compared.

The analysis included a closer look at the techniques and the cost-benefit. Even the increased assistance time and the delay for the ship owners have been looked at.

2 THE HARBOURS

The following harbours have been contacted during the study (in descending order with descending latitude): Kalix, Luleå, Piteå, Skellefteå, Umeå, Rundviks, Husum, Örnsköldviks, Härnösands, Söråkers, Sundsvall, Skärnäs, Söderhamns, Skutskärs, Gävle, Hargshamn, Hallstavik.

The harbours can be categorised into the way there are situated. Some ports are situated at rivers or in river mouths which results in a steady stream of water in the harbour basin. Others are situated more or less on archipelagos or islands and are thus not affected by steady streams caused by rivers, but can be more affected by currents or drifting ice. Another port layout is the closed harbour basin with no streams and currents and hardly affected at all by drift ice due to its protection. The last one is an unprotected harbour and open to the sea, with only a small number of outlying islands. The layout can hold relevance for the suitability of ice handling methods and the steady streams for instance can be seen as a natural ice handling method. The harbours on the Swedish east coast are characterised by a low water depth. The maximum water depth at the quays is on the average only about 10 meters at all surveyed harbours.

In most of the ports the traffic volume decreases slightly or not at all during winter time. This is often due to the fact that the same ships are calling at the port year around and meet the requirements of the common local ice restrictions. In some ports the amount is significantly reduced by about one-third. Those harbours are mainly situated in the middle of Sweden. Table 1 shows the traffic for selected months calling at Piteå harbour.

Table 1: Traffic volume in the port of Piteå 2006

Month	**No. of Ships**
January	37
February	25
March	29
April	23
May	33
July	40
Average	**30**

Traffic density is an important factor concerning icebreaking. Regular port calls reduce the amount of ice breaking required, because the ice channel stays unfrozen between the ship movements.

3 ICE CONDITIONS

3.1 Ice conditions in the Baltic Sea

Due to its isolated character, the Baltic Sea has a low salinity which varies from 0% to 2%. The water with the lowest salinity is found in the northern part of the Bay of Bothnia and close to the mouth of the Neva River in the Gulf of Finland. The low salinity is based on a low exchange of water to the Northern Sea (water changed once in 25 years (Liukkonen, 2006) and on the discharge of several rivers into the Baltic Sea. The Baltic Sea is very shallow with an average depth of 55 m and a maximum depth of 459 m. These factors influence the ice characteristics, like consistency, porosity, growth, structure and mechanics. Snow can constitute up to 50% of the total ice thickness and 35% of the sea ice mass can be composed of metamorphic snow (Granskog et. al., 2006).

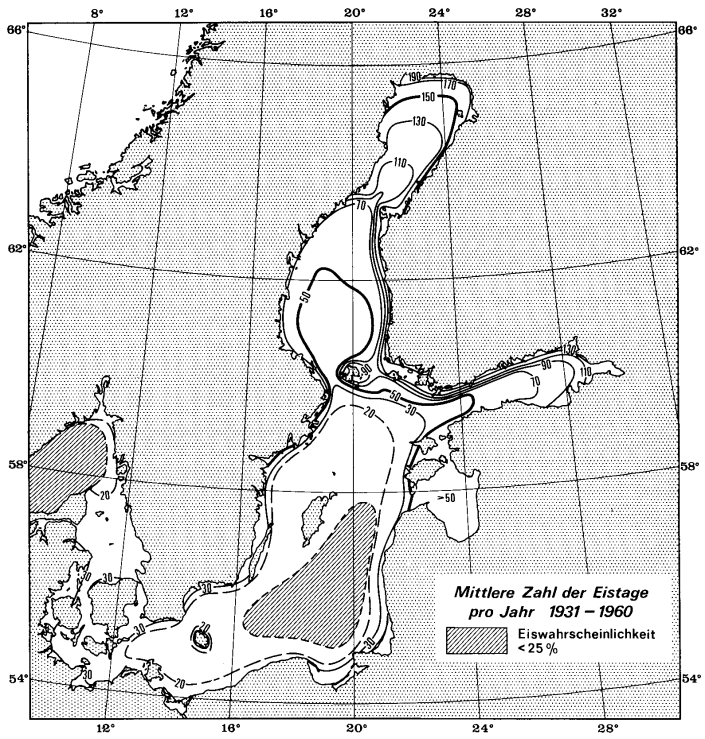

Figure 1: Average days with ice per year (Dietrich and Schott, 1974)

The Baltic Sea extends about 390.000 m^2 and has a long open-water season in most locations. The sub-arctic location of the Bay of Bothnia gives its northern part an average number of 190 days with ice, while in the southern Baltic Sea the occurrence of sea ice is more unlikely. In an average winter, ice growth starts in the Bay of Bothnia in the end of November while further south in the Gulf of Bothnia the growth starts in the beginning of January. This shows that the ice grows southwards in the Bay and Gulf of Bothnia, while it grows westwards in the Gulf of Finland. The ice in the Baltic reaches its maximum extent usually at the end of February or in the beginning of March. In the middle of May even the northern-most part of the Bay of Bothnia is free of ice.

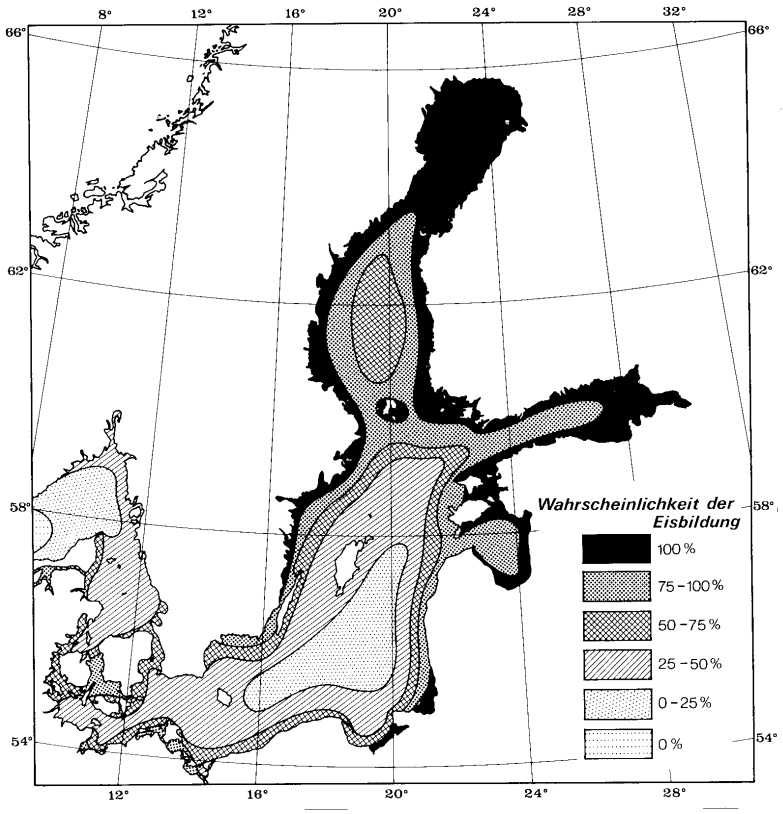

Figure 2: Probability of ice occurrence (Dietrich and Schott, 1974).

The variations from one winter to another are tremendous and it is important to describe the variation of the severity of a winter in the Baltic. The Swedish Maritime Association (Sjöfartsverket, 2008) defines the border between a mild and a normal winter at 98 000 km^2 and the one between normal and severe at 193 000 km^2, which can be seen in Figure 3.

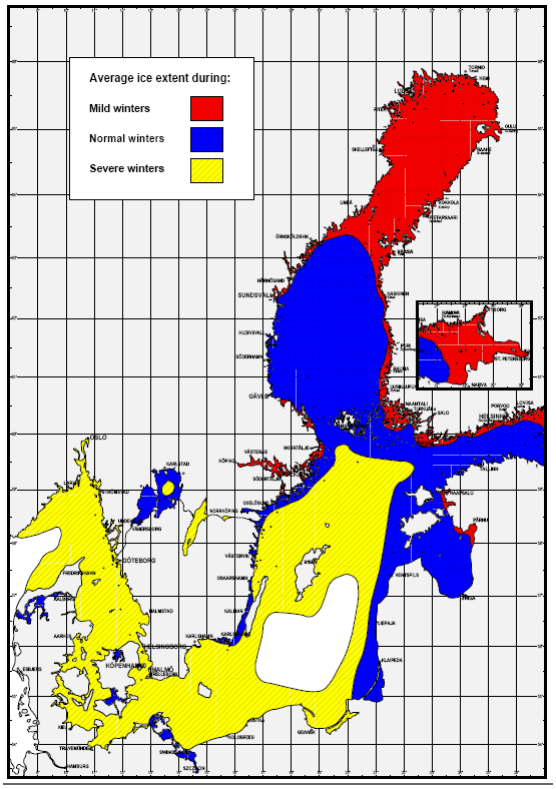

Figure 3: Average ice extent during mild, normal and severe winters (Source: SMHI, 2008)

The variations depend on the weather conditions. Important parameters are the mean temperature and the variation in temperature, wind velocity, direction and their variation. It is important to notice that these parameters do not only influence the ice conditions for the whole Baltic Sea, even in a particular region they can make a difference. The ice conditions can be severe at one location whilst the situation everywhere else is not extraordinary.

The worst ice conditions in the Baltic Sea occur in the northern part of the Bay of Bothnia and in the eastern part of the Gulf of Finland. The fact that there is almost no tide influences the ice coverage across the Baltic Sea. As described above all the ice in the Baltic Sea is first-year ice. The low salinity makes the ice stronger and more difficult to break than ice with high salinity.

The maximum ice thickness of level ice which has been measured is more than 1.2 m in the north, while on average the ice thickness exceeds rarely 40 cm (Kalliosaari and Seinä, 1987). Broken ice in channels can freeze again and build brash ice. Brash ice thicknesses up to 6-7 meters have been measured (Sandkvist, 1986).

High ice pressure against coasts, landfast ice or slower drifting ice, can cause the creation of ice ridges. Ice floes pile up and the ridges can become several meters thick, mainly under water and are an obstacle to the ice-going ships. Also the ice

pressure itself can prove dangerous to a ship stuck in the compressive ice field and is a potential source of damage.

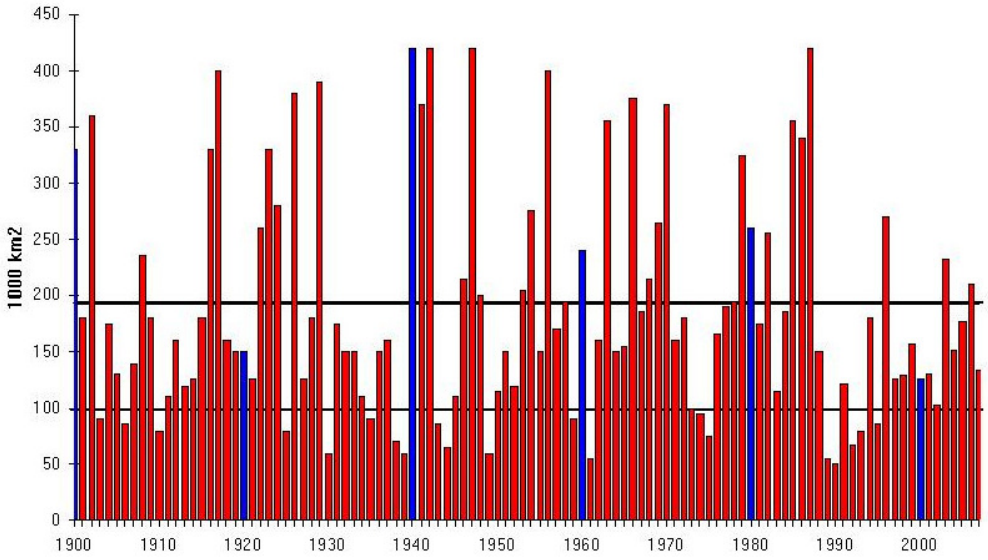

Figure 4: Ice spread in the Baltic Sea 1900-2007, in 1000 km^2 (Sjöfartsverket, 2008 c)

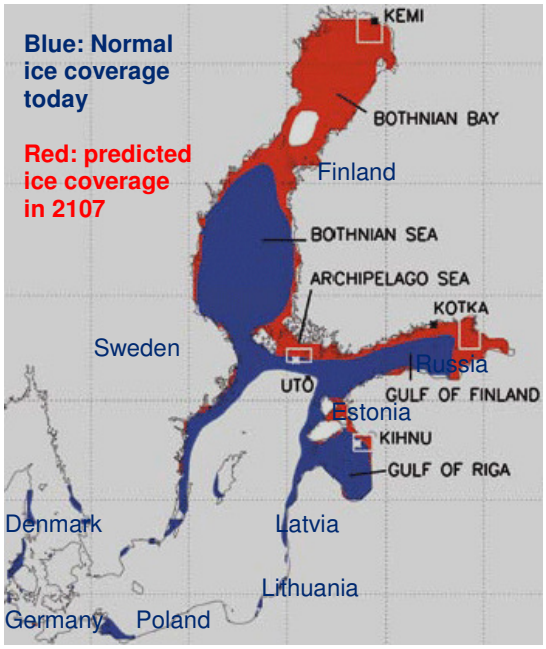

Figure 5: 100 years perspective of the ice occurrence in the Baltic Sea (SMHI, 2006)

Due to global climate change, the Swedish Meteorological and Hydrological Institute (SMHI) predicts a different ice situation for the future with a lower ice

probability. The estimated average ice coverage in 100 years time is shown in Figure 5.

3.2 Ice conditions in the Swedish harbours

The ice-cover starts in the harbours even a bit earlier than in the open sea, due to the shallower water and the protection afforded by the archipelagos. In the north of Sweden the harbours experience ice even in mild winters, while the harbours in the Bay of Bothnia can expect ice in normal winters. In extreme winters, like the winter of 1987, even harbours on the Swedish west cost can experience ice. The ports in the northern part of the Bay of Bothnia are ice bound for approximately six months in a normal winter, while further south in the Gulf of Bothnia ports experience an ice-bound period of about three months.

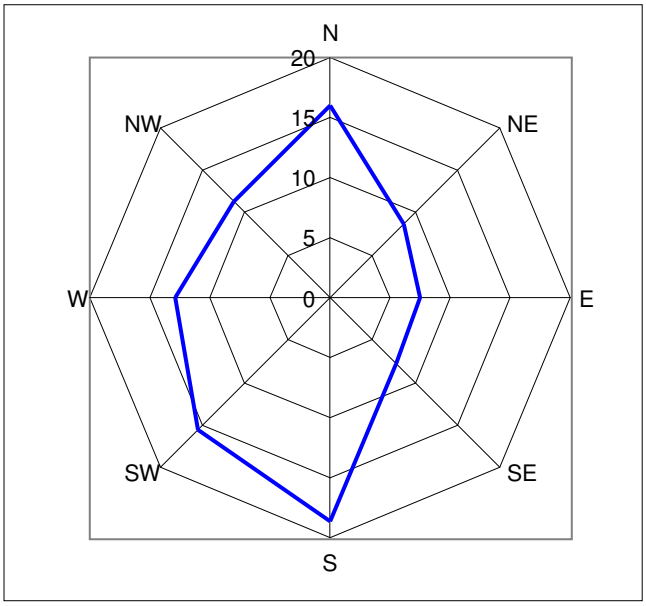

Figure 6: Frequency of wind direction [%] along the Swedish east coast. The mean is taken over 6 different stations between "Rödkallen" and "Svenska Högarna" (Calculated with source data from Alexandersson 2006)

It may be generally said that the ice conditions in the harbours are most of the time reflected well in the ice charts published by SMHI. The situation might be even better for shipping, because the ice surrounding the quays is landfast and static due to the protecting archipelagos. In ports situated in river mouths the streams from rivers drive the ice out of the harbour in spring time.

Even though winds, especially storms with wind from the east, can worsen the situation for many harbours and their access ice channels (exception: for Kalix southerly winds are the worst). Statistics, which are presented in Figure 6, show

that the west winds dominate along the Swedish east coast. The wind forces the ice then to drift towards the Finnish coast, which eases the situation for the Swedish harbours. Strong winds, which occur regularly in winter time (Figure 7), lead to ice cracks at certain positions, ridges then occur and ice pressure makes it difficult to keep the navigational channels free from ice.

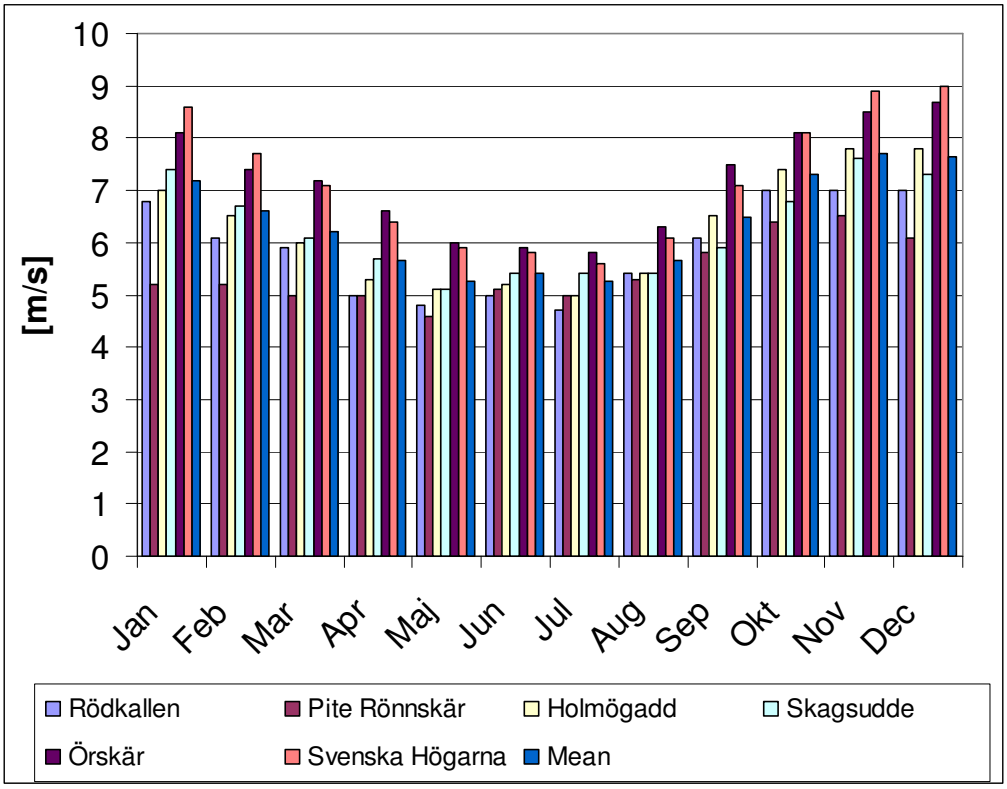

Figure 7: Average wind velocity [m/s] for selected stations along the Swedish east coast, divided by months. Source data taken: Alexandersson 2006.

The length of the winter season was put by the interview partners at the average to 4 months, a bit longer in the north, a bit shorter in the south. It is important to note that for many port authorities the ice season only starts when a lot of icebreaking is required. In the north a thin layer of ice does not therefore signal the beginning of the winter season. The ice season starts usually in the beginning/ middle of December and ends by the middle/ end of April. The worst ice situation is experienced most of the time in the end of February/ beginning-middle of March which corresponds to the end of ice growth.

Even though it is difficult to put a number on it, because of the significant variations in ice thickness from year to year, the average ice thickness was estimated to be about 30-50 cm in the northern harbours down to 20-30 cm in the southern ports. Local variations can be sizeable as well with a low ice thickness at some quays compared to the ice thickness out at the ice channel. Important to note

is that in most of the interviews it was mentioned that the most recent winters have been mild and the length of the ice season was shortened and the maximum and average ice thickness reduced compared to the long term experience. Half of the port managers and tugboat captains based that on global climate change, while the other half said that that can be based on variations from year to year as well.

4 ORGANISATION OF THE ICEBREAKING SERVICES IN THE SWEDISH WATERS

In the Swedish waters ice breaking is organised by the Swedish Maritime Administration (Sjöfartsverket) in cooperation with the Finnish Maritime Administration (Merenkulkulaitos). The ice-breaking management unit in Gothenburg issues restrictions, monitors operating conditions, informs shipping stakeholders about ice traffic conditions and allocates icebreakers to work areas, even though the commanders of icebreakers work relatively independently in their fields (Sjöfartsverket 2008 a).

Winter navigation has been regulated for several decades by the Finnish and the Swedish Maritime Administration. These restrictions have been adopted in 2004 by HELCOM. The restrictions are intended to avoid delays to vessels and to keep shipping running. Depending on the severity of the regional ice conditions the state-owned ice breakers of Sweden and Finland only support ships which meet the requirements for the region. The requirements have been established with respect to the ice classification, i.e. hull strength and the power to mass ratio.

All vessels passing particular waypoints and boundaries to ice-covered waters need to have a certain ice classification specified by the authorities according to the ice conditions. The ships are registered in the icebreaker's computer system and can be observed, guided and in difficult ice situations even instructed. In connection with the weather forecast and the ice charts icebreaking and convoys are planned. For a convoy several ships are collected at waiting positions and they are assisted by the icebreakers.

While in the Finnish winter harbours the state ice breakers force the route all the way to the quays in the ports, in Sweden the harbour authorities themselves are responsible for providing ice free fairways from the closest navigational channel to the quay, i.e. in the archipelago-protected waters. If it is really necessary the state icebreakers even break the whole way in. In the Swedish harbours the authorities' own or hired tugboats are used for icebreaking purposes. The port authority knows in advance when a ship is expected in the harbour, not least due to the good teamwork between ship's agent, ship owner, icebreaker service and stevedore. The icebreaking tug is then instructed to break the channel anew, if necessary. a lot of icebreaking has to be done, especially close to the quay and in addition often a turning area has to be broken free.

4.1 Ice restrictions for vessels in the Baltic Sea

The navigation in the winter is restricted for several decades by the Finnish and the Swedish Maritime Administration. These restrictions have been adopted in 2004 by HELCOM. The restrictions are meant to avoid delays of vessels and to keep the ship traffic running. Depending on the severity of the regional ice conditions the Governmental ice breakers of Sweden and Finland support just ships which meet the requirements for the region. The requirements are with respect to the ice classification, i.e. hull strength and power relative to the size.

4.2 Costs for the harbour in winter time

The harbours try to cover the costs for the icebreaking costs by increased port dues, which are often doubled for the time when there is a reasonable risk for ice in the harbour (common: 1. December – 30. April). In some of the ports the increase is only 50-60 %, while in two ports, which are industrial ports, no extra costs are taken from the calling ships. This is due to the fact, that most of the ships are chartered by the same company, owning the port.

It proved often difficult to get an exact picture of the costs incurred by the harbour due to icebreaking and winter navigation. The investment costs in stronger quay constructions, ice-strengthened tugboats or non temperature-sensitive cranes are difficult to estimate. Where ice-reducing techniques were installed, they had been often there for such a long time period that it was difficult to get records about the initial costs. Even the running costs for the increased amount of bunkers for the icebreaking tugs were seldom recorded. The easiest extra cost to get a grip on was the price for the tugboats chartered from tugboat companies. The contracts are often long term (5-10 years) and are sometimes fixed expenses, but more often consisting of a fixed price plus wages per hour for the ice breaking. In some harbours even the operating costs and costs for maintenance for the surface flow generators are part of the contract with the tugboat company.

Still one can say that the additional income due to increased port dues seldom cover the expenses for icebreaking. Often this requisite cover depends on the severity of the winter. In mild winters with a reduced number of hours the icebreaking tug has to serve will make that the port has no financial loss due to the ice.

The maritime shipping of goods year-round in the Baltic Sea is a fundamental prerequisite for a functioning industry. The companies avoid expensive stock-keeping, which would cost a lot more than the extra expenses due to winter navigation. Supply of goods for many regions is based on the maritime shipping and exports are made from the Baltic harbours to the whole world. A

benefit for the ports is that they are to some extent able to compete with ports which are ice-free.

The costs for the icebreaking and winter navigation for the ports depends on the size of the harbour, the location of the harbour, the traffic volume, the length of the fairway which has to be kept ice-free, etc.

In Finland the costs for icebreaking for the port owner are estimated to be between 0.2…0.3 million USD in an average winter, mainly for the harbour icebreaker and sanding and snow clearance. Total costs in Finland are estimated to be 4 million USD in an average winter up to 8 million USD in a severe winter (Laasonen 2000).

5 ICE CONTROL MEASURES/ ICE CONTROL TECHNIQUES

"By definition, the ice control techniques are methods for reducing the growth of ice in navigational areas and on structures in navigational channels and in harbours, and methods for breaking ice and keeping the broken ice away from navigational channels." (Tsinker, 1995).
The methods might be classified into mechanical, thermal, chemical and natural. Solutions consist of ice suppression, ice breaking, ice diversion and ice removal/ disposal. In the following only the control measures which are currently used in Sweden are described and analysed.

5.1 Choice of ice-handling methods

The ice-handling methods should be installed according to the operational point of view and the method should mitigate the interference with harbour and vessel operations (Tsinker, 1995). The tolerable interference of the ice depends on the requirements of the vessels. For loading and unloading Roll-on-Roll-off ships (RoRo) need to berth directly on the RoRo quay while general cargo ships often do not need to go all the way to the quay, because the cranes are able to bridge a gap due to ice jammed between vessel and quay. The choice of ice-handling methods can be categorised according to the following aspects:

- Effectiveness
- Environmental impact
- Reliability
- Investment requirements
- Construction and testing
- Cost effectiveness

5.2 Mechanical ice control methods

5.2.1 Icebreaking with harbour tugboats

The most common method to break the ice in Swedish harbours is by harbour tugs. Every harbour has access to an icebreaking tugboat. A typical tugboat has the following dimensions:
L = 27 m, B = 7.8 m, D = 4 m, P = 1 550 kW, 38 years old
The boats are characterised by a higher power performance compared to their non-reinforced colleagues that do not perform icebreaking duties

The state-owned icebreakers service the shipping traffic to the border to the open sea – protected water. The distances, the harbour tugboats need to keep free from ice vary from harbour to harbour. The shortest distance is only one nautical mile (Husum hamn), while the longest is almost 20 nm (Hallstavik). On average an ice channel has to be broken along a length of 8.5 nm. These long distances can only be broken by tugs; no other ice control technique would be as effective or more economical. In most of the ports the ice channel can be broken by the tugboat with one turn, this means sailing in and out once. Usually attempts are made to keep the navigational channels and traffic areas open with the icebreaking tug while the rest of the ice-cover should stay as intact as possible.

Figure 8: Winter navigation in the port of Luleå

The extra time it takes to take a vessel into the harbour depends on the ice situation and the power of the vessel. While in general the loss can be negligible

in normal winters, the severe winters can increase the time significantly. Time losses occur usually not in the ice channel but at the berthing place or quay, where ice floes collect between the structures and the vessel. High pressure and loads occur and are a source of damage to vessel and structure. Almost every party interviewed mentioned that the most difficult part of the icebreaking and ice removal happens to be close to the quay. This is also the case where other ice control measures can be included in the ice management.

Figure 9: Icebreaking tugboats in Luleå

The tugboats do not only have to keep the ice channel free of ice before arrival and before departure of a vessel. A turning place has to be broken as well and as much ice as possible has to be broken and flushed away from the berthing places or quays. This is often the most intensive part of the icebreaking. They are most of the time on stand by position close to the vessel, to be able to quickly provide assistance.

During the berthing of a vessel it is common that the tugboat flushes away ice floes which have collected between quay and vessel to facilitate manoeuvring.

The ice channel can freeze if no regular traffic transits and icebreaking takes place. When the crushed ice in the channel freezes again, it can be more difficult to break the ice in the old channel compared to breaking a new channel; therefore sometimes several channels have to be broken. In almost all harbours it is sufficient to break just one ice channel, sometimes only parts like the turning position have to be moved. In converging conditions i.e. onshore wind, navigation becomes more difficult in the brash ice fields present in the ice channels.

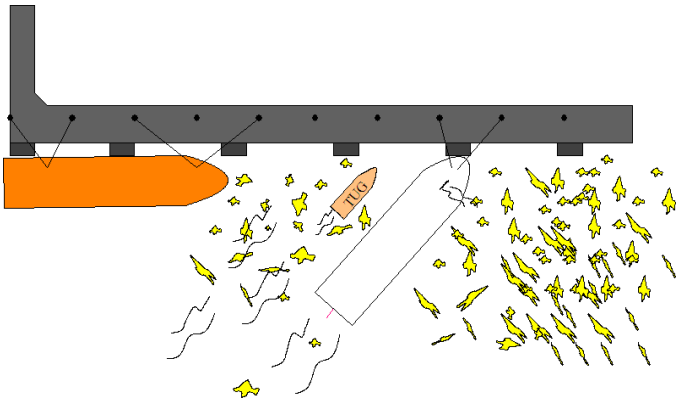

Figure 10: Tug flushing away ice

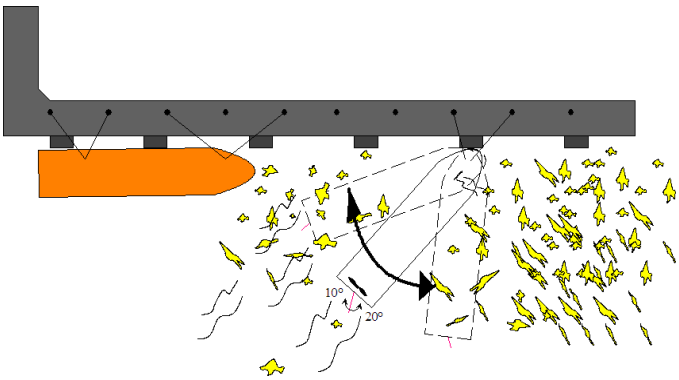

Figure 11: Clearing ice between vessel and quay while berthing

There were three main rough categories of problems mentioned concerning tugboat operations:

a) **Age**. On t average the tugboats used for icebreaking was almost 40 years old. The most recently built tugboat is "Viscaria" from Luleå Bogserbåt AB (launched 2000). It is difficult to find used tugboats which fulfill the necessary icebreaking requirements and new tugboats are too expensive for the ports with a purchase price of about 120-130 MSEK for a medium sized tug.
b) **Recruitment**. Timber towing formerly common along the whole coast is dying out. This implies that there are fewer personnel available with the training and experience necessary to man the tugboats. At the same time on the expectations of the crews are often higher than maybe necessary.
c) **Power**. While the fleet calling at the harbours has grown in size, the tugboat fleet has not been changed significantly and followed the growth which leads to partly underpowered tugs.

There is good cooperation with the state-owned icebreakers, which happen to break ridges that blockade harbour entrances. At the same time the tugboats break sometimes longer out than required if the state-owned icebreakers are busy.

5.2.2 Removing of ice by cranes

Cranes at the quay are very rarely used to lift away larger ice floes which have been collected close to docks or berthing places. They can lift up ice floes with weights around 18 tonnes.

5.2.3 Manual ice removal

During berthing ice floes in some ports are removed manually. Long sticks are used for this purpose.

5.3 Thermal ice control methods

5.3.1 Air bubbler system

An air bubbler system in a port can retard ice formation. They are mainly used for keeping dock and quay structures free from ice by suppressing ice growth by warming lower water levels. This water is brought to the surface forced by means of a bubble plume. The turbulence in the water and the heat energy then suppresses the formation of ice cover. The system consists of perforated pipes which are installed on the sea bed and connected to an air compressor. The compressor pressure used for the system needs to overcome the hydrostatic pressure and the frictional losses and is therefore dependant on the water depth of the bubbler outlet. For a successful installation the water at the bottom should be as warm as possible. The problem in many Swedish harbours is that they are so shallow, that the water temperature at the bottom is never as high as 4°C and hardly more than 0.1° or 0.2° over the freezing point. This makes the application of air bubbler systems very inefficient, difficult and expensive. In a Finnish study (Laasonen, 2000) it is described that an air volume of 10 l/s can be used for melting ice, 20-100 l/s can move aside broken ice. Further on it is stated that the airlines are sensitive to damage.

In one of the Swedish harbours an air bubbler system is used with a 5kW compressor. The system has been used for 2 seasons and the results are satisfactory. The system works along the quay and has two arms going out perpendicular to the quay with a length of 50 meters. About one meter between a moored vessel and the quay are kept free from ice by the system and the ice thickness is reduced. The harbour has pointed out that one of the major advantages is that the vessel does not freeze at the quay.

5.3.2 Waste water outflow

As many harbours are connected to industrial applications, waste water outflow from cooling systems is sometimes available but not always used. The warm water can be discharged into the required area, where even nozzles, air bubbler systems and diffusers can increase the spread. Most effective is warm water outflow with a temperature just above the freezing point and locally not too concentrated. In water with low salinity and waste water of temperatures more than 10°C, the warm water gets heavier than the surrounding water while cooling and sinks to the bottom.

A problem which has to be avoided is heat loss in non-ice-covered water that results in fog and icing on equipment. Therefore in an ideal situation the waste water outflow should allow a thin ice-cover to create, which can easily be broken by the tugboat.

The experiences with warm water outflows depend a lot on a careful design which has also been reported by a Finnish study (Laasonen, 2000). It is stated in this study that 10 MW thermal power should theoretically keep 10 hectares ice-free, in practice this is only 1-2 hectares. The waste water outflow is often a cost-free ice suppression method and can reduce the ice problems close to the quays. Advantages thus gained are that the icebreaking is eased, time losses reduced and the amount of damage on structures and vessels reduced.

At the same time the heat energy which could be used constitutes a valuable source for many other applications as well and might in the future no longer form a cost-free service for the harbours, alternatively more of the thermal energy might be removed effectively from the waste water.

In the port of Piteå a new factory for bio diesel is planned which could result in the availability of a lot of waste water (750 m3/min @ +10ºC). The planned factory has been approved by the authorities by April 2008. The planning process has not yet been completed and there might be a possibility to use the waste water as an icereducing measure in Piteå hamn.

Figure 12: Flow developers (Picture by Hargs Hamn AB)

5.3.3 Flow developers

Flow developers are employed to move or direct ice floes and broken ice away from quay structures. The most common type in the Baltic is the one with a propeller system. The most common application is at RoRo ramps, where a certain position has to be reached by the vessel to enable on- and offloading. The installation allows keeping a small part close to the quay free from broken ice by flushing parallel to the quay edge. In the literature minimum values of 30 kW (PIANC, 1984) for the engine power are set. In the Finnish study (Laasonen, 2000) it is described that the typical size is somewhat lower (10-30 kW) with an effect of 25-1000 m2. A problem which has been described is that damage occurred on the flow developer or the vessel and that some flow generators get lost fast by sinking or being flushed away.

5.3.4 Studies performed by Luleå Technical University

Various studies have been performed by researchers about thermal measures. Laboratory studies and full-scale trails have been performed with a combination of waste water and air bubble systems, mainly in the 80s and 90s. The main purpose has been to develop efficient ice reduction systems for winter navigation purposes. The main policy has been to utilize existing resources as waste energy in industrial spill water, water from sewage treatment plants, among others. The thermal conditions in the Baltic Sea brackish water regimes give opportunities to use considerable amounts of existing thermal energy from waste water with temperatures just above the freezing point.

In Piteå harbour a warm water outlet with 1MW and air bubble curtains were used to reduce the ice around a quay over an area of about 3600 m^2 (90 meter parallel with the quay, 40 meters out from the quay). The main principle was to establish a mixed box of water and air bubbles where the energy was exposed to the surface and also controlled by bubble curtains. The water was released 1.5 meters under the surface with 277/W/m^2 (10° C with 25 l/s). Two pipes with a diameter of 106 mm and a distance of 12 m from each other were used for the air bubbler system with holes at a distance of 1.36 m from each other. The air bubblers released about 100 l/s. In the beginning there was broken ice with a thickness of about 70 cm around the quays and a temperature at the bottom of about 0.2°C (13m - 19m deep water). After two days about 20% of the test area was free from ice, after 4 days about 50%. The temperature at the top three meters had increased by then with 0.1 - 0.2°C. Basic for a successful installation is that the water below the ice is in motion and that warm water is available.

A number of studies focused on ice reduction methods have been conducted, mainly by the Luleå technical University but also by and in cooperation with SSPA Sweden AB. The possibilities to use energy from Haparanda sewage treatment plant in order to reduce risks for ice jamming and hazardous ice piling in the Torne River mouth was studied by SSPA. The study showed that the ice growth and risk for jamming was considerably reduced when a controlled mix of the waste water with a temperature of at maximum +8 degrees with the river water was generated. The outlet was redesigned and instead of using an ordinary bottom located pipe outlet that generates a small and sometimes foggy open wake, the water was spread through a diffuser and mixed over a controlled width of the river. Energy based calculations showed considerably reduced ice thickness downstream the outlet position.

By a relocation of the outlet of sewage treatment waste water in the port of Luleå at least one terminal could be kept almost ice free during the winter period. The energy content of the outlet could be effectively used by a controlled mix with passing river water. The warm water was suggested to be let out through a diffuser located upstream the terminal.

5.4 Natural ice control methods

5.4.1 Snow

The snow works often as an ice suppressor. The snow insulates and prevents heat losses to the atmosphere. The constant snow cover can be about 30 cm in depth in the north of Sweden. At the same time, the snow cover obstructs the tugboats while breaking ice, because the resistance for icebreaking can be significantly increased by snow.

5.4.2 Stream

The streaming of rivers has, according to many of those interviewed, a very important part in the overall ice handling in the ports. Even though it can have a negative impact on the thermal ice-reducing measures and reduces their efficiency significantly, it reduces the rate of ice growth. It also helps the ice-breaking tug to wash away the broken ice out of the channel, along the quays, the berthing and the turning positions. The stream in the port of Luleå is reported to be 2 or 3 knots, sometimes even up to 4 knots strong.

5.4.3 Currents

The flow pattern in the harbour area can have a strong influence on the ice situation in the ports and can be compared to the streams described above.

5.4.4 Archipelagos

The archipelagos along the coast work in most of the harbours as an ice diversion. They help to keep the ice-cover intact and reduce ice pressures and ridges in the harbour area. They protect the channels and fairways from broken drifting ice.

Table 2: Ice control measures (PIANC, 1984)

	Alternatives	Effectiveness		Annual cost						
		Docks	Harbour	Docks	Harbour	Reliability	Safety	Environmental impact	Energy consumption	Experience
Thermal, chemical methods	Air bubbler	Yes	Low	Low	Low	High	High	Low	Low	Proven
	Thermal discharge where available	Yes	Yes	Low	Medium	High	High	Low	Low	Proven after few studies conducted
	Insulation	Yes	No	Medium	-	-	High	Some	Low	Unproven
Mechanical methods	Icebreaker	Yes	Yes	High	High	High	High	Low	High	Proven
	Air cushion vehicle	No	Yes	-	High	Medium	Limited	Noise	High	Proven
	Soviet LT8 device	No	Yes	-	High	High	High	Low	High	Proven
	Mechanical ice cutter	Yes	No	Yes	-	Low	Low	Low	Low	Little
Ice-stabilising structures	Navigational boom, artificial island	-	Yes	-	High	High	High	Low	-	Proven

5.5 Problems in winter navigation

One of the most demanding parts of the journey through the ice for a ship is the manoeuvring to the quay. Ice gets piled up close to the jetties and under the piers. Even with ice control measures in effect close to the quays, the arriving ship and the propeller streams fill up with ice again.

Icing

Icing is a phenomenon which occurs in ice-free waters with a low ambient temperature in connection with spray, snow or rain. The whole ship can be covered with ice which can be a danger for certain ship types, due to extra load on the ship. A more common problem is that for instance the hatch covers freeze and it can take a long time at the quay to unfreeze and open the covers. Also unfreezing the lashing on deck-stored containers can take some time and the mooring equipment might be harder to handle, which is often taken care by extra manning. The problem of icing is a more regular problem in the southern ports on the east coast of Sweden. Here the ports are often able to assist and de-ice the vessels by flushing away the icing.

Low temperatures

At low temperatures below freezing point, the impact resistance of steel is reduced. Hard contacts are common while manoeuvring close to the quay. Structural failure due to contact with ice, docks and fenders may occur at a

significantly lower level of impact in the cold climate. Cranes in the northern ports are often designed to withstand at least -30ºC, which is formulated in the "Helcom Recommandation 25/7".

Figure 13: Icing on a ship

Brash ice, which is a layer of round-shaped broken ice and slush often develops in winter time in the harbour and might freeze together. This layer increases the resistance compared to normal level ice and requires more power consumption and slows down traffic and berthing. This thick ice layer increases the resistance of the ship, thus increasing the demand for power to compensate. In addition, snow will increase resistance.

5.6 Damage and Risks in winter navigation

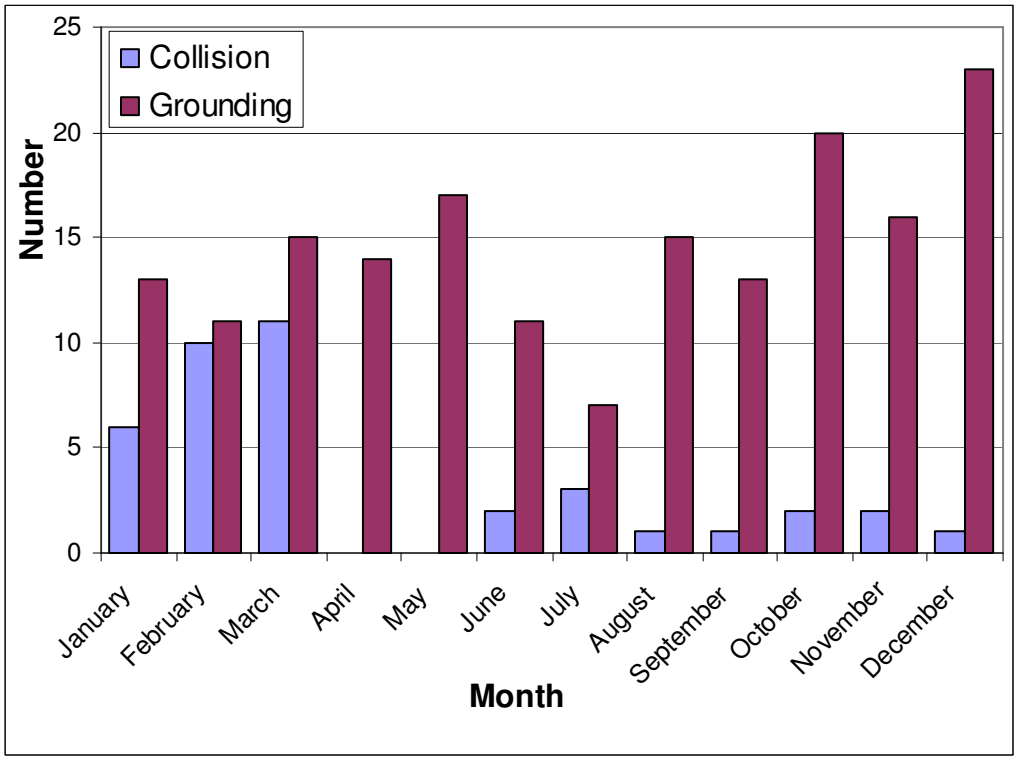

Figure 14: Collision and groundings divided by month (Kujala, 2007)

Damage

Improved icebreaker assistance, an improved advisory service from the icebreakers' management in guiding vessels through ice-affected areas and improved ice observations and reports has reduced the risk of damage (Transport Canada, 2005) at sea. The interviewed ports stated no damage has been reported in recent years, despite one based on a collision with a quay of a berthing vessel.

Much damage due to ice is detected at the end of the ice season or even later and damage due to ice occurs regularly on ships. The main source of damage in harbours is due to manoeuvring (Hänninen, 2003). The bilge keel might get damaged or ruptured while manoeuvring. Ice rubble can become several meters thick, especially close to the quays. Ice rubble can contain rocks and wood. The propeller, the rudder and the hull are exposed to this ice rubble and might get damaged, even though the most common damage to the propulsion units are due to reversing in ice. Controllable pitch (CP) propellers are sensitive to damage if the lube oil freezes due to deselecting the pitch servo while the ship is at the quay (Hüffmeier, 2006).

The probability of damage to ships can be directly connected to the severity of the winter. Still, the insurance club "Swedish" has reported only 4 incidents of ice damage valued at more than 10 000 USD in the last 10 years, 3 of

them involved damage to the propeller (Hultman, 2007). Inexperienced crews cause damage whilst reversing in ice (propeller and rudder) or following an icebreaker without due attention leading to a collision which is mirrored in the statistics in Figure 14.

5.6.1 Erosion and corrosion

The currents created by the propeller streams of vessels and tugboats lead to increased erosion and damage to the foundations of the piers and structures. Narrow and shallow sections of the fairway and the area under docks are exposed to these erosion problems forced by instantaneous large propeller flows.

The ice often abrades the protective coating from the quay structures. The unprotected parts may experience not only erosion but also corrosion. The tugboats are exposed to more corrosion problems during the winter season.

Damage to quay structures has been analysed in the ports. While in the beginning of year-round shipping damage occurred regularly on quays and quay structures, this problem is reduced today. The structures are exposed to ice forces which are due to pressure of the ice sheet through temperature variation (thermal ice pressure), pressure from the ice sheet through water level variations, dynamic pressure of drifting ice, pressure from pack-ice, vertical pressure from the ice sheet (Eriksson, 2007) and ice build up on vertical and horizontal surfaces due to icing. Also frost blasting can cause damage. The maintenance expenses are difficult to estimate and cannot solely be related to ice related damage.

5.6.2 Environmental aspects

Ice navigation changes the ice conditions with break-ups and accelerated brash ice due to refreezing. The natural ice cover is affected and the floe size decreased, the ice cover is more dynamic, the development of leads and ridges is encouraged.

Tugboats are utilized more in the winter time which leads to an increased consumption of bunkers. This results in an increased amount of carbon dioxide and other acid gases. Warm water has an influence on the environment. Beside the creation of fog, thermal ponds can also present an obstacle to migrating fishes, etc.

5.7 Swedish icebreaker management

The Swedish icebreaker division, a part of the Swedish Maritime Administration (SMA) is situated in Gothenburg. The cooperation with the harbours was described as very good. Support is given to each other both-way. Icebreaking includes a process of long planning so that the maritime traffic can flow easily. There is a good cooperation with the Finnish icebreaking service, which started as early as in the 1960ies.

The biggest challenge for the icebreaking management is to motivate and receive sufficient financial support for the icebreaking. The limited money sets most often the border. The public tends to forget fast that icebreaking is required in the Baltic Sea to keep the industry maintained and the population supplied.

The older generation of icebreakers in Sweden requires soon an upgrade and modernisation to break more fuel-efficiently and environmental friendly. Then these vessels could service another 20-25 years. Newbuildings of icebreakers all over Europe tend to be multipurpose vessels to lower the costs. Still a new vessel would cost about 1.5 billion SEK.

Most of the crews on arriving vessels the icebreakers get in contact with are used and prepared to sail through ice-covered waters. The amount of vessels with inadequate equipment has decreased. The amount of ships which need icebreaker assistance is reduced. Even though the cargo volume is growing, the number of ships transporting the cargo is reduced due to the fact that the ships are becoming bigger. The vessels have become better with the time based on higher demands by the authorities (ice class rules) and the just-in-time delivery which is required by many customers.

Damage which occur are often based on that the crew of a vessel is at a loss in a certain situation and does not know how to act in ice. The ship owners are certainly very interested in reducing damage and delay and there are ice training courses available. These courses are new and SMA and DNV work on a certification of these courses.

Damage on icebreakers are seldom and occur mainly by rear-end collisions. The docking of the icebreakers is therefore according to the classification societies, every 5 years.

- To avoid damage on vessels and icebreakers the SMA (Stenberg, 1994) the following factors need to be improved:
- Amount of misjudgements of the icebreaker performance to sail through an area with ice ridges.
- Amount of misjudgements of the following vessels to reduce speed within the given distance.

- Inattentiveness concerning the distances in a convoy.
- Failure or wrong orientation to judge the performance of the icebreaker in changed ice conditions by the crews of following vessels.
- Bad communication while change of watch concerning the ice conditions and the performance of the crews in the following vessels to sail through ice.
- Misjudgement of the breaking performance of the vessels in the convoy.

The crew of the icebreakers consists of about 17-20 men per vessel, year-round. In the winter season the crews are strengthen by people who get a temporary employment.

The environmental impact of icebreaking is mainly based on the fuel consumption. All vessels fulfil the requirements set for 2020 with 0.5% sulphur content in the fuel. Atle, the newest Swedish icebreaker is equipped with a catalyser. Another impact is due to the broken ice which is moving more compared to unbroken idle ice.

In Finland the law is different from the one in Sweden. Due to a lower traffic volume which incorporates a lower rhythm of incoming and outgoing vessels and a lower number of icebreaking tugboats, the state-owned icebreakers are also used to break the ice all the way to the quays. The costs for the icebreaking in Finland are much higher than the one in Sweden, an hour with an icebreaker costs almost twice as much there.

In the future a closer cooperation between the icebreakers of all states bordering the Baltic Sea might be possible, which could lead to an even more efficient service for the maritime traffic.

5.8 Comments of other stakeholders

5.8.1 Ship owners and shippers

The costs for increased port dues and increased bunker consumption are often part of the total calculation. The increased investment costs for a 5000 ton vessel with ice class 1A are about 500 000 € with a newbuilding price of 10 M€, corresponding to a 5 % higher investment.

In Finland the costs for icebreaking for the ship owner are estimated to be between 1200…1300 USD for a single shipment in the port, due to delays in berthing, extra use of the harbour icebreaker, damage to the ship, larger fuel consumption and the manual removal of ice and snow from decks. Total costs for ship owners in Finland are estimated to be 6 million USD in an average winter up to 12 million USD in a severe winter (Laasonen 2000).

Part of the ship owner's perspective is also the route planning and management. Ports further to the south have been chosen when possible for route service to avoid the more severe ice conditions in the north.

5.8.2 Problems mentioned by ship owners and shippers

A shortage of icebreakers has been observed in stringent winters; regionally last in the Gulf of Finland 2003, when waiting times appeared for the shipping traffic. If the restriction reaches a certain level, fewer vessels are available which fulfil the requirements and the rates increase unless one has contracted rates. Delay times mentioned above have been negligible in the last decade, with for instance no delay of more than 1 hour in about 2300 total calls (about 550 in ice conditions) (Erixon, 2008). If delay occurred this was due to shortage of icebreaker capacity accompanied by waiting times for the vessels (Toonen, 2008) and less regular information on ice tracks and waypoints.
Due to the series of mild winters the young officers do not get training on how to sail and manoeuvre in ice conditions, which is a concern for the ship owners.

5.8.3 Insurances

It is hardly possible for the insurance companies to identify the claims really caused by ice (Seltmann, 2008). Claims are reported with the main claim types: fire/explosion, grounding, contact, ice, heavy weather, special damage and engine. The "ice" claims type group alone does not suffice for this purpose, as also e.g. "grounding", "contact" or other claims may well have been caused by ice. In addition the number of ice claims registered is very small such that this group alone does not give a sufficient statistical basis for further analysis.
Generally one can say that there is some increased frequency of "ice" claims in severe winters.

No information have been available of details such as which part of the vessel is damaged, the geographical area where the accident occured or the actual cause.

6 IMPROVEMENTS AND FUTURE OF WINTER NAVIGATION

During the interviews some aspects were addressed significantly improving winter navigation. The regulations regarding winter navigation in the Baltic Sea have stopped badly equipped and poorly prepared vessels from entering the ice-covered waters. Restrictions on the power and ice-strength of the vessel and a steady renewal program for the fleet with more powerful ships have reduced the problems within the problems. The crews of the ship are in general better prepared than previously had been the case, even though a decay of experience can be observed due to the series of mild winters. Some ports have received more powerful tugboats which has eased the situation. The series of mild winters in recent years has reduced the amount of problems as well and if one implicates climate change as a reason, this has eased the situation as well. The ports often expressed a desire for better support, both technically and financially, for the future. Icebreaking all the way to the quay by the state-owned icebreakers as well as financial support by the Swedish government or EU to compensate for the competitive disadvantages due to extra costs would be desirable.

7 CONCLUSIONS

This study was performed by SSPA Sweden AB in order to find out the current state of the art of ice handling in ports. The use of various kinds of ice control techniques is usually taken care of by each port themselves. All seaports along the Swedish coast facing ice on a regular basis were asked to give an overview on the ice situation in their port. The basic ice handling methods were collected and analysed. The chief goal was to evaluate the efficiency of the ice handling methods, successful methods as well as less successful ones. Other problems connected to winter navigation in harbours were reviewed as well, such as scope and nature of damage, the delays for ship owners, costs for ship-owners and ports, and finally to discover ways of speeding up the winter traffic in ports. The study was part of the Interreg ice project co-ordinated by the Luleå Technical University and carried out during the winter of 2007-2008.

8 ACKNOWLEDGMENTS

We would like to thank the sponsors of the INTERREG project and Lennart Fransson, coordinator, Luleå Technical University. We would like to express our gratitude to all the port authorities, harbour masters, tugboat captains, companies and authorities who supported us with information.

REFERENCES

Alexandersson, H., Vindstatistik för Sverige 1961-2004 (In Swedish), SMHI Meteorologi Nr 121, 2006.

Dietrich, G. and Schott, F., Meereskunde der Ostsee (In German), published by L. Magaard and G. Rheinheimer, pp. 61–66, Springer, Berlin, Heidelberg, New York, 1974.

Eriksson, M., Reparation av isskydd, Piteå Hamn (In Swedish), Examensarbete, Luleå tekniska universitetet, 2007.

Erixon, S., Shippers view on winter navigation, Svenska Cellulosa Aktiebolaget, Personal correspondence, 2008.

Granskog, M., Kaartokallio, H., Kuosa, H., Thomas, D., Vainio, J., Sea ice in the Baltic Sea – A review, Estuarine, Coastal and Shelf Science Volume 70, Issues 1-2, October 2006, Pages 145-160, 2006.

Gullne, U., Sjöfartsverket, Icebreaking division, Personal correspondence, 2008.

Hänninen, S., Incidents and Accidents in Winter Navigation in the Baltic Sea, Winter 2002 – 2003, Winter Navigation Research Board, Research Report No 54, Helsinki , 2003.

Hosmann, N., Winter Navigation, Ahlmark Lines AB, Personal correspondence, 2008.

Hüffmeier, J. Design of an ice-going LNG carrier, Project work, Hamburg-Harburg Technical University, Hamburg 2006.

Hultman, A., Ice damages, Swedish Club, Personal correspondence, 2008.

Kalliosaari, S. and Seinä, A., Jäätalvet 1981-85 Suomen merialueilla (Ice Winters 1981-85 at the Finnish Territorial Waters), Finnish Institute of Marine Research (in Finnish), publication No. 254, Helsinki 1987.

Kujala, P., Meri-Kotka activities to improve the safety of marine traffic in the Gulf of Finland, International Seminar on The Safety of Ice Navigation and

Environment Protection in the Gulf of Finland 20th and 21st of November 2007 in Kotka, 2007.

Laasonen, J., Nyman, T., Rytkönen, J., Ice management in Finnish ports, (In Finnish) Publications of the Ministry of Transport and Communications 19/2000, Helsinki 2000.

Liukkonen, S., Technical Requirements for year-round Baltic Sea Tanker Traffic, SMM Conference 2006, Hamburg 2006.

PIANC, Ice Navigation, Report of a working group of the Permanent Technical Committee II, Supplement to Bulletin no 46, Brussels 1984.

Sandkvist, J., Brash Ice Behaviour in frequented Ship Channels, Licentiate Thesis, Series A no 139, Luleå University, Luleå 1986.

Sandkvist, J. and Häggkvist, K., Isreducering I torneälvens mynning – Optimalt nyttjande av varmt vatten, förslag till tekniskt lösning. SSPA report 6310-1 for the National Rescue Services Board, SSPA Sweden AB, 1991.

Seltmann, A., Accident statistics, CEFOR, Personal correspondence, 2008.

Sjöfartsverket, Homepage:
http://www.sjofartsverket.se/templates/SFVXPage____1076.aspx, 2008 a.

Sjöfartsverket, Homepage:
http://www.sjofartsverket.se/templates/SFVXPage____913.aspx, 2008 b.

Sjöfartsverket, Homepage:
http://www.sjofartsverket.se/templates/SFVXPage____5670.aspx, 2008 c.

SMHI, Homepage: http://www.smhi.se/oceanografi/iceservice/iceextent_col.pdf, 2008.

SMHI, Krympande isar i Östersjön (In Swedish), Medvind No. 4, 2006, Swedish Meteorological and Hydrological Institute, 2006.

Stenberg, J., Typiska tillbudssituationer vid isbrytning (In Swedish), Sjöfartsverket, 1994.

Toonen, A., Winter time shipping, Wijnne & Barends' Cargadoors- en Agentuurkantoren BV, Personal correspondence, 2008.

Transport Canada, Winter Navigation on the River and Gulf of St. Lawrence, Practical Notebook for Marine Engineers and Deck Officers, Marine Safety 901, Cap-Diamant, Québec 2005.

Tsinker, G., Marine Structures in cold Regions, Marine Structures Engineering: Specialized Applications, Springer, London 1995.

8.1 Interviews and Correspondences

Stig Forslund, Kalix kommun, 2008.
Leif Åhberg and **Ulf Petterson** Luleå Hamn AB, 2007.
Leif Öhman and **Per Nyström**, Piteå Hamn AB, 2007.
Göran Hillberg, Skellefteå Hamn, 2007.
Olle Eriksson, Boliden AB, 2007.
Curt Kristoffersson, Umeå Hamn AB, 2008.
Sten Olov Andersson, SCA Timber AB, Rundviks sågverk, 2008.
Mikael Johansson, M-real Sverige AB, Husum, 2008.
Conny Sallander, Örnsköldviks Hamn, 2008.
Olof Johansson, Härnösands Hamn, 2008.
Johan Stén, Delta Terminal Söråkers Hamn, 2008.
Håkan O. Hedlund, Kent Bovin, Sundsvalls Hamn AB, 2008.
Staffan Eriksson and **Lars Hamrin**, Skärnäs Terminal AB, 2007.
Tommy Eriksson, Söderhamns Stuveri & Hamn AB, 2008.
Lars Forsling, Port of Gävle AB, 2008.
Håkan Nilsson, Hargs Hamn, 2008.
Sven Olsson, Roslagsbogser AB, 2008.
Ulf Berglund, Holmen Paper AB, Hallstavik, 2008.

Appendix

Tug boats			Dimensions					Building year	Bollard pull	Speed	Main engine	
Harbour	**Name**	**Owner**	Length o.a	Breadth	Draught	Brutto tonnage	Netto tonnage		[ton]	[kn]	EHK	kW
Luleå	Victoria	Luleå Bogserbåts AB	27.0	9.5	4.7	239		1979	25	12	2640	1941
Karlsborg	Viscaria	Luleå Bogserbåts AB	36.1	12.0	6.2	603	181	2000	62	14	6120	4500
Piteå	Valkyria	Luleå Bogserbåts AB	32.3	9.7	5.2	312		1977	35	13.5	3520	2588
Skärnäs	B/B Skärnäs	Skärnäs Terminal	30.0	8.4	4.5	239	71	1964			1680	1235
Skellefteå	Aitik	Skellefteå Kommun	29.2	9.0	4.3	266		1969			2475	1820
Sundsvall	Bull	Sundsvalls Hamn AB	32.2	9.0	4.8	271		1972			2475	1820
Umeå	Kronö	Umeå Hamn AB	34.6	9.2	5.0	368		1970			2600	1912
Söråkers	J.A. Enhörning	Timrå Bogserings & Bärgnings AB	16.7	5.5	2.7	51.04	14.42	1961			495	364
Härnösands	B/F Max	Norrlands Sjöentreprenads	21.4	6.5	3.3			1967			720	529
Gävle	Järven	Noås Nordmuddring AB	30.8	8.4	4.8	236		1973	20	13	2100	1544
Örnsköldviks	Frans Michael	Noås Nordmuddring AB	31.4	8.2	4.0	212	63	1917	20	12	1800	1324
Husum	Kämpe	M-Real Sverige AB	29.6	9.2	4.3	296		1977			2642	1943
Hargshamn	Hallsta III	Roslagsbogser AB	15.1	4.6	2.3	20		1954			328	241
Hallstavik	Leam	Noås Nordmuddring AB	22.0	6.6	3.7	111	33	1959	16	12	1200	882
Rundvik	Axel	Rundviks Rederi AB	26.7	8.5	4.2	219		1967			2462	1810
Average			27.7	8.3	4.3	245.9	72.5	1967	30	13	2217	1630
Max			36.1	12.0	6.2	603.0	181.0	2000	62	14	6120	4500
Min			15.1	4.6	2.3	20.0	14.4	1917	16	12	328	241

Database Norströmsgrund

Lennart Fransson, Håkan Thun

PROJECT REPORT

Database Norströmsgrund

Manual for how to use the database for the lighthouse Norströmsgrund (1999-2003)

Lennart Fransson

Håkan Thun

Luleå University of Technology
Department for Civil & Environmental Engineering
Division of Structural Engineering

Preface

The following report is a part of the project ”Ismekanikk og havnedrift i islagte farvann” (Nordkalotten INTERREG III A Nord).

In this report it is described how data from field tests at the Lighthouse Norströmsgrund is structured in a database. Field tests were conducted during the years 1999-2003 within two EU-projects.

Luleå, april 2008

Lennart Fransson and Håkan Thun

Table of Contents

1 General information about the lighthouse Norströmsgrund

The lighthouse Norströmsgrund is located in a subarctic region at position 65° 6.6' N and 22° 19.3' E – about 35 nautical miles southeast of Luleå in Sweden – at the edge of the land fast ice of the Swedish coast and the drifting ice in the northern part of the Gulf of Bothnia.

The lighthouse has a total height of 42.3 m, has a diameter of about 5 m (7.2 m at waterline) and is placed at a water depth of approximately 13 m. The lighthouse consists of nine floors with a helicopter platform on the top, see Figure 1.

Figure 1 Photograph of the lighthouse Norströmsgrund.

The lighthouse is owned by the Swedish Maritime Administration (Sjöfartsverket) and is unmanned and hosts a Racon and a small white position light.

During common winters the lighthouse Norströmsgrund is located in the transition zone of the land fast ice and the high dynamic drift ice of the northern bay of Bothnia (Bottenviken). A common level ice thickness is about 40-60 cm while rafted ice of more than 1m thickness will be found. Due to the high dynamic ice situation hummock ice fields and pressure ridges are present with a high frequency. The keel depth of the ridges often exceeds 6m. This depth let the ridges ground at the caisson of the lighthouse.

Note: the text presented in this report are to some extent extracts from the logbook, reports etc. produced within the EU-projects LOLEIF/STRICE.

2 Introduction to the database

In this short report the background to the database and how to use the database, are described. The database contains about 21GB (080401) of data and consists of a number of web pages and could be found at the website:

http://www.ltu.se/norstromsgrund

The basic idea how to use the database is first to choose a date when ice load measurements have been performed and combine this with other data as temperature, wind direction and finally perform an analysis. There are no "force-deformation" graphs available, so every researcher has to analyse the data by them selves.

In appendix A an extract from the database is presented (the two first years).

3 The structure of the database

The first web page (index.htm) of the database is shown in Figure 1 (version 080401). On this page a photograph of the lighthouse can be seen together with some general information about the lighthouse (the dimensions, the geographic location and so on). At the bottom of the page there are links to the five years when measurements have been performed and by selecting one of them the user is guided to the actual data for this particular year.

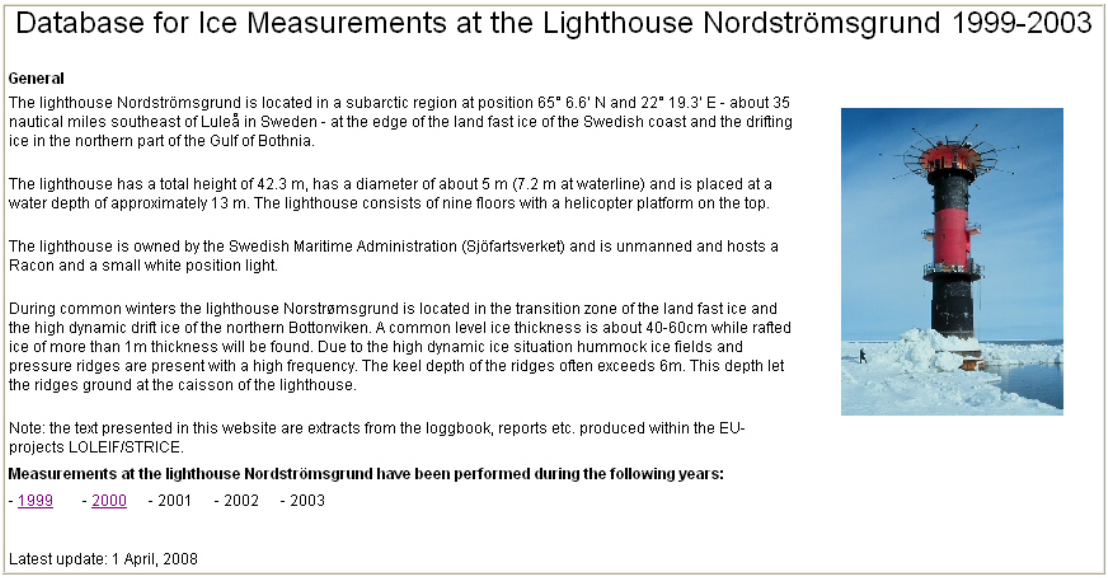

Figure 1 The "starting" page for the database (version 080401).

If, for example, the year 2000 is chosen the information in Figure 2 is shown. The web page begins with some general information for this particular year, like for how long time the measurements were performed, how many load panels that were used and so on.

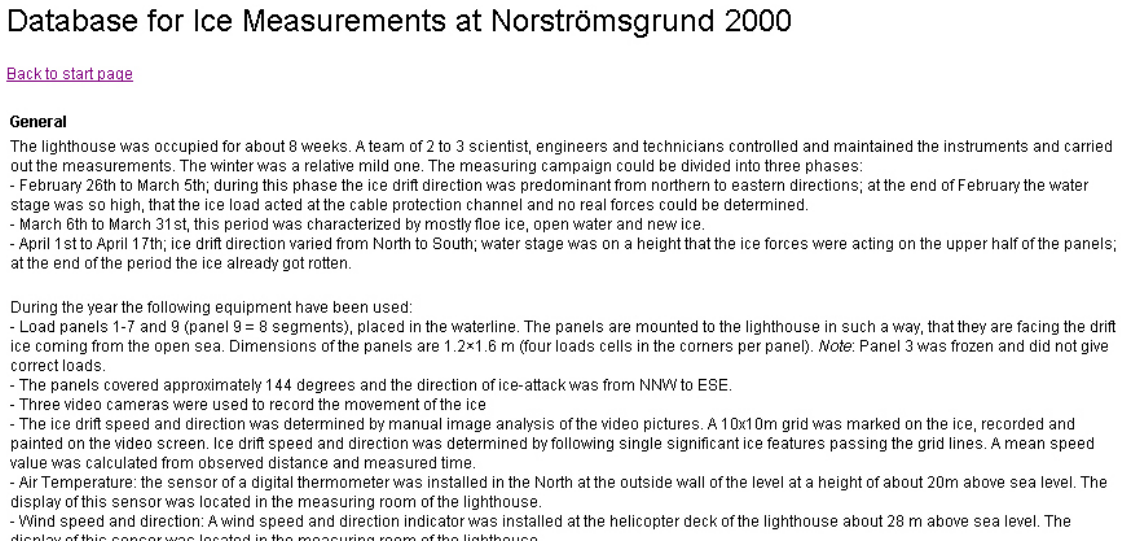

Figure 2 General information about actual year is presented at the top of the page.

The web page continues with the different measurements that were performed during the season (besides the ice load measurements), like:

- meteorological data (wind speed, wind direction, temperature etc.)
- ice charts
- ice thickness
- ice strength
- photographs

Before the actual database begins a list is shown with the dates when load measurements have been performed, see Figure 3 for the year 2000. By selecting one of the dates the user is redirected to the table/database for this day. The content of this table is an extract from the logbook that was written by the staff that was performing the measurements during this day.

Measured data during the year 2000 has been compiled for the following dates:

Table 1 - Data for the 1st of March	Table 6 - Data for the 7th of March	Table 11 - Data for the 1st of April	Table 16 - Data for the 13th of April
Table 2 - Data for the 3rd of March	Table 7 - Data for the 16th of March	Table 12 - Data for the 3rd of April	Table 17 - Data for the 14th of April
Table 3 - Data for the 4th of March	Table 8 - Data for the 18th of March	Table 13 - Data for the 4th of April	Table 18 - Data for the 17th of April
Table 4 - Data for the 5th of March	Table 9 - Data for the 26th of March	Table 14 - Data for the 5th of April	
Table 5 - Data for the 6th of March	Table 10 - Data for the 31st of March	Table 15 - Data for the 12th of April	

Figure 3 Table showing the dates when measurements have been performed.

As an example: if the link for 3rd of March is selected, the table in Figure 4 is shown. At the left side of the table, in the first column, the label ”Event No.” could be found. This label corresponds to the original data files. The second column is labelled “Date” and in the third column, the time column, it is written when measuring of the load has taken place (“Load Measuring, time period, start end”). These time and date labels could be used to correlate other data that has been measured during the same event (wind speed, wind direction etc.). If the event “0303_0200” is used as an example it could be seen in the table that the load has been measured between 16.10-20.23 and that this data has been saved in a file called ”0303_020.txt”. This “txt-file” is an ascii-file that could be selected and downloaded and used in a suitable analysis tool. A movie of the event is also available. During this sequence the wind direction has been easterly (E=East). Beneath the table explanations could be found.

Table 2 - Data for the 3rd of March. [TOP]

Event No.	Date	Load Meauring, time period		Ice Thickness	Ice formation	Failure mode	Ice drift		Load data	Video	Wind		Air temp.	Sampling rate	Remark
		Start	End		b)	c)	Speed	Direction		a)	Speed	Direction			
	2000-03-03	7:50:00	-	-	OW	-	-	-	-	-	9	W	-8.6	-	Data file Sonar: 00303, Data file EM: 000303,
	2000-03-03	12:20:00	-	-	-	-	-	S	-	-	-	-	-7.0	-	ice movement from South, very slow speed; n addional pipes at EM-frame
	2000-03-03	12:30:00	16:10:00	-	-	B + BU	-	-	-	-	-	-	-	1	started longterm measurement; started laser of the panel; bending + buckling failure, see c
	2000-03-03	13:00:00	-	-	-	-	-	-	-	-	-	-	-	-	started EM-Measurements
	2000-03-03	13:12:00	-	-	-	-	-	-	-	-	-	-	-	-	throw a marker onto the ice for speed determ 2-11
0303_0020	2000-03-03	16:10:00	20:23:00	-	-	-	-	E	0303_020.txt	0303_0021.mpg 0303_0022.mpg	-	-	-	-	started new measurement;
	2000-03-03	16:35:00	-	-	R	-	-	-	-	-	6	E	-	-	ridging in the East infront of the lighthouse, 2-
	2000-03-03	18:35:00	-	0.35	-	-	0.20	E	-	0303_0023_24_25.mpg	13	E	-9.2	-	-
	2000-03-03	18:50:00	-	0.35	-	C	0.17	E	-	0303_0023_24_25.mpg	-	-	-	-	-
0303_0040	2000-03-03	20:23:00	1:31:00	0.38	-	-	0.20	E	03032023.txt	0303_0041.mpg 0303_0042.mpg	-	-	-9.6	-	started new measurement;

Figure 4 Table showing data for one day.

Appendix A. Extract from the Database (1999 and 2000)

Database for Ice Measurements at the Lighthouse Norströmsgrund 1999-2003

General

The lighthouse Norströmsgrund is located in a subarctic region at position 65° 6.6' N and 22° 19.3' E - about 35 nautical miles southeast of Luleå in Sweden - at the edge of the land fast ice of the Swedish coast and the drifting ice in the northern part of the Gulf of Bothnia.

The lighthouse has a total height of 42.3 m, has a diameter of about 5 m (7.2 m at waterline) and is placed at a water depth of approximately 13 m. The lighthouse consists of nine floors with a helicopter platform on the top.

The lighthouse is owned by the Swedish Maritime Administration (Sjöfartsverket) and is unmanned and hosts a Racon and a small white position light.

During common winters the lighthouse Norströmsgrund is located in the transition zone of the land fast ice and the high dynamic drift ice of the northern Gulf of Bothnia (Bottenviken). A common level ice thickness is about 40-60 cm while rafted ice of more than 1 m thickness will be found. Due to the high dynamic ice situation hummock ice fields and pressure ridges are present with a high frequency. The keel depth of the ridges often exceeds 6 m. This depth let the ridges ground at the caisson of the lighthouse.

Note: the text presented in this website are extracts from the loggbook, reports etc. produced within the EU-projects LOLEIF/STRICE.

Measurements at the lighthouse Nordströmsgrund have been performed during the following years:

- 1999 - 2000 - 2001 - 2002 - 2003

Latest update: 1 April, 2008

Database for Ice Measurements at Norströmsgrund 1999

Back to start page

General

During the year the following equipment have been used:
- Load panels 1-7 and 9 (panel 9 = 8 segments), placed in the waterline. Dimensions of the panels are 1.2×1.6 m (four loads cells in the corners per panel)
- The panels covered approximately 144 degrees and the direction of ice-attack was from NNW to ESE.
- Ice thickness was measured by drilled holes.
- Three video cameras were used to record the movement of the ice
- Calibration parameters for the panels could be found here: calibration.doc

Notations in the data files:
- SumPan1 = The sum of the load from all load cells in each panel (kN).
- Panel 91 = The load for the individual load cells for panel 9, in this case for load cell 1 (of eight). SumPan9 is the total sum for panel 91 to panel 98.

Ice charts

The following ice charts are available for the time period:
- ice990207.pdf
- ice990221.pdf
- ice990323.pdf
- ice990423.pdf

Ice thickness

The ice thickness was measured by LTU during the period April 9th to April 12th (holes were drilled). The survey was done along the broken channel performed by the lighthouse when the ice came to a stop and the ice situation was stable. Select: Ice Thickness2.doc

Ice Compressive strength

During the period April 7th to April 12th 1999 five cores were taken in the vicinity of the lighthouse (core diameter 200 mm). Ice temperature, density and salinity profiles were determined. A thin section was cut, a crystal structure analysis performed and the crystal size was determined. Cubic specimen of a size of 45×90×150 cm were cut but with a bandsaw and uniaxial compression tests were performed at the lighthouse with the load direction perpendicular to the ice growth direction. The temperature of the specimen during the testing was approximately the collection temperature.
- core_A.xls
- core_B.xls
- core_C.xls
- core_D.xls
- core_E.xls

Measured data during the year 1999 has been compiled for the following dates:

Table 1 - Data for the 15th of February
Table 2 - Data for the 10th of April
Table 3 - Data for the 12th of April
Table 4 - Data for the 18th of April

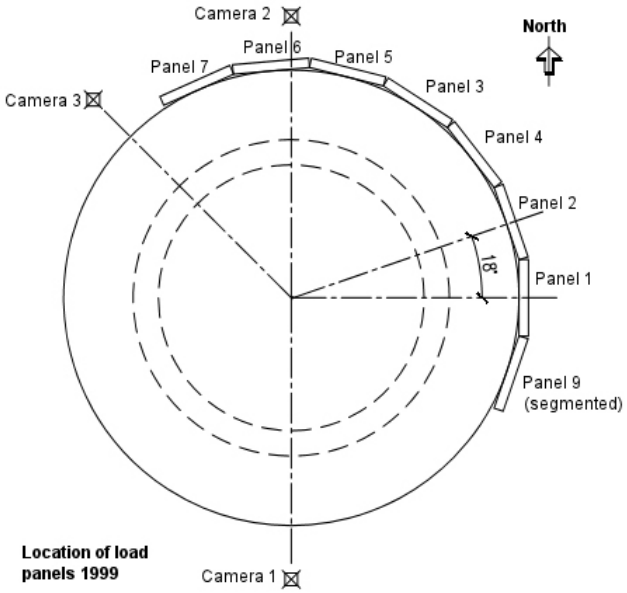

Illustration showing the location of load panels mounted on the lighthouse.

Table 1 - Data for the 15th of February 1999. [TOP]

Event No.	Date	Load Meauring, time period		Video	Ice Thickness	Ice formation	Failure mode	Ice drift		Load data	Wind		Air temp.	Sampling rate	Remark
	a	Start	End	a)	a	b)	c)	Speed	Direction	a	Speed	Direction	a	a	a
1502_010	1999-02-15	16:27:00	17:28:00	-	0.2 - 0.3 m	R	C	0.2	SSE	1502_100.txt	-	S	-	-	strong wind from southern directions; ice cover starts to move; loads on segmented panel (9) and panel 1 + 2; failure mode is crushing with bending incorporated; ridged ice with level ice floes incorporated; real time video with camcorder kn; 17:09 start of realtime video recording camera 2. Pictures 1_28-1_37
1502_011	1999-02-15	17:28:00	18:30:00	-	-	-	-	-	-	-	-	-	-	-	-
1502_012	1999-02-15	18:30:00	19:30:00	-	-	-	C	-	S	-	-	-	-	25	strong vibrations; small loads on segmented panel (9); real time video still running
		18:53:00		-	-	R	-	-	-	-	-	-	-	-	ridge is passing the lighthouse
		19:02:00		-	-	-	-	-	-	-	-	-	-	-	ice wedge in front the lighthouse in the south; no load on panels
		19:07:00		-	-	-	-	-	-	-	-	-	-	-	radial crack in the south is dividing the ice cover in two parts
		19:10:00		-	-	-	-	-	-	-	-	-	-	-	new ice floe is hitting the lighthouse and turns to the east

		19:17:00		-	-	-	C	-	-	-	-	-	-	-	new ice floe is reaching the lighthouse;crushing with tooth pasting in the south; panel 9 in contact with ice
		19:19:00		-	-	-	B	-	-	-	-	-	-	-	bending mode event; radial cracks
		19:21:00		-	-	-	B	-	-	-	-	-	-	-	radial + circumferential cracks
1502_013	1999-02-15	19:31:00	21:28:00	-	thin	L	-	-	S	-	-	-	-	-	thin level ice without any ridges
		19:36:00		-	-	-	B	-	S	-	-	-	-	-	deloading cycles due to occurrence of cracks in the south
		19:57:00		-	-	-	-	-	-	-	-	-	-	-	thicker ice is reaching the lighthouse but no significant load on panels
1502_014	1999-02-15	21:28:00	23:48:00	-	-	-	-	-	S	-	-	-	-	10	ice starts to move again from the south; no load on panels
1502_015	1999-02-15	23:48:00	8:23:00	-	-	-	-	-	-	-	-	-	-	-	start long term measurement

a) Camera 1, 2 and 3, positions see illustraion above.
b) L = Level ice, H= Hummocked ice, R= Rigged ice
c) C= Crushing, B= Bending, S= Splitting
d) Temperature measured at Rödkallen by SMHI. Position 5 km from

Table 2 - Data for the 10th of April 1999. [TOP]

Event No.	Date	Load Meauring, time period		Video	Ice Thickness	Ice formation	Failure mode	Ice drift		Load data	Wind		Air temp.	Sampling rate	Remark
	a	Start	End	a)	a	b)	c)	Speed	Direction	a	Speed	Direction	da	a	a
1004_031	1999-04-10	0:17:00	1:17:00	1004_010.mpg	abt. 1 m	L	C	0.13	N	1004_010.txt	10			-	
1004_032	1999-04-10	1:17:00	2:17:00	-	-	L	C	0.11	NNW	-	-	-		-	01:35 Start real time recording of camera 1
1004_033	1999-04-10	2:18:00	3:18:00	-	abt. 0.6 m	L	C	-	-	-	8		1.4	-	
1004_034	1999-04-10	3:18:00	4:18:00	-	-	L	C	-	-	-	-	-	-	-	real time recording stopped
1004_035	1999-04-10	4:18:00	9:00:00	1004_050.mpg	-	-	C	0.15	NNE	1004_050.txt	-	-	-	-	04:45 passing rubble ice field
1004_036	1999-04-10	9:00:00	10:00:00	-	-	-	C	0.11	NNW	-	-	-	-	-	
		9:56:00	-	-	-	-	-	-	-	-	-	-	-	-	
1004_037	1999-04-10	10:00:00	11:00:00	-	-	-	C	-	NNW	-	-	-	-	-	
1004_038	1999-04-10	11:00:00	12:00:00	-	-	-	-	-	NNW	-	-	-	-	-	
		11:30:00	-	-	-	-	-	-	W	-	-	-	-	-	no loads on panels
		11:45:00	-	-	-	-	-	0.05	NW	-	-	-	-	-	
1004_039	1999-04-10	12:00:00	13:00:00	-	-	-	-	-	NNW	-	-	-	-	-	
		12:48:00	-	-	-	-	-	-	-	-	-	-	-	-	very slow ice movement; almost stopped
1004_040	1999-04-10	13:00:00	14:00:00	-	-	-	-	-	-	-	-	-	-	-	sampling frequency = 10Hz
		13:30:00	-	-	-	-	-	-	N	-	-	-	-	-	slow ice movement; load on panel 3; Foto of broken channel
		13:40:00	-	-	-	-	-	-	-	-	-	-	-	-	wind speed and ice drift speed is increasing
1004_041	1999-04-10	14:00:00	15:03:00	-			C	0.05	N	-	-	NE to E	-	-	sampling frequency = 10Hz
		14:23:00	-	-	-	-	-	-	-	-	-	-	-	-	passing a ridge; zero forces due to release crack; pile up on the lighthouse abt. 6m; see photos; see video camera 1+3; in data plot see 14:15 - 14:20
1004_042	1999-04-10	15:03:00	17:00:00	1004_110.mpg	-	-	B	0.05	N	1004_110.txt 1004_120.txt	-	-	-	-	due to pile up in front of lighthouse upward bending failure
		15:45:00	-	-	-	-	C	-	-	-	-	-	-	-	the grounded ice went off; pure crushing; two times great vibrations
		16:03:00	-	-	-	-	-	-	NE	-	-	-	-	-	very high vibrations; highest loads on panel 3;
1004_043	1999-04-10	17:00:00	18:16:00	-	-	-	-	-	NE	-	-	-	-	-	
		17:36:00	-	-	-	-	-	-	ENE	-	-	-		-	ice has stopped

a) Camera 1, 2 and 3, positions see illustraion above.
b) L = Level ice, H= Hummocked ice, R= Rigged ice
c) C= Crushing, B= Bending, S= Splitting
d) Temperature measured at Rödkallen by SMHI. Position 5 km from

Table 3 - Data for the 12th of April 1999. [TOP]

Event No.	Date	Load Meauring, time period		Video	Ice Thickness	Ice formation	Failure mode	Ice drift		Load data	Wind		Air temp.	Sampling rate	Remark
a	a	Start	End	a)	a	b)	c)	Speed	Direction	a	Speed	Direction	a	a	a
1204_061	1999-04-12	0:05:00	12:00:00						W					1	small forces on panel 6, no loads on panel 5 + 3
		0:33:00													first load on panel 5

		1:04:00													ice movement stopped
1204_062	1999-04-12	12:08:00	0:00:00											1	

a) Camera 1, 2 and 3, positions see illustraion above.
b) L = Level ice, H= Hummocked ice, R= Rigged ice
c) C= Crushing, B= Bending, S= Splitting
d) Temperature measured at Rödkallen by SMHI. Position 5 km from

Table 4 - Data for the 18th of April 1999. [TOP]

Event No.	Date	Load Meauring, time period		Video	Ice Thickness	Ice formation	Failure mode	Ice drift		Load data	Wind		Air temp.	Sampling rate	Remark
a	a	Start	End	a)	a	b)	c)	Speed	Direction	a	Speed	Direction	a	a	a
1804_120	1999-04-18	0:16:00	7:00:00	1804_100.mpg						1804_100.txt					unconfined ice condition; open water in the east of the lighthouse (see camera 1)
		0:24:00													cracks in front of panel 5
		0:30:00													broken ice in front of panel 5 + 6; open water in front of panel 3
		0:36:00			0.3 - 0.5m				NNE		5 - 8	NNE			weak ice
		1:00:00													static load; more or less no movement; unconfined condition
		1:12:00										NNE			wind seems to increase; one can hear that the ice is failing somewhere else but not at the lighthouse; maybe some rafting or ridging
		1:25:00											+0.4		ice situation is still the same
1804_121	1999-04-18	7:00:00	11:50:00					very small	ENE		8 - 10	NE	-0.4	10	very small movement; more or less static load condition; ice movement was from ENE the last 2 hours with crushing failure
		9:14:00									abt. 5	NE	+0.2		rain; no ice movement; no load on panels
		11:50:00													ice has moved backwards; no load on panels; open water all around the lighthouse; stopped measurement; took new zero
1804_122	1999-04-18	11:56:00	23:59:00								2 - 3	NE	+1.6	1	no ice movement; rain; snow and ice surface is melting
		13:50:00							ENE		3 - 5	NNE	+1.6		ice is coming back from ENE (see camera 1+2); fog
		15:50:00									5	NNE	+2.2		static load on all panels; highest load on panel 5; sunshine; see photos; see camera 1+ 2; see picture, 21+22
		17:00:00											+1.8		the same scenario; the same weather condition; a ridge is directed towards panel 3 (see photo #25) ; photo #23 + #24 show under water part of old location. pictures 23-25
		18:55:00									5 - 7	N	+2.6		the same scenario; wind speed is a little increasing; still static load condition
		20:00:00									3 - 5	N			ice is moving away from the lighthouse; no load on panels. Picture 26
		21:00:00													ice is drifting parallel to the lighthouse from east to west; no load on the panels
		21:06:00			abt. 0.5m	R			ENE		3 - 5	NNE			weak ice
		21:45:00													static load condition; laser scanner data every 5 min for 1 h (21:12 - 22:12)
		22:13:00					B								bending failure in the east
		22:50:00													ice movement from south to north; no load on panels

a) Camera 1, 2 and 3, positions see illustraion above.
b) L = Level ice, H= Hummocked ice, R= Rigged ice
c) C= Crushing, B= Bending, S= Splitting
d) Temperature measured at Rödkallen by SMHI. Position 5 km from

Database for Ice Measurements at Norströmsgrund 2000

Back to start page

General

The lighthouse was occupied for about 8 weeks. A team of 2 to 3 scientist, engineers and technicians controlled and maintained the instruments and carried out the measurements. The winter was a relative mild one. The measuring campaign could be divided into three phases:
- February 26th to March 5th; during this phase the ice drift direction was predominant from northern to eastern directions; at the end of February the water stage was so high, that the ice load acted at the cable protection channel and no real forces could be determined.
- March 6th to March 31st, this period was characterized by mostly floe ice, open water and new ice.
- April 1st to April 17th; ice drift direction varied from North to South; water stage was on a height that the ice forces were acting on the upper half of the panels; at the end of the period the ice already got rotten.

During the year the following equipment have been used:
- Load panels 1-7 and 9 (panel 9 = 8 segments), placed in the waterline. The panels are mounted to the lighthouse in such a way, that they are facing the drift ice coming from the open sea. Dimensions of the panels are 1.2×1.6 m (four loads cells in the corners per panel). *Note*: Panel 3 was frozen and did not give correct loads.
- The panels covered approximately 144 degrees and the direction of ice-attack was from NNW to ESE.
- Three video cameras were used to record the movement of the ice
- The ice drift speed and direction was determined by manual image analysis of the video pictures. A 10x10m grid was marked on the ice, recorded and painted on the video screen. Ice drift speed and direction was determined by following single significant ice features passing the grid lines. A mean speed value was calculated from observed distance and measured time.
- Air Temperature: the sensor of a digital thermometer was installed in the North at the outside wall of the level at a height of about 20m above sea level. The display of this sensor was located in the measuring room of the lighthouse.
- Wind speed and direction: A wind speed and direction indicator was installed at the helicopter deck of the lighthouse about 28 m above sea level. The display of this sensor was located in the measuring room of the lighthouse.

Notations in the data files:
- SumPan1 = The sum of the load from all load cells in each panel (kN).
- Panel 91 = The load for the individual load cells for panel 9, in this case for load cell 1 (of eight). SumPan9 is the total sum for panel 91 to panel 98.
- In a second step the resultant force acting on the lighthouse was computed from the individual total forces of the panels. Because the panels are measuring the normal forces only, these were split into there components referring to a fixed N – E co-ordination system of the lighthouse. Forces induced by ice movement from North towards South, Fx, and East towards West, Fy, are defined positive.

Metrological Data

Meteorological data, Loleif_2000_environmental_data.xls, were manually sampled, documented in the log-book. Frequency distribution calculations were performed on wind speed and direction as well as ice drift speed and direction.
- air temperature, select: Air_Temperature_Time_Series_Winter_2000.jpg
- wind speed: Wind_Speed_Histogram_Winter_2000.jpg, Wind_Speed_Time_Series_Winter_2000.jpg
- wind direction: Wind_Direction_Histogram_Winter_2000.jpg, Wind_Direction_Time_Series_Winter_2000.jpg, Wind2000_Polar.jpg
- ice drift speed: Ice_Drift_Speed_Histogram_Winter_2000.jpg, Ice_Drift_Speed_Time_Series_Winter_2000.jpg,
- ice drift direction: Ice_Drift_Direction_Histogram_Winter_2000.jpg, Ice2000_Polar.jpg
- water stage: Water_Stage_Time_Series_Winter_2000.jpg

Ice charts

The following ice charts are available for the time period:
- ice000222.pdf
- ice000301.pdf
- ice000307.pdf
- ice000403.pdf
- ice000410.pdf
- ice000424.pdf
- ice000428.pdf

Ice thickness

As described earlier, the ice thickness was determined by:
- an echo sounder system located in 6-7 m water depth on the caisson of the lighthouse profiling the subsurface of the ice.
- an electromagnetic device and a laser distance meter profiling the surface and the subsurface of the ice.

In case of level ice, rafted ice and refrozen broken ice the results of both systems were in good agreement. For hummock ice and pressure ridges the sonar system gives the real subsurface of the ice, consolidated and unconsolidated part, while the ice thickness shown by the EM-device is presenting a value which is less then the subsurface determined by the echo sounder but larger then the consolidated layer.

- EM measurements 2000
- Sonar measurements 2000

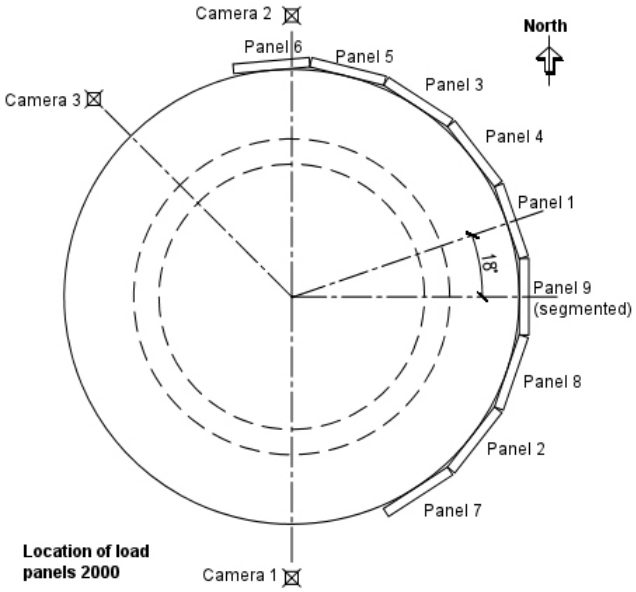

Illustration showing the location of load panels mounted on the lighthouse.

Ice Compressive strength

One set of uniaxial compressive strength tests were performed on a test frame which was brought to the lighthouse by LTU. The tests were carried out directly after sampling the ice at an air temperature close to 0°C. Ten specimen were tested, eight having the load applied perpendicular to the growth direction and two specimen were tested with applied load parallel to the growth direction. The ice temperature of the specimen was near the melting point at about –0.2 °C. The average strain rate during the tests was about 2 x 10-4 s-1 . In Ice_mech_prop_2000.xls the results of these tests are compiled together with the specimen geometry, the loading direction and the sampling section.

Pictures have been taken the following dates:

- 2000-03-03 - 2000-03-20 - 2000-03-26 - 2000-03-31 - 2000-04-05
- 2000-03-15 - 2000-03-21 - 2000-03-27 - 2000-04-01
- 2000-03-17 - 2000-03-23 - 2000-03-29 - 2000-04-02
- 2000-03-18 - 2000-03-25 - 2000-03-30 - 2000-04-03

Measured data during the year 2000 has been compiled for the following dates:

Table 1 - Data for the 1st of March
Table 2 - Data for the 3rd of March
Table 3 - Data for the 4th of March
Table 4 - Data for the 5th of March
Table 5 - Data for the 6th of March
Table 6 - Data for the 7th of March
Table 7 - Data for the 16th of March
Table 8 - Data for the 18th of March
Table 9 - Data for the 26th of March
Table 10 - Data for the 31st of March
Table 11 - Data for the 1st of April
Table 12 - Data for the 3rd of April
Table 13 - Data for the 4th of April
Table 14 - Data for the 5th of April
Table 15 - Data for the 12th of April
Table 16 - Data for the 13th of April
Table 17 - Data for the 14th of April
Table 18 - Data for the 17th of April

Table 1 - Data for the 1st of March. [TOP]

Event No.	Date	Load Meauring, time period		Ice Thickness	Ice formation	Failure mode	Ice drift		Load data	Video	Wind		Air temp.	Sampling rate	Remark
	a	Start	End		b)	c)	Speed	Direction		a)	Speed	Direction			
0103_0010	2000-03-01	5:00:00	10:40:00	-	-	-	-	-	01030500.txt	-	-	-	-8.0	-	Data file Sonar: 00301, Data file EM: 000301, Data file Laser: 01032000
	2000-03-01	5:07:00	-	0.50	CP	C	0.10	NE	-	-	-	-	-	-	water stage has dropped a little, all panels are showing forces
	2000-03-01	8:00:00	-	-	FI	-	-	-	-	-	-	E	-6.0	-	wind direction changed to E (very weak); end of closed pack ice; now floe ice
	2000-03-01	9:45:00	-	-	-	-	0.11	SE	-	-	4	E	-5.4	-	ice drift direction has changed to SE, snowfall
	2000-03-01	10:00:00	-	-	-	-	-	S	-	-	-	-	-	-	ice drift direction is from south to north

	2000-03-01	10:40:00	-	-	-	-	-	SW	-	-	-	-	-0.4	-	ice drift direction is now from SW to NE; no load on panels; stopped force, em + laser measurements
	2000-03-01	17:46:00	21:30:00	-	-	C	0.15	NNE	01031746	-	9	N	-10.0	-	started new measurement; still high water level; zero for sonar abt. 7.1m; zero for laser abt. 26m; drifting snow
	2000-03-01	21:20:00	-	0.45	-	C	0.20	ENE	-	-	-	-	-11.2	-	-
0103_0030	2000-03-01	21:30:00	0:00:00	-	-	-	-	-	01032130.txt	0103_0030.mpg	-	-	-	30	started new measurement.
	2000-03-01	23:52:00	-	-	OW	-	-	-	-	-	-	-	-	-	water level measured by sonar 7.02 m during open water phase

a) Camera 1, 2 and 3, positions see illustraion above.
b) L = Level ice, H= Hummocked ice, R= Ridged ice, CP= Closed pack, FI= Floe ice, OW= Open water, BI=Broken ice, TNI= Thin new ice, FR= Finger raftning, TI=Thin ice, RI= Refrozen ice, LF=Large floes, UI= Uniform ice, U=Unconfined, RC= Release crack, NI= New ice, PU=Pile up, G= Grounded, TLI= thin level ice, RFI=Refrozen broken ice, OC= Open channel
c) C= Crushing, B= Bending, S= Splitting, SL=Static load, M=Mixed, BU= buckling, CR=Creep
d) Temperature measured at Rödkallen by SMHI. Position 5 km from

Table 2 - Data for the 3rd of March. [TOP]

Event No.	Date	Load Meauring, time period		Ice Thickness	Ice formation	Failure mode	Ice drift		Load data	Video	Wind		Air temp.	Sampling rate	Remark
	a	Start	End		b)	c)	Speed	Direction		a)	Speed	Direction	a	a	
	2000-03-03	7:50:00	-	-	OW	-	-	-	-	-	9	W	-8.6	-	Data file Sonar: 00303, Data file EM: 000303, Data file Laser: 03032000
	2000-03-03	12:20:00	-	-	-	-	-	S	-	-	-	-	-7.0	-	ice movement from South, very slow speed; no wind, sunshine; installed addional pipes at EM-frame
	2000-03-03	12:30:00	16:10:00	-	-	B + BU	-	-	-	-	-	-	-	1	started longterm measurement; started laser + sonar; water level is abt. top of the panel; bending + buckling failure, see camera 1+2
	2000-03-03	13:00:00	-	-	-	-	-	-	-	-	-	-	-	-	started EM-Measurements
	2000-03-03	13:12:00	-	-	-	-	-	-	-	-	-	-	-	-	throw a marker onto the ice for speed determination; took 4 photos, 2-8 to 2-11
0303_0020	2000-03-03	16:10:00	20:23:00	-	-	-	-	E	0303_020.txt	0303_0021.mpg 0303_0022.mpg	-	-	-	-	started new measurement;
	2000-03-03	16:35:00	-	-	R	-	-	-	-	-	6	E	-	-	ridging in the East infront of the lighthouse, 2-12
	2000-03-03	18:35:00	-	0.35	-	-	0.20	E	-	0303_0023_24_25.mpg	13	E	-9.2	-	-
	2000-03-03	18:50:00	-	0.35	-	C	0.17	E	-	0303_0023_24_25.mpg	-	-	-	-	-
0303_0040	2000-03-03	20:23:00	1:31:00	0.38	-	-	0.20	E	03032023.txt	0303_0041.mpg 0303_0042.mpg	-	-	-9.6	-	started new measurement;

a) Camera 1, 2 and 3, positions see illustraion above.
b) L = Level ice, H= Hummocked ice, R= Ridged ice, CP= Closed pack, FI= Floe ice, OW= Open water, BI=Broken ice, TNI= Thin new ice, FR= Finger raftning, TI=Thin ice, RI= Refrozen ice, LF=Large floes, UI= Uniform ice, U=Unconfined, RC= Release crack, NI= New ice, PU=Pile up, G= Grounded, TLI= thin level ice, RFI=Refrozen broken ice, OC= Open channel
c) C= Crushing, B= Bending, S= Splitting, SL=Static load, M=Mixed, BU= buckling, CR=Creep
d) Temperature measured at Rödkallen by SMHI. Position 5 km from

Table 3 - Data for the 4th of March. [TOP]

Event No.	Date	Load Meauring, time period		Ice Thickness	Ice formation	Failure mode	Ice drift		Load data	Video	Wind		Air temp.	Sampling rate	Remark
	a	Start	End	a	b)	c)	Speed	Direction		a)	Speed	Direction	a	a	a
	2000-03-04	1:31:00	7:55:00	-	-	-	-	NE	-	-	-	-	-9.6	-	Data file laser: 04032000, data file sonar: 00304, data file EM: 000304. started new measurement
	2000-03-04	1:48:00	-	-	-	-	0.30	-	-	-	-	-	-	-	-
	2000-03-04	1:55:00	-	-	-	-	-	-	-	-	15	N	-	-	snowfall
	2000-03-04	1:57:00	-	-	-	-	-	-	-	-	-	-	-	-	zero for sonar abt. 7m
	2000-03-04	2:00:00	-	-	-	-	-	-	-	-	-	-	-	-	rafting at lighthouse, several layer
	2000-03-04	7:55:00	-	-	-	-	-	-	-	-	-	-	-	-	stopped measurement
	2000-03-04	10:56:00	-	-	-	-	-	NE	-	-	15	N	-7.6	-	alldata back up; still only slush and pancake ice, no forces on panels, sonar, laser +

															em are recording, no load recording
	2000-03-04	12:30:00	-	-	-	-	-	-	-	-	-	-	-	-	zero for sonar 6.7m ??
0403_0020	2000-03-04	13:47:00	15:45:00	-	TNI	C	0.3	NE	0403_020.txt	-	18	N	-5.8	10	started new measurement; very weak ice
	2000-03-04	15:45:00	-	-	-	-	-	-	-	--	20	N	-	-	stopped force reording; to much open water, no ice
	2000-03-04	21:43:00	-	-	-	-	-	-	-	-	-	-	-	-	stopped TL-recording
	2000-03-04	21:45:00	-	-	-	-	-	NE	-	-	20	N	-	-	started TL-recording 72h mode; only broken ice floes and slush ice; no forces are recorded
	2000-03-04	23:10:00	-	-	OW	-	-	-	-	-	-	-	-	-	zero for sonar abt. 6.6m ??
	2000-03-04	23:20:00	8:00:00	-	-	-	-	-	-	-	-	-	-	10	started new force recording

a) Camera 1, 2 and 3, positions see illustraion above.
b) L = Level ice, H= Hummocked ice, R= Ridged ice, CP= Closed pack, FI= Floe ice, OW= Open water, BI=Broken ice, TNI= Thin new ice, FR= Finger raftning, TI=Thin ice, RI= Refrozen ice, LF=Large floes, UI= Uniform ice, U=Unconfined, RC= Release crack, NI= New ice, PU=Pile up, G= Grounded, TLI= thin level ice, RFI=Refrozen broken ice, OC= Open channel
c) C= Crushing, B= Bending, S= Splitting, SL=Static load, M=Mixed, BU= buckling, CR=Creep
d) Temperature measured at Rödkallen by SMHI. Position 5 km from

Table 4 - Data for the 5th of March. [TOP]

Event No.	Date	Load Meauring, time period		Ice Thickness	Ice formation	Failure mode	Ice drift		Load data	Video	Wind		Air temp.	Sampling rate	Remark
	a	Start	End	a	b)	c)	Speed	Direction		a)	Speed	Direction	a	a	a
0503_0010	2000-03-05	0:26:00	-	-	TI	-	-	NE	0503_010.txt	-	20	N	-7.8	10	thin ice, breaking into floes at the lighthouse. Data file Sonar: 00305, Data file EM: 000305, Data file Laser: 05032000
	2000-03-05	0:29:00	-	-	-	C	0.30	-	-	-	-	-	-	-	crushing at panel 5+6 in the north, open lead in the east
	2000-03-05	0:47:00	-	-	-	C	-	-	-	-	-	-	-	-	no real confinement, ice floes are beaking into parts at the lighthouse
	2000-03-05	0:52:00	-	0.40	-	C	0.30	NE	-	0503_0011.mpg	-	-	-	-	confined condition
	2000-03-05	1:17:00	-	-	-	-	0.30	NE	-	0503_0011.mpg	-	-	-	-	-
	2000-03-05	5:15:00	-	-	-	-	0.40	NE	-	0503_0013.mpg	-	-	-	-	-
	2000-03-05	5:30:00	-	-	-	-	-	-	-	0503_0013.mpg	-	-	-	-	Lulea water level = -20
	2000-03-05	8:00:00	-	-	BI	-	-	E	-	-	18	N	-9.0	-	stopped force reording, no forces, only broken ice
	2000-03-05	8:15:00	11:12:00	-	NI	-	0.40	NE	-	-	-	-	-	10	started new force recording
	2000-03-05	8:21:00	-	0.05	FR	-	-	-	-	-	-	-	-	-	-
	2000-03-05	8:24:00	-	-	-	-	-	-	-	-	-	-	-	-	stopped em-measurement
	2000-03-05	8:35:00	-	-	-	-	-	-	-	-	-	-	-	-	started new em-recording, short open water period zero sonar abt. 6.7m
	2000-03-05	8:39:00	-	-	H	-	0.35	NE	-	-	-	-	-	-	less confinement
	2000-03-05	11:12:00	-	-	OW	-	-	-	-	-	-	-	-	-	stopped force recording; open water around the lighthouse; took new zero nu050300.sp8
	2000-03-05	12:17:00	13:24:00	-	-	-	-	-	05031217.txt	-	-	-	-	-	start force measurement
	2000-03-05	13:24:00	-	-	-	-	-	-	-	-	-	-	-	-	stopped force measurement
	2000-03-05	13:49:00	-	-	OW	-	-	-	-	-	-	-	-	-	sonar zero = 6.75 m
	2000-03-05	15:37:00	16:49:00	-	-	-	-	-	-	-	-	-	-	-	start force measurement
	2000-03-05	16:49:00	-	-	OW	-	-	-	-	-	-	-	-	-	stopped force measurement; sonar zero = 6.76 m
	2000-03-05	19:00:00	23:42:00	-	-	-	0.30	NE	-	-	10	NE	-7.6	10	start force measurement
	2000-03-05	23:42:00	-	-	-	-	-	-	-	-	-	-	-	-	stopped force measurement

	2000-03-05	23:47:00	8:47:00	-	FI	-	v	-	-	-	-	NE	-9.4	-	Start force measurement; low winds; sonar zero = 6.79, Lulea water stage = +4

a) Camera 1, 2 and 3, positions see illustraion above.
b) L = Level ice, H= Hummocked ice, R= Ridged ice, CP= Closed pack, FI= Floe ice, OW= Open water, BI=Broken ice, TNI= Thin new ice, FR= Finger raftning, TI=Thin ice, RI= Refrozen ice, LF=Large floes, UI= Uniform ice, U=Unconfined, RC= Release crack, NI= New ice, PU=Pile up, G= Grounded, TLI= thin level ice, RFI=Refrozen broken ice, OC= Open channel
c) C= Crushing, B= Bending, S= Splitting, SL=Static load, M=Mixed, BU= buckling, CR=Creep
d) Temperature measured at Rödkallen by SMHI. Position 5 km from

Table 5 - Data for the 6th of March. [TOP]

Event No.	Date	Load Meauring, time period		Ice Thickness	Ice formation	Failure mode	Ice drift		Load data	Video	Wind		Air temp.	Sampling rate	Remark
	a	Start	End	a	b)	c)	Speed	Direction		a)	Speed	Direction	a	a	a
	2000-03-06	8:47:00	-	-	NI	-	-	SSW	-	-	10	S	-10.6	-	Data file laser: 06032000, data file sonar: 00306, data file EM:000306. stopped all measurements, backup data;
	2000-03-06	12:22:00	-	-	OW	-	-	-	-	-	13	S	-	-	sonar zero = 7.10 m, Lulea water stage = +37
	2000-03-06	13:40:00	-	-	-	-	-	S	-	-	13	S	-	-	started laser+EM measurement; pnly panel 7+2 catch very low forces; snow
	2000-03-06	13:45:00	16:00:00	-	-	-	0.30	SSE	06031345.txt	-	-	-	-	10	started force measurement
	2000-03-06	14:40:00	-	-	-	-	0.20	SSE	-	-	-	-	-	-	-
	2000-03-06	15:18:00	-	-	-	-	0.20	SSE	-	-	-	-	-	-	-
	2000-03-06	15:50:00	-	-	-	-	0.22	S	-	-	-	-	-	-	-
	2000-03-06	16:00:00	18:54:00	-	-	-	-	-	06031600.txt	-	-	-	-	30	started force measurement
	2000-03-06	17:10:00	-	-	-	-	0.16	ESE	-	-	13	S	-8.6	-	-
	2000-03-06	18:16:00	-	-	H	-	0.17	SSE	-	-	-	-	-	-	loghthouse is vibrating
	2000-03-06	18:20:00	-	-	-	-	-	-	-	-	-	-	-	-	EM stopped with runtime error, saved data and restarted
	2000-03-06	18:34:00	-	-	-	-	0.10	SE	-	-	-	-	-	-	-
	2000-03-06	18:40:00	-	-	-	-	0.10	-	-	-	-	-	-	-	-
	2000-03-06	18:50:00	-	-	PU	-	-	-	-	-	9	S	-8.2	-	grounded ice pile up in the south, see camera 2; ridge is grounded at sonar too; no forces on panels; ice is going threw the pile not on top of the pile. Pictures 15, 16, 17.
	2000-03-06	18:54:00	-	-	-	-	-	-	-	-	-	-	-	-	stopped force measurement
	2000-03-06	19:00:00	19:59:00	-	-	BU	-	S	06031900.txt	-	-	-	-	-	started new force measurement; buckling infront of the pile
	2000-03-06	19:08:00	-	-	-	-	-	-	-	-	-	-	-	-	-
	2000-03-06	19:18:00	-	-	-	-	-	-	-	-	-	-	-	-	ice wedge disappeares; Lulea water stage = +59
	2000-03-06	19:24:00	-	-	-	-	-	-	-	-	-	-	-	-	part of the grounded ice wedge is still in place
	2000-03-06	19:28:00	-	-	-	-	0.06	ESE	-	-	-	-	-	-	-
	2000-03-06	19:35:00	-	-	H	-	0.06	SE	-	-	7	S	-8.6	-	-
	2000-03-06	19:46:00	-	0.30	L	-	-	-	-	-	-	-	-	-	-
	2000-03-06	19:57:00	-	-	-	-	0.10	SE	-	-	-	-	-	-	-
	2000-03-06	20:00:00	20:57:00	-	-	-	-	-	06032000.txt	-	-	-	-	10	started new force recording
	2000-03-06	20:06:00	-	-	-	-	0.05	-	-	-	-	-	-	-	-
	2000-03-06	20:42:00	-	-	-	-	-	-	-	-	-	-	-	-	ice movement stopped
	2000-03-06	20:54:00	-	-	-	-	-	E	-	-	-	-	-	-	very small drift speed, almost static load condition

	2000-03-06	21:00:00	6:33:00	-	-	-	-	-	-	-	-	-	-	1	started longterm force recording

a) Camera 1, 2 and 3, positions see illustraion above.
b) L = Level ice, H= Hummocked ice, R= Ridged ice, CP= Closed pack, FI= Floe ice, OW= Open water, BI=Broken ice, TNI= Thin new ice, FR= Finger raftning, TI=Thin ice, RI= Refrozen ice, LF=Large floes, UI= Uniform ice, U=Unconfined, RC= Release crack, NI= New ice, PU=Pile up, G= Grounded, TLI= thin level ice, RFI=Refrozen broken ice, OC= Open channel
c) C= Crushing, B= Bending, S= Splitting, SL=Static load, M=Mixed, BU= buckling, CR=Creep
d) Temperature measured at Rödkallen by SMHI. Position 5 km from

Table 6 - Data for the 7th of March. [TOP]

Event No.	Date	Load Meauring, time period		Ice Thickness	Ice formation	Failure mode	Ice drift		Load data	Video	Wind		Air temp.	Sampling rate	Remark
	a	Start	End	a	b)	c)	Speed	Direction		a)	Speed	Direction	a	a	a
	2000-03-07	6:33:00	9:00:00	-	-	C	0.10	NE	07030633.txt	-	9	N	-9.6	30	Data file laser: 07032000, data file sonar: 00307, data file EM: 000307.start new force recording
	2000-03-07	6:48:00	-	-	-	-	0.11	NE	-	-	-	-	-	-	-
	2000-03-07	7:15:00	-	-	-	-	-	-	-	-	-	-	-	-	Lulea water stage = +53
	2000-03-07	8:25:00	-	-	R	-	-	-	-	-	-	-	-11.8	-	-
	2000-03-07	9:00:00	11:07:00	-	-	-	0.15	NNE	07030900.txt	-	-	-	-12.2	30	start new force recording
	2000-03-07	9:10:00	-	-	H	-	0.15	N	-	-	7	N	-	-	hummocked ice
	2000-03-07	10:36:00	-	-	R	-	-	NE	-	-	-	-	-	-	problem with load cell 3 of panel 1; passing a ridge
	2000-03-07	10:45:00	-	-	G	-	0.20	N	-	-	10	N	-10.4	-	sunshine; grounded ice wedge in the north. Pictures: 20 - 24
	2000-03-07	11:07:00	13:45:00	-	G	-	0.26	N	07031107.txt	-	11	N	-	30	start new force recording; Lulea water stage is +45; still ice wedge in the North
	2000-03-07	11:55:00	-	-	-	-	0.20	N	-	-	-	-	-	-	problem with load cell 3 of panel 1 solved,
	2000-03-07	12:30:00	-	-	RC	-	-	-	-	-	-	-	-	-	EM-Computer restarted after shut down; one file has length 0; release crack in the north
	2000-03-07	13:45:00	-	-	-	-	-	-	-	-	-	-	-	-	stopped measurement; very thin ice is coming; start installation of acc. and inc.
	2000-03-07	17:15:00	-	-	-	-	-	-	-	-	-	-	-	-	restarted laser and sonar collection, sonar reading 7.12 m facing thin ice
	2000-03-07	18:20:00	-	-	-	-	-	-	-	-	-	-	-	-	acc. and inc. are connected
	2000-03-07	19:38:00	20:00:00	-	-	-	-	N	-	-	-	-	-	-	start new force recording, now with acc. + inc. (Test)
	2000-03-07	20:00:00	21:00:00	-	-	-	0.15	NNW	-	-	13	W	-	30	start new force recording
	2000-03-07	21:18:00	-	-	-	-	-	-	-	-	-	-	-10.0	-	-
	2000-03-07	21:00:00	22:40:00	-	-	-	-	W	-	-	-	-	-	10	start new force recording
	2000-03-07	22:40:00	-	-	-	-	-	W	-	-	-	-	-	-	stop force measurement

a) Camera 1, 2 and 3, positions see illustraion above.
b) L = Level ice, H= Hummocked ice, R= Ridged ice, CP= Closed pack, FI= Floe ice, OW= Open water, BI=Broken ice, TNI= Thin new ice, FR= Finger raftning, TI=Thin ice, RI= Refrozen ice, LF=Large floes, UI= Uniform ice, U=Unconfined, RC= Release crack, NI= New ice, PU=Pile up, G= Grounded, TLI= thin level ice, RFI=Refrozen broken ice, OC= Open channel
c) C= Crushing, B= Bending, S= Splitting, SL=Static load, M=Mixed, BU= buckling, CR=Creep
d) Temperature measured at Rödkallen by SMHI. Position 5 km from

Table 7 - Data for the 16th of March. [TOP]

Event No.	Date	Load Meauring, time period		Ice Thickness	Ice formation	Failure mode	Ice drift		Load data	Video	Wind		Air temp.	Sampling rate	Remark
	a	Start	End	a	b)	c)	Speed	Direction		a)	Speed	Direction	a	a	a
	2000-03-16	8:34:00	-	0.10	TLI	-	-	NW	-	-	6	NE	-7.0	-	Data file laser: 16032000, data file sonar; 00316.measured water level = 23 cm below top of the panel
	2000-03-16	8:52:00	12:02:00	-	-	-	-	-	-	-	-	-	-	-	started new force recording

	2000-03-16	10:50:00	-	0.10	-	B	0.01	ENE	-	-	6	NNW	-	-	-
	2000-03-16	11:07:00	-	-	-	-	-	-	-	-	-	-	-	-	-
	2000-03-16	12:02:00	15:06:00	-	-	CR	-	-	-	-	-	-	-	1	started long term measurement
	2000-03-16	12:07:00	-	-	-	-	-	-	-	-	4	NNW	-4.2	-	-
	2000-03-16	15:06:00	-	-	-	-	-	-	-	-	-	-	-	-	stopped force recording; nothing was happening during the last 2 hours
	2000-03-16	18:00:00	-	-	-	-	-	NE	-	-	6	N	-3.2	-	ice starts to move from N ---> S
	2000-03-16	18:20:00	21:05:00	-	-	-	-	-	-	-	-	-	-	1	started long term measurement
	2000-03-16	19:40:00	-	-	-	B	-	E	-	-	6	N	-3.6	-	very slow ice drift speed; almost static load condition
	2000-03-16	21:05:00	21:57:00	-	-	B	0.01	E	-	-	-	-	-5.4	30	started new force recording
	2000-03-16	21:17:00	-	-	-	-	-	-	-	-	6	NNW	-	-	water level abt. 30 cm below top of the panels
	2000-03-16	21:57:00	-	-	-	-	-	-	-	-	-	-	-	-	stopped force recording
1603_0050	2000-03-16	22:00:00	-	-	-	-	-	-	-	-	-	-	-	1	started long term measurement
	2000-03-16	22:29:00	-	0.10	-	B	0.04	E	-	-	-	-	-	-	weak ice

a) Camera 1, 2 and 3, positions see illustraion above.
b) L = Level ice, H= Hummocked ice, R= Ridged ice, CP= Closed pack, FI= Floe ice, OW= Open water, BI=Broken ice, TNI= Thin new ice, FR= Finger raftning, TI=Thin ice, RI= Refrozen ice, LF=Large floes, UI= Uniform ice, U=Unconfined, RC= Release crack, NI= New ice, PU=Pile up, G= Grounded, TLI= thin level ice, RFI=Refrozen broken ice, OC= Open channel
c) C= Crushing, B= Bending, S= Splitting, SL=Static load, M=Mixed, BU= buckling, CR=Creep
d) Temperature measured at Rödkallen by SMHI. Position 5 km from

Table 8 - Data for the 18th of March. [TOP]

Event No.	Date	Load Meauring, time period		Ice Thickness	Ice formation	Failure mode	Ice drift		Load data	Video	Wind		Air temp.	Sampling rate	Remark
	a	Start	End	a	b)	c)	Speed	Direction		a)	Speed	Direction	a	a	a
	2000-03-18	0:00:00	8:00:00	-	-	-	-	-	-	-	-	-	-	-	Data file laser: 18032000, data file sonar: 00318, data file EM: 000318.
	2000-03-18	8:00:00	-	-	BI	-	-	SSW	-	-	-	-	-3.6	-	stop force recording
	2000-03-18	9:25:00	-	-	BI	-	-	S	-	-	6	S	-3.6	-	-
	2000-03-18	15:07:00	17:20:00	-	-	-	-	-	18031508.txt	-	-	-	-	10	start new force recording
	2000-03-18	15:20:00	-	-	-	-	-	-	-	-	-	-	-	-	water level abt. 18 cm below top of the panels
	2000-03-18	17:20:00	20:27:00	-	-	-	0.12	NE	18031720.txt	-	6	N	-	10	start new force recording; unconfined condition; lot of open water patches; cracks are running towards open water patches
	2000-03-18	17:40:00	-	-	-	-	-	-	-	-	-	-	-	-	open water at sonar; reading = 6.98
	2000-03-18	17:45:00	-	-	-	-	-	-	-	-	-	-	-	-	stop TL-recording
	2000-03-18	17:48:00	-	-	-	-	-	-	-	-	-	-	-	-	start TL-recording; em reading over open water = 2.7 m
	2000-03-18	18:05:00	-	0.18	L	B	-	NE	-	-	-	-	-	-	-
	2000-03-18	18:25:00	-	0.15	-	-	0.08	-	-	-	-	-	-	-	-
	2000-03-18	18:57:00	-	0.15	-	B	0.09	ENE	-	-	-	-	-	-	weak ice
	2000-03-18	19:10:00	-	0.15	-	-	0.09	ENE	-	-	5	N	-6.8	-	-
	2000-03-18	20:27:00	-	0.16	-	B	-	-	-	-	-	-	-	-	very slow ice movement; creeping; stopped force recording for data back up
	2000-03-18	23:45:00	-	-	OW	-	-	-	-	-	-	-	-	-	sonar reading = 6.96; em reading = 2.91

a) Camera 1, 2 and 3, positions see illustraion above.
b) L = Level ice, H= Hummocked ice, R= Ridged ice, CP= Closed pack, FI= Floe ice, OW= Open water, BI=Broken ice, TNI= Thin new ice, FR= Finger raftning, TI=Thin ice, RI= Refrozen ice, LF=Large floes, UI= Uniform ice, U=Unconfined, RC= Release crack, NI= New ice, PU=Pile up, G= Grounded, TLI= thin level ice, RFI=Refrozen broken ice, OC= Open channel
c) C= Crushing, B= Bending, S= Splitting, SL=Static load, M=Mixed, BU= buckling, CR=Creep
d) Temperature measured at Rödkallen by SMHI. Position 5 km from

Table 9 - Data for the 26th of March. [TOP]

Event No.	Date	Load Meauring, time period		Ice Thickness	Ice formation	Failure mode	Ice drift		Load data	Video	Wind		Air temp.	Sampling rate	Remark
	a	Start	End	a	b)	c)	Speed	Direction		a)	Speed	Direction	a	a	a
	2000-03-26	3:05:00	-	-	-	-	-	-	-	-	-	-	-	-	Data file laser: 26032000,data file sonar: 00326, data file EM: 000326. stop and restart em system
	2000-03-26	4:05:00	-	-	-	-	-	-	-	-	-	-	-	-	time change, summer time, was done automatically for force recording; all other systems will be set manually
	2000-03-26	8:54:00	-	-	-	-	-	-	-	-	-	-	-	-	stop and restart em system
	2000-03-26	8:55:00	-	-	-	-	-	-	-	-	-	-	-	-	stop force recording
2603_0020	2000-03-26	8:58:00	15:00:00	-	RFI	-	-	NE	-	-	7	N	-	1	start new force recording
	2000-03-26	12:30:00	-	-	-	-	-	-	-	-	-	-	-	-	em system failed
	2000-03-26	15:00:00	-	-	-	-	-	-	-	-	-	-	-	-	stop all recordings
	2000-03-26	15:05:00	18:57:00	-	-	-	-	-	-	-	-	-	-	-	start all systems; all clocks now on summertime; ecxept sonar and TL-video
	2000-03-26	15:24:00	-	-	-	-	-	-	-	-	-	-	-	-	em system failed
	2000-03-26	18:57:00	-	-	OW	-	-	-	-	-	3	W	-3.4	1	start new ice force recording
	2000-03-26	21:56:00	4:06:00	-	-	-	W	-	-	-	-	-	-	-	-

a) Camera 1, 2 and 3, positions see illustraion above.
b) L = Level ice, H= Hummocked ice, R= Ridged ice, CP= Closed pack, FI= Floe ice, OW= Open water, BI=Broken ice, TNI= Thin new ice, FR= Finger raftning, TI=Thin ice, RI= Refrozen ice, LF=Large floes, UI= Uniform ice, U=Unconfined, RC= Release crack, NI= New ice, PU=Pile up, G= Grounded, TLI= thin level ice, RFI=Refrozen broken ice, OC= Open channel
c) C= Crushing, B= Bending, S= Splitting, SL=Static load, M=Mixed, BU= buckling, CR=Creep
d) Temperature measured at Rödkallen by SMHI. Position 5 km from d) Temperature measured at Rödkallen by SMHI. Position 5 km from

Table 10 - Data for the 31st of March. [TOP]

Event No.	Date	Load Meauring, time period		Ice Thickness	Ice formation	Failure mode	Ice drift		Load data	Video	Wind		Air temp.	Sampling rate	Remark
	a	Start	End	a	b)	c)	Speed	Direction		a)	Speed	Direction	a	a	a
	2000-03-31	0:01:00	-	-	-	-	-	NNE	-	-	10	NW	2.6	10	Data file laser: 31032000, data file sonar: 00331. start new force recording
	2000-03-31	9:39:00	20:25:00	-	-	-	-	ENE	-	-	4	NE	-2.2	10	start new force recording
	2000-03-31	11:28:00	-	-	-	-	0.06	E	-	-	3	E	-2.0	-	-
	2000-03-31	13:03:00	-	-	-	-	-	ESE	-	-	-	-	1.6	-	calm wind
	2000-03-31	18:32:00	-	-	-	-	-	-	-	-	-	-	-	-	new tape in TL-recorder
	2000-03-31	20:25:00	-	-	-	-	-	-	-	-	-	-	-	-	stop force recording
3103_0030	2000-03-31	20:32:00	0:00:00	-	-	-	-	-	3103_030.txt	-	-	-	-	-	-
	2000-03-31	23:05:00	-	-	-	-	-	-	-	-	-	-	-	-	snowfall

a) Camera 1, 2 and 3, positions see illustraion above.
b) L = Level ice, H= Hummocked ice, R= Ridged ice, CP= Closed pack, FI= Floe ice, OW= Open water, BI=Broken ice, TNI= Thin new ice, FR= Finger raftning, TI=Thin ice, RI= Refrozen ice, LF=Large floes, UI= Uniform ice, U=Unconfined, RC= Release crack, NI= New ice, PU=Pile up, G= Grounded, TLI= thin level ice, RFI=Refrozen broken ice, OC= Open channel
c) C= Crushing, B= Bending, S= Splitting, SL=Static load, M=Mixed, BU= buckling, CR=Creep
d) Temperature measured at Rödkallen by SMHI. Position 5 km from

Table 11 - Data for the 1st of April. [TOP]

Event No.	Date	Load Meauring, time period		Ice Thickness	Ice formation	Failure mode	Ice drift		Load data	Video	Wind		Air temp.	Sampling rate	Remark
	a	Start	End	a	b)	c)	Speed	Direction		a)	Speed	Direction	a	a	a
0104_0010	2000-04-01	0:00:00	07:15	-	-	-	-	-	-	-	-	-	-	-	Data file sonar:00401.asc , data file Laser: 01042000

	2000-04-01	1:00:00	-	-	-	-	-	-	-	-	-	-	-	-	Laser scanner restarted after overflow error; strong vibrations
0104_0020	2000-04-01	7:15:00	10:49:00	-	-	-	-	-	0104_020.txt	-	-	-	-	10	start new force recording
	2000-04-01	7:53:00	-	-	RI	-	-	NNE	-	-	13.0	N	-6.2	-	refrozen broken ice + channel; small ridges incorporated
	2000-04-01	8:57:00	-	-	-	-	0.3	NE	-	-	13.1	N	-	-	camera 3 is pointing towards North
	2000-04-01	10:15:00	-	-	-	-	-	-	-	-	-	-	-	-	started real time video
0104_0030	2000-04-01	10:49:00	12:15:00	0.13	-	-	-	-	0104_030.txt	-	13.9	NNE	-7.8	100	started new force recording; ice thickness of some floes abt. 25 cm
	2000-04-01	12:15:00	-	-	-	-	-	-	-	-	-	-	-	-	stopped force recording; new zero 010400.sp8
0104_0040	2000-04-01	12:17:00	16:36:00	-	OW	-	-	-	-	-	12.5	-	-7.2	10	started new force recording
0104_0050	2000-04-01	16:36:00	18:15:00	0.20	LF	-	-	NE	0104_050.txt	0104_0054.mpg 0104_0055.mpg	12.9	N	-5.2	100	started new force recording
0104_0060	2000-04-01	18:15:00	18:19:00	-	-	-	-	-	-	-	12.5	NNE	-5.2	10	started new force recording
0104_0070	2000-04-01	18:19:00	19:59:00	-	-	-	-	-	0104_060.txt	-	-	-	-	100	started new force recording
0104_0080	2000-04-01	19:59:00	21:09:00	-	-	-	-	-	0104_070.txt	-	-	-	-	100	started new force recording
0104_0090	2000-04-01	21:09:00	22:18:00	-	-	-	-	-	0104_080.txt	-	-	-	-	100	started new force recording
	2000-04-01	22:18:00	0:14:00	-	-	-	-	-	0104_090.txt	-	-	-	-	100	started new force recording
	2000-04-01	22:20:00	-	0.20	UI	-	-	-	-	-	10.6	N	-7.0	-	-

a) Camera 1, 2 and 3, positions see illustraion above.
b) L = Level ice, H= Hummocked ice, R= Ridged ice, CP= Closed pack, FI= Floe ice, OW= Open water, BI=Broken ice, TNI= Thin new ice, FR= Finger raftning, TI=Thin ice, RI= Refrozen ice, LF=Large floes, UI= Uniform ice, U=Unconfined, RC= Release crack, NI= New ice, PU=Pile up, G= Grounded, TLI= thin level ice, RFI=Refrozen broken ice, OC= Open channel
c) C= Crushing, B= Bending, S= Splitting, SL=Static load, M=Mixed, BU= buckling, CR=Creep
d) Temperature measured at Rödkallen by SMHI. Position 5 km from

Table12 - Data for the 3rd of April. [TOP]

Event No.	Date	Load Meauring, time period		Ice Thickness	Ice formation	Failure mode	Ice drift		Load data	Video	Wind		Air temp.	Sampling rate	Remark
	a	Start	End	a	b)	c)	Speed	Direction		a)	Speed	Direction	a	a	a
0304_0010	3000-04-03	0:00:00	9:58:00	-	-	-	-	-	-	-	-	-	-	-	Data file sonar:00403.asc , data file Laser: 03042000
0304_0020	3000-04-03	9:58:00	12:34:00	0.20	-	-	-	-	0304_020.txt	-	-	-	-6.4	10	start new force recording; ice thickness of large floes is abt 30to35cm; between large floes 5-15cm
	3000-04-03	11:13:00	-	-	-	-	-	-	-	-	-	-	-	-	large floe is pressing on panel 8+9
	3000-04-03	11:42:00	-	-	-	-	-	SSE	-	-	6.0	E	-5.8	-	-
0304_0030	3000-04-03	12:34:00	14:25:00	0.18	-	-	-	-	0304_030.txt	-	-	-	-	100	start new force recording
	3000-04-03	13:13:00	-	0.13	-	-	-	-	-	-	-	-	-	-	-
0304_0040	3000-04-03	14:25:00	17:50:00	-	-	-	-	-	0304_040.txt	-	-	-	-	10	start new force recording
	3000-04-03	15:12:00	-	-	-	-	-	-	-	-	-	-	-	-	restart sonar system after pc crash
	3000-04-03	17:50:00	-	-	-	SL	-	-	-	-	-	-	-	-	stopped measurements, cable of panel 1 was broken in connection box, O.K. again; synchronized time, 2 min difference loleif 1 --- loleif3 (l1 = 17:50 l3 = 17:52), 1 h loleif1 --- TL recorder; new tape in TL recorder
	3000-04-03	18:08:00	-	-	-	-	-	-	-	-	-	-	-	-	start TL recording 72h mode Tape #12
0304_0050	3000-04-03	18:10:00	21:52:00	-	-	SL	-	-	-	-	-	-	-	1	start ice force recording; still static load condition
	3000-04-03	18:12:00	-	-	-	-	-	-	-	-	-	-	-	-	start laser scanner data collection; corrected date and time; date set to 03.04. Was 06.04.
	3000-04-03	18:14:00	-	0.60	-	SL	-	-	-	-	6.9	E	-3.8	-	water level = 1.05m, top of poygon steel shield; drilled two holes, ice thickness measured to 60 cm, but before it was probably only 30 cm when the ice was still moving
0304_0060	3000-04-03	21:52:00	23:02:00	-	-	C	0.18	SE	0304_060.txt	0304_0061.mpg	-	-	-	30	start new force recording; ice starte to move again
	3000-04-03	23:02:00	-	-	FL	-	-	SE	-	-	8.4	SE	-4.2	10	start new force recording; drifting snow

a) Camera 1, 2 and 3, positions see illustraion above.
b) L = Level ice, H= Hummocked ice, R= Ridged ice, CP= Closed pack, FI= Floe ice, OW= Open water, BI=Broken ice, TNI= Thin new ice, FR= Finger raftning, TI=Thin ice, RI= Refrozen ice, LF=Large floes, UI= Uniform ice, U=Unconfined, RC= Release crack, NI= New ice, PU=Pile up, G= Grounded, TLI= thin level ice, RFI=Refrozen broken ice, OC= Open channel
c) C= Crushing, B= Bending, S= Splitting, SL=Static load, M=Mixed, BU= buckling, CR=Creep
d) Temperature measured at Rödkallen by SMHI. Position 5 km from

Table 13 - Data for the 4th of April. [TOP]

Event No.	Date	Load Meauring, time period		Ice Thickness	Ice formation	Failure mode	Ice drift		Load data	Video	Wind		Air temp.	Sampling rate	Remark
	a	Start	End	a	b)	c)	Speed	Direction		a)	Speed	Direction	a	a	a
	2000-04-04	7:45:00	-	-	-	-	0.12	SSE	-	-	8.7	SE	-3.2	-	Data file laser: 04042000, data file sonar: 00404.asc, data file EM: 000404.stop force recording; snow
	2000-04-04	7:51:00	10:44:00	-	-	-	-	-	-	-	-	-	-	10	start new force recording
	2000-04-04	9:05:00	-	-	-	-	0.10	SSE	-	-	6.6	SE	-1.4	-	-
	2000-04-04	10:44:00	-	-	-	-	-	SW	-	-	6.4	SSE	0.0	-	Stopped force recording, zero condition for panels; took new zero
	2000-04-04	13:20:00	-	-	-	-	-	-	-	-	3.6	N	-1.0	-	-
	2000-04-04	13:42:00	16:54:00	-	-	-	-	N	-	-	-	-	-	1	slow drift speed
	2000-04-04	15:00:00	-	-	-	-	-	-	-	-	-	-	-	-	EM system installed and calibration running; unfortuneately over edge of 60cm thick floe laser=1.7m
	2000-04-04	16:00:00	-	-	-	-	-	-	-	-	-	-	-	-	EM measurement started at 0.5 Hz, currently over floe edge. dEM = 3.00m Laser 1.7m above water level
	2000-04-04	16:20:00	-	-	-	-	-	N	-	-	5.8	N	-	-	ice starts to move from N ---> S
0404_0040	2000-04-04	16:54:00	19:35:00	-	U	-	-	NE	-	-	6.5	N	-2.6	10	started new force recording; release cracks due to open water around
	2000-04-04	17:30:00	-	0.25	U	-	-	-	-	-	-	-	-	-	typical ice thickness 25cm; water level 1m below "Stahlkante"; unconfined ice, braking into fragments infront of us; some buckling at ice thickness of 10cm

	2000-04-04	18:54:00	-	-	G	-	-	-	-	-	-	-	-	-	grouded wedge infront of lighthouse in NE
	2000-04-04	19:10:00	-	-	OC	-	-	-	-	-	5.8	N	-3.6	-	open channel filled with broken ice pieces infront of lighthouse
0404_0050	2000-04-04	19:35:00	21:00:00	-	-	-	0.20	ENE	0404_040.txt	-	6.0	N	-	10	start new force recording
	2000-04-04	19:48:00	-	0.13	-	B	0.20	E	-	-	-	-	-	-	bending failure due to lot of snow on ice surface; release crack opens again
	2000-04-04	19:58:00	-	-	-	-	-	-	-	-	-	-	-	-	snow load is to high, initiates the bending failure, no crushing; detail analysis of short crushing sequences
	2000-04-04	20:25:00	-	-	-	C	-	-	-	-	-	-	-	-	-
	2000-04-04	21:00:00	23:00:00	-	-	-	-	E	0404_050.txt	-	9.3	N	-4.2	10	start new force recording
	2000-04-04	21:02:00	-	0.20	-	RC	-	-	-	-	-	-	-	-	release crack i East
	2000-04-04	21:07:00	-	-	RI	-	0.17	E	-	-	-	-	-	-	refrozen deformed ice
	2000-04-04	22:45:00	-	0.15	-	-	0.20	E	-	-	8.7	N	-4.6	-	drifting snow
	2000-04-04	22:51:00	-	-	-	RC	-	-	-	-	-	-	-	-	-
	2000-04-04	23:00:00	-	-	-	-	-	-	-	-	-	-	-	10	start new force recording
	2000-04-04	23:35:00	-	-	OW	-	-	-	-	-	-	-	-	-	sonar zero reading 6.65m
	2000-04-04	23:48:00	-	-	-	-	-	-	-	-	-	-	-	-	EM stopped and restarted

a) Camera 1, 2 and 3, positions see illustraion above.
b) L = Level ice, H= Hummocked ice, R= Ridged ice, CP= Closed pack, FI= Floe ice, OW= Open water, BI=Broken ice, TNI= Thin new ice, FR= Finger raftning, TI=Thin ice, RI= Refrozen ice, LF=Large floes, UI= Uniform ice, U=Unconfined, RC= Release crack, NI= New ice, PU=Pile up, G= Grounded, TLI= thin level ice, RFI=Refrozen broken ice, OC= Open channel
c) C= Crushing, B= Bending, S= Splitting, SL=Static load, M=Mixed, BU= buckling, CR=Creep
d) Temperature measured at Rödkallen by SMHI. Position 5 km from

Table 14 - Data for the 5th of April. [TOP]

Event No.	Date	Load Meauring, time period		Ice Thickness	Ice formation	Failure mode	Ice drift		Load data	Video	Wind		Air temp.	Sampling rate	Remark
	a	Start	End	a	b)	c)	Speed	Direction		a)	Speed	Direction	a	a	a
0504_0010	2000-04-05	0:00:00	8:08:00	-	-	-	-	-	-	-	-	-	-	-	Data file laser: 05042000, data fle sonar: 00405.asc, data file em: 000405
	2000-04-05	8:00:00	-	-	R	-	-	NNE	-	-	9.0	N	-6.0	-	-
	2000-04-05	8:05:00	-	-	-	-	-	-	-	-	-	-	-	-	stop force recording
	2000-04-05	8:08:00	9:04:00	-	-	-	-	-	-	-	-	-	-	1	start new force recording
0504_0030	2000-04-05	9:04:00	10:22:00	-	H	M	0.20	NNE	0504_030.txt	-	-	-	-	10	start new force recording
	2000-04-05	9:09:00	-	-	-	-	0.20	N	-	-	9.0	N	-	-	-
	2000-04-05	9:18:00	-	-	-	-	-	-	-	-	-	-	-	-	EM stopped for back up
	2000-04-05	9:34:00	-	-	-	-	0.20	NW	-	-	-	-	-	-	-
	2000-04-05	9:55:00	-	0.20	-	C	-	-	-	-	-	-	-	-	lot of cracks with open water; sonar zero reading 6.56m
	2000-04-05	10:22:00	-	-	OW	-	-	-	-	-	9.0	N	-	-	slush ice doesn't allow a zero for sonar; snow; stop force recording
0504_0040	2000-04-05	10:26:00	11:00:00	0.33	-	C	0.29	NNE	0504_040.txt	-	-	-	-6.6	10	start new force recording
	2000-04-05	10:36:00	-	-	-	-	-	-	-	-	-	-	-	-	EM restartet; approximate offset Zi=0.9m Sw=3.2ppt
	2000-04-05	10:42:00	-	-	-	-	-	-	-	-	-	-	-	-	open crack infront of lighthouse
	2000-04-05	10:52:00	-	-	-	-	0.30	NE	-	-	-	-	-	-	-
0504_0050	2000-04-05	11:00:00	12:00:00	-	-	-	-	-	0504_050.txt	-	-	-	-	30	start new force recording
	2000-04-05	11:13:00	-	-	-	-	0.00	-	-	-	-	-	-	-	ice movement stopped
	2000-04-05	11:27:00	-	0.30	-	C	0.30	NNE	-	-	10.9	N	-6.6	-	-
	2000-04-05	11:34:00	-	-	R	-	-	-	-	-	-	-	-	-	passing a ridge; rubble pile initiates bending failure
	2000-04-05	11:39:00	11:44:00	-	-	-	-	-	-	-	-	-	-	-	no sonar data; camera 3 adjusted
	2000-04-05	11:46:00	-	-	R	-	-	-	-	-	-	-	-	-	passing a ridge
	2000-04-05	11:55:00	-	-	-	-	0.35	N	-	-	11.9	N	-6.6	-	-

0504_0060	2000-04-05	12:00:00	13:00:00	-	-	C	0.30	N	0504_060.txt	-	-	-	-	100	start new force recording
	2000-04-05	12:06:00	-	-	-	-	0.33	N	-	-	-	-	-	-	-
	2000-04-05	12:10:00	-	-	-	-	0.33	-	-	-	-	-	-	-	-
	2000-04-05	12:15:00	-	0.25	-	-	-	-	-	-	12.3	N	-6.4	-	ice thickness estimation from J. Schwarz
	2000-04-05	12:37:00	-	-	U	-	-	-	-	-	11.8	N	-6.2	-	unconfined ice condition due to crack in North
	2000-04-05	12:45:00	-	-	-	-	-	-	-	-	-	-	-	-	EM stopped
0504_0070	2000-04-05	13:00:00	14:00:00	-	-	-	-	-	-	-	-	-	-	30	start new force recording
	2000-04-05	13:49:00	-	0.40	L	C	0.33	NE	-	0504_0078.mpg	-	-	-	-	strong vibrations
	2000-04-05	13:51:00	-	-	-	-	-	-	-	0504_0079.mpg	-	-	-	-	EM restarted
	2000-04-05	13:59:00	-	-	RC	-	-	-	-	-	-	-	-	-	-
0504_0080	2000-04-05	14:00:00	15:00:00	-	-	-	-	-	0504_080.txt	-	10.9	N	-6.4	30	start new force recording
	2000-04-05	14:22:00	-	0.50	-	C	0.30	N	-	0504_0081.mpg	-	-	-	-	-
	2000-04-05	14:27:00	-	0.55	R	B	-	-	-	-	-	-	-	-	pssig thicker ice; ridge ???; ice does not have real strength, old ice with lot of snow on top (J.S.). #20 - #25
0504_0090	2000-04-05	15:00:00	16:00:00	-	-	M	0.30	N	0504_090.txt	-	12.5	N	-6.4	30	start new force recording; bending failure incorporated in crushing events
	2000-04-05	15:06:00	-	0.35	-	-	-	-	-	0504_0091_92.mpg 0504_0093.mpg	-	-	-	-	-
	2000-04-05	15:48:00	-	-	RI	C	0.30	N	-	-	11.0	N	-6.4	-	refrozen broken ice; crushing event
0504_0100	2000-04-05	16:00:00	17:30:00	-	-	C	-	-	0504_100.txt	-	-	-	-	30	start new force recording
	2000-04-05	17:24:00	-	-	-	-	-	-	-	-	-	-	-	-	EM restarted
0504_0110	2000-04-05	17:30:00	19:00:00	-	-	C	0.30	N	0504_110.txt	-	12.3	N	-	30	start new force recording
	2000-04-05	18:00:00	-	-	-	-	0.30	NNW	-	-	13.0	-	-	-	water level measurements: 2.2m = distance water surface ---> concret platform, 1.2m = distance water surface ---> steel shield, 0.7m = distance water surface ---> top of panel; sonar zero reading = 6.4m
	2000-04-05	18:20:00	-	-	R	-	-	-	-	-	-	-	-	-	passing consolidated ridge; forces are increasing
	2000-04-05	18:50:00	-	-	-	-	0.27	NNW	-	-	12.0	NW	-5.4	-	-
	2000-04-05	19:00:00	19:27:00	-	-	-	-	-	-	-	-	-	-	30	start new force recording
	2000-04-05	19:27:00	-	-	U	-	-	-	-	-	-	-	-	-	stopped force recording; unconfined condition, open leads; performed data back up
	2000-04-05	23:34:00	-	-	-	-	-	-	-	-	-	-	-	-	EM stopped, system above edge of channel
	2000-04-05	23:36:00	-	-	-	-	0.45	NW	-	-	14.4	W	-5.2	-	EM restarted over channel edge
	2000-04-05	23:48:00	-	-	-	-	-	-	-	-	-	-	-	-	EM stopped for the night

a) Camera 1, 2 and 3, positions see illustraion above.
b) L = Level ice, H= Hummocked ice, R= Ridged ice, CP= Closed pack, FI= Floe ice, OW= Open water, BI=Broken ice, TNI= Thin new ice, FR= Finger raftning, TI=Thin ice, RI= Refrozen ice, LF=Large floes, UI= Uniform ice, U=Unconfined, RC= Release crack, NI= New ice, PU=Pile up, G= Grounded, TLI= thin level ice, RFI=Refrozen broken ice, OC= Open channel
c) C= Crushing, B= Bending, S= Splitting, SL=Static load, M=Mixed, BU= buckling, CR=Creep
d) Temperature measured at Rödkallen by SMHI. Position 5 km from

Table15 - Data for the 12th of April. [TOP]

Event No.	Date	Load Meauring, time period		Ice Thickness	Ice formation	Failure mode	Ice drift		Load data	Video	Wind		Air temp.	Sampling rate	Remark
	a	Start	End	a	b)	c)	Speed	Direction		a)	Speed	Direction	a	a	a
	2000-04-12	8:19:00	-	-	FI	-	-	S	-	-	7.4	SE	1.8	-	Data file laser: 12042000, data file sonar: 00412.asc, data file EM: 000412. stop force recording; snow
	2000-04-12	10:05:00	-	-	-	-	-	-	-	-	-	-	-	-	open water at sonar, reading = 6.59
	2000-04-12	10:30:00	-	-	OW	-	-	-	-	-	8.7	SE	1.4	-	took new zero for panels, nu120400.sp8
	2000-04-12	11:01:00	13:00:00	-	-	-	-	-	-	-	-	-	1.2	10	start new force recording; weak ice
	2000-04-12	12:04:00	-	-	-	M	0.08	S	-	-	-	-	-	-	ice thickness varies a lot, sonar shows up to 1m; weak ice
	2000-04-12	13:00:00	15:05:00	-	-	-	-	SSE	-	-	6.3	SE	2.0	10	start new force recording, weak ice

1204_0040	2000-04-12	15:05:00	17:00:00	-	-	M	0.10	SSE	1204_040.txt	-	6.1	SE	1.8	10	start new force recording; mixed failure mode, bending and crushing, mostly bending
1204_0050	2000-04-12	17:00:00	18:36:00	-	L	B	-	SSE	1204_050.txt	-	4.7	S	1.6	10	start new force recording
	2000-04-12	17:09:00	-	-	-	-	-	-	-	-	-	-	-	-	restarted TL-recorder, new tape
	2000-04-12	17:10:00	-	-	-	-	-	-	-	-	-	-	-	-	em system failed
	2000-04-12	17:14:00	-	-	-	-	-	-	-	-	-	-	-	-	restarted em system
	2000-04-12	18:36:00	-	-	-	-	-	-	-	-	-	-	-	-	stop force recording; set up addional accelerometers
	2000-04-12	20:30:00	-	-	-	-	-	-	-	-	-	-	0.6	-	accelerometers are installed, Acc_1 = Level 1, Acc_2 = Level 3, Acc_3 = Level 6 (are still at level 8 but will be removed), Acc_4 = Level 8; no ice movement; calm wind
1204_0060	2000-04-12	22:30:00	0:00:00	-	-	SL	-	-	-	-	1.9	SE	1.6	1	start long term force recording

a) Camera 1, 2 and 3, positions see illustraion above.
b) L = Level ice, H= Hummocked ice, R= Ridged ice, CP= Closed pack, FI= Floe ice, OW= Open water, BI=Broken ice, TNI= Thin new ice, FR= Finger raftning, TI=Thin ice, RI= Refrozen ice, LF=Large floes, UI= Uniform ice, U=Unconfined, RC= Release crack, NI= New ice, PU=Pile up, G= Grounded, TLI= thin level ice, RFI=Refrozen broken ice, OC= Open channel
c) C= Crushing, B= Bending, S= Splitting, SL=Static load, M=Mixed, BU= buckling, CR=Creep
d) Temperature measured at Rödkallen by SMHI. Position 5 km from

Table 16 - Data for the 13th of April. [TOP]

Event No.	Date	Load Meauring, time period		Ice Thickness	Ice formation	Failure mode	Ice drift		Load data	Video	Wind		Air temp.	Sampling rate	Remark
	a	Start	End	a	b)	c)	Speed	Direction		a)	Speed	Direction	a	a	a
1304_0010	2000-04-13	0:00:00	8:30:00	-	-	-	-	-	-	-	-	-	-	1	Data file laser: 13042000, data file sonar: 00413.asc, data file em: 000413
	2000-04-13	8:30:00	-	-	-	SI	0.00	-	-	-	4.7	NE	0.4	-	stop all recordings to back up data; laser recording failed overnight; stabil ice conditions, small loads on panel 3+5, no load on other panels
	2000-04-13	10:50:00	-	-	-	-	-	-	-	-	4.7	NE	2.2	-	no ice movement, small static load on panel 3,5 + 4
	2000-04-13	11:18:00	-	-	-	-	-	-	-	-	-	-	-	-	start sonar, laser and em data recording
1304_0020	2000-04-13	11:20:00	13:29:00	-	-	SL	0.00	-	-	-	-	-	-	1	start long term force recording
	2000-04-13	11:30:00	-	-	-	-	-	-	-	-	-	-	-	-	measured ice thickness at em location 3 times to 32cm, freeborad = 0 cm; saw horizotally splitted ice; have taken 4 samples; water level = 63 cm below top of the panels
1304_0030	2000-04-13	13:29:00	14:31:00	-	-	-	-	-	-	1304_0031_32.mpg 1304_0033.mpg	-	-	-	30	start new force recording
	2000-04-13	13:40:00	-	0.28	-	B	0.05	NE	-	1304_0031_32.mpg	5.6	NNE	1.4	-	fog; water- and ice Temperature -0.2°C; Air temperature over the ice = 0.4 °C. Pictures: #15, #16 + #17
	2000-04-13	14:31:00	-	-	-	-	-	-	-	1304_0034.mpg	-	-	-	-	stop force recording; ice movement has stopped
1304_0040	2000-04-13	14:33:00	-	-	-	SL	0.00	-	-	-	6.6	NNE	1.4	1	start new force recording; took pictures from crushed ice samples. pictures: #23 - #26
	2000-04-13	15:30:00	-	-	-	-	-	-	-	-	-	-	-	-	stop and restart em recording; file name was wrong 04121117---->04131117
	2000-04-13	17:30:00	-	-	-	SL	0.00	-	-	-	6.6	N	-	-	no ice movement, static load condition; sunshine
1304_0050	2000-04-13	18:24:00	19:52:00	-	-	-	-	NE	1304_050.txt	-	-	-	-	30	start new force recording; ice starts to move again; em system failed, stop em recording
	2000-04-13	18:26:00	-	0.30	-	SL	-	NE	-	-	6.8	N	1.0	-	restarted em system; no real ice movement, static load; large ice wedge infront of the lighthousein NE, on the left + right side of this wedge ice is passing by; only friction forces are transmitted to the panels. Pictures: #27 + #28
	2000-04-13	19:52:00	-	-	-	-	-	-	-	-	-	-	-	-	stop force recording, to much open water around the lighthouse
1304_0060	2000-04-13	20:10:00	20:34:00	-	R	-	-	-	1304_060.txt	-	6.8	N	-0.2	30	start new force recording; passing a ridge; crack is opening in the NE

	2000-04-13	20:25:00	-	-	-	-	-	-	-	-	-	-	-	-	ice movement stopped; same scenario is described at 18:26 h
	2000-04-13	20:34:00	-	-	-	-	-	-	-	-	-	-	-	-	stop force recording; no movement is expected in the near future
	2000-04-13	21:14:00	-	-	-	-	-	-	-	-	8.3	N	-0.2	-	no ice movement, zero conditio, took new zero nu130400.sp8; em over open water reading = -0.33, laser reading over ice floe = 26.33
1304_0070	2000-04-13	22:07:00	23:05:00	-	-	-	-	-	1304_070.txt	-	-	-	-	10	start new force recording; ice starts to move again
1304_0080	2000-04-13	23:05:00	0:00:00	-	-	SL	-	-	-	-	7.2	N	-0.6	1	start new force recording

a) Camera 1, 2 and 3, positions see illustraion above.
b) L = Level ice, H= Hummocked ice, R= Ridged ice, CP= Closed pack, FI= Floe ice, OW= Open water, BI=Broken ice, TNI= Thin new ice, FR= Finger raftning, TI=Thin ice, RI= Refrozen ice, LF=Large floes, UI= Uniform ice, U=Unconfined, RC= Release crack, NI= New ice, PU=Pile up, G= Grounded, TLI= thin level ice, RFI=Refrozen broken ice, OC= Open channel
c) C= Crushing, B= Bending, S= Splitting, SL=Static load, M=Mixed, BU= buckling, CR=Creep
d) Temperature measured at Rödkallen by SMHI. Position 5 km from

Table 17 - Data for the 14th of April. [TOP]

Event No.	Date	Load Meauring, time period		Ice Thickness	Ice formation	Failure mode	Ice drift		Load data	Video	Wind		Air temp.	Sampling rate	Remark
	a	Start	End	a	b)	c)	Speed	Direction		a)	Speed	Direction	a	a	a
1404_0010	2000-04-14	0:00:00	1:36:00	-	-	-	-	-	-	-	-	-	-	-	Data file laser: 14042000, data file sonar: 00414.asc, data file em: 000414
	2000-04-14	1:30:00	-	-	-	-	-	ENE	-	-	-	-	-	-	restarted laser scanner after failure
1404_0020	2000-04-14	1:36:00	2:03:00	-	-	-	-	-	1404_020.txt	-	-	-	-	30	start new force record
	2000-04-14	1:38:00	-	-	-	-	-	-	-	-	7.6	N	-0.6	-	several release cracks occured
	2000-04-14	1:40:00	-	-	-	-	-	-	-	-	-	-	-	-	rafting process infront of the lighthouse in the East at a stationary floe; in the North ice cover is passing, in the South is open water
	2000-04-14	1:50:00	-	-	-	B	0.08	ENE	-	-	-	-	-	-	-
	2000-04-14	1:55:00	-	-	-	-	-	-	-	-	-	-	-	-	ice floe has stopped again in the ENE; static load condition esp. On panel 8 + 9; open water in the South
1404_0030	2000-04-14	2:03:00	8:30:00	-	-	-	-	-	1404_030.txt	-	7.6	N	-0.6	10	start new force recording
	2000-04-14	2:10:00	-	-	-	SL	-	-	-	-	-	-	-	-	static load on panel 8; laser reading = 26.03; sonar reading = 4.33; em ice thickness abt. 70cm
1404_0040	2000-04-14	8:30:00	9:13:00	-	-	-	-	-	1404_040.txt	-	9.5	NNE	0.2	30	start new force recording
	2000-04-14	8:37:00	-	-	-	B	-	-	-	-	-	-	-	-	semi static load condition in NE
	2000-04-14	8:41:00	-	-	-	B	0.10	SE	-	-	-	-	-	-	new release cracks
	2000-04-14	8:46:00	-	-	-	B	-	-	-	-	-	-	-	-	unconfined condition; radial + circon. cracks see camera 2+3
	2000-04-14	8:52:00	-	-	-	-	0.08	-	-	-	-	-	-	-	release crack in the North, ice movement stops
	2000-04-14	9:05:00	-	-	-	-	-	SE	-	-	-	-	-	-	ice starts to move again; release crack in the South is leading to open water in the South; ice movement stops again
	2000-04-14	9:07:00	-	-	-	B	-	-	-	-	-	-	-	-	ice starts to move again; unconfined condition; open water in the South
1404_0050	2000-04-14	9:13:00	10:50:00	-	-	-	-	SE	1404_050.txt	1404_0051.mpg 1404_0052.mpg 1404_0053.mpg	-	-	0.6	10	start mnew force recording; still unconfined condition; lot of open water patches around
	2000-04-14	10:45:00	-	-	-	-	-	E	-	-	8.6	NE	0.6	-	ice wedge infront of the lighthouse in the East; ice is passing by in the North and the South; nearly no forces
1404_0060	2000-04-14	10:50:00	13:03:00	-	-	-	-	-	1404_060.txt	-	-	-	-	10	start new force recording; ice situation is clearly to be seen at camera 1 + 2; sonar reading at open water = 6.61; stop em and back up em data
	2000-04-14	11:05:00	-	-	-	-	-	-	-	-	-	-	-	-	restarted em system
	2000-04-14	11:10:00	-	-	-	-	-	-	-	-	-	-	-	-	stop laser and back up data
	2000-04-14	11:17:00	-	-	-	-	-	-	-	-	-	-	-	-	restarted laser data collection
	2000-04-14	12:00:00	-	0.30	-	B	0.11	ESE	-	-	7.8	NE	1.0	-	better confinement, but still release cracks in the South; single bending events

	2000-04-14	12:38:00	-	-	-	B	0.10	ESE	-	-	-	-	1.0	-	snow
	2000-04-14	12:40:00	-	-	-	C	-	-	-	-	-	-	-	-	see camera 3
	2000-04-14	12:41:00	-	-	-	B	-	-	-	-	-	-	-	-	bending failure with radial release crack in NE
	2000-04-14	12:44:00	-	-	-	B	-	-	-	-	-	-	-	-	bending failure with rad + circon cracks, see camera 1 + 2 + 3
	2000-04-14	12:47:00	-	-	R	-	-	-	-	-	-	-	-	-	-
	2000-04-14	12:51:00	-	-	-	B	-	-	-	-	-	-	-	-	very slow ice movement; bending failure in NE
	2000-04-14	13:03:00	-	-	-	-	-	-	-	-	-	-	-	-	stop ice force recording; ice movement has stopped
1404_0070	2000-04-14	13:06:00	16:25:00	-	-	-	-	-	1404_070.txt	-	9.2	NE	0.6	10	start new force rcording
	2000-04-14	15:05:00	-	1.15	-	SL	0.00	-	-	-	8.8	NE	0.4	-	snow; static load condition on panel 7 + 2; ice thickness em = 1.2 m; ice thickness sonar = 1.1m
1404_0080	2000-04-14	16:25:00	16:55:00	0.18	L	-	0.15	ESE	-	-	7.3	NE	0.2	30	start new force recording; unconfined condition due to open water in the North
	2000-04-14	16:34:00	-	-	-	-	-	-	-	-	-	-	-	-	em system failed
	2000-04-14	16:36:00	-	-	-	B	-	-	-	-	-	-	-	-	restarted em system; release crack in the East splits the ice flow ---> no confinement
	2000-04-14	16:44:00	-	-	-	M	-	E	-	-	-	-	-	-	still unconfined condition due to open water in the North; mixed failure mode, crushing + bending; see camera 1. picture #30
	2000-04-14	16:55:00	-	-	-	-	-	-	-	-	-	-	-	-	stop force recording; open water now in North and South; no confinement
	2000-04-14	17:00:00	-	-	-	-	-	-	-	-	-	-	-	-	ice movement has stopped
1404_0090	2000-04-14	18:13:00	3:21:00	-	-	-	-	-	-	-	6.3	NE	-0.2	1	start long term force recording
	2000-04-14	18:18:00	-	-	-	-	-	-	-	-	-	-	-	-	ice thickness em = 80-90cm sonar = 1.3-1.4m
	2000-04-14	18:25:00	-	-	-	-	-	-	-	-	-	-	-	-	-
	2000-04-14	20:00:00	-	-	-	-	-	-	-	-	7.9	NE	-0.4	-	no ice movement; nearly no load on panels
	2000-04-14	22:39:00	-	-	-	-	-	-	-	-	-	-	-	-	stop em data recording
	2000-04-14	22:40:00	-	-	-	-	-	-	-	-	-	-	-	-	restart em system

a) Camera 1, 2 and 3, positions see illustraion above.
b) L = Level ice, H= Hummocked ice, R= Ridged ice, CP= Closed pack, FI= Floe ice, OW= Open water, BI=Broken ice, TNI= Thin new ice, FR= Finger raftning, TI=Thin ice, RI= Refrozen ice, LF=Large floes, UI= Uniform ice, U=Unconfined, RC= Release crack, NI= New ice, PU=Pile up, G= Grounded, TLI= thin level ice, RFI=Refrozen broken ice, OC= Open channel
c) C= Crushing, B= Bending, S= Splitting, SL=Static load, M=Mixed, BU= buckling, CR=Creep
d) Temperature measured at Rödkallen by SMHI. Position 5 km from

Table 18 - Data for the 17th of April. [TOP]

Event No.	Date	Load Meauring, time period		Ice Thickness	Ice formation	Failure mode	Ice drift		Load data	Video	Wind		Air temp.	Sampling rate	Remark
	a	Start	End	a	b)	c)	Speed	Direction		a)	Speed	Direction	a	a	a
	2000-04-17	0:05:00	7:00:00	-	FI	-	-	E	-	-	5.4	E	1.4	1	Data file laser: 17042000, data file sonar:v, data file EM: 000417. different floe sizes
	2000-04-17	0:18:00	-	-	FI	-	-	E	-	-	5.9	SE	1.4	1	-
	2000-04-17	7:00:00	8:00:00	-	-	mixed; b+c	0.15	SE	-	-	9.5	ESE	1.8	10	very weak ice ; sunshine
	2000-04-17	7:09:00	-	0.25	-	-	-	-	-	-	-	-	-	-	ice wedge in the east
	2000-04-17	7:14:00	-	-	R	-	-	-	-	-	-	-	-	-	passing ridged area
	2000-04-17	7:17:00	-	-	-	-	-	-	-	-	-	-	-	-	ice wedge inront of the lighthouse
	2000-04-17	7:20:00		0.14	-	-	-	-	-	-	-	-	-	-	ice wedge in the south
	2000-04-17	7:42:00	-	-	-	-	-	-	-	-	-	-	-	-	ice stopped; release crack and open water in the north; sonar zero reading = 6.48 m; low ice forces due to already rotten ice. Picture 7; 8; 9 of No. 4
	2000-04-17	7:48:00	-	-	small R	-	-	-	-	-	-	-	-	-	ice starts to move again; passing small ridge; small vibration on lighthouse

	2000-04-17	7:51:00	-	-	RC	-	-	-	-	-	-	-	-	-	release cracks are opening in NE and SE => ice wedge in the north; open water in E, S and W,
1704_0040	2000-04-17	8:00:00	9:00:00	-	-	-	-	SE	-	--	9.9	E	2.0	10	unconfined ice condition, lot of open water patches of different sizes don't allow continious ice movement and higher loads on panels; no study state is reached
	2000-04-17	8:55:00	-	0.5	-	mixed, c + b	-	-	-	-	-	-	2.0	-	better ice; more confinement
	2000-04-17	9:00:00	10:10:00	-	-	-	-	-	1704_040.txt	-	-	-	-	10	-
	2000-04-17	9:03:00	-	-	-	mixed, c + b	0.18	SE	-	-	9.9	SE	-	-	release crack; forming of wedges infront of the lighthouse leads to decreasing of forces
	2000-04-17	9:11:00	-	-	-	mixed, c + b	-	-	-	-	-	-	-	-	-
	2000-04-17	9:14:00	-	-	-	C	-	-	-	-	-	-	-	-	crushing event
	2000-04-17	9:20:00	-	-	R	-	-	-	-	-	-	-	-	-	passing a ridge
	2000-04-17	9:21:00	-	-	RC	-	-	-	-	-	-	-	-	-	ice movement stopped; release crack in the south is opening
	2000-04-17	10:12:00	11:17:00	-	-	-	-	-	-	-	11	E	2.4	1	open water in the south; no ice movement; static load condition on northern panels 6,5+3
	2000-04-17	11:12:00	-	-	-	-	-	-	-	-	-	-	-	-	ice moves again, but the lighthouse is now in an open lead; it is still some grounded ice in place; see camera 3
	2000-04-17	11:15:00	-	-	-	-	-	-	-	-	-	-	-	-	new ice floe is hitting the lighthouse from the south
	2000-04-17	11:17:00	12:13:00	-	-	mixed, c + b	-	SSE	-	-	-	-	-	10	ice movement stopped and started again; unconfined condition due to release crack in the East; mixed failure mode in the south
	2000-04-17	11:19:00	-	-	-	-	-	-	-	-	-	-	-	-	large radial crack opens in the south
	2000-04-17	11:24:00	-	-	-	-	-	-	-	-	-	-	-	-	another release crack opens in the south
	2000-04-17	11:38	-	-	-	-	-	-	-	-	11.6	E	2.4	-	still unconfined ice condition, lot of open water patches; coverage abt. 8/10 to 9/10
	2000-04-17	11:43	-	0.10	-	-	0.20	SE	-	-	-	-	-	-	-
	2000-04-17	11:48	-	0.18	-	M	0.25	SE	-	-	-	-	-	-	mixed failure mode, bending + crushing
	2000-04-17	11:51	-	-	-	-	-	-	-	-	-	-	-	-	release crack in SE
	2000-04-17	12:13	-	-	-	-	-	-	-	-	11.6	E	1.6	-	stop force recording; very havy rain; high voltage in the air; thunder protection starts to work
	2000-04-17	12:55	-	-	-	-	-	-	-	-	10.5	SE	1.6	-	restarted em system
	2000-04-17	13:10	13:46	0.10	L	C	0.22	SE	-	-	-	-	-	10	start new force recording; confined ice condition; ice thickbess might be even less then 10 cm
	2000-04-17	13:15	-	0.22	-	-	-	-	-	-	-	-	-	-	ice is getting thicker now
	2000-04-17	13:16	-	-	-	M	-	-	-	-	-	-	-	-	bending + crushing failure; no vibration
	2000-04-17	13:19	-	-	-	-	-	-	-	-	-	-	-	-	ice wedge in the South
	2000-04-17	13:33	-	-	-	-	0.20	SE	-	-	-	-	2.2	-	-
	2000-04-17	13:40	-	-	-	-	-	-	-	-	-	-	-	-	radial crack in the South is opening; no load on panel 7 + 2
	2000-04-17	13:46	-	-	-	-	-	-	-	-	-	-	-	-	all panels are free of load; stop force recording
	2000-04-17	13:49	-	-	-	-	-	-	-	-	-	-	-	-	took new zero nu170400.sp8; sonar zero reading = 6.59; em = 1.37; laser = 1.88
	2000-04-17	14:08	14:21	-	H	-	0.20	SE	-	-	12.2	SE	2.2	30	start new force recording; rafted and ridged ice is hitting the lighthouse and splitted in the South
	2000-04-17	14:14	-	-	-	M	-	-	-	-	-	-	-	-	bending + crushing; release crack in the South
	2000-04-17	14:21	-	-	-	-	-	-	-	-	-	-	-	-	stop force recording; open crack has a length of several hundred meters
	2000-04-17	15:02	15:21	-	-	-	0.25	S	-	-	-	-	2.2	30	start new force recording; release crack is opening in the South
	2000-04-17	15:07	-	-	-	B	-	-	-	-	11.6	SE	-	-	still release cracks in the SE towards open leads

	2000-04-17	15:17	-	-	-	-	-	-	-	-	-	-	-	-	sonar open water reading = 6.63
	2000-04-17	15:21	-	-	-	-	-	-	-	-	-	-	-	-	stop force recording
1704_0090	2000-04-17	15:28	16:04	-	-	-	-	SSE	1704_090.txt	-	-	-	-	30	start new force recording
	2000-04-17	15:30	-	-	-	M	-	-	-	-	-	-	-	-	first ice contact; small crushing event followed by bending failure; unconfined condition
	2000-04-17	15:32	-	-	-	M	-	-	-	-	-	-	-	-	crushing and bending; em shows ice thickness of abt. 60 cm, due to unconfinement in the NE sonar is not showing the real ice thickness; load on panel 7, 2, 8, 9 + 1
	2000-04-17	15:36	-	0.55	-	M	-	-	-	-	-	-	-	-	lighthouse is vibrating a little; crushing + bending failure; em shows ice thickness of abt. 50-60cm
	2000-04-17	15:40	-	0.40	-	C	0.22	S	-	-	-	-	-	-	-
	2000-04-17	15:50	-	-	R	C	-	-	-	-	-	-	-	-	crushing through a ridge; thicker ice behind the ridge abt. 80 cm, 2 layers ???
	2000-04-17	15:53	-	-	R	C	-	-	-	-	-	-	-	-	passing the next ridged area; em shows ice thickness up to 2 m and even more
	2000-04-17	15:56	-	-	R	C	-	-	-	-	-	-	-	-	em shows ice thickness of more then 3m; still crushing; lighthouse is vibrating
	2000-04-17	15:57	-	-	R	-	-	-	-	-	-	-	-	-	got stock in the ridge;
	2000-04-17	16:00	-	-	-	-	-	-	-	-	-	-	-	-	release crack in the South; ice starts to move again; sail will pass the em
	2000-04-17	16:04	-	-	-	-	-	-	-	-	-	-	-	-	stop force recording due to long open lead in the South
	2000-04-17	16:15	-	-	-	-	-	-	-	-	10.6	SSE	1.8	-	still open lead in the South
	2000-04-17	17:30	-	0.20	-	M	-	SW	-	-	12.3	SW	1.0	-	ice is turning more and more to the west; no forces can be measured
	2000-04-17	18:12	-	-	-	-	-	-	-	-	-	-	-	-	stop em recording, back up data
	2000-04-17	18:21	-	-	-	-	-	-	-	-	-	-	-	-	sonar open water reading = 6.71
	2000-04-17	19:46	-	-	-	-	-	WSW	-	-	12.4	S	1.4	-	-
	2000-04-17	21:40	-	-	-	-	-	WSW	-	-	12.3	S	1	-	rotten ice with a lot of melt puddles

a) Camera 1, 2 and 3, positions see illustraion above.
b) L = Level ice, H= Hummocked ice, R= Ridged ice, CP= Closed pack, FI= Floe ice, OW= Open water, BI=Broken ice, TNI= Thin new ice, FR= Finger raftning, TI=Thin ice, RI= Refrozen ice, LF=Large floes, UI= Uniform ice, U=Unconfined, RC= Release crack, NI= New ice, PU=Pile up, G= Grounded, TLI= thin level ice, RFI=Refrozen broken ice, OC= Open channel
c) C= Crushing, B= Bending, S= Splitting, SL=Static load, M=Mixed, BU= buckling, CR=Creep
d) Temperature measured at Rödkallen by SMHI. Position 5 km from